Automation and Control Engineering Series

Sliding Mode Control in Electro-Mechanical Systems

Second Edition

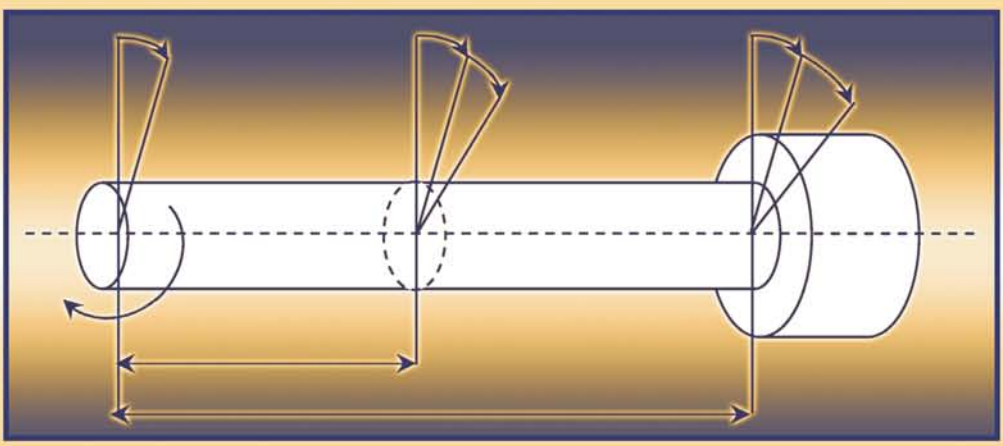

Vadim Utkin
Jürgen Guldner
Jingxin Shi

CRC Press
Taylor & Francis Group

Sliding Mode Control in Electro-Mechanical Systems

Second Edition

AUTOMATION AND CONTROL ENGINEERING

A Series of Reference Books and Textbooks

Series Editors

FRANK L. LEWIS, PH.D.,
FELLOW IEEE, FELLOW IFAC
Professor
Automation and Robotics Research Institute
The University of Texas at Arlington

SHUZHI SAM GE, PH.D.,
FELLOW IEEE
Professor
Interactive Digital Media Institute
The National University of Singapore

Sliding Mode Control in Electro-Mechanical Systems, Second Edition, *Vadim Utkin, Jürgen Guldner, and Jingxin Shi*

Optimal Control: Weakly Coupled Systems and Applications, *Zoran Gajić, Myo-Taeg Lim, Dobrila Skatarić, Wu-Chung Su, and Vojislav Kecman*

Intelligent Systems: Modeling, Optimization, and Control, *Yung C. Shin and Chengying Xu*

Optimal and Robust Estimation: With an Introduction to Stochastic Control Theory, Second Edition, *Frank L. Lewis; Lihua Xie and Dan Popa*

Feedback Control of Dynamic Bipedal Robot Locomotion, *Eric R. Westervelt, Jessy W. Grizzle, Christine Chevallereau, Jun Ho Choi, and Benjamin Morris*

Intelligent Freight Transportation, *edited by Petros A. Ioannou*

Modeling and Control of Complex Systems, *edited by Petros A. Ioannou and Andreas Pitsillides*

Wireless Ad Hoc and Sensor Networks: Protocols, Performance, and Control, *Jagannathan Sarangapani*

Stochastic Hybrid Systems, *edited by Christos G. Cassandras and John Lygeros*

Hard Disk Drive: Mechatronics and Control, *Abdullah Al Mamun, Guo Xiao Guo, and Chao Bi*

Autonomous Mobile Robots: Sensing, Control, Decision Making and Applications, *edited by Shuzhi Sam Ge and Frank L. Lewis*

Neural Network Control of Nonlinear Discrete-Time Systems, *Jagannathan Sarangapani*

Quantitative Feedback Theory: Fundamentals and Applications, Second Edition, *Constantine H. Houpis, Steven J. Rasmussen, and Mario Garcia-Sanz*

Fuzzy Controller Design: Theory and Applications, *Zdenko Kovacic and Stjepan Bogdan*

Chaos in Automatic Control, *edited by Wilfrid Perruquetti and Jean-Pierre Barbot*

Differentially Flat Systems, *Hebertt Sira-Ramirez and Sunil Kumar Agrawal*

Sliding Mode Control in Electro-Mechanical Systems

Second Edition

Vadim Utkin
Ohio State University
Columbus, Ohio, U.S.A.

Jürgen Guldner
BMW Group
Munich, Germany

Jingxin Shi
TTTech
Hettershausen, Germany

CRC Press
Taylor & Francis Group
Boca Raton London New York

CRC Press is an imprint of the
Taylor & Francis Group, an **informa** business

CRC Press
Taylor & Francis Group
6000 Broken Sound Parkway NW, Suite 300
Boca Raton, FL 33487-2742

Printed in the United States of America on acid-free paper
10 9 8 7 6 5 4 3 2 1

International Standard Book Number-13: 978-1-4200-6560-2 (Hardcover)

Visit the Taylor & Francis Web site at
http://www.taylorandfrancis.com

and the CRC Press Web site at
http://www.crcpress.com

"To the memory of my parents, who gave me a good start and illuminate my way now"–V.U.
"To my family, who always supports me strongly" –J.G.
"To my wife, my mother, and the memory of my father" –J.S.

Contents

Preface to the Second Edition

The authors accepted enthusiastically the opportunity offered by Taylor & Francis to publish a second edition of our book for two reasons: On the one hand, the proposal itself means that the interest in sliding mode control has remained at a high level even 10 years after publication of the first edition. On the other hand, it is a good opportunity to include new results into the book related to both the control design methodology and applications.

The chapters and sections related to the new theoretical developments embrace results on second order sliding mode with continuous control actions, state observers with simple binary sensors, and methods of analysis and chattering suppression—the phenomenon known to be the main obstacle for sliding mode control implementation. The above list is complemented by design principles for simultaneous estimation of state and parameters of electric motors and for designing multiphase power converters with chattering (ripple) suppression.

Results in automotive application of sliding mode control are presented in the concluding chapter.

Vadim Utkin, Jürgen Guldner, and Jingxin Shi

Authors

Vadim Utkin, PhD, DSc

Vadim Utkin is a graduate of the Moscow Power Institute (Diplomized Engineer) and received his PhD and Doctor of Sciences degrees from the Institute of Control Sciences, Moscow, Russia. He was with the Institute of Control Sciences since 1960 and served as Head of the Discontinuous Control Systems Laboratory from 1973 to 1994. Currently, he holds a joint professor position in the Electrical and Mechanical Engineering Departments of The Ohio State University. He has also held visiting positions at universities in the United States, Japan, Italy, and Germany.

Professor Utkin is one of the originators of the concepts of variable structure systems and sliding mode control. From 1975 to 1978, he was in charge of an international project between his institute of Control Sciences and Energoinvest (Sarajevo) on the sliding mode control of induction motors. Direct current, induction, and synchronous drives with sliding mode control have been applied for metal-cutting machine tools, process control, and electric cars.

Professor Utkin is an author and coauthor of five books and 300 papers. His current research interests are control of infinite-dimensional plants, including flexible manipulators, sliding modes in discrete-time systems and microprocessor implementation of sliding mode control, control of electric drives and alternators, robotics, and automotive control. As the Ford Chair Professor of Electromechanical Systems from 1994 to 2001, he has been a principle investigator with automotive companies on several projects on automotive engines and alternators control, and on power distribution control of hybrid electric vehicle.

Professor Utkin is an Honorary Doctor of University of Sarajevo. In 1972, he was awarded the Lenin Prize (the highest scientific award in the former Union of Soviet Socialist Republics); in 2003, he received the Oldenburger medal of the American Society of Mechanical Engineers; and in 2005, he was presented with the Humboldt award of the German government. He is an Institute of Electrical and Electronics Engineers (IEEE) fellow.

Professor Utkin was chairman of the International Program Committee of the 1990 International Federation of Automatic Control Congress (Tallinn, Estonia); currently, he is an associate editor of the *International Journal of Control* and a member of the Technical Committee of IEEE on Variable Structure and Sliding Mode Control.

Jingxin Shi

Jingxin Shi graduated from Beijing University of Aeronautics and Astronautics. From 1988 to 1998, he worked as a visiting scholar and research engineer (permanent employee) for the German Aerospace Center, Institute for Robotics and System Dynamics. He was one of the key engineers of German-D2 space robotic program ROTEX (Robot Technology Experiment, in which the robot flew on board American space shuttle Columbia in May, 1993). From 1999 to 2001, he worked for dSPACE GmbH as a resident engineer at the BMW Research Center, Munich, Germany. Since mid-2001, he has been a senior engineer of TTTech Germany GmbH for vehicle dynamics control.

Mr. Shi received the Best Paper Award during "26th International Symposium on Industrial Robots" in 1995. His research areas include control and hardware-in-the-loop simulation of electric drives, robotic manipulators, and vehicle dynamics.

Jürgen Guldner, PhD

Jürgen Guldner received an MS in Electrical Engineering from Clemson University in 1992 and a PhD in Controls and Robotics from the Technical University of Munich, Germany, in collaboration with the German Aerospace Center, in 1995. His research focused on sliding mode control and its application to robotics. During a postdoctoral fellowship with the Partners for Advanced Transit and Highways Program at the University of California at Berkeley, he extended application of sliding mode control to automotive steering.

In 1997, Dr. Guldner joined the BMW Technik GmbH (Munich, Germany) to lead research projects on automotive by-wire systems. He transferred to BMW AG's Research and Development Center in 2001 to head the Advanced Product Engineering Group for Chassis Control Systems. In late 2003, he was appointed head of the Product Engineering Department for Active and Passive Roll Stabilization and Engine Mounts.

From 2006 to 2008, Dr. Guldner was responsible for the development of vehicle systems and vehicle integration as chief engineer at the BMW Hybrid Technology Corporation. Since 2009, he has been with BMW Manufacturing Corporation preparing the production launch of BMW's first active hybrid vehicle.

1

Introduction

In the course of the entire history of automatic control theory, the intensity of investigation of systems with discontinuous control actions has been maintained at a high level. In particular, at the first stage, relay, or "on-off' regulators, ranked highly for design of feedback systems. The reason was twofold: ease of implementation and high efficiency of hardware. Monographs by Flugge-Lotz [1953] and Tsypkin [1955] were most obviously the first theoretical generalizations of the wide diversity of analysis and design methods for relay systems.

In systems with control as a discontinuous state function, so-called "sliding modes" may arise. The control action switches at high frequency should the sliding mode occur in the system. The study of sliding modes embraces a wide range of heterogeneous areas from pure mathematical problems to application aspects.

Systems with sliding modes have proven to be an efficient tool to control complex high-order nonlinear dynamic plants operating under uncertainty conditions, a common problem for many processes of modern technology. This explains the high level of research and publication activity in the area and unremitting interest of practicing engineers in sliding mode control during the past two decades.

1.1. Examples of Dynamic Systems with Sliding Modes

Sliding modes as a phenomenon may appear in a dynamic system governed by ordinary differential equations with discontinuous right-hand sides. The term sliding mode first appeared in the context of relay systems. It may happen that the control as a function of the system state switches at high (theoretically infinite) frequency, and this motion is called sliding mode. It may be enforced in the simplest first-order tracking relay system with the state variable $x(t)$:

$$\dot{x} = f(x) + u$$

with the bounded function $f(x)$, $|f(x)| < f_0$ = constant and the control as a relay function (Figure 1.1) of the tracking error $e = r(t) - x$; $r(t)$ is the reference input, and u is given by

$$u = \begin{cases} u_0 \text{ if } e > 0 \\ -u_0 \text{ if } e < 0 \end{cases} \quad \text{or} \quad u = u_0 \text{sign}(e),\ u_0 = const$$

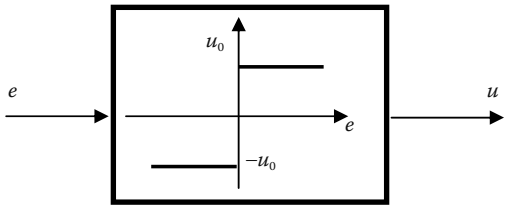

FIGURE 1.1
Relay control.

The values of e and $\frac{de}{dt} = \dot{e} = \dot{r} - f(x) - u_0 \text{sign}(e)$ have different signs if $u_0 > f_0 + |\dot{r}|$.

It means that the magnitude of the tracking error decays at a finite rate, and the error is equal to zero identically after a finite time interval T (Figure 1.2). The argument of the control function, e, is equal to zero, which is the discontinuity point. For any real-life implementation attributable to imperfections in switching device, the control switches at high frequency or takes intermediate values for continuous approximation of the relay function. The motion for $t > T$ is called sliding mode.

Formally, sliding mode may appear not only in a control system with discontinuous control but in any dynamic system with discontinuities in the motion equations. In the simple mechanical example system with Coulomb friction depicted in Figure 1.3, the right-hand side is a discontinuous function of the state.

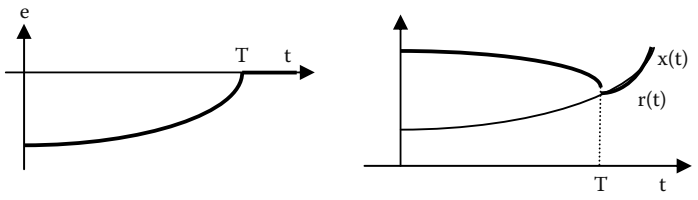

FIGURE 1.2
Sliding mode tracking control.

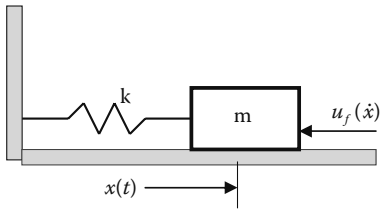

FIGURE 1.3
Mechanical system with Coulomb friction.

The motion equation is given by

$$m\ddot{x} + kx = -u_f(\dot{x})$$

where $x(t)$ is the displacement, k is the spring stiffness, and the friction force is a discontinuous function of the speed:

$$u_f = u_0 \text{sign}(\dot{x}), \quad u_0 = const.$$

If $u_0 < k|x|$, then the friction force takes one of the extreme values and the motion is described by nonhomogenous differential equations with the right-hand side equal to u_0 or $-u_0$. For $u_0 > \text{k}|x(t_0)|$ and $\dot{x}(t_0) = 0$, the mass sticks and $\dot{x}(t) \equiv 0$, $x(t) \equiv x(t_o)$ for $t > t_0$. This motion may be referred to as sliding mode because, similar to the previous example, the argument of the discontinuous function $u_f = u_0 \text{sign}(\dot{x})$ is equal to zero identically.

The third example illustrates sliding motions in an electric system: an alternating current/direct current voltage converter (see Figure 1.4) with dynamics equations

$$\frac{di_g}{dt} = \frac{V_g}{L}\sin(\omega t) - \frac{v_0}{L}u,$$
$$\frac{dv_0}{dt} = -\frac{v_0}{RC} + \frac{i_g}{C}u$$

where the input voltage $v_g = V_g \sin(\omega t)$ and the switches s_{1A}, s_{2A}, s_{1B}, and s_{2B} constitute the control input:

$$u = \begin{cases} 1 \text{ if } S_{1A} \text{ and } S_{2B} \text{ are closed} \\ -1 \text{ if } S_{1B} \text{ and } S_{2A} \text{ are closed} \end{cases}.$$

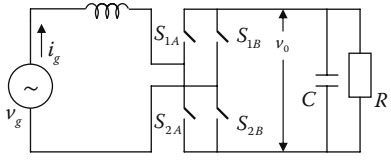

FIGURE 1.4
AC/DC voltage converter.

The switching logic should be found such that the output voltage v_0 is equal to the desired value $v_d(t)$. It seems reasonable to switch the function u depending on the sign of the tracking error $v_e = v_d - v_0$:

$$u = \begin{cases} 1 & \text{if } (v_d - v_0)i_g > 0 \\ -1 & \text{if } (v_d - v_0)i_g < 0 \end{cases} \quad \text{or } u = \text{sign}[(\,(v_d - v_0)i_g\,].$$

Calculate the time derivative of the tracking error as

$$\dot{v}_e = \dot{v}_g + \frac{v_0}{RC} - \frac{|i_g|}{C}\text{sign}(v_e).$$

If $|i_g| > \left|\frac{v_0}{R} + C\dot{v}_g\right|$, then v_e and $\dot{v}_e$ have different signs, hence the error v_e will vanish after finite time interval T and will be equal to zero identically afterward. The plots $v_e(t)$, $v_0(t)$, and $v_d(t)$ are similar to those of $e(t)$, $x(t)$, and $r(t)$ on Figure 1.2. As for the first-order example, ideal tracking is provided attributable to enforcing sliding mode.

1.2. Sliding Modes in Relay and Variable Structure Systems

The ideas underlying modern analysis and design methods for "sliding mode control" (SMC) may be found in the publications of the early 1930s. Figure 1.5 illustrates the so-called vibration control studied by Kulebakin [1932] in the context of voltage control for a DC generator of an aircraft.

Notice that the output voltage is close to the set point as a result of discontinuous feedback and high-frequency switching in the excitation winding. It seems that 1930s-era "vibration control" is just the same as our contemporary sliding mode control.

The second example from the 1930s (Figure 1.6) concerns relay systems with sliding modes for controlling the course of a ship [Nikolsky 1934]. It is amazing that the paper published more than 60 years ago was written in the language of modern control theory: "phase plane," "switching line," and even sliding mode.

In all the examples, except for the last one, the phenomenon sliding mode was revealed and discussed in time domain, although this term was not used directly. However, for analysis and design of sliding mode control, the state space method looks much more promising.

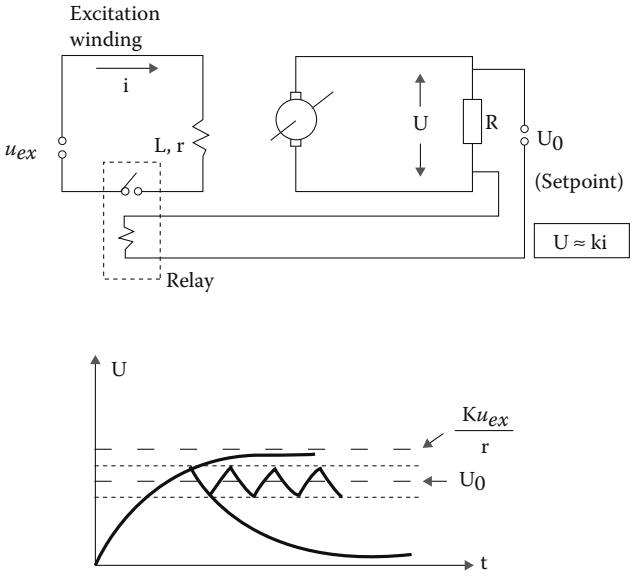

FIGURE 1.5
Vibration control of DC generator.

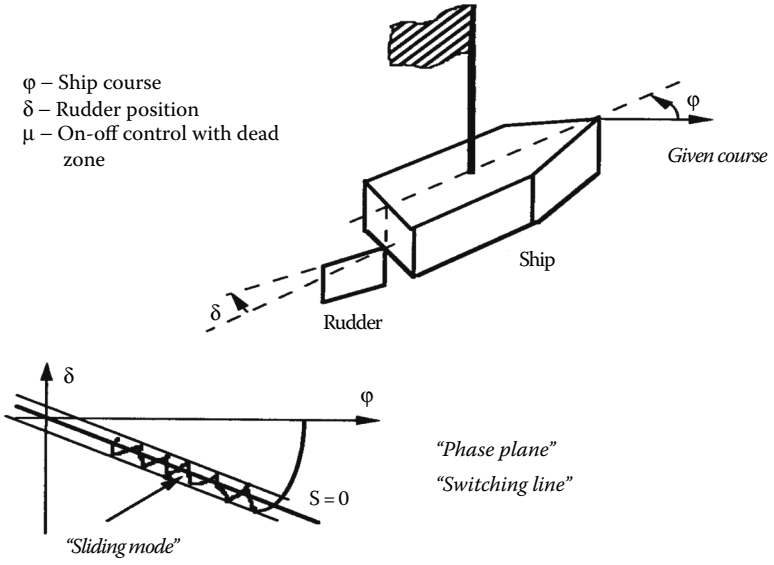

FIGURE 1.6
Sliding mode control of ship course.

The conventional example to demonstrate sliding modes in terms of the state space method is a second-order time-invariant relay system:

$$\begin{aligned} &\ddot{x} + a_2\dot{x} + a_1 x = u + f(t), \\ &u = -M\text{sign}(s), \quad s = \dot{x} + cx, \end{aligned} \tag{1.2.1}$$

where M, a_1, a_2, c are constant parameters, and $f(t)$ is a bounded disturbance.

The system behavior may be analyzed in the state plane $(x, \dot{x})$. The state plane in Figure 1.7 is shown for $a_1 = a_2 = 0$. The control u undergoes discontinuities at the switching line $s = 0$, and the state trajectories are constituted by two families: the first family corresponds to $s > 0$ and $u = -M$ (upper semiplane), and the second corresponds to $s < 0$ and $u = M$ (lower semiplane). Within the sector $m - n$ on the switching line, the state trajectories are oriented toward the line. Having reached the sector at some time t_1, the state cannot leave the switching line. This means that the state trajectory will belong to the switching line for $t > t_1$. This motion with state trajectories in the switching line is called sliding mode. Because, in the course of sliding mode, the state trajectory coincides with the switching line $s = 0$, its equation may be interpreted as the motion equation, i.e.,

$$\dot{x} + cx = 0. \tag{1.2.2}$$

It is important that its solution $x(t) = x(t_1)e^{-c(t-t_1)}$ depends on neither the plant parameters nor the disturbance. This so-called "invariance" property looks promising for designing feedback control for the dynamic plants operating under uncertainty conditions.

We have just described an ideal mathematical model. In real implementations, the trajectories are confined to some vicinity of the switching line. The

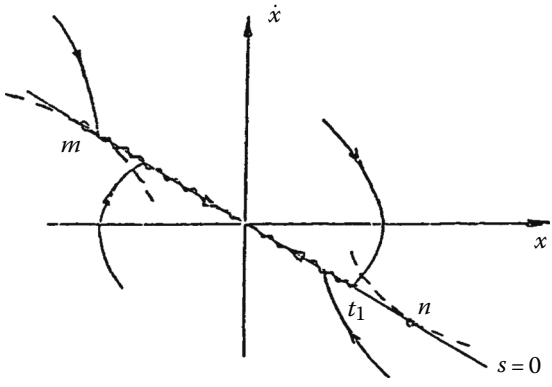

FIGURE 1.7
State plane of the second-order relay system.

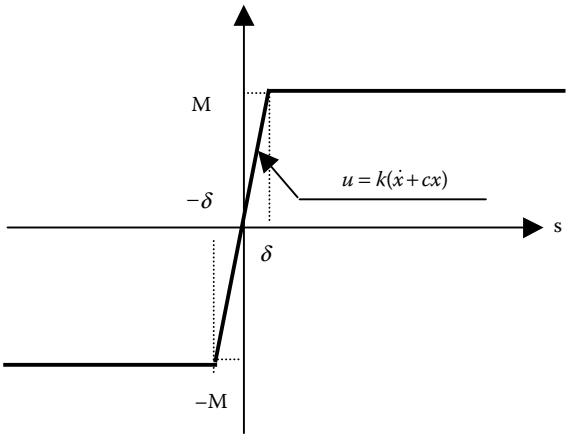

FIGURE 1.8
Continuous approximation of discontinuous control.

deviation from the ideal model may be caused by imperfections of switching devices such as small delays, dead zones, or hysteresis, which may lead to high-frequency oscillations as shown in Figure 1.6. The same phenomenon may appear as a result of small time constants of sensors and actuators having been neglected in the ideal model. This phenomenon, referred to as "chattering," was a serious obstacle to the use of sliding modes in control systems, and special attention will be paid to chattering suppression methods in Chapter 8. Note that the state trajectories are also confined to some vicinity of the switching line for continuous approximation of a discontinuous relay function (Figure 1.8) as well. In a δ vicinity of the line $s = 0$, control is the linear state function with a high gain k, and the eigenvalues of the linear system are close to $-k$ and $-c$. This means that the motion in the vicinity consists of the fast component decaying rapidly and the slow component coinciding with solution to the ideal sliding mode (Equation 1.2.2).

Sliding modes became a principle operation mode in variable structure systems or systems consisting of a set of continuous subsystems with a proper switching logic. For example, the second-order systems

$$\begin{aligned} &\ddot{x} - ax = u, \quad a > 0, \\ &u = -k \ |x| \ \text{sign}(s), \\ &s = cx + \dot{x}, \quad k > 0, \ c > 0 \end{aligned}$$

consists of two unstable linear structures (see Figure 1.9).

By varying the system structure along the switching lines $s = 0$ and $x = 0$ and enforcing sliding mode, the system becomes asymptotically stable (Figure 1.10). The switching line is reached for any initial conditions. If the

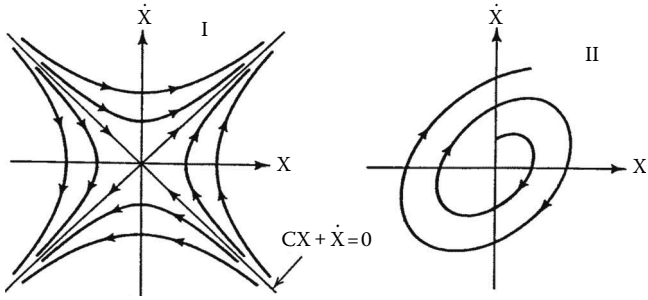

FIGURE 1.9
Variable structure system consisting of two unstable subsystems.

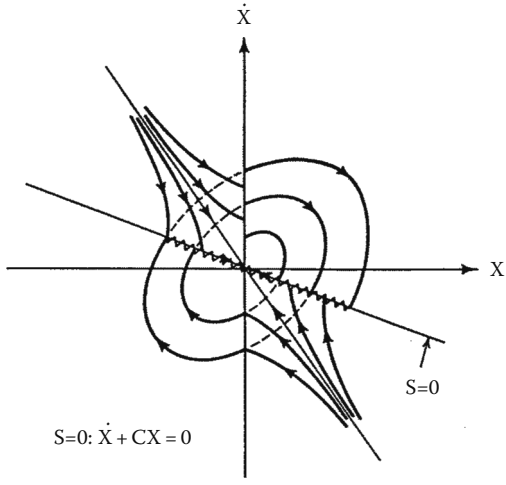

FIGURE 1.10
State plane of variable structure system.

slope of the switching line is lower than that of the asymptote of the structure I ($c < c_0$), than the state trajectories are oriented toward the line and sliding mode may start at any point of $s = 0$. Similar to the relay system, the sliding mode is governed by the first-order Equation 1.2.2 with the solution $x(t) = x(t_1)e^{-c(t-t_1)}$. Again, the solution depends on neither the plant parameters nor any disturbances to which the plant may be subjected.

The examples of relay and variable structure systems demonstrated order reduction and invariance with respect to plant uncertainties of the systems with sliding modes. Use of these properties was the key idea of variable

structure theory at the first stage when only single-input-single-output systems with motion equations in canonical space were studied [Emelyanov et al. 1970]. A control variable $x = x_1$ and its time derivatives $x^{(i-1)} = x_i$, $i = 1,\ldots, n$ are components of a state vector in the canonical space:

$$\begin{aligned} \dot{x}_i &= x_{i+1}, \qquad i = 1,\ldots,n-1 \\ \dot{x}_n &= -\sum_{i=1}^{n} a_i(t)x_i + f(t) + b(t)u, \end{aligned} \tag{1.2.3}$$

where $a_i(t)$ and $b_i(t)$ are unknown parameters and $f(t)$ is an unknown disturbance.

Control undergoes discontinuities on some plane $s(x) = 0$ in the state space:

$$u = \begin{cases} u^+(x,t) & \text{if } s(x) > 0 \\ u^-(x,t) & \text{if } s(x) < 0, \end{cases}$$

where $u^+(x, t)$ and $u^-(x, t)$ are continuous state functions, $u^+(x, t) \neq u^-(x, t)$ and $s(x) = \sum_{i=1}^{n} c_i x_i$, $c_n = 1$, and $c_1 \ldots c_{n-1}$ are constant coefficients. The discontinuous control was selected such that the state trajectories are oriented toward the switching plane $s = 0$; hence, sliding mode arises in this plane (Figure 1.11). Once sliding mode has begun, the motion trajectories of system (Equation 1.3) are in the switching surface,

$$x_n = -\sum_{i=1}^{n-1} c_i x_i.$$

Substitution into the $(n-1)$th equation yields the sliding mode equations

$$\begin{aligned} \dot{x}_i &= x_{i+1}, \qquad i = 1,\ldots,n-2 \\ \dot{x}_{n-1} &= -\sum_{i=1}^{n-1} c_i x_i \quad \text{or} \quad x^{(n-1)} + c_{n-1}x^{(n-2)} + \ldots + c_1 = 0. \end{aligned} \tag{1.2.4}$$

The motion equation is of reduced order and depends on neither the plant parameters nor the disturbance. The desired dynamics of the sliding mode may be assigned by a proper choice of the parameters of switching plane c_i.

Although the invariance property is very useful, it did create the illusion that any control problem can be easily solved by enforcing the sliding mode in the system. The main problem is that the space of state derivatives is a mathematical idealization, and ideal differentiators can hardly be implemented. As a result, another extreme appeared reflecting a certain pessimism over

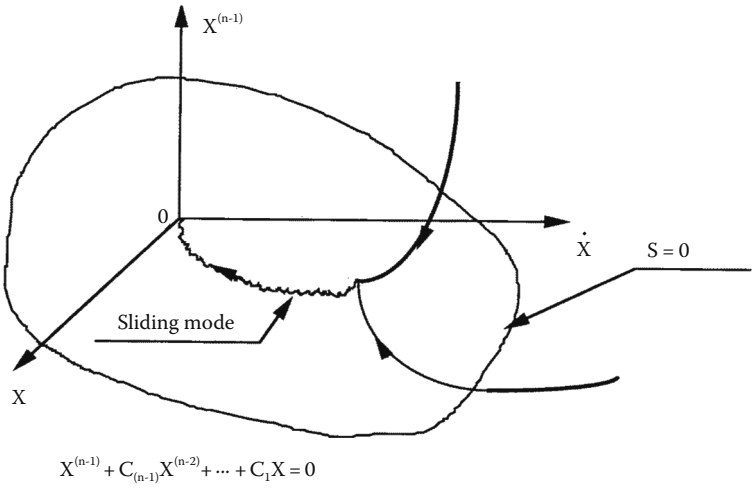

FIGURE 1.11
Sliding mode in canonical state space.

the practical possibility of implementing of variable structure systems with sliding modes. However, the refusal to use sliding modes in control systems proved to be unreasonable as well.

In modern technological processes, it is common that control and system output may be vector-valued quantities, and only some components of the state vector are accessible for measurement. The canonical space approach did not give any recipe how the control may be designed in such situations. The second stage of variable structure system studies was dedicated to the development of design methods for systems with motion equations in an arbitrary state space with vector control action and vector variable to be controlled [Utkin 1983]. The basic idea underlying the majority of control methods is enforcing multidimensional sliding modes.

1.3. Multidimensional Sliding Modes

In the previous examples of control systems with sliding modes, the control was a scalar state function, and the sliding mode was governed by a differential equation with the order by one less than the order of the original system. So we may assume that sliding motion may appear in an intersection of several surfaces if the control is a vector-valued quantity and each component undergoes discontinuities in its own switching surface. The planar motion of a point mass m with Coulomb friction (Figure 1.12) may serve as an example of such sliding mode.

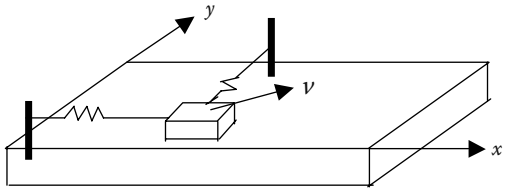

FIGURE 1.12
Mechanical system with Coulomb friction on a plane.

The motion in the orthogonal frame (x, y) is governed by the fourth-order system:

$$x = x_1, \quad y = y_1,$$
$$\begin{cases} \dot{x}_1 = x_2 \\ m\dot{x}_2 = -kx_1 - F_x \\ \dot{y}_1 = y_2 \\ m\dot{y}_2 = -ky_1 - F_y, \end{cases}$$

where both springs have the same stiffness k, $F_x = \dfrac{x_2}{\sqrt{x_2^2 + y_2^2}}$ and $F_y = \dfrac{y_2}{\sqrt{x_2^2 + y_2^2}}$ are (x, y)– components of the friction force vector $F = -Mv / \|v\|$, $M = const$, v is a speed vector with components x_2 and y_2, and $\|v\| = \sqrt{x_2^2 + y_2^2}$.

The magnitude of the friction force is equal to M for $v \neq 0$. F undergoes discontinuities when x_2 and y_2 are equal to zero simultaneously. If at initial time $v = 0$ (i.e., $x_2 = 0$ and $y_2 = 0$) and the maximal value of the friction force exceeds the spring force, $M > k\sqrt{x_1^2 + y_1^2}$, then the mass is stuck and $v \equiv 0$ for the additional motion.

Thus, beyond the intersections of two surfaces $x_2 = 0$ and $y_2 = 0$, the friction force is a continuous state function, and, in the domain $M > k\sqrt{x_1^2 + y_1^2}$, the state trajectories ($x_1(t) = const$, $y_1(t) = const$) belong to this manifold. This motion may be called the "two-dimensional sliding mode" in the intersection of two discontinuity surfaces.

The next example illustrates two-dimensional sliding mode in a control system with a two-dimensional control vector:

$$\begin{aligned} \dot{x}_1 &= x_2 \\ \dot{x}_2 &= x_3 + f_1(t) + u_1 \\ \dot{x}_3 &= f_2(t) + u_2 \end{aligned} \tag{1.3.1}$$

where $f_1(t)$ and $f_2(t)$ are unknown bounded disturbances with a known range of variation.

The components of the control undergo discontinuities in two planes of the three-dimensional state:

$$u_1 = -M_1 \operatorname{sign}(s_1),\ s_1 = x_1 + x_2,$$

$$u_2 = -M_2 \operatorname{sign}(s_2),\ s_2 = x_1 + x_2 + x_3,$$

where M_1, M_2 are positive constant values. If $M_2 > |x_2 + x_3 + f_1(t) + f_2(t)| + M_1$, then the values s_2 and $\dot{s}_2 = x_2 + x_3 + u_1 - M_2 \operatorname{sign}(s_2)$ have different signs. Hence, the plane $s_2 = 0$ is reached after a finite time interval, and then sliding mode with state trajectories in this plane will start (see Figure 1.13). For this motion, $x_3 = -x_1 - x_2$, and the sliding mode is governed by the second-order equation:

$$\begin{cases} \dot{x}_1 = x_2 \\ \dot{x}_2 = -x_1 - x_2 + f_1(t) + u_1. \end{cases}$$

Again, for $M_1 > |-x_1 + f_1(t)|$, the values s_1 and $\dot{s}_1 = -x_1 + f_1(t) - M_1 \operatorname{sign}(s_1)$ have different signs, and, after a finite time interval, the state will reach the intersection of the planes $s_1 = 0$ and $s_2 = 0$. The additional motion will be in this manifold (straight line formed by intersection of the two planes), and its first-order equation may be derived by substituting $-x_1$ for x_2 (because $s_1 = 0$) into the first equation to obtain $\dot{x}_1 = -x_1$.

The two-dimensional sliding mode is asymptotically stable, its order is by two less than that of the original system, and the motion does not depend on the disturbances $f_1(t)$ and $f_2(t)$.

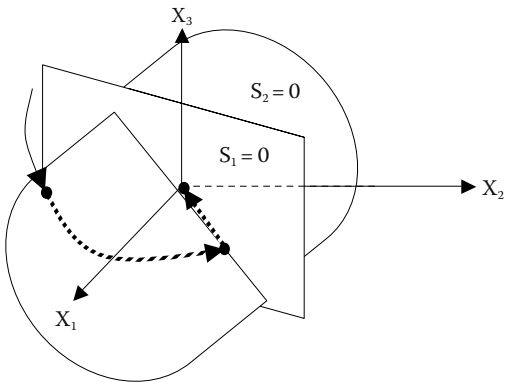

FIGURE 1.13
Two-dimensional sliding mode.

1.4. Outline of Sliding Mode Control Methodology

The examples of the control systems in the previous sections let us outline the main reasons why enforcing sliding modes is a promising method to control high-order nonlinear dynamic plants operating under uncertainty conditions.

In this book, we will deal mainly with processes described by nonlinear differential equations in an arbitrary n-dimensional state space with m-dimensional vector control actions (see Figure 1.14):

$$\dot{x} = f(x,t,u), \tag{1.4.1}$$

with $x \in \Re^n$, $f \in \Re^n$, $u \in \Re^m$, and t denoting the time. The control is selected as a discontinuous function of the state. For example, each component of the control u_i may undergo discontinuities on some nonlinear surface $s_i(x) = 0$ in the state space:

$$u_i = \begin{cases} u_i^+(x,t) & \text{if } s_i(x) > 0 \\ u_i^-(x,t) & \text{if } s_i(x) < 0 \end{cases} \quad i = 1,\ldots,m, \tag{1.4.2}$$

where $u_i^+(x,t)$ and $u_i^-(x,t)$ are continuous state functions, with $u_i^+(x,t) \neq u_i^-(x,t)$ and $s_i(x)$' s being continuous state functions.

Similar to the example with two-dimensional sliding mode in the intersection of two discontinuity planes in Section 1.3, we may expect that sliding mode may occur in the intersection of m surfaces $s_i(x) = 0$, ($i = 1,\ldots,m$), and the order of the motion equations is by m less than that of the original system. In

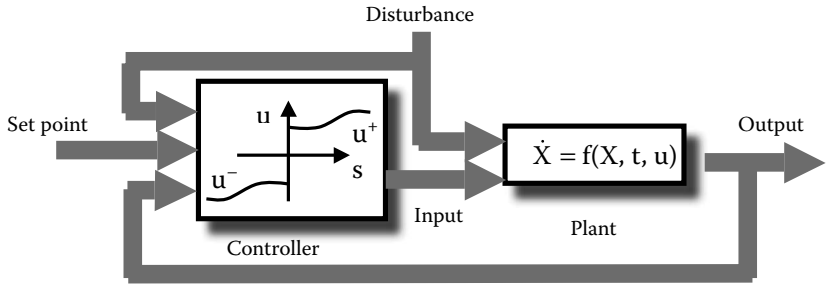

FIGURE 1.14
Systems with sliding mode control.

connection with control of high-dimensional plants, great interest is attached to design methods permitting decoupling the overall system motions into independent partial components. As we can see, enforcing sliding modes in systems with discontinuous control enables order reduction, which results in decoupling and simplification of the design procedure.

Furthermore, the element implementing a discontinuous function $u(x)$ has the input $s(x)$ close to zero during sliding mode (see Figure 1.15), whereas its output takes finite values (to be precise, the average value of the output because it contains a high-frequency component).

This means that the element implements high (theoretically infinite) gain, which is the conventional tool to suppress the influence of disturbances and uncertainties in the plant behavior. Unlike continuous high-gain control systems, the invariance effect is attained using finite control actions.

Our brief discussion of the motions in systems with sliding modes has shown that (1) the order of the system is reduced, and (2) sensitivity with respect to parameter variation and disturbances may be reduced should sliding mode occur.

As was demonstrated in the previous sections, the order reduction and invariance properties are feasible easily in second-order systems with motion equations in the canonical space. The sliding mode dynamics depend on the switching surface equations and do not depend on control. Hence, the design procedure should consist of two stages. First, the equation of the manifold with sliding mode is selected to design the desired dynamics of this motion in accordance with some performance criterion. Then, the discontinuous control should be found such that the state would reach the manifold and sliding mode exists in this manifold. As a result, the design is decoupled into two subproblems of lower dimension, and, after a finite time interval preceding the sliding motion, the system will possess the desired dynamic behavior.

We have dwelt on the main reasons for using sliding modes in control systems and outlined the sliding mode control design methodology. The basic design concept of the control methods studied in this book will focus on

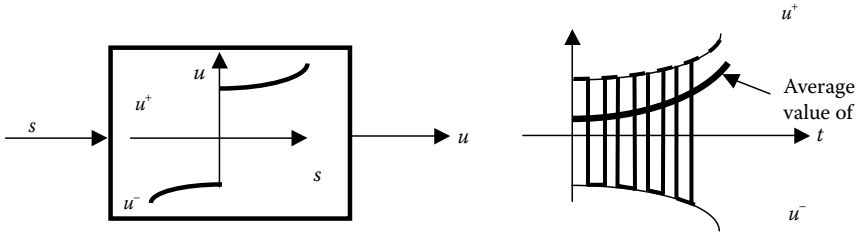

FIGURE 1.15
Sliding mode for high gain implementation.

enforcing sliding modes. Decoupling or invariance (or both) will be inherent in the majority of the proposed design techniques.

The decoupling and invariance properties make sliding mode methodology an efficient tool to control complex electrical and mechanical dynamic processes governed by high-order differential equation with bounded information on parameters and disturbances. An induction motor and multilink manipulator with unknown load torque and inertia and with position, speed or torque to be controlled are examples of such processes. The design methods for control of (1) pure mechanical systems with a force or torque as control actions such as manipulators and mobile robots, (2) pure electrical systems such as power converters, and (3) electromechanical systems such as electric motors will be developed in the book.

It is worth mentioning an implementation aspect of sliding mode control. Widely used electrical servomechanisms are controlled by power electronic converters. When using them, it seems reasonable to turn to control algorithms with discontinuous control actions, because only an on-off operation is admissible for such converters and discontinuities in control are dictated by the very nature of the converter elements.

References

Emelyanov S, Utkin V, Tarin V, Kostyleva N, Shubladze A, Ezerov V, Dubrovsky E. 1970. *Theory of Variable Structure Control Systems* (in Russian). Moscow: Nauka.

Flugge-Lotz I. 1953. Discontinuous Automatic System. New York: Princeton University Press.

Kulebakin V. 1932. "On Theory of Vibration Controller for Electric Machines" (in Russian). *Theor Exp Electron* 4.

Nikolski G. 1934. "On Automatic Stability of a Ship on a Given Course" (in Russian). *Proc Central Commun Lab* 1:34–75.

Tsypkin Y. 1955. *Theory of Relay Control Systems* (in Russian). Moscow: Gostechizdat.

Utkin V. 1983. "Variable Structure Systems: Present and Future." *Automat Remote Control* 9:1105–1120.

2

Mathematical Background

Sliding mode control is in the class of nonlinear control systems and inherently introduces discontinuities into the control loop. However, most tools for system analysis and control synthesis were developed for "continuous" linear and nonlinear systems. Consequently, these tools are not applicable to "discontinuous" methods such as sliding mode control and variable structure systems.

This chapter provides the mathematical background of the most important tools developed for discontinuous systems, in particular for the design of sliding mode control. Because this book is mainly intended to provide sufficient tools for practical control design in real-life applications, the interested reader is referred to the study by Utkin [1992] for a more detailed mathematical description of sliding mode techniques.

2.1. Problem Statement

The sketch of design methods discussed in Section 1.3 assumed that the properties of sliding modes in canonical spaces (Equation 1.2.3) would be preserved for arbitrary systems. These properties—order reduction and invariance—were revealed after the sliding mode equation had been derived. It was an easy problem because the equation of a switching surface was also the equation of sliding mode (see Equations 1.2.2 and 1.2.4). This is not the case for systems with motion equations with respect to arbitrary state variables. The analytical problems arising in such systems with sliding modes may be illustrated with the help of a linear second-order system,

$$\begin{aligned} \dot{x}_1 &= a_{11}x_1 + a_{12}x_2 + b_1u + d_1f(t) \\ \dot{x}_2 &= a_{12}x_1 + a_{22}x_2 + b_2u + d_2f(t) \end{aligned} \tag{2.1.1}$$

with relay control $u = -M\text{sign}(s)$, $s = c_1x_1 + c_2x_2$. All parameters a_{ij}, b_i, d_i, c_i $(i, j = 1, 2)$, M are constant, and $f(t)$ is a bounded disturbance.

Similar to relay systems in canonical space, the state trajectories in the state plane (x_1, x_2) may be oriented toward the switching line $s = 0$, and sliding mode arises along this line. To analyze the system behavior in sliding mode the question "what is the motion equation?" should be answered. In contrast to the second-order systems in canonical space, $x_2 = -c_2^{-1}c_1x_1$ resulting from $s = 0$ is not a motion equation. For the particular case $b_1 = 0$, substitution of

$-c_2^{-1}c_1x_1$ for x_2 into the first equation of Equation 2.1.1 lets us derive the first-order sliding mode equation

$$\dot{x}_1 = (a_{11} - a_{12}c_2^{-1}c_1)x_1 + d_1 f(t).$$

As we can see, the order reduction property takes place but invariance with respect to the disturbance does not, because the right-hand side of the motion equation depends on $f(t)$ directly.

The example has shown the fundamental problems related to mathematical models of sliding modes in systems described in the general form (Equations 1.4.1 and 1.4.2). To determine conditions for sliding mode to be insensitive to system uncertainties, special mathematical methods will need to be developed.

Next, having derived the sliding mode equations, the desired dynamics may be assigned by proper choice of the discontinuity surfaces equations as the first stage of the design procedure outlined in Section 1.4. The second stage implies selection of the discontinuous control inputs to enforce sliding mode in the intersection of the surfaces. To solve this problem, the conditions for sliding mode to exist should be obtained. For systems with scalar control, this condition may be interpreted easily from a geometrical point: the state trajectories should be oriented toward the discontinuity surface in its vicinity, or the variable describing deviation from the surface and its time derivative should have opposite signs. The components of the two-dimensional control in the third-order system (Equation 1.3.1) were designed based on these conditions. For the general case, the problem of enforcing sliding mode in the intersection of a set of discontinuity surfaces cannot be reduced to sequential treatment of scalar subproblems. This may be illustrated by a third-order controllable system with a two-dimensional control vector

$$\begin{aligned} \dot{x}_1 &= x_3 \\ \dot{x}_2 &= -x_3 + u_1 - 2u_2 \\ \dot{x}_3 &= -x_3 + 2u_1 + u_2, \end{aligned} \tag{2.1.2}$$

$$\begin{aligned} u_1 &= -\operatorname{sign}(s_1), \quad & s_1 &= x_1 + x_2, \\ u_2 &= -\operatorname{sign}(s_2), \quad & s_2 &= x_1 + x_3. \end{aligned}$$

The analysis of the condition for sliding mode to exist in the intersection of the discontinuity surfaces may be performed in terms of motion projection on subspace (s_1, s_2):

$$\begin{aligned} \dot{s}_1 &= -\operatorname{sign}(s_1) + 2\operatorname{sign}(s_2) \\ \dot{s}_2 &= -2\operatorname{sign}(s_1) - \operatorname{sign}(s_2). \end{aligned}$$

The state trajectories are straight lines in the state plane (s_1, s_2) (see Figure 2.1). It is clear from the picture that, for any point on $s_1 = 0$ or $s_2 = 0$,

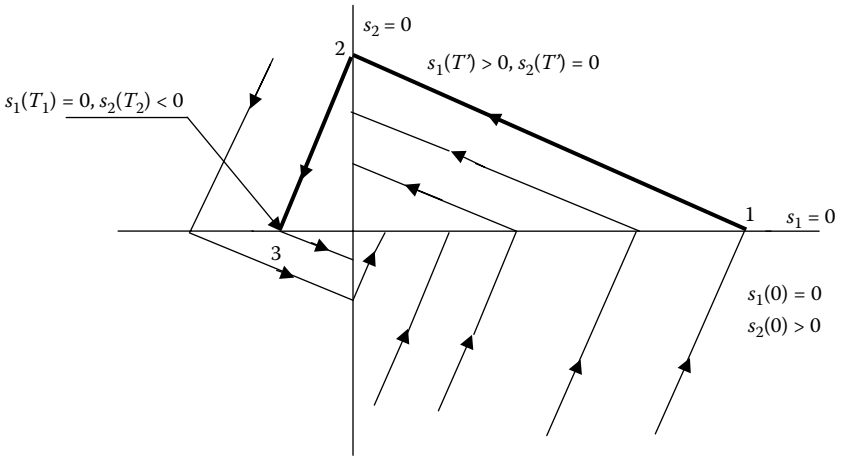

FIGURE 2.1
Sliding mode in the system with two-dimensional control.

the state trajectories are not oriented toward the line; therefore, sliding mode does not exist at any of the switching lines taken separately. At the same time, the trajectories converge on the intersection of them: the origin in the subspace (s_1, s_2). Let us calculate the time needed for the state to reach the origin. For initial conditions $s_1(0) = 0,\ s_2(0) > 0$ (point 1),

$$\begin{aligned} \dot{s}_1 &= 1 \\ \dot{s}_2 &= -3 \end{aligned} \quad \text{for } 0 < t < T',$$

and $s_2(T') = 0,\ \ T' = \frac{1}{3}s_2(0),\ s_1(T') = \frac{1}{3}s_2(0)$ at point 2. For the additional motion,

$$\begin{aligned} \dot{s}_1 &= -3 \\ \dot{s}_2 &= -1 \end{aligned} \quad \text{for } T' < t < T' + T'',$$

$$s_1(T' + T'') = 0,\ \ T'' = \frac{1}{9}s_2(0),\ \ s_2(T' + T'') = -\frac{1}{9}s_2(0) \text{ or}$$

$$s_2(T_1) = -\frac{1}{9}s_2(0),\ \ T_1 = T' + T'' = \frac{4}{9}s_2(0) \quad \text{at point 3.}$$

This means that

$$|s_2(T_i)| = (\frac{1}{9})^i |s_2(0)|, \quad s_1(T_i) = 0,$$

$$\Delta T_i = T_i - T_{i-1} = \frac{4}{9}s_2(T_{i-1}) = \frac{4}{9}(\frac{1}{9})^{i-1}s_2(0), \text{ for } i = 1, 2, \ldots, \text{ and } T_0 = 0.$$

Because

$$\lim_{i\to\infty}[s_2(T_i)]=0,\quad s_1(T_i)=0,\quad \lim_{i\to\infty}=\lim_{i\to\infty}\sum_{i=1}^{\infty}\Delta T_i \;=\; \frac{4}{9}s_2(0)\frac{1}{1-1/9}=\frac{1}{2}s_2(0),$$

the state will reach the manifold $(s_1, s_2)=0$ after a finite time interval, and thereafter sliding mode will arise in this manifold as in all the above systems with discontinuous scalar and vector controls. The example illustrates that the conditions for two-dimensional sliding mode to exist cannot be derived from analysis of scalar cases. Even more, sliding mode may exist in the intersection of discontinuity surfaces, although it does not exist on each of them taken separately.

In addition to the problems of mathematical model and invariance conditions for the general case, we face one more problem of mathematical flavor: the existence conditions for multidimensional sliding modes should be derived. The mathematical models and existence conditions for sliding modes will be studied in this chapter, and the invariance conditions will be addressed in the chapter dedicated to the design methods for sliding mode control.

2.2. Regularization

The first mathematical problem in the context of our plan to use sliding modes for designing feedback control systems is the problem of mathematical description of this motion. It arises as a result of discontinuities in the control inputs and hence in right-hand sides of the motion differential equations. Discontinuous systems are not a subject of the conventional theory of differential equations dealing with continuous state functions.* The conventional theory does not answer even the fundamental questions: whether the solution exists and whether the solution is unique. Formally, even for our simple examples of second-order systems in canonical form (Equation 1.2.1), our method of deriving the sliding mode equations was not legitimate. The solution $x(t)=x(t_1)e^{-c(t-t_1)}$ should satisfy the original differential equation (Equation 1.2.1) rather than the heuristically written equation (Equation 1.2.2). Direct substitution of $x(t)$ into Equation 1.2.1 leads to $s(t)=0$ and $(1-a_2+a_1)x(t_1)e^{-c(t-t_1)}\stackrel{?}{=}-M\ \mathrm{sign}(0)+f(t)$. Because the function $\mathrm{sign}(\cdot)$ is not defined at zero point, we cannot check whether the solution $x(t)$ is correct.

* Strictly speaking, the most conventional method requires the right-hand sides of a differential equation to consist of functions $f(x)$ satisfying the Lipschitz condition $\|f(x_1)-f(x_2)\|<L\|x_1-x_2\|$ with some positive number L, referred to as the Lipschitz constant, for any x_1 and x_2. The condition implies that the function does not grow faster than some linear one, which is not the case for discontinuous functions if x_1 and x_2 are close to a discontinuity point.

In situations in which conventional methods are not applicable, the common approach is to use different methods of regularization or replacing the original problem by a closely similar one for which familiar methods are applicable. For systems with discontinuous controls, the regularization approach has a simple physical interpretation. Uncertainty of system behavior at the discontinuity surfaces appears because the motion Equations 1.4.1 and 1.4.2 are an ideal system model. Nonideal factors, such as small imperfections of switching devices (delay, hysteresis, small time constants) and unmodeled dynamics of sensors and actuators, are neglected in the ideal model. Incorporating them into the system model makes discontinuity point isolated in time and eliminates ambiguity in the system behavior. Next, small parameters characterizing all these factors are assumed to tend to zero. If the limit of the solutions exists with the small parameters tending to zero, then they are taken as the solutions to the equations describing the ideal sliding mode. Such a limit procedure is the "regularization" method for deriving sliding mode equations in the dynamic systems with discontinuous control.

To illustrate the regularization method, we consider a linear time-invariant system with one control input, being a scalar relay function of a linear combination of the state components:

$$\dot{x} = Ax + bu, \quad x \in \Re^n, \tag{2.2.1}$$

where A and b are $n \times n$ and $n \times 1$ constant matrices, $u = M\text{sign}(s)$, M is a scalar positive constant value, and $s = cx$, $c = (c_1, c_2, ..., c_n) = \text{const}$.

As in the examples in Chapter 1 and Section 2.1, the state trajectories may be oriented in a direction toward the switching plane $s(x) = 0$ in the state space $x^T = (x_1, x_2, ..., x_n)$. Hence, the sliding mode occurs in the plane (Figure 2.2), and the motion equation should be found. A similar problem was left unanswered for system Equation 2.1.1.

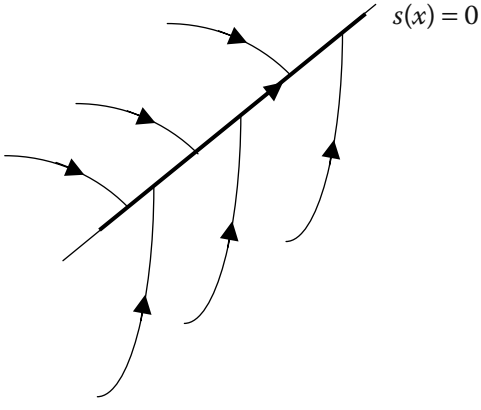

FIGURE 2.2
Sliding mode in a linear system.

Following the regularization procedure, small imperfections of a switching device should be taken into account. If a relay device is implemented with a hysteresis loop with the width 2Δ (see Figure 2.3), then the state trajectories oscillate in a Δ vicinity of the switching plane (see Figure 2.4). The value of Δ is assumed to be small such that the state trajectories may be approximated by straight lines with constant state velocity vectors $Ax + bM$ and $Ax - bM$ in the vicinity of some point x on the plane $s(x) = 0$.

Calculate times Δt_1 intervals and Δt_2 and increments Δx_1 and Δx_2 in the state vector for transitions from point 1 to point 2 and from point 2 to point 3, respectively:

$$\Delta t_1 = \frac{2\Delta}{\dot{s}^+} = \frac{-2\Delta}{cAx + cbM},$$
$$\Delta x_1 = (Ax + bM)\Delta t_1 = (Ax + bM)\frac{-2\Delta}{cAx + cbM}.$$

Similarly, for the second interval,

$$\Delta t_2 = \frac{2\Delta}{\dot{s}^-} = \frac{2\Delta}{cAx - cbM},$$
$$\Delta x_2 = (Ax - bM)\Delta t_2 = (Ax - bM)\frac{2\Delta}{cAx - cbM}.$$

Note that, by our assumption, sliding mode exists in the ideal system; therefore, the values s and $\dot{s}$ have opposite signs, i.e., $\dot{s}^+ = cAx + cbM < 0$ and $\dot{s}^- = cAx - cbM > 0$. This implies that both time intervals Δt_1 and Δt_2 are positive. Note that the inequalities may hold if $cb < 0$.

The average state velocity within the time interval $\Delta t = \Delta t_1 + \Delta t_2$ may be found as

$$\dot{x}_{av} = \frac{\Delta x_1 + \Delta x_2}{\Delta t} = Ax - (cb)^{-1}bcAx.$$

The next step of the regularization procedure implies that the width of the hysteresis loop Δ should tend to zero. However, we do not need to calculate $\lim_{\Delta \to 0}(\dot{x}_{av})$: the limit procedure was performed implicitly when we assumed that state trajectories are straight lines and the state velocities are constant. This is the reason why $\dot{x}_{av}$ does not depend on Δ. As it follows from the more accurate model, the sliding mode in the plane $s(x) = 0$ is governed by

$$\dot{x} = (I_n - (cb)^{-1}bc)Ax \tag{2.2.2}$$

with initial state $s[x(0)] = 0$ and I_n being an identity matrix. It follows from Equations 2.2.1 and 2.2.2 that

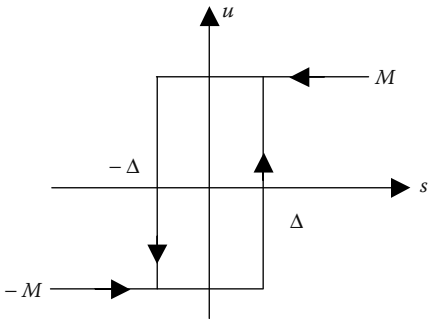

FIGURE 2.3
Relay with hysteresis.

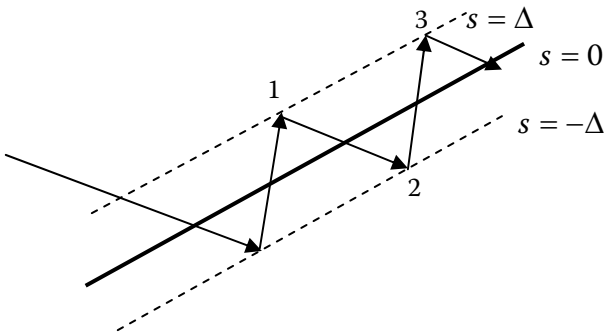

FIGURE 2.4
Oscillations in a vicinity of the switching surface.

$$\dot{s} = c(I_n - (cb)^{-1}bc)Ax \equiv 0.$$

Hence, the state trajectories of the sliding mode are oriented along the switching plane. The condition $s[x(0)] = 0$ enables one to reduce the system order by one. To obtain the sliding mode equation of $(n-1)$th order, one of the components of the state vector, let it be x_n, may be found as a function of the other $n-1$ components and substituted into the system (Equation 2.2.2). Finally, the last equation for x_n can be disregarded.

Applying the above procedure to the second-order system (Equation 2.1.1) results in a first-order sliding mode equation along the switching line $s = c_1x_1 + c_2x_2 = 0$:

$$\dot{x}_1 = \left(a_{11} - a_{12}c_2^{-1}c_1 - (cb)^{-1}b_1(ca^1 - ca^2c_2^{-1}c_1)\right)x_1 + \left(d_1 - b_1(cb)^{-1}(cd)\right)f,$$

where $c = (c_1, c_2)$, $b^T = (b_1, b_2)$, $(a^1)^T = (a_{11}, a_{21})$, $(a^2)^T = (a_{12}, a_{22})$, $d^T = (d_1, d_2)$, and cb and c_2 are assumed to be different from zero. As we can see for this general case of a linear second-order system, the sliding mode equation is of reduced order and depends on the plant parameters, disturbances, and coefficients of the switching line equation but does not depend on control.

For the systems in canonical form in Equations 1.2.1 and 1.2.3, the above regularization method may serve as validation that the reduced order sliding mode Equations 1.2.2 and 1.2.4 depend on neither plant parameters nor disturbances.

Exactly the same equations for our examples result from regularization based on an imperfection of "delay" type [Andre and Seibert 1956a,b]. It is interesting to note that nonlinear systems of an arbitrary order with one discontinuity surface were studied in this paper, and the motion equations proved to be the same for both types of imperfections: hysteresis and delay. This result may be easily interpreted in terms of relative time intervals for control input to take each of two extreme values. For a system of an arbitrary order with scalar control,

$$\dot{x} = f(x,u), \quad x, f \in \Re^n, \quad u(x) \in \Re, \tag{2.2.3}$$

$$u(x) = \begin{cases} u^+(x) & \text{if } s(x) > 0 \\ u^-(x) & \text{if } s(x) > 0, \end{cases}$$

where the components of vector f, scalar functions $u^+(x), u^-(x)$ and $s(x)$ are continuous and smooth, and $u^+(x) \neq u^-(x)$. We assume that sliding mode occurs on the surface $s(x) = 0$ and try to derive the motion equations using the regularization method. Again, let the discontinuous control be implemented with some imperfections of unspecified nature; control is known to take one of the two extreme values, $u^+(x)$ or $u^-(x)$, and the discontinuity points are isolated in time. As a result, the solution exists in the conventional sense, and it does not matter whether we deal with small hysteresis, time delay, or time constants neglected in the ideal model.

Like for the system (Equation 2.2.1) with hysteresis imperfection, the state velocity vectors $f^+ = f(x,u^+)$ and $f^- = f(x,u^-)$ are assumed to be constant for some point x on the surface $s(x) = 0$ within a short time interval $[t, t + \Delta t]$. Let the time interval Δt consist of two sets of intervals Δt_1 and Δt_2 such that $\Delta t = \Delta t_1 + \Delta t_2$, $u = u^+$ for the time from the set Δt_1 and $u = u^-$ for the time from the set Δt_2. Then the increment of the state vector after time interval Δt is found as

$$\Delta x = f^+ \Delta t_1 + f^- \Delta t_2$$

and the average state velocity as

$$\dot{x}_{av} = \frac{\Delta x}{\Delta t} = \mu f^{+} + (1-\mu) f^{-},$$

where $\mu = {}^{\Delta t_1}\!/_{\Delta t}$ is relative time for control to take value u^{+} and $(1-\mu)$ to take value u^{-}, $0 \le \mu \le 1$. To get the vector $\dot{x}$ the time Δt should be tended to zero. However, we do not need to perform this limit procedure, because it is hidden in our assumption that the state velocity vectors are constant within time interval Δt; therefore, the equation

$$\dot{x} = \mu f^{+} + (1-\mu) f^{-} \tag{2.2.4}$$

represents the motion during sliding mode. Because the state trajectories during sliding mode are in the surface $s(x) = 0$, the parameter μ should be selected such that the state velocity vector of the system (Equation 2.2.4) is in the tangential plane to this surface, or

$$\dot{s} = \text{grad}[s(x)] \cdot \dot{x} = \text{grad}[s(x)][\mu f^{+} + (1-\mu) f^{-}] = 0, \tag{2.2.5}$$

$$\text{with grad}[s(x)] = \left[{}^{\partial s}\!/_{\partial x_1} \ \ldots \ {}^{\partial s}\!/_{\partial x_n} \right].$$

The solution to Equation 2.2.5 is given by

$$\mu = \frac{\text{grad}(s) \cdot f^{-}}{\text{grad}(s) \cdot (f^{-} - f^{+})}. \tag{2.2.6}$$

Substitution of Equation 2.2.6 into Equation 2.2.4 results in the sliding mode equation

$$\dot{x} = f_{sm}, \quad f_{sm} = \frac{(\text{grad } s) \cdot f^{-}}{(\text{grad } s) \cdot (f^{-} - f^{+})} f^{+} - \frac{(\text{grad } s) \cdot f^{+}}{(\text{grad } s) \cdot (f^{-} - f^{+})} f^{-}, \tag{2.2.7}$$

representing the motion in sliding mode with initial condition $s[x(0)] = 0$. Note that sliding mode occurs in the surface $s(x) = 0$; therefore, the functions s and $\dot{s}$ have different signs in the vicinity of the surface (Figure 2.5) and $\dot{s}^{+} = (\text{grad } s) \cdot f^{+} < 0$, $\dot{s}^{-} = (\text{grad } s) \cdot f^{-} > 0$. As follows from Equation 2.2.6, the condition $0 \le \mu \le 1$ for parameter μ holds. It is easy to check the condition $\dot{s} = (\text{grad } s) \cdot f_{sm} = 0$ for the trajectories of system (Equation 2.2.7) and to show that they are confined to the switching surface $s(x) = 0$. As could be expected, direct substitution of grad $s = c$, $f^{+} = Ax + bu^{+}$ and $f^{-} = Ax + bu^{-}$ into Equation 2.2.7 results in the sliding mode Equation 2.2.2 derived for the linear system in Equation 2.2.1 with the discontinuity plane $s(x) = cx = 0$ via hysteresis regularization.

It is interesting to note that the above regularization method for deriving the sliding mode equation may be considered as a physical interpretation of the famous Filippov method. The method is intended for solution continuation

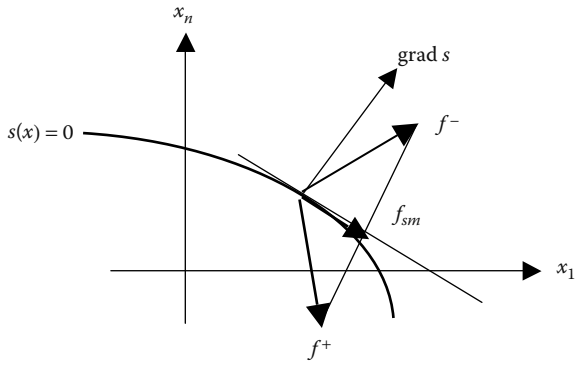

FIGURE 2.5
Sliding mode equation by Filippov's method.

at a discontinuity surface for differential equations with discontinuous right-hand sides [Filippov 1988]. According to this method, the ends of all state velocity vectors in the vicinity of a point on a discontinuity surface should be complemented by a minimal convex set, and state velocity vector of the sliding motion should belong to this set. In our case, we have two points, ends of vectors f^+ and f^-, and the minimal convex set is the straight line connecting their ends (see Figure 2.5). The equation of this line is exactly the right-hand side of Equation 2.2.4. The intersection of the line with the tangential plane defines the state velocity vector in the sliding mode *fsm*, or the right-hand side of the sliding mode equation. It is clear that the result of Filippov's method coincides with the equation derived by the regularization approach.

The regularization methods discussed above and the methods studied by Andre and Zeibert [1956a,b] were developed under rather restrictive assumptions: a special class of imperfections (delay or hysteresis) in which control may take only two extreme values, with scalar control and one discontinuity surface. The general regularization concept embracing a wider class of imperfections (such as continuous approximation of a discontinuous function) and sliding modes in the intersection of several surfaces is regularization via "boundary layer" [Utkin 1971, 1992]. We describe the idea of the boundary layer approach for an arbitrary system with vector control:

$$\dot{x} = f(x,u), \quad x, f \in \Re^n, \quad u(x) \in \Re^m, \tag{2.2.8}$$

$$u(x) = \begin{cases} u^+(x) & \text{for } s(x) > 0 \\ u^-(x) & \text{for } s(x) < 0 \end{cases} \text{(componentwise)}.$$

The components of vector $s(x)^T = [s_1(x) \ldots s_m(x)]$ are m smooth functions, and the ith component of the control undergoes discontinuities on the ith

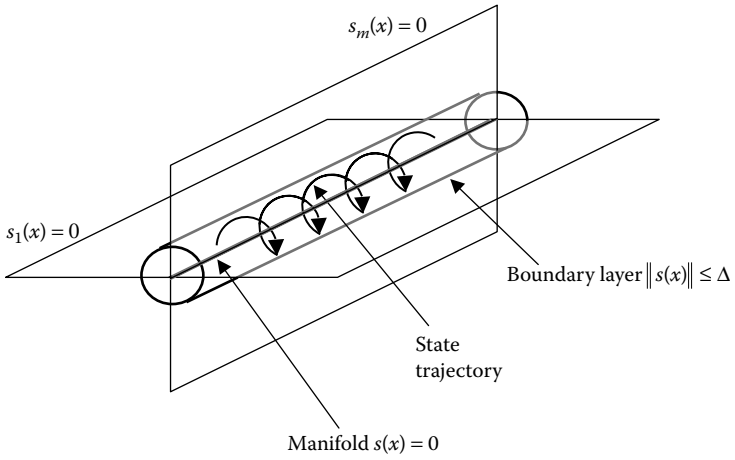

FIGURE 2.6
Sliding mode equation by boundary layer method.

surface $s_i(x) = 0$. Similar to sliding mode in the intersection of two planes in Equation 2.1.2, sliding mode may occur in the manifold $s(x) = 0$. To obtain the sliding mode equations, the ideal control in Equation 2.2.8 is replaced by a new control $\tilde{u}$ such that the solution to Equation 2.2.8 with this control exists in the conventional sense. Because of the substitution, the trajectories are not confined to the manifold $s(x) = 0$ but run in its boundary layer with the width $\Delta > 0$ (see Figure 2.6):

$$\|s(x)\| \le \Delta, \quad \|s\| = (s^T s)^{1/2}.$$

The imperfections taken into account in the control $\tilde{u}$ are not specified, and it is only known that the solution to Equation 2.2.8 with the new control exists in the conventional sense. As a rule, real-life imperfections belong to this class (including hysteresis, time delay, and small time constants neglected in the ideal model).

The core idea of the boundary layer regularization method is as follows. If the limit of the solution to Equation 2.2.8, with $u = \tilde{u}$ and the width of the boundary layer tending to zero, exists and is unique and does not depend on the type of imperfections and the way of tending Δ to zero, i.e., is independent of the limit procedure in

$$\lim_{\Delta \to 0} x(t, \Delta) = x^*(t) \tag{2.2.9}$$

then the function $x^*(t)$ is taken as the solution to Equation 2.2.8 with ideal sliding mode. Otherwise, we should recognize that the motion equations beyond the discontinuity manifold do not let us derive unambiguously the

equations for the motion in the manifold. The particular cases of regularization for the systems with scalar discontinuous control handled in this section have shown that Equation 2.2.7 is the "right" model of sliding mode. More general cases will be discussed in the next section using the boundary layer approach.

2.3. Equivalent Control Method

From a methodological point of view, it is convenient to develop a procedure for deriving the sliding mode equations for the system in Equation 2.2.8, first using heuristic method and then analyzing whether they can be taken as the motion model based on the boundary layer regularization approach.

We assume that the initial state vector of the system in Equation 2.2.8 is in the intersection of all discontinuity surfaces, i.e., in the manifold $s(x) = 0$, and sliding mode occurs with the state trajectories confined to this manifold for $t > 0$.

Because motion in the sliding implies $s(x) = 0$ for $t > 0$, we may assume that $ds / dt = \dot{s} = 0$ as well. Hence, in addition to $s(x) = 0$, the time derivative $\dot{s}(x) = 0$ may be used to characterize the state trajectories during sliding mode. The fast switching control u is an obstacle for using conventional methods, so disregard the control discontinuities and calculate the vector u such that time derivative of vector s on the state trajectories of Equation 2.2.8 is equal to zero:

$$\dot{s}(x) = G \cdot f(x, u) = 0, \tag{2.3.1}$$

where $G = (\partial s / \partial x)$ is $m \times n$ matrix with gradients of functions $s_i(x)$ as rows. Let a solution to the algebraic Equation 2.3.1 exist. The solution $u_{eq}(x)$ will further be referred to as "equivalent control." This continuous function is substituted for the discontinuous control u into the original system in Equation 2.2.8:

$$\dot{x} = f(x, u_{eq}). \tag{2.3.2}$$

It is evident that, for initial conditions $s(x(0)) = 0$ in compliance with Equation 2.3.1, additional motion governed by Equation 2.3.2 will be along the state trajectories in the manifold $s(x) = 0$ like in sliding mode in the system in Equation 2.2.8. Equation 2.3.2 is taken as the equation of sliding mode in the intersection of m discontinuity surfaces $s_i(x) = 0$, $(i = 1, ..., m)$. The procedure of deriving the equation will be referred to as the "equivalent control method."

From a geometrical point of view, the equivalent control method means replacement of discontinuous control on the intersection of switching

surfaces by a continuous one such that the state velocity vector lies in the tangential manifold. For example, in the system with scalar control (Equation 2.2.3), this vector may be found as the intersection of the tangential plane and the locus $f(x,u)$ with control u running from u^- to u^+ (see Figure 2.7).

The intersection point defines the equivalent control u_{eq} and the right-hand side $f(x,u_{eq})$ in the sliding mode Equation 2.1.2. Note that the right-hand side $f(x,u_{eq})$ of the motion equation resulting from the equivalent control method does not coincide with that of Filippov's method (f_{sm} in Equation 2.9 and Figure 2.5). They are equal if the system (Equation 2.2.3) with scalar control is linear with respect to control $f(x,u)=f_0(x)+b(x)u$ (f_0 and b are n-dimensional vectors). Then the locus $f(x,u)$ of the equivalent control method (Figure 2.7) coincides with a minimal convex set (the straight line connecting the end of vectors f^+ and f^-) of Filippov's method. The discrepancy reflects the fact that different ways of regularization lead to different sliding mode equations in systems with nonlinear functions of control input in motion equations [Utkin 1972].

We apply the equivalent method procedure to so-called affine systems, i.e., nonlinear systems with right-hand sides in the motion Equation 2.2.8 as linear functions of the control input u,

$$\dot{x} = f(x) + B(x)u, \quad x, f(x) \in \Re^n, \quad B(x) \in \Re^{n\times m}, \quad u(x) \in \Re^m, \tag{2.3.3}$$

$$u(x) = \begin{cases} u^+(x) & \text{for } s(x) > 0 \\ u^-(x) & \text{for } s(x) < 0 \end{cases} \text{(componentwise)}, \; s(x)^T = [s_1(x) \ldots s_m(x)].$$

Similar to the system in Equation 2.2.8, each surface $s_i(x)=0$ is the set of discontinuity points for corresponding control component u_i. Equation 2.3.1 of the equivalent control method for the system in Equation 2.3.2 is of form

$$\dot{s} = Gf + GBu_{eq} = 0, \tag{2.3.4}$$

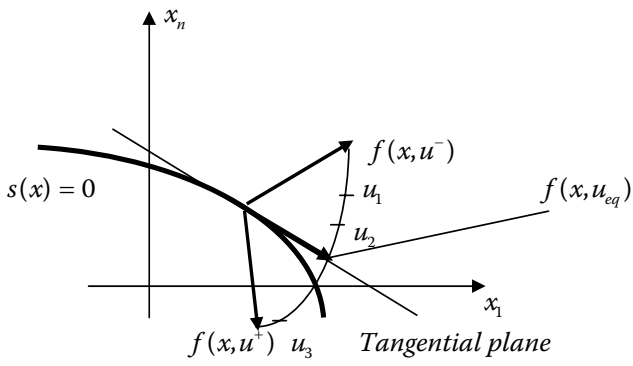

FIGURE 2.7
Equivalent control method for nonlinear systems with scalar control.

where $G = (\partial s/\partial x)$.

Assuming that matrix GB is nonsingular for any x, find the equivalent control $u_{eq}(x)$ as the solution to Equation 2.3.4

$$u_{eq}(x) = -\left(G(x)B(x)\right)^{-1} G(x) f(x)$$

and substitute $u_{eq}(x)$ into Equation 2.14 to yield the sliding mode equation as

$$\dot{x} = f(x) - B(x)\left(G(x)B(x)\right)^{-1} G(x) f(x). \tag{2.3.5}$$

Equation 2.3.5 is taken as the equation of sliding mode in the manifold $s(x) = 0$. The equation has been postulated. According to our concept, the question whether it is a right model of the motion in sliding mode may be answered involving the regularization method based on introduction of a boundary layer of the manifold $s(x) = 0$. For the affine systems (Equation 2.3.3), the sliding mode equation is found uniquely in the framework of the method, and it coincides with Equation 2.3.5 resulting from the equivalent control method. This statement is substantiated by Utkin [1971] under general assumptions related to smoothness and growth rate for the functions f, B, u^+, u^-, and s. According to these results, the condition in Equation 2.2.9 holds, which means that any solution in the boundary layer $x(t, \Delta)$ tends to a solutions $x^*(t)$ of Equation 2.3.5 regardless of what kind of imperfection caused the motion in the boundary layer and in what way the boundary layer is reduced to zero.

Formally, the equivalent control method may be applied to systems that are nonlinear with respect to control as well. As was mentioned, the result differs from the equations of Filippov's method even for systems with scalar control.

Attempts to show that this or that method is right by using the regularization approach have been unsuccessful because the sliding mode equations resulting from the limit procedure depend on the nature of introduced imperfections and the way of tending them to zero. For example, sliding modes in relay systems with small delay or hysteresis in a switching device are governed by the equation of Filippov's method, but, for a piecewise smooth continuous approximation of a discontinuous function, they are governed by the equation of the equivalent control method. The reader may find the details of sliding mode analysis in nonlinear systems with explanations of the reasons of ambiguity in the work of Utkin [1992].

Qualitatively, the result for affine systems may be explained in terms of a system block diagram (Figure 2.8). In compliance with the equivalent control method, the time derivative $\dot{s}$ is formally set to be equal to zero (Equation 2.3.4). For the motion in a boundary layer, s is a small value of order Δ, but $\dot{s}$ takes finite values and does not tend to zero with Δ. This means that real control does not satisfy the Equation 2.3.4 and may be found as

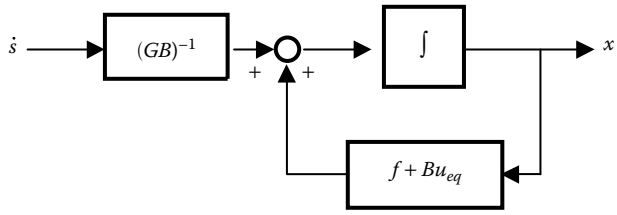

FIGURE 2.8
Equivalent control method for affine systems.

$$u = u_{eq} + (GB)^{-1}\dot{s}.$$

The motion equation in the boundary layer is governed by

$$\dot{x} = f + Bu_{eq} + (GB)^{-1}\dot{s}.$$

It differs from the ideal sliding Equation 2.3.5 by the additional term $(BG)^{-1}\dot{s}$. In terms of block diagrams, any dynamic system may be represented as a series of integrators, and it is natural to assume that an output of each of them may be estimated by an upper bound of the integral of an input.

In our case, the input is $\dot{s}$ and its integral s tends to zero with $\Delta \to 0$. Therefore, the response to this input tends to zero. This explains why the solution with the boundary layer reduced to zero tends to that to the equation of the equivalent control method. Of course, this is not the case for the systems with nonlinear functions of control in motion equations; indeed, generally speaking, $\int_0^t h(\dot{s})d\tau$ does not tend to zero even if s does and $h(0) = 0$. For example, if $s = -(1/\omega)\cos\omega t$, $\dot{s} = \sin\omega t$, then s tends to zero with $\omega \to \infty$ but $\int_0^t [(\dot{s})^2 d\tau$ does not.

Uniqueness of sliding mode equations in affine systems explains why the major attention is paid to this class in theory of sliding mode control. It is worth noting that systems nonlinear with respect to a state vector and linear with respect to a control input are the most common in practical applications.

2.4. Physical Meaning of Equivalent Control

The motion in sliding mode was regarded as a certain idealization. It was assumed that the control changes at high, theoretically infinite, frequency

such that the state velocity vector is oriented precisely along the intersection of discontinuity surfaces. However, in reality, various imperfections make the state oscillate in some vicinity of the intersection, and components of control are switched at finite frequency alternatively taking the values $u_i^+(x)$ and $u_i^-(x)$. These oscillations have high frequency and slow components. The high frequency is filtered out by a plant under control, whereas its motion in sliding mode is determined by the slow component. Conversely, sliding mode equations were obtained by substitution of equivalent control for the real control. It is reasonable to assume that the equivalent control is close to the slow component of the real control, which may be derived by filtering out the high-frequency component by a low-pass filter. Its time constant should be sufficiently small to preserve the slow component undistorted but large enough to eliminate the high-frequency component. As shown previously by Utkin [1992], the output of a low-pass filter

$$\tau\dot{z} + z = u$$

tends to the equivalent control:

$$\lim_{\tau\to 0,\ \Delta/\tau\to 0} z = u_{eq}.$$

This way of tending z to u_{eq} is not something involved but naturally follows from physical properties of the system. Indeed, the vicinity of a discontinuity manifold of width Δ, where the state oscillates, should be reduced to make the real motion close to ideal sliding mode. For reduction of Δ, the switching frequency f of the control should be increased; otherwise, the amplitude of oscillations would exceed Δ because $\Delta \approx 1/f$. To eliminate the high-frequency component of the control in sliding mode, the frequency should be much higher than $1/\tau$, or $1/f << \tau$; hence, $\Delta << \tau$. Finally, the time constant of the low-pass filter should be made to tend to zero because the filter should not distort the slow component of the control. Thus, the conditions $\tau \to 0$ and $\Delta/\tau \to 0$ (which implies $\Delta \to 0$) should be fulfilled to extract the slow component equal to the equivalent control and to filter out the high-frequency component.

It is interesting that the equivalent control depends on plant parameters and disturbances that may be unknown. For example, let us assume that sliding mode exists on the line $s = 0$ in the system in Equation 2.1.1:

$$\ddot{x} + a_2\dot{x} + a_1 x = u + f(t),$$
$$u = -M\text{sign}(s), \quad s = \dot{x} + cx,$$

where M, a_1, a_2, c are constant parameters, and $f(t)$ is a bounded disturbance. Equivalent control is the solution to the equation $\dot{s} = -a_2\dot{x} - a_1 x + u + f(t) = 0$ with respect to u under condition $s = 0$, or $\dot{x} = -cx$:

$$u_{eq} = (-a_2 c + a_1)x - f(t).$$

As we can see, the equivalent control depends on parameters a_1, a_2, and disturbance $f(t)$. Extracting equivalent control by a low-pass filter, this information may be obtained and used for improvement of feedback control system performance. Furthermore, this opportunity will be used in Chapter 6 for designing state observers with sliding modes and in Chapter 8 for chattering suppression.

2.5. Existence Conditions

The methods developed in the previous section enable us to write down the sliding mode equation should sliding mode occur in a system. If the sliding mode exhibits the desired dynamic properties, the control should be designed such that this motion is enforced. Hence, the conditions for sliding mode to exist should be derived: the second mathematical problem in the analysis of sliding mode as a phenomenon. For the systems with scalar control studied in this chapter and Chapter 1, the conditions were obtained from geometrical considerations: the deviation from the switching surface s and its time derivative should have opposite signs in the vicinity of a discontinuity surface $s = 0$ [Barbashin 1967] or

$$\lim_{s\to+0} \dot{s} < 0, \text{ and } \lim_{s\to-0} \dot{s} > 0. \tag{2.5.1}$$

For the system in Equation 1.2.1, the domain of sliding mode (sector $m - n$ on the switching line) (see Figure 1.7) was found based on geometric considerations. It may be found analytically from Equation 2.5.1 as

$$\dot{s} = (-c^2 + a_2 c - a_1)x - M\text{sign}(s) + f(t),$$

and the domain of sliding for bounded disturbance $|f(t)| < f_0$ is given by

$$|x| < \frac{M - f_0}{|-c^2 + a_2 c - a_1|}.$$

As was demonstrated in Equation 2.1.2, for existence of sliding mode in an intersection of a set of discontinuity surfaces $s_i(x) = 0, (i = 1, ..., m)$, it is not necessary to fulfill inequalities (Equation 2.5.1) for each of them. The example showed that the trajectories converge to the manifold $s^T = [s_1 ... s_m] = 0$ and reach it after a finite time interval similarly to the systems with scalar control. The term "converge" means that we deal with the problem of stability of the origin in m-dimensional subspace $(s_1, ..., s_m)$; therefore, the existence conditions may be formulated in terms of stability theory.

In addition, a nontraditional condition, "finite time convergence," should take place. This last condition is important to distinguish systems with

sliding modes from continuous systems with state trajectories converging to some manifold asymptotically. For example, the state trajectories of the system $\ddot{x} - x = 0$ converge to the manifold $s = \dot{x} - x = 0$ asymptotically because $\dot{s} = -s$; however, it would hardly be reasonable to call the motion in $s = 0$ sliding mode.

In the sequel, we examine the conditions for sliding mode to exist for affine systems (Equation 2.3.3). To derive the conditions, stability of the motion projection on subspace s governed by the differential equation

$$\dot{s} = Gf + GBu \tag{2.5.2}$$

should be analyzed.

The control Equation 2.3.3

$$u(x) = \begin{cases} u^+(x) & \text{for } s(x) > 0 \\ u^-(x) & \text{for } s(x) > 0 \end{cases} \text{(componentwise)}, \; s(x)^T = [s_1(x) \ldots s_m(x)]$$

may be represented as

$$u(x) = u_0(x) + U(x)\text{sign}(s), \tag{2.5.3}$$

where $u_0(x) = \dfrac{u^+(x) + u^-(x)}{2}$, $U(x)$ is a diagonal matrix with elements $U_i(x) = \dfrac{u_i^+(x) - u_i^-(x)}{2}$ for $i = 1, \ldots, m$, and the discontinuous control sign(s) takes the form of a componentwise sign function

$$\text{sign}(s)^T = [\text{sign}(s_1) \ldots \text{sign}(s_m)]. \tag{2.5.4}$$

Then the motion projection on subspace s is governed by

$$\dot{s} = d(x) - D(x)\text{sign}(s), \tag{2.5.5}$$

with $d = Gf + GBu_0$, $D = -GBU$. To find the stability conditions of the origin $s = 0$ for nonlinear system (Equation 2.5.5), i.e., the conditions for sliding mode to exist, we will follow the standard methodology for stability analysis of nonlinear systems and try to find a Lyapunov function. At the same time, we should remember that the right-hand side in the motion equation is discontinuous and not defined in the points in which arguments of the sign functions are equal to zero. To illustrate that the problem needs subtle treatment, let us turn to the example in Equation 2.1.2 in Section 2.1 with the equation of motion projection on subspace (s_1, s_2) given by

$$\begin{aligned} \dot{s}_1 &= -\text{sign}\, s_1 \; + \; 2\text{sign}\, s_2 \\ \dot{s}_2 &= -2\text{sign}\, s_1 \; - \; \text{sign}\, s_2. \end{aligned}$$

The time derivative of the positive definite Lyapunov function candidate $V = |s_1| + |s_2|$ along the system trajectories,

$$\dot{V} = \frac{\partial V}{\partial s_1}\dot{s}_1 + \frac{\partial V}{\partial s_{21}}\dot{s}_2 = \text{sign}(s_1)(-\text{sign } s_1 \ + \ 2\text{sign } s_2) + \text{sign}(s_2)(-2\text{sign } s_1 \ - \ \text{sign } s_2) = -2,$$

is negative definite, and we may conclude that the origin of the state plane (s_1, s_2) is asymptotically stable. Figure 2.1 shows that this is the case. The time needed for the state to reach the origin is calculated as $T = V(0)/|\dot{V}| = V(0)/2 = |s_2(0)|/2$ for initial condition $s_1(0) = 0, \ \ s_2(0) \neq 0$. The result coincides with the reaching time found by the point-to-point transform method in Section 2.1.

However, the conclusion on asymptotic stability made for the example is not always correct. The time derivative of the positive definite Lyapunov function candidate

$$V = 4|s_1| + |s_2|$$

along the trajectories of another example system

$$\dot{s}_1 = -2\text{sign } s_1 \ - \text{sign } s_2$$
$$\dot{s}_2 = -2\text{sign } s_1 \ + \ \text{sign } s_2$$

is negative

$$\dot{V} = \frac{\partial V}{\partial s_1}\dot{s}_1 + \frac{\partial V}{\partial s_2}\dot{s}_2 = -7 - 6\text{sign}(s_1)\text{sign}(s_2)$$

everywhere except at the discontinuity surfaces. However, it does not testify to stability. As can be seen in the state plane shown in Figure 2.9, the state trajectories reach the plane $s_1 = 0$ on which sliding mode occurs (the existence conditions in Equation 2.5.1 hold in this plane). Following the equivalent control method, the motion equation may be obtained by finding $[\text{sign}(s_1)]_{eq}$ from equation $\dot{s}_1 = 0$ and substituting it into the second equation. This results in sliding equation $\dot{s}_2 = 2\text{sign}(s_2)$ with unstable solution and s_2 tending to infinity.

Instability of the motion along the plane $s_1 = 0$ means that no sliding mode occurs in the intersection of the discontinuity surfaces $s_1 = 0$ and $s_2 = 0$. The trajectories intersect the surfaces $V = const.$ from outside everywhere except for the corner points with $s_1 = 0$, and the trajectories of sliding mode in $s_1 = 0$ diverge through these points. In the first example in Figure 2.1, sliding mode occurs on none of the discontinuity surfaces; therefore, the discontinuity points of the right-hand side in motion equations are isolated. This is the reason for decreasing of the Lyapunov function and difference in signs of V and $\dot{V}$, suggesting asymptotic stability of the origin in subspace (s_1, s_2) and existence of sliding mode in the intersection of planes $s_1 = 0$ and $s_2 = 0$. However, as evidenced by the second example in Figure 2.9, knowledge of the signs of a piecewise smooth function and its derivative, generally speaking, is not sufficient to ascertain that sliding mode does exist.

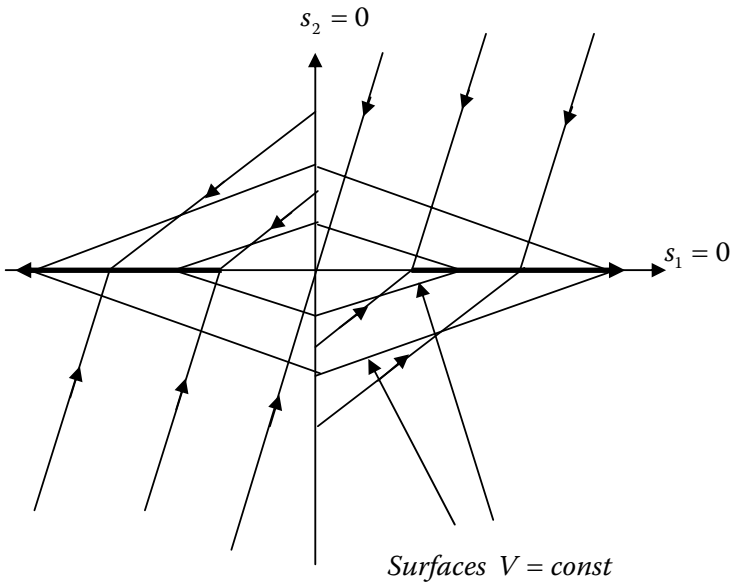

FIGURE 2.9
s—plane of the system with two-dimensional control.

To be able to use a Lyapunov function in the form of the sum of absolute values whenever sliding mode occurs on some of the discontinuity surfaces, the corresponding components of discontinuous control should be replaced by their equivalent ones, and only then the time derivative of the Lyapunov function should be found.

Definition 2.1

The set $S(x)$ in the manifold $s(x) = 0$ is the domain of sliding mode, if for the motion governed by Equation 2.5.6, the origin in the subspace s is asymptotically stable with finite convergence time for each x from $S(x)$.

Definition 2.2

Manifold $s(x) = 0$ is referred to as sliding manifold if sliding mode exists at each point, or $S(x) = \{x : s(x) = 0\}$.

Theorem 2.1

If the matrix D in the equation

$$\dot{s} = -D\text{sign}(s) \tag{2.5.6}$$

is positive definite

$$D + D^T > 0, \tag{2.5.7}$$

then the origin $s = 0$ is an asymptotically stable equilibrium point with finite convergence time. □

Proof 2.1

Let the sum of absolute values of s_i

$$V = \text{sign}(s)^T s > 0 \tag{2.5.8}$$

be a Lyapunov function candidate. Partition vector s into two subvectors $s^T = (s^k)^T (s^{m-k})^T$, assuming that sliding mode occurs in the intersection of k discontinuity surfaces, $s^k = 0$, whereas the components of vector s^{m-k} are different from zero.

According to the equivalent control method, vector $\text{sign}(s^k)$ in the motion equation must be replaced by the function $[\text{sign}(s^k)]_{eq}$ such that $\dot{s}^k = 0$. Because $s^k = 0$ in sliding mode, the time derivative of V in Equation 2.5.8 consists of $(m - k)$ terms:

$$\begin{aligned} \dot{V} &= \frac{d}{dt}\left((\text{sign}(s^{m-k}))^T s^{m-k}\right) \\ &= \left(\text{sign}(s^{m-k})\right)^T \dot{s}^{m-k}. \end{aligned}$$

The value of $\left(\text{sign}(s^k)\right)_{eq}^T \dot{s}^k$ is equal to zero in sliding mode; therefore,

$$\dot{V} = \left(\text{sign}(s^k)\right)_{eq}^T \dot{s}^k + \left(\text{sign}(s^{m-k})\right)^T \dot{s}^{m-k}.$$

Replacing vector $\dot{s}$ with its value form (Equation 2.5.6) and vector $\text{sign}(s^k)$ with $\left(\text{sign}(s^k)\right)_{eq}$, we have

$$\dot{V} = -z^T D z = -z^T \frac{D + D^T}{2} z,$$

where $z^T = \left(\text{sign}(s^k)\right)_{eq}^T \left(\text{sign}(s^{m-k})\right)^T$. Because matrix D is positive definite (Equation 2.5.7), $\dot{V} \le -\lambda_{\min} \|z\|^2$, $\lambda_{\min} > 0$ is the minimal eigenvalue of matrix $\frac{D + D^T}{2}$, $\|z\| = \sqrt{z^T z}$.† Because at initial time, at least one of the components of

† Of course, generally speaking $Q \ne \frac{Q + Q^T}{2}$ but $z^T Q z = z^T \frac{Q + Q^T}{2} z$.

vector s is different from zero and one of the components of vector z is equal to +1 or –1, $\|z\| \geq 1$, the Lyapunov function (Equation 2.5.8) decays at a finite rate

$$\dot{V} \leq -\lambda_{\min}. \tag{2.5.9}$$

The condition in Equation 2.5.9 means that V and vector s vanish after a finite time interval, and the origin $s = 0$ is an asymptotically stable equilibrium point with finite convergence time. □

The two second-order examples were studied in this section. For both of them, time derivatives of positive definite Lyapunov functions of "sum of absolute values" type were negative definite everywhere except at the discontinuity surfaces.

For the first second-order example in this section, $D = \begin{pmatrix} 1 & -2 \\ 2 & 1 \end{pmatrix}$ and matrix $D + D^T > 0$ is positive definite, which testifies to stability (Figure 2.1). The second system with $D = \begin{pmatrix} 2 & 1 \\ 2 & -1 \end{pmatrix}$ is unstable (Figure 2.9), and matrix $D + D^T = \begin{pmatrix} 4 & 3 \\ 3 & -2 \end{pmatrix}$ is not positive definite.

The sufficient stability (or sliding mode existence) condition formulated in Theorem 2.1 for the system in Equation 2.5.6 can be easily generalized for the case in Equation 2.5.2 or 2.5.5. For $s(x) = 0$ to be a sliding manifold, it is sufficient that, for any $x \in S$, $S\{x : s(x) = 0\}$,

$$\begin{aligned} &D(x) + D^T(x) > 0, \\ &\lambda_0 > d_0\sqrt{m} \text{ with } \lambda_{\min}(x) > \lambda_0 > 0, \\ &\|d(x)\| < d_0, \end{aligned} \tag{2.5.10}$$

where $\lambda_{\min}(x)$ is the minimal eigenvalue of $\dfrac{D + D^T}{2}$, λ_0 is a constant positive value, and d_0 is an upper estimate of vector $d(x)$ in Equation 2.5.5.

The time derivative of Lyapunov function (Equation 2.4.8) along the trajectories of Equation 2.5.2 is of the form similar to Equation 2.5.9:

$$\begin{aligned} \dot{V} &= z^T d(x) - z^T \frac{D + D^T}{2} z \\ &\leq \|z\|\|d(x)\| - \lambda_{\min} \end{aligned}.$$

The components of vector z are either $\text{sign}(s_i)$ or $[\text{sign}(s_i)]_{eq}$. As shown in Section 2.3, the equivalent control is an average value of discontinuous control, and this value is a continuous function varying between the two extreme values of the discontinuous control. This means that $\left|(\text{sign}(s_i))_{eq}\right| \leq 1$;

hence, the norm of m-dimensional vector z with components from the range ±1 does not exceed $\sqrt{m}$ and

$$\dot{V} \le d_0\sqrt{m} - \lambda_0 < 0. \tag{2.5.11}$$

Because the Lyapunov function decays at a finite rate, it vanishes and sliding mode occurs after a finite time interval.

Remark 2.1

If inequality (Equation 2.5.11) holds for any x, then it simultaneously is "the reaching condition," i.e., the condition for the state to reach the sliding manifold from any initial point.

Remark 2.2

Upper and lower estimates of $d(x)$ and $\lambda_{\min}(x)$, respectively, may depend on x. Then the condition for sliding manifold to exist and the reaching condition is of the form

$$\dot{V} \le \|d(x)\|\sqrt{m} - \lambda_{\min}(x) < -v_0, \tag{2.5.12}$$

where v_0 is constant positive value.

Remark 2.3

Functions $d(x)$ and $D(x)$ depend on control Equations 2.5.3 and 2.5.5. The value of $\lambda_{\min}(x)$ may be increased by increasing the difference between $u_i^+(x)$ and $u_i^-(x)$ without varying $u_0(x)$ and $d(x)$. Then the condition in Equations 2.5.11 and 2.5.12 can be fulfilled.

General Remark for Chapter 2

When studying the equations of sliding modes and conditions for this motion to exist, only time-invariant systems were handled, but all results are valid for time-varying systems as well. The difference for a time-varying switching manifold $s(x,t) = 0$ is as follows: to find the equivalent control, Equation 2.3.4 should be complemented by an additional term $\partial s(x,t)/\partial t$,

$$\dot{s} = Gf + GBu_{eq} + \partial s(x,t)/\partial t = 0,$$

and its solution $u_{eq} = -(GB)^{-1}(Gf + \partial s/\partial t)$ should be substituted into Equation 2.3.3 regardless of whether functions f and B in motion Equation 2.3.3 depend on time or are time invariant.

References

Andre J, Seibert P. 1956a. "Über Stückweise Lineare Differential-Gleichungen, die bei Regelungsproblemen Auftreten I" (in German). *Arch der Math* 7.

Andre J, Seibert P. 1956b. "Über Stückweise Lineare Differential-Gleichungen, die bei Regelungsproblemen Auftreten II" (in German). *Arch der Math* 7.

Barbashin E. 1967. *Introduction to the Theory of Stability* (in Russian). Moscow: Nauka.

Filippov A. 1988. *Differential Equations with Discontinuous Right-Hand Sides*. Durdrecht, The Netherlands: Kluwer Publishers.

Utkin V. 1971. "Equations of Slipping Regimes in Discontinuous Systems I." *Automat Remote Control* 32:1897–1907.

Utkin V. 1972. "Equations of Slipping Regimes in Discontinuous Systems II." *Automat Remote Control* 33:211–219.

Utkin V. 1992. *Sliding Modes in Control and Optimization*. London: Springer-Verlag.

3

Design Concepts

The key idea of the design methodology for sliding mode control was outlined in Chapter 1 (Section 1.4). According to this idea, any design procedure should consist of two stages. As established in Chapter 2, sliding modes are governed by a reduced order system depending on the equations of some discontinuity surfaces. The first stage of design is the selection of the discontinuity surfaces such that sliding motion would exhibit desired properties. The methods of conventional control theory, such as stabilization, eigenvalue placement, and dynamic optimization, may be applied at this stage. The second stage is to find discontinuous control to enforce sliding mode in the intersection of the surfaces selected at the first stage. The second problem is of reduced order as well because its dimension is equal to the number of discontinuity surfaces, which is usually equal to the dimension of control.

Partitioning of the overall motion into two motions of lower dimensions—the first motion preceding sliding mode within a finite time interval and the second motion being sliding mode with the desired properties—may simplify the design procedure considerably. In addition, sliding modes may be insensitive with respect to unknown plant parameters and disturbances, although the invariance property does take place for any system, as demonstrated for the system in Equation 2.1.1 in Chapter 2 (Sections 2.1 and 2.2). In this chapter, different sliding mode control design methods based on the decoupling principle will be developed and special attention will be paid to the class of the system with invariant sliding motions.

3.1. Introductory Example

As an example of sliding mode control design, a multilink manipulator may be considered under the assumption that each link is subjected to a control force or torque. The system motion is represented by a set of interconnected second-order equations:

$$M(q)\ddot{q} + f(\dot{q}, q, t) = u,$$

where q and u are vectors of the same dimension of generalized states and force or torque control components, respectively, $M(q)$ is a positive-definite inertia matrix, and $f(q, \dot{q}, t)$ is a function depending on the system geometry,

the velocity vector, unknown parameters, and disturbances. The motion equation may be represented as

$$\dot{p} = v, \quad M(p)\dot{v} = -f(p, v, t) + u$$

with $q = p$, $\dot{q} = v$.

If sliding mode is enforced in the manifold $s = cp + v = 0$, then

$$\dot{p} = -cp.$$

(Formally, equivalent control u_{eq} should be found from equation $\dot{s} = 0$, substituted into the second equation, and then v should be replaced by $-cp$; it will result in the above equation with respect to p). Assigning the eigenvalues of the sliding mode equation by a proper choice of matrix c, the desired rate of convergence of $p = q$ and $v = \dot{q}$ (note that $s = cp + v = 0$) to zero may be determined. To enforce the sliding mode with the desired dynamics, convergence of the motion projection on subspace

$$\dot{s} = c\dot{p} + \dot{v} = cv - M^{-1}f + M^{-1}u$$

should be provided. The inertia matrix as well as its inverse, M^{-1}, are positive definite. It follows from Theorem 2.1 of Section 2.4 that the discontinuous control

$$u = -U(q, \dot{q})\text{sign}(s), \quad U(q, \dot{q}) > 0$$

with sufficiently high value of scalar function $U(q, \dot{q})$ enforces sliding motion in manifold $s = 0$. Only an upper bound of function $f(q, \dot{q}, t)$ and low estimate of minimal eigenvalue of M^{-1} (see Remarks 2.2 and 2.3 in Section 2.4) are needed for the design of the control stabilizing the mechanical system operating under uncertainty condition with the desired rate of convergence. Of course, it should be mentioned that the solution has been obtained in the framework of an ideal model with known state vector (p^T, v^T) and assuming that the control forces may be implemented as discontinuous state functions.

3.2. Decoupling

In the sequel, we will deal with affine systems

$$\dot{x} = f(x, t) + B(x, t)u, \quad x, f \in \Re^n, \quad B(x) \in \Re^{n \times m}, \quad u(x) \in \Re^m, \tag{3.2.1}$$

$$u(x)=\begin{cases}u^{+}(x,t) & \text{if } s(x)>0\\ u^{-}(x,t) & \text{if } s(x)>0\end{cases}\ \text{(componentwise)},\ s(x)^{T}=[s_1(x)\ldots s_m(x)],$$

with the right-hand side of Equation 3.2.1 being a linear function of control.

To obtain the equation of sliding mode in manifold $s(x) = 0$ under the assumption that matrix GB (matrix $G = \{\partial s/\partial x\}$ with rows as gradients of the components of vector s is nonsingular the equivalent control

$$u_{eq}(x, t) = -(G(x)\, B(x, t))^{-1}\, G(x)\, f(x, t)$$

should be substituted into Equation 3.1 for the control $u(x)$ to yield

$$\begin{aligned}\dot{x} &= f_{sm}(x,t),\\ f_{sm}(x,t) &= f(x,t)-B(x,t)\big(G(x)B(x,t)\big)^{-1}G(x)f(x,t).\end{aligned}\tag{3.2.2}$$

Because $s(x) = 0$ in sliding mode, this system of m algebraic equations may be solved with respect to m component of the state vector constituting subvector x_2:

$$x_2 = s_0(x_1),\ \ x_2 \in \Re^m,\ \ x_1 \in \Re^{n-m},\ \ x^T = [x_1^T \quad x_2^T]\ \text{and}\ s(x) = 0.$$

Replacing x_2 by $s_0(x_1)$ in the first $n - m$ Equation 3.2.2 yields a reduced order sliding mode equation,

$$\dot{x}_1 = f_{1sm}\big(x_1, s_0(x_1), t\big),\tag{3.2.3}$$

where $f_{sm}^T(x,t) = f_{sm}^T(x_1, x_2, t) = [f_{1sm}^T(x_1, x_2, t) \quad f_{2sm}^T(x_1, x_2, t)]$.

The motion Equation 3.2.3 depends on function $s_0(x_1)$, i.e., on the equation of the discontinuity manifold. Function $s_0(x_1)$ may be handled as m-dimensional control for the reduced order system. It should be noted that the design problem is not a conventional one because right-hand sides in Equations 3.2.2 and 3.2.3 depend not only on the discontinuity manifold equation but on the gradient matrix G as well. If a class of functions $s(x)$ is preselected, for instance linear functions or in the form of finite series, then both $s(x)$, G and, as a result, the right-hand sides in Equation 3.2.3 depend on the set of parameters to be selected when designing the desired dynamics of sliding motion.

The second-order system (Equation 2.1.1) with a scalar control

$$\begin{aligned}\dot{x}_1 &= a_{11}x_1 + a_{12}x_2 + b_1u + d_1f(t)\\ \dot{x}_2 &= a_{12}x_1 + a_{22}x_2 + b_2u + d_2f(t)\\ u &= -M\text{sign}(s),\ s = c_1x_1 + c_2x_2\end{aligned}$$

may serve as an example. As shown in Section 2.2, sliding mode along the switching line $s = c_1x_1 + c_2x_2 = 0$ is governed by the first-order equation

$$\dot{x}_1 = \left(a_{11} - a_{12}c_2^{-1}c_1 - (cb)^{-1}b_1(ca^1 - ca^2c_2^{-1}c_1)\right)x_1 + \left(d_1 - b_1(cb)^{-1}(cd)\right)f(t),$$

where $c = [c_1\ c_2]$, $b^T = [b_1\ b_2]$, $(a^1)^T = [a_{11}\ a_{21}]$, $(a^2)^T = [a_{12}\ a_{22}]$, $d^T = [d_1\ d_2]$, and cb and c_2 are assumed to be different from zero. The equation may be rewritten in the form

$$\dot{x}_1 = \left(a_{11} - a_{12}c_1^* - (c^*b)^{-1}b_1(c^*a^1 - c^*a^2c_1^*)\right)x_1 + \left(d_1 - b_1(c^*b)^{-1}(c^*d)\right)f(t)$$

with $c^* = [c_1^*\ \ 1]$, and $c_1^* = c_2^{-1}c_1$. Hence, only one parameter c_1^* should be selected to provide the desired motion of the first-order dynamics in our second-order example. The second stage of the design procedure is selection of discontinuous control enforcing sliding mode in manifold $s(x) = 0$, which has been chosen at the first stage. The condition for sliding mode to exist is equivalent to stability condition of the motion projection on subspace s

$$\dot{s} = Gf + GBu \tag{3.2.4}$$

with a finite convergence time (see Section 2.4).

Generally speaking, matrix $-(GB + (GB)^T)$ is not positive definite; therefore, the stability cannot be provided by increasing the elements of matrix U as it is recommended in Remark 2.3 of Section 2.4 for control (Equation 3.2.1). Let the positive-definite function

$$V = 0.5\, s^T s > 0$$

be a Lyapunov function candidate. Its time derivative along the system trajectories is of the form

$$\dot{V} = s^TGf + s^TGBu. \tag{3.2.5}$$

Assuming that matrix GB is nonsingular, select the control u as a discontinuous function

$$u = -U(x)\text{sign}(s^*) \text{ with } s^* = (GB)^T s, \tag{3.2.6}$$

where $U(x)$ is a scalar positive function of the state. Then Equation 3.2.5 is of form

$$\dot{V} = s^TGf - U\left|s^*\right|,$$

where $|s^*| = (s^*)^T \operatorname{sign}(s^*)$, or

$$\dot{V} = (s^*)^T (GB)^{-1} Gf - U|s^*|.$$

Because $|s^*| \geq \|s^*\|$ is attributable to $\sum_{i=1}^{m} |s_i^*| \geq \left(\sum_{i=1}^{m} (s_i^*)^2 \right)^{1/2}$, it follows from Equation 3.2.6 that

$$\dot{V} \leq |s^*| |(GB)^{-1} Gf| - U|s^*|.$$

If an upper estimate $F \geq |(GB)^{-1} Gf|$ is known, then $\dot{V} < 0$ for $U > F$, the motion is asymptotically stable and sliding mode is enforced in the system. Later it will be proven that the time interval preceding sliding mode is finite and may be decreased by increasing the magnitude $U(x)$ of the discontinuous control. Sliding mode occurs in the manifold $s^* = 0$. The transformation (Equation 3.2.6) is nonsingular; therefore, the manifolds $s = 0$ and $s^* = 0$ coincide and sliding mode takes place in the manifold $s = 0$, which was selected to design sliding motion with the desired properties.

The design procedure has been decoupled into two independent subproblems of lower dimensions m and $n - m$. Decoupling is feasible because the sliding mode equations do not depend on control but they do depend on the sliding manifold equation. When designing a switching manifold, only one constraint should be taken into account: matrix GB should be nonsingular. Exact knowledge of plant parameters and disturbances (vector f and matrix B) is not needed; only knowledge of an upper bound F is sufficient to enforce sliding mode in manifold $s^* = 0$. Matrix $B(x, t)$ is needed to calculate vector s^* in Equation 3.2.6. However, the range of parameter variation in matrix $B(x, t)$ may be found such that sliding mode can be enforced without exact knowledge of these parameters.

First, we will show that any $m \times m$ transformation matrix Q in

$$s^* = Q(x)s$$

fits if $(Q^{-1})^T GB = L(x)$ is a matrix with a dominant diagonal

$$|l_{ii}| > \sum_{\substack{j=1 \\ j \neq i}}^{m} |l_{ij}|, \quad \text{or } \alpha_i = |l_{ii}| - \sum_{\substack{j=1 \\ j \neq i}}^{m} |l_{ij}|, \quad \alpha_i > 0 \quad \text{for any } i = 1, \ldots, m.$$

Indeed, for control $u = -U(x)(\operatorname{sign}(L))(\operatorname{sign}(s^*))$ with sign$L$ being a diagonal matrix with elements $\operatorname{sign}(l_{ii})$,

$$\dot{V} = (s^*)^T (Q^{-1})^T Gf - U(s^*)^T L(\text{sign}(L))(\text{sign}(s^*))$$
$$= \sum_{i=1}^{m} s_i^* q_i - U \sum_{i=1}^{m} \left(|s_i^*| (|l_{ii}| + \sum_{\substack{j=1 \\ j \neq i}}^{m} l_{ij} \text{sign}(l_{ij} s_i^* s_j^*) \right),$$

where q_i are elements of vector $(Q^{-1})^T Gf$. The time derivative of the Lyapunov function is negative, i.e., sliding mode is enforced in $s^* = 0$ if

$$U(x) > \max_i |q_i(x,t)| / \alpha_i.$$

To illustrate the design method for the system in Equation 3.2.1, assume that matrix B consists of a known nominal part and unknown variation $B = B_0 + \Delta B$. Then for $Q = (GB_0)^T$, matrix L is of form $L = I_m + \Delta L$, $\Delta L = (GB_0)^{-1} G\Delta B$ (I_m is $m \times m$ identity matrix). This form enables finding admissible range of variations in matrix B: the sum of absolute values on any row of matrix ΔL should not exceed 1. Hence, sliding mode can be enforced with control Equation 3.2.6 in systems with unknown parameters in the input matrix $B(x, t)$.

3.3. Regular Form

The two-stage design procedure—selection a switching manifold and then finding control enforcing sliding mode in this manifold—becomes simpler for systems in so-called "regular form." The regular form for an affine system (Equation 3.2.1) consists of two blocks:

$$\begin{aligned} \dot{x}_1 &= f_1(x_1, x_2, t) \\ \dot{x}_2 &= f_2(x_1, x_2, t) + B_2(x_1, x_2, t)u, \end{aligned} \tag{3.3.1}$$

where $x_1 \in \Re^{n-m}$, $x_2 \in \Re^m$, and B_2 is an $m \times m$ nonsingular matrix, i.e., $\det B_2 \neq 0$. The first block does not depend on control, whereas the dimension of the second block coincides with that of the control.

The design is performed in two stages as well. First, m-dimensional state vector x_2 is handled as the control of the first block and designed as a function of the state x_1 of the first block in correspondence with some performance criterion

$$x_2 = -s_0(x_1). \tag{3.3.2}$$

Again, we deal with a reduced order design problem. At the second stage, discontinuous control is to be selected to enforce sliding mode in the manifold

$$s(x_1, x_2) = x_2 + s_0(x_1) = 0. \tag{3.3.3}$$

After sliding mode occurs in the sliding manifold (Equation 3.3.3), the condition (Equation 3.3.2) holds, and the additional motion in the system will be governed by the differential equation

$$\dot{x}_1 = f_1\left(x_1, -s_0(x_1), t\right) \tag{3.3.4}$$

with the desired dynamic properties.

The design of the discontinuous control may be performed using the methods of Section 3.1 with $x^T = [x_1^T \quad x_2^T]$, $f^T = [f_1^T \quad f_2^T]$, $B^T = [0_{m\times(n-m)} \quad B_2^T]$, $G = [G_1 \; I_m]$, $G_1 = \{\partial s_0/\partial x_1\}$ being an $m \times (n - m)$ matrix.

Note the following characteristics for the design in the regular form:

1. In contrast to Equations 3.2.2 and 3.2.3, the sliding mode equation does not depend on gradient matrix G, which makes the design problem at the first stage a conventional one: design of m-dimensional control x_2 in $(n - m)$-dimensional system with state vector x_1.
2. Calculation of the equivalent control to find the sliding mode equation is not needed.
3. The condition $\det(GB) = \det(B_2) \neq 0$ holds. (Recall that this condition is needed to enforce sliding mode in the preselected manifold $s(x) = 0$.)
4. Sliding mode is invariant with respect to functions f_2 and B_2 in the second block.

These characteristics suggest that we should find a coordinate transformation reducing the original affine system (Equation 3.2.1) to the regular form (Equation 3.3.1) before designing sliding mode control. We will confine ourselves to systems with scalar controls. The methods related to systems with vector control may be found in the work of Luk'yanov and Utkin [1981]. We assume that, in a system,

$$\begin{aligned} &\dot{x} = f(x,t) + b(x,t)u, \\ &x \in \Re^n, \;\; u \in \Re, \;\; f^T = [f_1, \ldots, \; f_n], \end{aligned} \tag{3.3.5}$$

$b(x, t)$ is an n-dimensional vector with components $b_i(x, t)$, $i = 1,\ldots,n$. Assume that at least one of them, let it be $b_n(x, t)$, is different from zero for any x and t

$$b_n(x, t) \neq 0.$$

Let a solution to an auxiliary system of $(n-1)$th order,

$$dx_i/dx_n = b_i/b_n,\ i = 1,\ldots,n,\ x^T = (x_1,\ldots,x_n), \tag{3.3.6}$$

be a set of functions:

$$x_i = \varphi_i(x_n, t),\ i = 1,\ldots,n-1. \tag{3.3.7}$$

Let us introduce the nonsingular coordinate transformation

$$y_i = x_i - \varphi_i(x_n, t),\ i = 1,\ldots,n-1. \tag{3.3.8}$$

According to Equations 3.3.5 through 3.3.8, the motion equations with respect to new state vector $(y_1,\ldots,y_{n-1}, x_n)$ are of the form

$$\begin{aligned}
\dot{y}_i &= \dot{x}_i - \frac{d\varphi_i(x_n,t)}{dx_n}\dot{x}_n \\
&= \dot{x}_i - \frac{dx_i}{dx_n}\dot{x}_n = f_i + b_i u - \frac{b_i}{b_n}(f_n + b_n u) \\
&= f_i - \frac{b_i}{b_n} f_n, \qquad i = 1,\ldots,n-1 \\
\dot{x}_n &= f_n + b_n u.
\end{aligned}$$

Replacing x_i by $y_i + \varphi_i(x_n)$ leads to motion equations

$$\begin{aligned}
\dot{y} &= f^*(y, x_n, t), \\
\dot{x}_n &= f_n^*(y, x_n) + b_n^*(y, x_n, t)u,
\end{aligned} \tag{3.3.9}$$

where y and f^* are $(n-1)$-dimensional vectors, and f_n^* and b_n^* are scalar functions. The system with respect to y and x_n is in the regular form (Equation 3.3.1) with $(n-1)$th and first-order blocks.

For a particular case with b_i depending only on one coordinate x_n, the state transformation may be found in the explicit form

$$y_i = x_i - \int_0^{x_n} \frac{b_i(\gamma, t)}{b_n(\gamma, t)} d\gamma. \tag{3.3.10}$$

The system with respect to the new variables is in the regular form (Equation 3.3.9) as well.

3.4. Invariance

Consider a control system with time-varying parameters operating in the presence of disturbances. Given reference inputs may be treated as disturbances if the deviations of control variables from the inputs are included into a state vector. The possibility of designing systems with invariant sliding motions in canonical spaces was discussed in the introduction to Chapter 1.

Let variable x_1 and its time derivatives $x_1^{i-1} = x_i$, $i = 2,\ldots,n$ be components of a state vector in the canonical space. Then the motion equations of a single-input-single-output system in canonical space are of the form

$$\begin{aligned} \dot{x}_i &= x_{i+1}, \qquad i = 1,\ldots,n-1 \\ \dot{x}_n &= -\sum_{i=1}^{n} a_i(t)x_i + f(t) + b(t)u, \end{aligned} \tag{3.4.1}$$

where $a_i(t)$ and $b(t)$ are bounded parameters with known range $|a_i(t)| \le a_{i0}$, $|b(t)| \ge b_0$, $f(t)$ is a bounded disturbance $|f(t)| \le f_0$ with a_{i0}, b_0, f_0 being known scalar numbers. Let the control be a discontinuous state function

$$u = -(\alpha|x| + M)\text{sign}(s), \quad |x| = \sum_{i=1}^{n} |x_i|, \quad s = \sum_{i=1}^{n} c_i x_i,$$

where α, M, and c_i are constant values and $c_n = 1$. Calculate the time derivative of function s as

$$\dot{s} = \sum_{i=1}^{n} (c_{i-1} - a_i)x_i - b(\alpha|x| + M)\text{sign}(s) \text{ with } c_0 = 0.$$

The conditions for the state to reach plane $s = 0$ in the state space and for sliding mode to exist (see Equation 2.4.1) are fulfilled if

$$b_0\alpha > \max(c_{i-1} - a_{i0}),\ i = 1,\ldots,n,\ b_0M > f_0.$$

After a finite time interval, sliding mode occurs in the plane $s = 0$. To obtain the sliding mode equation, $x_n = -\sum_{i=1}^{n-1} c_i x_i$ should be substituted into the $(n-1)$th equation of the system in Equation 3.4.1 and the last one should be disregarded:

$$\begin{aligned} \dot{x}_i &= x_{i+1}, \qquad i = 1,\ldots,n-2 \\ \dot{x}_{n-1} &= -\sum_{i=1}^{n-1} c_i x_i. \end{aligned}$$

The sliding mode equation is invariant to the plant parameter variations and the disturbance, and its dynamics are determined by the roots of the characteristic equation

$$p^{n-1} + c_{n-1}p^{n-2} + \cdots + c_2 p + c_1 = 0,$$

which may be shaped by a proper choice of coefficients c_i in the equations of the discontinuity surface.

However, technical difficulties involved in obtaining time derivatives of the plant output x_1 are the major obstacles for implementation of such specific sliding modes. At the same time, by means of both scalar and vector control, invariant sliding modes can be enforced in the spaces whose coordinates may not only be derivatives but arbitrary physical variables as well.

Let us formulate the invariance conditions for arbitrary affine systems of the form in Equation 3.2.1:

$$\dot{x} = f(x,t) + B(x,t)u + h(x,t), \tag{3.4.2}$$

where vector $h(x, t)$ characterizes disturbances and parameter variations that should not affect the feedback system dynamics. In compliance with the equivalent control method (see Section 2.3), the solution to $\dot{s} = G(f + Bu + h) = 0$ with respect to control,

$$u_{eq} = -(GB)^{-1}(f + h)$$

should be substituted into the system Equation 3.4.2 to yield

$$\dot{x} = f - B(GB)^{-1}Gf + (I_n - B(GB)^{-1}G)h. \tag{3.4.3}$$

Let range $B(x, t)$ be a subspace formed by the base vectors of matrix $B(x, t)$ for each point (x, t). Sliding mode is invariant with respect to vector $h(x, t)$ if

$$h(x, t) \in \text{range}(B(x, t)). \tag{3.4.4}$$

The condition in Equation 3.4.4 means that there exists vector $\gamma(x, t)$ such that

$$h(x, t) = B(x, t)\,\gamma(x, t). \tag{3.4.5}$$

Direct substitution of vector $h(x, t)$ in the form of Equation 3.4.5 into Equation 3.4.3 demonstrates that the sliding motion in any manifold $s(x) = 0$ does not depend on perturbation vector $h(x, t)$. As follows from the design methods in Sections 3.1 and 3.2, an upper estimate of this vector is needed to enforce the sliding motion. The condition in Equation 3.4.5 generalizes the invariance condition obtained by Drazenovic [1969] for linear systems.

3.5. Unit Control

The objective of this section is to demonstrate a design method for discontinuous control enforcing sliding mode in some manifold without individual selection of each component of control as a discontinuous state function. The approach implies design of control based on a Lyapunov function selected for a nominal (feedback or open-loop) system. The control is to be found such that the time derivative of the Lyapunov function is negative along the trajectories of the system with perturbations caused by uncertainties in the plant model and environment conditions.

The roots of the above approach may be found in papers by Gutman and Leitmann published in the 1970s [Gutman and Leitmann 1976; Gutman 1979]. The design idea may be explained for an affine system:

$$\dot{x} = f(x,t) + B(x,t)u + h(x,t), \tag{3.5.1}$$

with state and control vectors $x \in \Re^n$, $u \in \Re^m$, state-dependent vectors $f(x, t)$, $h(x, t)$, and control input matrix $B(x,t) \in \Re^{n\times m}$. The vector $h(x, t)$ represents the system uncertainties, and its influence on the control process should be rejected. The equation

$$\dot{x} = f(x,t) \tag{3.5.2}$$

represents an open-loop nominal system that is assumed to be asymptotically stable with a known Lyapunov function candidate

$$V(x) > 0,$$
$$W_o = dV/dt\big|_{h=0,u=0} = \text{grad}(V)^T f < 0, \text{grad}(V)^T = \left[\frac{\partial V}{\partial x_1} \ldots \frac{\partial V}{\partial x_n}\right]. \tag{3.5.3}$$

The perturbation vector $h(x, t)$ is assumed to satisfy the matching conditions (Equation 3.4.4); hence, there exists vector $\gamma(x, t) \in R^m$ such that

$$h(x, t) = B(x, t)\ \gamma(x, t). \tag{3.5.4}$$

$\gamma(x, t)$ may be an unknown vector with known upper scalar estimate $\gamma_0(x, t)$,

$$\|\gamma(x,t)\| < \gamma_o(x,t). \tag{3.5.5}$$

Calculate the time derivative of Lyapunov function $V(x)$ along the trajectories of the perturbed system (Equations 3.5.2 through 3.5.5) as

$$W = dV/dt = W_o + \text{grad}(V)^T B(u + \gamma). \tag{3.5.6}$$

For control u depending on the upper estimate of the unknown disturbance, chosen as

$$u = -\rho(x,t)\frac{B^T \operatorname{grad}(V)}{\left\|B^T \operatorname{grad}(V)\right\|}, \tag{3.5.7}$$

with a scalar function $\rho(x, t) > \gamma_0(x, t)$ and

$$\left\|B^T \operatorname{grad}(V)\right\|^2 = \left(\operatorname{grad}(V)^T B\right)\left(B^T \operatorname{grad}(V)\right),$$

the time derivative of the Lyapunov function,

$$\begin{aligned} W &= W_o - \rho(x,t)\left\|B^T \operatorname{grad}(V)\right\| + \operatorname{grad}(V)^T B\gamma(x,t) \\ &< W_o - \left\|B^T \operatorname{grad}(V)\right\|[\rho(x,t) - \gamma_0(x,t)] \\ &< 0 \end{aligned}$$

is negative. This implies that the perturbed system with control (Equation 3.5.7) is asymptotically stable as well.

Two important features should be underlined for the system with control (Equation 3.5.7):

1. Control (Equation 3.5.7) undergoes discontinuities in $(n - m)$-dimensional manifold $s(x) = B^T \operatorname{grad}(V) = 0$ and is a continuous state function beyond this manifold. This is the principle difference between control (Equation 3.5.7) and all the control inputs in the previous sections with individual switching functions for each control component.
2. The disturbance $h(x, t)$ is rejected because of enforcing sliding mode in the manifold $s(x) = 0$. Indeed, if the disturbance (Equation 3.5.4) is rejected, then control u should be equal to $-\gamma(x, t)$ which is not generally the case for the control (Equation 3.5.7) beyond the discontinuity manifold $s(x) = B^T \operatorname{grad}(V) \neq 0$. It means that sliding mode occurs in the manifold $s = 0$, and the equivalent value of control u_{eq} is equal to $-\lambda(x, t)$.

   Note that the norm of control (Equation 3.5.7) with the gain $\rho(x, t) = 1$

$$\left\|\frac{B^T \operatorname{grad}(V)}{\left\|B^T \operatorname{grad}(V)\right\|}\right\|$$

   is equal to one for any value of the state vector. It explains the term "unit control" for the control (Equation 3.5.7).

Later on, unit control was used directly with a Lyapunov function at the second stage of the conventional two-stage design procedure for sliding mode control: selection of a sliding manifold $s(x) = 0$ and enforcing sliding mode in this manifold [Ryan and Corless 1984; Dorling and Zinober 1986]. The manifold $s(x) = 0$ was selected in compliance with some performance criterion and the control was designed similar to that of Equation 3.5.7:

$$u = -\rho(x,t)\frac{D^T s(x)}{\left\|D^T s(x)\right\|}, \tag{3.5.8}$$

with $D = GB$, $G = \{\partial s/\partial x\}$, and D was assumed to be nonsingular.

The equation of the motion projection of the system in Equation 3.5.1 on the subspace s is of form

$$\dot{s} = G(f + h) + Du. \tag{3.5.9}$$

The conditions for the trajectories to converge to the manifold $s(x) = 0$ and for sliding mode to exist in this manifold may be derived based on a Lyapunov function candidate

$$V = \frac{1}{2}s^T s > 0. \tag{3.5.10}$$

Find the time derivative of Lyapunov function (Equation 3.5.10) along the trajectories of the system in Equation 3.5.9 with control Equation 3.5.8:

$$\begin{aligned}\dot{V} &= s^T G(f + h) - \rho(x,t)\left\|D^T s(x)\right\| \\ &= [s^T D][D^{-1}G(f + h)] - \rho(x,t)\left\|D^T s(x)\right\| \\ &\le \left\|D^T s(x)\right\|\left[\left\|D^{-1}G(f + h)\right\| - \rho(x,t)\right].\end{aligned}$$

For $\rho(x,t) > \left\|D^{-1}G(f + h)\right\|$, the value of $\dot{V}$ is negative; therefore, the state will reach the manifold $s(x) = 0$. Next, we will show that, if $\rho(x,t) - \left\|D^{-1}G(f + h)\right\| \ge \rho_0 > 0$ (ρ_0 is constant value), then $s(x)$ vanishes and sliding mode occurs after a finite time interval. Preliminarily, we estimate $\left\|D^T s(x)\right\|$:

$$\|s\| = \left\|(D^T)^{-1}D^T s\right\| \le \left\|(D^T)^{-1}\right\|\left\|D^T s\right\| \text{ and } \left\|D^T s\right\| \ge \left\|(D^T)^{-1}\right\|^{-1}\|s\|.$$

Thus, $\dot{V} \le -\left\|(D^T)^{-1}\right\|^{-1}\rho_0\|s\|$, and, because $V = \frac{1}{2}\|s\|^2$, $\|s\| = \sqrt{2V}$ leads to

$$\dot{V} < -\eta V^{1/2}, \eta = \sqrt{2}\left\|(D^T)^{-1}\right\|^{-1}\rho_0.$$

The solution to the differential inequality $V(t)$ is nonnegative and is bounded by

$$V(t) < \left(-\frac{\eta}{2} t + \sqrt{V_0} \right)^2, V_0 = V(0).$$

Because the solution vanishes after some $t_s < \frac{2}{\eta}\sqrt{V_0}$, the vector s vanishes as well and sliding mode starts after a finite time interval.

Again, the principle difference should be underlined in motions preceding the sliding mode in $s(x) = 0$ for the conventional componentwise control and unit control design methods. For the conventional method, the control undergoes discontinuities should any of the components of vector s change sign, whereas the unit control is a continuous state function until the manifold $s(x) = 0$ is reached.

3.6. Second-Order Sliding Mode Control

3.6.1. Preliminary Remarks

The systems with scalar control

$$\dot{x} = f(x,t) + b(x,t)u, \quad x, f, b \in !^n,$$
$$u(x) = \begin{cases} u^+(x) \text{ if } s(x) > 0 \\ u^-(x) \text{ if } s(x) < 0 \end{cases}, \; u^+, \; u^-, s \text{ are continuous scalar functions.} \tag{3.6.1}$$

will be treated in this section.

Time derivative of s is a discontinuous state function (or $(grad(s))^T b \neq 0$), and sliding mode is enforced on the surface $s(x) = 0$. The above condition means that the relative degree with respect to function $s(x)$ is equal to one, i.e., the derivative of $s(x)$ depends directly on control $u(x)$. Of course, generally speaking, the control system is designed to control some output variable $y(x)$, and the relative degree with respect to the output should not be equal to one. It depends on the structure of the plant and does not depend on the controller. For enforcing sliding mode, relative degree with respect to $s(x)$ equal to one can be provided by selecting it as a state function or, as we will see in Section 9.2, a function of the state of a dynamic controller.

The principal design idea of sliding mode control implies generating reduced order motion in some manifold $s(x) = 0$ with the desired properties. The question of interest is, "Can a similar effect be reached for cases with a relative degree greater than one, i.e., when the time derivative of $s(x)$ is continuous, but $\ddot{s}(x)$ is a discontinuous state function and the control input

is a continuous state function?" If true, the range of applications of sliding mode control will be increased because not all actuators can operate with discontinuous inputs. For example, high-frequency switching in an output may result in damage of valves in hydraulic actuators. This chattering problem will be addressed in Chapter 8.

In numerous publications, different design methods were offered for these cases, and the authors referred to these methods as "high-order sliding mode control." For a survey, see the work of Levant [2007]. The design methods will be discussed in this chapter except for the cases when high-order sliding modes can be easily interpreted in terms of the conventional sliding modes (or first-order sliding modes). For example, conventional sliding mode occurs in the switching line $cx + \dot{x} = 0$ in the system in Equation 1.2.1 studied in the introductory chapter. If $s_0 = x$ denotes the switching function, then $\dot{s}_0$ is continuous, whereas $\ddot{s}_0$ is discontinuous, but it is hardly reasonable to call the conventional sliding mode in the point $x = \dot{x} = 0$ second-order sliding mode. Similarly, sliding mode in the origin of the canonical space of the system in Equation 1.2.3 should not be referred to as the nth order sliding mode with respect to $s_0 = x$, or the $(n - 1)$th order with respect to $s_1 = cx + \dot{x}$, and so on.

As a final remark of this section, the problem of sliding mode existence in the system with continuous control will be addressed. The design objective is the same as in first-order sliding mode system, e.g., Equation 1.2.2: the state trajectories should be in the manifold $s(x) = 0$. If the right-hand side of the motion equation satisfies the Lipschitz condition (which is not the case for control as a discontinuous state function), then the manifold $s(x) = 0$ cannot be reached for arbitrary initial conditions as a result of uniqueness of solutions. However, it can happen if control is a continuous non-Lipschitzian function. Indeed, let the continuous control in the system in Equations 2.3.3 and 2.3.4 with $GB = I$ be of form

$$u = -u_0 \frac{s}{\|s\|^{1/2}} + u_{eq}, \ \lim_{\|s\| \to 0} \frac{s}{\|s\|^{1/2}} = 0 \tag{3.6.2}$$

Then the time derivative of Lyapunov function $V = \frac{1}{2} s^T s > 0$ is

$$\dot{V} = -\|s\|^{3/2} < 0 \text{ and } \dot{V} = -(2V)^{3/4}. \tag{3.6.3}$$

The solution of Equation 3.6.3 $V(t) = (V_0^{1/4} - 2^{-5/4} t)^4$ is equal to zero for $t \geq 2^{5/4} V_0^{5/4}$. It means that the trajectories of the system with continuous control belong to the manifold $s(x) = 0$ after a finite time interval. The motion is similar to that of the systems with discontinuous control: it is reasonable to call this motion sliding mode.

3.6.2. Twisting Algorithm

The system in Equation 3.6.1 is assumed to have a relative degree with respect to $s(x)$ equal to one. Then discontinuous control can be designed such that sliding mode occurs on the surface $s(x) = 0$. If because of technological conditions control actions have to be continuous, the problem can be solved by inserting a dynamic block, for instance an integrator, between discontinuous control and the system input:

$$\dot{u} = v. \tag{3.6.4}$$

It is assumed that the time derivative $\dot{s}$ is available, and v is designed as a discontinuous function of s and $\dot{s}$.

Of course, this assumption means that the relative degree of the system has not been changed and still is equal to one. The problem of reducing s to zero can be easily solved based on the conventional sliding mode $v = v_0 signS, S = \dot{s} + cs$ with v_0 being constant or a continuous state function. Because $\dot{S}$ is discontinuous, sliding mode can be enforced on $S = 0$, which means that $s \to 0$. As discussed in Section 3.6.1, it is hardly reasonable to refer to sliding mode in point $s = \dot{s} = 0$ as the second-order sliding mode. Conventional sliding mode can be enforced on the line $S = \dot{s} + c\sqrt{s} = 0$. Similar to Equation 3.6.3, the solution to this equation is reduced to zero after a finite time. The finiteness of the reaching time served as the argument for several authors to label the conventional sliding mode in the point $s = \dot{s} = 0$ "second-order sliding mode."

One more interesting modification of the control algorithm for the system in Equations 3.6.1 and 3.6.4 was proposed under the assumption that the point $s = \dot{s} = 0$ is reached after a finite time interval, but sliding mode does not occur at this first stage of motion. Illustrate the design idea for the case $(grad(s))^T b = 1$. Control $v = -M_0 sign(s) - M_1 sign(\dot{s})$, M_0, M_1 are positive constant values, then $\ddot{s} = F(x,t,u) - M_0 sign(s) - M_1 sign(\dot{s})$, $F(x, t, u)$ is a continuous function of all arguments, $|F(x, t, u)| \le F_0$, F_0 is a constant value, $M_0 > M_1 + F_0$, $M_1 > F_0$. Although the control undergoes discontinuities on $\dot{s} = 0$, sliding mode cannot exist on this switching line, if $s \neq 0$, because $M_0 > M_1$ and $\ddot{s}$ does not change sign.

Calculate time derivative of positive definite Lyapunov function $V = 2\sqrt{\frac{1}{2}\dot{s}^2 + M_0 |s|}$:

$$\dot{V} = \frac{\dot{s}F - M_1 |\dot{s}|}{\sqrt{\frac{1}{2}\dot{s}^2 + M_0 |s|}} \le -\frac{M' |\dot{s}|}{\sqrt{\frac{1}{2}\dot{s}^2 + M_0 |s|}} < 0, \quad M' = M_1 - F_0 > 0.$$

Because the condition $\dot{s} = 0$ cannot hold for any finite interval with $s \neq 0$, the motion in the subspace $(s, \dot{s})$ is asymptotically stable, and, starting from a

finite time instant for any initial conditions, both state components will be bounded. Next, the finite time convergence to the origin will be shown. Time derivative of V can be written as:

$$\dot{V} = -\frac{M'}{\sqrt{\frac{1}{2} + M_0 \frac{|s|}{\dot{s}^2}}} < 0.$$

For $\frac{|s|}{\dot{s}^2} \le k, k = const$ beyond domain D on the plane $(s, \dot{s})$, see Figure 3.1 with boundaries $S_I = \dot{s} - \varepsilon\sqrt{s} = 0$ and $S_{II} = \dot{s} + \varepsilon\sqrt{s} = 0$, $\varepsilon = 1/\sqrt{k}$,

$$\dot{V} \le -M' \frac{1}{\sqrt{\frac{1}{2} + M_0 k}} = -\alpha < 0, \tag{3.6.5}$$

and the Lyapunov function decays at finite rate.

Without loss of generality, the motion starting in semiplane $s > 0$ will be studied only. It follows from differentiation of S_I and S_{II} that $\dot{S}_I = -M_0 - M_1 + F(x,t,u) + \frac{1}{2}\varepsilon^2$ on $S_I = 0$ and $\dot{S}_{II} = -M_0 + M_1 + F(x,t,u) + \frac{1}{2}\varepsilon^2$

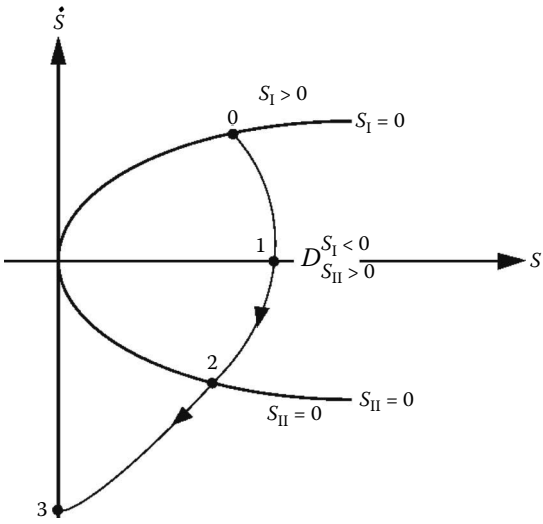

FIGURE 3.1
State trajectory in the plane $(s, \dot{s})$.

on $S_{II}=0$ are negative for some value of $\varepsilon > 0$. This means that state trajectories can penetrate into domain D through line $S_I = 0$ and leave it through line $S_{II} = 0$ only. For initial conditions on $S_I = 0$ (s_0 and $\dot{s}_0 = \varepsilon\sqrt{s_0}$, point 0)

the state trajectory crosses axis S at time t_1 ($s_1 = s(t_1)$, $\dot{s}_1 = \dot{s}(t_1) = 0$, point 1),

then $S_{II} = 0$ at time $t_1 + t_2$ ($s_2 = s(t_1 + t_2)$, $\dot{s}_2 = \dot{s}(t_1 + t_2) = -\varepsilon\sqrt{s_2}$, point 2),

and then axis $\dot{s}$ at time $t_1+t_2+t_3$ ($s_3 = s(t_1+t_2+t_3) = 0$, $\dot{s}_1 = \dot{s}(t_1+t_2+t_3)$, point 3).

Further it will be shown that the average rate of decreasing of the Lyapunov function V is negative and does not depend on the system state.

The system Equation 3.6.4 for s > 0 can be represented in the form

$$\ddot{s} = -m, \quad m = \begin{cases} m_1 & \text{if } S_I < 0, \dot{s} > 0 \\ m_2 & \text{if } S_{II} > 0, \dot{s} < 0 \\ m_3 & \text{if } S_{II} < 0, \dot{s} < 0. \end{cases}$$

Calculate the values of the state variables at point 1,2,3 and t_1, t_2, t_3 assuming that m_1, m_2, m_3 are constant, and keeping in mind that the solution for each interval is of form $s(t) = m_i/2\, t^2 + c_1 t + c_2$, $\dot{s} = m_i t + c_1$, $i = 1, 2, 3$, c_1 and c_2 depend on initial and boundary conditions:

$$t_1 = \frac{\varepsilon\sqrt{s_0}}{m_1}, \; t_2 = \varepsilon\sqrt{s_0}\sqrt{\frac{1 + \dfrac{\varepsilon^2}{2m_1}}{m_2^2 + \dfrac{\varepsilon^2}{2} m_2}}. \tag{3.6.6}$$

It follows from Equations 3.6.4 and 3.6.6 that

$$t_1 + t_2 \le \beta_1 \varepsilon\sqrt{s_0}, \quad \beta_1 = \frac{1}{M_0 + M_1 - F_0} + \sqrt{\frac{1 + \dfrac{\varepsilon^2}{2(M_0 + M_1 - F_0)}}{(M_0 - M_1 - F_0)^2 + \dfrac{\varepsilon^2}{2}(M_0 - M_1 - F_0)}}. \tag{3.6.7}$$

For the point 2

$$s_2 = s(t_1 + t_2) = s_0 \frac{1 + \dfrac{\varepsilon^2}{2m_1}}{1 + \dfrac{\varepsilon^2}{2m_2}},\ \dot{s}_2 = \dot{s}(t_1 + t_2) = -\varepsilon\sqrt{s_0}\sqrt{\frac{1 + \dfrac{\varepsilon^2}{2m_1}}{1 + \dfrac{\varepsilon^2}{2m_2}}}$$

and

$$s_2 = s(t_1 + t_2) \geq \beta_2 s_0,\quad \beta_2 = \frac{1 + \dfrac{\varepsilon^2}{2(M_0 + M_1 + F_0)}}{1 + \dfrac{\varepsilon^2}{2(M_0 - M_1 - F_0)}}. \tag{3.6.8}$$

The time t_3 for the third interval can be found as a solution to the equation $-m_3\frac{t^2}{2} - \varepsilon\sqrt{s_2}t + s_2 = 0$:

$$t_3 = \frac{2\sqrt{s_2}}{\varepsilon + \sqrt{\varepsilon^2 + 2m_3}}$$

and as follows from Equations 3.6.4 and 3.6.8:

$$t_3 \geq \beta_3\sqrt{s_0},\ \beta_3 = \frac{2\sqrt{\beta_2}}{\varepsilon + \sqrt{\varepsilon^2 + 2(M_0 - M_1 + F_0)}}. \tag{3.6.9}$$

For initial conditions at point 0, average value of the time derivative of the Lyapunov can be estimated for time interval $[0, t_1 + t_2 + t_3]$ taking into account that for time interval $[0, t_1 + t_2]$ it is nonpositive:

$$\dot{V}_{av} < \frac{1}{t_1 + t_2 + t_3}(-\alpha t_3). \tag{3.6.10}$$

As follows from (3.6.7–3.6.10) the upper estimate of the average rate of decaying V is negative and does not depend on the state

$$\dot{V}_{av} < -\alpha_0,\quad \alpha_0 = const = \frac{\alpha\beta_3}{\varepsilon\beta_1 + \beta_2} > 0.$$

This estimate is valid for trajectories with arbitrary $|F(x,t,u)| \leq F_0$ starting from any point of domain D since they run between the trajectories of the system with different combinations of extreme values of m_i.

The above analysis let us make the conclusion:

> Beyond the domain D for any value of the state vector the Lyapunov function decays at finite rate greater than α, for any initial conditions in the boundary of D or in its inner part the average rate is also finite greater than α_0. This means that under the condition
>
> $$M_0 > M_1 + F_0,\ M_1 > F_0$$
>
> the origin in the plane $(s, \dot{s})$ is reached after a finite time interval and then the second order sliding mode starts. It follows from the motion equations that the time functions $S(t)$ and $\dot{s}(t)$ cannot remain sign-constant; they have interlacing zeros. Therefore the sliding mode control algorithm discussed in this section is called "twisting."

3.6.3. Super-Twisting Algorithm

Similar to the twisting algorithm, the super-twisting sliding mode control algorithm [Levant 2007] relies on inserting an integrator into the control loop, such that control becomes a continuous time function. However, in contrast to the twisting algorithm, the time derivative of function s is not needed. As a result, the relative degree of the system is increased. Nevertheless, the new control design methodology allows enforcing the second-order sliding mode after a finite time interval and suppressing unknown disturbances with bounded time derivatives. The design idea of the super-twisting control again will be illustrated for the system in Equation 3.6.1 assuming that $(grad(s))^T b = 1$.

For the system in Equation 3.6.1 with continuous control,

$$\begin{aligned} &u = -a\sqrt{|s|}sign(s) + v, \\ &\dot{v} = -Msign(s),\ a > 0,\ M > 0,\ a, M - const \end{aligned} \tag{3.6.11}$$

find the second time derivative of s:

$$\ddot{s} = -a\frac{\dot{s}}{2\sqrt{|s|}} - Msign(s) + \dot{f}(t), \tag{3.6.12}$$

where $f(t)$ is a function of the state and disturbances,

$$|\dot{f}| \le f_0 - const.$$

The Lyapunov function in Section 3.6.2

$$V = 2\sqrt{\frac{1}{2}\dot{s}^2 + M|s|}$$

will be used for stability analysis. Its time derivative for the system in Equation 3.6.12 is of form

$$\dot{V} = \frac{-a\dfrac{\dot{s}^2}{2|s|} + \dfrac{\dot{s}}{\sqrt{|s|}}\dot{f}}{\sqrt{\dfrac{\dot{s}^2}{2|s|} + M}}. \tag{3.6.13}$$

Further analysis is similar to that in the previous section. If $\dfrac{\dot{s}^2}{|s|} > \varepsilon^2$, $\varepsilon > 0 - const$ and

$$\dot{f}_0 < \frac{1}{2}a\varepsilon\gamma,\ \gamma = const,\ \gamma < 1 \tag{3.6.14}$$

then the Lyapunov function decays at a finite rate beyond domain D on the plane $(s, \dot{s})$ (Figure 3.1) with boundaries $S_I = \dot{s} - \varepsilon\sqrt{s} = 0$ and $S_{II} = \dot{s} + \varepsilon\sqrt{s} = 0$:

$$\dot{V} \le -\frac{1}{2}a(1-\gamma)\frac{\varepsilon^2}{\sqrt{\dfrac{1}{2}\varepsilon^2 + M}} < 0. \tag{3.6.15}$$

(Again, it is assumed that $s > 0$.) Motion Equation 3.6.12 in the domain D may be written in the form

$$\ddot{s} = -Msign(s) + F(x,u,t), \quad |F(x,u,t)| \le \frac{a}{2}\varepsilon + \dot{f}_0.$$

Analysis of the motion in the domain D can be done similarly to that in section 3.6.2 assuming that

$$M_1 = M,\ M_2 = 0,\ F_0 = \frac{a}{2}\varepsilon + \dot{f}_0,\ M > F_0. \tag{3.6.16}$$

It means that the estimates in Equations 3.6.7 and 3.6.8 are valid for control in Equation 3.6.11. Function $-\dfrac{a}{2}\dfrac{\dot{s}}{\sqrt{|s|}}$ is positive for the part of the trajectories 2-3, therefore t_3 can be estimated from equation $\ddot{s} = -M - \dot{f}_0$ similarly to the estimate in Equation 3.6.9:

$$t_3 \ge \beta_3\sqrt{s_0},\ \beta_3 = \frac{2\sqrt{\beta_2}}{\varepsilon + \sqrt{\varepsilon^2 + 2(M + \dot{f}_0)}}. \tag{3.6.17}$$

The upper estimate of $\dot{V}$ in the domain D follows from Equations 3.6.13 and 3.6.14:

$$\dot{V} < a\frac{\gamma^2\varepsilon^2}{4\sqrt{M}}. \tag{3.6.18}$$

The average rate of the Lyapunov function on the trajectory 0-1-2-3 can be estimated from Equations 3.6.7, 3.6.8, 3.6.15, 3.6.17, and 3.6.18:

$$\dot{V} < [a\frac{\gamma^2\varepsilon^2}{4\sqrt{M}}(t_1+t_2) - a(1-\gamma)\frac{\varepsilon^2}{\sqrt{\varepsilon^2+M}}t_3]/(t_1+t_2+t_3)$$
$$= \frac{a\frac{\gamma^2\varepsilon^3\beta_1}{4\sqrt{M}} - a(1-\gamma)\frac{\varepsilon^2}{\sqrt{\varepsilon^2+M}}\beta_3}{\varepsilon\beta_1+\beta_3} < -\alpha_0.$$

Since β_1 and β_3 are not equal to zero with $\varepsilon = 0$, there exists a pair ε and γ such that $\alpha_0 > 0$ which means that the Lyapunov functions decay at a finite rate. Hence the second order sliding mode in the origin of the state plane $(s, \dot{s})$ will occur with after a finite time interval in the system with disturbance satisfying the conditions in Equations 3.6.14 and 3.6.16. The advantages of the super-twisting control with the second order sliding mode are: a continuous control suppressing arbitrary disturbances with bounded time derivative; there is no need to use the derivative of a switching function.

References

Dorling CM, Zinober ASI. 1986. "Two Approaches to Sliding Mode Design in Multivariable Variable Structure Control Systems." *Int J Control* 44:65–82.

Drazenovic B. 1969. "The Invariance Conditions for Variable Structure Systems." *Automatica* 5:287–295.

Gutman S. 1979. "Uncertain Dynamic Systems: A Lyapunov Min-Max Approach." *IEEE Trans Automatic Control* AC-24:437–449.

Gutman S, Leitmann G. 1976. "Stabilizing Feedback Control for Dynamic Systems with Bounded Uncertainties." *Proc IEEE Conf Decision Control* pp. 94–99.

Levant A. 2007. "Principles of 2-sliding Mode Design." *Automatica* 43:576–586.

Luk'yanov A, Utkin V. 1981. "Methods of Reducing Equations for Dynamic Systems to a Regular Form." *Automation Remote Control* 42:413–420.

Ryan EP, Corless M. 1984. "Ultimate Boundness and Asymptotic Stability of a Class of Uncertain Systems via Continuous and Discontinuous Feedback Control." *IMA J Math Cont Inf* 1:222–242.

4

Sliding Mode Control of Pendulum Systems

The design of sliding mode control for nonlinear multivariable systems has been extensively studied in many books and papers. The design procedure of such high-order nonlinear control systems may be complicated and varies from case to case. The objective of this chapter is to develop design methods for nonlinear mechanical systems governed by a set of second-order equations. The proposed approach assumes that the control systems can be transformed into a regular form (see Section 3.2), which enables decoupled control design. The control laws are illustrated for different inverted pendulum systems.

4.1. Design Methodology

When controlling mechanical systems, we deal with a set of interconnected second-order nonlinear differential equations:

$$J(q)\ddot{q} = f(q,\dot{q}) + Bu, \tag{4.1.1}$$

where $q \in \Re^n$, $u \in \Re^m$, u is a vector of control forces and torques, elements of matrix B are equal to either 0 or 1, rank $(B) = m$. In particular, for rotational mechanical systems, $J(q)$ is an inertia matrix. The system may be underactuated, i.e., it has fewer inputs than degrees of freedom, and/or is unstable.

The system in Equation 4.1.1 may be represented in the form of $2n$ equations of first order with respect to vectors $q_1 = q$ and $q_2 = \dot{q}_1$, and then the regular form approach can be applied. Here, we will generalize the approach for systems consisting of blocks governed by the second-order equations. Then it can directly be applied to nonlinear mechanical systems (Equation 4.1.1).

The inertia matrix $J(q)$ in mechanical systems is nonsingular, and B has full rank matrix; hence, $J^{-1}(q)B$ has full rank as well. The components of vector q may be reordered such that, in the motion equations,

$$\begin{aligned}
&\ddot{q}_1 = \tilde{f}_1(q,\dot{q}) + \tilde{B}_1(q)u \\
&\ddot{q}_2 = \tilde{f}_2(q,\dot{q}) + \tilde{B}_2(q)u \\
&q = \begin{bmatrix} q_1 \\ q_2 \end{bmatrix},\ q_1 \in \Re^{n-m},\ q_2 \in \Re^m,\ \begin{bmatrix} \tilde{f}_1 \\ \tilde{f}_2 \end{bmatrix} = J^{-1}f,\ \begin{bmatrix} \tilde{B}_1 \\ \tilde{B}_2 \end{bmatrix} = J^{-1}B,\ \det(\tilde{B}_2) \neq 0.
\end{aligned} \tag{4.1.2}$$

According to the regular form technique, as discussed in Section 3.2, a coordinate transformation $z = \phi(q) \in \Re^{n-m}$, $y = q_2$ with continuously differentiable function $\varphi(q)$ should be found such that the condition

$$\frac{\partial \phi(q)}{\partial q} J^{-1} B = 0$$

is fulfilled. Then $\dot{z} = \frac{\partial \phi(q)}{\partial q}\dot{q}$, $\ddot{z} = \frac{\partial}{\partial q}\left(\frac{\partial \phi(q)}{\partial q}\dot{q}\right)\dot{q} + \frac{\partial \phi(q)}{\partial q} J^{-1}(f + Bu)$ and the mechanical system equation is reduced to the regular form consisting of a set of second-order equations:

$$\begin{aligned} \ddot{z} &= f_1(z, y, \dot{z}, \dot{y}) \\ \ddot{y} &= f_2(z, y, \dot{z}, \dot{y}) + B_2(z, y)u, \qquad \det(B_2) \neq 0. \end{aligned} \tag{4.1.3}$$

For the regular form with blocks consisting of first-order equations (Section 3.2), the state of the low block was handled as control in the top block. The desired dependence between the two subvectors was provided by enforcing sliding mode.

In our case, the top block equation in Equation 4.1.3 depends on both vectors y and $\dot{y}$. This fact introduces some peculiarities that should be taken into account when designing sliding mode control. Furthermore, stabilization tasks for different types of mechanical systems will be studied. It is assumed that the origin in a system state space is an equilibrium point of an open-loop system:

$$f_1(0, 0, 0, 0) = 0,$$

$$f_2(0, 0, 0, 0) = 0.$$

4.1.1. Case 4.1

First, the stability of the system zero dynamics with vector y as an output is checked. They are governed by the first equation in Equation 4.1.3 with $y = 0$, $\dot{y} = 0$:

$$\ddot{z} = f_1(z, 0, \dot{z}, 0). \tag{4.1.4}$$

If they are stable, then sliding mode is enforced in the manifold $s = \dot{y} + cy = 0$ with scalar parameter $c > 0$. It is a simple task because rank $(B_2) = m$ and any method of enforcing sliding modes in Sections 3.1 and 3.3 is applicable. After sliding mode starts in the manifold $s = 0$, the state y tends to zero as

a solution to $\dot{y} + cy = 0$, and, hence, because of stability of zero solution of Equation 4.1.4, z decays as well.

4.1.2. Case 4.2

Now stability of the system zero dynamics with vector z as an output is checked. If $z(t) \equiv 0$, then the zero dynamics equation are obtained from the top block of Equation 4.1.3:

$$f_1(0, y, 0, \dot{y}) = 0. \tag{4.1.5}$$

Note that the zero dynamics are a set of first-order equations, whereas they are a set of second-order equations in Case 4.1. If the zero dynamics are stable, then sliding mode is enforced in the manifold

$$s = f_1 + c_1 z + c_2 \dot{z} = 0.$$

After sliding mode starts,

$$f_1 = -c_1 z - c_2 \dot{z}, \tag{4.1.6}$$

and the equation for z in Equation 4.1.3 is of the form

$$\ddot{z} = -c_1 z - c_2 \dot{z}. \tag{4.1.7}$$

For positive scalar parameters c_1 and c_2, the solution to Equation 4.1.7 tends to zero, and then $y(t)$ as a solution to Equation 4.1.6 tends to zero as well. This stabilization method for systems with stable zero dynamics is applicable if

$$\operatorname{rank}\left(\frac{\partial f_1}{\partial \dot{y}} B_2 \right) \geq \dim(s) = \dim(z). \tag{4.1.8}$$

Then $\dot{s} = F(z, y, \dot{z}, \dot{y}) + \dfrac{\partial f_1}{\partial \dot{y}} B_2 u$ (F is a function independent of the control u), and, as shown in Section 3.2, sliding mode can be enforced. Generally speaking, this condition holds if $\dim(z) \leq \dim(y)$.

4.1.3. Case 4.3

We assume that function f_1 in Equation 4.1.3 does not depend on $\dot{y}$, i.e., $f_1 = f_1(z, y, \dot{z})$. If the condition in Equation 4.1.6 holds, then z and $\dot{z}$ tend to zero. After z decays, y is found from the algebraic equation $f_1(0,y,0) = 0$. Because the origin of the state space is the equilibrium point, $f_1(0,0,0) = 0$,

coordinate y tends to zero as well. To provide the condition in Equation 4.1.6, the switching manifold is selected as

$$s = \dot{s}_1 + \alpha s_1 = 0, \quad \alpha > 0,$$

with $s_1 = f_1 + c_1 z + c_2 \dot{z}$. The time derivative of s_1 and s are of form $\dot{s}_1 = \frac{\partial f_1}{\partial y}\dot{y} + F_1(z, y, \dot{z})$, where function $F_1(z, y, \dot{z})$ depends on neither $\dot{y}$ nor control, and $\dot{s} = F(z, y, \dot{z}, \dot{y}) + \frac{\partial f_1}{\partial y} B_2 u$, where function $F(z, y, \dot{z}, \dot{y})$ does not depend on control. As for Case 4.2, sliding mode can be enforced in the manifold $s = 0$ if the condition in Equation 4.1.8 holds. In sliding mode, $s_1(t)$ decays as a solution to the equation $\dot{s}_1 + \alpha s_1 = 0$. This means that the condition in Equation 4.1.6 holds, and $z(t), \dot{z}(t)$, and $y(t)$ tend to zero.

4.1.4. Case 4.4

Let us assume that the condition in Equation 4.1.8 holds and consider the special case of function f_1:

$$f_1 = f_{11}(y)\dot{y} + f_{12}(z, y, \dot{z}),$$

which is linear with respect to $\dot{y}$ and the zero dynamics governed by $f_{11}(y)\dot{y} + f_{12}(0, y, 0) = 0$ are unstable (otherwise the design method of Case 4.2 is applicable). Then the first equation of Equation 4.1.3 with respect to new variables,

$$z_1 = \dot{z} - g(y), \quad z_2 = z, \quad z_1, z_2 \in \Re^{n-m},$$

is transformed to

$$\begin{aligned} \dot{z}_1 &= f'_{12}(z_1, z_2, y) + f_{11}(y)\dot{y} - \frac{\partial g}{\partial y}\dot{y}, \\ \dot{z}_2 &= z_1 + g(y), \\ \frac{\partial g}{\partial y} &= \left\{ \frac{\partial g_i}{\partial y_j} \right\}, \quad \begin{matrix} i = 1, \ldots, n-m \\ j = 1, \ldots, m \end{matrix} \end{aligned} \tag{4.1.9}$$

$$f'_{12}(z_1, z_2, y) = f_{12}\big(z_2, y, z_1 + g(y)\big).$$

If the function $g(y)$ is a solution to the partial differential equation

$$\frac{\partial g}{\partial y} = f_{11}(y), \tag{4.1.10}$$

then the system in Equation 4.19 is reduced to

$$\dot{p} = F(p, y), \quad p = \begin{bmatrix} z_1 \\ z_2 \end{bmatrix}, \quad f = \begin{bmatrix} f'_{12}(z_1, z_2, y) \\ z_1 + g(y) \end{bmatrix}. \tag{4.1.11}$$

In the reduced order system in Equation 4.1.11, the state of the second block in Equation 4.1.3 y is handled as $(n - m)$-dimensional control. For instance, it may be selected

$$y = -s_0(p) \tag{4.1.12}$$

such that the system

$$\dot{p} = F\big(p, -s_0(p)\big)$$

is asymptotically stable. The relationship in Equation 4.1.12 is valid if sliding mode is enforced in the manifold

$$s = y + s_0(p) = 0.$$

Similar to Case 4.2, this can be done because Equation 4.1.8 holds by our assumption.

Remark 4.1

The design procedures for Cases 4.2 through 4.4 were developed under the assumption in Equation 4.1.8. If this condition does not hold, a multistep procedure may be applied similar to that described by Luk'yanov and Dodds [Luk'yanov 1993; Luk'yanov and Dodds 1996].

An example of a two-step design will be described in Section 5.6 for linear time-varying systems. Three nonlinear pendulum systems based on the above design procedures will be studied in the following section. The specific design procedures for selecting a sliding manifold and discontinuous control for a cart pendulum, a double-inverted pendulum, and a rotational inverted pendulum will be demonstrated. The theoretical studies will be complemented by simulation and experimental results.

4.2. Cart Pendulum

Figure 4.1 shows the physical model of a cart-pendulum system. M and m are masses of the cart and the inverted pendulum, respectively. l is the distance from the center of gravity of the link to its attachment point. The coordinate x

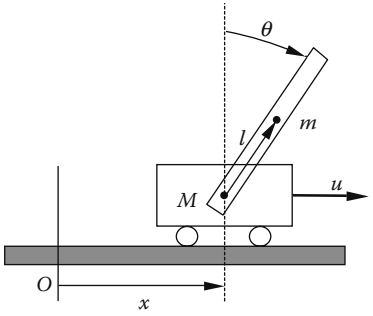

FIGURE 4.1
The cart-pendulum system.

represents the position of the cart on the horizontal axis to a fixed point, and θ is the rotational angle of the pendulum. Using the method of Lagrangian equations, one can easily show that the dynamic equations of the cart pendulum [Mori, Nishihara, and Furuta 1976] are

$$\begin{cases} (M+m)\ddot{x} + ml\ddot{\theta}\cos\theta - ml\dot{\theta}^2\sin\theta = u \\ \dfrac{4}{3}ml\ddot{\theta} + m\ddot{x}\cos\theta - mg\sin\theta = 0. \end{cases} \tag{4.2.1}$$

The goal of the control is to stabilize the system in a position in which the pendulum is in the unstable vertical position $\theta = 0$ and the cart is at a given point on the straight line $x = 0$ under the action of the control force u. It is assumed that the parameters and the state vector are available. For convenience of design, we first rewrite the given system in Equation 4.2.1 with respect to the second derivatives of the coordinates x and θ as

$$\begin{cases} \ddot{x} = \dfrac{1}{k}\left(-mg\cos\theta\sin\theta + \dfrac{4}{3}u^*\right) \\ \ddot{\theta} = \dfrac{1}{kl}\left((M+m)g\sin\theta - u^*\cos\theta\right), \end{cases} \tag{4.2.2}$$

where

$$k = \frac{4}{3}(M+m) - m\cos^2\theta > 0$$

and

$$u^* = u + ml\dot{\theta}^2\sin\theta. \tag{4.2.3}$$

The system in Equation 4.2.2 with scalar control u^* is in the form of Equation 4.1.2 with

$$\begin{bmatrix} \tilde{B}_1 \\ \tilde{B}_2 \end{bmatrix} = \begin{bmatrix} \dfrac{4}{3k} \\ -\dfrac{\cos(\theta)}{kl} \end{bmatrix}.$$

To reduce the system to the regular form of Equation 4.2.2, coordinate transformation

$$y = \phi(x, \theta)$$

should be found such that the second-order differential equation with respect to y does not depend on the control u^*. The solution to the problem is given in Section 3.2. According to Equations 3.2.5 and 3.2.8,

$$\begin{aligned} y &= \phi(x, \theta) \\ &= x - \varphi(\theta), \end{aligned} \tag{4.2.4}$$

where $\varphi(\theta)$ is a solution to the equation $\dfrac{d\varphi}{d\theta} = \dfrac{\tilde{B}_1}{\tilde{B}_2}$ or

$$\frac{d\varphi}{d\theta} = -\frac{4l}{3\cos(\theta)}.$$

The coordinate transformation in Equation 4.2.4 with the solution to this equation

$$\varphi(\theta) = -\frac{4}{3} l \ln \frac{1 + \tan(\theta/2)}{1 - \tan(\theta/2)}$$

results in

$$\dot{y} = \dot{x} + \frac{4}{3} l \frac{\dot{\theta}}{\cos\theta}$$

and

$$\ddot{y} = \ddot{x} + \frac{4}{3} l \frac{\ddot{\theta}}{\cos\theta} + \frac{4}{3} l \frac{\sin\theta \dot{\theta}^2}{\cos^2\theta}. \tag{4.2.5}$$

The regular form of the system obtained from Equations 4.2.2 and 4.2.5 is in the form

$$\begin{aligned} \ddot{y} &= G(\theta,\dot{\theta})\tan\theta \\ \ddot{\theta} &= v(\theta,u^*) \end{aligned}, \tag{4.2.6}$$

where

$$G(\theta,\dot{\theta}) = \frac{g}{k}\left(\left(\frac{4}{3}-\cos^2\theta\right)m+\frac{4}{3}M\right)+\frac{4}{3}l\frac{\dot{\theta}^2}{\cos\theta}$$

and

$$v(\theta,u^*) = \frac{1}{kl}\left((M+m)g\sin\theta - u^*\cos\theta\right). \tag{4.2.7}$$

Control of the nonlinear system (Equation 4.2.6) may be found as outlined below.

Step 1: Consider the first equation of the system in Equation 4.2.6. The function denoted as $G(\theta,\dot{\theta})$ is positive for any values of the arguments if $-\frac{\pi}{2} < \theta < \frac{\pi}{2}$. The function $\tan(\theta)$ is handled as control based on the choice proposed in Equation 4.1.6. For this intermediate control, select $\tan(\theta)$ as linear combination of y and $\dot{y}$,

$$\tan(\theta) = -\alpha_1 s_2 \quad \alpha_1 > 0, \quad s_2 = y + \dot{y}, \tag{4.2.8}$$

then, the upper equation of the system in Equation 4.2.6 is represented as

$$\begin{aligned} \dot{y} &= -y + s_2 \\ \dot{s}_2 &= -y - (\alpha_1 G(\theta,\dot{\theta}) - 1)s_2. \end{aligned}$$

The time derivative of the Lyapunov function candidate

$$V = \frac{1}{2}(y^2 + s_2^2),$$

with $V = 0$ at the origin $(y, s_2) = (0,0)$ is $\dot{V} = -y^2 - (\alpha_1 G - 1)s_2^2$. Because $G(\theta,\dot{\theta}) > 0$ for $-\frac{\pi}{2} < \theta < \frac{\pi}{2}$, we observe that $\dot{V} < 0$ for $\alpha_1 G > 1$, i.e., design parameter α_1 should be chosen such that $\alpha_1 > 1/G > 0$ for any t. Hence, the equilibrium point is asymptotically stable with $y \to 0$ and $s_2 \to 0$ as $t \to \infty$. Consequently, $(x, \theta) \to (0, 0)$ as $t \to \infty$, as follows from Equations 4.2.4 and 4.2.8.

To implement intermediate control (Equation 4.2.8), control u^* will be designed such that the function $s_1 = \tan\theta + \alpha_1(y + \dot{y}) \to 0$ as $t \to \infty$ then $\tan\theta \to -\alpha_1(y + \dot{y})$.

Step 2: The function s_1 tends to zero asymptotically, if it is a solution to differential equation

$$\dot{s}_1 = -\frac{\alpha}{\cos^2\theta} s_1$$

or

$$s(\theta, \dot{\theta}, y, \dot{y}) = (\cos^2\theta)\dot{s}_1 + \alpha s_1 = 0,$$

with $s_1 = \tan\theta + \alpha_1(y + \dot{y})$ and $\dot{s}_1 = \dfrac{1}{\cos^2\theta}\dot{\theta} + \alpha_1(\dot{y} + G\tan\theta)$.

Step 3: To assign the control law such that

$$s = \dot{\theta} + \alpha_1 \cos^2\theta(\dot{y} + G\tan\theta) + \alpha s_1 = 0,$$

calculate the time derivative of the function s along the solutions of Equation 4.2.6:

$$\dot{s} = \Psi(\theta, \dot{\theta})v + F(\theta, \dot{\theta}, \dot{y}), \tag{4.2.9}$$

where

$$\Psi(\theta, \dot{\theta}) = 1 + \frac{8}{3}\alpha_1 l(\sin\theta)\dot{\theta}$$

and

$$F(\theta, \dot{\theta}, y) = \alpha_1(\cos^2\theta)G\tan\theta + \alpha\dot{s}_1 + \alpha_1[G - 2(\cos\theta\sin\theta)\dot{y} - 2G\sin^2\theta]\dot{\theta}$$
$$+\alpha_1\cos\theta\sin\theta\left(\frac{2gm}{k}\cos\theta\sin\theta + \frac{4}{3}l\dot{\theta}^2\frac{\sin\theta}{\cos^2\theta}\right)\dot{\theta}.$$

The state reaches the surface $s = 0$ for any initial conditions, and sliding mode exists at any point of the surface if the deviation from the surface s and its time derivative have opposite signs. This condition is satisfied if

$$v = -v_o \text{sign}(s\Psi(\theta, \dot{\theta})) \tag{4.2.10}$$

where

$$v_o \geq \frac{1}{|\Psi|_{\min}}|F|_{\max}.$$

Finally, the real control is obtained from Equations 4.2.10, 4.2.7, and 4.2.3:

$$u = \frac{1}{\cos\theta}\left(\left((M+m)g\sin\theta - ml\cos\theta\sin\theta\dot{\theta}^2\right) + klv_o sign(s\Psi)\right).$$

It should be noticed that sliding mode may disappear, if $\Psi = 0$, because $\dot{s}$ in Equation 4.2.9 does not depend on control v for $\Psi = 0$. On one hand, the function Ψ is positive for the domain $\frac{8}{3}\alpha_1 l(\sin\theta)\dot{\theta} > -1$, including the origin. On the other hand, for the domain,

$$\frac{9}{64\alpha_1^2 l^2}\frac{\cos\theta}{\sin^2\theta} > (\sin\theta)v_o, \tag{4.2.10}$$

a system trajectory may intersect the surface $\Psi = 0$ once only. To derive this condition, calculate time derivative of the function Ψ on system trajectories for the points on the surface $\Psi = 0$:

$$\dot{\Psi} = \frac{8}{3}\alpha_1 l\left((\cos\theta)\dot{\theta}^2 + (\sin\theta)\ddot{\theta}\right) = \frac{8}{3}\alpha_1 l\left(\frac{9}{64\alpha_1^2 l^2}\frac{\cos\theta}{\sin^2\theta} - (\sin\theta)v_o sign(s\Psi)\right).$$

It is clear that $\dot{\Psi} > 0$ if the condition in Equation 4.2.10 holds, and it can be fulfilled by a proper choice of α_1 for the range

$$-\pi/2 < \theta < \pi/2.$$

4.3. Rotational Inverted Pendulum Model

A rotational inverted pendulum system as described by Widjaja [1994] is considered in this section. Figure 4.2 shows the plant consisting of a rotating base and a pendulum.

m_1 and J_1 are mass and inertia of the pendulum, l_1 is the distance from the center of gravity of the link to its pivot point, g is the gravity acceleration, and C_1 is the frictional constant between the pendulum and the rotating base. The coordinate θ_0 represents the rotational angle of the base with respect to some horizontal axis (usually defined as the starting position), and θ_1 is the rotational angle of the pendulum with respect to the vertical axis. $\theta_0 = 0$ refers to the unstable equilibrium point.

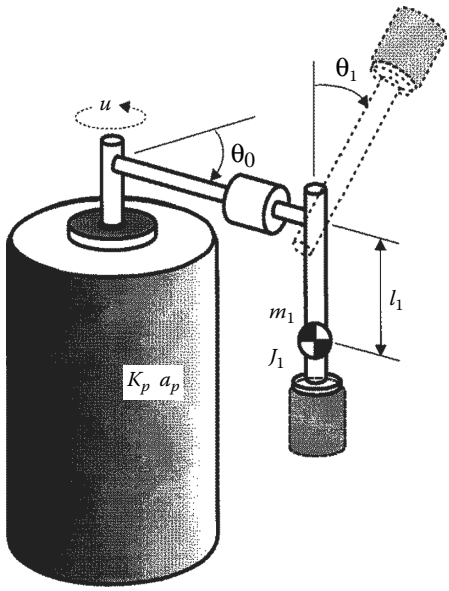

FIGURE 4.2
Inverted pendulum with rotating base.

The dynamic equations of the system are represented by

$$\begin{aligned}\ddot{\theta}_0 &= -a_p\dot{\theta}_o + K_p u \\ \ddot{\theta}_1 &= -\frac{C_1}{J_1}\dot{\theta}_1 + \frac{m_1 g l_1}{J_1}\sin\theta_1 + \frac{K_1}{J_1}\ddot{\theta}_0\end{aligned} \tag{4.3.1}$$

The upper equation is a simplified model of the permanent magnet DC motor used to drive the rotating base with constants a_p and K_p. The bottom equation of the system in Equation 4.3.1 is the dynamics of the pendulum. K_1 is a proportionality constant. The sign of K_1 depends on the position of the pendulum: $K_1 < 0$ inverted position and $K_1 > 0$ for noninverted position. The applied armature voltage u is the only control input of the system.

As addressed by Widjaja [1994], the inverted pendulum system includes several control problems: swing-up, balancing, and both swing-up and balancing. In this section, we will concentrate on a sliding mode controller for balancing the pendulum. The swing-up algorithm in the experiments will be directly taken from the work by Widjaja [1994]. First, we will try to stabilize the system such that the pendulum is in the unstable vertical position $\theta_1 = 0$ and allow the base to be at an arbitrary fixed position. Then, the design method will be generalized to drive both the pendulum and the rotating base to the equilibrium point $\theta_1 = \theta_0 = 0$ and maintain it there.

4.4. Rotational Inverted Pendulum

4.4.1. Control of the Inverted Pendulum

Notice, first, that in the system in Equation 4.3.1 rewritten in the form

$$\begin{aligned}\ddot{\theta}_0 &= -a_p\dot{\theta}_o + K_p u \\ \ddot{\theta}_1 &= -\frac{C_1}{J_1}\dot{\theta}_1 + \frac{m_1 g l_1}{J_1}\sin\theta_1 - \frac{K_1}{J_1}a_p + \frac{K_1}{J_1}K_p u,\end{aligned} \tag{4.4.1}$$

the control u is multiplied by constant coefficients. Because $B(x)$ in this case is a constant matrix, a linear transformation needed to reduce the system into the regular form can easily be found:

$$y = \theta_o - \frac{J_1}{K_1}\theta_1. \tag{4.4.2}$$

Differentiating Equation 4.4.2 results in

$$\dot{y} = \dot{\theta}_o - \frac{J_1}{K_1}\dot{\theta}_1, \tag{4.4.3}$$

and the motion equations are the regular form

$$\begin{aligned}\ddot{y} &= \frac{C_1}{K_1}\dot{\theta}_1 - \frac{m_1 g l_1}{K_1}\sin\theta_1 \\ \ddot{\theta}_1 &= -\frac{a_p K_1}{J_1}\dot{y} - \left(\frac{C_1}{J_1} + a_p\right)\dot{\theta}_1 + \frac{m_1 g l_1}{J_1}\sin\theta_1 + \frac{K_1 K_p}{J_1}u.\end{aligned} \tag{4.4.4}$$

Let us first consider the lower subsystem of the regular form in Equation 4.4.4 and try to stabilize the system with respect to $\theta_1 = 0$. If the discontinuous control $u = -M\,\mathrm{sign}(s)$ is applied with $s = \dot{\theta}_1 + \alpha\theta_1$; $\alpha > 0$, both $\dot{\theta}_1 \to 0$ and $\theta_1 \to 0$ as $t \to \infty$ after sliding mode is enforced in the plane $s = 0$. However, the zero dynamics of the pendulum from the upper equation of Equation 4.4.4 are governed by $\ddot{y} = 0$; hence, $y \to \infty$ as $t \to \infty$, and the system is unstable. Therefore, the conventional design approach (Case 4.1 in Section 4.1) does not work for the pendulum system if the control should stabilize the inverted pendulum in the unstable vertical position with an arbitrary fixed position of the rotating base, $\theta_0 = const$.

Now we design a sliding mode controller for the pendulum system based on the procedure of Case 4.2 in Section 4.1. Consider the upper equation of

the system in Equation 4.4.4. According to Equation 4.1.6, the sliding manifold should be selected as

$$\frac{C_1}{J_1}\dot{\theta}_1 - \frac{m_1 g l_1}{J_1}\sin\theta_1 = -\alpha_1(y + \dot{y}).$$

Hence, the upper subsystem is stable,

$$\ddot{y} = -\alpha_1(y + \dot{y}),$$

for a positive constant α_1. Both $y \to 0$ and $\dot{y} \to 0$ as $t \to \infty$, but, as follows from the upper equation of Equation 4.4.4, the zero dynamics of the reduced order system,

$$\dot{\theta}_1 = \frac{m_1 g l_1}{C_1}\sin\theta_1, \qquad \frac{m_1 g l_1}{C_1} > 0,$$

are unstable. Case 4.2 in Section 4.1 is not applicable and does not work. We now combine the ideas of Cases 4.3 and 4.4 to stabilize the pendulum.

Step 1: Following the approach of Case 4.4, introduce a new variable,

$$x = \dot{y} - \frac{C_1}{K_1}\theta_1, \tag{4.4.5}$$

such that the right-hand side of the upper block in the motion equations would not depend on the time derivative of the state variable of the botton block. Because $\dot{x} = \ddot{y} - \dfrac{C_1}{K_1}\dot{\theta}_1$, substitution of $\ddot{y}$ from the system in Equation 4.4.4 yields

$$\begin{aligned}
\dot{x} &= -\frac{m_1 g l_1}{K_1}\sin\theta_1 \\
\ddot{\theta}_1 &= -\frac{a_p K_1}{J_1}x - \frac{a_p C_1}{J_1}\theta_1 - \left(\frac{C_1}{J_1} + a_p\right)\dot{\theta}_1 + \frac{m_1 g l_1}{J_1}\sin\theta_1 + \frac{K_1 K_p}{J_1}u.
\end{aligned} \tag{4.4.6}$$

The right-hand side of the upper equation in the system in Equation 4.4.6 does not depend on $\dot{\theta}_1$. Then, following the approach of Case 4.3, select the control such that the condition

$$\frac{m_1 g l_1}{K_1}\sin\theta_1 = \alpha_1 x \tag{4.4.7}$$

holds. The reduced order system becomes

$$\dot{x} = -\alpha_1 x,$$

with $x \to 0$ as $t \to \infty$ for positive constant α_1. In addition, because x decay exponentially, we can conclude from Equations 4.4.7, 4.4.5, and 4.4.3 that functions θ_1, $\dot{y}$, $\dot{\theta}_1$, and $\dot{\theta}_o$ all decay exponentially as well. As a result, the desired system dynamics with $(\dot{\theta}_o, \theta_1) \to (0,0)$ as $t \to \infty$ are obtained, and the rotating base remains at a fixed position ($\theta_0 = const.$).

Step 2: The condition in Equation 4.4.7 holds if the function

$$s_1 = \frac{m_1 g l_1}{K_1} \sin\theta_1 - \alpha_1 x = 0. \tag{4.4.8}$$

The derivative of s_1 does not depend on the control u,

$$\dot{s}_1 = \frac{m_1 g l_1}{K_1} \cos\theta_1 \dot{\theta}_1 + \alpha_1 \frac{m_1 g l_1}{K_1} \sin\theta_1,$$

but decays to zero if

$$\dot{s}_1 = -\alpha\, s_1$$

or

$$\frac{m_1 g l_1}{K_1} \cos\theta_1 \dot{\theta}_1 + \alpha_1 \frac{m_1 g l_1}{K_1} \sin\theta_1 = -\alpha s_1; \quad \alpha > 0.$$

Step 3: This condition is satisfied if sliding mode is enforced in the surface

$$s = \dot{s}_1 + \alpha s_1 = \frac{m_1 g l_1}{K_1} \cos\theta_1 \dot{\theta}_1 + \alpha_1 \frac{m_1 g l_1}{K_1} \sin\theta_1 + \alpha s_1 = 0. \tag{4.4.9}$$

Sliding mode exists if the functions s and $\dot{s}$ have opposite signs. Because only the derivative of $\dot{\theta}_1$ depends on the control force u, the function $\dot{s}$ may be represented in the form

$$\dot{s} = \frac{m_1 g l_1}{K_1} \cos\theta_1 \ddot{\theta}_1 + \psi_1(x, \theta_1, \dot{\theta}_1) = \frac{K_p m_1 g l_1}{J_1} \cos\theta_1 u + \tilde{\psi}_1(x, \theta_1, \dot{\theta}_1),$$

where Ψ_1 and $\tilde{\psi}_1$ are functions of the system states. Notice that the function $\cos\theta_1$ is positive for the pendulum angle $-\pi/2 < \theta_1 < \pi/2$. The condition for existence of the sliding mode is satisfied if

$$u = -u_o \,\mathrm{sign}(s), \tag{4.4.10}$$

where

$$u_o \geq \frac{J_1}{K_p m_1 g l_1 \cos\theta_1} |\psi_1'|_{\max}.$$

Once the state trajectories of sliding mode are confined to the switching manifold $s = 0$ after a finite time interval $s_1 \to 0$ and $x \to 0$ as $t \to \infty$. The desired dynamic behavior with $\theta_0 \to const$ and $\theta_1 \to 0$ as $t \to \infty$ is guaranteed.

4.4.2. Control of the Base Angle and Inverted Pendulum

We have just shown that the system can be stabilized with respect to $\theta_1 = 0$ and $\dot{\theta}_0 = 0$ by introducing a new variable of x. Design of the control system for stabilizing both the pendulum and the rotating base at the equilibrium point $(\theta_0, \theta_1) = (0,0)$ is performed as follows.

Step 1: The first equation of Equations 4.4.6 and 4.4.5 constitute the system similar to Equation 4.1.11 in the design method of Case 4.4:

$$\begin{aligned} \dot{x} &= -\frac{m_1 g l_1}{K_1} \sin\theta_1 \\ \dot{y} &= x + \frac{C_1}{K_1}\theta_1. \end{aligned} \tag{4.4.11}$$

The state component θ_1 in the system in Equation 4.4.11 is handled as control. If the last term of the upper equation satisfies

$$\sin\theta_1 = -\lambda_1(x + y), \tag{4.4.12}$$

with constant λ_1, then the system is equivalent to

$$\begin{aligned} \dot{x} &= -a_1\lambda_1(x + y) \\ \dot{y} &= x + a_2\lambda_1 h(\theta_1)(x + y), \end{aligned} \tag{4.4.13}$$

where constants a_1 and a_2 for the interval pendulum angle $-\pi/2 < \theta_1 < \pi/2$ are positive because they are defined as

$$\alpha_1 = -\frac{m_1 g l_1}{K_1} > 0, \qquad \alpha_2 = -\frac{C_1}{K_1} > 0; \quad K_1 < 0. \tag{4.4.14}$$

h is a function of the pendulum angle θ_1, $h(\theta_1) = \theta_1/\sin\theta_1$. Stability of the system in Equation 4.4.13 is analyzed using the Lyapunov function candidate

$$V = \frac{1}{2}(x + y)^2 + \frac{1}{2}x^2,$$

with the time derivative along the solutions of the system in Equation 4.4.13:

$$\dot{V} = (x+y)(\dot{x}+\dot{y}) + x\dot{x} - \left(a_1 - a_2 h(\theta_1)\right)\lambda_1 (x+y)^2 + x(x+y) - a_1\lambda_1 x(x+y).$$

The function $\dot{V}(t)$ is negative semidefinite,

$$\dot{V} = -\left(a_1 - a_2 h(\theta_1)\right)\lambda_1 (x+y)^2 \le 0,$$

if

$$\lambda_1 = \frac{1}{a_1} > 0$$

and the coefficient

$$\left(a_1 - a_2 h(\theta_1)\right) > 0. \tag{4.4.15}$$

The function $h(\theta_1)$ satisfies the inequalities

$$1 \le h(\theta_1) < \pi/2, \tag{4.4.16}$$

for pendulum angle $-\pi/2 < \theta_1 < \pi/2$. Combining the inequalities in Equations 4.4.15 and 4.4.16 and substituting a_1 and a_2 from Equation 4.4.14, one obtains a sufficient condition for the pendulum system to be stable as

$$\frac{m_1 g l_1}{C_1} > \pi/2.$$

From a practical point of view, because the inverted pendulum is designed to rotate freely around its pivot, the frictional constant C_1 is much less than the torque ($m_1 g l_1$) of the pendulum itself. Therefore, the condition in Equation 4.4.15 holds for a real pendulum system. Moreover, if $\dot{V} = 0$ or $x + y = 0$, it follows from Equation 4.4.13 that x is a constant value but $y \to \infty$ as $t \to \infty$ if this constant value is different from zero. Therefore, the system in Equation 4.4.13 can maintain the $\dot{V} = 0$ condition only at the equilibrium point $(x,y) = (0,0)$. It is shown that the equilibrium point is asymptotically stable in the large with $x \to 0$ and $y \to 0$ as $t \to \infty$. Consequently, as follows from Equations 4.4.12 and 4.4.2, $(\theta_0,\theta_1) \to (0,0)$ as $t \to \infty$, which is control objective.

Step 2: Following the same procedure as described in the previous case, Equation 4.4.12 holds if the function

$$s_1 = \sin\theta_1 + \lambda_1(x + y) = 0.$$

The function s_1 satisfies the linear first-order differential equation

$$\dot{s}_1 = -\lambda s_1, \quad \lambda > 0,$$

if

$$\cos\theta_1\dot{\theta}_1 + \lambda_1(\dot{x} + \dot{y}) = -\lambda s_1, \tag{4.4.17}$$

because, in this case,

$$\dot{s}_1 = \cos\theta_1\dot{\theta}_1 + \lambda_1(\dot{x} + \dot{y}).$$

Step 3: To satisfy Equation 4.4.17, sliding mode should be enforced in the switching surface

$$s = \dot{s}_1 + \lambda s_1 = \cos\theta_1\dot{\theta}_1 + \lambda_1(\dot{x} + \dot{y}) + \lambda s_1 = 0.$$

The time derivative of the function s is of the form

$$\dot{s} = \cos\theta_1\ddot{\theta}_1 + \psi_2(x, y, \theta_1, \dot{\theta}_1) = \frac{K_1K_p}{J_1}\cos\theta_1 u + \tilde{\psi}_2(x, y, \theta_1, \dot{\theta}_1),$$

where Ψ_2 and $\tilde{\Psi}_2$ are functions of the system states. The function $\cos\theta_1$ is positive, and parameter K_1 is negative for the pendulum angle $-\pi/2 < \theta_1 < \pi/2$. The condition for existence of sliding mode (the functions s and $\dot{s}$ need to have opposite signs) is satisfied if

$$u = u_o \,\text{sign}(s) \;\text{ with }\quad u_o \geq \frac{-J_1}{K_1K_p\cos\theta_1}\left|\tilde{\psi}_2\right|_{\max}.$$

After sliding mode occurs on the surface $s = 0$, $s_1 \to 0$ and $(x,y) \to (0,0)$ as $t \to \infty$. Finally, the desired dynamic behavior, $(\theta_0,\theta_1) \to (0,0)$ as $t \to \infty$ is obtained.

4.5. Simulation and Experiment Results for Rotational Inverted Pendulum

Both simulation and experimental results for stabilizing the rotational inverted pendulum system will be presented in this section. Special emphasis will be placed on robustness by investigating the ability of the sliding mode controllers for significant plant parameter variations.

The experimental setup was developed, and it is currently available for both undergraduate and graduate control system laboratories at The Ohio State University.

Figure 4.3 describes the complete hardware setup configuration of the inverted pendulum system. The real-time control system mainly consists of three parts: the controller, interface circuits, and the pendulum system. Two optical encoders are used to measure the angular positions of both the pendulum and the base. All parameters of the inverted pendulum system are listed in Table 4.1, and they are determined experimentally by identification techniques [for more details, see Widjaja 1994].

The inverted pendulum system allows the user to change the system parameters or add disturbances by attaching containers of various size and contents to the end of the pendulum. A container of metal bolts and water will later be added to the pendulum in the set of experiments. The mass of the container and its contents significantly change the system parameters, whereas the motion of the water within the container acts as a disturbance to the system.

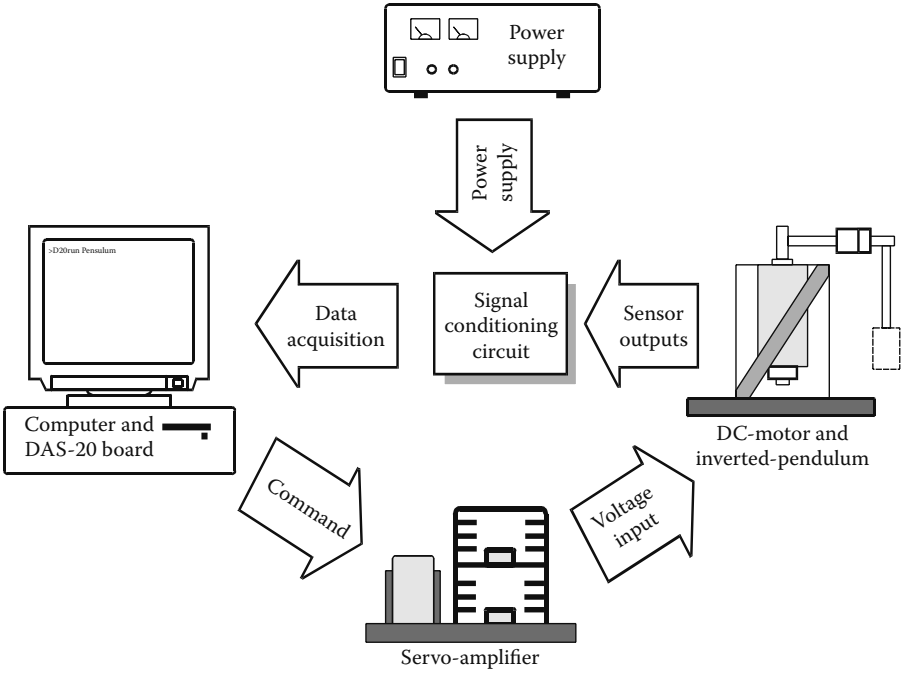

FIGURE 4.3
Hardware setup configuration of the pendulum system.

TABLE 4.1

Parameters of the Rotational Inverted Pendulum System

Parameters/Values	Parameters/Values
$l_1 = 0.113\ m$	$m_1 = 8.6184 \times 10^{-2}\ kg$
$g = 9.8066\ m/s^2$	$J_1 = 1.301 \times 10^{-3}\ N \cdot m \cdot s^2$
$a_p = 33.04$	$C_1 = 2.979 \times 10^{-3}\ N \cdot m \cdot s/rad$
$K_p = 74.89$	$K_1 = \begin{cases} -1.9 \times 10^{-3}, & \text{if } -\pi/2 < \theta_1 < \pi/2 \\ 1.9 \times 10^{-3}, & \text{otherwise} \end{cases}$

Figure 4.4 shows the simulation results for stabilizing both the pendulum and the rotating base using the LQR technique with $u = 0.7\theta_o + 1.0\dot{\theta}_o + 10.8\theta_1 + 0.7\dot{\theta}_1$. The pendulum is first swung up with the

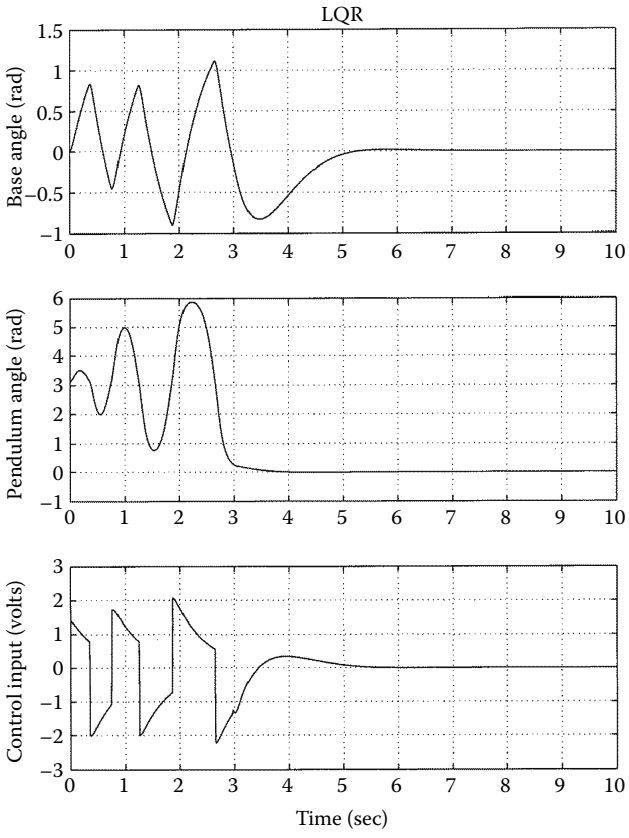

FIGURE 4.4
Simulation results by LQR.

swing-up algorithm, and then the LQR begins to take over the control when the rotational angle of the pendulum is within the range of $|\theta_1| \leq 0.3rad$. The experimental results for nominal conditions by using the LQR has been provided previously [Widjaja 1994; Ordonez, Zumberge, Spooner, and Passino 1997].

We will focus on the performance of the inverted pendulum system using our previously developed sliding mode controllers. Two case studies of the control objectives will be presented: stabilizing the pendulum at $\theta_1 = 0$ with $\dot{\theta}_o = 0$, and stabilizing both the pendulum and the rotating base with respect to the equilibrium point $\theta_1 = \theta_o = 0$.

4.5.1. Stabilization of the Inverted Pendulum

The simulation results using the control laws developed in this section are shown in Figure 4.5. The required information for calculating the control

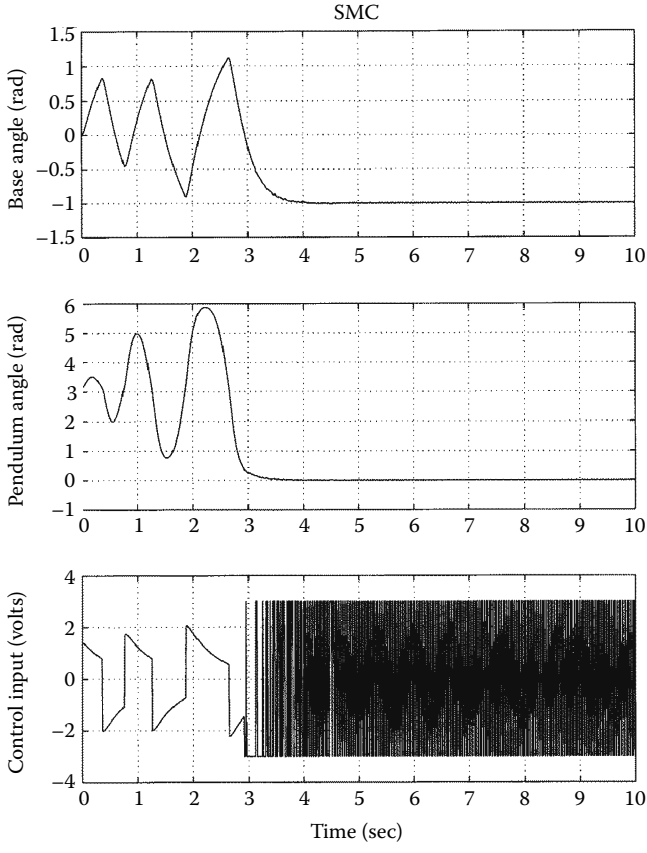

FIGURE 4.5
Simulation results by SMC for stabilizing the pendulum.

input is Equations 4.4.2, 4.4.5, 4.4.8, 4.4.9, and 4.4.10. As can be seen, the pendulum angle is driven to zero, and the rotating base at the same time remains at a fixed position (its angular velocity equals to zero) with the selected input gains $\lambda_1 = 0.08$, $\lambda = 100$, and $u_0 = 3$.

The discontinuous controller was implemented for real-time control of the pendulum. We observed that, as a result of the sampling issue of the discrete-time control system, in practice, the ideal sliding mode control cannot be implemented. Besides, as presented in many publications [Utkin 1978; Kwatny and Siu 1987; Bartolini 1989], the chattering that appears as a high-frequency oscillation at the vicinity of the desired manifold may be excited by unmodeled high-frequency dynamics of the system. To suppress the chattering, the saturating continuous approximation [Slotine and Sastry 1983; Burton and Zinober 1986] (see also Chapters 8 and 9) will be used to replace the ideal switching at the vicinity of the switching manifold. This results in a tradeoff between accuracy and robustness.

Figures 4.6 through 4.8 show the experimental results of the SMC for stabilizing the pendulum with different loads attached to the end of the pendulum. The sampling time for the control system is $\Delta t = 5ms$, and it is fixed for other experimental results in the later figures. The control law using a continuous approximation by a sinusoidal function is designed as

$$u = \begin{cases} u_o \sin\left(\dfrac{\pi}{2\delta} s\right), & \text{if } |s| \le \delta \\ u_o \text{sign}(s), & \text{otherwise} \end{cases}, \tag{4.5.1}$$

where δ is the allowable maximum width of the continuous zone from the desired ideal sliding manifold $s = 0$. It can be easily shown that the ideal discontinuous control is implemented if $\delta = 0$. The larger the value of δ, the less invariance to system uncertainties is anticipated, although the less chattering in the system states is accomplished. The input gains of the SMC pendulum system are selected as $\lambda_1 = 0.08$, $\lambda = 400$, $u_0 = 2.5$.

As can be seen in Figure 4.6 for the nominal plant, the pendulum angle is stabilized close to zero. The control force input, as we expected, swings up the pendulum from the beginning, switches to the SMC at time around 1.5 sec, and then stays in the δ zone $|u| < u_0 = 2.5$ after 2 sec. It should be noted that the system is stabilized at the point $(\dot{\theta}_o, \theta_1) = (0, 0)$ and it is marginally stable with respect to $(\dot{\theta}_o, \theta_1)$. It explains why the position of the rotating base is slowly drifting (θ_o is not constant). Similar results were obtained when the same controller is used to drive the pendulum with both the water (Figure 4.7) and the metal bolts (Figure 4.8). We observe that the controller can still manage the balance of the inverted pendulum quite well without saturation of the control input. The interesting differences include the following: small ripples are generated as a result of the distributed disturbance from the water in Figure 4.7, the average values of the control input in both cases gradually converge to zero when disturbances get settled at the final time

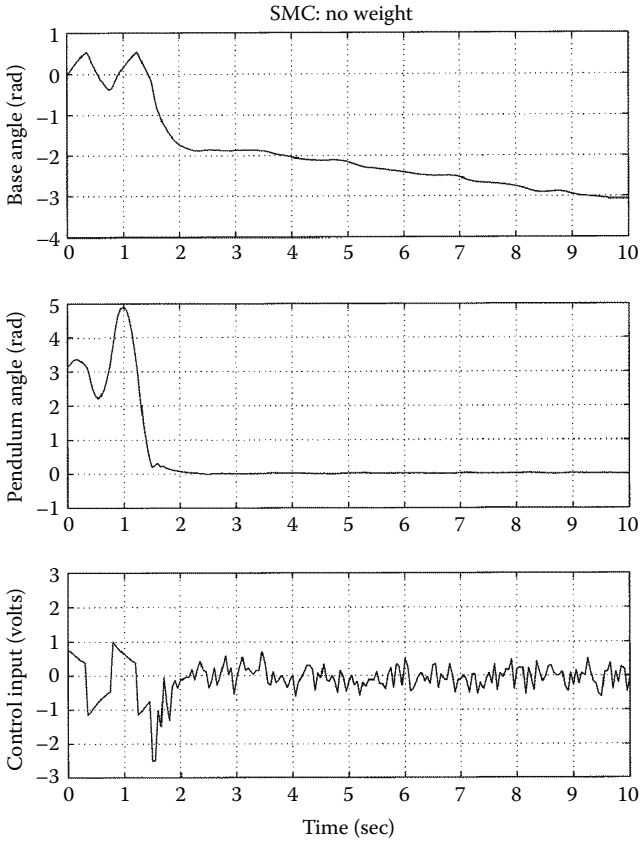

FIGURE 4.6
Experimental results by SMC: no weight.

10 sec, and a smaller amplitude of the control input is observed at the steady state when additional weight, the metal bolts, are added to the system as shown in Figure 4.8.

4.5.2. Stabilization of the Inverted Pendulum and the Base

The sliding mode control for stabilizing both the pendulum and the base will be designed following Equations 4.4.2, 4.4.3, 4.4.5, and 4.4.8 through 4.4.10. The simulation results for control (Equation 4.4.10) with the gains $\lambda_1 = 0.08$, $\lambda = 800$, and $u_0 = 3$ are shown in Figure 4.9.

Figure 4.10 shows the experimental results of the SMC for the nominal pendulum using the modified controller in Equation 4.5.1 with $\lambda_1 = 0.08$, $\lambda = 800$, and $u_0 = 2.5$. For a small value of δ, we observe that the control input

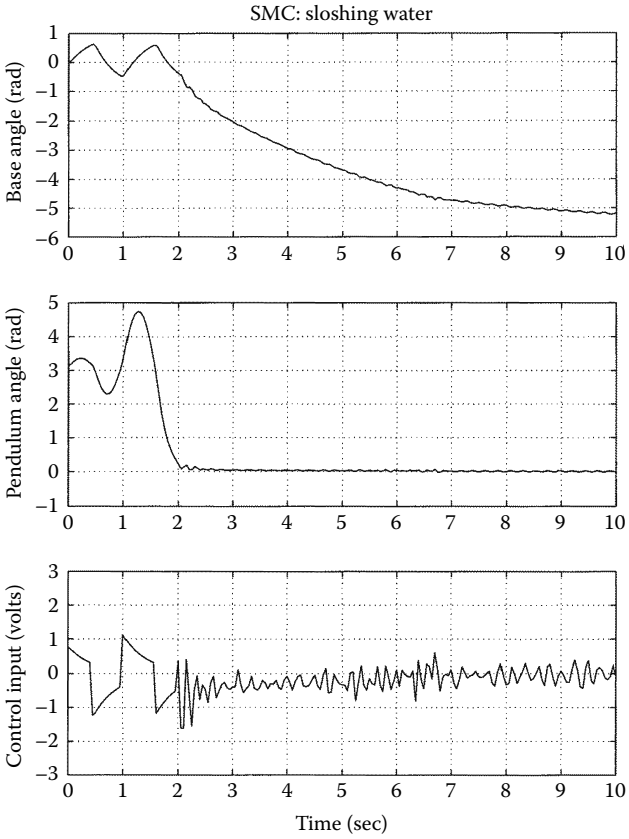

FIGURE 4.7
Experimental results by SMC: sloshing water.

is still similar to the discontinuous control in Figure 4.5, although its switching frequency is considerably reduced. As a result, chattering exists in both of the state responses. The results for a larger value of δ are shown in Figure 4.11. The control input is no longer saturated and varies between the extreme values $\pm$ 2.5.

The most interesting experimental results are depicted in Figures 4.12 and 4.13. The controller is able to provide convergence of the pendulum with both metal bolts and sloshing water using the same gains for the control input. The system states are stabilized at the vicinity of the equilibrium point (θ_0,θ_1) = (0,0). The low-amplitude oscillations similar to Figure 4.7 under the effect of sloshing water dynamics is still observed in Figure 4.12, where the control input has an average value close to zero. We observe an underdamped system response in Figure 4.12 for the pendulum with metal bolts. The control

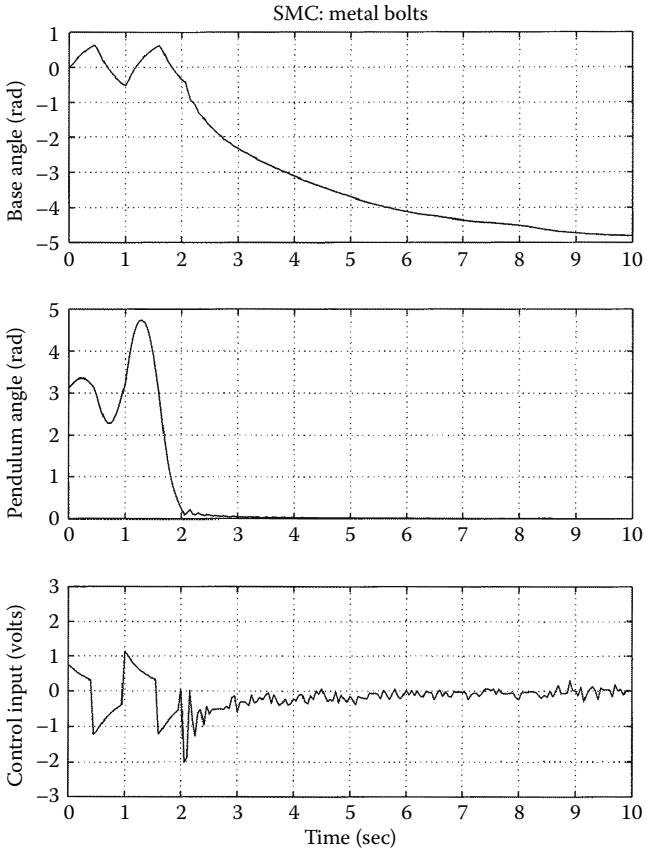

FIGURE 4.8
Experimental results by SMC: metal bolts.

input oscillations are relatively large at the beginning of the process compared with Figure 4.8, but then they decrease to the same level after a couple of seconds when both the pendulum and the rotating base get settled.

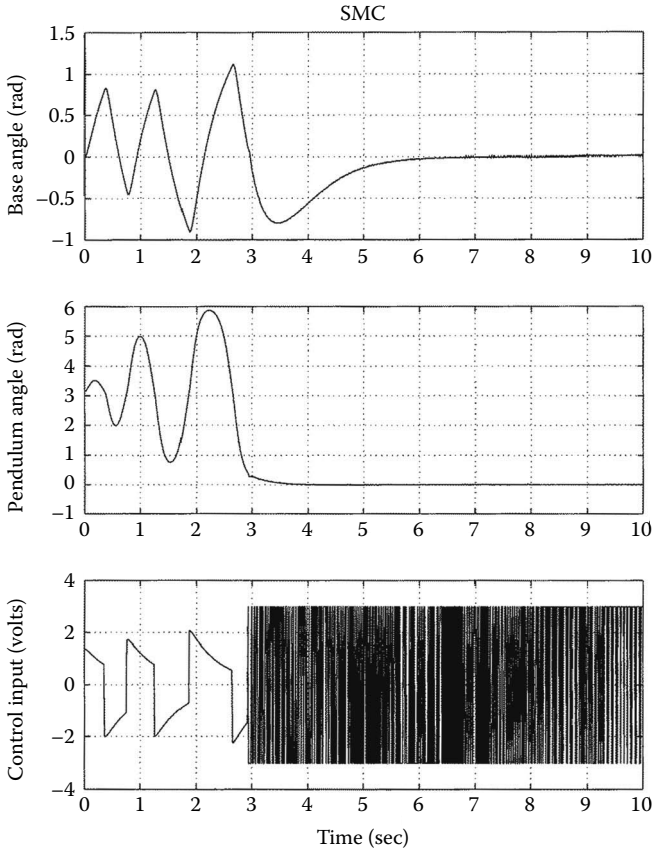

FIGURE 4.9
Simulation results by SMC for stabilizing both the pendulum and the base.

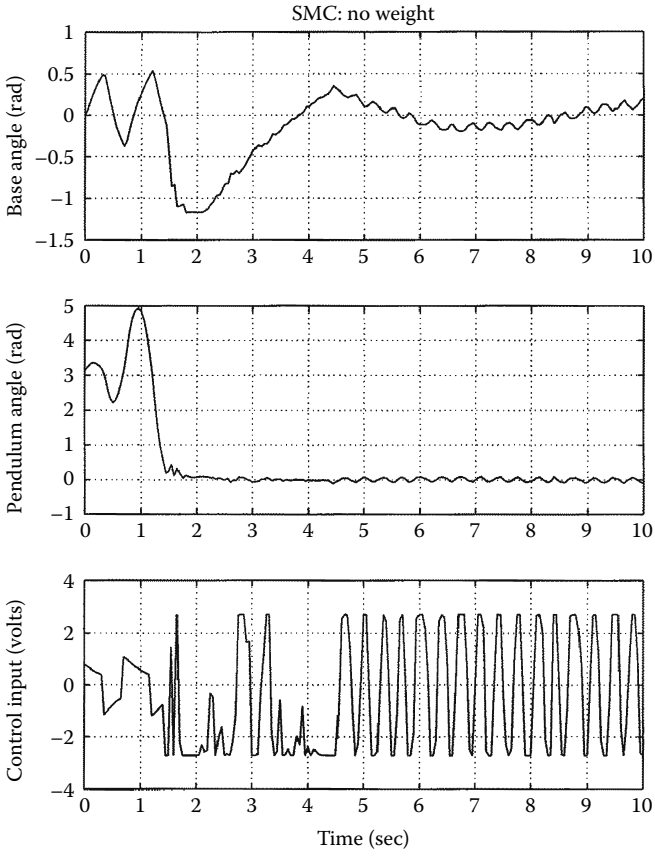

FIGURE 4.10
Experimental results by SMC: no weight.

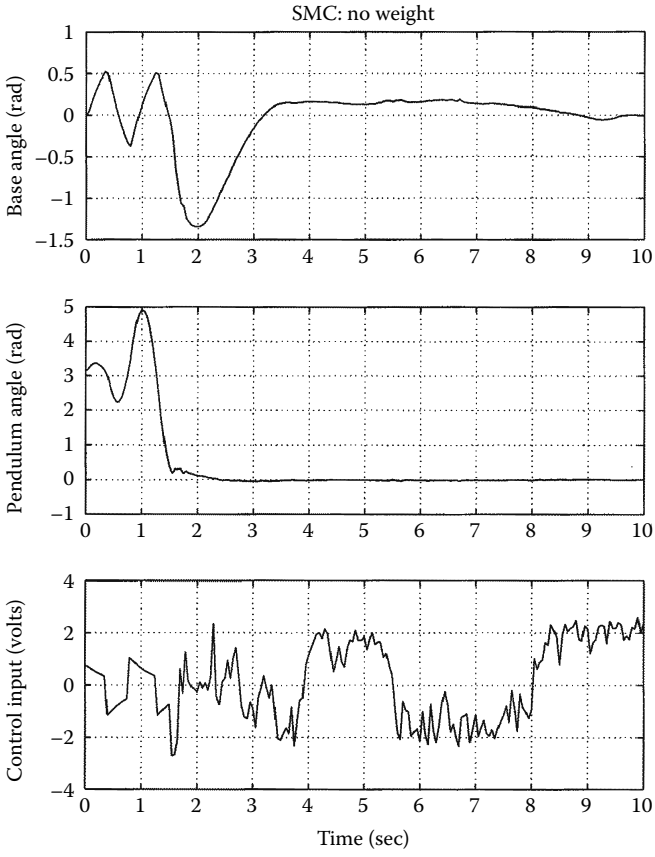

FIGURE 4.11
Experimental results by SMC: no weight.

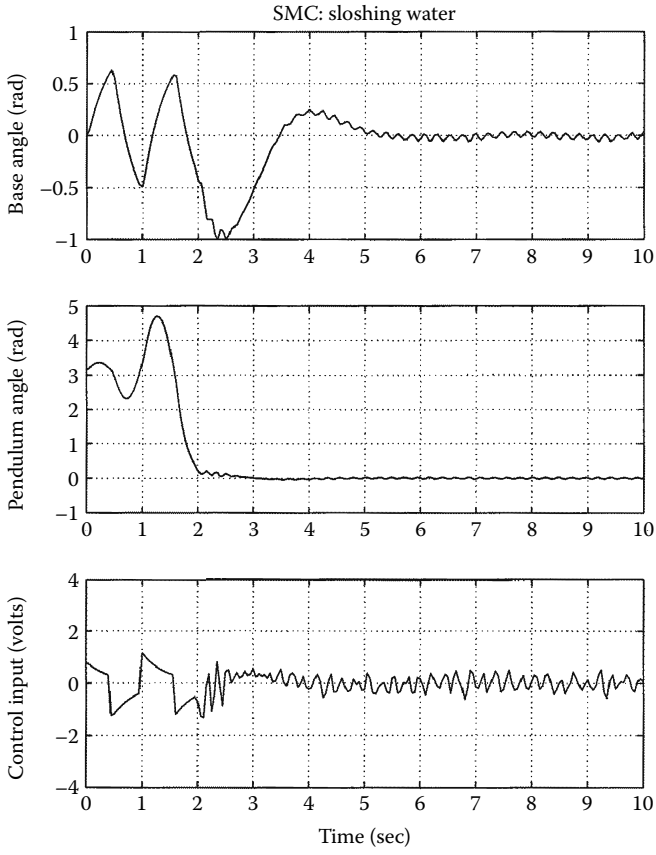

FIGURE 4.12
Experimental results by SMC: sloshing water.

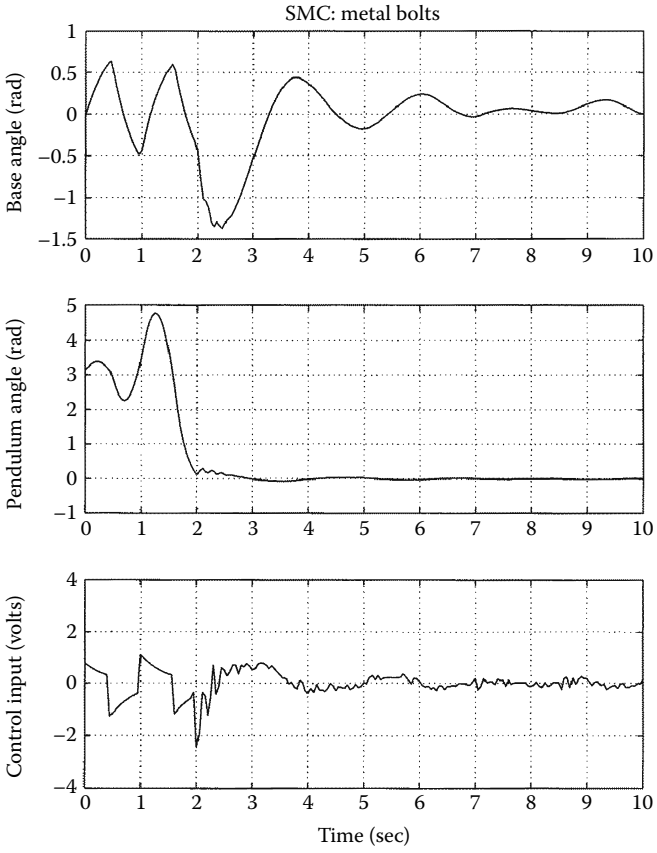

FIGURE 4.13
Experimental results by SMC: metal bolts.

References

Bartolini G. 1989. "Chattering Phenomena in Discontinuous Control Systems." *Int J Syst Sci* 20:2471–2481.

Burton JA, Zinober ASI. 1986. "Continuous Approximation of Variable Structure Control." *Int J Syst Sci* 17:875–885.

Kwatny HG, Siu TL. 1987. "Chattering in Variable Structure Feedback Systems." Proceedings of the International Federation of Automatic Control 10th World Congress, Tokyo, Japan.

Ledgerwood T, Misawa E. 1992. "Controllability and Nonlinear Control of Rotational Inverted Pendulum," in *Advances in Robust and Nonlinear Control Systems*, edited by E. Misawa. *ASME J Dyn Syst Control* 43:81–88.

Luk'yanov AG. 1993. "Optimal Nonlinear Block-Control Method." Proceedings of the Second European Control Conference, Groningen, The Netherlands.

Luk'yanov AG, Dodds SJ. 1996. "Sliding Mode Block Control of Uncertain Nonlinear Plants." Proceedings of the International Federation of Automatic Control World Congress, San Franciso, CA.

Mori S, Nishihara H, Furuta K. 1976. "Control of Unstable Mechanical System: Control of Pendulum." *Int J Control* 23:673–692.

Ordonez R, Zumberge J, Spooner JT, Passino KM. 1997. "Adaptive Fuzzy Control: Experiments and Comparative Analyses." *IEEE Trans Fuzzy Syst* 5:167–188.

Slotine JJ, Sastry SS. 1983. "Tracking Control of Nonlinear Systems Using Sliding Surfaces, with Application to Robot Manipulators." *Int J Control* 38:465–492.

Utkin VI. 1992. *Sliding Modes in Control and Optimization*. London: Springer-Verlag.

Widjaja M. 1994. *Intelligent Control for Swing Up and Balancing of an Inverted Pendulum System*. Master's thesis, The Ohio State University, Columbus, OH.

5

Control of Linear Systems

The objective of this chapter is to demonstrate the sliding mode control design methodology for linear systems. Reducing system equations to the regular form will be performed as a preliminary step in all design procedures. The core idea is to use the methods of linear control theory for reduced-order equations and to use different methods of enforcing sliding modes with the desired dynamics.

5.1. Eigenvalue Placement

We start with the conventional problem of linear control theory: eigenvalue placement in a linear time invariant multidimensional system

$$\dot{x} = Ax + Bu, \tag{5.1.1}$$

where x and u are n- and m-dimensional state and control vectors, respectively, A and B are constant matrices, rank(B) = m. The system is assumed to be controllable.

For any controllable system, there exists a linear feedback $u = Fx$ (F being a constant matrix) such that the eigenvalues of the feedback system, i.e., of matrix $A + BF$, take the desired values, and, as a result, the system exhibits desired dynamic properties [Kwakernaak and Sivan 1972].

Now we will show that the eigenvalue task may be solved in the framework of sliding mode control technique dealing with a reduced order system. As demonstrated in Section 3.2, the design becomes simpler for systems represented in regular form. Because rank(B) = m, matrix B in Equation 5.1.1 may be partitioned (after reordering the state vector components) as

$$B = \begin{bmatrix} B_1 \\ B_2 \end{bmatrix}, \tag{5.1.2}$$

where $B_1 \in \Re^{(n-m)\times m}$, $B_2 \in \Re^{m\times m}$ with $\det B_2 \neq 0$. The nonsingular coordinate transformation

$$\begin{bmatrix} x_1 \\ x_2 \end{bmatrix} = Tx, \quad T = \begin{bmatrix} I_{n-m} & -B_1 B_2^{-1} \\ 0 & B_2^{-1} \end{bmatrix} \tag{5.1.3}$$

reduces the system Equations 5.1.1 and 5.1.2 to regular form

$$\begin{aligned}\dot{x}_1 &= A_{11}x_1 + A_{12}x_2\\ \dot{x}_2 &= A_{21}x_1 + A_{22}x_2 + u,\end{aligned} \tag{5.1.4}$$

where $x_1 \in \Re^{(n-m)}$, $x_2 \in \Re^m$, and A_{ij} are constant matrices for $i, j = 1, 2$. It follows from controllability of (A, B) that the pair (A_{11}, A_{12}) is controllable as well [Utkin and Young 1978]. Handling x_2 as an m-dimensional intermediate control in the controllable $(n - m)$-dimensional first subsystem of Equation 5.1.4, all $(n - m)$ eigenvalues may be assigned arbitrarily by a proper choice of matrix C in

$$x_2 = -Cx_1.$$

To provide the desired dependence between components x_1 and x_2 of the state vector, sliding mode should be enforced in the manifold

$$s = x_2 + Cx_1 = 0, \tag{5.1.5}$$

where $s^T = (s_1,\ldots,s_m)$ is the difference between the desired and real values of x_2.

After sliding mode starts, the motion is governed by a reduced order system with the desired eigenvalues

$$\dot{x}_1 = (A_{11}x_1 - A_{12}C)x_1 \tag{5.1.6}$$

For a piecewise linear discontinuous control

$$u = -(\alpha(|x| + \delta)\text{sign}(s), \tag{5.1.7}$$

with $|x| = \sum_{i=1}^{n} |x_i|$, $\text{sign}(s)^T = [\text{sign}(s_1) \ldots \text{sign}(s_m)]$, whereas α and δ are constant positive values, calculate the time derivative of positive definite function $V = \frac{1}{2}s^T s$

$$\begin{aligned}\dot{V} &= s^T\left((CA_{11} + A_{21})x_1 + (CA_{12} + A_{22})x_2\right) - (\alpha|x| + \delta)|s|\\ &\le |s|\left|(CA_{11} + A_{21})x_1 + (CA_{12} + A_{22})x_2\right| - (\alpha|x| + \delta)|s|.\end{aligned}$$

It is evident that there exists such value of α that for any δ the time derivative $\dot{V}$ is negative, which validates convergence of the state vector to manifold $s = 0$ in Equation 5.1.5 and existence of sliding mode with the desired dynamics. The time interval preceding the sliding motion may be decreased by increasing parameters α and δ in control (Equation 5.1.7).

A similar result may be obtained in the system with unit control (see Section 3.4):

$$u = -(\alpha|x| + \delta)\frac{s}{\|s\|}, \quad \|s\| = (s^T s)^{1/2}, \tag{5.1.8}$$

which undergoes discontinuities on manifold $s = 0$ in contrast to control (Equation 5.1.7) with discontinuity points on each surface $s_i = 0$ ($i = 1,\ldots,m$). The time derivative of V for the system in Equation 5.1.4 with control in Equation 5.1.8 is of the form

$$\begin{aligned}\dot{V} &= s^T\left((CA_{11} + A_{21})x_1 + (CA_{12} + A_{22})x_2\right) - (\alpha|x| + \delta)\|s\| \\ &\le \|s\|\left|(CA_{11} + A_{21})x_1 + (CA_{12} + A_{22})x_2\right| - (\alpha|x| + \delta)\|s\|.\end{aligned}$$

Again, there exists α such that $\dot{V}$ is negative for any δ and states reach manifold $s = 0$ after a finite time interval.

If the system is not reduced to the regular form, the manifold $s = Cx$ (C being an $m \times (n - m)$ matrix) may be selected in terms of the original system (Equation 5.1.1) based on the equivalent control method approach and the conditions for sliding mode to exist (Sections 2.3 and 2.4). Assume that sliding mode in $s = 0$ has the desired dynamic properties and matrix CB is not singular. Then

$$\dot{s} = CAx + CBu,$$

and the time derivative of Lyapunov function $V = \frac{1}{2}s^T s$ is of the form

$$\dot{V} = s^T CAx + s^T CBu.$$

If matrix $(CB + (CB)^T)$ is positive definite, then discontinuous control

$$u = -M(x)\text{sign}(s),$$

with $M(x) = (\alpha|x| + \delta)$ and sufficiently high but finite α and an arbitrary value of δ leads to sliding mode after a finite time interval. (The proof is similar to the one for nonlinear systems in Section 3.2).

For an arbitrary matrix CB, control should be selected in compliance with the method of Section 3.2:

$$u = -U(x)\text{sign}(s^*),\ s^* = (CB)^T s.$$

The time derivative of Lyapunov function candidate $V = \frac{1}{2}s^T s$ for the system with $U(x) = (\alpha|x| + \delta)$,

$$\dot{V} = (s^*)^T (CB)^{-1} CAx - |s^*|(\alpha|x| + \delta)$$
$$\leq |s^*| |(CB)^{-1} CAx| - |s^*|(\alpha|x| + \delta)$$

is negative definite for sufficiently high α and an arbitrary value of δ as well.

Finally, it is interesting to note that, for systems with the nonlinear unit control, a sliding mode existence condition may be derived by the algebraic stability criteria developed for linear systems. Indeed, if CB is a Hurwitz matrix, then Lyapunov equation $(CB)P + P^T(CB) = -I_m$ has a positive definite solution $P > 0$, and the time derivative of Lyapunov function candidate $V = \frac{1}{2} s^T P s > 0$ in the system with control $u = M(x)\frac{s}{\|s\|}$ may be found as

$$\dot{V} = s^T PAx + M(x) s^T P(CA) \frac{s}{\|s\|}$$
$$= s^T PAx + M(x) s^T \frac{P(CA) + (CA)^T P}{2} \frac{s}{\|s\|}$$
$$\leq \|s\| \|PAx\| - \frac{1}{2} M(x) \|s\|.$$

If function $M(x) = (\alpha|x| + \delta)$, then $\dot{V}$ is negative and sliding mode occurs after a finite time interval (see Section 3.5).

5.2. Invariant Systems

One of the main objectives of designing feedback control systems is to reduce sensitivity with respect to disturbances and plant parameter variations. As shown in Section 3.3, sliding modes in any manifold are invariant to those factors if they act in a control space (Equations 3.4.4 and 3.4.5). For linear systems

$$\dot{x} = (A + \Delta A(t))x + Bu + Qf(t), \quad f(t) \in \Re^l, \tag{5.2.1}$$

the invariance conditions were formulated in terms of system and input matrices in the work by Drazenovic [1969]: sliding modes in any manifold are invariant with respect to parameter variations $\Delta A(t)$ and disturbance vector $f(t)$ if

$$\Delta A \in \text{range}(B), Q \in \text{range}(B),$$

or there exist matrices Λ_A and Λ_Q (constant or time varying) such that

$$\Delta A = B\Lambda_A,\ Q = B\Lambda_Q. \tag{5.2.2}$$

If the conditions in Equation 5.2.2 hold, then the regular form for Equation 5.2.1 is similar to Equation 5.1.4,

$$\dot{x}_1 = A_{11}x_1 + A_{12}x_2$$
$$\dot{x}_2 = A_{21}x_1 + A_{22}x_2 + u + \Lambda_A x + \Lambda_Q f(t).$$

Selecting discontinuous control in the form (Equation 5.1.7) with manifold (Equation 5.1.5) leads to the sliding mode equation (Equation 5.1.6) with desired dynamics and invariance property. Assuming that the ranges of plant parameter variations and an upper bound of the disturbance vector f_0 ($\|\Lambda_Q f(t)\| \le f_0$) are known, $s = 0$ can be made a sliding manifold in the system with control (Equation 5.1.7) under the additional condition

$$\delta \ge f_0. \tag{5.2.3}$$

A similar approach may be applied to decouple l interconnected systems

$$\dot{x}_i = A_i x_i + \sum_{\substack{j=1 \\ j\neq i}}^{l} A_{ij}x_j + B_i u_i, \quad i = 1,...,l,$$

where $x_i \in \Re^{n_i}$, $u_i \in \Re^{m_i}$, and A_i, B_i, and B_i are constant matrices.

Interconnection terms may be handled as disturbances, and the invariance conditions may be reformulated for each subsystem:

$$A_{ij} \in \text{range}(B_i).$$

Discontinuous control in the ith system

$$u_i = -(\alpha_i + \delta_i)|x|\text{sign}(s_i),\ \ x^T = (x_i^T,...,x_l^T),\ \ s_i = C_i x_i,\ \ C_i = \text{const.},\ \ s_i \in \Re^{m_i},$$

with sufficiently high but finite values α_i enforces sliding mode in manifold $s_i = 0$ governed by an $(n_i - m_i)$ order equation that does not depend on the states of the other subsystems. The dynamics of each subsystem may be designed by a proper choice of matrices C_i in the equations of the sliding manifolds.

5.3. Sliding Mode Dynamic Compensators

The value of δ should exceed an upper estimate of a disturbance vector (Equation 5.2.3) in discontinuous control (Equation 5.1.7) designed to reject

disturbances. To soften the control action, it would be desirable to reduce the control amplitude in sliding mode if the magnitude of the disturbance decreases. Usually, disturbances are not accessible for measurement, which is the main obstacle for designing a control system with the above property. Nevertheless, the formulated task is solvable if rather fuzzy a priori knowledge on a class of disturbances is available.

Let the disturbance in motion Equation 5.2.1 with $\Delta A = 0$ satisfy the invariance condition in Equation 5.2.2 and let Q be a constant matrix. Then the system may be represented in the regular form

$$\begin{aligned} \dot{x}_1 &= A_{11}x_1 + A_{12}x_2 \\ \dot{x}_2 &= A_{21}x_1 + A_{22}x_2 + u + \Lambda_Q f(t), \end{aligned} \tag{5.3.1}$$

and the equation of sliding mode in manifold $s = Cx_1 + x_2 = 0$ (Equation 5.1.6) does not depend on the disturbance vector. Assume that the components of vector $f(t)$ cannot be measured and a "disturbance model" is taken in the form of a time-varying linear dynamic system:

$$f^{(k)} + \sum_{i=1}^{k-1} \theta_i(t) f^{(i)} = 0. \tag{5.3.2}$$

The scalar coefficients $\theta_i(t)$ can vary arbitrarily over bounded intervals

$$|\theta_i(t)| \le \vartheta_{i0}. \tag{5.3.3}$$

It is assumed that neither initial conditions nor functions $\theta_i(t)$ are measured, and only ranges ϑ_{i0} are known. Equation 5.3.2 embraces a rather wide class of disturbances. For example, for $k = 2$, it includes exponential and harmonic functions, polynomials of any finite power (beginning from a certain time), all kinds of products of these functions, etc.

The controller is designed as a dynamic system with control u as an output

$$u^{(k)} + \sum_{i-0}^{k-1} d_i u^{(i)} = v, \tag{5.3.4}$$

where d_i are constant scalar coefficients whose choice is dictated by convenience of implementation only.

The input v will be selected as a piecewise linear function of the controller and system states. Each of m control channels of the system has a kth-order dynamic element, the total order of the system being equal to $n + mk$. The state coordinate of the additional dynamic system can be measured.

Let us write the motion equations of the extended system in the space consisting of $x_1, x_2, \ldots, x_{k+2}$, if

$$\dot{x}_i = x_{i+1}, i = 2, \ldots, k+1. \tag{5.3.5}$$

Because $\dot{x}_2 = x_3$, it follows from the second equation of Equation 5.3.1 that

$$u = x_3 - A_{21}x_1 - A_{22}x_2 - \Lambda_Q f. \tag{5.3.6}$$

Differentiating Equation 5.3.6 k times and substituting the right-hand sides of Equations 5.3.1, 5.3.5, and 5.3.6 for the time derivatives of x_i and u, we obtain

$$u^{(i)} = x_{i+3} + \sum_{j=1}^{i+2} A_j^i x_j - \Lambda_Q f^{(i)}, \quad i = 1,\ldots,k-1, \tag{5.3.7}$$

$$u^{(k)} = \dot{x}_{k+2} + \sum_{j=1}^{k+2} A_j^k x_j - \Lambda_Q f^{(k)}, \tag{5.3.8}$$

where A_j^i and A_j^k are constant matrices. By substituting the values of derivatives $u^{(i)}$ from Equations 5.3.7 and 5.3.8 into Equation 5.3.4 and replacing the kth derivative of the disturbance vector in accordance with Equation 5.3.2 by a linear combination of vectors $f,\ldots,f^{k-1}$, we obtain

$$\dot{x}_{k+2} = \sum_{i=1}^{k+2} A_i x_i + \sum_{i=0}^{k-1} (d_i - \theta_i(t))\Lambda_Q f^{(i)} + v, \tag{5.3.9}$$

where A_i are constant matrices.

Bearing in mind that vectors $\Lambda_Q f^{(i)}$ ($i = 0,\ldots,k-1$) may be computed from Equation 5.3.7, Equation 5.3.9 may be represented as

$$\dot{x}_{k+2} = \sum_{i=1}^{k+2} \bar{A}(t)_i x_i + \sum_{i=0}^{k-1} (d_i - \theta_i(t))u^{(i)} + v, \tag{5.3.10}$$

where $\bar{A}_i(t)$ are matrices depending on $\theta_i(t)$ and, consequently, time. Introduce notations

$$\bar{x}^T = [\bar{x}_1^T \quad \bar{x}_2^T], \quad \bar{x}_1^T = [x_1^T \ \ldots \ x_{k+1}^T], \quad \bar{x}_2 = x_{k+2}, \quad \bar{u}^T = [u^T \ \dot{u}^T \ldots \ (u^{(k-1)})^T],$$
$$\sum_{i=0}^{k-1} (d_i - \theta_i(t))u^{(i)} = \theta(t)\bar{u}, \quad \theta = [(d_1 - \theta_i(t) \ \ldots \ (d_i - \theta_{k-1}(t)]$$

and rewrite the first equation in Equation 5.3.1 and Equations 5.3.5 and 5.3.10 as

$$\begin{aligned} \frac{d\bar{x}_1}{dt} &= \bar{A}_{11}\bar{x}_1 + \bar{A}_{12}\bar{x}_2 \\ \frac{d\bar{x}_2}{dt} &= \bar{A}_{21}(t)\bar{x}_1 + \bar{A}_{22}(t)\bar{x}_2 + \theta(t)\bar{u} + v, \end{aligned} \tag{5.3.11}$$

where $\bar{A}_{11}$ and $\bar{A}_{12}$ are constant matrices, and $\bar{A}_{21}(t)$, $\bar{A}_{22}(t)$, and $\theta(t)$ are time-varying matrices with bounded elements because the coefficients $\theta_i(t)$ (Equation 5.3.3) were assumed to be bounded.

The system (Equation 5.3.11) is in regular form, and, by handling $\bar{x}_2$ as an intermediate control in the first block, the desired dynamics may be assigned by a proper choice of matrix C in $\bar{x}_2 = -C\bar{x}_1$. Then, following the design methodology of Section 3.2, sliding mode is enforced in the manifold $s = \bar{x}_2 + C\bar{x}_1 = 0$ by control

$$v = -\left(\alpha(|\bar{x}_1| + |\bar{x}_2| + |\bar{u}|) + \delta\right)\text{sign}(s). \tag{5.3.12}$$

Indeed, time derivative of Lyapunov function candidate $V = \frac{1}{2}s^T s$

$$\dot{V} = s^T\left((C\bar{A}_{11} + \bar{A}_{21})\bar{x}_1 + (C\bar{A}_{12} + \bar{A}_{22})\bar{x}_{21} + \theta\bar{u}\right) - \left(\alpha(|\bar{x}_1| + |\bar{x}_2| + |\bar{u}|) + \delta\right)|s|$$

is negative for a sufficiently high but finite value of α and any δ. After a finite time interval, sliding mode governed by

$$\frac{d\bar{x}_1}{dt} = (\bar{A}_{11} - \bar{A}_{12}C)\bar{x}_1 \tag{5.3.13}$$

will occur with the desired dynamics and invariance properties with respect to disturbances.

The objective of the design was to decrease the magnitude of control with decreasing disturbances without measurement of the disturbances. This is the case for our system: in the solution to Equation 5.3.13, $\bar{x}_1(t)$and $\bar{x}_2(t)$ tend to zero, which means that functions $u^{(i)}$ tend to $-\Lambda_Q f^{(i)}$ (Equation 5.3.7); because $u^{(i)}$ ($i = 1,\ldots,k-1$) are components of vector $\bar{u}$, and the control v (Equation 5.3.12) decreases with the disturbances. The output of the additional dynamic system u is a continuous function and tends to $-\Lambda_Q f$, which leads to disturbance rejection. In real systems, often there is no need to introduce an additional dynamic system; its part may be played by actuators with outputs usually accessible for measurement. Then, an actuator input is the control to be designed, and its magnitude depends on disturbances and their derivatives.

Example 5.1

The disturbance rejection method will be illustrated with a second-order system in which the plant and actuator are integrators (Figure 5.1).

An external disturbance $f(t)$ is applied to the plant and is not accessible for measurement. The control u is designed as a piecewise linear function of the controlled value $x = x_1$, which should be reduced to zero but also of the actuator output y. Then the behavior of the plant and the system is governed by the systems of the first and second order, respectively,

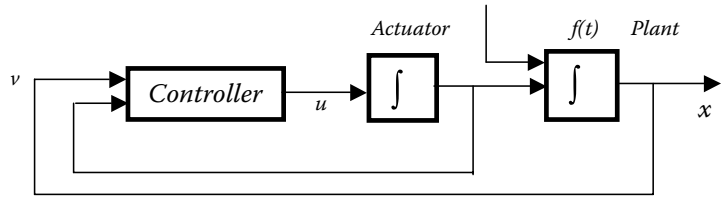

FIGURE 5.1
Sliding mode dynamic compensator in a second-order system.

$$\begin{aligned} u &= x_2 - f \text{ and} \\ \dot{x}_1 &= x_2 \\ \dot{x}_2 &= \upsilon - \dot{f}. \end{aligned} \tag{5.3.14}$$

Select control for the system in Equation 5.3.14 in the form similar to Equation 5.3.12 $v = -(\alpha|x_1| + \beta|u| + \delta)\text{sign}(s)$, with α, β, and $c > 0$ being constant coefficients. The control low may be also written as

$$\upsilon = -\Psi x_1 - \Psi_u u - \delta \text{ sign}(s),$$

where $\Psi = \alpha \text{ sign}(x_1 s)$ and $\Psi_u = \beta \text{ sign}(us)$. The system in Equation 5.3.14 is governed by piecewise linear differential equations

$$\begin{aligned} \dot{x}_1 &= x_2 \\ \dot{x}_2 &= -\Psi x_1 - \Psi_u x_2 - \delta \text{ sign}(s) + \Psi_u f + \dot{f}. \end{aligned}$$

As shown for a similar second-order system with no disturbance in Section 2.1 (with $f(t) \equiv 0$), the coefficients of control can be selected such that the state reaches the switching line and sliding mode is enforced at each point of this line. After some finite time interval, the state tends to zero in sliding mode with motion equation $\dot{x} + cx = 0$. The state planes of the two unstable linear structures of the system are shown in Figure 1.9, and the state plane of the asymptotically stable system with variable structure is shown in Figure 1.10. If $f(t) \neq 0$, singular points ($\dot{x}_1 = \dot{x}_2 = 0$) of each of the four linear structures, corresponding to the four combinations of $\pm\alpha$ and $\pm\beta$, are shifted from the origin. The magnitudes and signs of the shifts are dependent on coefficients α, β, and disturbance $f(t)$. Figure 5.2.A and Figure 5.2.B separately shows right and left semiplanes of the system state plane for the area $|x_2| \leq f(t)$, where, by virtue of the plant equation, $\text{sign}(u) = -\text{sign}(\dot{f}(t))$. The first-order actuator takes part of an additional dynamic system (Equation 5.3.4); therefore, the disturbance $f(t)$ is assumed to satisfy the conditions in Equation 5.3.2 for $k = 1$:

$$\dot{f} = \theta(t) f, \quad |\theta(t)| \leq \beta.$$

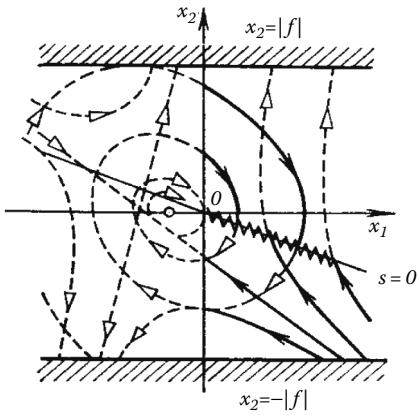

FIGURE 5.2A
Right, semiplane of state plane.

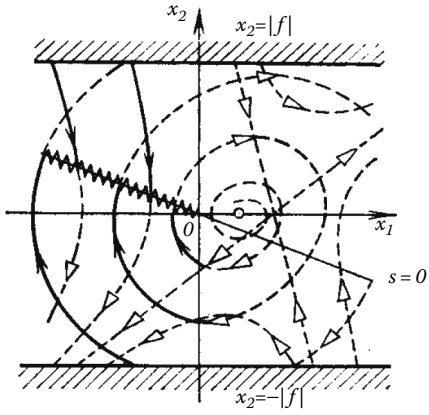

FIGURE 5.2B
Left, semiplane of state plane.

As can be seen from the state plane, the singular points are shifted such that the state trajectories in the vicinity of the switching line $s = 0$ are directed toward it and sliding mode occurs in the system.* The same conclusion can be made analytically. Because $\text{sign}(u) = -\text{sign}(f(t))$, the term $\Psi_u f$ in the motion equation is equal to $-\beta|f|\text{sign}(s)$ and for the points $x_2 = -cx_1$ on the switching line

$$\dot{s} = (-c^2 + \Psi_u - \Psi)x_1 - \delta\ \text{sign}(s) - \beta|f|\ \text{sign}(s) + \dot{f}.$$

* Strictly speaking, the curves of Figure 5.2 are not state trajectories because the disturbance makes the system time varying. Each curve should be regarded as the locus of points for which, at each fixed time, the tangential to the curve coincides with state velocity vector.

The values of s and $\dot{s}$ have opposite signs, or the conditions in Equation 2.4.1 for sliding mode to exist hold for $\alpha > c^2 + \beta$ and an arbitrary positive δ. Thus, the change of signs in the main and local feedback enables one to reject unmeasured disturbances.

5.4. Ackermann's Formula

Ackermann's formula enables us to determine a linear state-feedback scalar control law in explicit form resulting in a system with desired eigenvalues [Ackermann 1992]. A similar task arises when designing sliding model control in linear systems with a linear discontinuity surface because the corresponding sliding mode equation is linear and depends on the coefficients of the surface equation.

The traditional approach to sliding mode control design implies transforming the linear system into the regular form (Section 5.1) consisting of two blocks and handling the state vector of one of the blocks as a fictitious control.

In this section, the design method of scalar sliding mode control rests on Ackermann's formula and is oriented toward obtaining a discontinuity plane equation in explicit form as well in terms of the original system without transforming it into regular form [Ackermann and Utkin 1998]. For a linear plant operating under uncertainty conditions, the control enforces sliding motions governed by a linear equation with the desired eigenvalue placement and independent of disturbance.

Consider a controllable system described by a differential equation,

$$\dot{x} = Ax + b\big(u + f(x,t)\big), \tag{5.4.1}$$

where x is an n-dimensional state vector, u is a scalar control, A and b are known matrix and vector, and $f(x,t)$ is a nonlinear disturbance with known upper bound $|f(x,t)| < f_0(x,t)$. As follows from Equation 5.4.1, the control and disturbance vectors (bu and bf) are collinear, so the invariance condition (Equation 5.2.2) is satisfied, and, consequently, the sliding mode in any plane is invariant with respect to the disturbance.

The design of sliding mode control in Equation 5.4.1 implies the selection of a plane $s = c^T x = 0$ (c^T is an n-dimensional constant row vector) and consequently design of the control enforcing the sliding mode in $s = 0$. The sliding mode equation is of the $(n-1)$th order and does not depend on the disturbance. The desired dynamic properties may be provided by a proper

choice of the vector c. Traditionally, the sliding mode equation is derived first and then the conventional methods of the linear theory are applied.

As mentioned above, the aim of this section is to show how the vector c may be found in an explicit form without the sliding motion equation using Ackermann's formula, as far as the eigenvalue placement task is concerned.

The desired eigenvalues $\lambda_1, \lambda_2,\ldots,\lambda_n$ of linear system $\dot{x} = Ax + bu_a$ may be assigned using Ackermann's formula [Ackermann 1992]

$$u_a = -k^T x,\ k^T = e^T P(A), \tag{5.4.2}$$

where

$$e^T = [0 \ldots 0\ 1][b\ Ab \ldots A^{n-1}b]^{-1}$$

$$P(\lambda) = (\lambda - \lambda_1)(\lambda - \lambda_2)\ldots(\lambda - \lambda_{n-1})(\lambda - \lambda_n).$$

Suppose now that the real or pairwise conjugate complex values $\lambda_1, \lambda_2,\ldots,\lambda_{n-1}$ are the desired eigenvalues of the sliding mode.

Theorem 5.1

If

$$c^T = e^T P_1(A) \tag{5.4.3}$$

with $P_1(\lambda) = (\lambda - \lambda_1)(\lambda - \lambda_2)\ldots(\lambda - \lambda_{n-1}) = p_1 + p_2\lambda + \ldots + p_{n-1}\lambda^{n-2} + \lambda^{n-1}$, then $\lambda_1, \lambda_2,\ldots,\lambda_{n-1}$ are the eigenvalues of the sliding mode dynamics in the plane $s = c^T x = 0$. □

Proof 4.1

According to Ackermann's formula (Equation 5.4.2), $\lambda_1, \lambda_2,\ldots,\lambda_n$ are eigenvalues of the matrix $A^* = A - bk^T$, with λ_n being an arbitrary value. Vector c^T is a left eigenvector of A^* corresponding to λ_n. Indeed, as follows from Equations 5.4.2 and 5.4.3

$$c^T A^* = c^T A - c^T b e^T P(A).$$

Because

$$\begin{aligned} c^T b &= e^T P_1(A) b \\ &= [0 \quad 0 \quad \cdots \quad 0 \quad 1][b \quad Ab \quad \cdots \quad A^{n-1}b]^{-1}[b \quad Ab \quad \cdots \quad A^{n-1}b][p_1 \quad p_2 \quad \cdots \quad 1]^T \\ &= 1 \end{aligned} \tag{5.4.4}$$

and $P(A) = P_1(A)(A - \lambda_n I)$,

$$c^T A^* = c^T A - e^T P_1(A)(A - \lambda_n I),$$

which reduces with Equation 5.4.3 to

$$c^T A^* = \lambda_n c^T \tag{5.4.5}$$

and means that c^T is a left eigenvalue of A^*, correspodning to eigenvalue λ_n. The system $\dot{x} = (A - bk^T)x + b\left[u - u_a + f(x,t)\right]$ is now transformed such that $s = c^T x$ becomes the last state and the first $n - 1$ states $x^* = [x_1 \quad x_2 \quad \cdots \quad x_{n-1}]^T$ remain unchanged, i.e.,

$$\begin{bmatrix} x^* \\ s \end{bmatrix} = \begin{bmatrix} I & 0 \\ c^T & \end{bmatrix} x = Tx$$

For T to be invertible, the last component of c^T must be nonzero. Because this vector is nonzero, the condition can always be satisfied by reordering the components of the state vector x. Under the conditions in Equations 5.4.4 and 5.4.5, the transformed system is

$$\dot{x}^* = A_1 x^* + a_s s + b^*\left(u - u_a + f(x,t)\right) \tag{5.4.6}$$

$$\dot{s} = \lambda_n s + u - u_a + f(x,t), \tag{5.4.7}$$

where

$$\begin{bmatrix} A_1 & a_s \\ 0 & \lambda_n \end{bmatrix} = T\left(A - bk^T\right)T^{-1}, \quad \begin{bmatrix} b^* \\ 1 \end{bmatrix} = Tb.$$

The spectrum of matrix A_1 consists of desired eigenvalues $\lambda_1, \lambda_2, \ldots, \lambda_{n-1}$.

To derive the sliding mode equation in the plane $s = 0$, the solution to the algebraic equation $\dot{s} = 0$ with respect to u should be substituted into Equation 5.4.6. It results in the motion of equation

$$\dot{x}^* = A_1 x^* \tag{5.4.8}$$

with the desired dynamics, independent of the unknown disturbance $f(x,t)$. □

The result has a transparent geometric interpretation. Vector c^T is a left eigenvector of the matrix A^* corresponding to the eigenvalue λ_n. This means that the plane $s = c^T x = 0$ is an invariant subspace of A^* with the motion determined by the previously selected set of $(n - 1)$ eigenvalues $\lambda_1, \lambda_2, \ldots, \lambda_{n-1}$. If sliding mode is enforced in the plane $s = c^T x = 0$, then it exhibits the desired dynamics. Note that the design of the plane $s = c^T x = 0$ does not imply assign-

ing the eigenvalue λ_n; it only appears in the proof of the theorem and may take an arbitrary value.

The discontinuous control u is designed to enforce sliding mode in the plane $s = 0$. This implies that the conditions in Equation 2.4.1 should be satisfied, i.e., the values of s and $\dot{s}$ should have different signs in some vicinity of the plane,

$$\begin{aligned} \dot{s} &= c^T Ax + u + f(x,t) \\ u &= -M(x,t)\text{sign}(s), \end{aligned} \tag{5.4.9}$$

where $M(x,t)$ is chosen such that

$$M(x,t) > |C^T Ax| + f_0(x,t).$$

If the control may take only two extreme values $+M_0$ or $-M_0$ (which is common in applications), then Equation 5.4.9 with $M(x,t) = M_0$ enforces a sliding mode in the plane $s = 0$ governed by Equation 5.4.8 as well. Of course, the domain of initial conditions and the disturbance should be bounded.

Example 5.2

Let $\lambda = -1$ be the desired eigenvalue of sliding motion for the second-order system

$$\dot{x} = Ax + b\big(u + f(x,t)\big),$$

where

$$A = \begin{bmatrix} 0 & 0 \\ 0 & 1 \end{bmatrix}, \quad b = \begin{bmatrix} 1 \\ 1 \end{bmatrix}, \quad x = \begin{bmatrix} x_1 \\ x_2 \end{bmatrix}.$$

According to Equation 5.4.3,

$$c^T = [0 \;\; 1][b \;\; Ab]^{-1} P_1(A),\ P_1(A) = A + I,$$

$$c^T = [-1 \;\; 2]$$

and the sliding surface equation is of the form (note that $c^T b = 1$) $s = -x_1 + 2x_2 = 0$. By the equivalent control method, the solution to the system $s = 0$, $\dot{s} = 0$ with respect to x_2 and u

$$u_{eq} = -x_1 - f(x_1,t), \quad x_2 = \frac{1}{2}x_1$$

should be substituted into the original system to derive the sliding motion equation $\dot{x}_1 = -x_1$. The sliding mode is determined by the eigenvalue $\lambda = -1$ and does not depend on the disturbance $f(x,t)$.

The design procedure based on *Ackermann's* formula is summarized as follows.

Step 1: The desired spectrum of the sliding motion $\lambda_1, \lambda_2, \ldots \lambda_{n-1}$ is selected.

Step 2: The equation of the discontinuity plane $s = c^T x = 0$ is found as

$$c^T = e^T(A - \lambda_1 I)(A - \lambda_2 I)\ldots(A - \lambda_{n-1} I).$$

Step 3: The discontinuous control (Equation 5.4.9) is designed.

Remark 5.1

It follows from Equation 5.4.9 that sliding mode may be enforced in an unperturbed system by

$$u = -(\alpha \|x\| + \delta)\text{sign}(s)$$

with some finite positive number α and any positive δ. The control tends to zero in the system with asymptotically stable sliding modes.

5.4.1. Simulation Results

The design procedure will be demonstrated for sliding mode stabilization of an inverted pendulum (Figure 5.3) subjected to a bounded unknown disturbance force.

The linearized motion equations are of the form [Kortüm and Lugner 1994]

$$\dot{x} = Ax + b\big(u + f(t)\big),$$

where

$$A = \begin{bmatrix} 0 & 0 & 1 & 0 \\ 0 & 0 & 0 & 1 \\ 0 & a_{32} & 0 & 0 \\ 0 & a_{42} & 0 & 0 \end{bmatrix}, \quad b = \begin{bmatrix} 0 \\ 0 \\ b_3 \\ b_4 \end{bmatrix}, \quad x = \begin{bmatrix} x \\ \alpha \\ \dot{x} \\ \dot{\alpha} \end{bmatrix}$$

and

$$\begin{aligned} a_{32} &= -3(c - mga) / a(4M_t + m), \\ a_{42} &= -3(M_t + m)(c - mga) / a^2 m(4M_t + m), \\ b_3 &= 4 / (4M_t + m), \\ b_4 &= 3 / (4M_t + m). \end{aligned}$$

M_t and m are masses of the trolley and pendulum, a is the pendulum length, c is the spring stiffness, $g = 9.81m/s^2$, u and $f(t)$ are control and disturbance forces, and $|f(t)| \le f_0 = \text{const}$, in which f_0 is assumed to be known.

Sliding mode control is designed for $M_t = 5$, $m = 1$, $a = 1$, $c = 1$. Let $\lambda_1 = -1$, $\lambda_2 = -2$, $\lambda_3 = -3$ be the desired eigenvalues of sliding motion. According to Equation 5.4.3, the discontinuity plane equation

$$s = c^T x = 0,$$

$$c^T = [0\ 0\ 0\ 1][b\ Ab\ A^2b\ A^3b]^{-1}\ (A + I)(A + 2I)(A + 3I),$$

I is an identity matrix,

$$c^T = [-4.77\ 48.4\ -8.75\ 18.7].$$

The control is assumed to take two extreme values only:

$$u = -M_0 \text{sign}(s),\ M_0 = \text{const}.$$

As follows from the above studies, for any $M_0 > f_0$, there exits a domain of initial conditions such that sliding mode is enforced in the plane $s = 0$.

The simulation examples are given for sliding mode control with

$$M_0 = 40 \text{ and } f(t) = f_0 \sin(3t),\ f_0 = 0.5.$$

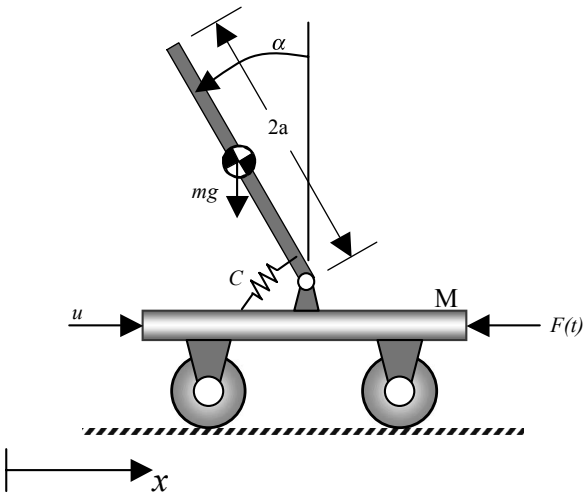

FIGURE 5.3
Inverted pendulum with trolley system.

Figure 5.4 shows the stabilization process for initial conditions $x(0) = 0.5$, $\alpha(0) = 0.2$, $\dot{x}(0) = 0$, $\dot{\alpha}(0) = 0$. Sliding mode occurs after a finite time interval, and, thereafter, both coordinates x and α do not depend on the time-varying disturbance and tend to zero.

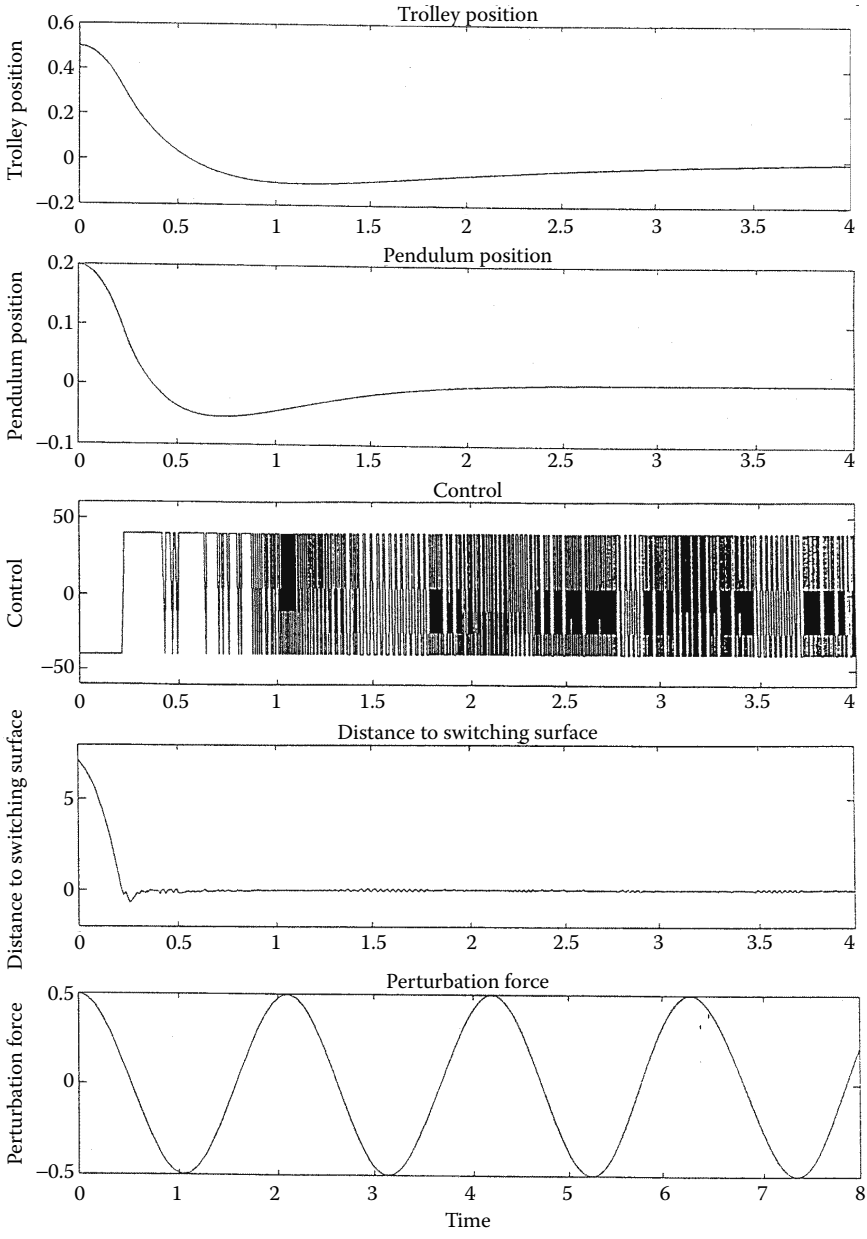

FIGURE 5.4
Sliding mode control of inverted pendulum, $x(0) = 0.5$, $\alpha(0) = 0.2$.

The system without feedback is unstable and control is bounded; therefore, the motion may turn to be unstable should initial conditions be increased. The system is still stable for $\alpha(0) = 0.38$ (Figure 5.5) and becomes unstable with $\alpha(0) = 0.39$ (Figure 5.6). As mentioned in Remark 5.1, sliding mode may be enforced in an unperturbed system ($f(t) = 0$) for arbitrary initial conditions with piecewise linear control

$$u = -\beta(|x| + |\dot{x}| + |\alpha| + |\dot{\alpha}| + \delta)\text{sign}(s),$$

where β, δ are positive values and some finite β and arbitrary δ.

The simulation results with $\beta = 30$, $\delta = 0$, $x(0) = 1$, $\dot{x}(0) = 0$, $\alpha(0) = 1$, $\dot{\alpha}(0) = 0$ are shown in Figures 5.5 through 5.7.

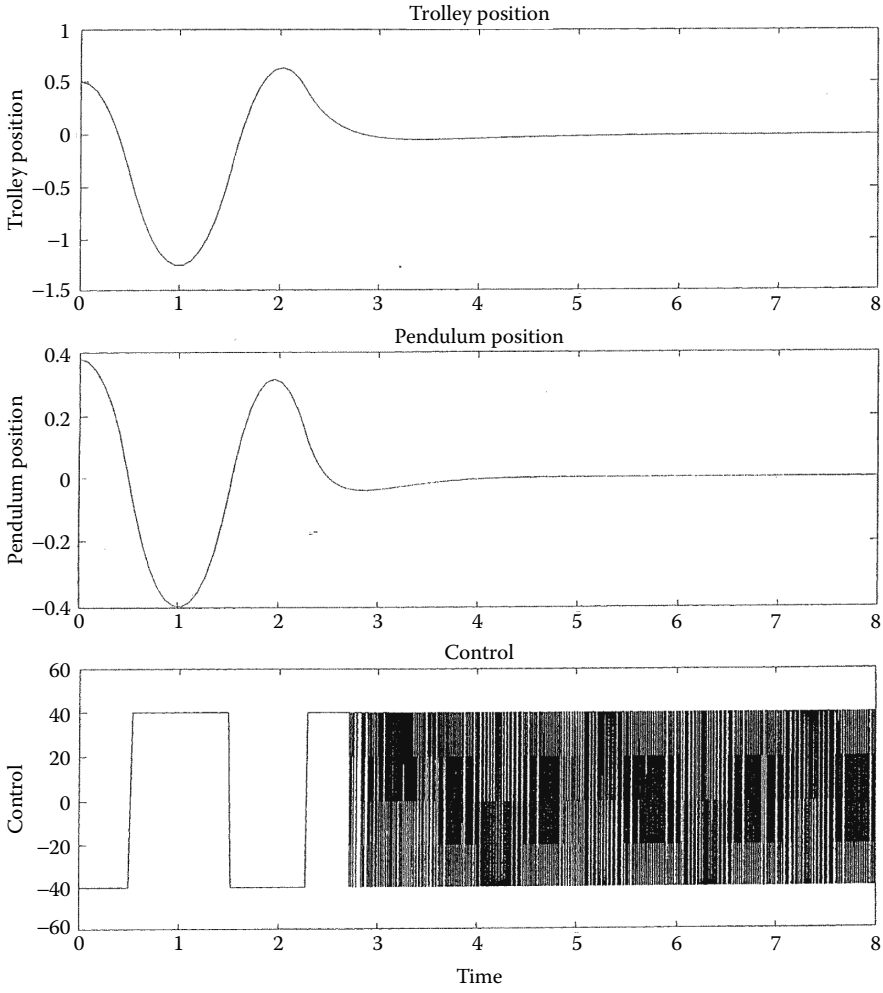

FIGURE 5.5
Both the state vector and control tend to zero in sliding mode.

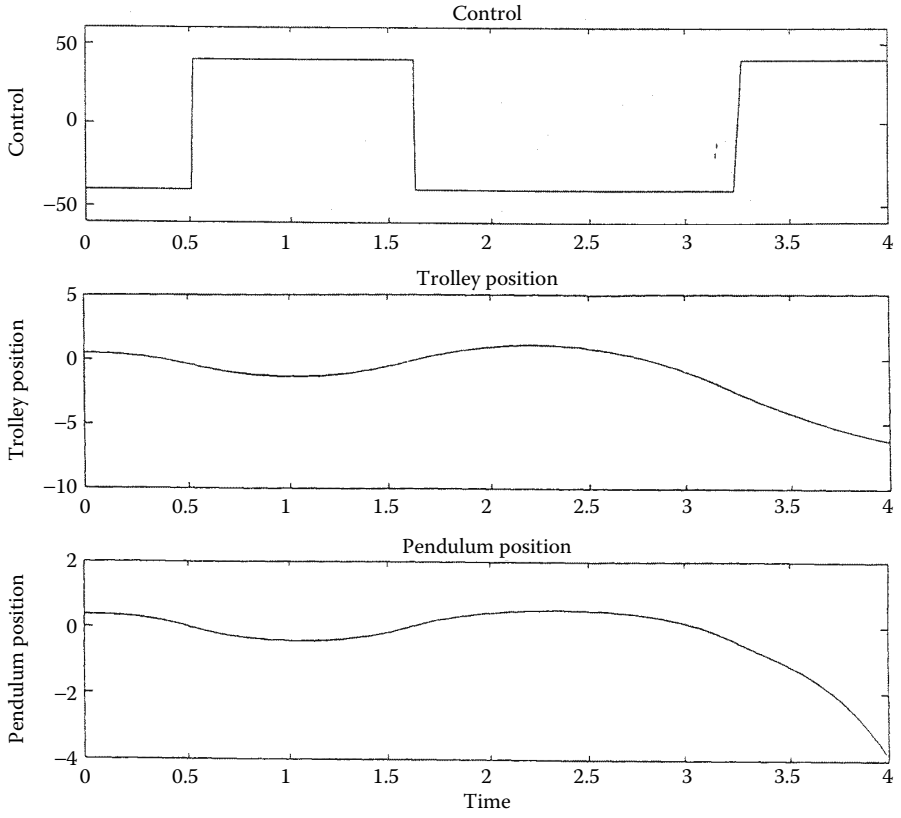

FIGURE 5.6
Sliding mode control of inverted pendulum $\alpha(0) = 0.39$.

5.5. Output Feedback Sliding Mode Control

Implementation of the design methods developed in the previous sections implies that all components of a state vector have to be accessible for measurement. However, this is not the case for many practical situations. Two approaches may be studied for these cases. The first method is the design of state observers to restore the state vector using available measurements of some states, and the second method is to derive a class of systems such that the control task may be solved by designing a static output feedback controller. The second approach to sliding mode control design under incomplete information on the system states is studied in this section. The observer design methods are studied in Chapter 6.

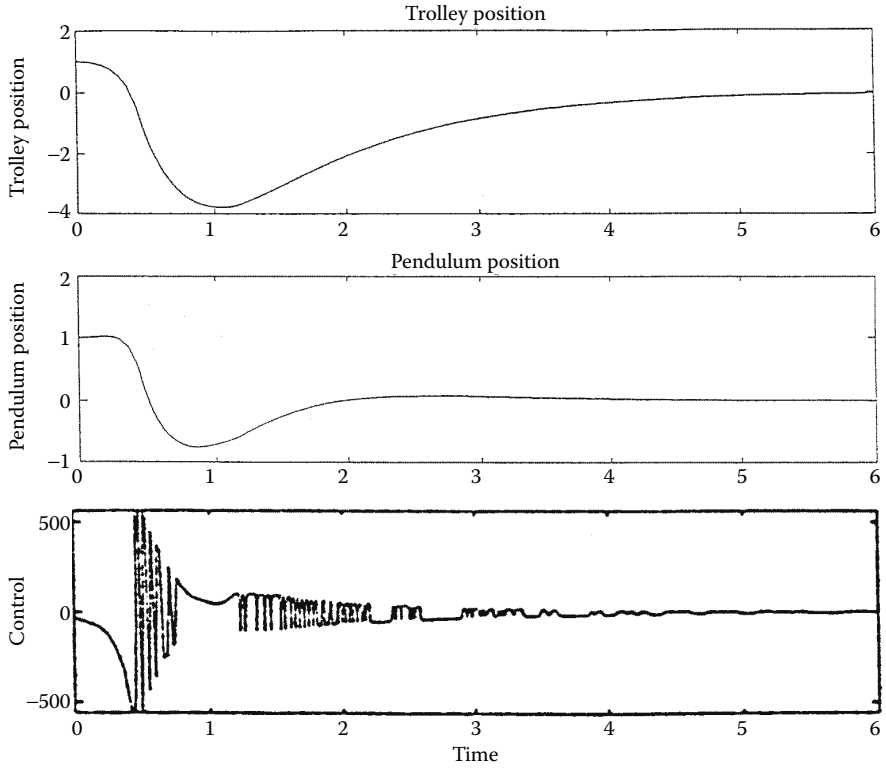

FIGURE 5.7
Sliding mode control of inverted pendulum; unperturbed system with state-dependent control magnitude.

It is assumed that, for the system

$$\dot{x} = Ax + B\,u \tag{5.5.1}$$

$$y = Cx \tag{5.5.2}$$

with l-dimensional output vector y,

1. The pair (A, B) is controllable and the pair (A, C) is observable.
2. Rank $B = m$ and rank $C = l$.
3. $l > m$.

The system (Equations 5.5.1 and 5.5.2) is referred to as output pole assignable if the eigenvalues of matrix $A + BLC$ or of a feedback system with linear control $u = Ly$ (L is a constant $m \times l$ matrix) take any desired values. The class of such linear systems may be found based on the well-known result by Kimura [1975]:

Theorem 5.2

If the system (Equations 5.5.1 and 5.5.2) is controllable and observable and satisfies the relation

$$n \le l + m - 1, \tag{5.5.3}$$

then it is pole assignable by gain output feedback. □

There exists a nonsingular coordinate transformation reducing the system to regular form (see also Section 3.2)

$$\begin{bmatrix} \dot{x}_1 \\ \dot{x}_2 \end{bmatrix} = \begin{bmatrix} A_{11} & A_{12} \\ A_{21} & A_{22} \end{bmatrix} \begin{bmatrix} x_1 \\ x_2 \end{bmatrix} + \begin{bmatrix} 0 \\ I_m \end{bmatrix} u, \tag{5.5.4}$$

where the pair (A_{11}, A_{12}) is controllable. Equation 5.5.2 is transformed into

$$y = \begin{bmatrix} C_1 & C_2 \end{bmatrix} \begin{bmatrix} x_1 \\ x_2 \end{bmatrix} = C_1 x_1 + C_2 x_2, C_1 \in \Re^{l \times (n-m)}, \quad C_2 \in \Re^{l \times m}.$$

If C_2 is a matrix with full rank, then it may be represented in the form (with reordering the components of vector x_2 if needed)

$$C_2 = \begin{bmatrix} C_{21} \\ C_{22} \end{bmatrix}, C_{21} \in \Re^{(l-m) \times m}, \quad C_{22} \in \Re^{m \times m}, \quad \det(C_{22}) \neq 0,$$

and for a nonsingular matrix

$$P = \begin{bmatrix} I_{l-m} & -C_{21} C_{22}^{-1} \\ 0 & C_{22}^{-1} \end{bmatrix}$$

$$y^* = Py = \begin{bmatrix} PC_1 & PC_2 \end{bmatrix} x = \begin{bmatrix} C_{11} & 0 \\ C_{21} & I_m \end{bmatrix} \begin{bmatrix} x_1 \\ x_2 \end{bmatrix}.$$

The switching manifold $s = 0$ in sliding mode control is defined as

$$s = Fy^* = \begin{bmatrix} F_1 & I_m \end{bmatrix} \begin{bmatrix} C_{11} x_1 \\ C_{21} x_1 + x_2 \end{bmatrix} = (F_1 C_{11} + C_{21}) x_1 + x_2,$$

where $F \in R^{m \times l}$, $F_1 \in R^{m \times (l-m)}$.

The control input is selected as a discontinuous function of the output

$$u = -K \cdot \operatorname{sign}(s) \quad K = \operatorname{diag}\begin{bmatrix} k_1 & k_2 & \cdots & k_m \end{bmatrix}.$$

The control gains k_i are chosen such that

$$k_i > |f_i|, f^T = [f_1,\ldots,f_m], f = [(F_1C_{11} + C_{21})A_{11} + A_{21}]x_1 + [(F_1C_{11} + C_{21})A_{12} + A_{22}]x_2,$$

which means that the time derivative of Lyapunov function candidate $V = \frac{1}{2}s^T s$

$$\dot{V} = s^T f - s^T K \cdot \text{sign}(s) < 0$$

is negative definite, and sliding mode will be enforced after a finite time interval.

In sliding mode, $s = 0$ and

$$x_2 = -(F_1C_{11} + C_{21})x_1. \tag{5.5.5}$$

Substituting Equation 5.5.5 into Equation 5.5.4 yields

$$\dot{x}_1 = (A_{11} - A_{12}C_{21})x_1 + A_{12}\upsilon, \tag{5.5.6}$$

where $\upsilon = -F_1C_{11}x_1 = -F_1y_1 \in R^m$ is handled as a control input. The original system in Equations 5.5.1 and 5.5.2 in sliding mode is replaced by the reduced order system in Equation 5.5.6 and $s = 0$

$$\dot{x}_1 = A^* x_1 + A_{12}\upsilon \tag{5.5.7}$$

$$y_1 = C_{11}x_1, \tag{5.5.8}$$

where $A^* = (A_{11} - A_{12}C_{21})$, and pair (A^*, A_{12}) is controllable as a result of controllability of pair (A_{11}, A_{12}).

Now we deal with a pole placement task for a reduced order controllable system with an $(l - m)$-dimensional output vector. The condition of Kimura's Theorem 5.2 may be reformulated for eigenvalue placement of system (Equations 5.5.7 and 5.5.8):

Theorem 5.3

If the original system in Equations 5.5.1 and 5.5.2 is controllable and the system in Equations 5.5.7 and 5.5.8 is observable and satisfies the relation

$$(n - m) \le (l - m) + m^* - 1 \quad m^* = \text{rank } A_{12}, \tag{5.5.9}$$

then it is pole assignable by gain output feedback. □

Under the condition in Equation 5.5.9, there exists matrix F_1 such that eigenvalues of sliding mode equation

$$\dot{x}_1 = (A^* - A_{12}F_1C_{11})x_1 \tag{5.5.10}$$

takes the desired values.

Because $m^* \le m$, the condition in Equation 5.45 $n \le l + m^* - 1$ means that the original system (Equations 5.5.1 and 5.5.2) is pole assignable by gain output feedback if the reduced-order system (Equations 5.5.7 and 5.5.8) is pole assignable.

If the pair (C_{11}, A^*) is not observable, the same procedure is applicable to the observable part of x_1. The unobservable system (Equations 5.5.7 and 5.5.8) may be presented in the form [Kwakernaak and Sivan 1972]

$$\begin{bmatrix} \dot{x}_1' \\ \dot{x}_1'' \end{bmatrix} = \begin{bmatrix} A_{11}^* & 0 \\ A_{21}^* & A_{22}^* \end{bmatrix} \begin{bmatrix} x_1' \\ x_1'' \end{bmatrix} + \begin{bmatrix} A_{12}' \\ A_{12}'' \end{bmatrix} \upsilon$$
$$y_1 = C_{11}' x_1'$$

with an observable pair (C_{11}', A_{11}^*). Then the upper subsystem is pole assignable if it satisfies the condition in Equation 5.5.9, whereas the eigenvalues of the second subsystem are those of A_{21}^* and can be changed under no conditions.

Remark 5.2

The above eigenvalue placement method is applicable for systems with plant parameter variations and disturbances (Equation 5.2.1)

$$\dot{x} = (A + \Delta A)x + B\,u + Qf,$$
$$y = Cx.$$

If the invariance conditions in Equation 5.2.2 hold, then the motion in sliding mode depends on neither ΔA nor $f(t)$ is and governed by Equation 5.5.10 as well.

Example 5.3

Assumption: The original system is pole assignable but the sliding mode control system is not pole assignable:

$$\begin{bmatrix} \dot{x}_1 \\ \dot{x}_2 \\ \dot{x}_3 \\ \dot{x}_4 \end{bmatrix} = \begin{bmatrix} 0 & 1 & 1 & 0 \\ 1 & 0 & 2 & 0 \\ 0 & 0 & 0 & 0 \\ 0 & 0 & 0 & 0 \end{bmatrix} \begin{bmatrix} 0 & 0 \\ 0 & 0 \\ 1 & 0 \\ 0 & 1 \end{bmatrix} + \begin{bmatrix} u_1 \\ u_2 \end{bmatrix},$$

$$\begin{bmatrix} y_1 \\ y_2 \\ y_3 \end{bmatrix} = \begin{bmatrix} 1 & 0 & 0 & 0 \\ 0 & 0 & 1 & 0 \\ 0 & 0 & 0 & 1 \end{bmatrix} \begin{bmatrix} x_1 \\ x_2 \\ x_3 \\ x_4 \end{bmatrix}, n = 4,\ m = 2,\ l = 3.$$

This system is controllable and observable. The relation in Equation 5.5.9 is satisfied. The switching manifold is designed as

$$s = \begin{bmatrix} f_1 & 1 & 0 \\ f_2 & 0 & 1 \end{bmatrix} \begin{bmatrix} y_1 \\ y_2 \\ y_3 \end{bmatrix} = 0$$

with parameters f_1 and f_2 to be selected.

The reduced order system is

$$\begin{bmatrix} \dot{x}_1 \\ \dot{x}_2 \end{bmatrix} = \begin{bmatrix} 0 & 1 \\ 1 & 0 \end{bmatrix} \begin{bmatrix} x_1 \\ x_2 \end{bmatrix} + \begin{bmatrix} 1 & 0 \\ 2 & 0 \end{bmatrix} \upsilon$$
$$y_1 = \begin{bmatrix} 1 & 0 \end{bmatrix} \begin{bmatrix} x_1 \\ x_2 \end{bmatrix} \quad . \tag{5.5.11}$$

This system is controllable and observable as well, but the relation in Equation 5.5.9 is not satisfied, because $\text{rank} \begin{bmatrix} 1 & 0 \\ 2 & 0 \end{bmatrix} = m^* = 1$ and $n > l + m^* - 1$.

It is impossible to locate poles arbitrarily. Substituting $\upsilon = F_1 y = -(f_1, f_2)^T x_1$ into Equation 5.5.11 yields

$$\begin{bmatrix} \dot{x}_1 \\ \dot{x}_2 \end{bmatrix} = \begin{bmatrix} -f_1 & 1 \\ 1 - 2f_1 & 0 \end{bmatrix} \begin{bmatrix} x_1 \\ x_2 \end{bmatrix}.$$

Because one parameter is free, only one pole may be located arbitrarily.

Example 5.4

Assumption: Both the original system and the system with the sliding mode control are pole assignable:

$$\begin{bmatrix} \dot{x}_1 \\ \dot{x}_2 \\ \dot{x}_3 \\ \dot{x}_4 \end{bmatrix} = \begin{bmatrix} 0 & 1 & 1 & 0 \\ 1 & 0 & 0 & 1 \\ 0 & 1 & 0 & 0 \\ 0 & 0 & 0 & 0 \end{bmatrix} \begin{bmatrix} 0 & 0 \\ 0 & 0 \\ 1 & 0 \\ 0 & 1 \end{bmatrix} + \begin{bmatrix} u_1 \\ u_2 \end{bmatrix}$$

$$\begin{bmatrix} y_1 \\ y_2 \\ y_3 \end{bmatrix} = \begin{bmatrix} 1 & 0 & 0 & 0 \\ 0 & 2 & 1 & 0 \\ 0 & 0 & 0 & 1 \end{bmatrix} \begin{bmatrix} x_1 \\ x_2 \\ x_3 \\ x_4 \end{bmatrix}, n = 4,\ m = 2,\ l = 3.$$

This system is controllable and observable and satisfies the relation in Equation 5.5.9. The switching manifold is

$$s = \begin{bmatrix} f_1 & 1 & 0 \\ f_2 & 0 & 1 \end{bmatrix} \begin{bmatrix} y_1 \\ y_2 \\ y_3 \end{bmatrix} = 0.$$

The reduced order system,

$$\begin{bmatrix} \dot{x}_1 \\ \dot{x}_2 \end{bmatrix} = \begin{bmatrix} 0 & -1 \\ 1 & 0 \end{bmatrix} \begin{bmatrix} x_1 \\ x_2 \end{bmatrix} + \begin{bmatrix} 1 & 0 \\ 0 & 1 \end{bmatrix} \upsilon$$

$$y_1 = \begin{bmatrix} 1 & 0 \end{bmatrix} \begin{bmatrix} x_1 \\ x_2 \end{bmatrix}$$

is controllable and observable and satisfies the relation in Equation 5.5.9; therefore, it is pole assignable. Indeed, any eigenvalues of the system with control $\upsilon = -F_1 y_1 = -(f_1, f_2)^T x_1$

$$\begin{bmatrix} \dot{x}_1 \\ \dot{x}_2 \end{bmatrix} = \begin{bmatrix} f_1 & -1 \\ 1+f_2 & 0 \end{bmatrix} \begin{bmatrix} x_1 \\ x_2 \end{bmatrix}$$

may be assigned by a proper choice of coefficients f_1 and f_2.

5.6. Control of Time-Varying Systems

Design of desired dynamics of time-varying control systems is a considerably more difficult task than that for the systems with constant parameters, because the properties of time-varying systems cannot be interpreted in terms of their eigenvalues. Decoupling system motions into motions of lower dimension enables one to simplify the control design. Therefore, it is of interest to apply sliding mode control methodology to reduce the order of the motion equations. We will follow the so-called "block control principle" [Drakunov et al. 1990] for reducing the original design problem to a set of independent problems with lower dimensions.

In time-varying system

$$\dot{x} = A(t)x + B(t)u, \quad x \in \Re^n, \quad u \in \Re^m, \quad \text{rank}(B) = m, \tag{5.6.1}$$

let the elements of $A(t)$ and $B(t)$ be bounded with time derivatives of proper orders. Similar to Equations 5.1.1 and 5.1.2, it is assumed that matrix $B(t)$ may be represented in the form

$$B(t) = \begin{bmatrix} B_1(t) \\ B_2(t) \end{bmatrix} \text{and } \det(B_2(t) \neq 0 \text{ for any } t.$$

The nonsingular coordinate transformation

$$\begin{bmatrix} \dot{x}_1 \\ \dot{x}_2 \end{bmatrix} = TAT^{-1} \begin{bmatrix} x_1 \\ x_2 \end{bmatrix} + T \begin{bmatrix} B_1 \\ B_2 \end{bmatrix} u + \dot{T}T^{-1} \begin{bmatrix} x_1 \\ x_2 \end{bmatrix}$$
$$\begin{bmatrix} x_1 \\ x_2 \end{bmatrix} = Tx, \quad T = \begin{bmatrix} I_{n-m} & -B_1 B_2^{-1} \\ 0 & B_2^{-1} \end{bmatrix}, \tag{5.6.2}$$

reduces the system Equations 5.6.1 to the regular form consisting of two blocks:

$$\begin{aligned} \dot{x}_1 &= A_{11}x_1 + A_{12}x_2 \\ \dot{x}_2 &= A_{21}x_1 + A_{22}x_2 + u, \end{aligned} \tag{5.6.3}$$

where $x_1 \in \Re^{(n-m)}$, $x_2 \in \Re^m$, and A_{ij} are time-varying matrices ($i,j = 1, 2$).

The state vector x_2 of the second block in Equation 5.6.3 is handled as control for the first block. x_2 should be selected as a function of the state vector x_1 to shape the desired dynamics of the first block. We will confine our choice to linear functions with time-varying gains

$$x_2 = -C(t)x_1, \quad C(t) \in \Re^{m \times (n-m)}. \tag{5.6.4}$$

Shaping desired dynamics of the system

$$\dot{x}_1 = (A_{11} - A_{12}C)x_1$$

in accordance with some performance criterion is reduced to design of the linear time-varying system of the $(n - m)$th order with the feedback matrix $C(t)$. This task is easier than the original one of nth order with control u being a linear function of the full state vector $x^T = [x_1^T \; x_2^T]$.

If the matrix $C(t)$ is found, then discontinuous control enforcing sliding mode in the manifold

$$s = x_2 + C(t)x_1 = 0, \; s^T = (s_1, s_2, \ldots, s_m) \tag{5.6.5}$$

should be designed. The equation of the motion projection on subspace s in the system with control

$$u = -\left(\alpha(|x_1| \; + \; |x_2|) + \delta\right)\text{sign}(s)$$

is of form

$$\dot{s} = (CA_{11} + A_{21} + \dot{C})x_1 + (CA_{12} + A_{22})x_2 - \big(\alpha(|x_1| + |x_2|) + \delta\big)\text{sign}(s),$$

where α and δ are positive constants. The coefficient α may be found such that, for any positive δ, the conditions in Equation 2.4.1 hold for any function s_i. Then sliding mode exists on each plane $s_i = 0$ and their intersection $s = 0$.

Although design of desired dynamics in sliding mode is easier than for the original system, we deal with a time-varying system, and special methods should be used for stabilization. We will discuss one of them resulting in exponentially stable time-varying systems.

The idea of the design procedure is to decouple the first system in Equation 5.6.3 with intermediate control x_2 into two subsystems similarly to transformation in Equation 5.6.2 applied to the original system. If $m \le n - m$ and rank $(A_{12}) = m$, then the first system in Equation 5.6.3 may be transformed into

$$\begin{aligned} \dot{x}_1' &= A_{11}'x_1' + A_{12}'x_1'' \\ \dot{x}_1'' &= A_{21}'x_1' + A_{22}'x_1'' + x_2, \quad x_1' \in \Re^{n-2m}, \quad x_1'' \in \Re^m, \end{aligned} \tag{5.6.6}$$

where

$$\begin{bmatrix} x_1' \\ x_1'' \end{bmatrix} = T_1 x_1, \quad T_1 = \begin{bmatrix} I_{n-2m} & -B_1'(B_2'')^{-1} \\ 0 & (B_2'')^{-1} \end{bmatrix}, \quad A_{12} = \begin{bmatrix} B_1' \\ B_2' \end{bmatrix}, \quad \det(B_2') \neq 0. \tag{5.6.7}$$

Vector x_1'' in the first subsystem of Equation 5.6.7 is handled as control, and it is assumed that $\text{rank}(A_{12}') = n - 2m$. Then for any matrix $A_1(t)$

$$\dot{x}_1' = A_1 x_1' \tag{5.6.8}$$

if

$$x_1'' = -C_1(t)x_1', \tag{5.6.9}$$

where $C_1 = (A_{12}')^+(A_{11}' - A_1)$ with $(A_{12}')^+$ being the pseudoinverse to A_{12}':

$$A_{12}'(A_{12}')^+ = I_{n-2m}.$$

The condition in Equation 5.6.9 holds if

$$s_1 = x_1'' + C_1(t)x_1' \tag{5.6.10}$$

tends to zero. The equation for s_1 is derived from Equations 5.6.6 and 5.6.9,

$$\dot{s}_1 = S'x_1' + S''x_1'' + x_2$$

with matrices S' and S'' depending on the elements of Equations 5.6.6 and 5.6.9 and their time derivatives.

For any matrix $A_2(t)$,

$$\dot{s}_1 = A_2 s_1 \tag{5.6.11}$$

if

$$x_2 = A_2 s_1 - S' x_1' - S'' x_1''. \tag{5.6.12}$$

Because vectors x_1, x_1', x_1'' and s_1 are correlated through nonsingular transformations in Equations 5.6.7 and 5.6.9, Equation 5.6.12 may be presented as

$$x_2 = -C(t)x_1, \tag{5.6.13}$$

with $C(t)$ depending on the matrices A and B in the original systems in Equation 5.6.1, their time derivatives, and matrices A_1 and A_2.

The condition in Equation 5.6.13 holds if control u in Equation 5.6.1 is designed as a discontinuous function of the state enforcing sliding mode in the manifold

$$s = x_2 + C(t)x_1 = 0.$$

The above design procedure with control

$$u = -\left(\alpha(|x_1| + |x_2|) + \delta\right)\text{sign}(s)$$

is applicable for this task. After sliding mode in $s = 0$ occurs, the conditions in Equations 5.6.12 and 5.6.13 hold and s_1 will be governed by autonomous Equation 5.6.11. As follows from the first equation of Equation 5.6.6 and 5.6.8 through 5.6.10,

$$\dot{x}_1' = A_1 x_1' + A_{12}' s. \tag{5.6.14}$$

The system dynamics in sliding mode are determined by differential Equations 5.5.11 and 5.6.14 or by matrices A_1 and A_2, which may be selected by the designer. For example, they may be assigned constant with spectra such that exponential convergence at the desired rate is provided.

Generalization of the design method for the cases $\text{rank}(A_{12}) < m$ and $\text{rank}(A_{12}') < n - 2m$ may be found in the work by Drakunov et al. [1990]. It is shown there that exponential stability of sliding mode may be provided for controllable time-varying systems.

References

Ackermann J. 1992. *Sampled-Data Control Systems*. Berlin: Springer-Verlag.

Ackermann J, Utkin V. 1998. "Sliding Mode Control Design Based on Ackermann's Formula." *IEEE Trans Automatic Control* 43: 234–237.

Drakunov SV, Izosimov DB, Luk'yanov AG, Utkin VA, Utkin VI. 1990. "Block Control Principle I." *Automation Remote Control* 51:601–609.

Drazenovic B. 1969. "The Invariance Conditions in Variable Structure Systems." *Automatica* 5:287–295.

Kimura H. 1975. "Pole Assignment by Gain Output Feedback." *IEEE Trans Automatic Control* 20:509–516.

Kortuem W, Lugner P. 1994. *Systemdynamik und Regelung von Fahrzeugen. Einfuehrung und Beispiele.* Berlin: Springer-Verlag.

Kwakernaak H, Sivan R. 1972. *Linear Optimal Control Systems*. New York: Interscience.

Utkin V, Young K-KD. 1978. "Methods for Constructing Discontinuity Planes in Multidimensional Variable Structure Systems." *Automation Remote Control 39:1466–1470.*

6

Sliding Mode Observers

All design methods of the previous chapters, except for Section 5.5, were developed under the assumption that the state vector is available. In practice, however, only a part of its components may be measured directly. The output feedback sliding mode control method of Section 5.5 is applicable to rather limited types of systems. An alternative approach is designing asymptotic observers, which are dynamic systems for estimating all the components of the state vector using those measured directly. First, we will study the conventional full-order and reduced order observers intended for linear time-invariant systems Next, we present sliding mode modifications for state observation of time-invariant [Utkin 1992] and time-varying systems with disturbance estimation [Hashimoto et al. 1990].

6.1. Linear Asymptotic Observers

The idea underlying observer design methods may be illustrated for a linear time-invariant system (Equation 5.1.1) as shown:

$$\dot{x} = Ax + Bu \tag{6.1.1}$$

with output vector

$$y = Cx,\ y \in \Re^l,\ C = const,\ \text{rank}(C) = l. \tag{6.1.2}$$

The pair (C, A) is assumed to be observable.

A linear asymptotic observer is designed in the same form as the original system (Equation 6.1.1) with an additional input depending on the mismatch between the real (Equation 6.1.2) and estimated values of the output vector:

$$\dot{\hat{x}} = A\hat{x} + Bu + L(C\hat{x} - y), \tag{6.1.3}$$

where $\hat{x}$ is an estimate of the system state vector, $L \in \Re^{n\times l}$ is an input matrix.

Of course the state vector of the observer $\hat{x}$ is available because the auxiliary dynamic system is implemented in a controller. The motion equation with respect to mismatch $\overline{x} = \hat{x} - x$ is of form

$$\dot{\overline{x}} = (A + LC)\overline{x}. \tag{6.1.4}$$

The behavior of the mismatch governed by homogenous Equation 6.1.4 is determined by eigenvalues of matrix $A + CL$. For observable systems, they may be assigned arbitrarily by a proper choice of input matrix L [Kwakernaak and Sivan 1972]. It means that any desired rate of convergence of the mismatch to zero or estimate $\hat{x}(t)$ to state vector $x(t)$ may be provided. Then any full state control algorithms with vector $\hat{x}(t)$ are applicable.

The order of the observer may be reduced because of the fact that rank(C) = l and the observed vector may be represented as

$$y = C_1 x_1 + C_2 x_2, \quad x^T = [x_1^T \; x_2^T], \quad x_1 \in \Re^{n-l}, \quad x_2 \in \Re^l, \quad \det(C_2) \neq 0.$$

It is sufficient to only design an observer for vector x_1, whereas the components of vector x_2 are calculated as

$$x_2 = C_2^{-1}(y - C_1 x_1). \tag{6.1.5}$$

Write the equation of the system in Equations 6.1.1 and 6.1.2 in space (x_1, y),

$$\begin{aligned} \dot{x}_1 &= A_{11} x_1 + A_{12} y + B_1 u \\ \dot{y} &= A_{21} x_1 + A_{22} y + B_2 u, \end{aligned} \tag{6.1.6}$$

where $TAT^{-1} = \begin{bmatrix} A_{11} & A_{12} \\ A_{21} & A_{22} \end{bmatrix}$, $TB = \begin{bmatrix} B_1 \\ B_2 \end{bmatrix}$, $T = \begin{bmatrix} I_{n-l} & 0 \\ C_1 & C_2 \end{bmatrix}$ (the coordinate transformation is nonsingular, $\det(T) \neq 0$). The design of a reduced order observer rests on coordinate transformation

$$x' = x_1 + L_1 y, \tag{6.1.7}$$

and the system behavior is considered in the space (x', y). The coordinate transformation is obviously nonsingular for any L_1. The equation with respect to x' is obtained from Equations 6.1.5 through 6.1.7:

$$\begin{aligned} \dot{x}' &= (A_{11} + L_1 A_{21}) x' + A'_{12} y + (B_1 + L_1 B_2) u, \\ A_{12}' &= A_{12} L_1 + L_1 A_{22} - (A_{11} + L_1 A_{21}) L_1. \end{aligned}$$

The observer is designed in the form of a dynamic system of the ($n - l$)th order

$$\dot{\hat{x}}' = (A_{11} + L_1 A_{21}) \hat{x}' + A'_{12} y + (B_1 + L_1 B_2) u, \tag{6.1.8}$$

with $\hat{x}'$ as an estimate of the state vector x'. The mismatch $\bar{x}' = \hat{x}' - x'$ is governed by

$$\dot{\bar{x}}' = (A_{11} + L_1 A_{21}) \bar{x}'. \tag{6.1.9}$$

Again, if the original system is observable, the eigenvalues of matrix $A_{11} + L_1 A_{21}$ may be assigned arbitrarily [Kwakernaak and Sivan 1972]. It means that $\bar{x}'$ tends to zero and $\hat{x}'$ tends to x' at any desired rate. The components of the state vector x_1 and x_2 are thus found from Equations 6.1.5 and 6.1.7.

6.2. Observers for Linear Time-Invariant Systems

Let us proceed to the design of a state observer with inputs as discontinuous functions of mismatches in which motion preceding sliding mode and motion in the intersection of discontinuity surfaces may be handled independently. The observer is described by differential equations

$$\begin{aligned} \dot{\hat{x}}_1 &= A_{11}\hat{x}_1 + A_{12}\hat{y} + B_1 u + L_1 v \\ \dot{\hat{y}} &= A_{21}\hat{x}_1 + A_{22}\hat{y} + B_2 u - v, \end{aligned} \tag{6.2.1}$$

where $\hat{x}_1$ and $\hat{y}$ are the estimates of the system state,

$$v = M\text{sign}(\hat{y} - y), \quad M > 0, \quad M = \text{const.}$$

The vectors $\hat{x}_1$, $\hat{y}$, and, therefore, $\hat{y} - y$ are measured.

The discontinuous vector function $\nu \in \Re^l$ is chosen such that sliding mode is enforced in the manifold $\bar{y} = \hat{y} - y = 0$ and the mismatch between the output vector y and its estimate $\hat{y}$ is reduced to zero. A matrix L_1 must be found such that the mismatch $\bar{x}_1 = \hat{x}_1 - x_1$ between x_1 and its estimate $\hat{x}_1$ decays at the desired rate. Equations with respect to $\bar{x}_1$ and $\bar{y}$ are obtained from Equations 6.1.6 and 6.2.1:

$$\begin{aligned} \dot{\bar{x}}_1 &= A_{11}\bar{x}_1 + A_{12}\bar{y} + L_1 v \\ \dot{\bar{y}} &= A_{21}\bar{x}_1 + A_{22}\bar{y} - v, \\ v &= M \cdot \text{sign}(\bar{y}). \end{aligned} \tag{6.2.2}$$

As shown in Section 2.4, the sliding mode is enforced in the manifold $\bar{y} = 0$ if the matrix multiplying ν in the second equation of Equation 6.2.2 is negative definite and M takes high but finite value. It is the case for our system because ν is multiplied by a negative identity matrix. Hence, for bounded initial conditions, sliding mode can be enforced in manifold $\bar{y} = 0$. As follows from the equivalent control methods, the solution ν_{eq} to equation $\dot{\bar{y}} = 0$ should be substituted into the first equation of Equation 6.2.2 with $\bar{y} = 0$ to derive the sliding mode equation

$$\begin{aligned} v_{eq} &= A_{21}\bar{x}_1 \\ \dot{\bar{x}}_1 &= (A_{11} + L_1 A_{21})\bar{x}_1, \end{aligned} \tag{6.2.3}$$

which coincides with Equation 6.1.9. Hence, the desired rate of convergence of $\bar{x}_1$ to zero and convergence of $\hat{x}_1$ to x_1 can be provided by a proper choice of matrix L_1, and then x_2 is found from Equation 6.1.5.

The observer with the input as a discontinuous function of the mismatch (Equation 6.2.2) in sliding mode is equivalent to the reduced order observer (Equation 6.1.8). However, if the plant and observed signal are affected by noise, the nonlinear observer may happen to be preferable as a result of filtering properties because its structure coincides with that of a Kalman filter [Drakunov 1983].

6.3. Observers for Linear Time-Varying Systems

6.3.1. Block-Observable Form

For time-varying system

$$\dot{x} = A(t)x + B(t)\ u \tag{6.3.1}$$

$$y = C(t)x, \tag{6.3.2}$$

where $x \in \Re^n$, $u \in \Re^m$, $y \in \Re^l$, the output vector $y(t)$ and matrices $A(t)$, $B(t)$, and $C(t)$ are assumed to be known. An observer is to be designed to estimate the state vector $x(t)$.

For any nonsingular transformation of the state x into (y_o^T, x_1^T), $y_o \in \Re^{l_0}$, $x_1 \in \Re^{n-l_0}$, Equation 6.3.1 is represented as follows:

$$\dot{y}_0 = A_{00}(t)y_o + A_{01}^*(t)x_1 + B_0(t)u \tag{6.3.3}$$

$$\dot{x}_1 = A_{10}^*(t)y_o + A_{11}^*(t)x_1 + B_1^*(t)u. \tag{6.3.4}$$

The system in Equations 6.3.3 and 6.3.4 with known vector y_0 is called the "block-observable form." Superscripts and subscripts in Equations 6.3.3 and 6.3.4 denote block matrices of the transformed system matrices A, B in Equation 6.3.1. The system in Equations 6.3.1 and 6.3.2 can be represented in block-observable form, if the rank l_0 and the principle minor position of the time-varying matrix $C(t)$ do not vary in time. In this case, after reordering vectors x and y, there exists $(l - l_0) \times l_0$ matrix $\Lambda_0(t)$ such that

$$C(t) = \begin{bmatrix} C_0(t) \\ \Lambda_0(t)C_0(t) \end{bmatrix}, \quad \text{rank}C_0(t) = l_0,$$

and $l_0 \times n$ matrix $C_0(t)$ is of the form

$$C_o(t) = [C_0'(t)\ \ C_0''(t)]$$

with nonsingular $l_0 \times l_0$ matrix $C_0''(t)$. Vector y_0 is found as

$$y_0 = C_o(t)x = C_0'(t)x_1 + C_0''(t)\, x_1^*,$$

where $x^T = [x_1^T \;\; x_1^{*T}]$ is transformed into $[y_o^T \;\; x_1^T]$

$$\begin{bmatrix} y_0 \\ x_1 \end{bmatrix} = T_0 \begin{bmatrix} x_1 \\ x_1^* \end{bmatrix} = \begin{bmatrix} C_0'' & C_0'' \\ I_{n-l_0} & 0 \end{bmatrix} \begin{bmatrix} x_1 \\ x_1^* \end{bmatrix}, \quad \det(T_0) \neq 0 \tag{6.3.5}$$

The output Equation 6.3.2 is written as

$$y = \begin{bmatrix} C_0 \\ \Lambda_0 C_0 \end{bmatrix} x = \begin{bmatrix} C_0 \\ \Lambda_0 C_0 \end{bmatrix} \begin{bmatrix} x_1 \\ x_1^* \end{bmatrix} = \begin{bmatrix} y_0 \\ \Lambda_0 y_0 \end{bmatrix} = \begin{bmatrix} I_{l_0} \\ \Lambda_0 \end{bmatrix} y_0,$$

where I_{l_0} is an identity matrix. Vector y_0 consists of linearly independent components of vector y, and the system can be transformed to the block-observable form using Equation 6.3.5.

The above procedure leads to block-observable forms for $0 < l_0 < n$. The $l_0 = 0$ case implies that the original system is unobservable (under the assumption that the position of the principle minor does not vary in time). For $l_0 = n$, the state vector may be obtained directly as a solution of the equation $y = C(t)x$.

Treating vector $A_{01}^*(t)x_1$ in Equation 6.3.3 as an output vector of the subsystem in Equation 6.3.4 and assuming that the rank and position of the principle minor of the matrix $A_{01}^*(t)$ do not vary in time, the subsystem in Equation 6.3.3 can be represented in block-observable form. The rank of $A_{01}^*(t)$ is equal to l_1 $(0 \le l_1 \le l_0)$. There exists $(l_0 - l_1) \times l_1$ matrix $\Lambda_1(t)$ such that

$$A_{01}^*(t) = \begin{bmatrix} C_1(t) \\ \Lambda_1(t)C_1(t) \end{bmatrix}$$
$$\text{rank} A_{01}^*(t) = l_1 \quad \text{rank}\; C_1(t) = l_1.$$

$C_1(t)$ is represented as

$$C_1(t) = \left[C_1'(t) \;\; C_1''(t)\right], \quad \det\; C''(t) \neq 0,$$

where $C_1'(t) \in \Re^{l_1 \times (n-l_0-l_1)}$, $C_1''(t) \in \Re^{l_1 \times l_1}$. Then $y_1(t)$ is

$$y_1(t) = C_1(t)x_1 = C_1'(t)x_2 + C_1''(t)x_2^*,$$

where $y_1 \in \Re^{l_1}$, $x_2 \in \Re^{n-l_0-l_1}$, and $x_2^* \in \Re^{l_1}$.

The transformation matrix of $x_1^T = \left(x_2^T, x_2^{*T}\right)$ into $\left(y_1^T, x_2^T\right)$ is

$$\begin{bmatrix} y_1 \\ x_2 \end{bmatrix} = \begin{bmatrix} C_1' & C_1'' \\ I_{n-l_1-l_0} & 0 \end{bmatrix} \begin{bmatrix} x_2 \\ x_2^* \end{bmatrix} = T_1 \begin{bmatrix} x_2 \\ x_2^* \end{bmatrix}, \quad \det(T_1) \neq 0.$$

Applying this transformation to the system in Equation 6.3.4, the following equation is obtained:

$$\begin{bmatrix} \dot{y}_1 \\ \dot{x}_2 \end{bmatrix} = T_1 A_{10}^* y_0 + \left(T_1 A_{11}^* T_1^{-1} + T_1 \dot{T}_1^{-1}\right) \begin{bmatrix} y_1 \\ x_2 \end{bmatrix} + T_1 B_1^* u, \tag{6.3.6}$$

where

$$T_1 A_{10}^* = \begin{bmatrix} A_{10} \\ A_{20}^* \end{bmatrix}, \quad \left(T_1 A_{11}^* T_1^{-1} + T_1 \dot{T}_1^{-1}\right) = \begin{bmatrix} A_{11} & A_{12}^* \\ A_{21}^* & A_{22}^* \end{bmatrix},$$
$$T_1 B_1^* = \begin{bmatrix} B_1 \\ B_2^* \end{bmatrix}.$$

Equation 6.3.6 is rewritten as

$$\dot{y}_1 = A_{10}(t) y_o + A_{11}(t) y_1 + A_{12}^*(t) x_2 + B_1(t) u$$
$$\dot{x}_2 = A_{20}^*(t) y_o + A_{21}^*(t) y_1 + A_{22}^*(t) x_2 + B_2^*(t) u.$$

The block in Equation 6.3.3 is rewritten as

$$\dot{y}_0 = A_{00}(t) y_o + A_{01}(t) y_1 + B_0(t) u, \tag{6.3.7}$$

where $A_{01}(t) = \begin{bmatrix} I_{l_1} \\ \Lambda_1(t) \end{bmatrix}$, rank $A_{01}(t) = l_1$.

For $l_1 < n - l_0$, the subsystem in Equation 6.3.4 can be represented in block-observable form again ($l_1 > 0$, otherwise the system in Equations 6.3.1 and 6.3.2 is unobservable). Because after each step the dimension of x_i is less than that of x_{i-1}, the procedure terminates after a finite number of steps.

Recall that the procedure is implementable if, in the block-observable form of the ith subsystem

$$\dot{y}_i = \sum_{j=0}^{i} A_{i,j}(t) y_j + A_{i,i+1}^*(t) x_{i+1} + B_i(t) u$$
$$\dot{x}_{i+1} = \sum_{j=0}^{i} A_{i,j}^*(t) y_j + A_{i+1,i+1}^*(t) x_{i+1} + B_{i+1}^*(t) u, \tag{6.3.8}$$

the rank and the position of the principle minor of the matrix $A^*_{i,i+1}(t)$ do not vary in time.

Finally, this procedure terminates after r steps and $y_r = C_r x_r = C''_r x^*_{r+1}$ $(x_{r+1} = 0)$. The rth subsystem is written as

$$\begin{aligned}\dot{y}_r &= A_{r0}(t)y_o + A_{r1}(t)y_1 + \cdots + A_{rr}(t)y_r + A^*_{r,r+1}(t)x_{r+1} + B_r u \\ &= \sum_{j=0}^{r} A_{r,j}(t)y_j + B_r(t)u.\end{aligned}$$

Similar to Equations 6.3.3 and 6.3.7, $A^*_{i,i+1}(t)x_{i+1}$ in Equation 6.3.8 may be replaced by $A_{i,i+1}(t)y_{i+1}$ as follows:

$$\dot{y}_i = A_i(t)y^*_i + A_{i,i+1}(t)y_{i+1} + B_i(t)u \quad (i = 1,\ldots,r-1) \tag{6.3.9}$$

$$\dot{y}_r = A_r(t)y^*_r + B_r(t)u, \tag{6.3.10}$$

where $A_i(t) = (A_{i1}, A_{i2}, \cdots, A_{ii})$, $y^{*T}_i = (y^T_0, y^T_1, \cdots, y^T_i)$, $y_i \in \Re^{l_i}$, rank $A_{i,i+1}(t) = l_{i+1}$, and $A_{i,i+1}$ is a full rank matrix. Then the system in Equations 6.3.9 and 6.3.10 is represented as a set of block observable forms,

$$\frac{d}{dt}\begin{bmatrix} y_0 \\ y_1 \\ y_2 \\ \vdots \\ \vdots \\ y_r \end{bmatrix} = \begin{bmatrix} A_{00} & A_{01} & 0 & 0 & \cdots & 0 \\ A_{10} & A_{11} & A_{12} & 0 & \cdots & 0 \\ A_{20} & A_{21} & A_{22} & A_{23} & \cdots & 0 \\ \vdots & \vdots & \vdots & \vdots & \ddots & \vdots \\ \vdots & \vdots & \vdots & \vdots & \cdots & A_{r-1,r} \\ A_{r0} & A_{r1} & A_{r2} & A_{r3} & \cdots & A_{rr} \end{bmatrix}\begin{bmatrix} y_0 \\ y_1 \\ y_2 \\ \vdots \\ \vdots \\ y_r \end{bmatrix} + \begin{bmatrix} B_0 \\ B_1 \\ B_2 \\ \vdots \\ \vdots \\ B_r \end{bmatrix} u,$$

with full rank matrices $A_{i,i+1}$.

6.3.2. Observer Design

Using the sliding mode approach, the design procedure for an observer for a time-varying system may be decoupled into r trivial and independent stabilization subproblems. Let the observer equation be of the form

$$\dot{\hat{y}}_i = A_i(t)\hat{y}^*_i + A_{i,i+1}(t)\hat{y}_{i+1} + B_i(t)u + v_i \quad (i = 0,\ldots,r-1), \tag{6.3.11}$$

$$\dot{\hat{y}}_r = A_r(t)\hat{y}^*_r + B_r(t)u + v_r. \tag{6.3.12}$$

Observer inputs v_i are designed as

$$v_0 = M_0 \text{sign}(y_0 - \hat{y}_0) \tag{6.3.13}$$

$$v_i = M_i \text{sign}(A^+_{i-1,i} z_i), \quad \tau_i \dot{z}_i + z_i = v_{i-1} \quad (i = 1, \ldots, r), \tag{6.3.14}$$

where the left pseudoinverse matrix $A^+_{i-1,i}$ ($A^+_{i-1,i} A_{i-1,i} = I_{l_i}$) exists, because $A_{i-1,i}$ is a full-rank matrix. Equations for mismatches $\tilde{y}_i = y_i - \hat{y}_i$ are

$$\frac{d}{dt}\begin{bmatrix} \overline{y}_0 \\ \overline{y}_1 \\ \overline{y}_2 \\ \vdots \\ \vdots \\ \overline{y}_r \end{bmatrix} = \begin{bmatrix} A_{00} & A_{00} & 0 & 0 & \cdots & 0 \\ A_{10} & A_{11} & A_{12} & 0 & \cdots & 0 \\ A_{20} & A_{21} & A_{22} & A_{23} & \cdots & 0 \\ \vdots & \vdots & \vdots & \vdots & \ddots & \vdots \\ \vdots & \vdots & \vdots & \vdots & \cdots & A_{r-1,r} \\ A_{r0} & A_{r1} & A_{r2} & A_{r3} & \cdots & A_{rr} \end{bmatrix} \begin{bmatrix} \overline{y}_0 \\ \overline{y}_1 \\ \overline{y}_2 \\ \vdots \\ \vdots \\ \overline{y}_r \end{bmatrix} - \begin{bmatrix} v_0 \\ v_1 \\ v_2 \\ \vdots \\ \vdots \\ v_r \end{bmatrix}.$$

For bounded initial conditions and any finite numbers $M_1, \ldots, M_r$ there exists a number such that, after a finite time interval, sliding mode occurs at the manifold $\overline{y}_0 = 0$ because each component of $\tilde{y}_0$ and its time derivative have different signs (Equation 2.4.1). According to the equivalent control method (Section 2.3), the solution of $\dot{\overline{y}}_0 = 0$ with $\overline{y}_0 = 0$

$$(v_0)_{\text{eq}} = [M_0 \text{sign}(\overline{y}_0)]_{eq} = A_{01} \overline{y}_1$$

should be substituted into Equation 6.3.14 to find the sliding mode equation. Then the output of the first-order filter z_1 approaches the equivalent control input v_{0eq}

$$\lim_{\tau_1 \to 0} z_1 = v_{0eq} = A_{01} \overline{y}_1 \text{ and } \overline{y}_1 = \lim_{\tau_1 \to 0} A^+_{01} z_1.$$

Similarly, $\overline{y}_2$can be found from the second block (subsystem with respect to $\overline{y}_1$)

$$\overline{y}_2 = \lim_{\tau_2 \to 0} A^+_{12} z_2$$

Consequently, sliding mode will occur at each block, and then all the subvectors $\overline{y}_1, \ldots, \overline{y}_r$ will converge to zero. Because $y_i = \hat{y}_i + \overline{y}_i$ $(i = 1, \ldots, r)$, all subvectors of the state vector $(y_1, \ldots, y_r)$ and correspondingly x will be found.

Remarks 6.1

1. The procedure is invariant with respect to $l_i \times (l_r + \ldots + l_i)$ matrices $A_i(t)$ $i = 0, \ldots, r$.
2. There is no need to enforce sliding mode in the last block because

$$v_{r-1,eq} = A_{r-1,r}(t) \overline{y}_r,$$

and the last subvectors y_r may be found as

$$y_r = \hat{y}_r + A^{+}_{r-1,r}(t)z_r.$$

3. At the presence of an unknown disturbance vector $f(t)$ in the last block

$$\dot{y}_r = A_r(t)y_r + B_r(t)u + f(t),\ \ f(t) \in \Re^{l_r},$$

the mismatch equation is of the form

$$\dot{\overline{y}}_r = A_r(t)\overline{y}_r + f(t) - v_r.$$

After sliding mode occurs in this subsystem, $\overline{y}_r = 0$ and

$$\nu_{req} = f(t) \text{ and } \lim_{\tau_f \to 0} z_f = v_{req} = f(t)$$

if $\tau_f \dot{z}_f + z_f = v_r$.

As a result, the last block enables one to find the equivalent disturbance vector, which includes external disturbances, parameter variations, and nonlinear state functions. This approach is developed in Chapter 8 as one of the methods for chattering suppression.

6.3.3. Simulation Results

As an example of the above observer design, let us consider the following time-varying system:

$$\dot{x} = A(t)x + B(t)\ u + f(t)$$

$$y = C(t)x,$$

where

$$A(t) = \begin{bmatrix} a_{00} & a_{01} & 0 & a_{03} \\ 0 & a_{11} & a_{12} & 0 \\ a_{20} & 0 & 0 & a_{23} \\ 0 & a_{31} & 0 & a_{33} \end{bmatrix},\ B(t) = \begin{bmatrix} b_{00} & 0 \\ 0 & b_{11} \\ 0 & 0 \\ 0 & 0 \end{bmatrix},$$

$$C(t) = \begin{bmatrix} c_{00} & c_{01} & 0 & 0 \\ 0 & c_{11} & 0 & 0 \end{bmatrix},\qquad f(t) = \begin{bmatrix} 0 & 0 & f_2 & f_3 \end{bmatrix}.$$

The elements of the coefficient matrices, the inputs, and the disturbances are as follows:

$$
\begin{aligned}
&a_{00} = -4 \cdot e^{-t} \qquad a_{01} = -2 + \sin(t/2 \\
&a_{11} = -5 \cdot \cos(0.3t) \quad a_{23} = -2 \cdot e^{-t} \\
&a_{31} = -1 - \frac{\sqrt{t+2}}{t+1} \qquad a_{33} = -2 \\
&a_{03} = a_{12} = a_{20} = -1 \\
&b_{00} = -3 \quad b_{11} = -5 \cdot e^{-t/5} \\
&c_{00} = 4 + \sin(t/2) \qquad c_{10} = 2 - e^{-t/5} \\
&c_{11} = -5 + \frac{1}{2}\sin(-0.3t) \\
&u_0 = 5\cos(t), u_1 = -3.
\end{aligned}
$$

For output matrix $C(t)$

$$
\operatorname{rank}\begin{bmatrix} c_{11} & c_{12} \\ 0 & c_{22} \end{bmatrix} = 2, \quad t \in [0, \infty).
$$

The rank and the principle minor position of the time-varying matrix $C(t)$ do not vary in time.

The block-observable form can be easily obtained following the above method,

$$
\frac{d}{dt}\begin{bmatrix} y_0 \\ y_1 \end{bmatrix} = \begin{bmatrix} A_{00} & A_{01} \\ A_{10} & A_{11} \end{bmatrix}\begin{bmatrix} y_0 \\ y_1 \end{bmatrix} + \begin{bmatrix} B_0 \\ B_1 \end{bmatrix} u + \begin{bmatrix} 0 \\ f \end{bmatrix},
$$

where

$$
\begin{aligned}
y_0 &= \begin{bmatrix} c_{00} & c_{01} \\ 0 & c_{11} \end{bmatrix}\begin{bmatrix} x_1 \\ x_2 \end{bmatrix}, \\
y_1 &= \begin{bmatrix} x_3 \\ x_4 \end{bmatrix}.
\end{aligned}
$$

The observer in Equations 6.3.11 through 6.3.14 for our system is the form

$$
\frac{d}{dt}\begin{bmatrix} \hat{y}_0 \\ \hat{y}_1 \end{bmatrix} = \begin{bmatrix} A_{00} & A_{01} \\ A_{10} & A_{11} \end{bmatrix}\begin{bmatrix} \hat{y}_0 \\ \hat{y}_1 \end{bmatrix} + \begin{bmatrix} B_0 \\ B_1 \end{bmatrix} u + \begin{bmatrix} v_0 \\ v_1 \end{bmatrix},
$$

where ν_0 and ν_1 are observer inputs

$$
\begin{aligned}
v_0 &= M_0 \text{sign}(y_0 - \hat{y}_0), \\
v_1 &= M_1 \text{sign}(A_{01}^{-1} z_1) \\
\tau_1 \dot{z}_1 + z_1(t) &= v_0(t) \\
z_1(0) &= 0.
\end{aligned}
$$

Simulations were performed for two cases.

6.3.4. Case 6.1: The System with Zero Disturbances

The initial value of system states are given by

$$
\begin{aligned}
x_0(0) = 5, \quad x_1(0) = 5, \\
x_2(0) = 5, \quad x_3(0) = 5
\end{aligned}.
$$

Because the disturbance is assumed to be zero, only the state estimation is considered. The initial values of the observer state are equal to zero.

Because the sampling interval T_s confines the switching frequency, the filter constant τ_1, which must theoretically approach zero, is selected as $4T_s$. The sampling interval is 100μs.

Figures 6.1.A and 6.1.B depict both the system states $x_2(t)$, $x_3(t)$ and the outputs $\hat{x}_2(t)$, $\hat{x}_3(t)$ of the sliding mode observer. As can be viewed from the figure, the estimated states converge to the real states rapidly. The gain matrices M_0 and M_1 are

$$
M_0 = \begin{bmatrix} 5 & 0 \\ 0 & 5 \end{bmatrix}, \quad M_1 = \begin{bmatrix} 10 & 0 \\ 0 & 10 \end{bmatrix}.
$$

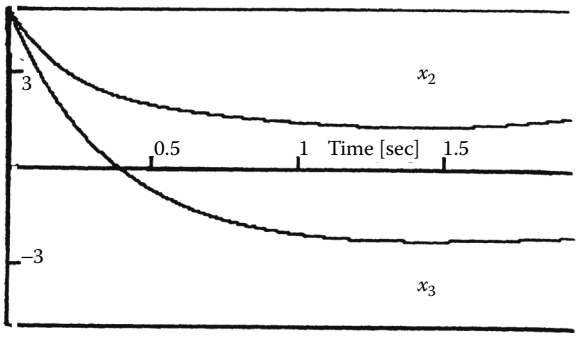

FIGURE 6.1.A
Real system state values.

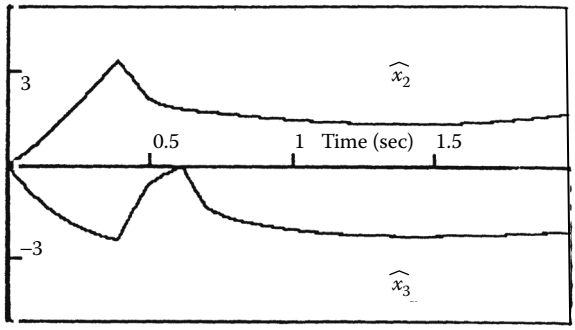

FIGURE 6.1.B
Estimated system state.

6.3.5. Case 6.2: The System with Disturbances

Because the unknown disturbances f_2, f_3 are to be estimated, the additional filter is introduced (see Remark 6.1, item 3):

$$\tau_f \dot{z}_f + z_f(t) = v_1(t),$$
$$z_f(0) = [0\ 0]^T.$$

The estimated disturbance is the output of the above filter

$$\hat{f}(t) = z_f(t), \hat{f}(t)^T = [\hat{f}_2(t)\ \ \hat{f}_3(t)].$$

The time constant τ_1 is chosen to be 500 μsec. Other conditions for simulation are the same as in Case 6.1.

By observing the estimation response from Figures 6.2.A and 6.2.B, it can be concluded that the unknown disturbances can be found by the sliding mode observer.

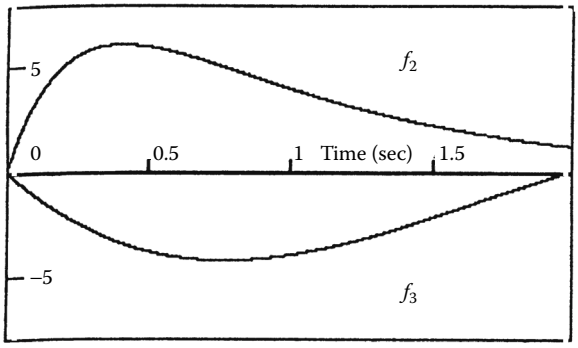

FIGURE 6.2.A
Real disturbances.

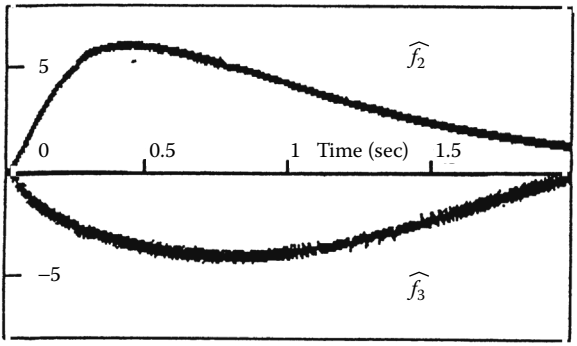

FIGURE 6.2.B
Estimated disturbances.

6.4. Observer for Linear Systems with Binary Output

As long as a linear system with an output as a linear function of the state is observable, the state variables can be estimated using conventional observers, although robustness to disturbance and modeling uncertainty need to be considered further. However, the conventional observer approach is not feasible when a binary sensor limits output information to the sign of the output. An example is the oxygen sensor of an air/fuel ratio control system for internal combustion engines. Its reading indicates only whether the control output is higher or lower than the desired value.

A design methodology for such systems was developed by Drakunov and Utkin [1995] and Kim, Rizzoni, and Utkin [1998]. The two-stage observer was proposed to consist of a discrete time-varying observer to estimate the states at each sensor switching instant and of a continuous system to estimate the state trajectory between the switching instants. Generally speaking, the observer equations are time varying, and the conventional eigenvalue placement methodology is not applicable. The observer design approach described below overcomes this difficulty and guarantees convergence.

6.4.1. Observer Design

Consider the system

$$\begin{aligned} \dot{x} &= Ax + Bu \\ y &= sign(Cx - b), \end{aligned} \tag{6.4.1}$$

where x is the state, u is the control and y is the scalar output, A, B, and C are constant matrices, and b is a scalar parameter. Let z_k be the state vector

at sensor switching instants and τ_k be the interval between switching instants:

$$\begin{aligned} z_k &= x(t_k) \\ \tau_k &= t_k - t_{k-1} \end{aligned}. \tag{6.4.2}$$

If the z_k values are known exactly for the entire process, the estimation of the states becomes an initial-value problem with known initial conditions: if all the states are available at every sensor switching instants

$$y = z_k, \tag{6.4.3}$$

then estimation of the continuous state variables during the sensor switching interval becomes the initial value problem with the state variables at the switching instant t_k as the initial condition. Consequently, the state trajectory until the next sensor switching instant t_{k+1} can be calculated by

$$x(t) = e^{A(t-\tau_k)}z_k + \int_{t_k}^{t_{k+1}} e^{A(t-\tau)}Bu(\tau)d\tau \quad \text{for } t_k \le t \le t_{k+1}. \tag{6.4.4}$$

However, if information on the z_k values is limited, as is the case with the binary sensor measurement, a discrete observer is needed to estimate the discrete sequence z_k. Then, the continuous states $x(t)$ can be obtained by using the discrete estimation as an initial value during the sensor switching intervals (i.e., the time interval between t_k and t_{k+1}) according to Equation 6.4.4. Now the measurement equation becomes

$$y_k = sign(Cz_k - b). \tag{6.4.5}$$

As mentioned above, the observer design procedure is divided into two steps. The first step consists of estimating the state variables at each switching instant of the binary sensor, i.e., $\hat{z}_k$= estimation of z_k at time t_k. The second step consists of estimating the states between the sensor switching times, i.e., $\hat{x}(t)$is equal to estimation of $x(t)$ for the time interval between t_k and t_{k+1}. This two-step procedure leads to a continuous estimate of the state variables for the entire process.

Using the definition given in Equation 6.4.3, the discrete system (defined only at sensor switching instant) can be expressed as follows:

$$z_k = e^{A\tau_{k-1}}z_{k-1} + \int_{t_{k-1}}^{t_k} e^{A(t_k-\tau)}Bu(\tau)d\tau. \tag{6.4.6}$$

A discrete observer can be designed to estimate the sequence z_k. In this case, the updates of the estimates of these discrete state variables occur in

nonuniformly distributed time intervals (time between t_{k-1} and t_k), which are the intervals between binary sensor switching times. Because at switching instants $Cz_k = b$ for any k, the discrete observer can be constructed in the form

$$\hat{z}_k = e^{A\tau_{k-1}}\hat{z}_{k-1} + \int_{t_{k-1}}^{t_k} e^{A(t-\tau)}Bu(\tau)d\tau + L_{k-1}(C\hat{z}_{k-1} - b), \tag{6.4.7}$$

which results in the equation with respect to mismatch $\overline{z}_k = \hat{z}_k + z_k$, $C\hat{z}_k - b = c\overline{z}_k$

$$\overline{z}_k = (e^{A\tau_{k-1}} + L_{k-1}C)\overline{z}_{k-1} \quad . \tag{6.4.8}$$

Vector L_{k-1} should be selected such that this homogenous system is stable with the desired rate of convergence. The selection of the gain for this type of observer is not a trivial task because the system in question is time varying (because the sensor switching interval τ varies in time) and the conventional approach based on eigenvalue placement is not applicable. The observer design will be illustrated for the second-order system with $C = (1,0)$, $L_k^T = (l_{1k}, l_{2k})$ in Equation 6.4.8:

$$\begin{aligned}\overline{z}_{1k} &= (a_{11k-1} + l_{1k-1})\overline{z}_{1k-1} + a_{12k-1}\overline{z}_{12k-1}\\ \overline{z}_{2k} &= (a_{21k-1} + l_{2k-1})\overline{z}_{1k-1} + a_{22k-1}\overline{z}_{12k-1}\end{aligned},$$

where a_{ijk-1} are elements of matrix $e^{A\tau_{k-1}}$, $a_{12k-1} \neq 0$ –sufficient observability condition.

Coordinate transformation

$$s_k = \alpha_k\overline{z}_{1k} + \overline{z}_{2k},\ \alpha_k = {q - a_{22k-1}}\Big/{a_{12k-1}},\ |q| < 1$$

results in

$$\overline{z}_{1k} = (a_{11k-1} + l_{1k-1} - \alpha_{k-1}a_{12k-1})\overline{z}_{1k-1} + a_{12k-1}s_{k-1}$$

$$s_k = [\alpha_k(a_{11k-1} + l_{1k-1} - \alpha_{k-1}a_{12k-1}) + a_{21k-1} + l_{2k-1} - \alpha_{k-1}a_{22k-1}]\overline{z}_{1k-1} + qs_{k-1}.$$

For

$$l_{1k-1} = r - a_{11k-1} + \alpha_{k-1}a_{12k-1},\ |r| < 1,\ r = const$$

and

$$l_{2k-1} = -\alpha_k(a_{11k-1} + l_{1k-1} - \alpha_{k-1}a_{12k-1}) - a_{21k-1} + \alpha_{k-1}a_{22k-1},$$

the observer motion is governed by

$$\bar{z}_{1k} = r\bar{z}_{1k-1} + a_{12k-1}s_{k-1}$$
$$s_k = qs_{k-1}.$$

Since $\lim s_k = 0$ and $\lim \bar{z}_{1k} = 0$ with $k \to \infty$, the state of the observer tends to the system state with the desired rate defined by q and r. In the second stage, the state values are found for any time between switching instants following Equation 6.4.4.

Remark 6.2

A similar methodology can be applied to systems with delayed binary observation:

$$\dot{x}(t) = Ax(t) + Bu(t)$$
$$y(t) = sign[Cx(t-\theta) - b], \ \theta = const > 0.$$

Design of the observer for the system

$$\dot{x}(t-\theta) = Ax(t-\theta) + Bu(t-\theta)$$
$$y(t) = sign[Cx(t-\theta) - b]$$

is identical to Equation 6.4.1 with t replaced by $t - \theta$; therefore, the observer proposed in this section can be used to find the value of $x(t - \theta)$. Finally, the convolution equation

$$x(t) = e^{A\theta}x(t-\theta) + \int_{t-\theta}^{t} e^{A(t-\tau)}Bu(t-\tau)d\tau$$

can be used for calculating the current value of the state vector.

References

Drakunov S. 1983. "On Adaptive Quasi-optimal Filter with Discontinuous Parameters." *Automation Remote Control* 44:1167–1175.

Drakunov S, Utkin V. 1995. "Discrete Event Sliding Mode Observers for Continuous Time Systems." Proceedings of the 34th Conference of Decision and Control, New Orleans, LA.

Hashimoto H, Utkin VI, Jian-Xin X, Suzuki H, Harashima F. 1990. "VSS Observer for Linear Time Varying System." Proceedings of the Industrial Electronics, Control, and Instrumentation Conference, Pacific Grove, CA.

Kim Y-W, Rizzoni G, Utkin VI. 1998. "Automotive Engine Diagnosis and Control via Nonlinear Estimation." *Control Systems* 18:84–89.

Kwakernaak H, Sivan R. 1972. *Linear Optimal Control Systems*. New York: Interscience.

Utkin VI. 1992. *Sliding Modes in Control and Optimization*. London: Springer-Verlag.

7

Integral Sliding Mode

The robustness property of conventional sliding mode control with respect to variations of system parameters and external disturbances can only be achieved after the occurrence of sliding mode. During the reaching phase, however, there is no guarantee for robustness. Integral sliding mode seeks to eliminate the reaching phase by enforcing sliding mode throughout the entire system response. Different from the conventional design approach, the order of the motion equation in integral sliding mode is equal to the order of the original system rather than reduced by the dimension of the control input. As a result, robustness of the system can be guaranteed starting from the initial time instant. Uniform formulations of this new sliding mode design principle will be developed in this chapter. It is shown with examples that this generalized scheme of integral sliding mode enables a wide scope of application areas, including control in robotics and electric drives. The concept of integral sliding mode can also be extended to construct a new type of perturbation estimator that solves the chattering problem without loss of robustness and control accuracy. Additional details on integral sliding mode can be found in the work of Utkin and Shi [1996].

7.1. Motivation

Sliding mode plays a dominant role in variable structure systems (VSS) theory. The core idea of designing VSS control algorithms consists of enforcing sliding mode in some manifold of state space. Traditionally, these manifolds are constructed as the intersection of hyper-surfaces in the state space. This intersection domain is normally called switching manifold. Once the system reaches the switching plane, the structure of the feedback loop is adaptively altered to slide the system state along the switching plane; the system response depends thereafter on the gradient of the switching plane and remains insensitive to variations of system parameters and external disturbances under so-called matching conditions (Section 3.3). The order of the motion equation in sliding mode is equal to $(n - m)$, with n being the dimension of the state space and m the dimension of the control input. However, during the reaching phase, i.e., before sliding mode occurs, the system possesses no such insensitivity property; therefore, insensitivity can not be ensured throughout an entire response.

As an extension of traditional sliding mode schemes, the concept of integral sliding mode concentrates on robustness during the entire response. The order of the motion equation in this new type of sliding mode is equal to the dimension of the plant model. Therefore, sliding mode is established without a reaching phase, implying that the invariance of the system to parametric uncertainty and external disturbances is guaranteed starting from the initial time instant. This chapter generalizes the sliding mode control concept and emphasizes the background philosophy used for developing such new variable structure systems.

We assume that there already exists an ideal system consisting of a nominal plant model and a properly designed feedback control. To this existing controller, a discontinuous term is added based on integral sliding mode to ensure the desired performance despite parametric uncertainty and external disturbances. Design examples in some application areas are given to illustrate the methodology of this design philosophy. The basic idea of integral sliding mode for linear systems can be found in the work of Ackermann and Utkin [1994].

Integral sliding mode may also be used to prevent chattering in a control loop, often caused by controller discontinuities exciting unmodeled dynamics. For chattering prevention, the discontinuous control term is low-pass filtered before being fed to the plant, thus moving the discontinuity to an auxiliary control loop without unmodeled dynamics to be excited. The filtered control acts as a perturbation compensator and preserves the invariance property of sliding mode. The chattering prevention aspect of integral sliding mode is discussed in detail in Section 8.5.

This chapter only deals with uncertainties that satisfy the matching conditions. For systems with unmatched uncertainties, the readers are referred to the work of Cao and Xu [2004] and Castaños and Fridman [2006].

7.2. Problem Statement

For a given dynamic system represented by the following state space equation

$$\dot{x} = f(x) + B(x)u, \tag{7.2.1}$$

with $x \in \Re^n$ being the state vector and $u \in \Re^m$ being the control input vector ($rank\ B(x) = m$), suppose there exists a feedback control law $u = u_0(x)$, normally a continuous control, such that the system in Equation 7.2.1 can be stabilized in a desired way (e.g., its state trajectory follows a reference trajectory with a given accuracy). We denote this ideal closed-loop system as

$$\dot{x}_0 = f(x_0) + B(x_0)u_0, \tag{7.2.2}$$

where x_0 represents the state trajectory of the ideal system under control u_0. However, in practical applications, the system in Equation 7.2.1 operates under uncertainty conditions that may be generated by parameter variations, unmodeled dynamics, and external disturbances. Under this consideration, the real trajectory of the closed-loop control system may be summarized by

$$\dot{x} = f(x) + B(x)u + h(x,t), \tag{7.2.3}$$

in which vector $h(x,t)$ comprises the perturbation attributable to parameter variations, unmodeled dynamics, and external disturbances and is assumed to fulfill the matching condition (see Section 3.4)

$$h(x,t) \in \text{span}\{B(x)\}, \tag{7.2.4}$$

or equivalently,

$$h(x,t) = B(x)u_h \text{ with } u_h \in \Re^m. \tag{7.2.5}$$

In other words, control u is assumed to be able to influence all components of vector $h(x,t)$ via control matrix $B(x)$.

Assume that $h(x,t)$ is bounded and an upper bound can be found as

$$\left|h_i(x,t)\right| \le h_i^+(x,t),\ i = 1,\ \ldots,\ n, \tag{7.2.6}$$

with $h_i^+(x,t)$ being known positive scalar functions. The control design challenge thus becomes the following: find a control low $u(x,t)$ such that the trajectories of the system in Equation 7.2.3 satisfy $x(t) \equiv x_0(t)$ starting from the initial time instant, i.e., $x(0) = x_0(0)$.

7.3. Design Principles

For the system in Equation 7.2.3, first redesign the control law to be

$$u = u_0 + u_1, \tag{7.3.1}$$

where $u_0 \in \Re^m$ is the "ideal control" defined in Equation 7.2.2, and $u_1 \in \Re^m$ is designed to reject the perturbation term $h(x,t)$. Substitution of the control law in Equation 7.3.1 into Equation 7.2.3 yields

$$\dot{x} = f(x) + B(x)u_0 + B(x)u_1 + h(x,t). \tag{7.3.2}$$

Furthermore, define a sliding manifold as

$$s = s_0(x) + z, \text{ with } s,\ s_0(x),\ z \in \Re^m, \tag{7.3.3}$$

which consists of two parts: the first part $s_0(x)$ may be designed as a linear combination of the system states, similar to the conventional sliding mode design; the second part z introduces the integral term and will be determined below.

The philosophy of integral sliding mode is as follows: to achieve $x(t) \equiv x_0$ (t) at all time $t > 0$, the equivalent control of u_1, denoted by u_{1eq}, should fulfill

$$B(x)u_{1eq} = -h(x,t), \tag{7.3.4}$$

or, in terms of Equation 7.2.5,

$$u_{1eq} = -u_h. \tag{7.3.5}$$

The equivalent control u_{1eq} accurately describes the system trajectories when sliding along the manifold $s(x) = 0$ in Equation 7.3.3. See also Section 2.3 or the work by Utkin [1992] for details of the mathematical derivation of equivalent control.

To adequately define auxiliary variable $z(x,t)$ in Equation 7.3.3 to achieve Equation 7.3.5, set the time derivative $\dot{s}$ equal to zero,

$$\dot{s} = \dot{s}_0(x) + \dot{z} = \frac{\partial s_0}{\partial x}\left\{ f(x) + B(x)u_0(x) + B(x)u_{1eq}(x) + B(x)u_h \right\} + \dot{z} = 0. \tag{7.3.6}$$

To ensure the requirement in Equation 7.3.5, define

$$\dot{z} = -\frac{\partial s_0}{\partial x}\left\{ f(x) + B(x)u_0(x) \right\},\ z(0) = -s_0(x(0)), \tag{7.3.7}$$

where initial condition $z(0)$ is determined based on the requirement $s(0) = 0$. In other words, sliding mode is to occur starting from the initial time instant. Because Equation 7.3.5 is satisfied, the motion equation of the system in sliding mode will be

$$\dot{x} = f(x) + B(x)u_0(x), \tag{7.3.8}$$

as if the perturbation term $h(x,t)$ did not exist, identical to the ideal system trajectories (Equation 7.2.2).

Definition 7.1: Integral Sliding Mode

A sliding mode is said to be an integral sliding mode if its motion equation is of the same order as the original system (i.e., the order of sliding motion is

equal to n). The control u_1 in Equation 7.3.1 is defined to enforce sliding mode along the manifold (Equation 7.3.3) via discontinuous

$$u_1 = -M(x)\,\text{sign}(s), \tag{7.3.9}$$

where control gain $M(x)$ can be selected as a scalar function or even a constant to simplify the control design. Based on Equations 7.3.3, 7.3.7, and 7.3.9, the time derivative of s can be calculated as

$$\dot{s} = \frac{\partial s_0}{\partial x} B(x) u_h - \frac{\partial s_0}{\partial x} B(x) M(x)\,\text{sign}(s). \tag{7.3.10}$$

In the above equation, s_0 should be selected such that matrix $\frac{\partial s_0}{\partial x} B(x)$ is nonsingular during the entire system response. Then, the control gain $M(x)$ should be selected depending on the property of $\frac{\partial s_0}{\partial x} B(x)$ such that sliding mode is enforced in the manifold $s = 0$ (see Sections 2.5 and 3.2).

7.4. Perturbation and Uncertainty Estimation

A crucial part of the nature of sliding mode control schemes is the control discontinuity. In closed loop, the "switching" in the control action often results in high-frequency oscillations in practical implementations. Fast dynamics, like those of actuators and sensors, which were neglected in the control design process, are excited by the sliding mode control switches, occurring at high but finite frequencies. This phenomenon, common to all high-gain control systems, is referred to as chattering.

Several methods have been presented in the literature to alleviate chattering. The key idea is to limit the controller gain or the controller bandwidth. A detailed discussion of the causes of chattering and the various tools to prevent this phenomenon can be found in Chapter 8. The remainder of this section is devoted to a brief description of using integral sliding mode to design perturbation estimators, rejecting overall system perturbations that satisfy the matching condition, with the chattering level being significantly reduced.

As mentioned above, high-gain controllers are frequently limited by loop dynamics, especially by actuator dynamics preventing direct implementation of sliding mode schemes. Conversely, discontinuous control inputs are often prescribed by the nature of the system, e.g., by conventional pulse width modulation (PWM) units in power electronics. To resolve such seemingly contradictory specifications, recall that the actual effect of a discontinuous controller on a given plant is equal to the average of the control action, the so-called equivalent control (see Section 2.3).

With this in mind, reformulate the integral sliding mode principle in Section 7.3 in terms of a perturbation estimator. Instead of Equation 7.3.1, change the control input to

$$u = u_0 + u_{1eq}. \tag{7.4.1}$$

However, the control in Equation 7.4.1 cannot be implemented directly because the equivalent value of discontinuous control u_1 depends on unknown disturbance $h(x,t)$ in Equation 7.2.3. It was shown in Section 2.4 that the equivalent value of a discontinuous control is equal to the average value measured by a first-order linear filter, with the discontinuous control as its input. The time constant of the filter should be sufficiently fast such that the plant and disturbance dynamics are allowed to pass through the filtering without significant phase lag. Therefore, substitute $u_{1eq} = u_{1av}$ with u_{1av} defined by

$$\mu \dot{u}_{1av} + u_{1av} = u_1, \tag{7.4.2}$$

where the time constant μ should be selected small enough not to distort the slow component of the switched action, equal to u_{1eq}. In most practical applications, the frequency spectrum of perturbation to be compensated for does not overlap with the high-frequency components of the switching unit.

One may be tempted to ask the following: if the discontinuity in the real control path is smoothed, how can sliding mode be generated? Furthermore, does u_{1av} (= u_{1eq}) still cancel the perturbation term u_h? As shown in the sequel, these questions can be answered positively, if the discontinuous control u_1 is shifted from the plant input to the input of an auxiliary dynamic system.

Similar to Equations 7.3.3 and 7.3.7, redesign the switching function

$$s = s_0(x) + z, \tag{7.4.3}$$

with z defined in

$$\dot{z} = -\frac{\partial s_0}{\partial x}\left\{ f(x) + B(x)u - B(x)u_1 \right\},\ z(0) = -s_0(x(0)). \tag{7.4.4}$$

The time derivative of sliding variable s in Equation 7.4.3 can be calculated as

$$\begin{aligned} \dot{s} &= \frac{\partial s_0}{\partial x}\left\{ f(x) + B(x)u + B(x)u_h \right\} - \frac{\partial s_0}{\partial x}\left\{ f(x) + B(x)u - B(x)u_1 \right\} \\ &= \frac{\partial s_0}{\partial x} B(x)u_h + \frac{\partial s_0}{\partial x} B(x)u_1. \end{aligned} \tag{7.4.5}$$

Design the same discontinuous control for u_1 as shown in Equation 7.3.9 and assume that matrix $\frac{\partial s_0}{\partial x} B(x)$ is nonsingular during the entire system response; sliding mode can be enforced in the system using methods given in Sections 2.5 and 3.2.

Solving for u_1 after setting $\dot{s} = 0$ in Equation 7.4.5 reveals that $u_{1eq} = -u_h$ holds as well, implying that u_{1av} $(= u_{1eq})$ is indeed an estimate of the perturbation term u_h. In this case, Equation 7.4.4 can be interpreted as an internal dynamic process for generating sliding mode defined by Equation 7.4.3; discontinuity appears only in the internal process; thus, no chattering is excited in the real control path. Moreover, because u_{1av} cancels the perturbation u_{1h} without precise knowledge of the system model and associated parameters, a high degree of robustness is maintained. The information needed for this control scheme is the upper bound of the perturbation. From a conceptual point of view, integral sliding mode is used here only for estimating the system perturbation rather than for the purpose of control. The control action to the real plant will be continuous and is significantly enhanced by the perturbation compensator.

7.5. Examples

Four application examples will be presented in the following sections. The main content of each section and the significance of each application example are listed in Table 7.1.

TABLE 7.1

Application Examples and Their Significance

Application	Significance of the Application Example
7.5.1. Linear time-invariant systems	Linear time-invariant systems are special case of the proposed general design principle
7.5.2. Control of robot manipulators	Robust control of rigid-body robots under parameter uncertainties
7.5.3. Pulse-width modulation for electric drives	Design philosophy of integral sliding mode can be directly applied to practical systems
7.5.4. Robust current control for permanent-magnet synchronous motors	Version 1 : Robust current control of permanent-magnet synchronous motors Version 2 : Utilization of proposed perturbation estimator to achieve advanced performance

7.5.1. Linear Time-Invariant Systems

Consider a controllable linear time-invariant system with scalar control

$$\dot{x} = Ax + B\big(u + d(x,t)\big), \tag{7.5.1}$$

with state vector $x \in \Re^n$, scalar control $u \in \Re$, known system matrix $A \in \Re^{n\times n}$, $B \in \Re^n$, and $d(x,t)$ being a nonlinear perturbation with known upper bound

$$\left|d(x,t)\right| < d^+(x,t). \tag{7.5.2}$$

Design control u as stated in Equation 7.3.1 as $u = u_0 + u_1$, where u_0 is predetermined such that system $\dot{x} = Ax + Bu_0$ follows a given trajectory with desired accuracy. For example, u_0 may be designed as linear static feedback control $u_0 = -k^T x$, $k \in \Re^{n\times 1}$, in which gain vector k can be determined by pole-placement or linear-quadratic Gaussian methods.

For pole-placement design, Ackermann's formula (Section 5.4) may be used. Assuming that the desired eigenvalues for system $\dot{x} = Ax + Bu_0$ are $\lambda_1, \lambda_2, ..., \lambda_n$, the control gain k^Tcan be determined explicitly depending on Ackermann's formula

$$k^T = \boldsymbol{e}^T P(\boldsymbol{A}), \tag{7.5.3}$$

where $\boldsymbol{e}^T = (0, ..., 0, 1)(B, AB, ..., A^{n-1}B)^{-1}$ and $P(\cdot)$ is the characteristic polynomial of the system, defined by $P(\lambda) = (\lambda - \lambda_1)(\lambda - \lambda_2)...(\lambda - \lambda_{n-1})(\lambda - \lambda_n)$.

According to Equations 7.3.3 and 7.3.7, design the sliding manifold as

$$s = C^T x + z = 0, C \in \Re^n, \tag{7.5.4}$$

with

$$\dot{z} = -C^T\left(Ax + Bu_0\right), \quad z(0) = -C^T x(0). \tag{7.5.5}$$

Particularly, vector $C \in \Re^n$ may be selected to be equal to $B \in \Re^n$, resulting in

$$s = B^T x + z, \tag{7.5.6}$$

and

$$\dot{z} = -B^T Ax - (B^T B)u_0, \quad z(0) = -B^T x(0). \tag{7.5.7}$$

The time derivative of s can be calculated as

$$\dot{s} = (B^T B)\big(u_1 + d(x,t)\big). \tag{7.5.8}$$

Solving for u_1 by formally setting $\dot{s} = 0$ shows that $u_{1eq} = -d(x,t)$. Thus, the motion equation in sliding mode coincides with that of the ideal system $\dot{x} = Ax + Bu_0$ without perturbation $d(x,t)$. Furthermore, because $s(0) = B^T x(0) + z(0) = 0$, sliding mode will occur from the initial time instant $t = 0$.

For a controllable linear time-invariant system ($B \neq 0$), $C^T B = B^T B > 0$ holds and the second part of the control, u_1, can be designed as

$$u_1 = -m_0(x)\,\mathrm{sign}(s), \tag{7.5.9}$$

where $m_0(x) > d^+(x,t)$ should be satisfied such that the function s and $\dot{s}$ have different signs, implying that sliding mode can be enforced. For systems in which only discontinuous control inputs are allowed, e.g., for switching controlled devices such as power converters, the control input can be designed as

$$u = -m_0\,\mathrm{sign}(s), \tag{7.5.10}$$

instead of the $u = u_0 + u_1$. To enforce sliding mode, control gain m_0 should satisfy

$$m_0 > |u_0| + d^+(x,t). \tag{7.5.11}$$

Integral sliding mode may also be called "full order sliding mode" [see Ackermann and Utkin 1994].

7.5.2. Control of Robot Manipulators

The model of a rigid body robot manipulator (see Section 12.1) with n degrees of freedom can be written as

$$M(q)\ddot{q} + N(q,\dot{q}) = \tau, \tag{7.5.12}$$

where $M \in \Re^{n\times n}$ is the mass matrix, $N \in \Re^{n\times 1}$is the vector including centrifugal, Coriolis, and gravity forces, $q \in \Re^{n\times 1}$ represents the joint angle vector, and $\tau \in \Re^{n\times 1}$ denotes the joint torque vector.

Using the so-called "computed torque method" based on the nominal model without perturbations, the required nominal joint torque for the tracking control of the joint position is defined as

$$\tau_0 = M_0(q)(\ddot{q}_d - K_D\dot{q}_e - K_P q_e) + N_0(q,\dot{q}), \tag{7.5.13}$$

where M_0, N_0 are the nominal values of M, N, $K_P \in \Re^{n\times n}$, $K_D \in \Re^{n\times n}$ are positive definite diagonal gain matrices determining the closed-loop performance, and the tracking error is defined as $q_e(t) = q(t) - q_d(t)$, with $\begin{bmatrix} q_d(t) & \dot{q}_d(t) & \ddot{q}_d(t) \end{bmatrix}$ being the desired trajectory and its time derivatives.

Substituting Equation 7.5.13 into Equation 7.5.12 under the assumption of exact knowledge of the model parameters, i.e., $M = M_0$ and $N = N_0$, the resulting closed-loop error dynamics are given by

$$\ddot{q}_e + K_v \dot{q}_e + K_p q_e = 0, \tag{7.5.14}$$

implying that tracking error $q_e(t)$ tends to zero asymptotically.

However, for a real robot with uncertain parameters $M \neq M_0$ and $N \neq N_0$, the error dynamics are perturbed as shown

$$\ddot{q}_e + K_D \dot{q}_e + K_P q_e = M_0^{-1} \tau_p, \tag{7.5.15}$$

where τ_p is given by

$$\tau_p = \left(\bar{M} \ddot{q} + \bar{N} \right), \tag{7.5.16}$$

with $\bar{M} = M_0 - M$ being the parameter error for matrix $M(q)$ and $\bar{N} = N_0 - N$ being the parameter error for vector $N(q, \dot{q})$. Thus, no matter how the constant matrices K_p and K_D are chosen, the tracking error $q_e(t)$ will not tend to zero.

To suppress the perturbation caused by modeling uncertainty, design a robust controller based on the proposed integral sliding mode principle and show that the ideal closed-loop error dynamics as given by Equation 7.5.14 can still be achieved.

Because the disturbance torque τ_p contains $\ddot{q}$, which is a function of the control input $\tau = \tau_0 + \tau_1$, to design the control input τ_1 rejecting the system disturbance, it is necessary to reformulate the system model such that the resulting disturbance term is not a function of the control input τ_1. The ideal robot dynamics with $M = M_0$, $N = N_0$, and $\tau = \tau_0$ can be rewritten in terms of the error dynamics as

$$\ddot{q}_{e0} = -M_0^{-1} N_0 + M_0^{-1} \tau_0 - \ddot{q}_d. \tag{7.5.17}$$

For the real system (Equation 7.5.12) under control $\tau = \tau_0 + \tau_1$, error dynamics similar to the ideal tracking error (Equation 7.5.17) can be derived as

$$\ddot{q}_e = -M^{-1} N + M^{-1} \tau - \ddot{q}_d. \tag{7.5.18}$$

According to the proposed integral sliding mode design method in Equations 7.3.3 and 7.3.7, let the switching function be $s = s_0 + z$ with

$$s_0 = \begin{bmatrix} C & I \end{bmatrix} \begin{bmatrix} q_e \\ \dot{q}_e \end{bmatrix}, \tag{7.5.19}$$

and

$$\dot{z} = -\begin{bmatrix} C & I \end{bmatrix} \begin{bmatrix} \dot{q}_e \\ -M_0^{-1}N_0 + M_0^{-1}\tau_0 - \ddot{q}_d \end{bmatrix}, \; z(0) = -Cq_e(0) - \dot{q}_e(0), \qquad (7.5.20)$$

where $C \in \Re^{n\times n}$ is a positive definite gain matrix and $I \in \Re^{n\times n}$ is an $n \times n$ unit matrix.

The time derivative of vector $s(t)$ can then be obtained by differentiation of Equation 7.5.19 with substitution of error dynamics (Equation 7.5.18) and auxiliary variable z as defined in Equation 7.5.20,

$$\dot{s} = \dot{s}_0 + \dot{z} = \zeta_1 + \zeta_2\tau_0 + M^{-1}\tau_1, \qquad (7.5.21)$$

where $\zeta_1 = (M_0^{-1}N_0 - M^{-1}N)$ and $\zeta_2 = (M^{-1} - M_0^{-1})$ are due to the mismatches between the nominal parameters M_0 and N_0, and the real system parameters $M(q)$ and$N(q,\dot{q})$, viewed as system perturbations similar to Equation 7.5.16 in Equation 7.5.15. In the following, we assume that vector $\zeta_1 + \zeta_2\tau_0$ is norm bounded.

Note that, for the derivation of Equation 7.5.21, the joint torque is composed of two additive parts as shown

$$\tau = \tau_0 + \tau_1, \qquad (7.5.22)$$

with τ_0 already defined in Equation 7.5.13 and τ_1 being the discontinuous part to reject the system perturbations. Define

$$\tau_1 = -\Gamma_0 \operatorname{sign}(s), \qquad (7.5.23)$$

where Γ_0 is a positive constant and design a Lyapunov function candidate $V = \frac{1}{2}s^T s$. The time derivative of V along the solutions of Equation 7.5.21 is given by

$$\dot{V} = s^T\dot{s} = s^T(\zeta_1 + \zeta_2\tau_0) - s^T M^{-1}\Gamma_0 \operatorname{sign}(s). \qquad (7.5.24)$$

Because the kinetic energy of a robot, i.e., $\frac{1}{2}\dot{q}^T M(q)\dot{q}$, is always positive for $\|\dot{q}\| \neq 0$, matrix $M(q)$ is positive definite, and the inverse matrix $M(q)^{-1}$ is positive definite as well. One of the sufficient conditions for $\dot{V} < 0$ is to select the control gain Γ_0 as

$$\Gamma_0 > \frac{1}{\rho}\|\zeta_1 + \zeta_2\tau_0\|, \qquad (7.5.25)$$

where ρ is a positive number smaller than $\lambda_{\min}\left(M^{-1}\right)$, the smallest eigenvalue of matrix $M(q)^{-1}$. Under the above condition, sliding mode will be enforced in finite time. Definition of the initial conditions in Equation 7.5.20

as $z(0) = -Cq_e(0) - \dot{q}_e(0)$ eliminates the reaching time to the sliding manifold. Once sliding mode occurs and the system is confined to the manifold $s(t) = 0$, the equivalent control of τ_1 can be used to examine the system behavior. The equivalent control is obtained by formally setting $\dot{s} = 0$, yielding

$$\tau_{1eq} = -M(\zeta_1 + \zeta_2 \tau_0). \tag{7.5.26}$$

Substitution of $\tau = \tau_0 + \tau_{1eq}$ in Equation 7.5.12 with equivalent control (Equation 7.5.26) leads to the motion equation during sliding mode, which can be simplified as

$$M_0(q)\ddot{q} + N_0(q, \dot{q}) = \tau_0. \tag{7.5.27}$$

Control τ_0 in Equation 7.5.13 thus achieves the ideal closed-loop error dynamics (Equation 7.5.14) as if perturbations caused by the parametric uncertainty did not exist.

7.5.3. Pulse-Width Modulation for Electric Drives

In contrast to the examples in Sections 7.5.1 and 7.5.2, the integral sliding mode design philosophy is directly exploited to implement the PWM in an electric drive system instead of applying Equations 7.3.3 and 7.3.7. Without loss of generality, an electric drive supplied by a power converter can be described by the affine dynamic system like

$$\dot{x} = f(x) + B(x)u, \tag{7.5.28}$$

where $x \in R^n$ represents the current and flux components, and $u \in R^m$ is the control voltages taking only two values, $-u_0$ and $+u_0$, with u_0 being the DC-Bus (also called DC-link or link) voltage. For field-oriented control design (see Chapter 10), Equation 7.5.28 is often transformed into a rotating coordinate system aligned with one of the flux vectors (rotor flux or stator flux). Using a transformation matrix T, a nonlinear projector with sinusoidal entries, the system Equation 7.5.28 may be transformed into the new coordinate system, denoted as (d, q):

$$\dot{x}_{dq} = f_{dq}(x_{dq}) + B_{dq}(x_{dq})u_{dq}, \tag{7.5.29}$$

where u_{dq} is the new control input in coordinate system (d, q). Suppose that the control u_{dq} has been determined to satisfy the given specifications. The task then is to transform the control u_{dq} back to the original coordinate system using the inverse transformation T^{-1} (if matrix T is not a square matrix, the pseudo-inverse will be used; see Chapter 10). Denote this transformed control as u^* and let

$$u^* = T^{-1}u_{dq}. \tag{7.5.30}$$

Now the question arises, how to obtain the actual control u for the system in Equation 7.5.28, which may only take two discontinuous values $-u_0$ and $+u_0$ and should be exactly equivalent to u^*?

The solution is to make the equivalent value of the control u to be equal to the equivalent value of u^*, i.e. $u_{eq} = u^*_{eq}$. Design a sliding mode manifold

$$s = \int_0^t \left(u^*(\zeta) - u(\zeta)\right) d\zeta = 0, \tag{7.5.31}$$

with associated control u

$$u = u_0 \,\text{sign}(s). \tag{7.5.32}$$

For a Lyapunov function candidate $V = \frac{1}{2} s^T s$, the time derivative of V is given by

$$\dot{V} = s^T \dot{s} = s^T u^* - s^T u_0 \,\text{sign}(s). \tag{7.5.33}$$

It is obvious that sliding mode can be enforced if the DC-Bus voltage satisfies $u_0 > \|u^*\|$, or, in other words, the DC-Bus voltage should be high enough to enforce the desired motion.

An example of applying sliding mode PWM to the current control of permanent-magnet synchronous motors can be found in Section 10.2.3.

7.5.4. Robust Current Control for Permanent-Magnet Synchronous Motors

For high-performance operation of permanent-magnet synchronous motors (PMSM), current control may be implemented using the so-called field-oriented control (FOC) approach (see Chapter 10 for more details). From a control point of view, this control approach uses a state transformation, after which the decoupling and linearization tasks can be performed easily. However, high-performance FOC needs precise knowledge of the motor parameters. Practically, those parameters cannot be known exactly because, first, the model used for FOC is a simplified motor model; second, the motor parameters are normally obtained by an identification procedure in which errors are always present; and third, these parameters may vary with the rotor position and ambient temperature. As a result, the motor torque and the motor flux cannot be controlled independently, resulting in torque pulsation and lower efficiency.

Two solutions exist for solving this problem, namely, adaptive control and robust control. Adaptive control recursively calculates the motor parameters depending on the state measurements, whereas robust control tries to suppress the parameter uncertainty using high control gains. The former involves a high computational overhead and an additional convergence

problem, while the latter may result in low control efficiency and may excite high frequency unmodeled dynamics. In the following, we propose two versions of control approaches based on integral sliding mode. These control strategies belong to the category of robust control. However, as one can see from the second version of the control design based on the perturbation estimation described in Section 7.4, the control approach is actually an adaptation to the system perturbation, resulting in continuous control actions suitable to interface with a conventional PWM unit.

In the (d, q) synchronously rotating reference frame (see Section 10.2.2 for the details of modeling a PMSM in different coordinate frames), the voltage equations of a PMSM are expressed by the following nonlinear differential equations

$$\frac{di_d}{dt} = \frac{1}{L}u_d - \frac{R}{L}i_d + \omega_e i_q,$$

$$\frac{di_q}{dt} = \frac{1}{L}u_q - \frac{R}{L}i_q - \omega_e i_d - \lambda\omega_e, \tag{7.5.34}$$

with the definitions shown in Table 7.2.

In practice, parameters L, R, and λ are not known exactly. For the control design, the nominal values of these parameters, denoted as L_0, R_0, and λ_0, are used. In the ideal case with $L = L_0$, $R = R_0$, and $\lambda = \lambda_0$, we may exploit FOC to design the current controller. For the motor currents $i_d(t)$ and $i_q(t)$ to track desired current references $i_d^*(t)$ and $i_q^*(t)$, control voltages $u_d = u_{d0}$ and $u_q = u_{q0}$ can be designed to achieve the desired performance

$$\left|i_d(t) - i_d^*(t)\right| < \varepsilon_d, \quad \left|i_q(t) - i_q^*(t)\right| < \varepsilon_q, \forall\ t > t_0, \tag{7.5.35}$$

where ε_d, ε_q, and t_0 are specified by the control designer. As an example, the pole-placement design can be performed based on the known motor parameters and the closed-loop poles can be placed arbitrarily.

TABLE 7.2

Variables of PMSM Motor Model

Variables	Physical Meaning	Variables	Physical Meaning
i_d	d-axis stator current	i_q	q-axis stator current
u_d	d-axis stator voltage	u_q	q-axis stator voltage
ω_e	Electrical angular velocity	R	Armature resistance
L	Armature inductance	λ	Flux linkage of permanent magnet

In practice, however, $L \neq L_0$, $R \neq R_0$, and $\lambda \neq \lambda_0$, and the above FOC design may result in an unacceptable control error. To suppress the parameter uncertainty, the control voltages are augmented to

$$u_d = u_{d0} + u_{d1},$$

$$u_q = u_{q0} + u_{q1}. \tag{7.5.36}$$

For the first version of the control design, u_{d1} and u_{q1} are selected discontinuous to suppress the perturbation caused by discrepancies between the true motor parameters and the nominal motor parameters (the latter were used for FOC design by $u_d = u_{d0}$ and $u_q = u_{q0}$):

$$u_{d1} = -M_d \operatorname{sign}(s_d),$$

$$u_{q1} = -M_q \operatorname{sign}(s_q), \tag{7.5.37}$$

where M_d and M_q are the control gains to be determined later. The switching functions s_d and s_q are now designed based on the proposed integral sliding mode control

$$s_d = s_{d0} + z_d,$$

$$s_q = s_{q0} + z_q, \tag{7.5.38}$$

in which s_{d0} and s_{q0} are selected as $s_{d0} = i_d - i_d^*$, $s_{q0} = i_q - i_q^*$; z_d and z_q are given as follows

$$\dot{z}_d = -\left(\frac{1}{L_0}u_{d0} - \frac{R_0}{L_0}i_d + \omega_e i_q\right) + \frac{di_d^*}{dt},$$

$$z_d(0) = -\left(i_d(0) - i_d^*(0)\right),$$

$$\dot{z}_q = -\left(\frac{1}{L_0}u_{q0} - \frac{R_0}{L_0}i_q - \omega_e i_d - \lambda_0\omega_e\right) + \frac{di_q^*}{dt},$$

$$z_q(0) = -\left(i_q(0) - i_q^*(0)\right), \tag{7.5.39}$$

with i_d^*, i_q^* and their time derivatives being provided by an outer control loop, e.g., a speed control loop. Now let us analyze the system stability and determine the discontinuous control gains M_d and M_q. First, we deal with the d component. Taking the time derivative of s_d yields

$$\dot{s}_d = \dot{s}_{d0} + \dot{z}_d = \frac{1}{L}u_{d1} + \varepsilon_1 u_{d0} - \varepsilon_2 i_d, \tag{7.5.40}$$

where $\varepsilon_1 = (1/L - 1/L_0)$ and $\varepsilon_2 = (R/L - R_0/L_0)$. Substitute Equation 7.5.37 into Equation 7.5.40 to obtain

$$\dot{s}_d = -\frac{M_d}{L} sign(s_d) + (\varepsilon_1 u_{d0} - \varepsilon_2 i_d). \tag{7.5.41}$$

To enforce sliding mode in Equation 7.5.41, the discontinuous control gain M_d can be selected as

$$M_d > \max\left\{L\left|\varepsilon_1 u_{d0} - \varepsilon_2 i_d\right|\right\}. \tag{7.5.42}$$

The right-hand side of the above inequality is assumed to be bounded. Once sliding mode is achieved, $s_d = 0$ holds; the equivalent control of u_{d1} compensates exactly for the perturbation in terms of u_{hd} (see Equations 7.2.5 and 7.3.5),

$$(u_{d1})_{eq} = -u_{hd} = -L(\varepsilon_1 u_{d0} - \varepsilon_2 i_d). \tag{7.5.43}$$

Similar derivations hold for the q component, where $\dot{s}_q$ can be given as

$$\dot{s}_q = \dot{s}_{q0} + \dot{z}_q = \frac{1}{L}u_{q1} + \varepsilon_1 u_{q0} - \varepsilon_2 i_q - \varepsilon_3 \omega_e, \tag{7.5.44}$$

in which ε_1 and ε_2 are the same as for the d component in Equation 7.5.40 and $\varepsilon_3 = (\lambda - \lambda_0)$. Substitution of Equation 7.5.37 into Equation 7.5.44 yields

$$\dot{s}_q = -\frac{M_q}{L} sign(s_q) + (\varepsilon_1 u_{q0} - \varepsilon_2 i_q - \varepsilon_3 \omega_e). \tag{7.5.45}$$

Enforcing sliding mode in Equation 7.5.45 requires

$$M_q > \max\left\{L\left|\varepsilon_1 u_{q0} - \varepsilon_2 i_q - \varepsilon_3 \omega_e\right|\right\}. \tag{7.5.46}$$

Again, the equivalent control of u_{q1} compensates exactly the perturbation in terms of u_{hq}:

$$(u_{q1})_{eq} = -u_{hq} = -L(\varepsilon_1 u_{q0} - \varepsilon_2 i_q - \varepsilon_3 \omega_e). \tag{7.5.47}$$

It should be noted that, unlike M_d, control gain M_q depends on the electrical rotor speed ω_e if the flux linkage λ is not known precisely.

Because the DC-Bus voltage of a drive system is always limited, the amplitude of the control voltages, i.e., $\sqrt{u_d^2 + u_q^2}$, is also limited, implying that M_d and M_q cannot be selected arbitrarily: increasing M_q leads to a decrease of M_d.

As long as inequalities in Equations 7.5.42 and 7.5.46 hold, sliding mode can be enforced. Otherwise, stability of sliding mode is not guaranteed, which means that the parameter uncertainties cannot be fully compensated. This is one of the drawbacks of the first version of control design.

Another drawback of the first version algorithm lies in the fact that the resulting controllers u_d and u_q are difficult to be implemented by a conventional PWM unit, because they contain a discontinuous part. It should be noted that the standard FOC relies on a PWM unit to adopt the continuous controller u_{d0} and u_{q0} for the discontinuous control voltages of PMSM motors. However, u_d and u_q as defined in Equation 7.5.36 are a mixture of continuous and discontinuous parts. After the coordinate transformation, i.e., from the (d, q) frame to the stator (α, β) frame resulting in u_α and u_β (and if necessary further to the phase coordinate frame resulting in u_a, u_b and u_c), they should be applied to the PWM unit. If these controls contain a discontinuous part, the associated sudden jumps in the PWM duty ratio may be harmful to the used power converter.

Now let us modify the control design such that the above-mentioned drawbacks will be solved, resulting in the second version of control approach based on the perturbation estimator, as discussed in Section 7.4.

The controls u_d and u_q are of similar form to Equation 7.5.36:

$$u_d = u_{d0} + \tilde{u}_{d1},$$

$$u_q = u_{q0} + \tilde{u}_{q1}, \tag{7.5.48}$$

where the continuous functions $\tilde{u}_{d1}$ and $\tilde{u}_{q1}$ are low-pass filtered values of discontinuous controls u_{d1} and u_{q1}. The discontinuous controls u_{d1} and u_{q1} are designed to have the same form as given by Equation 7.5.37:

$$u_{d1} = -M_d \operatorname{sign}(s_d),$$

$$u_{q1} = -M_q \operatorname{sign}(s_q). \tag{7.5.49}$$

The switching functions s_d and s_q are of the same form as Equation 7.5.38:

$$s_d = s_{d0} + z_d,$$

$$s_q = s_{q0} + z_q, \tag{7.5.50}$$

where the integral terms z_d and z_q, following Equation 7.4.4, are now becoming

$$\dot{z}_d = -\left(\frac{1}{L_0}u_d - \frac{R_0}{L_0}i_d + \omega_e i_q - \frac{u_{d1}}{L_0}\right) + \frac{di_d^*}{dt},$$

$$z_d(0) = -\left(i_d(0) - i_d^*(0)\right),$$

$$\dot{z}_q = -\left(\frac{1}{L_0}u_q - \frac{R_0}{L_0}i_q - \omega_e i_d - \lambda_0\omega_e - \frac{u_{q1}}{L_0}\right) + \frac{di_q^*}{dt},$$

$$z_q(0) = -\left(i_q(0) - i_q^*(0)\right). \tag{7.5.51}$$

The time derivatives of $\dot{s}_d$ and $\dot{s}_q$ are, respectively,

$$\dot{s}_d = -\frac{M_d}{L_0}\text{sign}(s_d) + \left(\varepsilon_1(u_{d0} + \tilde{u}_{d1}) - \varepsilon_2 i_d\right),$$

$$\dot{s}_q = -\frac{M_q}{L_0}\text{sign}(s_q) + \left(\varepsilon_1(u_{q0} + \tilde{u}_{q1}) - \varepsilon_2 i_q - \varepsilon_3\omega_e\right). \tag{7.5.52}$$

The conditions for enforcing sliding mode in Equation 7.5.52 are

$$M_d > \max\left\{L_0\left|\varepsilon_1(u_{d0} + \tilde{u}_{d1}) - \varepsilon_2 i_d\right|\right\},$$

$$M_q > \max\left\{L_0\left|\varepsilon_1(u_{q0} + \tilde{u}_{q1}) - \varepsilon_2 i_q - \varepsilon_3\omega_e\right|\right\}. \tag{7.5.53}$$

After the occurrence of sliding mode, the equivalent control can be written as

$$(u_{d1})_{eq} = -L_0\left(\varepsilon_1(u_{d0} + \tilde{u}_{d1}) - \varepsilon_2 i_d\right),$$

$$(u_{q1})_{eq} = -L_0\left(\varepsilon_1(u_{q0} + \tilde{u}_{q1}) - \varepsilon_2 i_q - \varepsilon_3\omega_e\right). \tag{7.5.54}$$

In practice, the equivalent control can be obtained by applying low-pass filters with u_{d1} and u_{q1} as the filter inputs, and $\tilde{u}_{d1}$ and $\tilde{u}_{q1}$ as the filter outputs (see Section 2.4). Thus, for the controller implementation, the disturbance compensation terms $\tilde{u}_{d1}$ and $\tilde{u}_{q1}$ can be obtained as

$$\tilde{u}_{d1} = (u_{d1})_{eq} = lowpass(u_{d1}),$$

$$\tilde{u}_{q1} = (u_{q1})_{eq} = lowpass(u_{q1}). \tag{7.5.55}$$

Based on Equation 7.5.55 and $\tilde{u}_{d1}$ and $\tilde{u}_{q1}$ from Equation 7.5.54, resulting in

$$\tilde{u}_{d1} = -L(\varepsilon_1 u_{d0} - \varepsilon_2 i_d),$$

$$\tilde{u}_{q1} = -L(\varepsilon_1 u_{q0} - \varepsilon_2 i_q - \varepsilon_3 \omega_e). \tag{7.5.56}$$

They are exactly the same as the perturbation terms identified in the first version of current control (see Equations 7.5.43 and 7.5.47). The above derivations show that the system perturbations are indeed compensated by $\tilde{u}_{d1}$ and $\tilde{u}_{q1}$.

Now $\tilde{u}_{d1}$ and $\tilde{u}_{q1}$ are continuous and thus acceptable for the PWM unit. Because the dynamics defined by Equation 7.5.51, which contain the discontinuous controls u_{d1} and u_{q1}, are calculated in the control computer, u_{d1} and u_{q1} are not sent to the real control path, so that M_d and M_q are independent from the DC-Bus voltage and can be selected as high as required to enforce sliding mode.

Remark 7.1

If the resulting $\tilde{u}_{d1}$ and $\tilde{u}_{q1}$ are too high such that $\sqrt{u_d^2 + u_q^2}$ exceeds the DC-Bus voltage, the system perturbations cannot be compensated completely. However, the perturbation estimation given by Equation 7.5.56 remains true. This case indicates that the system disturbances are too large and cannot be fully compensated by any control algorithm.

Another example of using the perturbation estimation concept will be given in Chapter 12, showing the effectiveness of this control scheme in the torque control of a flexible robot joint. In this application, the mass of inertia of the motor rotor and of the link, the joint stiffness, and the frictions at both motor and link sides are assumed to be unknown.

7.6. Summary

This chapter has developed a new sliding mode design concept: integral sliding mode. The proposed uniform formulation of the integral sliding mode enables a wide scope of applications. The main advantage of this new design principle is that the robustness provided by sliding mode can be guaranteed throughout an entire response of the system starting from the initial time instant. We emphasized the basic idea and the background philosophy used to develop such a new sliding mode design approach. Furthermore, application examples of practical systems were discussed in detail. The chattering effect, which was a major drawback of sliding mode control, is reduced using the proposed algorithms, while preserving the robustness and the accuracy of the control system.

References

Ackermann J, Utkin VI. 1994. "Sliding Mode Control Design Based on Ackermann Formula." Proceedings of the IEEE Conference on Decision and Control, Orlando, FL.

Cao W, Xu J. 2004. "Nonlinear Integral-Type Sliding Mode Surface for Both Matched and Unmatched Uncertain Systems." *IEEE Trans Automatic Control* 49:1355–1360.

Castaños F, Fridman L. 2006. "Analysis and Design of Integral Sliding Manifolds for Systems with Unmatched Perturbations." *IEEE Trans Automatic Control* 51:853–858.

Utkin VI. 1992. *Sliding Modes in Control and Optimization*. London: Springer-Verlag.

Utkin VI, Shi J. 1996. "Integral Sliding Mode in Systems Operating under Uncertainty Conditions." Proceedings of the IEEE Conference on Decision and Control, Kobe, Japan.

8

The Chattering Problem

Almost ever since sliding mode ideas have been put forward, the audible noise some sliding mode controllers exhibit has irritated control engineers and often has led to resentments, even rejection of the technique. The phenomenon is best known as chattering. Two main causes have been identified: First, fast dynamics in the control loop, which were neglected in the system model, are often excited by the fast switching of sliding mode controllers. Second, digital implementations in microcontrollers with fixed sampling rates may lead to discretization chatter.

This chapter concentrates on the first cause, the unmodeled dynamics in the control loop, and introduces multiple methods to reliably prevent chattering. Sliding mode in discrete-time systems without discretization chatter is discussed in Chapter 9.

8.1. Problem Analysis

The term chattering describes the phenomenon of finite-frequency, finite-amplitude oscillations appearing in many sliding mode implementations. These oscillations are caused by the high-frequency switching of a sliding mode controller exciting unmodeled dynamics in the closed loop. "Unmodeled dynamics" may be those of sensors and actuators neglected in the principal modeling process because they are generally significantly faster than the main system dynamics. However, because "ideal" sliding mode systems are infinitely fast, all system dynamics should be considered in the control design.

Fortunately, preventing chattering usually does not require a detailed model of all system components. Rather, a sliding mode controller may be first designed under idealized assumptions of no unmodeled dynamics. In a second design step, possible chattering is to be prevented by one of the methods discussed in this chapter. The solution of the chattering problem is of great importance when exploiting the benefits of a sliding mode controller in a real-life system. To some extent, chattering, without proper treatment in the control design, has been a major obstacle for implementation of sliding mode to a wide range of applications. It should be noted that the switching action itself as the core of a continuous-time sliding mode system is *not* referred to as chattering because, in the ideal case, the switching is intended and its frequency tends to infinity; chattering, in the terminology of this book, describes undesired system oscillations with finite frequency caused by system imperfections.

This section seeks to provide an in-depth analysis of the chattering problem. Both analytical and numerical studies are used to examine how unmodeled dynamics in a closed system with a controller discontinuity are excited, leading to oscillations in the system trajectory.

8.1.1. Example System: Model

A simple first-order plant with second-order unmodeled actuator dynamics is used as an example for illustration purposes throughout this section. For clarity of presentation, we refrain from using a more complex system such as the inverted pendulum. The model of the first-order example system with state and output $x(t)$ is given by:

$$\dot{x}(t) = ax(t) + d(x,t) + bw(t), \tag{8.1.1}$$

where $a^- \le a \le a^+$ and $0 < b^- \le b \le b^+$ are unknown parameters within known bounds, $w(t)$ is the control variable, and disturbance $d(t)$ is assumed to be uniformly bounded for all operating conditions (x, t) as $|d(x, t| \le d^+$. Control variable $w(t)$ is the output of an unmodeled actuator with stable dynamics dominated by second-order

$$w(t) = \frac{\omega^2}{p^2 + 2\omega p + \omega^2} u(t) = \frac{1}{(\mu p + 1)^2} u(t), \tag{8.1.2}$$

where $u(t)$ is the actual control input to plant (Equation 8.1.1) and p denotes the Laplace variable. In Equation 8.1.2 and in the sequel, a mixed representation of time domain and frequency (Laplace) domain functions is used for ease of presentation, although not formally correct. For example, it is understood in Equation 8.1.2 that time-domain control variable $w(t)$ is the output of the low-pass filter described by the inverse of the Laplace-transfer function in p with time-domain input $u(t)$.

In Equation 8.1.2, $\omega > 0$ is the unknown actuator bandwidth with $\omega >> a$ in Equation 8.1.1. The small time constant $\mu = \frac{1}{\omega} > 0$ was substituted to symbolize that the actuator dynamics are assumed to be significantly faster than the system dynamics (Equation 8.1.1).

The goal of control is to make state and output $x(t)$ of the system in Equation 8.1.1 track a desired trajectory $x_d(t)$ with a known amplitude bound as $|x_d(t)| \le x_d^+$ and a known bound on the rate of change $|\dot{x}_d(t)| \le v_d^+$. The parameters for the exemplary simulations in this section are $a = 0.5$, $b = 1$, $d(t) = 0.2 \sin(10t) + 0.3 \cos(20t) \le 0.5$, $\omega = 50$, thus $\mu = 0.02$, with a limit on available control resources of $|u(t)| \le 2.01$ and a desired trajectory $x_d(t) = \sin(t)$, i.e., $x_d^+ = 1$ and $v_d^+ = 1$. Note that with $a > 0$, the example plant in Equation 8.1.1 is unstable.

8.1.2. Example System: Ideal Sliding Mode

Standard sliding mode control design for the ideal plant (Equation 8.1.1), i.e., neglecting actuator dynamics (Equation 8.1.2) by setting $w(t) = u(t)$, defines the sliding variable as

$$s(t) = x_d(t) - x(t) \tag{8.1.3}$$

and the associated sliding mode controller as

$$w(t) = M \text{ sign } s(t). \tag{8.1.4}$$

Stability of the closed-loop system and tracking of desired $x_d(t)$ are manifested by examination of the Lyapunov function candidate*

$$V(t) = \frac{1}{2b} s^2(t). \tag{8.1.5}$$

Differentiation of Equation 8.1.5 along the system trajectories (Equation 8.1.1) under control $w(t)$ Equation 8.1.4 and without the actuator dynamics of Equation 8.1.2 yields

$$\begin{aligned} \dot{V}(t) &= \frac{1}{b} s(t)\dot{s}(t) \\ &= g(x, x_d, t)s(t) - M|s(t)|, \end{aligned} \tag{8.1.6}$$

where the term $g(x, x_d, t) = \dfrac{\dot{x}_d(t) - ax(t) - d(t)}{b}$ is upper bounded by

$$|g(x, x_d, t)| \le g^+ = \frac{v_d^+ + a^+ x_d^+ + d^+}{b^-} \tag{8.1.7}$$

under the assumption that $x(t) \approx x_d(t)$. For $M \ge g^+ + \dfrac{\xi}{\sqrt{2b^-}}$ with scalar $\xi > 0$, substitution of the control law in Equation 8.1.4 into Equation 8.1.6 leads to

$$\dot{V}(t) \le -\xi V^{1/2}(t), \tag{8.1.8}$$

* Although stability analysis in this simple example does not require detailed derivation via a Lyapunov function, this method is used for uniformity of presentation throughout the chapter.

which testifies to convergence to $s(t) = 0$ within finite time (see also Section 3.4 for more details): solution of Equation 8.1.8 for an arbitrary initial condition $V(0) > 0$ yields

$$V(t) = \left(-\frac{\xi}{2} t + V^{1/2}(0) \right)^2, \tag{8.1.9}$$

which implies that $V(t)$ is identical to zero after finite time $t_{sm} \geq \frac{2}{\xi} V^{1/2}(0)$. Reaching time t_{sm} is a conservative estimate of the maximum time necessary to reach $s(t) = 0$. In practice, sliding mode often occurs earlier.

Subsequently, the system is invariantly confined to the manifold $s(t) = 0$ in Equation 8.1.3 despite parametric uncertainty in a and b and unknown disturbance $d(x, t)$. A block diagram of the ideal sliding mode system is shown in Figure 8.1.

The behavior of plant (Equation 8.1.1) in sliding mode under control (Equation 8.1.4) can be examined using the equivalent control method (see also Section 2.3). Because $s(t)$ is invariantly identical to zero after reaching the sliding manifold, $\dot{s}(t)$ can be formally set to zero. Solving

$$\begin{aligned} \dot{s}(t) &= \dot{x}_d(t) - \dot{x}(t) \\ &= b\big(g(x,t) - w(t)\big) \\ &\equiv 0 \end{aligned} \tag{8.1.10}$$

for the continuous equivalent control yields

$$w_{\text{eq}}(t) = g(x, t), \tag{8.1.11}$$

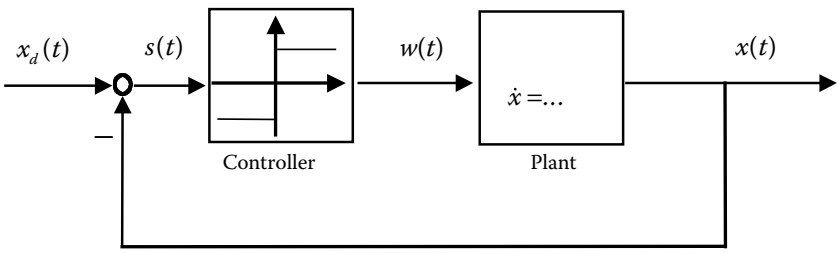

FIGURE 8.1
Block diagram of ideal sliding mode control loop. A discontinuous controller forces the output $x(t)$ of the plant to exactly track the desired trajectory $x_d(t)$. No chattering occurs because the control loop is free of unmodeled dynamics.

which can be viewed as an average of the discontinuous control $w(t)$ in Equation 8.1.4. Applying equivalent control $w_{\text{eq}}(t)$ to plant (Equation 8.1.1) would result in exactly the same motion trajectory as applying discontinuous control $w(t)$ (Equation 8.1.4), which, however, is not possible because $g(x, t)$ contains unknown terms. Substitution of $w_{eq}(t)$ into Equation 8.1.1 validates the exact tracking performance in sliding mode with $x_d(t) = x(t)$.

For the simulation of Equation 8.1.1 under control Equation 8.1.4 with $M = 2.01$ in Figure 8.2, initial condition $x(0) = 1$ was chosen. After reaching the sliding manifold $s(t) = 0$ at $t \approx 0.45$ sec, system trajectory $x(t)$ coincides exactly with desired $x_{\text{d}}(t)$, and control $w(t)$ is switched at very high frequency, creating a solidly black area. For illustration, equivalent control $w_{eq}(t)$ in Equation 8.1.11 is shown as a white line in this black area in Figure 8.2.b. Setting the parameter bounds to $a^- = a^+ = a = 0.5$ and $b^- = b^+ = b = 1.0$ results in $g^+ = 2$, which leads to slow convergence to $s(t) = 0$ attributable to small $\xi \approx 0.014$. This slow convergence was chosen to illustrate the reaching process.

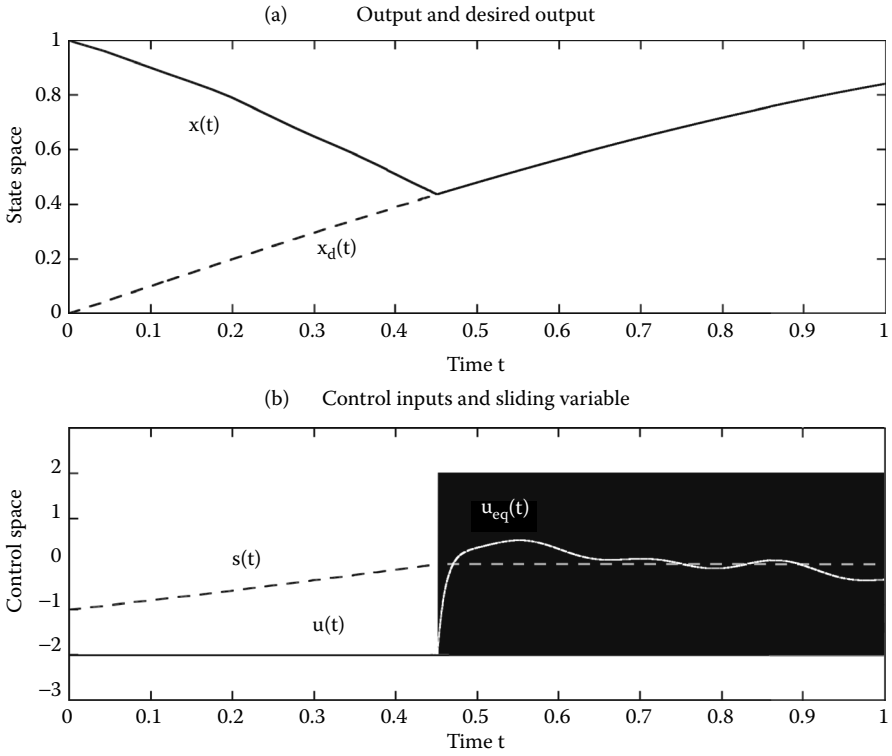

FIGURE 8.2
Ideal sliding mode in first-order system. State $x(t)$ converges to desired $x_d(t)$ in finite time, i.e., $s(t) = 0$ after $t \approx 0.45$ sec. Thereafter, control $u(t)$ switches with infinite frequency and shows as a black area. Equivalent control $u_{\text{eq}}(t)$ is drawn as a dashed line.

8.1.3. Example System: Causes of Chattering

In a practical application, unmodeled dynamics in the closed-loop-like actuator (Equation 8.1.2) often prevent ideal sliding mode to occur and cause fast, finite amplitude oscillations. Figure 8.3 shows a block diagram of the closed control loop, including the previously neglected actuator dynamics.

To study the causes of these oscillations, first revisit the differences between continuous and discontinuous systems. In accordance with singular perturbation theory [for a comprehensive survey, see Kokotovic 1984] for systems with continuous motion equations, fast motion components like those of actuators for large ω in Equation 8.1.2 decay rapidly provided they are stable (as is the case for $\omega > 0$). The slow motion component of plant (Equation 8.1.1) thus continuously depends on the steady-state solution of Equation 8.1.2. In other words, the algebraic solution of Equation 8.1.2 for $\mu \to 0$ may be substituted into Equation 8.1.1 as an approximation, and continuous control design may very well neglect the actuator dynamics. In the case of Equation 8.1.2, $w = u$ results as assumed in Figures 8.1 and 8.2.

In systems with discontinuities, the solution to the motion equation depends on the small time constants of fast components as well. However, unlike in systems with continuous control, discontinuities in the control excite the unmodeled dynamics, which lead to oscillations in the state vector. This phenomenon is also referred to as chattering in control literature. These oscillations are known to result in low control accuracy, high heat losses in electrical power circuits, and high wear of moving mechanical parts.

Figure 8.4 shows the chattering behavior of system Equation 8.1.1 under control $w(t)$ of Equation 8.1.4 but with actuator dynamics in Equation 8.1.2 in the loop as shown in Figure 8.3. The top graph depicts output $x(t)$ oscillating around desired $x_d(t)$ after $t \approx 0.5$ sec. In the bottom graph, control $u(t)$, shown as a solid line, switches with finite frequency, whereas output $w(t)$ of the actuator, shown as a dotted line, clearly is not able to follow the steps in control command $u(t)$. Note that an increase of the actuator bandwidth would increase the frequency of the square-wave behavior of $u(t)$ but would not

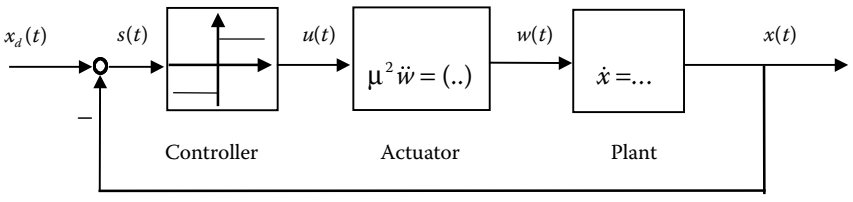

FIGURE 8.3
Control loop with actuator dynamics neglected in ideal control design. Sliding mode does not occur because the actuator dynamics are excited by the fast switching of the discontinuous controller, leading to chattering in the loop.

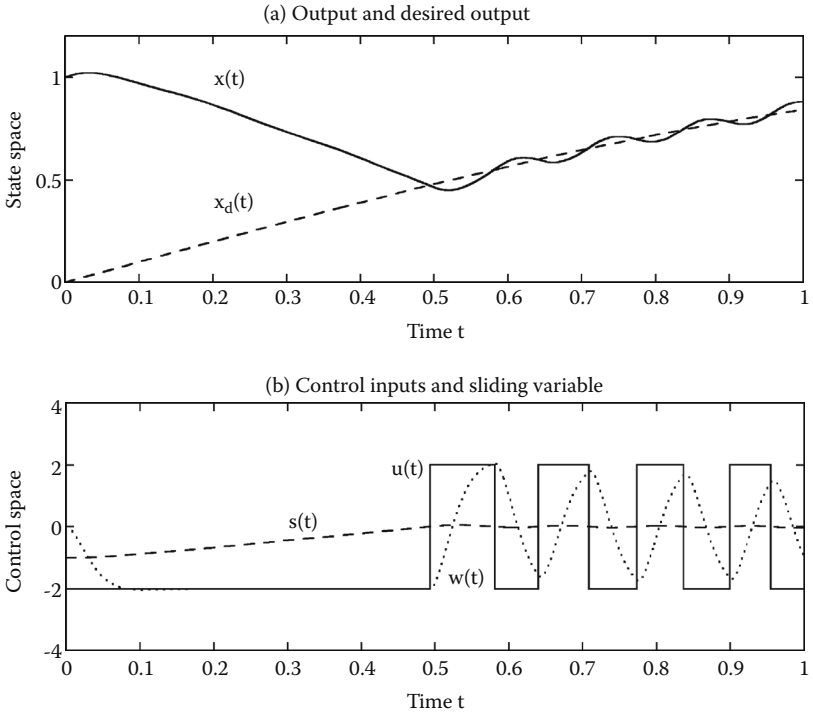

FIGURE 8.4
Chattering in first-order system with second-order actuator dynamics under discontinuous control. After switches in control $u(t)$, actuator output $w(t)$ lags behind, leading to oscillatory system trajectories.

be able to eliminate the oscillations. In fact, in case of a mechanical device performing oscillations as in Figure 8.4 at high frequency, audible noise often results, which led to the name chattering and is extremely harmful to mechanical system components.

For additional study of the nature of the oscillations, consider the situation immediately after a switch in control $u(t)$ from $u(t_{sw}^-) = -M$ to $u(t_{sw}^+) = M$ at time t_{sw}. Immediately after the switch, input $u(t_{sw}^+)$ and output $w(t_{sw}^+)$ of the actuator differ by $2M$. Although the discrepancy between $u(t)$ and $w(t)$ decreases after the switch at a rate faster than the motion of system Equation 8.1.1, $u(t)$ and $w(t)$ are not "close" in the sense of singular perturbation theory [see also Utkin 1993]. Consequently, the small time constants cannot be neglected when examining the behavior of a system with discontinuities in the motion equation.

Consider the system trajectories in Figure 8.4. Initially, $x(t)$ converges to $x_d(t)$ until $t \approx 0.5$ sec. Thereafter, instead of tracking $x_d(t)$ exactly as in the

ideal case shown in Figure 8.2, $x(t)$ goes through cycles of divergence and convergence. This suggests that the manifold $s(t) = x_d(t) - x(t) = 0$ is attractive for large deviations, but the trajectories might diverge in some small vicinity $\varepsilon(\mu)$ of $s(t) = 0$, where scalar ε depends on the bandwidth of the unmodeled actuator dynamics (Equation 8.1.2). The motion trajectory is ultimately confined to this vicinity, i.e., $|s(t)| \le \varepsilon$; however, inside the ε vicinity, oscillations of finite frequency and finite amplitude occur.

Stability for large deviations, i.e., for $|s(t)| > \varepsilon$, can be illustrated using the fact that $u(t)$ is constant for $|s(t)| > \varepsilon$. The actuator dynamics (Equation 8.1.2) decay rapidly because they are stable and $w(t) \approx u(t)$ after some short time interval. In the example of Figure 8.4, the actuator dynamics have decayed after less than 0.1 sec. Hence, the stability analysis (Equations 8.1.5 through 8.1.8) can be used to establish convergence of the system trajectories to $s(t) = 0$ until the first switching of $u(t)$ takes place, at $t \approx 0.5$ sec in the example in Figure 8.4.

To examine the subsequent system behavior, assume steady-state conditions with $u(t) = w(t) = -M$ for $|s(t)| > \varepsilon$. The step response of the actuator for the first switch at t_{sw} from $u(t) = -M$ to $u(t) = +M$ at $s(t) = 0$ is given by

$$w(t) = M\left(1 - 2\left(\frac{t - t_{sw}}{\mu} + 1\right)e^{-\frac{t-t_{sw}}{\mu}}\right). \tag{8.1.12}$$

For some initial time interval $\Delta t = t - t_{sw}$, actuator output $w(t) < u(t) = M$ and $\dot{V}(t) > 0$ in Equation 8.1.6 results for the case $g(x, x_d, t)s(t) > 0$. Only after the decay of the exponential term in Equation 8.1.12, i.e., after $\Delta t(\mu)$, $|w(t)| > g^+$ is established once more and $\dot{V}(t) < 0$ testifies to the convergence to sliding manifold $s(t) = 0$. During the time interval Δt, the maximum deviation from ideal tracking can be approximated by

$$|\Delta s| \le \varepsilon(\mu) = (g^+ + M)\Delta t(\mu). \tag{8.1.13}$$

Similar derivations hold for the next switch from $u(t) = +M$ to $u(t) = -M$.

Summarizing the above shows that, in the nonideal system, $s(t)$ is converging toward zero for $|s(t)| > \varepsilon$. For large deviations from the sliding manifold , system (Equation 8.1.1) with unmodeled dynamics (Equation 8.1.2) under control (Equation 8.1.4) behaves similar to the ideal system, converging to the sliding manifold. Hence, its motion is ultimately confined to $|s(t)| \le \varepsilon$ after some finite time interval. Inside the $\varepsilon(\mu)$ vicinity, stability cannot be guaranteed. In fact, temporary divergence can be shown for $|s(t)| < \varepsilon$.

To qualitatively illustrate the influence of unmodeled dynamics on the system behavior, consider the simplest case $a = 0$, $d(x, t) = 0$, $b = 1$, $x_d(t) = 0$ in Equations 8.1.1 and 8.1.3 as shown in Figure 8.5.

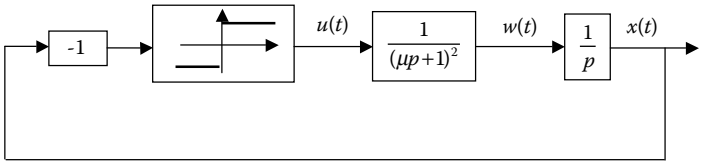

FIGURE 8.5
Block diagram illustrating divergence within ε vicinity of sliding manifold.

The motion equations may be written in the form

$$\begin{aligned} \dot{x} &= w \\ \dot{w} &= v \\ \dot{v} &= -\frac{2}{\mu} v - \frac{1}{\mu^2} w + \frac{1}{\mu^2} u. \end{aligned} \tag{8.1.14}$$

For the control $u = -M \operatorname{sign}(x)$, the sign-varying Lyapunov function

$$V = x\nu - 0.5w^2 \tag{8.1.15}$$

has a negative time derivative

$$\dot{V} = x\left(-\frac{2}{\mu} v - \frac{1}{\mu^2} w + \frac{1}{\mu^2} u \right) \tag{8.1.16}$$

for small magnitudes of ν and w. This means that the motion is unstable in an $\varepsilon(\mu)$-order vicinity of the manifold $s(x) = x = 0$.

Alternatively to Figure 8.5, the block diagram of the system in Equation 8.1.14 may be represented in the form depicted in Figure 8.6.

The motion equations may now be written as

$$\begin{aligned} \dot{x}^* &= -M \operatorname{sign}(x) \\ \mu^2 \ddot{x} + 2\mu\dot{x} + x &= x^*. \end{aligned} \tag{8.1.17}$$

Sliding mode cannot occur in the systems because the time derivative $\dot{x}$ is a continuous time function and cannot have its sign opposite to x in the vicinity of the point $x = 0$ where the control undergoes discontinuities.

The value of $\dot{x}^*$ is bounded, and, as follows from the singular perturbation theory [see Kokotovic, O'Malley, and Sannuti 1976; Kokotovic 1984], the difference between x and x^* is of μ order. The signs of x and x^* coincide beyond the $\varepsilon(\mu)$ vicinity of $s(x) = x = 0$, hence the magnitudes of x^* and x decrease, i.e., the state trajectories converge to this vicinity and after a finite time interval t_1 the state remains in the vicinity. According to the analysis of Equations 8.1.14, the motion in the vicinity of $x = 0$ is unstable.

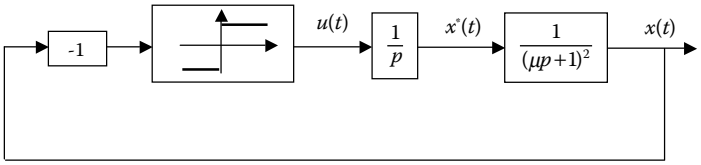

FIGURE 8.6
Alternative representation of block diagram.

The fact of local instability explains why chattering may appear in the systems with discontinuous controls at the presence of unmodeled dynamics. The high-frequency oscillations in the discontinuous control system may be analyzed in time domain as well.

These brief periods of divergence occur after switches of the control input variable $u(t)$ when the output $w(t)$ of the actuator is unable to follow the abrupt change of the control command. The proposed solutions to the chattering problem thus focus on either avoiding control discontinuities in general or move the switching action to a controller loop without any unmodeled dynamics. After introducing the Describing Function to analyze the frequency and amplitude of chattering, the remainder of this chapter will discuss various types of chattering prevention schemes and examine their respective benefits.

8.1.4. Describing Function Method for Chattering Analysis

For analyzing the influence of mismatch in modeling from neglecting the small time constants of actuators and sensors, the describing function method can be used to estimate the amplitude and frequency of chattering. Intuitively, the amplitude of chattering will be related to amplitude of discontinuous control.

Let us consider the following system with scalar control:

$$\begin{aligned} \dot{x} &= f(x) + l(x)u \quad (x \in \Re^n) \\ s &= s(x) \\ u &= -M(x)sign(s). \end{aligned} \tag{8.1.18}$$

The time derivative of s can be written as

$$\dot{s} = Gf + Glu, \quad G = \left\{ \frac{\partial s}{\partial s} \right\}^T. \tag{8.1.19}$$

When chattering occurs at high frequency, state components as well as terms Gf and Gl in Equation 8.1.19 may be considered to be constant for short time interval. Thus, the system in Equation 8.1.18 becomes

$$\dot{x} = a + bu \quad (x \in \Re^n), \tag{8.1.20}$$

where the vectors a and b are constant. The system in Equation 8.1.18 is used to analyze chattering qualitatively. For simplicity, the sliding surface is selected as

$$s = 0,\ s = cx, \tag{8.1.21}$$

where c is an $1 \times n$ row vector with constant elements. For $cb > 0$, the control input u becomes

$$u = \begin{cases} M & \text{for } s < 0 \\ -M & \text{for } s > 0, \end{cases} \tag{8.1.22}$$

where M is a positive constant. Now, let us assume that linear sensor dynamics with small time constant μ are disregarded in the model in Equation 8.1.20. The system state vector x is regarded as an input of the unmodeled subsystem with state vector z ($z \in \Re^m$):

$$\mu\dot{z} = Az + Bx. \tag{8.1.23}$$

The time constant μ is a sufficiently small, positive value, A and B are $m \times m$ and $m \times n$ matrices, respectively. The matrix A is assumed to have eigenvalues with negative real parts. Instead of the system state vector x, the controller will use a vector x^*($x^* \in \Re^n$), which is a linear combination of the elements in the sensor state vector z:

$$x^* = Hz, \tag{8.1.24}$$

where H is a constant $n \times m$ matrix. Because the controller is using x^*, rather than the vector x directly from the plant, the sliding mode surface (Equation 8.1.21) now becomes

$$s^* = cx^*. \tag{8.1.25}$$

With this alternative switching surface, the system in Equation 8.1.20 will be as follows:

$$\dot{x} = a + bu^*, \quad u^* = \begin{cases} M & \text{for } s^* < 0 \\ -M & \text{for } s^* > 0. \end{cases} \tag{8.1.26}$$

The entire system including sensor dynamics is depicted in Figure 8.7. In static mode, when the left-hand side of Equation 8.1.23 is zero, the vector x^* should follow the state x without any distortion. Therefore,

$$x^* = -HA^{-1}Bx, \tag{8.1.27}$$

$$-HA^{-1}B = I. \tag{8.1.28}$$

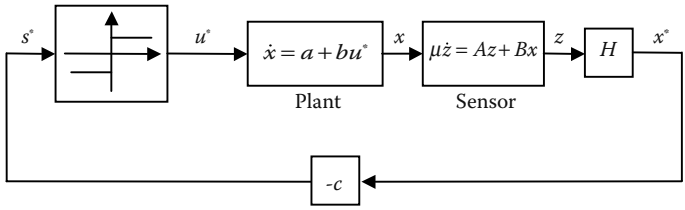

FIGURE 8.7
System with a fast sensor dynamics.

Note that A^{-1} exists because A has nonzero eigenvalues as assumed previously.

To implement the describing function method, Laplace transformation is applied to Equations 8.1.23 through 8.1.26:

$$\begin{aligned} s^*(p) &= G_u(p)u^*(p) + G_a a(p) \\ G_u(p) &= cH\left(\mu pI - A\right)^{-1} B\frac{b}{p}, \\ G_a(p) &= cH(\mu pI - A)^{-1} B\frac{1}{p}. \end{aligned} \tag{8.1.29}$$

In compliance with the describing function method, the solution of Equations 8.1.26 and 8.1.29 is assumed to be a harmonic function plus a constant (Figure 8.8):

$$s^*(t) = \alpha + \beta \sin \omega t, \ (\alpha < \beta), \tag{8.1.30}$$

where α, β, and ω are constant. Then, the first two terms of Fourier expansion of the input function $u^* = -Msign(s)$ can be found as follows:

$$u^*(t) = u_0^* + u_1^* \sin \omega t \tag{8.1.31}$$

$$u_0^* = \frac{\omega}{2\pi}\int_0^{2\pi/\omega} u^*(t)dt = -\frac{2}{\pi}M\sin^{-1}\frac{\alpha}{\beta} \tag{8.1.32}$$

$$u_1^* = \frac{\omega}{\pi}\int_0^{2\pi/\omega} u^*(t)\sin\omega t dt = -\frac{4M}{\pi}\cos\left(\sin^{-1}\frac{\alpha}{\beta}\right) = -\frac{4M}{\pi}\sqrt{1-\left(\frac{\alpha}{\beta}\right)^2}. \tag{8.1.33}$$

The relation between α and constant inputs u_0^* can be found replacing variable p in transfer functions by zero. Considering the condition in Equation 8.1.28, this results in

$$\alpha = \frac{1}{p}(cbu_0^* + ca)$$

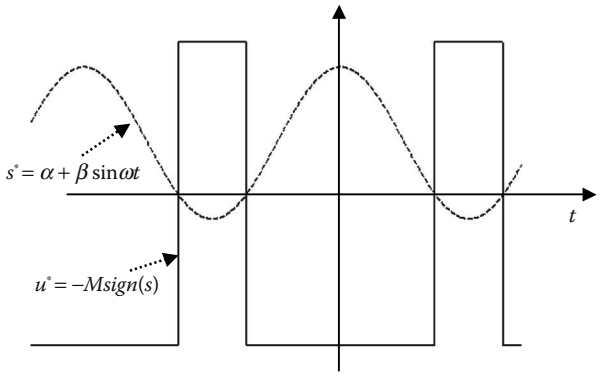

FIGURE 8.8
The switching function s^* and corresponding control input u^*.

Because $\frac{1}{p} \to \infty$ with $p \to 0$, the constant component of the function u^* is determined as

$$u_0^* = -\frac{ca}{cb}, \tag{8.1.34}$$

which is known as the equivalent control for the original system without unmodeled dynamics: the solution to $\dot{s} = ca + cbu = 0$ with respect to u. To find the amplitude of the harmonic component u_1^* in the control input, calculate $\frac{\alpha}{\beta}$ from Equations 8.1.34 and 8.1.32 and then substitute this value into Equation 8.1.33

$$u_1^* = -\frac{4M}{\pi} \cos\left(\frac{ca}{cb}\frac{\pi}{2M}\right). \tag{8.1.35}$$

It can be seen from Equation 8.1.35 that the amplitude of chattering depends on the value of M. Increasing M leads to increasing of the harmonic component in the input and, as a result, increasing the amplitude of chattering β in the output.

The chattering frequency can be found from balance of phases of the first harmonics in input and output variables:

$$-\frac{\pi}{2} + \arg\left[cH(j\omega^* I - A)^{-1} Bb\right] = \pm k\pi, \quad k = 0, 1, 2, \ldots, \tag{8.1.36}$$

where $\omega^* = \mu\omega$. If it is assumed that Equation 8.1.36 has a solution for $\omega^* = \tilde{\omega}$, then the chattering frequency can be written as $\omega = \frac{\tilde{\omega}}{\mu}$.

Because the amplitude of chattering depends on the magnitude of control, the intuitive way of chattering reduction is decreasing the control magnitude M but ensuring that sliding mode still exists.

8.2. Boundary Layer Solution

The boundary layer solution, proposed by Slotine and Sastry [1983] and Slotine [1984], seeks to avoid control discontinuities and switching action in the control loop. The control law in Equation 8.1.4 is replaced by a saturation function that approximates the sign(s) term in a boundary layer of the manifold $s(t) = 0$. Numerous types of saturation functions sat(s) have been proposed in the literature.

"In the large", i.e., for $|s(t)| > \varepsilon$, sat(s) = sign(s). However, in a small ε vicinity of the origin, the so-called boundary layer, sat(s) ≠ sign(s) is continuous. As an illustrative example, consider a simple linear saturation function

$$u(t) = \begin{cases} M\text{sign}\big(s(t)\big) & \text{for} \quad |s(t)| > \varepsilon \\ \\ \dfrac{M}{\varepsilon} s(t) & \text{for} \quad |s(t)| \le \varepsilon \end{cases}, \tag{8.2.1}$$

with linear proportional feedback gain $\dfrac{M}{\varepsilon}$ within the boundary layer in the vicinity of the origin, $|s(t)| \le \varepsilon$, and symmetrically saturated by M for $|s(t)| > \varepsilon$ outside the boundary layer. A block diagram of the example system under control (Equation 8.2.1) is shown in Figure 8.9.

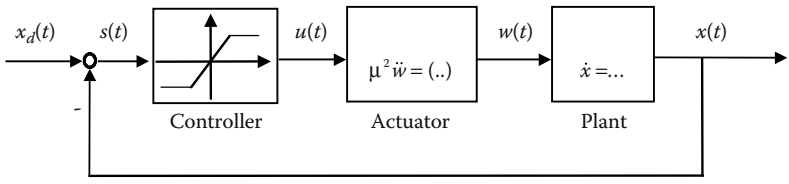

FIGURE 8.9
Saturation function replaces discontinuous controller. Instead of achieving ideal sliding mode, the system trajectories are confined to a boundary layer of the manifold $s(t) = 0$.

For a stability analysis, substitute Equation 8.2.1 into Equation 8.1.6 instead of Equation 8.1.4 to yield

$$\dot{V}(t) \le \begin{cases} -\xi V^{1/2}(t) & \text{for} \quad |s(t)| > \varepsilon \\ s(t)\left(g^{+} - \dfrac{M}{\varepsilon} s(t)\right) & \text{for} \quad |s(t)| \le \varepsilon \end{cases}. \tag{8.2.2}$$

Direct examination of Equation 8.2.2 shows similar stability properties as Equation 8.1.8 for $|s(t)| > \varepsilon$ and undetermined stability for $|s(t)| \le \varepsilon$. Hence, the system trajectories are guaranteed to converge to the boundary layer. Because within the boundary layer the system is continuous and linear in this simple example, linear control theory can be used to further study the stability. Substituting $u(t) = \dfrac{M}{\varepsilon} s(t)$ into Equations 8.1.2 and 8.1.1 with Equation 8.1.3 yields Laplace-domain expression:

$$\begin{aligned} &\left(\mu^2 p^3 + \mu(2 - a\mu)p^2 + (1 - 2a\mu)p + \left(b\frac{M}{\varepsilon} - a\right)\right)x(t) = h(x, x_d, t), \\ &h(x, x_d, t) = b\frac{M}{\varepsilon} x_d(t) + (\mu p + 1)^2 d(x, t), \end{aligned} \tag{8.2.3}$$

where $h(x, x_d, t)$ can be interpreted as a disturbance to the left-hand side of the first row in Equation 8.2.3. The Hurwitz stability bounds for the left-hand side of the first equation in Equation 8.2.3 are given as

$$a\mu < 1/2 \tag{8.2.4}$$

and

$$\frac{M}{\varepsilon} < \frac{2}{b\mu}(1 - a\mu)^2. \tag{8.2.5}$$

The first stability bound (Equation 8.2.4) states that the unmodeled dynamics have to be stable and faster than the system dynamics (Equation 8.1.1) themselves. The stability boundary (Equation 8.2.5) defines the highest feedback gain the system (Equation 8.1.1) with actuator dynamics (Equation 8.1.2) can sustain in the linear sense. Higher gains, in particular theoretically infinite gains of discontinuous sliding mode controllers, result in instability in the vicinity of $s(t) = 0$, causing chattering as shown in the previous section.

Furthermore, for oscillation-free trajectories with critically damped eigenvalues in Equation 8.2.3, $\frac{M}{\varepsilon} < \frac{3\sqrt{2}-4}{b\mu}(1-2a\mu)^2$ is required. It is interesting to note that, in this simple example, the boundary layer width ε depends almost linearly on the actuator time constant μ and inverse linearly on the available control resources M. In the simulation shown in Figure 8.10, ε = 0.1 was chosen, which leads to stable but less than critically damped eigenvalues. Consequently, small overshoot results when $x(t)$ converges to $x_d(t)$.

One of the benefits of the boundary layer approach is that sliding mode control design methodologies can be exploited to derive a continuous controller. The invariance property of sliding mode control is partially preserved in the sense that the system trajectories are confined to a δ(ε) vicinity of the sliding manifold $s(t) = 0$, instead of exactly to $s(t) = 0$ as in ideal sliding mode in Figures 8.1 and 8.2. Within the δ(ε) vicinity, however, the system behavior is not determined, i.e., further convergence to zero is not guaranteed. This type of control design is part of a class of robust controllers that satisfy the "globally uniform ultimate boundedness" condition proposed by Leitmann [1981]. Note that no real sliding mode takes place because the switching action is replaced by a continuous approximation.

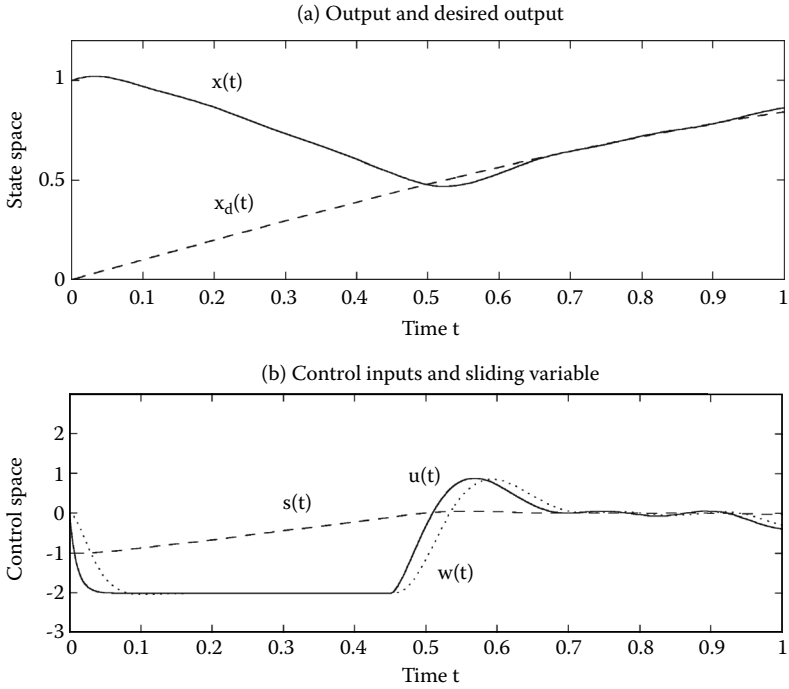

FIGURE 8.10
Saturation function approximating control discontinuity in boundary layer yields chattering free system trajectories. State $x(t)$ converges to desired $x_d(t)$, but does not track exactly as in ideal sliding mode.

8.3. Observer-Based Solution

The boundary layer approach discussed above avoids generating sliding mode by replacing the discontinuous switching action with a continuous saturation function. In many applications, however, control discontinuities are inherent to the system, e.g., in various voltage inputs of power converters or electric drives. When implementing a continuous controller, a technique such as PWM has to be exploited to adapt the control law to the discontinuous system inputs. In light of recent advances of high-speed circuitry and insufficient linear control methodologies for internally nonlinear high-order plants such as AC motors, sliding mode control has become increasingly popular. Commercially available electronic converters enable handling switching frequencies in the range of hundreds of kilohertz. Hence, it seems unjustified to bypass a system's discontinuous control inputs by converting a continuous controller, e.g., via a PWM scheme. Rather, such system specifications call for alternative methods to prevent chattering while preserving control discontinuities.

An asymptotic observer in the control loop can eliminate chattering despite discontinuous control laws. The key idea as proposed by Bondarev, Bondarev, Kostyleva, and Utkin [1985] is to generate ideal sliding mode in an auxiliary observer loop rather than in the main control loop. Ideal sliding mode is possible in the observer loop because it is entirely generated in the control software and thus does not contain any unmodeled dynamics. The main loop follows the observer loop according to the observer dynamics. Despite applying a discontinuous control signal with switching action to the plant, no chattering occurs and the system behaves as if an equivalent continuous control was applied. A block diagram for the example system of this chapter with an auxiliary observer is shown in Figure 8.11.

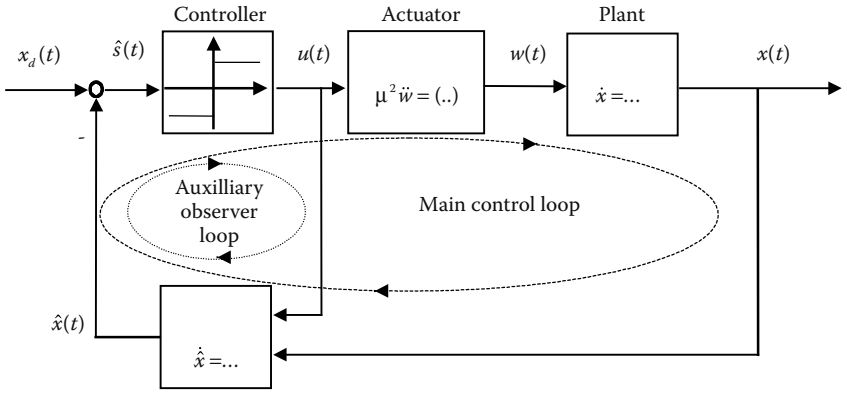

FIGURE 8.11
Control loop with auxiliary observer loop. Ideal sliding mode occurs in observer manifold $\hat{s}(t) = 0$ because the observer loop is free of unmodeled dynamics. The plant output $x(t)$ follows the observer output $\hat{x}(t)$ without chattering despite discontinuous control $u(t)$ applied to main loop with actuator dynamics.

Define a first-order observer for the example system in Equation 8.1.1 as

$$\dot{\hat{x}}(t) = ax(t) + bu(t) + L_1\bar{x}(t), \tag{8.3.1}$$

where L_1 is the linear feedback gain for the observation error $\bar{x}(t) = x(t) - \hat{x}(t)$. Exact knowledge of the system parameters a and b is assumed in Equation 8.3.1 for ease of presentation. In the case of parametric uncertainty, parameter estimates $\hat{a}$ and $\hat{b}$ replace a and b in Equation 8.3.1 and a more complex analysis results.

The linear dynamics of the observation error are governed by

$$\dot{\bar{x}}(t) = d(x, t) - L_1\bar{x}(t). \tag{8.3.2}$$

Error $\bar{x}(t)$ in Equation 8.3.2 is stable and bounded by

$$|\bar{x}(t)| \le \frac{d^+}{L_1}, \tag{8.3.3}$$

with the disturbance bounded by $|d(x, t)| \le d^+$. Introducing an observer sliding manifold

$$\hat{s}(t) = x_d(t) - \hat{x}(t) \tag{8.3.4}$$

allows definition of an ideal sliding mode controller for the observer loop as

$$u(t) = M \operatorname{sign} \hat{s}(t) \tag{8.3.5}$$

to replace Equations 8.1.3 and 8.1.4. Stability of the auxiliary observer loop is examined via a similar Lyapunov function candidate as in Equation 8.1.5,

$$\hat{V}(t) = \frac{1}{2b}\hat{s}^2(t). \tag{8.3.6}$$

Substitution of Equation 8.3.1 under control (Equation 8.3.5) into the time derivative of Equation 8.3.6 reveals

$$\begin{aligned}\dot{\hat{V}}(t) &= \frac{1}{b}\hat{s}(t)\dot{\hat{s}}(t) \\ &= \frac{1}{b}\left(\dot{x}_d(t) - ax(t) - L_1\bar{x}(t)\right)\hat{s}(t) - M|\hat{s}(t)| \\ &\le \frac{1}{b^-}\left(v_d^+ + a^+x_d^+ + d^+\right)|\hat{s}(t)| - M|\hat{s}(t)|,\end{aligned} \tag{8.3.7}$$

where observation error bound (Equation 8.3.3) was used to reduce the expression. Substitution of the bound of the independent observer error system of Equation 8.1.7 and condition $M \ge g^+ + \frac{\xi}{\sqrt{2b^-}}$ leads to

$$\dot{\hat{V}}(t) \le -\xi \hat{V}^{1/2}(t) \tag{8.3.8}$$

under similar assumptions as for Equation 8.1.8. Sliding mode is established in the observer loop after finite time as in Equation 8.1.9 and $\hat{s}(t) = 0$ holds exactly thereafter.

To examine the behavior of the overall system under sliding mode in the auxiliary observer loop, the equivalent control method is used. Solving

$$\dot{\hat{s}}(t) = \dot{x}_d(t) - ax(t) - bu(t) - L_1\bar{x}(t) \equiv 0 \tag{8.3.9}$$

for the equivalent control of input $u(t)$ yields

$$bu_{\text{eq}}(t) = \dot{x}_d(t) - ax(t) - L_1\bar{x}(t). \tag{8.3.10}$$

Substitution of Equation 8.3.10 into the plant Equation 8.1.1 with actuator dynamics (Equation 8.1.2) leads to

$$\begin{aligned} &\left(\mu^2 p^3 + \mu(2 - a\mu)p^2 + (1 - 2a\mu)p + L_1\right)x(t) = h^*(x, x_d, t), \\ &h^*(x, x_d, t) = (p + L_1)x_d(t) + (\mu p + 1)^2 d(x, t). \end{aligned} \tag{8.3.11}$$

Equation 8.3.11 is similar to Equation 8.2.3 except for two details. First, the desired trajectory $x_d(t)$ enters the disturbance function $h^*(x, x_d, t)$ in a different manner then $h(x, x_d, t)$. Second, left-hand side of stability bound Equation 8.2.5 is modified to

$$L_1 + a < \frac{2}{\mu}(1 - a\mu)^2. \tag{8.3.12}$$

The analytical similarities between the boundary layer approach and the asymptotic observer-based solution in this simple first-order example are also apparent in the system trajectories. Compare the simulation of the observer-based approach in Figure 8.12 with the boundary layer approach simulation in Figure 8.8. Both show similar behavior with a small overshoot when reaching the sliding manifold. Note that, for the observer-based solution, the observed state $\hat{x}(t)$ achieves ideal sliding mode with discontinuous switching action (black area in Figure 8.12), whereas the true state $x(t)$ follows according to the observer dynamics without exhibiting chattering.

The observer-based solution requires slightly more effort in the control design. However, in many control applications, observers for immeasurable states are vital parts of the overall system and can be readily included into

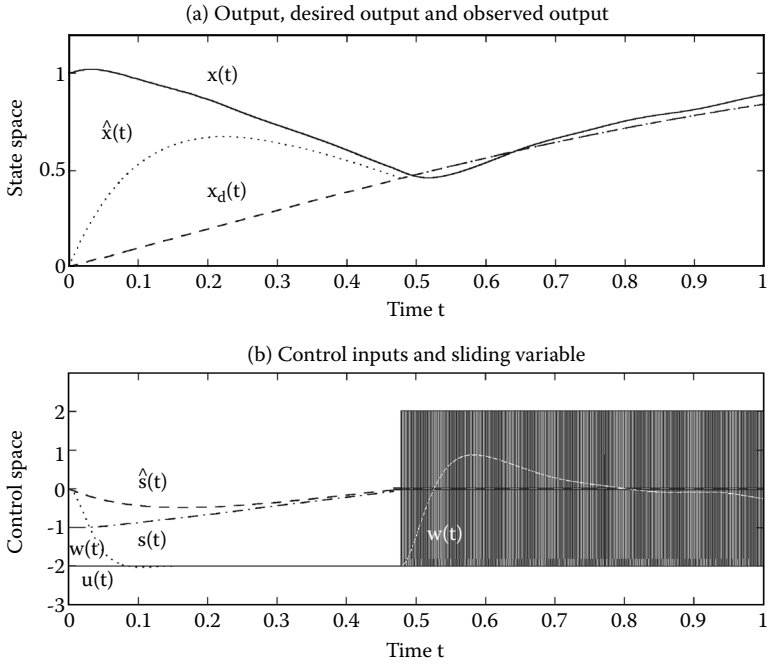

FIGURE 8.12
Observer in auxiliary control loop enables chattering free system trajectories despite discontinuous control switching after sliding manifold $\hat{s}(t) = 0$ is reached. Plant output $x(t)$ tracks observer output $\hat{x}(t)$ according to observer error dynamics.

the control design. Note that the design of the actual observer depends on the system specifications; both full-state and reduced order observers may be used. Furthermore, observers provide more flexibility. For instance, in the example studied in this chapter, the observer (Equation 8.3.1) may be extended to include an estimate of the disturbance under the assumption that $\dot{d}(t)$ is small as shown

$$\begin{aligned} \dot{\hat{x}}(t) &= ax(t) + \hat{d}(t) + bu(t) + L_1\bar{x}(t), \\ \dot{\hat{d}}(t) &= \qquad\qquad\qquad L_2\bar{x}(t), \end{aligned} \tag{8.3.13}$$

where L_1 and L_2 determine the observer dynamics. The simulation in Figure 8.13 shows that the tracking performance of the extended observer (Equation 8.3.13) is improved compared with the initial design (Equation 8.3.1), i.e., $\hat{x}(t)$ tracks $x(t)$ closer after the initial overshoot when reaching the sliding manifold.

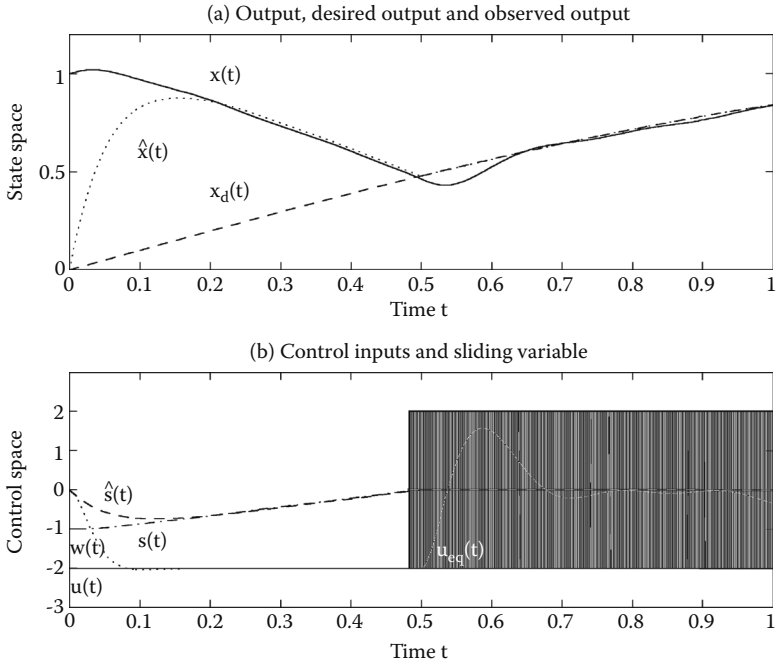

FIGURE 8.13
Tracking performance is improved by increasing the order of the observer in auxiliary control loop. After sliding manifold $\hat{s}(t) = 0$ is reached, plant output $x(t)$ tracks observer output $\hat{x}(t)$ and desired $x_d(t)$ closely.

8.4. Regular Form Solution

Both the boundary layer approach and the observer-based solution to the chattering problem assume that the unmodeled dynamics are completely unknown. In practical applications, however, at least partial information about unmodeled dynamics, in particular of actuators, is often available together with measurements of the actuator outputs. For example, for electric drives, models are readily available but may contain uncertain parameters. Thus, in the design of a controller for the overall system, these dynamics can be included into the control design to enhance the performance of the overall system.

Because the actuator dynamics and the plant dynamics are block separated, i.e., the output(s) of the actuator(s) are the input(s) to the plant, a cascaded control structure can be designed following the regular form approach or the block control principle (see Sections 3.2 and 5.6 or Drakunov et al. [1990a,b]). The basic idea is to design a cascaded controller in two steps. In the first step, a continuous controller is derived for the plant under the assumption that

the plant input(s) is (are) the actual control input(s) to the overall system, defining "desired" actuator output(s) w_d(t). In the second step, the actuator input(s) $u(t)$, i.e., the real control input(s) of the system, is (are) used to ensure the actuator output(s) track the desired output(s) exactly via sliding mode control with $w(t) = w_d$(t). This approach is a special case of cascaded control structures as applied to the block control principle [Drakunov et al. 1984, 1990a,b] and the integrator back-stepping method [Krstic, Kanellakopoulos, and Kokotovic 1995].

The regular form approach to prevent chattering is especially intriguing for systems with electrical actuators in which control input discontinuities are often imposed by the system specifications. Particularly for electromechanical systems, the benefits of sliding mode control can be fully exploited based on the wealth of available control designs for electric drives and power converters (described in Chapters 10 and 11).

Assume the main source of unmodeled dynamics in a control loop being the actuator as depicted in Figure 8.3. Further assume availability of a model for the actuator in Equation 8.1.2, e.g., with uncertain parameters as

$$w(t) = \frac{\hat{\omega}^2}{p^2 + 2\hat{\omega}p + \hat{\omega}^2} u(t) = \frac{1}{(\hat{\mu}p + 1)^2} u(t), \tag{8.4.1}$$

where $\hat{\omega} = 1/\hat{\mu}$ is an estimate for the actuator bandwidth, $u(t)$ is the control input to the overall system, and $w(t)$ is the measurable actuator output. For more realistic actuator dynamics, refer to Chapter 10. A block diagram of the complete control system is shown in Figure 8.14. Note that the regular form approach is not applicable to systems with unmodeled dynamics mainly introduced by sensors rather than by actuators because measurement of both input(s) and output(s) of the unmodeled dynamics is required. Because sensor input(s) are usually not available via measurement(s), other methods such as the observer-based approach should be used to prevent chattering.

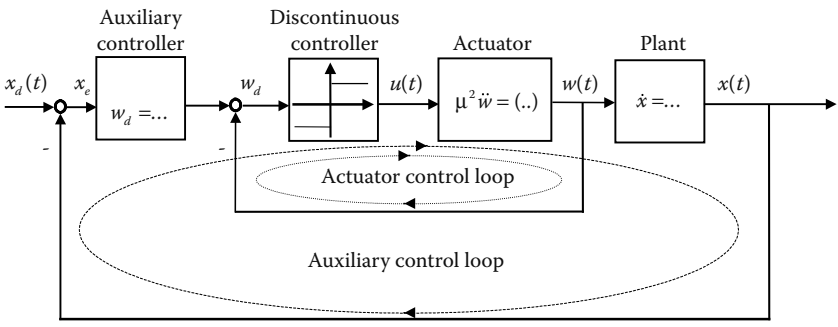

FIGURE 8.14
Cascaded controller with continuous auxiliary control and discontinuous actuator control loop.

In the first design step, a continuous auxiliary control law $w_d(t)$ is derived for plant (Equation 8.1.1) to track desired trajectory $x_d(t)$. Although any control design methodology, linear or nonlinear, can be used, it is important to ensure trackability in the face of limited bandwidth actuator dynamics. In other words, the rate of the auxiliary controller should be bounded as

$$\left|\dot{w}_d(t)\right| \le \dot{w}_d^+. \tag{8.4.2}$$

Depending on the order of the actuator dynamics, additional bounds on higher time derivatives of $w_d(t)$ might be necessary. For the example system (Equation 8.1.1), a first-order linear controller

$$w_d(t) = C(x_d(t) - x(t)) = Cx_e(t) \tag{8.4.3}$$

with proportional gain $C > 0$ may be used to yield error dynamics

$$\dot{x}_e(t) = b\left(-Cx_e(t) + g(x, x_d, t)\right), \tag{8.4.4}$$

where an upper bound g^+ for disturbance function $g(x, x_d, t)$ was given in Equation 8.1.7. Error dynamics (Equation 8.4.4) are stable but are disturbed by $g(x, x_d, t)$. If available, the performance of controller in Equation 8.4.3 can be improved by feedforward of a disturbance estimate $\hat{g}(x, x_d, t)$ as

$$w_d(t) = Cx_e(t) + \frac{1}{\hat{b}}\hat{g}(x, x_d, t). \tag{8.4.5}$$

The second design step is to drive the error $w_e(t) = w_d(t) - w(t)$ between desired $w_d(t)$ in Equations 8.4.3 or 8.4.5 and actual actuator output $w(t)$ to zero. Because this inner control loop is free of unmodeled dynamics, a discontinuous sliding mode controller can be designed as

$$u(t) = \left(\hat{\mu}p + 1\right)^2 w_d(t) + M \operatorname{sign} s(t) \tag{8.4.6}$$

with second-order sliding variable

$$s(t) = K\dot{w}_e(t) + w_e(t), \quad K > 0. \tag{8.4.7}$$

Control Equations 8.4.6 and 8.4.7 assume that the first and second time derivatives of $w_d(t)$ in Equations 8.4.3 or 8.4.5 and the first time derivative of the actuator output, $\dot{w}(t)$, are available, e.g., from an observer. Controller Equation 8.4.6 leads to the inner loop error dynamics

$$\mu^2\ddot{w}_e(t) + 2\mu\dot{w}_e(t) + w_e(t) + M \operatorname{sign} s(t) = p\left(\bar{\mu}^2 p + \bar{\mu}\right) w_d(t), \tag{8.4.8}$$

where $\bar{\mu} = \mu - \hat{\mu}$ is the estimation error of the actuator dynamics, and p is the Laplace variable. Following the conventional design methodology of sliding mode control, it can be shown that the values of $s(t)$ and $\dot{s}(t)$ have different signs for bounded $\dot{w}_d(t)$, $\ddot{w}_d(t)$ and high enough but finite magnitude of control resource M. Hence, sliding mode is enforced in the manifold $s(t) = 0$ with $w_e(t)$ decaying to zero as determined by K in Equation 8.4.7. Consequently, desired control Equations 8.4.3 or 8.4.5 is directly implemented to plant Equation 8.1.1.

In the simulation shown in Figure 8.15, the desired actuator output was limited according to the real actuator limits, i.e., $-M \le w_d(t) \le M$. The sliding variable in Equation 8.4.7 converges to zero within finite time. Thereafter, $s(t) = 0$ and the control switches at (theoretically) infinite frequency, resulting in the black solid area in Figure 8.15b. At the same time, $x(t)$ converges to desired $x_d(t)$, but tracking is not exact because of linear control Equation 8.4.3.

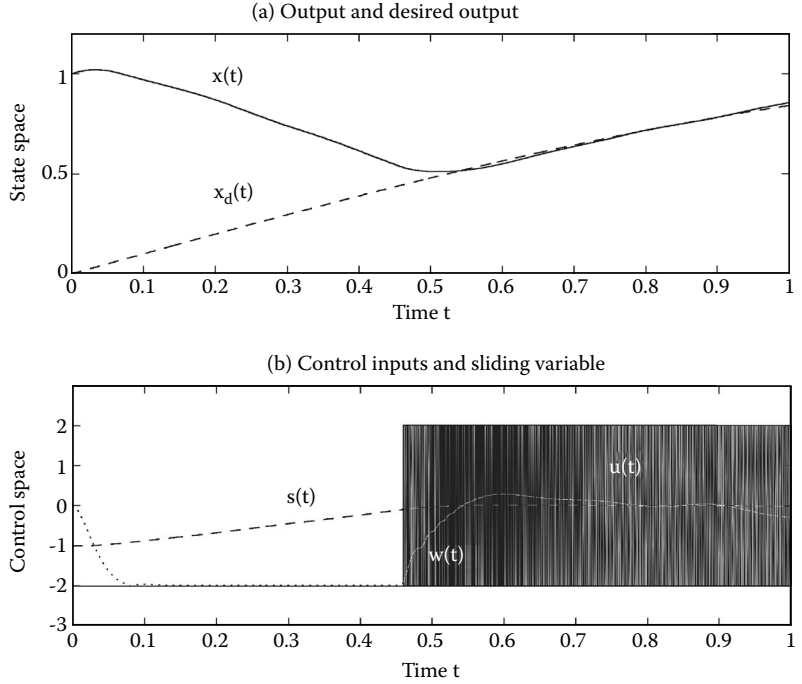

FIGURE 8.15
Cascaded controller structure to prevent chattering. Despite discontinuous control action in actuator control loop, plant output $x(t)$ follows desired trajectory $x_d(t)$ without oscillations.

8.5. Disturbance Rejection Solution

The regular form solution in the previous section relies on a continuous controller to achieve tracking of the desired trajectory $x_d(t)$ by the output $x(t)$ of plant Equation 8.1.1. The linear controller Equation 8.4.3 was augmented by an estimate of the disturbance $g(x, x_d, t)$ in Equation 8.4.5. Often, such an estimate is not readily accessible. The disturbance rejection approach discussed in this section provides means to obtain an accurate disturbance estimate while avoiding chattering in the main control loop. This approach can be viewed as a special case of so-called integral sliding mode. A more mathematical background of integral sliding mode is described in Chapter 7.

The main idea of disturbance rejection via sliding mode is to compose the overall controller of a continuous part and a discontinuous part, i.e.,

$$u(t) = u_c(t) + u_d(t). \tag{8.5.1}$$

The idea of combining a continuous and a discontinuous part for the control input has been used by many authors [for a survey see, DeCarlo, Zak, and Matthews 1988]. The continuous component $u_c(t)$ is used to control the overall behavior of the system, whereas the discontinuous component $u_d(t)$ is used to reject disturbances and to suppress parametric uncertainties. A block diagram is shown in Figure 8.16.

Assume that, for the example system in Equation 8.1.1, the desired trajectory $x_d(t)$ is known but the disturbance $d(x, t)$ is unknown. Also assume the parameter b to be known and parameter a to be entirely unknown.

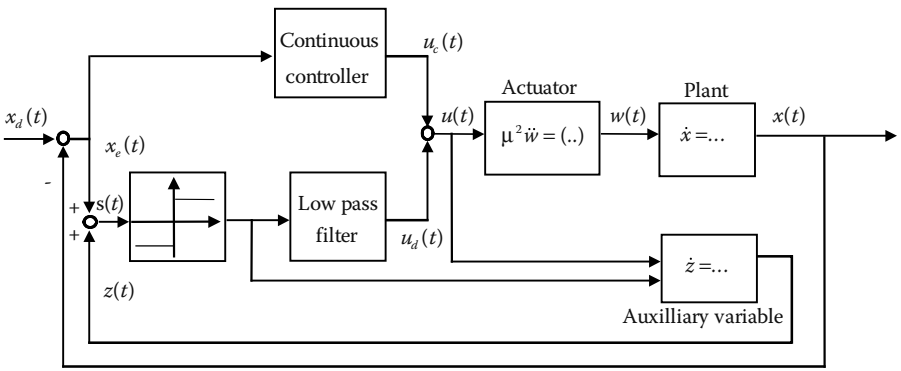

FIGURE 8.16
Disturbance rejection via sliding mode with auxiliary controller loop to avoid chattering. A continuous controller $u_c(t)$ is augmented by a disturbance rejection controller $u_d(t)$, derived from a low-pass-filtered discontinuous controller for an auxiliary control variable $z(t)$.

A continuous controller with linear feedback and feedforward of the desired trajectory $x_d(t)$ then can be designed as

$$u_c(t) = \frac{1}{b}\left(Cx_e(t) + \dot{x}_d(t)\right), \tag{8.5.2}$$

where $C > 0$ is a proportional feedback gain for the tracking error $x_e(t) = x_d(t) - x(t)$. Substitution of Equation 8.5.2 with the disturbance rejection term $u_d(t)$ being set to zero, i.e., $u(t) = u_c(t)$, into system dynamics (Equation 8.1.1) without actuator dynamics (Equation 8.1.2) yields stable error dynamics

$$\dot{x}_e(t) + Cx_e(t) = f(x,t), \tag{8.5.3}$$

which are perturbed by the disturbance function $f(x, t) = -ax(t) - d(x, t)$. Due to $f(x, t) \neq 0$, the tracking error $x_e(t)$ does not go to zero. A simulation in Figure 8.17 illustrates this with a "weak" feedback gain C, leading to imperfect tracking of the desired trajectory $x_d(t)$.

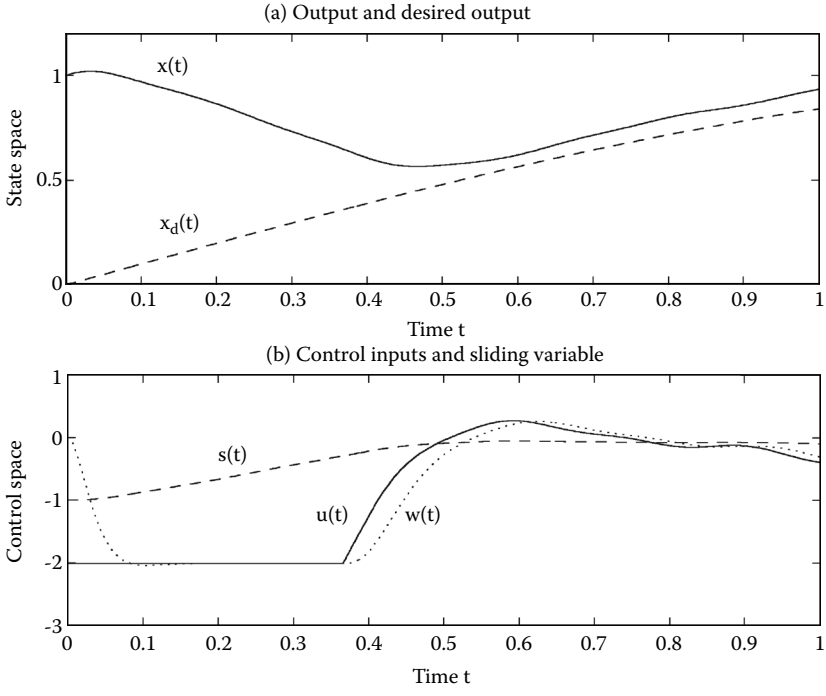

FIGURE 8.17
Linear feedback controller with feedforward of desired trajectory, $u_c(t)$, leads to inaccurate tracking of desired trajectory $x_d(t)$, because the closed-loop system (Equation 8.5.3) is perturbed by unknown plant dynamics $ax(t)$ and external disturbance $d(x,t)$.

To reduce the influence of disturbance $f(x, t)$ on the tracking performance, the second term in controller Equation 8.5.1 is designed as a disturbance estimator using sliding mode control. Define a sliding manifold as

$$s(t) = x_e(t) + z(t), \tag{8.5.4}$$

where $z(t)$ is an auxiliary sliding variable with

$$\dot{z}(t) = -\dot{x}_d(t) + bu(t) - bM \operatorname{sign} s(t). \tag{8.5.5}$$

Differentiation of the sliding variable $s(t)$ in Equation 8.5.4 and substitution of plant (Equation 8.1.1) and auxiliary sliding variable (Equation 8.5.5) yields

$$\begin{aligned} \dot{s}(t) &= \dot{x}_e(t) + \dot{z}(t) \\ &= -ax(t) - d(x,t) + b\big(u(t) - w(t)\big) - bM \operatorname{sign} s(t) \\ &< a^+ |x(t)| + d^+ + b\left| \left(\frac{\mu^2 p^2 + 2\mu p}{(\mu p + 1)^2} \right) u(t) \right| - bM \operatorname{sign} s(t). \end{aligned} \tag{8.5.6}$$

The third term in the right-hand side of the last row in Equation 8.5.6 is the mismatch between the actuator input and the actuator output and decays rapidly according to actuator dynamics (Equation 8.1.2). Note that this term can be fully eliminated if the actuator output is measurable and Equation 8.5.5 can be changed to

$$\dot{z}(t) = -\dot{x}_d(t) + bw(t) - bM \operatorname{sign} s(t). \tag{8.5.7}$$

Stability of the sliding manifold $s(t)$ can be established using Lyapunov function candidate

$$V(t) = \frac{1}{2} s^2(t). \tag{8.5.8}$$

Differentiation of Equation 8.5.8 and substitution of Equation 8.5.6 yields

$$\begin{aligned} \dot{V}(t) &= s(t)\dot{s}(t) \\ &< |s(t)| \left(a^+ |x(t)| + d^+ + b\mu \left| \left(\frac{\mu p^2 + 2p}{(\mu p + 1)^2} \right) u(t) \right| \right) - bM |s(t)|. \end{aligned} \tag{8.5.9}$$

Because the actuator time constant μ is assumed small, sliding mode exists for sufficiently large

$$M > \frac{1}{b}\left(a^+ |x(t)| + d^+ \right) \tag{8.5.10}$$

and $s(t) = 0$ after finite time. Choosing the initial conditions of the auxiliary sliding variable $z(t)$ in Equation 8.5.5 as $z(0) = -x_e(0)$ eliminates the reaching phase by setting $s(0) = 0$ in Equation 8.5.4. While the system is in sliding mode, the motion trajectories can be examined using the equivalent control method. Solving $\dot{s}(t) = 0$ in Equation 8.5.6 under the assumption $w(t) = u(t)$ for the discontinuity term yields the continuous equivalent control

$$\begin{aligned} u_{d_{\text{eq}}}(t) &= \frac{1}{b}\left(-ax(t) - d(x,t)\right) \\ &= \frac{f(x,t)}{b}, \end{aligned} \tag{8.5.11}$$

which delivers an exact estimate of the disturbance perturbing the error dynamics (Equation 8.5.3) of the system under continuous control alone. Thus, defining the second term in Equation 8.5.1 as

$$u_d(t) = u_{d_{\text{eq}}}(t) \tag{8.5.12}$$

leads to exact tracking with error dynamics

$$\dot{x}_e(t) + Cx_e(t) = 0 \tag{8.5.13}$$

instead of Equation 8.5.3 under $u(t) = u_c(t)$. Equation 8.5.13 ensures asymptotic tracking of $x_d(t)$ with disturbances. The equivalent control $u_{d_{\text{eq}}}(t)$ can be obtained by averaging the discontinuous switching component in the right-hand side of Equation 8.5.5, e.g., via a low pass

$$\begin{aligned} u_{d_{\text{eq}}}(t) &= u_{d_{ave}}(t) \\ u_{d_{ave}}(t) &= \frac{M}{(\varepsilon p + 1)} \operatorname{sign} s(t), \end{aligned} \tag{8.5.14}$$

where p denotes the Laplace variable and $\varepsilon > 0$ is a small time constant. Disturbance rejection controller $u_d(t)$ in Equation 8.5.14 is continuous. It was shown by Utkin [1992] that the low-pass average of the discontinuity term in Equation 8.5.14 equals the equivalent control (Equation 8.5.11). In systems with the ability to use discontinuous control inputs directly, the low-pass filter may be omitted completely.

The simulation in Figure 8.18 shows the improvement of the controller performance achieved by the disturbance estimator $u_d(t)$ compared with Figure 8.17. The bottom graph depicts the performance of the disturbance estimator and shows that $s(t) = 0$ at all times attributable to setting $z(0) = -x_e(0)$ and thus $s(0) = 0$. Estimation $u_{d_{ave}}(t)$ tracks the disturbance $f(x, t)$ consistently, with a small lag introduced by the averaging low pass in Equation 8.5.14.

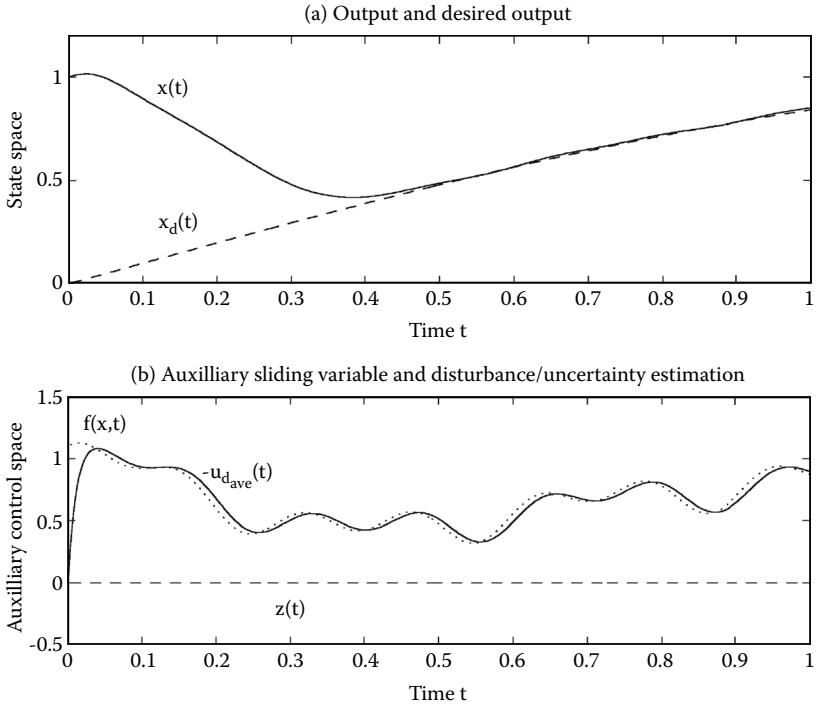

FIGURE 8.18
Performance of linear feedback controller with feedforward of desired trajectory, $u_c(t)$, is significantly improved by disturbance rejection controller $u_d(t)$ based on auxiliary variable $z(t)$ for estimating unknown plant dynamics $ax(t)$ and external disturbance $d(x, t)$ summarized as $f(x, t) = -ax(t) - d(x,t)$.

The closed-loop system is free of chattering despite the discontinuity in Equation 8.5.5 because the disturbance rejection term $u_d(t)$ is continuous. However, $x(t)$ tracks desired $x_d(t)$ exactly because of the rejection of disturbance $f(x, t)$, which also contains uncertainty in parameter a of the system in Equation 8.1.1. Note that the rejection of the parametric uncertainty does not assume constant system parameters but rather is able to also account for parameter variations.

8.6. State-Dependent Gain Method

This section provides an alternative way to suppress chattering without designing an additional system, e.g., an asymptotic observer that needs preliminary information of the system or plant. In Section 8.1.4, it was shown

that the magnitude of chattering is proportional to the gain M. Thus, the idea is to reduce the value of M without losing guarantee of existence of sliding mode. To support this idea, a state-dependent gain method is proposed [Lee and Utkin 2006]. The design idea will be illustrated for the second-order system with a state-dependent gain $M(x)$ in the sliding mode controller

$$\begin{aligned} \dot{x}_1 &= x_2 \\ \dot{x}_2 &= a_1 x_1 + a_2 x_2 + u \end{aligned} \tag{8.6.1}$$

$$\begin{aligned} s &= cx_1 + x_2 \\ u &= -M sign(s) \\ M &= M(x_1) = M_0(|x_1| + \delta), \end{aligned} \tag{8.6.2}$$

where c and M_0 are positive constant values, and δ is a sufficiently small, positive constant. Note that the gain M is not constant but a function of the state x_1. The constant M_0 should be selected to force sliding mode to occur along the switching surface. It may be found analytically from Equations 8.6.1 through 8.6.2:

$$\dot{s} = (a_1 - a_2 c - c^2)x_1 - M_0(|x_1| + \delta)sign(s). \tag{8.6.3}$$

Sliding mode exists if

$$|a_1 - a_2 c - c^2| \le M_0. \tag{8.6.4}$$

The approach based on state-dependent gain stems from the early publications on variable structure control of the 1960s [Emelyanov, Utkin Taran, Kostyleva, Shubladze, Ezerov, and Dubrovsky 1970].

Figure 8.19 demonstrates simulation results of the system (Equation 8.6.1) with constant and state-dependent gains in control

$$\begin{aligned} u_1 &= -M_0 sign(s) \\ u_2 &= -M_0(|x_1| + \delta)sign(s). \end{aligned} \tag{8.6.5}$$

It can be seen that the amplitude of the system input is significantly reduced by using the proposed controller compared with the result using conventional sliding mode control with a fixed gain M. In addition to the effect of chattering reducing, the state-dependent gain in control is expected to decrease the control effort. As the simulation shows, the both control algorithms result in the same trajectory for $x_1(t)$.

Now, second-order actuator dynamics

$$w(p) = \frac{1}{(\mu p + 1)^2} u(p)$$

are introduced into the system. At the presence of unmodeled dynamics, chattering arises but the magnitude of chattering is reduced by using state-dependent gain M as expected (Figure 8.20).

8.7. Equivalent Control-Dependent Gain Method

Any method would be helpful to suppress chattering if it can decrease the gain M while maintaining sliding mode. In the previous section, reducing M along with the system state was suggested. This methodology will hardly be applicable for nonlinear systems at the presence of unknown disturbances. As shown in Section 2.3, the motion in sliding mode is determined by the equivalent control u_{eq}, a solution to equation $\dot{s} = 0$ with respect to control. The function u_{eq} is an average value of the real discontinuous control, and, of course, the real control amplitude should be greater than $|u_{eq}|$. Conversely, u_{eq} can be easily obtained using a low-pass filter. Hence, the smallest allowable amplitude of the discontinuous control can be based on the equivalent control

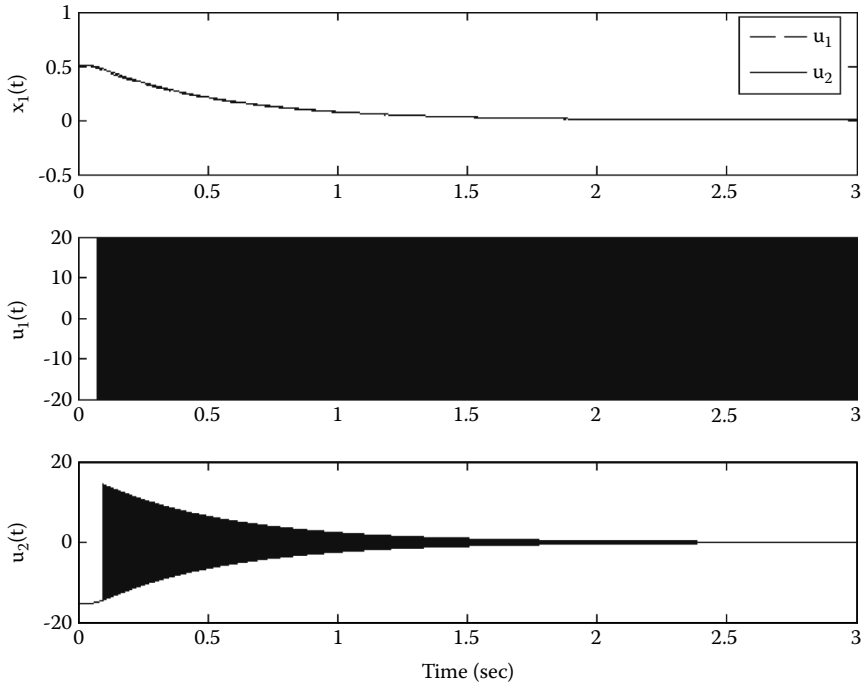

FIGURE 8.19
Simulation results for the system in Equation 8.6.1 with two different controllers.

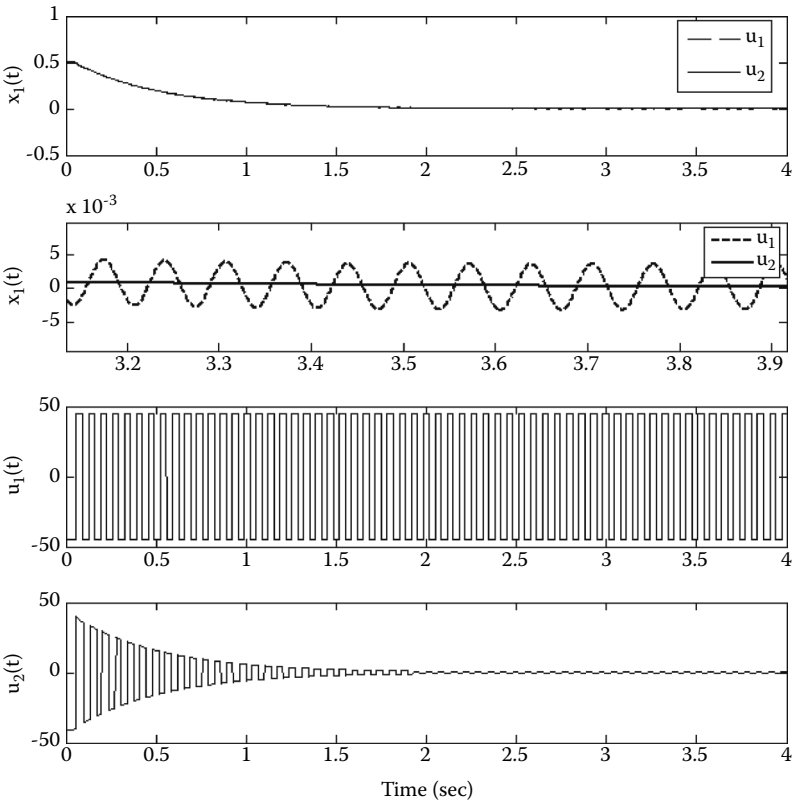

FIGURE 8.20
Chattering is reduced by using state-dependent gain in control.

obtained by low-pass filtering of the real, discontinuous control such that sliding mode is maintained once it has occurred [Lee and Utkin 2006].

Although the equivalent control-dependent gain method will be demonstrated for a first-order system, it is applicable for any system with scalar control.

For the following system,

$$\dot{x} = f(x,t) + u, \tag{8.7.1}$$

select control as a discontinuous function of equivalent control

$$u = -M(|\sigma| + \delta)sign(x), \tag{8.7.2}$$

where $M > |f(x,t)|$, δ is a positive constant value, and σ is the average value of $sign(s)$, which is equal to $[sign(x)]_{eq}$. The value of $[sign(s)]_{eq}$ can be found using a low-pass filter $\tau\dot{\sigma} + \sigma = sign(s)$ ($\tau << 1$).

Suppose that, at initial time $x(0) \neq 0$, then $sign(x) = \pm 1$, $|\sigma| = 1$ and functions $x(t)$ and $\dot{x}(t)$ have opposite signs; therefore, sliding mode will appear at point $x = 0$ after finite time interval. After sliding mode occurs, it will not disappear, as follows.

Lemma 8.1

The absolute value of equivalent control approximation σ is less than 1.

Proof 8.1

If sliding mode exists, $\dot{x}$ becomes zero and the equivalent control $sign(x)_{eq} = \sigma$:

$$\dot{x} = f(x) - M(|\sigma| + \delta)\sigma = 0. \tag{8.7.3}$$

1. If $f(x) > 0$, then $\sigma > 0$ and Equation 8.7.3 becomes

   $$M\sigma^2 + M\delta\sigma - f = 0,$$

   with the solution

   $$\sigma = \frac{-M\delta + \sqrt{(M\delta)^2 + 4Mf}}{2M}, \text{ or } \sigma = -\frac{\delta}{2} + \sqrt{\left(\frac{\delta}{2}\right) + \frac{f}{m}} = \frac{\frac{f}{M}}{\frac{\delta}{2} + \sqrt{\left(\frac{\delta}{2}\right)^2 + \frac{f}{M}}}.$$

   Hence, $0 < \sigma \leq \sqrt{\frac{f}{M}}$ because $M > |f(x)|$.

2. If $f(x) < 0$, then $\sigma < 0$. Similarly, Equation 8.7.3 is rewritten as $M\sigma_2 - M\delta\sigma + f = 0$. With the solution

   $$\sigma = \frac{\delta}{2} - \sqrt{\left(\frac{\delta}{2}\right)^2 - \frac{f}{M}} = -\frac{-\frac{f}{M}}{\frac{\delta}{2} + \sqrt{\left(\frac{\delta}{2}\right)^2 - \frac{f}{M}}}.$$

   Therefore, $-1 < -\sqrt{-\frac{f}{M}} < \sigma < 0$. Finally, $-1 < \sigma < 1$. □

The system dynamics (Equation 8.7.3) may be rewritten as

$$\begin{aligned}\dot{x} &= f(x) - M(|\sigma| + \delta)sign(x) \\ &= f(x) - M(|\sigma| + \delta)\{sign(x) - \sigma + \sigma\} \\ &= -M\{sign(x) - \sigma\}.\end{aligned}$$

Because $|\sigma| < 1$, x and $\dot{x}$ have different signs, sliding mode cannot disappear.

If $f(x, t)$ is reduced to zero during sliding mode, then control u tends to $-M\delta sign(x)$, which leads to a decreased control amplitude. As a result, the chattering will be attenuated.

Simulation results for the system (Equation 8.6.1) with control $u_1 = -M(|\sigma| + \delta)sign(s)$, $\sigma = [sign(s)]_{eq}$, and $u_2 = -Msign(s)$, ($M = const$) are shown in Figure 8.21. Chattering reduction is observed in the system with equivalent control-dependent gain.

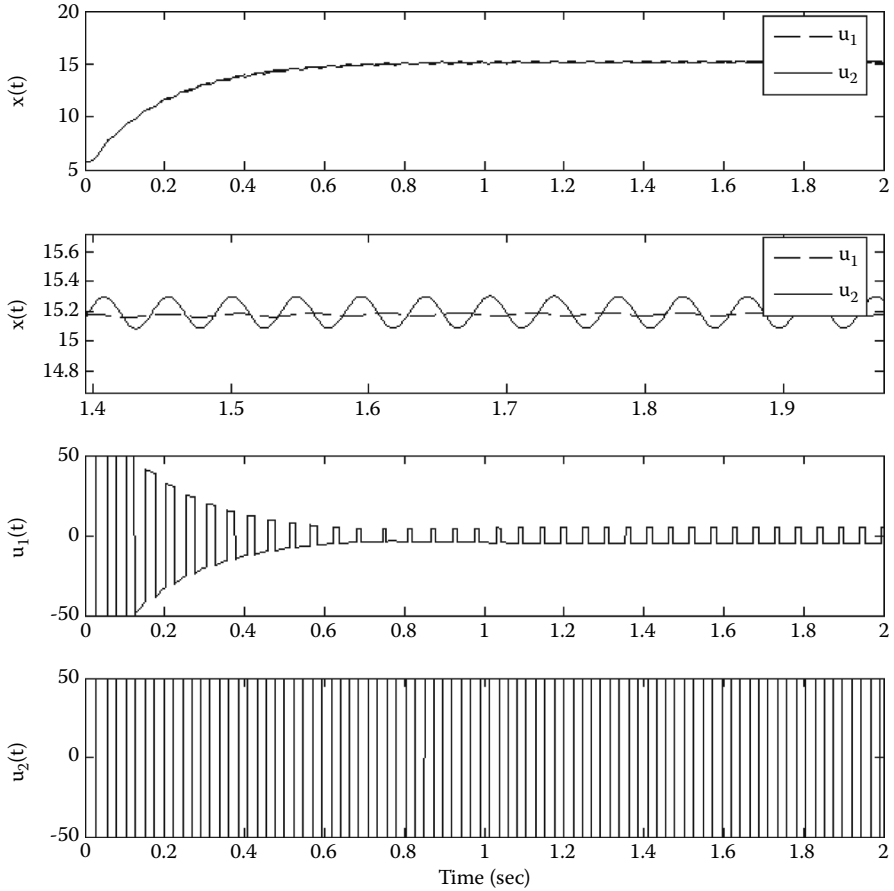

FIGURE 8.21
Comparison of chattering for equivalent control-dependent and constant gains.

8.8. Multiphase Chattering Suppression

8.8.1. Problem Statement

Although the introduction of state observers leads to a significant reduction of chattering, their application needs information about the process equations. The common way to implement sliding mode control is based on electronic power converters with "on/off" as the only admissible switching operation mode. An output of converters can take only two (or finite number of) values; therefore, the methodologies of Sections 8.5 and 8.6 are not applicable for chattering suppression. A natural way to reduce chattering is increasing switching frequency. However, it is not always possible as a result of limitation of switching frequency or losses in power converters. In addition, implementation of sliding modes in power converters results in frequency variations, which is unacceptable in many applications.

The challenge is to design a multiphase converter system based on a given, fixed switching frequency, reducing chattering to a desired level. This may be possible by providing a desired phase shift between phases for any loads and frequencies to implement the "harmonic cancellation" method. Attempts to apply this idea to PWM have been made such that phase shifts are interconnected and can be controlled, using a transformer with primary and secondary coils in different phases. Alternatively, the phase shift was obtained using delays, filters, or set of triangular inputs with selected delays [Miwa, Wen, and Schecht 1992; Xu, Wei, and Lee 2003; Woo, Lee, and Schuellein 2006]. Frequency control can be performed changing the width of a hysteresis loop in switching devices [Ngyuen and Lee 1995; Cortes and Alvarez 2002].

The approach in this section stems from the nature of the sliding mode control and provides a desired phase shift between phases for any frequency without any additional dynamic elements.

To formulate the problem statement, consider the system with scalar control,

$$\begin{aligned} \dot{x} &= f(x,t) + b(x,t)u \\ (x, f, b &\in \Re^n,). \end{aligned} \tag{8.8.1}$$

For system Equation 8.8.1, it is assumed that control should be designed as a continuous function of state variables $u_0(x)$. This situation is common for so-called "cascade control" used for electric motors with current as a control input. To implement the desired control, power converters often use PWM as a principle operation mode. Sliding mode is one of the tools to implement this mode based on the feedback approach as shown in Figure 8.22, which illustrates that the output u tracks the reference input $u_0(x)$ in sliding mode:

$$\begin{aligned} &s = u_0(x) - u,\ \dot{u} = v = Msign(s),\ M > 0, \\ &\dot{s} = g(x) - Msign(s),\ g(x) = [grad(u_0)]^T(f + bu). \end{aligned} \tag{8.8.2}$$

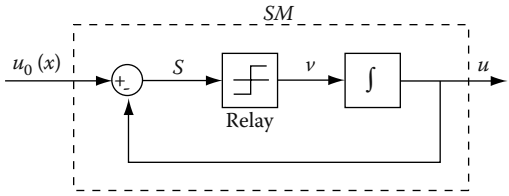

FIGURE 8.22
Sliding mode control for a simple power converter model.

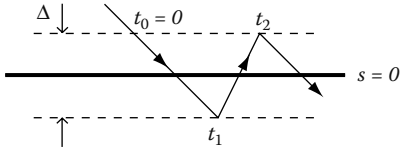

FIGURE 8.23
Oscillation in the vicinity of switching surface.

It is evident that sliding mode in the surface $s = 0$ with $u \equiv u_0(x)$ exists if $M > |g(x)|$. If the control is implemented with a hysteresis loop, chattering with oscillation amplitude $A = \frac{\Delta}{2}$ in s is illustrated in Figure 8.23.

Under the assumption that the switching frequency is high enough, the state x can be considered as constant within the time interval $[t_0, t_2]$, and the switching frequency is found as $f = \frac{1}{t_1 + t_2}$, where $t_1 = \frac{\Delta}{M - g(x)}, t_2 = \frac{\Delta}{M + g(x)}$. So, Δ can be selected as

$$\Delta = \frac{M^2 - g(x)^2}{2M} \frac{1}{f_{des}} \tag{8.8.3}$$

to maintain the switching frequency at the desired level f_{des}; however, the magnitude of oscillation may be unacceptable. The hysteresis loop can be implemented by a switching element with gain K_h as depicted in Figure 8.24.

Let us assume now that the desired control is implemented by m power converters, called "multiphase converter," with $s_i = \frac{u_0}{m} - u_i, (i = 1, 2, \ldots m)$ and $\frac{u_0}{m}$ as reference inputs as shown in Figure 8.25.

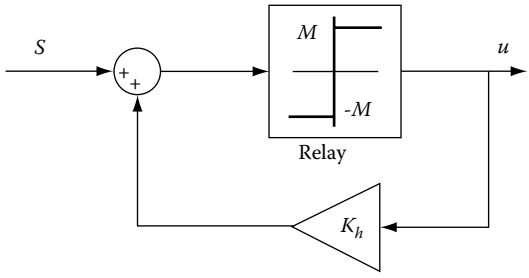

FIGURE 8.24
Implementation of hysteresis loop with width $\Delta = K_h M$.

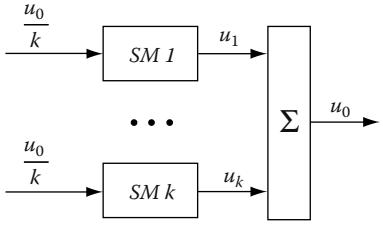

FIGURE 8.25
m-phase converter with evenly distributed reference input.

If each power converter operates properly, the output is equal to the desired control $u_0(x)$. Amplitude and frequency in each converter can be found as follows:

$$A = \frac{\Delta}{2}, f = \frac{M^2 - \left\{\frac{g(x)}{m}\right\}^2}{2M\Delta}. \tag{8.8.4}$$

The amplitude of chattering in u_0 depends on the oscillation in each converter phase, and, in the worst case, it can be m times higher than that of each converter. For the system in Figure 8.22, phases depend on initial conditions and cannot be controlled. However, as was demonstrated for the system in Equation 2.1.1 (see also Figure 2.1), switching instants or phase shift between oscillations in different control channels are not independent if the channels are interconnected. Hence, if discontinuous inputs of the integrators are interconnected, then the phases of oscillations will be interdependent, which gives hope to reduce the chattering amplitude in the output signal. First, it should be demonstrated that, by controlling phases, the output oscillation amplitude can be reduced.

Suppose that a multiphase converter with m phases is to be designed such that the period of chattering T is the same in each phase, and two subsequent phases have phase shift T/m. Because chattering is a periodic time function, it can be represented as Fourier series with frequencies

$$\omega_k = \omega \cdot k, \omega = \frac{2\pi}{T} (k = 1, 2, \cdots, \infty). \tag{8.8.5}$$

The effect of kth harmonic in the output signal is the sum of individual outputs from all of phases and can be easily calculated as follows:

$$\sum_{i=0}^{m-1} sin\left[\omega_k (t - \frac{2\pi}{\omega m} i)\right] = \sum_{i=0}^{m-1} Im\left[e^{j(\omega_k t - \frac{2\pi k}{m} i)}\right]$$
$$= Im(e^{j\omega_k t} Z), Z = \sum_{i=0}^{m-1} e^{-j\frac{2\pi k}{m} i}. \tag{8.8.6}$$

To find Z, let us consider the following equation:

$$Ze^{-j\frac{2\pi k}{m}} = \sum_{i=0}^{m-1} e^{-j\frac{2\pi k}{m}(i+1)} = \sum_{i'=1}^{m} e^{-j\frac{2\pi k}{m} i'}. \tag{8.8.7}$$

Because $Ze^{-j\frac{2\pi k}{m} i}\Big|_{i=m} = e^{-j\frac{2\pi k}{m} i}\Big|_{i=0}$, it follows from Equation 8.8.7,

$$Ze^{-j\frac{2\pi k}{m}} = Z.$$

The function $e^{-j\frac{2\pi k}{m}}$ is equal to one only if $\frac{k}{m}$ is integer or $k = m, 2m, \ldots$, which means that $Z = 0$ for all other cases. This analysis shows that all harmonics except for lm ($l = 1, 2, \ldots$) are suppressed in the output signal. As a result, the amplitude of chattering can be reduced to the desired level by increasing the number of phases, providing a desired phase shift between two subsequent phases from the methodology proposed in the previous section.

The above analysis lets us outline the design method for suppressing chattering: first select the width of the hysteresis loop in each phase in compliance with Equation 8.8.3 (or $K_h = \Delta/M$) to have the desired switching frequency. Then select the number of phases m and switching functions to provide the desired phase shifts T/m. The last problem will be addressed in the next section.

8.8.2. Design Principle

Let two power converters be implemented as shown in Figure 8.26, and the switching function for the second converter is proposed as $s_2^* = s_2 - s_1$: ($s_1 = u_0/2 - u_1$, $s_2 = u_0/2 - u_2$, $\nu_1 = Msign(s_1)$, and $\nu_2 = Msign(s_2^*)$).

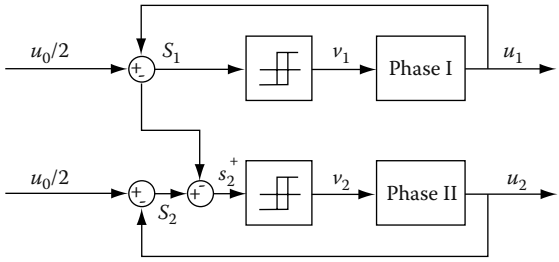

FIGURE 8.26
A controller model with two interconnected phases.

Then, time derivatives of s_1 and s_2^* become

$$\begin{aligned} s_1 &= a - M sign(s_1)\ (a = \frac{g(x)}{k}) \\ s_2^* &= M sign(s_1) - M sign(s_2^*). \end{aligned} \tag{8.8.8}$$

The system behavior in the plane s_1 and s_2^* is analyzed with the widths of hysteresis loops for the two sliding surfaces being Δ and $\alpha\Delta$, respectively. First, the case $a = 0$ and $\alpha = 1$ is considered. As can be seen from Figure 8.27, phase shift between ν_1 and ν_2 is equal to $\frac{T}{4}$ for any value of Δ, where T is the period of oscillations $T = \frac{2\Delta}{M}$.

It is evident that, for any initial conditions different from point 0 (for instance, 0′), the motion represented in Figure 8.27 will appear in time less than $\frac{T}{2}$. A similar analysis may be performed for the case $a \neq 0$ (of course $M > |a|$) and $\alpha \neq 1$. In Figure 8.28, s plane is demonstrated for $a > 0$ and $\alpha > 1$. Also, the period of oscillations T can be easily found from the equation with respect to s_1 as follows:

$$T = \frac{\Delta}{M - a} + \frac{\Delta}{M + a} = \frac{2M\Delta}{M^2 - a^2}. \tag{8.8.9}$$

From Figure 8.28 and Equation 8.8.8, it can be seen that the phase shift becomes

$$\phi = \frac{\alpha\Delta}{2M}, \tag{8.8.10}$$

which is equal to the time for changing s_2^* from $\frac{\alpha\Delta}{2}$ to $-\frac{\alpha\Delta}{2}$ or vice versa. The switching illustrated in Figure 8.28 takes place if

$$\frac{\alpha\Delta}{2M} \leq \frac{\Delta}{M + |a|}. \tag{8.8.11}$$

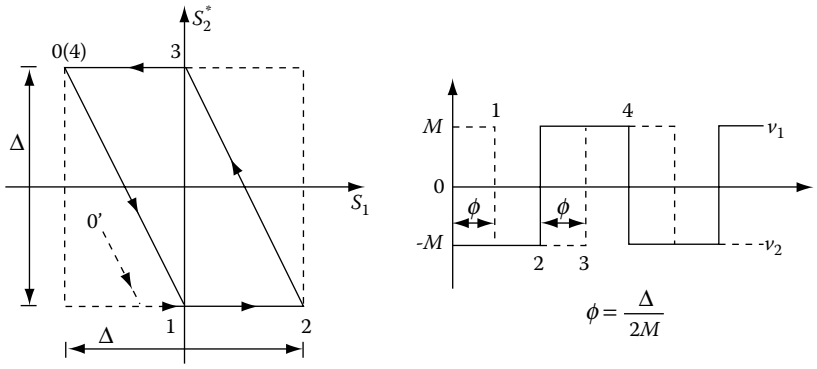

FIGURE 8.27
The system behavior in *s* plane with $\alpha = 1$.

Otherwise, for the trajectory starting from point 2 in Figure 8.28, ν_1 will switch from M to $-M$ before ν_2 switches from $-M$ to M at point 3.

As follows from this example, the phase shift between oscillations can be selected by proper choice of α for any switching frequency without using dynamic elements, e.g., transformers and filters.

Next, we show that the selection of the phase number depends on the range of the function a. First, the value α is calculated to provide the desired phase shift. Because ϕ must be equal to T/m, α can be found from Equations 8.8.9 through 8.8.11 as

$$\alpha = \frac{4M^2}{m(M^2 - a^2)}, \tag{8.8.12}$$

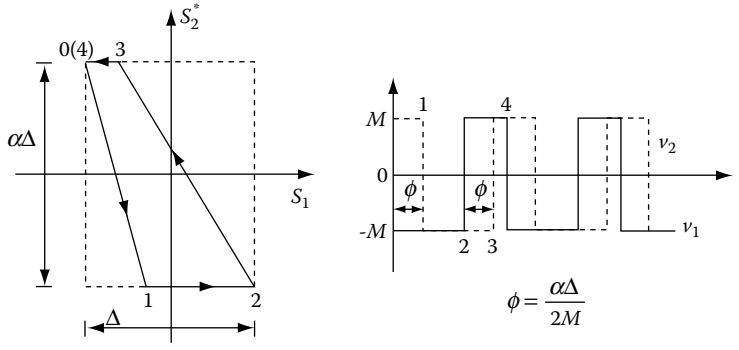

FIGURE 8.28
Control of the phase between ν_1 and ν_2.

where the function a is assumed to be bounded as $|a| < a_{\max} < M$. According to Equations 8.8.11 and 8.8.12 for a positive a, the following condition should hold:

$$\frac{4M^2}{m(M^2 - a^2)} \frac{\Delta}{2M} \leq \frac{\Delta}{M + a}.$$

or

$$m > \frac{2M}{M - a_{\max}}. \tag{8.8.13}$$

Similarly, it also can be shown that the same condition should hold for a negative a.

The above results may be summarized as the design procedure for the multiphase converter:

- Select the width of hysteresis loop as a state function such that the switching frequency in the first phase is maintained at the desired level.
- Determine the number of phases for a given range of function a variation.
- Find the parameter α as a function of a such that the phase shift between two subsequent phases is equal to $\frac{1}{m}$ of the oscillation period of the first phase.

Remark 8.1.

As follows from Equation 8.8.13, the following condition for a should hold:

$$|a| \leq M\left(1 - \frac{2}{m}\right)(m \geq 2)\cdot \tag{8.8.14}$$

If not, it can lead to the collapse of the switching sequence. Also, the frequency of the second phase may change. To preserve the switching sequence and frequency even in case $|a| > a_{max}\left(a_{max} = M\left(1 - \frac{2}{m}\right)\right)$, the condition in Equation 8.8.11 must be always fulfilled. Therefore, the function α should be selected as in Equation 8.8.12 for Equation 8.8.14 and in compliance with Equation 8.8.11, i.e.,

$$\alpha = \begin{cases} \dfrac{4M^2}{m(M^2 - a^2)} & if\ |a| < M\left(1 - \dfrac{2}{m}\right) \\ \dfrac{2M}{M + |a|} & if\ a_{max} < |a| < M. \end{cases} \tag{8.8.15}$$

Another version, called "master-slave mode," of multiphase converters is proposed here based on phase shift control with sliding mode. The approach implies frequency control in the first phase and open-loop control for the others as illustrated in Figure 8.29.

The first phase (master) is connected to the next phase (slave) through an additional first-order system as a shifter such that the discontinuous input v_2 for the slave has a desired phase shift from v_1 without changing switching frequency.

To demonstrate the design idea, a two-phase converter system similar to the one in Section 8.8.2 is considered. The equation of the first phase,

$$\dot{s}_1 = a - v_1, v_1 = Msign(s_1), \tag{8.8.16}$$

is complemented by the following equation of an additional first-order dynamic system:

$$\dot{s}_2^* = K(v_1 - v_2), v_2 = Msign(s_2^*). \tag{8.8.17}$$

The second phase cannot be governed by Equation 8.8.17 for $K \neq 1$, because the control input in any phase can take only the two values $+M$ and $-M$. The

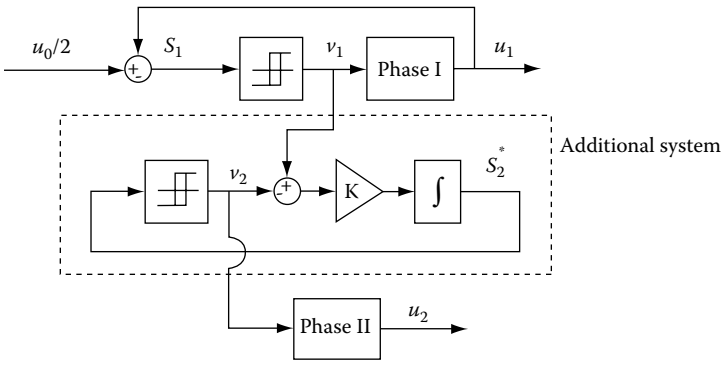

FIGURE 8.29
Two-phase power converter model in the master-slave mode.

analysis of the system behavior can be performed in the same manner as in the previous sections. With the width of hysteresis loop Δ, the phase shift between v_1 and v_2 becomes

$$\phi = \frac{\Delta}{2KM}, \tag{8.8.18}$$

whereas the phase shift from the earlier design principle can be found in Equation 8.8.10. Comparing Equation 8.8.10 with Equation 8.8.18, the value of K is found as $1/\alpha$ or

$$K = \frac{m(M^2 - a^2)}{4M^2}. \tag{8.8.19}$$

For multiphase converters, the desired control of each phase can be obtained similarly from the control of the previous phase; the input to kth phase, v_k, is a phase-shifted signal from the input to the previous phase v_{k-1}.

Remark 8.2

In the additional dynamic system (Equation 8.8.17), the width of hysteresis loop $\tilde{\Delta}$ ($\tilde{\Delta} = \alpha\Delta$) and the amplitude of both discontinuous functions $\tilde{M}$ ($\tilde{M} = \beta M$) may be chosen arbitrarily (α, β = const.). Then, the phase shift becomes

$$\tilde{\phi} = \frac{\alpha\Delta}{2K\beta M} = \frac{\Delta}{2\tilde{K}M}, \quad \left(\tilde{K} = \frac{K\beta}{\alpha}\right),$$

and $\tilde{K}$ should be selected properly from Equation 8.8.12.

Remark 8.3

Similar to the first version varying the width of a hysteresis loop, the desired phase shift cannot be provided by master-slave modification in Figure 8.29 if the condition in Equation 8.8.13 does not hold. However, for the master-slave version, the necessary phase shift can be gained by sequential connection of several "slaves" such that each of them has an admissible phase shift.

8.9. Comparing the Different Solutions

In applications of sliding mode control, unmodeled dynamics in the control loop are often excited by the discontinuous switching action of a sliding mode controller, leading to oscillations in the motion trajectory. Because of

the acoustic noise that such oscillations may cause in mechanical systems, this phenomenon is also referred to as chattering. This chapter studied the chattering problem and presented several solutions to reliably eliminate or significantly reduce chattering in the control loop. To successfully prevent chattering, these methods require some estimate of the time constant or the bandwidth of the unmodeled dynamics. Instead of achieving exact tracking performance as in ideal sliding mode, small tracking errors are tolerated.

In general, the achievable performance of a control system depends on the performance of sensors and actuators, availability of knowledge about the system, i.e., the quality of the system model, and the availability of measurements of system variables. For example, a system with a slow actuator cannot fully reject fast disturbances, regardless of the control design methodology used. A sliding mode controller under ideal conditions is able to fully exploit the system capabilities. Under realistic conditions, a chattering prevention scheme should be selected to meet the system specifications and to ensure good control performance.

The first method substitutes the discontinuity of a sliding mode controller by a saturation function and yields motion in a boundary layer of the sliding manifold instead of true sliding along the manifold. Effectively, sliding mode methodology is used to design a continuous high-gain controller that respects bounds on the control resources.

The second method shifts the switching action of the sliding mode controller into an auxiliary observer loop, thus circumventing unmodeled dynamics in the main loop and achieving ideal sliding mode in the observer loop. The plant follows the ideal trajectory of the observer according to the observer performance. Because the control input to the plant is still discontinuous, this method is ideal for systems that already have an observer in the control structure or for systems with inherently discontinuous control inputs such as voltage inputs of electric drives. Implementation of a continuous controller in a system with discontinuous inputs generally requires PWM, whereas direct implementation of sliding mode control with an observer avoids PWM.

The third method is mainly designed for systems in which some knowledge of the unmodeled dynamics and intermediate measurements are available, e.g., known actuator dynamics. Such systems consisting of separated blocks may be controlled with a cascaded control structure that avoids chattering by explicitly taking the unmodeled dynamics into account for the control design. In this sense, they are no longer unmodeled but rather part of the overall system model.

The fourth method combines a continuous and a discontinuous controller to achieved good performance without chattering. The continuous part controls the overall motion, whereas the task of the discontinuous part is to reject the influence of parametric uncertainty and disturbances. This method is a special case of integral sliding mode and is especially useful for systems with large uncertainties and/or disturbances.

The state- or equivalent-control-dependent gain methods are efficient tools to significantly reduce chattering. However, in many cases, they are not applicable because the actuators in the control systems are power converters with a finite number of output voltage values.

In addition, even without unmodeled dynamics, the switching frequency of power converters should be bounded as a result of heat losses during each switching, which is proportional to the square of the switched current. A multiphase sliding mode power converter is a feasible method for reducing both chattering and heat losses.

All methods possess their advantages and disadvantages, both of which depend on the system specifications. When designing a sliding mode controller for a given system, the chattering prevention method usually requires careful consideration of all details; unfortunately, no textbook solution exists to cope with all systems in a general manner.

References

Bondarev AG, Bondarev SA, Kostyleva NE, Utkin VI. 1985. "Sliding Modes in Systems with Asymptotic State Observers." *Automation Remote Control* 46:49–64.

Cortes D, Alvarez J. 2002. "Robust Sliding Mode Control for the Boost Converter." Power Electronics Congress, Technical Proceedings, Cooperative Education and Internship Program 2002, VIII IEEE International, Guadalajara, Mexico.

DeCarlo RA, Zak SH, Matthews GP. 1988. "Variable Structure Control of Nonlinear Multivariable Systems: A Tutorial." *Proc IEEE* 76:212–232.

Drakunov SV, Izosimov DB, Luk'yanov AG, Utkin VA, Utkin VI. 1984. "A Hierarchical Principle of the Control Systems Decomposition based on Motion Separation." Preprints of the Ninth International Federation of Automatic Control Congress, Budapest, Hungary.

Drakunov SV, Izosimov DB, Luk'yanov AG, Utkin VA, Utkin VI. 1990a. "Block Control Principle I." *Automation Remote Control* 51:601–609.

Drakunov SV, Izosimov DB, Luk'yanov AG, Utkin VA, Utkin VI. 1990b. "Block Control Principle II." *Automation Remote Control* 52:737–746.

Emelyanov S, Utkin V, Taran V, Kostyleva N, Shubladze A, Ezerov V, Dubrovsky E. 1970. *Theory of Variable Structure Systems* (in Russian). Moscow: Nauka.

Kokotovic PV. 1984. "Applications of Singular Perturbation Techniques to Control Problems." *SIAM Rev* 6:501–550.

Kokotovic PV, O'Malley RB, Sannuti P. 1976. "Singular Perturbations and Order Reduction in Control Theory." *Automatica* 12:123–132.

Krstic M, Kanellakopoulos I, Kokotovic P. 1995. *Nonlinear and Adaptive Control Design*. New York: Wiley-Interscience.

Lee H, Utkin VI. 2006. "Chattering Analysis." In *Advances in Variable Structure and Sliding Mode Control*. London: Springer-Verlag, 107–121.

Leitmann G. 1981. "On the Efficacy of Nonlinear Control in Uncertain Systems." *ASME J Dyn Syst Measure Control* 102:95–102.

Miwa B, Wen D, Schecht M. 1992. "High Efficiency Power Factor Correction Using Interleaving Techniques." IEEE Applied Power Electronics Conference, Boston, MA.

Nguyen VM, Lee CQ. 1995. "Tracking Control of Buck Converter using Sliding-Mode with Adaptive Hysteresis." Power Electronics Specialists Conference, PESC '95 Record, 26th Annual IEEE Conference, Atlanta, GA.

Slotine J-J. 1984. "Sliding Controller Design for Nonlinear Systems." *Int J Control* 40:421–434.

Slotine J-J, Sastry SS. 1983. "Tracking Control of Nonlinear Systems Using Sliding Surfaces, with Application to Robot Manipulators." *Int J Control* 38:465–492.

Utkin VI. 1992. *Sliding Modes in Control and Optimization*. Berlin: Springer-Verlag.

Utkin VI. 1993. "Application Oriented Trends in Sliding Mode Theory." Proceedings of the IEEE Industrial Electronics Conference, Maui, HI.

Woo W, Lee N-C, Schuellein G. 2006. "Multi-Phase Buck Converter Design with Two-Phase Coupled Inductors." Applied Power Electronics Conference and Exposition 2006, 21st Annual IEEE Conference, Seattle, WA.

Xu P, Wei J, Lee FC. 2003. "Multiphase Coupled-Buck Converter: A Novel High Efficient 12 V Voltage Regulator Module, Power Electronics." *IEEE Trans* 18:74–82.

9

Discrete-Time and Delay Systems

Sliding mode is a very powerful tool for control design. So far, this text has concentrated on sliding mode control design for continuous-time systems. However, in many practical problems, controllers are implemented in discrete time, e.g., using microprocessors. Similar to the development of linear systems theory in the 1960s and 1970s, the discretization process requires the approach to be rethought. This chapter seeks to develop a general concept for discrete-time sliding mode and presents linear systems as design examples. This new concept is further extended to systems with delays and distributed systems.

9.1. Introduction to Discrete-Time Systems

Most sliding mode approaches are based on finite-dimensional continuous-time models and lead to discontinuous control action. Once such a dynamic system is "in sliding mode," its motion trajectory is confined to a manifold in the state space, i.e., to the sliding manifold. Generally speaking, for continuous-time systems, this reduction of the system order may only be achieved by discontinuous control, switching at theoretically infinite frequency.

When challenged with the task of implementing sliding mode control in a practical system, the control engineer has two options:

- Direct, analog implementation of a discontinuous control law with a very fast switching device, e.g., with power transistors.
- Discrete implementation of sliding mode control, e.g., with a digital microcontroller.

The first method is only suitable for systems with a voltage input, allowing the use of analog switching devices. Most other systems are usually based on a discrete microcontroller-based implementation. However, a discontinuous control designed for a continuous-time system model would lead to chatter when implemented without modifications in discrete time with a finite sampling rate. This discretization chatter is different from the chattering problem caused by unmodeled dynamics as discussed in Chapter 8. Discretization chatter is attributable to the fact that the switching frequency

is limited to the sampling rate, but correct implementation of sliding mode control requires infinite switching frequency. The following example will illustrate the difference between ideal continuous-time sliding mode and direct discrete implementation with discretization chatter. The subsequent sections of this chapter are dedicated to the development of a discrete-time sliding mode concept to eliminate the chatter. This concept then is extended to systems with delays and distributed systems governed by differential-difference equations.

Example 9.1: Ideal Sliding Mode versus Discrete Implementation

Examine a first-order example system modeled in continuous time as

$$\dot{x}(t) = g\big(x(t)\big) + u(t), \tag{9.1.1}$$

with state $x(t)$, bounded dynamics $|g(x)| \le \bar{g}$, and control input $u(t)$. To enforce sliding mode on a manifold

$$\sigma = \{x: x(t) = 0\}, \tag{9.1.2}$$

a discontinuous control law may be designed as

$$u(t) = -u_0 \operatorname{sign} x(t), \tag{9.1.3}$$

with available control resources $u_0 > \bar{g}$. The usual Lyapunov-based stability analysis examines

$$V = \frac{1}{2}x^2(t) \tag{9.1.4}$$

along the trajectories of system (Equation 9.1.1) with control (Equation 9.1.3), leading to

$$\begin{aligned} \dot{V}(t) &= x(t)\big(g\big(x(t)\big) - u_0 \operatorname{sign} x(t)\big) \\ &\le -|x(t)|(u_0 - \bar{g}), \end{aligned} \tag{9.1.5}$$

which testifies to convergence to the manifold (Equation 9.1.2) within finite time. An example trajectory is shown in Figure 9.1 with $g(t) = \sin(t)$ and $u_0 = 2$, starting from initial conditions $x(t = 0) = 3$. At t_{sm} the system reaches the sliding manifold $x = 0$. Thereafter, the motion trajectory is invariantly confined to the manifold (Equation 9.1.2) via discontinuously switching control, illustrated in the bottom diagram of Figure 9.1 by a black rectangle.

A direct discrete implementation with sampling time Δt would result in

$$\begin{aligned} x_{k+1} &= x_k + (g_k + u_k)\Delta t, \\ u_k &= -u_0 \operatorname{sign} x_k, \\ k &= 1, 2, \ldots, \end{aligned} \tag{9.1.6}$$

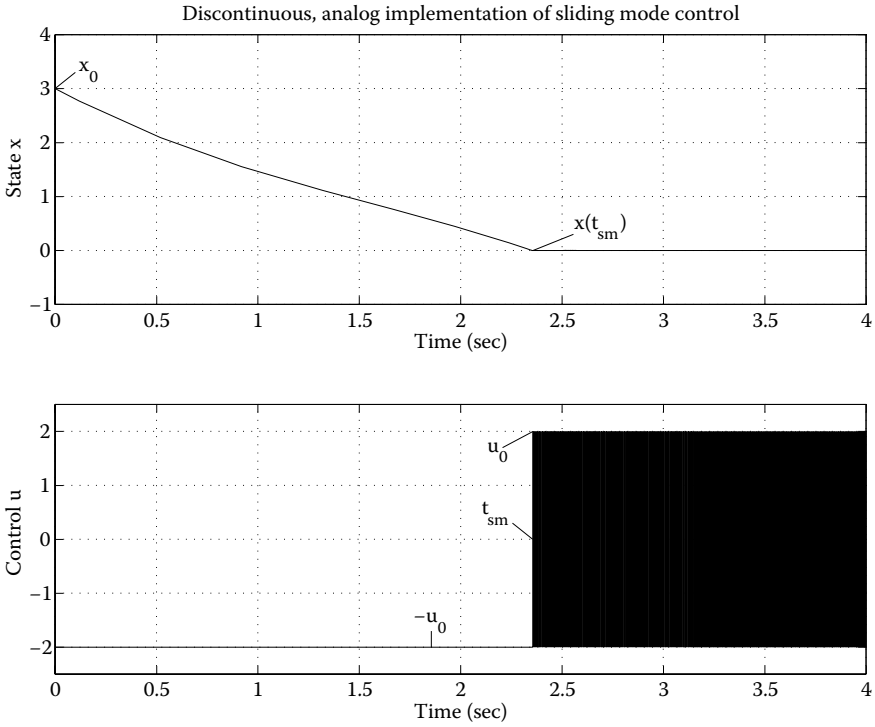

FIGURE 9.1
Ideal sliding mode in first-order example system achieved via direct, analog implementation of a discontinuous control law with infinitely fast switching.

where subscript k denotes the sampling points, e.g., the system state x_k at time instance $t_k = k\Delta t$. The motion trajectory may not reach the manifold $x = 0$ because control u_k is only calculated at the sampling points k, i.e., the switching frequency is limited by the sampling rate $1/\Delta t$. During the sampling interval Δt, the control is constant and the system behaves like an open-loop system [Kotta 1989].

The example with exaggerated large sampling time $\Delta t = 0.1$sec as depicted in Figure 9.2 illustrates the need to develop a discrete-time sliding mode algorithm rather than implementing Equation 9.1.6.

It should be noted that increasing the sampling rate decreases the amplitude of the discretization chatter and increases its frequency but may not eliminate this discrete-time phenomenon unless $\Delta t \to 0$. Moreover, the sampling rate of a control system should correspond to the fastest dynamics of the system instead of "wasting" computational power for the control algorithm's sake.

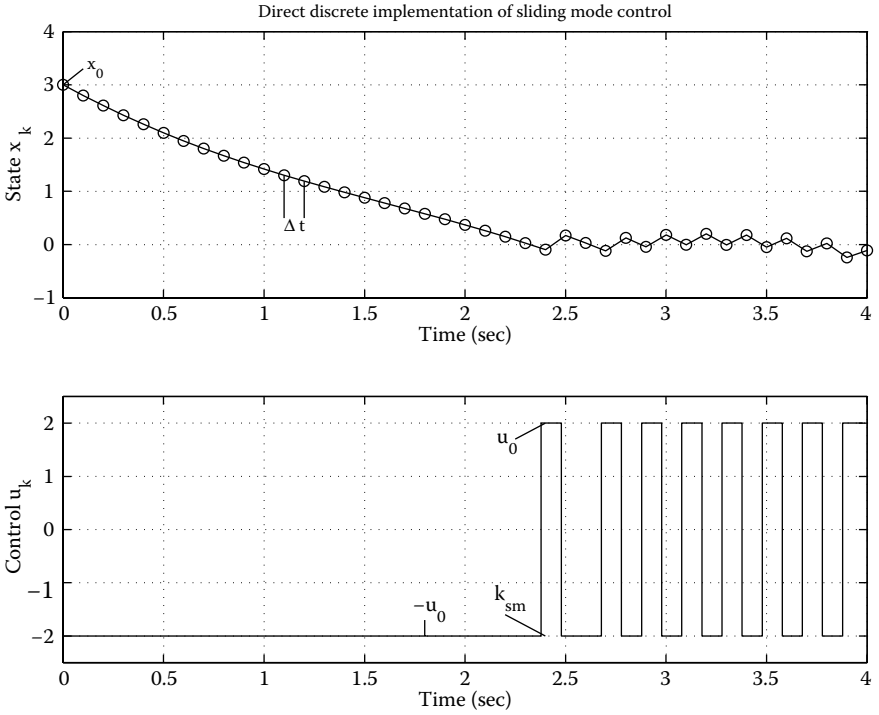

FIGURE 9.2
Direct implementation of sliding mode control in discrete time. Sampling instances are marked with small circles. Control u_k may only be switched at sampling instances, resulting in discretization chatter in the motion trajectory after reaching the vicinity of the sliding manifold at $t_{sm} = k_{sm}\Delta t$.

9.2. Discrete-Time Sliding Mode Concept

Before developing the concept of discrete-time sliding mode, let us revisit the principle of sliding mode in continuous-time systems with ideal discontinuous control from an engineering point of view. A more mathematical treatment may be found in the work of Utkin [1993] or Drakunov and Utkin 1990]. Rewrite Equation 9.1.1 as a general continuous-time system

$$\dot{x} = f(x, u, t), \tag{9.2.1}$$

with a discontinuous scalar control law

$$u = \begin{cases} u_0 & \text{if} \quad s(x) \geq 0 \\ -u_0 & \text{if} \quad s(x) < 0 \end{cases} \tag{9.2.2}$$

and sliding mode in some manifold $s(x) = 0$ (see also Figure 9.3).

$$x(t = 0)$$

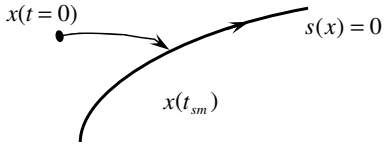

FIGURE 9.3
Motion trajectory of continuous-time system with scalar sliding mode control. Starting from initial point $x(t = 0)$, the trajectory reaches the sliding manifold $s(x) = 0$ within finite time t_{sm} and remains on the manifold thereafter.

Note the following observations characterizing the nature of sliding mode systems:

- The time interval between the initial point $t = 0$ and the reaching of the sliding manifold $\sigma = \{x: s(x) = 0\}$ at t_{sm} is finite, in contrast to systems with a continuous control law that exhibit asymptotic convergence to any manifold consisting of state trajectories.
- Once the system is "in sliding mode" for all $t \geq t_{sm}$, its trajectory motion is confined to the manifold $\sigma = \{x: s(x) = 0\}$, and the order of the closed-loop system dynamics is less than the order of the original uncontrolled system.
- After sliding mode has started at t_{sm}, the system trajectory cannot be backtracked beyond the manifold $\sigma = \{x: s(x) = 0\}$ like in systems without discontinuities. In other words, at any point $t_0 \geq t_{sm}$, it is not possible to determine the time instance t_{sm} or to reverse calculate the trajectory for $t < t_{sm}$ based on information of the system state at t_0.

However, during both time intervals before and after reaching the sliding manifold, the state trajectories are continuous time functions and the relation between two values of the state at the ends of a finite time interval $t = [t_0, t_0 + \Delta t]$ may be found by solving Equation 9.2.1 as

$$x(t_0 + \Delta t) = F(x(t_0)), \tag{9.2.3}$$

where $F(x(t))$ is a continuous function as well. When derived for each sampling point $t_j = k\Delta t$, $k = 1, 2, \ldots$, Equation 9.2.3 is nothing but the discrete-time representation of the continuous time prototype (Equation 9.2.1), i.e.,

$$x_{k+1} = F(x_k),\ x_k = x(k\Delta t). \tag{9.2.4}$$

Starting from time instance t_{sm}, the state trajectory belongs to the sliding manifold with $s(x(t))$, or for some $k_{sm} \geq \dfrac{t_{sm}}{\Delta t}$,

$$s(x_k) = 0,\ \forall k \geq k_{sm}. \tag{9.2.5}$$

It seems reasonable to call this motion "sliding mode in discrete time," or "discrete-time sliding mode." Note that the right-hand side of the motion equation of the system with discrete-time sliding mode is a continuous state function.

So far, we have generated a discrete-time description of a continuous-time sliding mode system. Next, we need to derive a discrete-time control law that may generate sliding mode in a discrete-time system. Let us return to the example in Equation 9.2.1 and suppose that, for any constant control input u and any initial condition $x(0)$, the solution to Equation 9.2.1 may be found in closed form, i.e.,

$$x(t) = F(x(0), u). \tag{9.2.6}$$

Now also assume that control u may be chosen arbitrarily. With the help of Equation 9.2.6, follow the procedure below:

1. At $t = 0$, select constant $u(x(t = 0), \Delta t)$ for a given time interval Δt such that $s(x(t = \Delta t)) = 0$.
2. Next, at $t = \Delta t$, find constant $u(x(t = \Delta t), \Delta t)$ such that $s(x(t = 2\Delta t)) = 0$.
3. In general, for each $k = 0, 1, 2,\ldots$, at $t = k\Delta t$ choose constant $u(x_k, \Delta t)$ such that $s(x_{k+1}) = 0$.

In other words, at each sampling point k, select u_k such that this control input, to be constant during the next sampling interval Δt, will achieve $s(x_{k+1}) = 0$ at the next sampling point $(k + 1)$. During the sampling interval, state $x(k\Delta t < t < (k + 1)\Delta t)$ may not belong to the manifold, i.e., $s(x(t)) \neq 0$ is possible for $k\Delta t < t < (k + 1)\Delta t$. However, the discrete-time system

$$\begin{aligned} x_{k+1} &= F(x_k, u_k) \\ u_k &= u(x_k) \end{aligned} \tag{9.2.7}$$

hits the sliding manifold at each sampling point, i.e., $s(x_{k+1}) = 0 \;\forall\; k = 0, 1, 2, \ldots$ is fulfilled.

Because $F(x(0), u)$ tends to $x(0)$ as $\Delta t \to 0$, the function $u(x(0), \Delta t)$ may exceed the available control resources u_0. As a result, the bounded control shown in the bottom diagram of Figure 9.4 steers state x_k to zero only after a finite number of steps k_{sm}. Thus, the manifold is reached after a finite time interval $t_{sm} = k_{sm}\Delta t$, and, thereafter, the state x_k remains on the manifold. In analogy to continuous-time systems, this motion may be referred to as discrete-time sliding mode. Note that sliding mode is generated in the discrete-time system with control $-u_0 \le u \le u_0$ as a continuous function of the state x_k and is piecewise constant during the sampling interval.

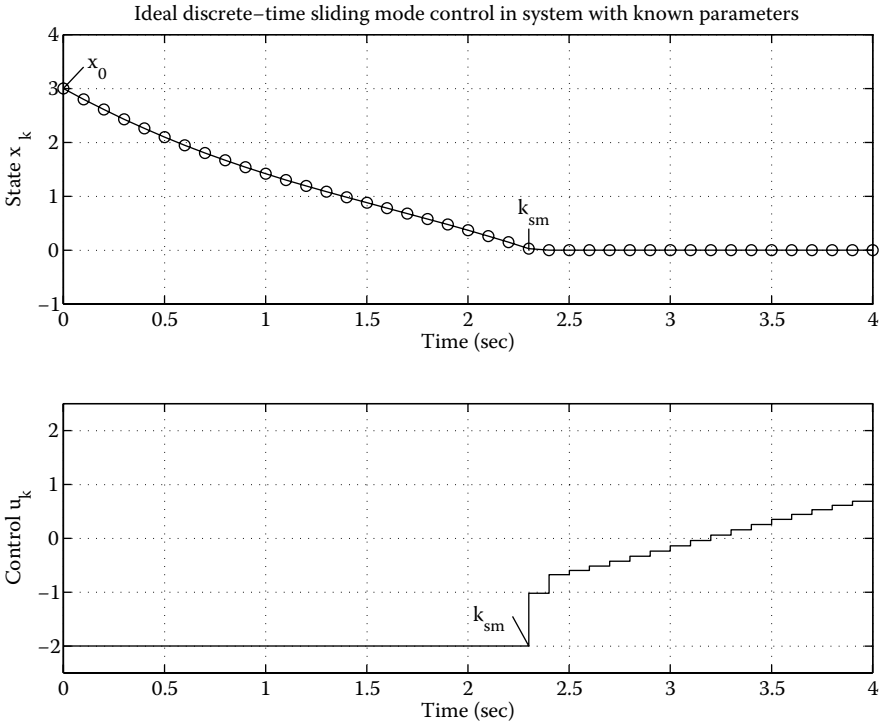

FIGURE 9.4
Proper implementation of sliding mode control in discrete time. Sampling instances are marked with small circles. Control u_k is selected as $-u_0 \le u_k \le u_0$ at each sampling instance to achieve $s(x_{k+1}) = 0$ as quickly as possible in accordance with the available control resources, resulting in chatter-free motion after reaching the sliding manifold at $t_{sm} = k_{sm}\Delta t$.

The above first-order example clarifies the definition of the term discrete-time sliding mode introduced by Drakunov and Utkin [1990] for an arbitrary finite-dimensional discrete-time system.

Definition 9.1: Discrete-Time Sliding Mode

In the discrete-time dynamic system

$$x_{k+1} = \mathrm{F}(x_k, u_k),\ x \in \Re^n,\ u \in \Re^m,\ m \le n, \tag{9.2.8}$$

discrete-time sliding mode takes place on a subset Σ of the manifold $\sigma = \{x: s(x) = 0\}$, $s \in \Re^m$, if there exists an open neighborhood $\aleph$ of this subset such that, for each $x \in \aleph$, it follows that $s(F(x_{k+1})) \in \Sigma$.

In contrast to continuous-time systems, sliding mode may arise in discrete-time systems with a continuous function in the right-hand side of the

closed-loop system equation. Nevertheless, the aforementioned characteristics of continuous-time sliding mode have been transferred to discrete-time sliding mode. The mathematical implications in terms of group theory may be found in the work by Drakunov and Utkin [Drakunov and Utkin 1990; Utkin 1993]. Practical issues will be discussed in the subsequent section using linear systems as an example.

9.3. Linear Discrete-Time Systems with Known Parameters

This section deals with discrete-time sliding mode control for linear time-invariant continuous-time plants. Let us assume that a sliding mode manifold is linear for an nth-order discrete-time system $x_{k+1} = F(x_k)$, *i.e.*, $s_k = Cx_k$, $C \in \Re^{m\times n}$ with m control inputs. According to Definition 9.1, the sliding mode existence condition is of the form

$$s_{k+1} = C(F(x_k)) \tag{9.3.1}$$

for any $x_k \in \aleph$. To design a discrete-time sliding mode control law based on the condition in Equation 9.3.1, consider the discrete-time representation of the linear time-invariant system

$$\dot{x}(t) = Ax(t) + Bu(t) + Dr(t), \tag{9.3.2}$$

with state vector $x(t) \in \Re^n$, control $u(t) \in \Re^m$, reference input $r(t)$, and constant system matrices A, B, and D. Transformation to discrete time with sampling interval Δt yields

$$x_{k+1} = A^*x_k + B^*u_k + D^*r_k, \tag{9.3.3}$$

where

$$A^* = e^{A\Delta t}, \quad B^* = \int_0^{\Delta t} e^{A(\Delta t - t)}B\,\mathrm{d}\,\tau, \quad D^* = \int_0^{\Delta t} e^{A(\Delta t - t)}D\,\mathrm{d}\,\tau \tag{9.3.4}$$

and the reference input $r(t)$ is assumed to be constant during the sampling interval Δt. In accordance with Equation 9.3.1, discrete-time sliding mode exists if the matrix CB^* has an inverse and the control u_k is designed as the solution of

$$s_{k+1} = CA^*x_k + CD^*r_k + CB^*u_k = 0. \tag{9.3.5}$$

In other words, control u_k should be chosen as

$$u_k = -(CB^*)^{-1}(CA^*x_k + CD^*r_k). \tag{9.3.6}$$

By analogy with continuous-time systems, the control law in Equation 9.3.6 yielding motion in the manifold $s = 0$ will be referred to as equivalent control. To reveal the structure of $u_{k_{eq}}$, let us represent it as the sum of two linear functions:

$$u_{k_{eq}} = -\left(CB^*\right)^{-1} s_k - \left(CB^*\right)^{-1}\left(\left(CA^* - C\right)x_k + CD^* r_k\right) \tag{9.3.7}$$

and

$$s_{k+1} = s_k + (CA^* - C)x_k + CD^* r_k + CB^* u_k. \tag{9.3.8}$$

As in the first-order example considered in the previous section, $u_{k_{eq}}$ may exceed the available control resources with $\Delta t \to 0$ for initial $s_k \neq 0$ because, attributable to $(CB^*)^{-1} \to \infty$, $(CB^*)^{-1}(CA^* - C)$ and $(CB^*)^{-1}CD^*$ take finite values. Hence, the real-life bounds for control u_k should be taken into account.

Suppose that the control can vary within $\|u_k\| \le u_0$ and the available control resources are such that

$$\left\|\left(CB^*\right)^{-1}\right\| \cdot \left\|\left(CA^* - C\right)x_k + CD^* r_k\right\| < u_0. \tag{9.3.9}$$

Note that, otherwise, the control resources are insufficient to stabilize the system.

The control

$$u_k = \begin{cases} u_{k_{eq}} & \text{for} \quad \left\|u_{k_{eq}}\right\| \le u_0 \\ u_0 \dfrac{u_{k_{eq}}}{\left\|u_{k_{eq}}\right\|} & \text{for} \quad \left\|u_{k_{eq}}\right\| > u_0 \end{cases} \tag{9.3.10}$$

complies with the bounds on the control resources. As shown above, $u_k = u_{k_{eq}}$ for $\left\|u_{k_{eq}}\right\| \le u_0$ yields motion in the sliding manifold s = 0. To proof convergence to this domain, consider the case $\left\|u_{k_{eq}}\right\| > u_0$ but in compliance with the condition in Equation 9.3.9. From Equations 9.3.7 through 9.3.10, it follows that

$$s_{k+1} = \left(s_k + \left(CA^* - C\right)x_k + CD^* r_k\right)\left(1 - \frac{u_0}{\left\|u_{k_{eq}}\right\|}\right) \quad with \quad u_0 < \left\|u_{k_{eq}}\right\|. \tag{9.3.11}$$

Thus,

$$\begin{aligned}\|s_{k+1}\| &= \left\|\left(s_k + \left(CA^* - C\right)x_k + CD^* r_k\right)\right\|\left(1 - \frac{u_0}{\left\|u_{k_{eq}}\right\|}\right) \\ &\le \|s_k\| + \left\|\left(CA^* - C\right)x_k + CD^* r_k\right\| - \frac{u_0}{\left\|\left(CB^*\right)^{-1}\right\|} \\ &< \|s_k\|\end{aligned} \tag{9.3.12}$$

as a result of Equation 9.3.9.

Hence, $\|s_k\|$ decreases monotonously and, after a finite number of steps, $\left\|u_{k_{eq}}\right\| < u_0$ is achieved. Discrete-time sliding mode will take place from the next sampling point onward.

Control (Equation 9.3.10) provides chatter-free motion in the manifold $s = 0$ as shown in Figure 9.4, in contrast to the direct implementation of discontinuous control in Figure 9.2, resulting in discretization chatter in the vicinity of the sliding manifold. Similar to the case of continuous-time systems, the equation $s = Cx = 0$ enables the reduction of system order, and the desired system dynamics in sliding mode can be designed by appropriate choice of matrix C.

9.4. Linear Discrete-Time Systems with Unknown Parameters

Complete information of the plant parameters is required for implementation of control in Equation 9.3.10, which may not be available in practice. To extend the discrete-time sliding mode concept to systems with unknown parameters, suppose that the system in Equation 9.3.5 operates under uncertainty conditions: the matrices A and D and the reference input r_k are assumed to be unknown and may vary in some ranges such that the condition in Equation 9.3.9 holds. Similar to Equation 9.3.10, the control law

$$u = \begin{cases} -\left(CB^*\right)^{-1} s_k & \text{for} \quad \left\|\left(CB^*\right)^{-1} s_k\right\| \le u_0 \\ -u_0 \dfrac{\left(CB^*\right)^{-1} s_k}{\left\|\left(CB^*\right)^{-1} s_k\right\|} & \text{for} \quad \left\|\left(CB^*\right)^{-1} s_k\right\| > u_0 \end{cases} \tag{9.4.1}$$

respects the bounds on the control resources. Furthermore, control (Equation 9.4.1) does not depend on the plant parameters A and D and the reference input r_k. Substitution of Equation 9.4.1 into the system equations of the previous section leads to

$$s_{k+1} = s_k\left(1 - \frac{u_0}{\left\|\left(CB^*\right)^{-1} s_k\right\|}\right) + \left(CA^* - C\right)x_k + CD^* r_k \quad \text{for} \quad u_0 < \left\|\left(CB^*\right)^{-1} s_k\right\|, \tag{9.4.2}$$

and, similar to Equation 9.3.12,

$$\begin{aligned}
\left\|s_{k+1}\right\| &\le \left\|s_k\right\|\left(1 - \frac{u_0}{\left\|\left(CB^*\right)^{-1} s_k\right\|}\right) + \left\|\left(CA^* - C\right)x_k + CD^* r_k\right. \\
&\le \left\|s_k\right\| - \frac{u_0\left\|s_k\right\|}{\left\|\left(CB^*\right)^{-1} s_k\right\|} + \left\|\left(CA^* - C\right)x_k + CD^* r_k\right\| \\
&\le \left\|s_k\right\| - \frac{u_0}{\left\|\left(CB^*\right)^{-1}\right\|} + \left\|\left(CA^* - C\right)x_k + CD^* r_k\right\| \\
&< \left\|s_k\right\|.
\end{aligned} \tag{9.4.3}$$

Hence, as for the case with complete knowledge of system parameters discussed in Section 9.3, the value of $\|s_k\|$ decreases monotonously, and, after a finite number of steps, control $\|u_k\| < u_0$ will be within the available resources. Substituting Equation 9.4.1 into Equation 9.3.8 results in

$$s_{k+1} = (CA^* - C)xk + CD^*rk. \tag{9.4.4}$$

Because the matrices $(CA^* - C)$ and CD^* are of Δt order, the system motion will be in a Δt-order vicinity of the sliding manifold $s = 0$. Figure 9.5 shows a simulation of the first-order Example 9.1 for unknown matrices A and D. Convergence to the vicinity of the sliding manifold is achieved in finite time; thereafter, the motion trajectory does not follow the sliding manifold exactly but rather remains within a Δt-order vicinity. This result is expected from systems operating under uncertainty conditions, because we are dealing with an open-loop system during each sampling interval. In contrast to discrete-time systems with direct implementation of discontinuous control as shown in Figure 9.2, this motion is free of discretization chatter.

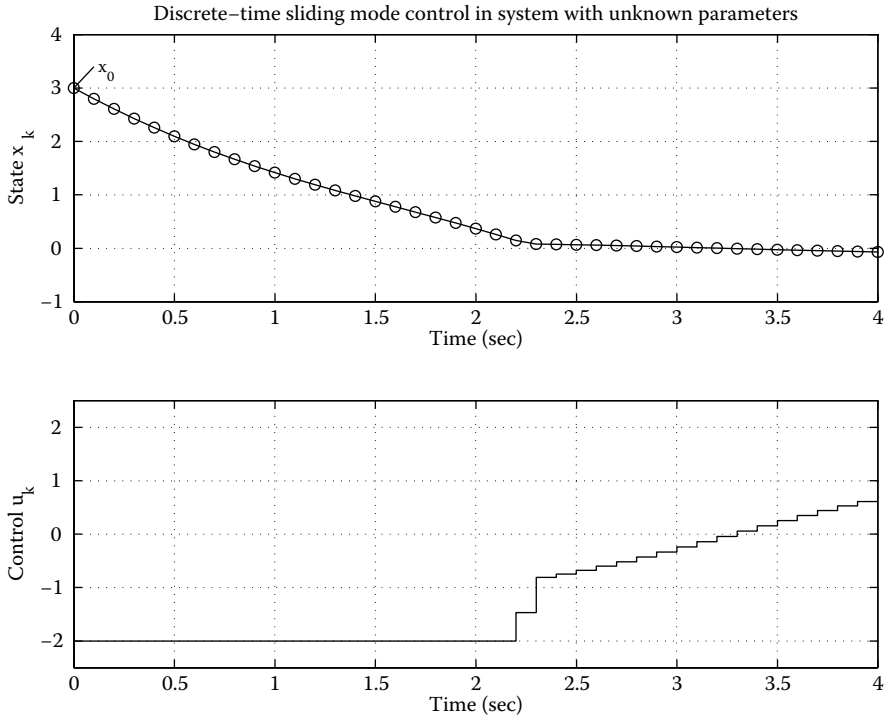

FIGURE 9.5
Discrete-time sliding mode control for system with uncertain parameters. Sampling instances are marked with small circles. Control u_k is selected as $-u_0 \le u_k \le u_0$ at each sampling instance such that $s(x_{k+1})$ approaches the vicinity of the sliding manifold in finite time and remains in the vicinity afterward with chatter-free motion.

9.5. Introduction to Systems with Delays and Distributed Systems

This section discusses design methods for systems described by difference and differential-difference equations. These types of equations may serve as mathematical models for dynamic systems with delays or for distributed systems with finite dimensional inputs and outputs. The following section presents the basic sliding mode control design methodology. A flexible shaft as an example for a distributed system is discussed in Section 9.7.

Consider a system modeled by differential-difference equations in regular form as

$$\dot{x}(t) = A_{11}x(t) + A_{12}z(t), \tag{9.5.1}$$

$$z(t) = A_{21}x(t-\tau) + A_{22}z(t-\tau) + B_0u(t-\tau), \tag{9.5.2}$$

where $x \in \Re^n$, $z \in \Re^k$, and $u \in \Re^m$. The pair (A_{11}, A_{12}) is assumed to be controllable, and the difference system Equation 9.5.2 is assumed invertible with output $\tilde{A}_{12}z(t)$, where $\tilde{A}_{12}$ consists of the basic rows of A_{12} in Equation 9.5.1.

Recall the sliding mode concept for discrete-time systems presented in Section 9.2 and in Definition 9.1. For differential-difference system as in Equations 9.5.1 and 9.5.2, sliding mode can be defined in a similar manner: sliding mode exists in some manifold σ if the state trajectories starting outside this manifold reach σ within finite time and all state trajectories that belong to the manifold σ at some time instance t_{sm} remain in σ for all $t \geq t_{sm}$.

System (Equations 9.5.1 and 9.5.2) is written in block-control form as described by Drakunov et al. [1990a,b] for ordinary differential equations (see also Section 3.2). The two-step design procedure first derives a desired control $z_d(x(t))$ for Equation 9.5.1 to yield the desired motion along a manifold $\sigma = \{x: S(x) = 0\}$ in this first block, assuming $z = z_d$. The second design step uses real control input $u(x, t)$ in Equation 9.5.2 to ensure that this assumption holds by enforcing sliding mode in the second block along manifold $\sigma_0 = \{x: z - z_d = 0\}$. In the overall system (Equations 9.5.1 and 9.5.2), sliding mode exists in the intersection of both manifolds as described by $\sigma \cap \sigma_0$.

9.6. Linear Systems with Delays

This section deals with linear systems with known parameters in analogy to Section 9.3. The extension to systems with unknown parameters follows similar procedures as for discrete-time systems in Section 9.4 and is omitted here.

As an example, consider a time-invariant linear system with a delay in the input variable

$$\dot{x}(t) = Ax(t) + Bu(t - \tau), \tag{9.6.1}$$

where $x \in \Re^n$, $u \in \Re^m$, $t > 0$, and the initial conditions are denoted by $x(0) = x_0$ and $u(\xi) = u_0(\xi)$ for $-\tau < \xi < 0$. The system in Equation 9.6.1 can be represented in differential-difference block-form (Equation 9.5.1 and 9.5.2) by setting $A_{11} = A$, $A_{12} = B$, $A_{21} = 0_{m\times n}$, $A_{22} = 0_{m\times m}$ and $B_0 = I_{m\times m}$:

$$\dot{x}(t) = A_{11}x(t) + A_{12}z(t), \tag{9.6.2}$$

$$z(t) = u(t - \tau). \tag{9.6.3}$$

First, design a smooth function $S(x) = (s_1(x), \ldots, s_i(x), \ldots, s_m(x)) \in \Re^m$ and a discontinuous control $z_d = \left(z_{d_1}(x), \ldots, z_{d_i}(x), \ldots, z_{d_m}(x)\right) \in \Re^m$ with components

$$z_{d_i}(x(t)) = \begin{cases} z_{d_i}^+(x(t)) & \text{for } s_i(x(t)) > 0 \\ z_{d_i}^-(x(t)) & \text{for } s_i(x(t)) < 0 \end{cases} \quad i = 1, 2, \ldots, m \tag{9.6.4}$$

such that, after a finite time interval, every trajectory belongs to the intersection $\sigma = \bigcap_{i=1}^{m} \sigma_i$ of the surfaces $\sigma_i = \{x: s_i(x) = 0\}$ and sliding mode exists thereafter. Second, to implement control Equation 9.6.4 in Equation 9.6.2, assign

$$u(t) = z_d(x(t + \tau)) \tag{9.6.5}$$

for Equation 9.6.3 to enforce sliding mode on the manifold $\sigma_0 = \{x: z - z_d = 0\}$. The values of $x(t + \tau)$ have to be extrapolated from the solution of Equation 9.6.2 as

$$x(t + \tau) = e^{At}x(t) + \int_0^{\tau} e^{At}Bu(t - \xi)\,d\xi. \tag{9.6.6}$$

Note that control $u(t)$ needs to be stored in the microcontroller for the time interval $[t, t - \xi]$.

Similar to discrete-time systems as discussed in Sections 9.2 through 9.4, control $u(t)$ is designed with preview such that $z(t + \tau) = z_d(t + \tau)$ at some future point, τ ahead of the current time instance t. In contrast to discrete-time systems, time t is continuous rather than sampled at discrete-time instances $k\Delta t$.

The system motion (Equations 9.6.2 through 9.6.2) in sliding mode along manifold σ_0 is described by

$$\dot{x}(t) = Ax(t) + Bz_d\left(x(t)\right). \tag{9.6.7}$$

Once sliding mode also occurs on the intersection $\sigma = \bigcap_{i=1}^{m} \sigma_i$ by design of Equation 9.6.4, sliding mode exists along the intersection of all $(m + 1)$ sliding manifolds $\Sigma = \sigma \cap \sigma_0 = \sigma = \bigcap_{i=1}^{m} \sigma_i$ with the desired dynamics of the system in Equation 9.6.1.

9.7. Distributed Systems

This section discusses a flexible shaft as an example for a distributed system. Because distributed systems can be described by similar differential-difference equations as systems with delays, the design methodology of Section 9.6 will be used.

Consider a flexible shaft with lengths l and inertial load J acting as a torsion bar as depicted in Figure 9.6. Let $e(t)$ be the absolute coordinate of the left end of the bar with input torque M and let $d(x, t)$ be the relative deviation at location $0 \le x \le$ l at time t. Hence, the absolute deviation of a point $0 < x < l$ at time t is described by $q(x, t) = e(t) + d(x, t)$ and governed by

$$\frac{\partial^2 q(x, t)}{\partial t^2} = a^2 \frac{\partial^2 q(x, t)}{\partial x^2}, \tag{9.7.1}$$

where a is the flexibility constant depending on the geometry and the material of the bar. The boundary conditions corresponding to the input torque M and the load inertia J are

$$M = -a^2 \frac{\partial q(0, t)}{\partial x}, \qquad J \frac{\partial^2 q(l, t)}{\partial t^2} = -a^2 \frac{\partial^2 q(l, t)}{\partial x^2}. \tag{9.7.2}$$

Consider the input torque F as the control input $u(t)$ and the load position $q(l, t)$ as the system output. To find the transfer function $W(p)$ via Laplace transform, assume zero initial conditions

$$q(x, 0) = 0, \qquad \frac{\partial q(x, 0)}{\partial t} = 0 \tag{9.7.3}$$

to yield

$$\begin{aligned} a^2 Q(0, p) &= -U(p), \\ p^2 Q(x, p) &= a^2 Q''(x, p), \\ a^2 Q'(l, p) &= -Jp^2 Q(l, p), \end{aligned} \tag{9.7.4}$$

where $Q(x, p)$ denotes the Laplace transform of $q(x, t)$ with spatial derivatives $Q'(x, p) = \dfrac{\partial Q(x, p)}{\partial x}$ and $Q''(x, p) = \dfrac{\partial^2 Q(x, p)}{\partial x^2}$, and $U(p)$ represents the Laplace

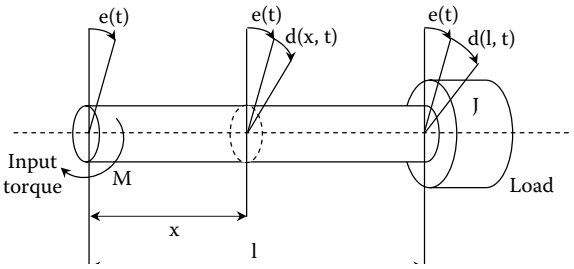

FIGURE 9.6
Flexible shaft with input torque M and load J acting as a torsion bar.

transform of input variable $u(t)$. The solution to the boundary value problem in Equation 9.7.4 is given by

$$Q(x,\,p) = -\frac{(1-\frac{J}{a}p)e^{-\frac{l-x}{a}p} + (1+\frac{J}{a}p)e^{\frac{l-x}{a}p}}{ap\left(-(1-\frac{J}{a}p)e^{-\frac{l}{a}p} + (1+\frac{J}{a}p)e^{\frac{l}{a}p}\right)}U(p) \tag{9.7.5}$$

from which $W(p)$ may be found by setting $x = l$ to yield

$$W(p) = \frac{2e^{-\tau p}}{ap\left(1+\frac{J}{a}p\right)+\left(1-\frac{J}{a}p\right)e^{-2\tau p}}, \tag{9.7.6}$$

where $\tau = l/a$ describes the "delay" between the left end and the right end of the bar. The corresponding differential-difference equation may be written in the form

$$J\ddot{q}(t) + Jq(t-\tau) + a\dot{q}(t) - a\dot{q}(t-2\tau) = 2u(t-\tau). \tag{9.7.7}$$

Denoting $x_1(t) = q(t)$, $x_2(t) = \dot{q}(t)$, and $z(t) = J\ddot{q}(t) + a\dot{q}(t)$, we obtain the motion equations as

$$\begin{aligned} \dot{x}_1(t) &= x_2(t) \\ \dot{x}_2(t) &= -\big(ax_2(t) + z(t)\big)/J \end{aligned} \tag{9.7.8}$$

$$z(t) = 2ax_2(t-2\tau) - z(t-2\tau) + 2u(t-\tau), \tag{9.7.9}$$

which correspond to the block structure in Equations 9.5.1 and 9.5.2. In the first design step, assign a desired control $z_d(t)$ for the first block as shown

$$z_d(t) = -M\ sign(kx_1(t) + x_2(t)),\ k > 0. \tag{9.7.10}$$

To achieve $z(t) = z_d(t)$ in the second design step, choose control input $u(t)$ as

$$u(t) = u_{eq}(t) = \frac{1}{2}\big(-2ax_2(t-\tau) + z(t-\tau) - M\,\mathrm{sign}\big(kx_1(t+\tau) + x_2(t+\tau)\big)\big). \tag{9.7.11}$$

The manifold $s(t) = z_d(t) - z(t) = 0$ is reached within finite time $t < \tau$ and sliding mode exists thereafter. If control $u(t)$ is bounded by $|\,u(t)| \le u_0$, choose

$$u(t) = \begin{cases} u_{eq}(t) & \text{for} \quad |u_{eq}(t)| \le u_0 \\ u_0 \operatorname{sign} u_{eq}(t) & \text{for} \quad |u_{eq}(t)| > u_0 \end{cases}, \tag{9.7.12}$$

and there exists an open domain containing the origin of the state space of the system in Equations 9.7.8 and 9.7.9 such that, for all initial conditions in this domain, sliding mode occurs along the manifold $s(t) = 0$. The values of $x_1(t + \tau)$ and $x_2(t + \tau)$ have to be calculated as the solution of Equation 9.7.8 with known input $z(t)$ from Equation 9.7.9 as shown in Equation 9.6.6. If only output $y(t) = x_1(t)$ is measurable but not its time derivative $\dot{y}(t) = x_2(t)$, an asymptotic observer should be used to estimate the state $x_2(t)$. For details of sliding mode control for systems with delays and for distributed systems, see the work of Drakunov and Utkin [Drakunov and Utkin 1990; Utkin 1993].

9.8. Summary

Wide use of digital controllers has created a need to generalize the sliding mode concept to discrete-time control systems, which raises the fundamental question: What is sliding mode in a discrete-time system? Discontinuous control in a continuous-time system may result in sliding mode in some manifold of the state space, whereas it results in chatter in a discrete-time implementation. Hence, we first defined the essence of sliding mode, constituting a general concept. In short, sliding mode exists in a manifold if the system trajectories reach this manifold in finite time and remain in the manifold thereafter. Mathematically speaking, the trajectory of a system in sliding mode is not invertible, i.e., after sliding mode has occurred, it is impossible to find the point in time and the state space location sliding mode started, nor is it possible to backtrack the system trajectory beyond this point.

Following this definition, sliding mode may be generated in discrete-time systems using a continuous control input. Design methods have been developed in this chapter and were extended to systems with delays and distributed systems. They enable decoupling of the overall dynamics into independent partial motion of lower dimension and low sensitivity to system uncertainties. For all systems, the motion trajectories are free of chatter, which has been the main obstacle for certain applications of discontinuous control action in systems governed by discrete and difference equations.

References

Drakunov SV, Utkin VI. 1990. "Sliding Mode in Dynamic Systems." *Int. Journal of Control* 55:1029–1037.

Drakunov SV, Izosimov DB, Luk'yanov AG, Utkin VA, Utkin VI. 1990a. "Block Control Principle I." *Automation Remote Control* 51:601–609.

Drakunov SV, Izosimov DB, Luk'yanov AG, Utkin VA, Utkin VI. 1990b. "Block Control Principle II." *Automation Remote Control* 52:737–746.

Kotta U. 1989. "Comments on the Stability of Discrete-Time Sliding Mode Control Systems." *IEEE Trans Automatic Control* 34:1021–1022.

Utkin VI. 1993. "Sliding Mode Control in Discrete-Time and Difference Systems." In *Variable Structure and Lyapunov Control,* edited by A. Zinober. London: Springer-Verlag.

10

Electric Drives

In recent years, much research effort has been devoted to the application of sliding mode control techniques to power electronic equipments and electrical drives. Interest in this control approach has emerged because of its potential for circumventing parameter variation effects under dynamic conditions with a minimum of implementation complexity. In electric drive systems, the existence of parameter changes caused by, for instance, winding temperature variation, converter switching effect, and saturation, is well recognized although infrequently accounted for. In servo applications, significant parameter variations arise from often unknown loads; for example, in machine tool drives and robotics, the moment of inertia represents a variable parameter depending on the load of the tool or the payload. Among the distinctive features claimed for sliding mode control are order reduction, disturbance rejection, strong robustness, and simple implementation by means of power converters. Hence, sliding mode is attributed to high potentials as a prospective control methodology for electric drive systems. The experience gained so far testifies to its efficiency and versatility. In fact, control of electric drives is one of the most challenging applications because of increasing interest in using electric servo-mechanisms in control systems, the advances of high-speed switching circuitry, as well as insufficient linear control methodology for inherent nonlinear high-order multivariable plants such as AC motors.

Implementation of sliding mode control by means of the most common electric components has turned out to be simple enough. The commercially available power converters enable handling powers of several dozen kilowatts at frequencies of several hundred kilohertz. When using converters of this type, confining their function to pulse-width modulations seems unjustified, and it is reasonable to turn to algorithms with direct discontinuous control actions. Introduction of discontinuities is dictated by the very nature of power converters.

This chapter consists of three main parts: sliding mode control of DC motors, permanent-magnet synchronous motors, and induction motors. These three types of electric motors are the most commonly used drive systems in industrial applications. All these drive systems have much in common: current control, speed control, observer design, and issues of sensorless control. As will be shown in each particular section, sliding mode control techniques are used flexibly to achieve the desired control performance, not only in controller design but also in observer design and estimation processes.

The basic framework of this chapter has been given previously [Utkin 1993; Sabanovic, Sabanovic, and Ohnishi 1993]. However, both the content and theoretical aspect have been extended considerably with respect to the above framework.

10.1. DC Motors

10.1.1. Introduction

To show the effectiveness of sliding mode techniques in the control of electric drives, we start with the most simple drive systems, i.e. DC-motor-based drive systems. This section is an extension of the sliding mode approaches applied to DC motors given by Utkin [1993]. Moreover, some implementation aspects will be enhanced, aiming at applications of theoretical derivations given in the proceeding chapters to real-life systems.

10.1.2. Model of the DC Motor

From the point of controllability, a DC motor with a constant excitation is the simplest electric drive. Figure 10.1 shows the structure of the electric circuit of a permanently excited DC motor.

The motor dynamics are governed by two coupled first-order equations with respect to armature current and shaft speed

$$L\frac{di}{dt} = u - Ri - \lambda_0\omega,$$

$$J\frac{d\omega}{dt} = k_t i - \tau_l, \tag{10.1.1}$$

where i is armature current, u is terminal voltage, ω is shaft speed, J is inertia of the motor rotor and load, R is armature resistance, L is armature inductance, λ_0 is back electromotive force (EMF) constant, k_t is torque constant, and τ_l is load torque.

Throughout this section, the motor parameters used to verify the design principles are as follows: L = 1.0 mH, R = 0.5 Ω, J = 0.001 kg·m^2, k_t = 0.008

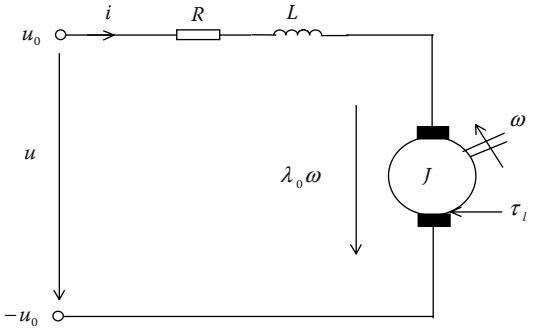

FIGURE 10.1
Electric model of a DC motor with permanent excitation.

Nm/A, $\lambda_0 = 0.001$ V·s/rad, and $\tau_l = B\omega$, with B being the coefficient of viscous friction equal to 0.01 Nm·s/rad. The supplied link voltage is $u_0 = 20$ V.

For speed control of a DC motor, a cascaded control structure usually is preferred, with an inner current control loop and an outer speed control loop. Control input u may be continuous or discontinuous, depending on the output power of the DC motor. For a low-power system, a continuous control may be selected. For a high-power system, a discontinuous control (e.g., in the form of PWM) has to be used because a continuous controlled voltage, whilst providing large current, is difficult to generate.

We concentrate on discontinuous control in the sequel of this chapter, because control discontinuities are the very nature of sliding mode control. Furthermore, discontinuous control of DC motors is universal in the sense that it can be used both for low-power systems and high-power systems. Figure 10.2 shows the typical control structure of a DC-motor-based drive system.

10.1.3. Current Control

At first, assume there exists an outer control loop providing a desired current i^*. Let us consider the current control problem by a defining switching function

$$s = i^* - i \tag{10.1.2}$$

as the error between the real, measured current i and the reference current i^* determined by the outer-loop controller. Design the discontinuous control as

$$u = u_0 \operatorname{sign}(s), \tag{10.1.3}$$

where u_0 denotes the supplied link voltage. As discussed in the previous chapters, to enforce the sliding mode, control gain u_0 should be selected such that $s\dot{s} < 0$. Now check this condition by evaluating $s\dot{s}$ and select u_0 as

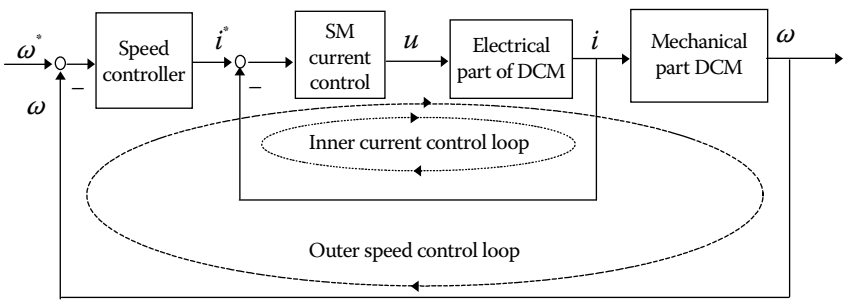

FIGURE 10.2
Cascaded control structure of DC motors. SM, sliding mode; DCM, DC motor.

$$s\dot{s} = s\left(\frac{di^*}{dt} + \frac{R}{L}i + \frac{\lambda_0}{L}\omega\right) - \frac{1}{L}u_0|s|,$$
$$u_0 > \left|L\frac{di^*}{dt} + Ri + \lambda_0\omega\right|, \tag{10.1.4}$$

then sliding mode can be enforced.

Examine inequality Equation 10.1.4. If the reference current is constant, the link voltage u_0 needed to enforce sliding mode should be higher than the voltage drop at the armature resistance plus the induced back EMF; otherwise the reference current i^* cannot be followed. Furthermore, reference current i^* may not vary arbitrarily; its time derivative di^*/dt should be bounded to ensure existence of sliding mode for a given link voltage u_0.

Figure 10.3 depicts a simulation result of the proposed current controller.

10.1.4. Speed Control

For the speed controller in an outer loop, the current control loop may be treated as an ideal current source, i.e., given a reference current i^*, it will be tracked immediately. This assumption may become true only for systems in

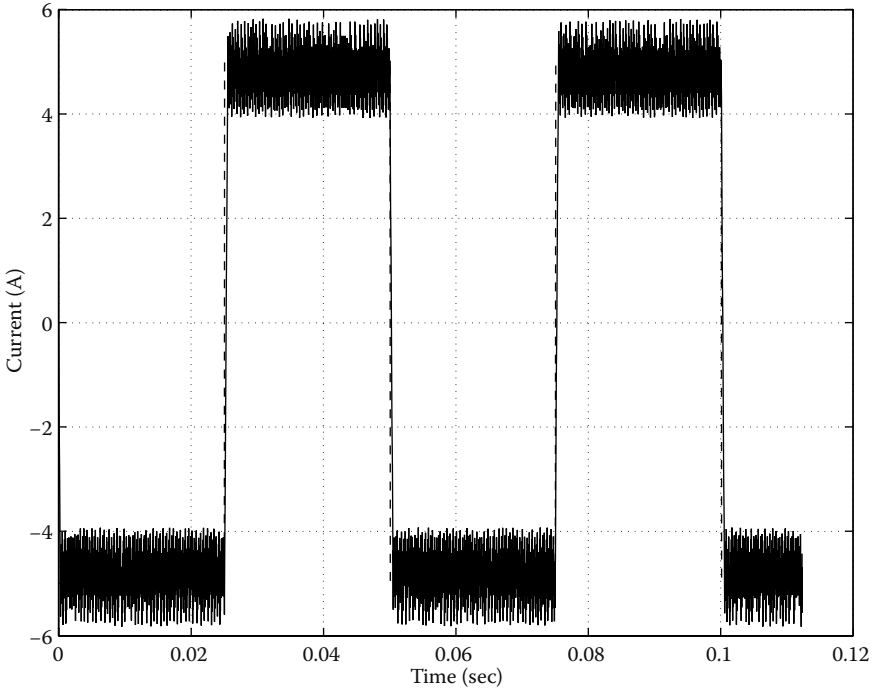

FIGURE 10.3
Current control of DC motor. Dashed line, reference current; solid line, real current.

which the electrical time constant is much smaller than the mechanical time constant or for systems in which the dynamic response of the speed control is not a critical problem. Any control design technique, linear or nonlinear, may be used for speed control: proportional-integral-derivative control or a more sophisticated methodology but without discontinuities such as a sliding mode controller. The reason is as follows: a sliding mode controller has already been used in the inner current control loop; thus, if we would use another sliding mode controller for speed control, the output of the speed controller i^* would be discontinuous, implying an infinite di^*/dt that destroys the inequality Equation 10.1.4 for any implementable u_0.

In many industrial systems, proportional-integral controllers are used with or without a feedforward compensation depending on the nature of the controlled system and the performance requirements. This type of controller is simple but may be sensitive to disturbances in the mechanical subsystem.

Suppose an exponential stability of the speed tracking error is desired and design

$$c(\omega^* - \omega) + (\dot{\omega}^* - \dot{\omega}) = 0, \tag{10.1.5}$$

where c is a positive constant determining the convergence rate. As follows from the motor mechanical Equation 10.1.1, the reference current i^* feeding to the inner current controller should be selected as

$$i^* = \frac{J}{k_t} c(\omega^* - \omega) + \frac{J}{k_t}\dot{\omega}^* - \frac{1}{k_t}\tau_l. \tag{10.1.6}$$

However, implementation of speed controller Equation 10.1.6 requires knowledge of the motor parameters J, k_t and the load torque τ_l, which are normally unknown.

10.1.5. Integrated Structure for Speed Control

To overcome the problems of the cascade control structure, we propose another control approach based on the sliding mode control principle to track a given speed trajectory. In this new control structure, the inner current controller is removed. Current control is achieved in an implicit manner. The advantages of this control structure lie in the fast dynamic response and high robustness with respect to disturbances in both the electrical and mechanical subsystems.

Let $\omega^*(t)$ be the reference shaft speed and $e = \omega^* - \omega$ be the speed tracking error. Define state variables $x_1 = e$ and $x_2 = \dot{e}$. The motion equation of the DC motor with respect to the states x_1, x_2 is given by

$$\begin{aligned} \dot{x}_1 &= x_2, \\ \dot{x}_2 &= -a_1 x_1 - a_2 x_2 + f(t) - bu, \end{aligned} \tag{10.1.7}$$

where $a_1 = k_t\lambda_0/(JL)$, $a_2 = R/L$, and $b = k_t/(JL)$ are constant values. The linear part of Equation 10.1.7 is perturbed by $f(t) = \ddot{\omega}^* + a_2\dot{\omega}^* + a_1\omega^* + R\tau_l/JL + \dot{\tau}_l/J$, depending on the desired speed and load torque disturbances. Because Equation 10.1.7 is a second-order system, the switching function is designed as

$$s = cx_1 + \dot{x}_1, \tag{10.1.8}$$

with c being a positive constant. The associated controller is defined as

$$u = u_0 \,\text{sign}(s), \tag{10.1.9}$$

where u_0 is the link voltage. According to the above equations, the speed tracking error x_1 decays exponentially after sliding mode occurs in the manifold $s = 0$, i.e.,

$$s = cx_1 + \dot{x}_1 = 0, \tag{10.1.10}$$

where constant c determines the rate of the convergence. The system motion in sliding mode is independent from parameters a_1, a_2, b and disturbances in $f(t)$. Similar to the case of current control, the link voltage u_0 should satisfy the condition

$$u_0 > \frac{1}{b}\left|cx_2 - a_1x_1 - a_2x_2 + f(t)\right| \tag{10.1.11}$$

for sliding mode to exist. Then, after a finite time interval, the system state will reach the sliding manifold (Equation 10.1.10). Thereafter, the system response depends only on the design parameter c.

Figures 10.4 through 10.6 show the simulation results of the proposed speed controller. The control gain c is selected as $c = 100$. Figure 10.4 depicts the response of the speed control. As illustrated in the figure, the speed transition time is about 0.05 sec. Figure 10.5 is the wave form of the motor current. Bear in mind that the motor current is not controlled explicitly; the ordinary behavior of the current is the result of the acceleration control. Figure 10.6 gives the response of the sliding variable s.

10.1.6. Observer Design

For the implementation of the control algorithm given in Equations 10.1.8 and 10.1.9, angular acceleration of the shaft is needed for calculating the sliding variable s in Equation 10.1.8 attributable to $x_2 = \dot{\omega}^* - \dot{\omega}$. However, in practice, the angular acceleration is not measured. Instead, the motor current i and the shaft velocity ω are normally available. Numerical differentiation of the speed signal may result in a high level of noise in the calculated acceleration signal. In this case, the acceleration signal may be calculated as

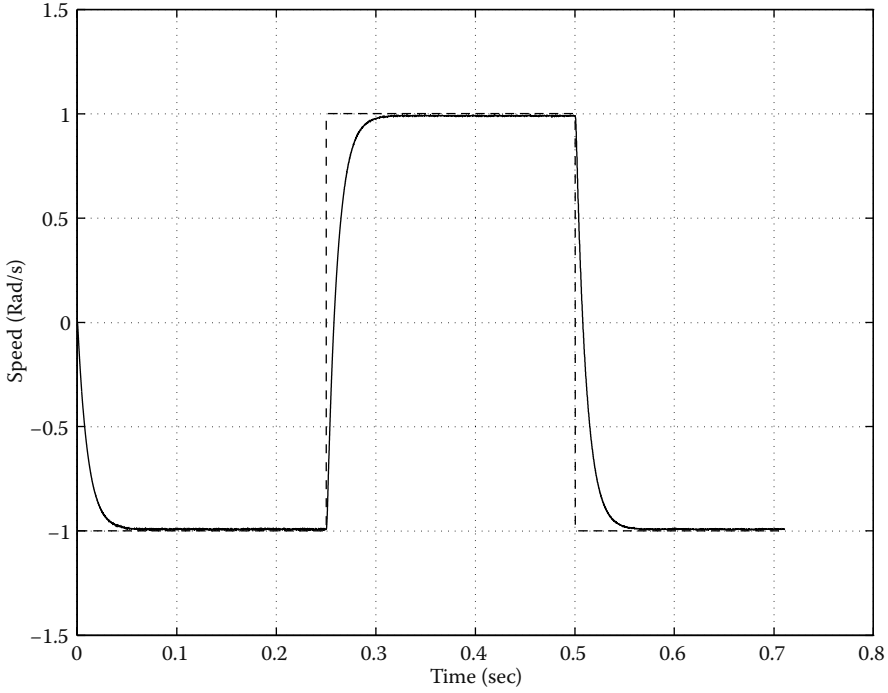

FIGURE 10.4
Speed response of the speed control. Dashed line, reference speed; solid line, real speed.

$$\dot{\omega} = \frac{1}{J} k_t i - \frac{1}{J} \tau_l, \tag{10.1.12}$$

where the load torque τ_l is assumed to be known; parameters J and k_t may be found by an identification process.

However, if the load torque is unknown or is varying under different working conditions, we may estimate it by making some assumptions that correspond to real-life conditions. For example, we may assume that the load torque changes very slowly, i.e., $\dot{\tau}_l = 0$. This condition means that the load torque is assumed to be constant. Practically, this assumption has great significance because it provides an equation for the observer design and enables one to estimate the load torque that varies "slowly" with the time. The word "slowly" is relative to the mechanical and the electrical time constant of the DC motor. An observer is proposed here for estimation of the load torque.

To involve the measured current and the velocity signals into the observer design, we use the design technique of Luenberger reduced-order asymptotic observer (see Section 6.1). An intermediate variable is introduced,

$$z = \tau_l + l\omega, \tag{10.1.13}$$

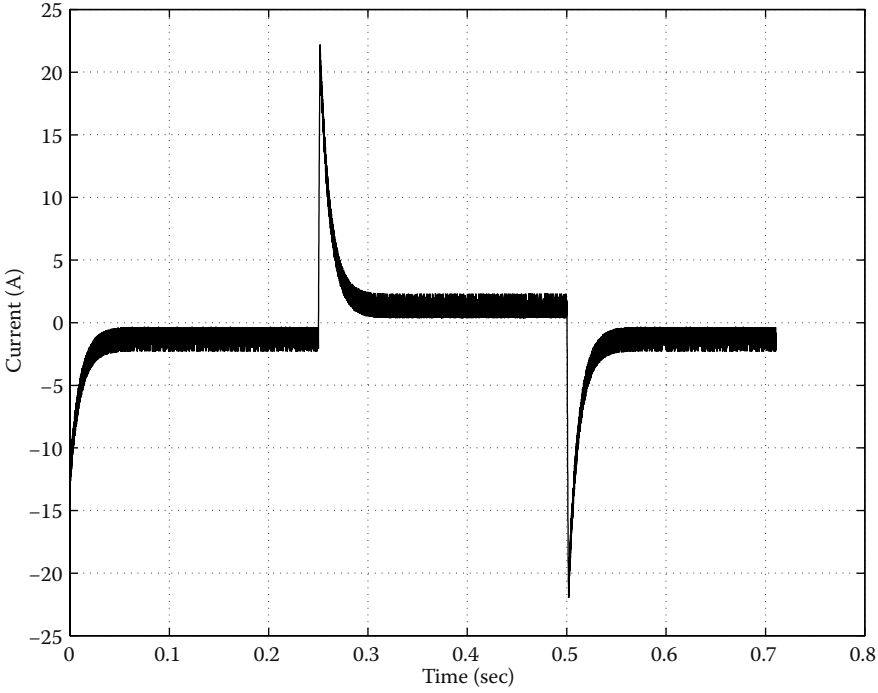

FIGURE 10.5
Current response of the speed controller.

where l is a constant observer gain. The motion equation for z, under the assumption $\dot{\tau}_l = 0$, is of form

$$\frac{dz}{dt} = l\dot{\omega} = \frac{1}{J}(-lz + l^2\omega + lk_t i). \tag{10.1.14}$$

Design an observer for the intermediate variable z as

$$\frac{d\hat{z}}{dt} = \frac{1}{J}(-l\hat{z} + l^2\omega + lk_t i). \tag{10.1.15}$$

The solution to the mismatch equation

$$\frac{d\bar{z}}{dt} = -\frac{l}{J}\bar{z}, \quad \text{with} \quad \bar{z} = \hat{z} - z \tag{10.1.16}$$

tends to zero exponentially, and the rate of convergence can be selected by a proper choice of the observer gain l. As a result, $\hat{z}$ will converge to z asymptotically, and the load torque can be estimated as

$$\tau_l = \hat{z} - l\omega. \tag{10.1.17}$$

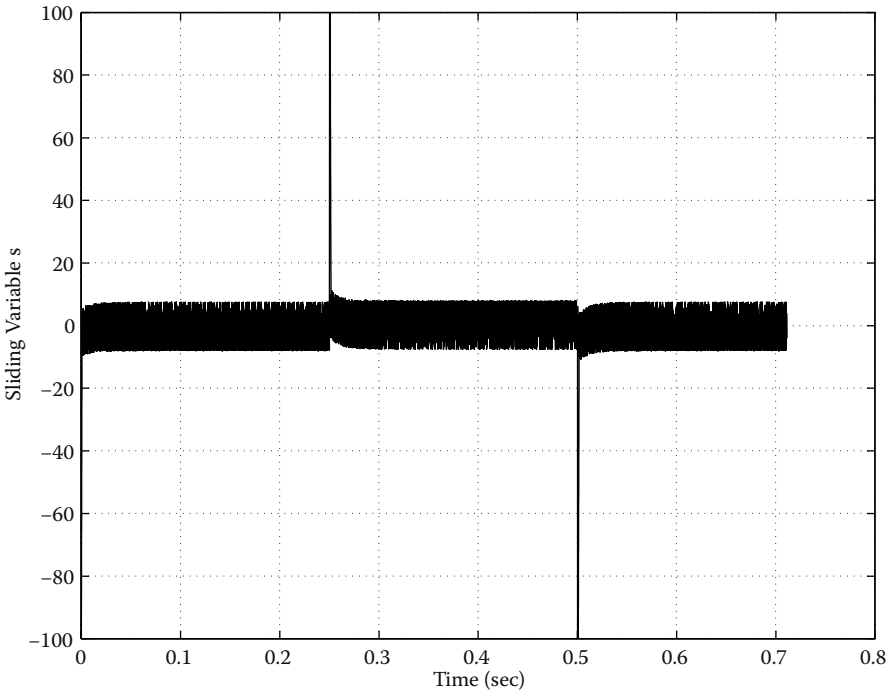

FIGURE 10.6
Response of the sliding variable *s* of the speed controller.

Now we are able to calculate the acceleration signal using Equation 10.1.12.

Estimation of the shaft acceleration can also be achieved by the following Luenberger observer (see Section 6.1) without explicitly involving knowledge of load torque:

$$\begin{aligned}\frac{d\hat{z}_1}{dt} &= \hat{z}_2 - l_1\left(\hat{\omega}-\omega\right),\\ \frac{d\hat{z}_2}{dt} &= \frac{k_t}{JL}\left(u - Ri - \lambda_0\hat{z}_1\right) - l_2\left(\hat{\omega}-\omega\right),\end{aligned} \tag{10.1.18}$$

where $\hat{\omega}$ is an estimate of the shaft speed, $\hat{z}_1 = \hat{\omega}$ and $\hat{z}_2 = \dot{\hat{\omega}}$, and l_1, l_2 are observer gains. Assumption $\dot{\tau}_l = 0$ was also used when deriving Equation 10.1.18. Denoting $\overline{z}_1 = \hat{z}_1 - z_1$ and $\overline{z}_2 = \hat{z}_2 - z_2$ as the mismatches between estimated and real quantities, the mismatch dynamics can be obtained as

$$\begin{aligned}\frac{d\overline{z}_1}{dt} &= \overline{z}_2 - l_1\overline{z}_1,\\ \frac{d\overline{z}_2}{dt} &= -\left(\frac{k_t\lambda_0}{JL} + l_2\right)\overline{z}_1.\end{aligned} \tag{10.1.19}$$

The characteristic polynomial of the above system is given by

$$p^2 + l_1 p + \left(\frac{k_t \lambda_0}{JL} + l_2 \right) = 0. \tag{10.1.20}$$

Obviously, the poles of the observer system can be placed arbitrarily by adjusting the observer gains l_1, l_2.

Figures 10.7 and 10.8 show the simulation results of the proposed estimation algorithms in Equations 10.1.12 through 10.1.17 for estimating the load torque as well as the shaft acceleration. The observer gain is designed to be $l = 40$. The mass of inertia J in the observer model is selected to have 10% difference from the real inertia in the motor model to generate a difference in the figures. Otherwise, the observer outputs and the model outputs would be too close to be distinguished.

10.1.7. Speed Control with Reduced-Order Model

As discussed in the previous sections, speed control of a DC motor requires control of either the motor current or the motor acceleration. However, in

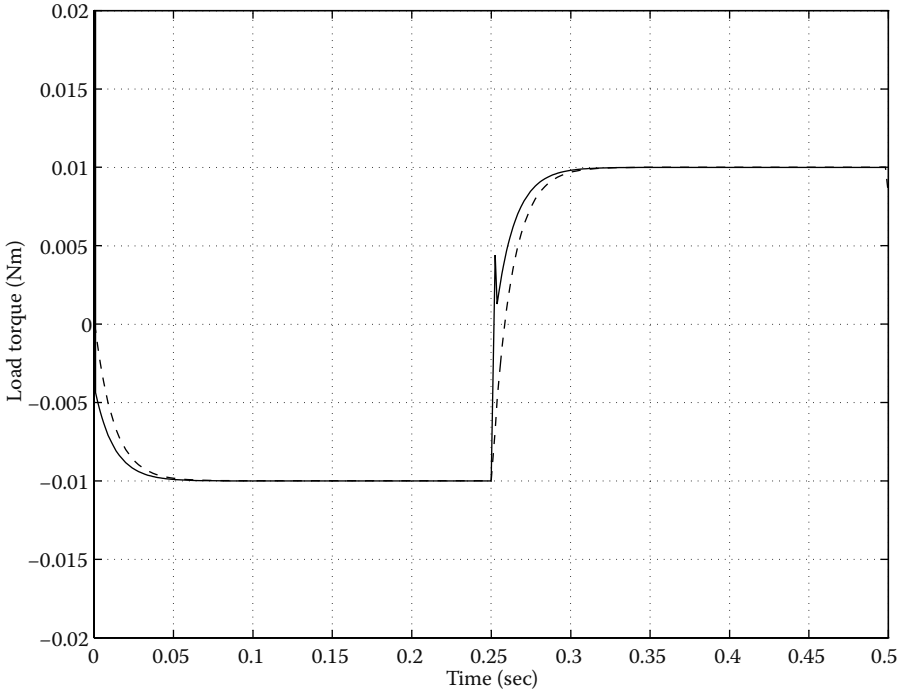

FIGURE 10.7
Real and observed load torque. Dashed line, real load torque; solid line, observed load torque.

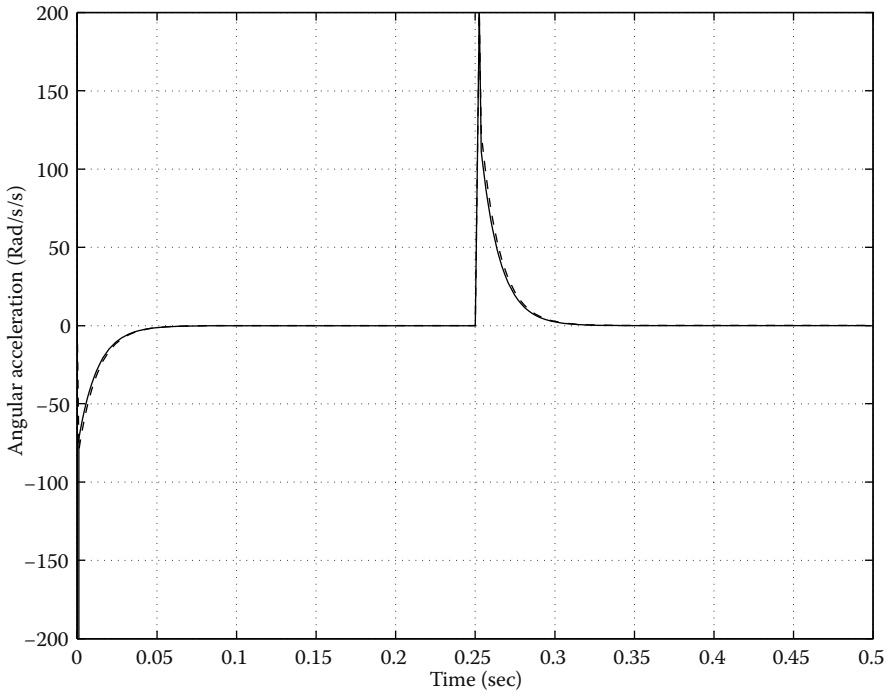

FIGURE 10.8
Real and observed shaft acceleration. Dashed line, real acceleration; solid line, observed acceleration.

some industrial systems, simple relay-controlled DC motors based only on speed measurement have been used. In this subsection, we will design simplified sliding mode control based only on speed measurement without estimation of other state components. Furthermore, the control methods proposed below will solve the chattering problem often encountered in those industrial systems.

Normally, the mechanical motion of a DC motor is much slower than the electromagnetic dynamics, implying that the relation $L << J$ holds. Suppose the speed tracking error is $\omega_e = \omega^* - \omega$; we may rewrite the DC motor model in terms of ω_e

$$\begin{aligned} L\frac{di}{dt} &= u - Ri - \lambda_0(\omega^* - \omega_e), \\ J\frac{d\omega_e}{dt} &= -k_t i + \tau_l + J\dot{\omega}^*. \end{aligned} \tag{10.1.21}$$

Calling on the theory of "singularly perturbed systems" [Kokotovic, O' Malley, and Sannuti 1976], we may formally let L be equal to zero because $L << J$. Solving for i from the resulting algebraic Equation 10.1.21 yields

$$i = -\frac{\lambda_0}{R}(\omega^* - \omega_e) + \frac{1}{R}u. \tag{10.1.22}$$

Substituting Equation 10.1.22 into Equation 10.1.21 results in

$$J\frac{d\omega_e}{dt} = \frac{k_t\lambda_0}{R}(\omega^* - \omega_e) - \frac{k_t}{R}u + \tau_l + J\dot{\omega}^*. \tag{10.1.23}$$

The above equation is a reduced-order (first-order) model of the DC motor system and can be used for the purpose of speed control without involving the knowledge of current and acceleration. The controller is designed as

$$u = u_0 \operatorname{sign}(\omega_e), \tag{10.1.24}$$

and the existence condition for the sliding mode $\omega_e = 0$ will be

$$u_0 > \left|\lambda_0\omega + \frac{\tau_l R}{k_t} + \frac{JR}{k_t}\dot{\omega}^*\right|. \tag{10.1.25}$$

However, in real-life systems under sliding mode control, neglected dynamics in the closed loop may result in the so-called chattering phenomenon. In the case of the speed controller (Equation 10.1.24), current i is assumed to be a linear function of the input voltage u in Equation 10.1.22 because of the assumption $L \approx 0$. From a macroscopic perspective, this assumption holds true. For high-frequency switching of the discontinuous input voltage u according to Equation 10.1.24, however, the electrical dynamics prevent armature current i from ideal tracking of voltage u, leading to chattering as explained in detail in Chapter 8. Moreover, the order reduction technique of the singular perturbation theory is formally not applicable to differential equations with discontinuous right-hand sides.

In a sliding mode controlled system with unmodeled dynamics, chattering can be bypassed by constructing the sliding manifold using observed states rather than direct measurements (see also Chapter 7). Bearing in mind the assumption $\dot{\tau}_l = 0$, design an asymptotic observer for estimating ω_e and τ_l as

$$\begin{aligned} J\frac{d\hat{\omega}_e}{dt} &= \frac{k_t\lambda_0}{R}(\omega^* - \hat{\omega}_e) - \frac{k_t}{R}u + \hat{\tau}_l + J\dot{\omega}^* - l_1(\hat{\omega}_e - \boldsymbol{\omega}_e), \\ \frac{d\hat{\tau}_l}{dt} &= -l_2(\hat{\omega}_e - \omega_e), \end{aligned} \tag{10.1.26}$$

where l_1 and l_2 are positive observer gains. The mismatch dynamics of the observer can be obtained as

$$J\dddot{\bar{\omega}}_e + \left(\frac{k_t\lambda_0}{R} + l_1\right)\ddot{\bar{\omega}}_e + \frac{l_2}{J}\dot{\bar{\omega}}_e = 0, \tag{10.1.27}$$

with $\bar{\omega}_e = (\hat{\omega}_e - \omega_e)$. Because all the coefficients in the above equation are positive, $\bar{\omega}_e$ will tend to zero asymptotically, and the desired convergence rate can be provided by selection of the constants l_1 and l_2. The discontinuous control using estimated state $\hat{\omega}_e$ will be

$$u = u_0 \,\text{sign}(\hat{\omega}_e). \tag{10.1.28}$$

The ideal sliding mode can be enforced if

$$u_0 > \left| \lambda_0(\omega^* - \hat{\omega}_e) + \frac{\hat{\tau}_l R}{k_t} + \frac{JR}{k_t}\dot{\omega}^* + \frac{l_1 R}{k_t}\bar{\omega}_e \right|. \tag{10.1.29}$$

Under this control scheme, chattering is eliminated, whereas the robustness provided by the sliding mode control is preserved within an accuracy of L/J (remember that the reduced-order equation was obtained under the assumption $L/J << 1$) . The sliding mode occurs in the observer loop, which does not contain unmodeled dynamics. The observer gains l_1 and l_1 should be chosen to yield mismatch dynamics (Equation 10.1.27) slower than the electrical dynamics of the DC motors to prevent chattering. Because the estimated $\hat{\omega}$ is close to ω, the real speed ω tracks the desired value ω^*. Figure 10.9 shows the control structure based on the reduced-order model and observed state.

Figure 10.10 shows a simulation result of the reduced-order speed control with measured speed (Equation 10.1.24). The high-frequency chattering is attributable to neglect of the fast dynamics, i.e., the dynamics of the electric part. Figure 10.11 depicts the response of the speed control with observed speed using Equation 10.1.26. The observer gains are selected as $l_1 = l_2 = 20$. As can be seen from the figures, the high-frequency chattering now has disappeared, confirming the theory described above.

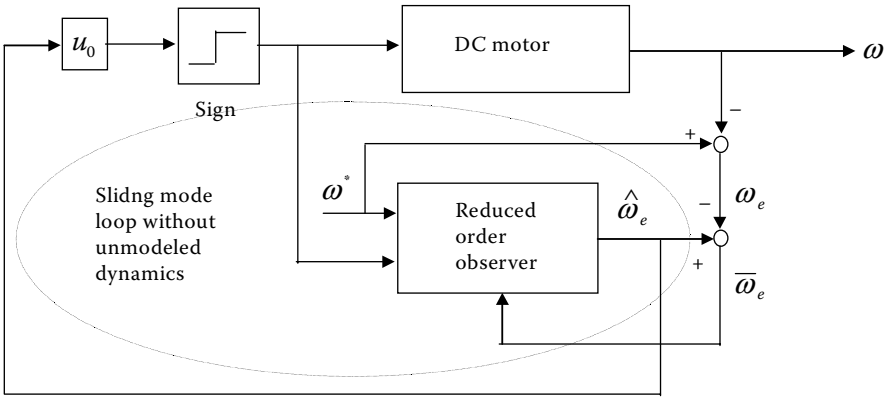

FIGURE 10.9
Speed control based on reduced-order model and observed state.

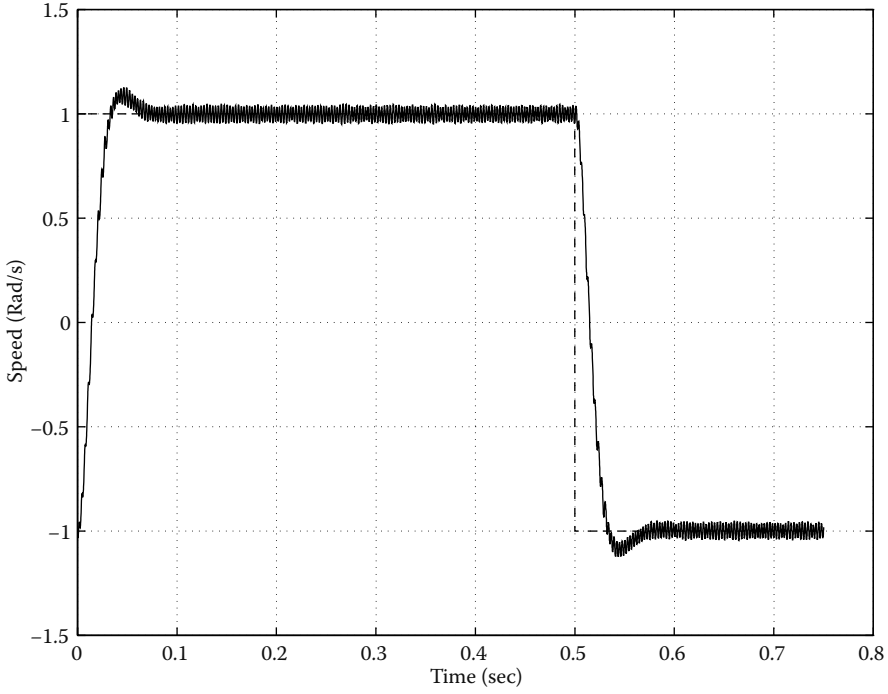

FIGURE 10.10
Reduced-order speed control with measured speed. Dashed line, reference speed; solid line, real speed.

10.1.8. Observer Design for Sensorless Control

Strictly speaking, the word "sensorless" is not correct because one must sense or measure some variable to obtain some information as the base of estimating the unknown variable(s). Normally, sensorless control of an electric drive implies that no sensor for any mechanical variable is necessary, but electrical variables such as motor current and voltage should be available. In the following, we treat the problem of estimating the motor speed and/or the load torque based on the motor current and voltage. The methodology used here is again based on the sliding mode design principle.

10.1.8.1. Estimation of the Shaft Speed

Design a current observer as follows:

$$L\,d\hat{i}/dt = u - R\hat{i} - l_1\,\mathrm{sign}(\bar{i}), \tag{10.1.30}$$

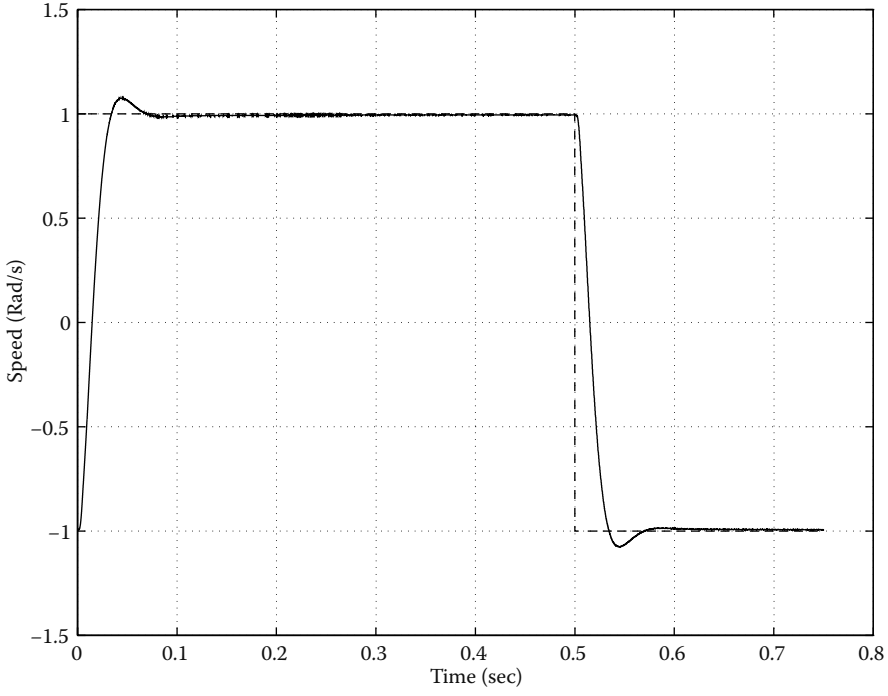

FIGURE 10.11
Reduced-order speed control with observed speed. Dashed line, reference speed; solid line, real speed.

where $\bar{i} = \hat{i} - i$ and $l_1 > 0$ is a constant observer gain. The dynamics of the mismatch $\bar{i}$ can be obtained by subtracting Equation 10.1.30 from the model equation given in Equation 10.1.1:

$$L d\bar{i}/dt = -R\bar{i} + \lambda_0 \omega - l_1 \operatorname{sign}(\bar{i}). \tag{10.1.31}$$

Now select the constant l_1 to enforce sliding mode ($s = \bar{i} = 0$) by applying the existence condition $s\dot{s} < 0$ to yield

$$l_1 > \left|\lambda_0 \omega - R\bar{i}\right|, \tag{10.1.32}$$

under which $\bar{i}$ will decay to zero in finite time. Using the concept of equivalent control (see Section 2.3), we obtain

$$L d\bar{i}/dt = -R\bar{i} + \lambda_0 \omega - (l_1 \operatorname{sign}(\bar{i}))_{eq} = 0, \tag{10.1.33}$$

and

$$(l_1 \operatorname{sign}(\bar{i}))_{eq} = -R\bar{i} + \lambda_0 \omega. \tag{10.1.34}$$

After the reaching phase of sliding mode, $\bar{i}$ is equal to zero, and, for known back-EMF constant λ_0 (which can be determined during the parameter identification), the motor speed can be obtained as

$$\omega = (l_1 \operatorname{sign}(\bar{i}))_{eq} / \lambda_0 . \tag{10.1.35}$$

Now the problem is how to determine the value of $(l_1 \operatorname{sign}(\bar{i}))_{eq}$. To determine an equivalent control, a low-pass filter may be used (see Section 2.4). Only first-order filters were analyzed in Section 2.4. In fact, the same methodology is applicable for higher-order low-pass filters, for example, an l-order low-pass filter such as

$$\begin{aligned} \mu \dot{x} &= Ax + B(l_1 \operatorname{sign}(\bar{i})), \\ y &= C^T x, \end{aligned} \tag{10.1.36}$$

where $A \in \Re^{l \times l}$, $B \in \Re^l$, and $C \in \Re^l$ are the filter parameters that satisfy $C^T A^{-1} B = -1$, $x \in \Re^l$ represents the state vector of the filter, and y is the filter output; small positive parameter $\mu << 1$ represents the filter time constant. Calling on the theory of singularly perturbed systems, if $\mu \to 0$, then $y \to (l_1 \operatorname{sign}(\bar{i}))_{eq}$.

So far, we have discussed the problem of estimating the speed signal. Once the speed signal is available, a speed controller may be constructed. Bearing in mind that the speed signal is obtained by passing the discontinuous control through a low-pass filter, high-frequency components of the discontinuous control may not be filtered out completely because of the limitation on the filter time constant (i.e., μ should be small enough). A sliding mode controller will no longer be suitable for speed control because of the high-frequency disturbances. It would be helpful if the speed control includes an integral term, e.g., a PI-type controller is appropriate. In this case, the controlled real speed will follow the mean value of the estimated speed.

10.1.8.2. Estimation of Load Torque

As the speed signal is available, estimated or measured, the load torque can also be obtained by applying the sliding mode technique to an observer. First, design a speed observer as follows:

$$J \frac{d\hat{\omega}}{dt} = k_t i - l_2 \operatorname{sign}(\bar{\omega}), \text{ with } \bar{\omega} = \hat{\omega} - \omega. \tag{10.1.37}$$

Suppose that the parameters J and k_t are known; then the mismatch $\bar{\omega}$ is governed by

$$J \frac{d\bar{\omega}}{dt} = \tau_l - l_2 \operatorname{sign}(\bar{\omega}), \tag{10.1.38}$$

where l_2 is a constant observer gain. Applying the existence condition for sliding mode to occur in $\bar{\omega} = 0$ yields

$$\bar{\omega}\dot{\bar{\omega}} = \frac{\tau_l}{J}\bar{\omega} - \frac{l_2}{J}|\bar{\omega}| < 0, \tag{10.1.39}$$

implying that $l_2 > |\tau_l|$ should hold. Because l_2 appears only in the observer algorithm, it can be selected high enough. Once sliding mode occurs, the load torque is equal to the equivalent control of the discontinuous term $l_2 \operatorname{sign}(\bar{\omega})$, i.e.,

$$\tau_l = (l_2 \operatorname{sign}(\bar{\omega}))_{eq}. \tag{10.1.40}$$

To extract the equivalent control given above, we need a low-pass filter again.

It should be noted that, during the derivations of the load torque observer, no assumption such as $\dot{\tau}_l = 0$ was made. Actually, this observer design scheme works as long as the spectrum of the load torque does not intersect with the spectrum of the high-frequency components of the switching action.

Figures 10.12 through 10.14 show the simulation results of the proposed observer algorithms for sensorless control. The observer gains are chosen as $l_1 = l_2 = 20000$. The low-pass filters for extracting the motor speed and the load torque are both of Butterworth type with second order. The cutoff frequencies of the low-pass filters are 1000 and 550 rad/sec, respectively. The motor is commanded to follow a block signal of reference speed. As shown in Figure 10.12, the estimated speed signal tracks the real speed signal very closely, as do the estimated acceleration and the estimated load torque.

10.1.9. Discussion

Generally speaking, uncertainties in the plant model of any observer design will cause the observed state to differ from the real state. If this observed state is used within the control loop, it may result in a control error. However, if the observer error is within a small range, the control error is also bounded by a similar small range, implying that the observed state may still be useful for increasing the control performance.

For implementation of an observer, the observer equation should be integrated in real time using a microprocessor or signal processor with a fixed sampling period. As a result, the system to be controlled is continuous in time, but the observer in the control computer is a discrete time system. Furthermore, the error of the integration will be large if the following applies:

1. The sampling period of the microprocessor is too large.
2. The integration algorithm is primitive.

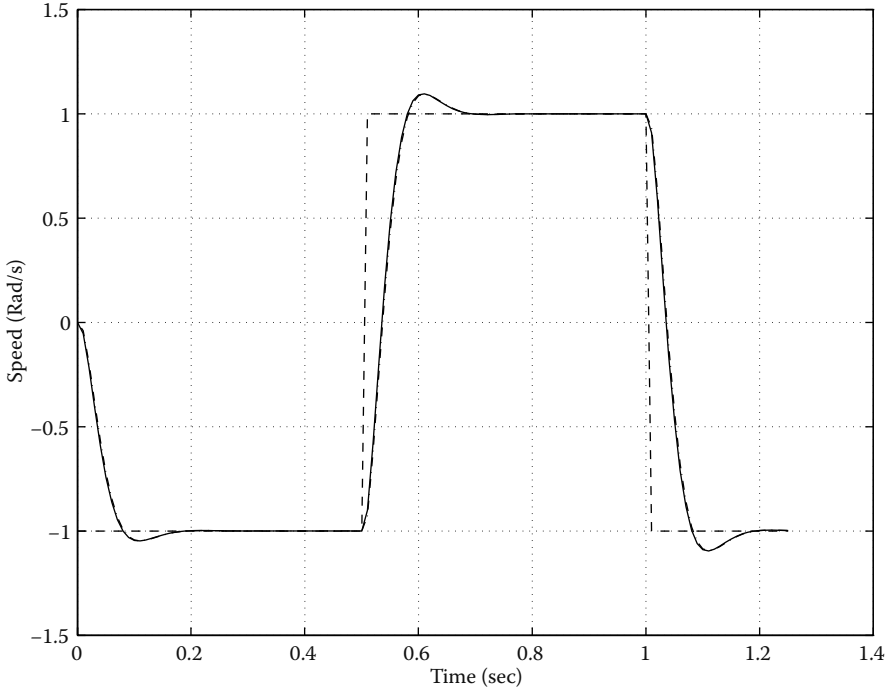

FIGURE 10.12
Response of the sliding mode speed observer. Dashed line, reference speed; solid line, real speed; dash-dotted line, observed speed.

3. The observer gain is too high.
4. The time constant of the observer system is too small.

The system accuracy may be improved by decreasing the sampling interval. However, for a larger sampling interval, more complex and efficient control algorithms may be implemented. The control engineer has to find a suitable tradeoff. Readers particularly interested in microprocessor implementation of sliding mode controllers and observers are encouraged to study Chapter 9 on discrete-time systems.

10.2. Permanent-Magnet Synchronous Motors

10.2.1. Introduction

Permanent-magnet synchronous motors (PMSMs) belong to the category of AC drives. The terminology "brushless DC motor," used in the fields of machine tools and robotics, often refers to a current-controlled PMSM.

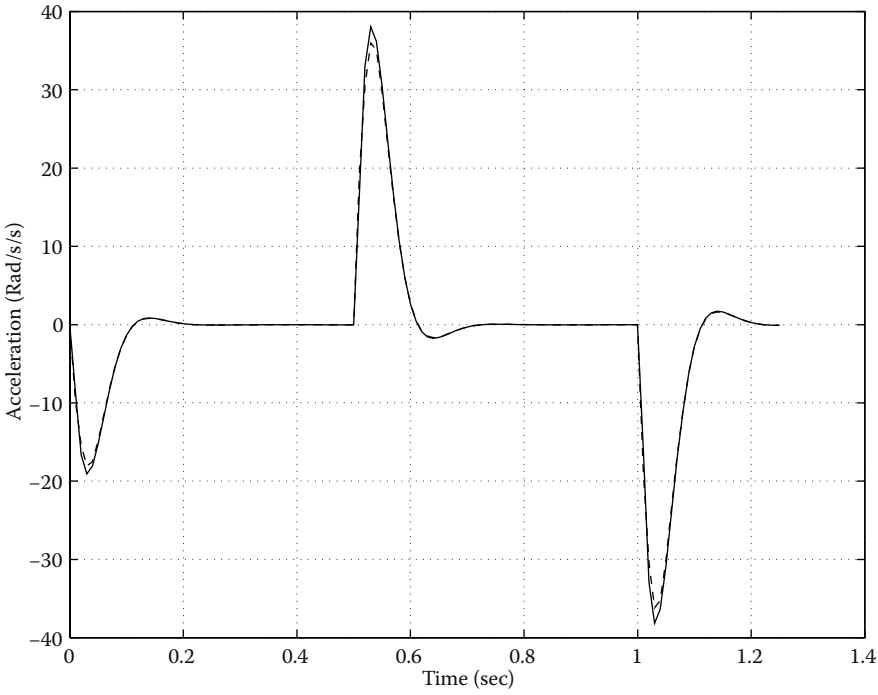

FIGURE 10.13
Observed acceleration versus real acceleration. Dashed line, observed acceleration; solid line, real acceleration.

It is interesting to point out that the discussion of the control problem of PMSMs in the field-oriented reference frame, referred to as (d, q) frame, is independent from the number of phases of a motor, i.e., no matter of a two-phase or a three-phase motor, they have the same structure in this coordinate frame. The differences lie only on the forward and backward transformations of the states and controls (here, currents and voltages). In fact, a model in the (d, q) frame is an uniform description of an AC device based on the electromagnetic principle including all types of AC drives and power converters. Control design methods performed in the (d, q) coordinates are called *field-oriented control* (FOC). FOC is sometimes referred to as "vector control," implying that a current vector should be controlled rather than only one current component as in the case of a pure DC motor. The principle of FOC was developed more than 30 years ago [Blaschke 1974]. From a control point of view, this control approach uses a state transformation, after which the decoupling and linearization tasks can be performed easily. Recently, because of the rapid progress in the technology of semiconductors, high-speed microprocessors as well as signal processors are massively introduced

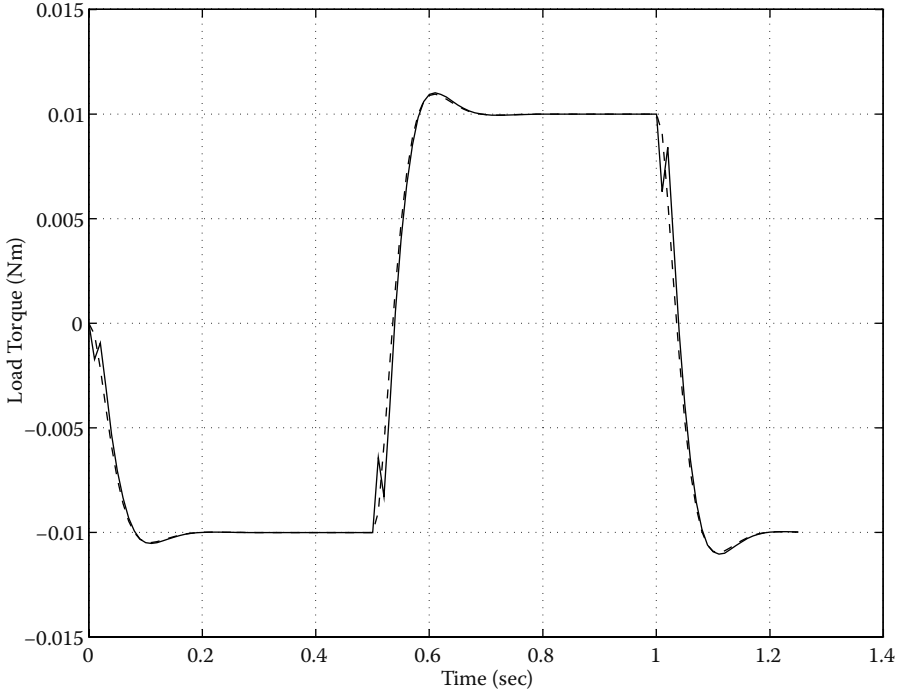

FIGURE 10.14
Observed load torque versus real load torque. Dashed line, observed load torque; solid line, real load torque.

in the area of electric drive systems. As a result, the concept of FOC has been implemented in many drive systems of AC machines. The remaining problem is robustness associated with parameter variations and load variations.

Theoretically, sliding mode control provides advantages over conventional control designs (e.g., decoupling, linearization, linear control, and PWM) because of the simple control structure and the robustness property of the sliding mode control principle. However, it is recognized that, in microprocessor-based implementations, the sampling interval and thus the minimum switching interval of the sliding mode controller, is much larger than the resolution of a hardware-based PWM. As a result, some deterioration in control performance was observed. This problem may be solved by discrete-time sliding mode control (see Chapter 9) in conjunction with hardware PWM techniques. Moreover, because the structure of a sliding mode controller is very simple, a nonmicroprocessor, purely hardware-based implementation is possible and often leads to favorable results. Hence, the effectiveness of the sliding mode control can be fully demonstrated without using PWM units.

10.2.2. Modeling of Permanent-Magnet Synchronous Motors

The structure of a PMSM-based drive system is shown in Figure 10.15. For sliding mode control design, it is convenient if the control inputs take values from the discrete set $\{-u_0, u_0\}$ instead of on-off signals from the discrete set $\{0, 1\}$. Let the six on-off signals be $\boldsymbol{s}_w = [s_{w1}\ s_{w2}\ s_{w3}\ s_{w4}\ s_{w5}\ s_{w6}]^T$ with $s_{w4} = 1 - s_{w1}$, $s_{w5} = 1 - s_{w2}$, and $s_{w6} = 1 - s_{w3}$, and the control inputs for sliding mode control design be $U_{gate} = [u_1\ u_2\ u_3]^T$, then the following relation holds

$$U_{gate} = u_0 G_w s_w, \text{ with } G_w = \begin{bmatrix} 1 & 0 & 0 & -1 & 0 & 0 \\ 0 & 1 & 0 & 0 & -1 & 0 \\ 0 & 0 & 1 & 0 & 0 & -1 \end{bmatrix}. \tag{10.2.1}$$

The backward transformation can be obtained as

$$\begin{aligned} s_{w1} &= 0.5(1 + u_1/u_0), \quad s_{w4} = 1 - s_{w1}, \\ s_{w2} &= 0.5(1 + u_2/u_0), \quad s_{w5} = 1 - s_{w2}, \\ s_{w3} &= 0.5(1 + u_3/u_0), \quad s_{w6} = 1 - s_{w3}. \end{aligned} \tag{10.2.2}$$

In general, the dynamic model of an AC motor can be established using physical laws

$$\begin{aligned} \boldsymbol{U} &= \boldsymbol{R}\boldsymbol{I} + \frac{d\Psi}{dt}, \\ \Psi &= \boldsymbol{L}\boldsymbol{I} + \Psi_M, \end{aligned} \tag{10.2.3}$$

where $\boldsymbol{U}$, $\boldsymbol{I}$, and Ψ are the voltage vector, the current vector, and the flux vector, respectively; $\boldsymbol{R}$ and $\boldsymbol{L}$ are the resistance matrix and the inductance

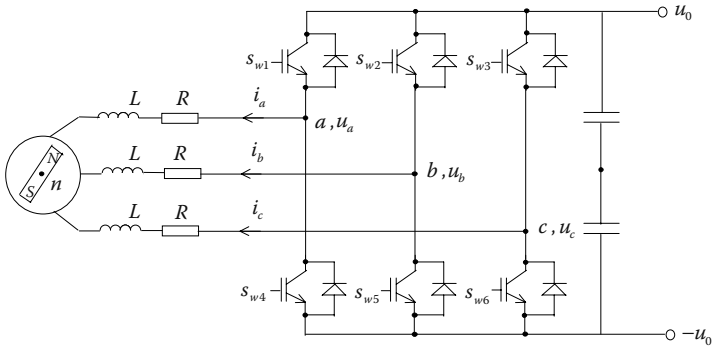

FIGURE 10.15
Structure of a PMSM drive system. *N* and *S* denote the magnetic north and south, respectively; *n* is the neutral point of the stator windings; u_a, u_b and u_c are the potential differences between points *a*, *b*, *c* and the neutral point *n*, respectively.

matrix, respectively; and Ψ_M is the flux vector caused by the permanent magnet, if applicable.

The system in Equation 10.2.3 is a general description of electromagnetic effects and is independent of the used coordinate system. For PMSMs, three reference frames are normally used for describing the dynamic behavior of a motor (see Figure 10.16): the phase frame, i.e., the (a, b, c) coordinate frame; the stator frame, i.e., the (α, β) coordinate frame; and the field-oriented frame, i.e., the (d, q) coordinate frame (same as the rotor coordinate frame for PMSMs).

For a symmetrical PMSM in the (a, b, c) coordinate, the flux components generated by the permanent magnet are given as

$$\begin{aligned} \Psi_{ma} &= \lambda_0 \cos \theta_e, \\ \Psi_{mb} &= \lambda_0 \cos (\theta_e - 2\pi/3), \\ \Psi_{mc} &= \lambda_0 \cos (\theta_e + 2\pi/3), \end{aligned} \tag{10.2.4}$$

where λ_0 is the flux linkage of the permanent magnet and θ_e is the electrical angular position of the motor rotor. The electrical motion equations of a PMSM, neglecting the reluctance effects, can be written as

$$\begin{aligned} \frac{di_a}{dt} &= -\frac{R}{L} i_a - \frac{1}{L} e_a + \frac{1}{L} u_a, \\ \frac{di_b}{dt} &= -\frac{R}{L} i_b - \frac{1}{L} e_b + \frac{1}{L} u_b, \\ \frac{di_c}{dt} &= -\frac{R}{L} i_c - \frac{1}{L} e_c + \frac{1}{L} u_c, \end{aligned} \tag{10.2.5}$$

where R is the winding resistance and L is the winding inductance, i_a, i_b, i_c are the phase currents, and u_a, u_b, u_c are the phase voltages. Furthermore, e_a, e_b, e_c are the induced EMF components of the following form:

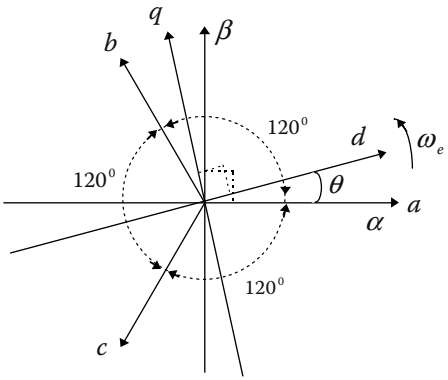

FIGURE 10.16
Coordinate systems of PMSM.

$$
\begin{aligned}
e_a &= \frac{d\Psi_{ma}}{dt} = -\lambda_0 \omega_e \sin\theta_e, \\
e_b &= \frac{d\Psi_{mb}}{dt} = -\lambda_0 \omega_e \sin(\theta_e - 2\pi/3), \\
e_c &= \frac{d\Psi_{mc}}{dt} = -\lambda_0 \omega_e \sin(\theta_e + 2\pi/3),
\end{aligned}
\tag{10.2.6}
$$

in which $\omega_e = d\theta_e/dt$ is the electrical angular speed of the rotor. The relationship between the phase voltages u_a, u_b, u_c and the discontinuous controls u_1, u_2, u_3 is given by

$$
[u_a \;\; u_b \;\; u_c]^T = A_{abc}^{123} [u_1 \;\; u_2 \;\; u_3]^T, \tag{10.2.7}
$$

where matrix A_{abc}^{123} is defined as

$$
A_{abc}^{123} = \frac{1}{3} \begin{bmatrix} 2 & -1 & -1 \\ -1 & 2 & -1 \\ -1 & -1 & 2 \end{bmatrix}. \tag{10.2.8}
$$

Note that matrix A_{abc}^{123} is a singular matrix implying that the phase voltages u_a, u_b, u_c are not independent. As shown later, the sum of u_a, u_b, u_c is equal to zero because of the physical configuration given in Figure 10.15.

The motor model in (α, β) coordinates can be obtained by either applying the definition given in Equation 10.2.3 or transforming the motor model from the (a, b, c) coordinate frame into the (α, β) frame. The electrical part of the motor model in this coordinate frame is

$$
\begin{aligned}
\frac{di_\alpha}{dt} &= -\frac{R}{L} i_\alpha - \frac{1}{L} e_\alpha + \frac{1}{L} u_\alpha, \\
\frac{di_\beta}{dt} &= -\frac{R}{L} i_\beta - \frac{1}{L} e_\beta + \frac{1}{L} u_\beta,
\end{aligned}
\tag{10.2.9}
$$

where $e_\alpha = -\lambda_0 \omega_e \sin\theta_e$ and $e_\beta = \lambda_0 \omega_e \cos\theta_e$ are the induced EMF components in the (α, β) coordinate frame; the stator currents $[i_\alpha \; i_\beta]^T$ and the stator voltages $[u_\alpha \; u_\beta]^T$ are defined as follows:

$$
\begin{aligned}
[i_\alpha \;\; i_\beta]^T &= A_{\alpha,\beta}^{a,b,c} [i_a \;\; i_b \;\; i_c]^T, \\
[u_\alpha \;\; u_\beta]^T &= A_{\alpha,\beta}^{a,b,c} [u_a \;\; u_b \;\; u_c]^T,
\end{aligned}
\tag{10.2.10}
$$

where $A_{\alpha,\beta}^{a,b,c}$ denotes the transformation matrix

$$
A_{\alpha,\beta}^{a,b,c} = 2/3 \begin{bmatrix} 1 & -1/2 & -1/2 \\ 0 & \sqrt{3}/2 & -\sqrt{3}/2 \end{bmatrix}. \tag{10.2.11}
$$

Because the rank of this matrix is two, the backward transformation has no unique solution. For the backward transformation of Equation 10.2.10, the concept of "pseudo-inverse (also called "Moore-Penrose inverse") of a matrix can be used. The pseudo-inverse of matrix $A_{\alpha,\beta}^{a,b,c}$, denoted as $\left(A_{\alpha,\beta}^{a,b,c}\right)^{+}$, is calculated as

$$\left(A_{\alpha,\beta}^{a,b,c}\right)^{+} = \left(A_{\alpha,\beta}^{a,b,c}\right)^{T}\left(A_{\alpha,\beta}^{a,b,c}\left(A_{\alpha,\beta}^{a,b,c}\right)^{T}\right)^{-1} = \frac{3}{2}\left(A_{\alpha,\beta}^{a,b,c}\right)^{T} = \begin{bmatrix} 1 & -1/2 & -1/2 \\ 0 & \sqrt{3}/2 & -\sqrt{3}/2 \end{bmatrix}^{T}. \tag{10.2.12}$$

It is easy to prove that $A_{\alpha,\beta}^{a,b,c}\left(A_{\alpha,\beta}^{a,b,c}\right)^{+}$ is a 2×2 unit matrix. As a result, the backward transformation of the stator currents and voltages can be given as

$$\begin{aligned} [i_a \;\; i_b \;\; i_c]^T &= \left(A_{\alpha,\beta}^{a,b,c}\right)^{+}[i_\alpha \;\; i_\beta]^T, \\ [u_a \;\; u_b \;\; u_c]^T &= \left(A_{\alpha,\beta}^{a,b,c}\right)^{+}[u_\alpha \;\; u_\beta]^T. \end{aligned} \tag{10.2.13}$$

The motor model in the (d, q) coordinate frame, which rotates synchronously with the motor rotor, can also be obtained by transforming the motor model from the (α, β) coordinate frame to (d, q) coordinates as shown:

$$\begin{aligned} \frac{di_d}{dt} &= -\frac{R}{L}i_d + \omega_e i_q + \frac{1}{L}u_d, \\ \frac{di_q}{dt} &= -\frac{R}{L}i_q - \omega_e i_d - \frac{1}{L}\lambda_0\omega_e + \frac{1}{L}u_q, \end{aligned} \tag{10.2.14}$$

where i_d and i_q are the stator currents in the (d, q) coordinate frame, and u_d and u_q are the stator voltages in the same coordinate frame. The term $\lambda_0\omega_e = e_q$ is the q component of the induced EMF generated by the permanent magnet, and the d component of the EMF e_d is equal to zero. Note the second equation in Equation 10.2.14. If the current component i_d could be made equal to zero, we would get exactly the behavior of a constant-excited DC motor. This is the main idea of field-oriented control: to decouple the motor dynamics such that the resulting system behaves like a DC motor. The current vector $[i_d \; i_q]^T$ and the voltage vector $[u_d \; u_q]^T$ can be transformed from the (α, β) coordinate frame

$$\begin{aligned} [i_d \;\; i_q]^T &= A_{d,q}^{\alpha,\beta}[i_\alpha \;\; i_\beta]^T, \\ [u_d \;\; u_q]^T &= A_{d,q}^{\alpha,\beta}[u_\alpha \;\; u_\beta]^T, \end{aligned} \tag{10.2.15}$$

in which matrix $A_{d,q}^{\alpha,\beta}$ is defined as

$$A_{d,q}^{\alpha,\beta} = \begin{bmatrix} \cos\theta_e & \sin\theta_e \\ -\sin\theta_e & \cos\theta_e \end{bmatrix}. \tag{10.2.16}$$

This matrix is an orthogonal matrix whose inverse is equal to its transpose. As a result, the backward transformation can be written as

$$\begin{aligned}[i_\alpha \;\; i_\beta]^T &= \left(A_{d,q}^{\alpha,\beta}\right)^T [i_d \;\; i_q]^T \\ [u_\alpha \;\; u_\beta]^T &= \left(A_{d,q}^{\alpha,\beta}\right)^T [u_d \;\; u_q]^T .\end{aligned} \tag{10.2.17}$$

The relationship between the (d, q) coordinate frame and the (a, b, c) coordinate frame can also be established. The phase currents i_a, i_b, i_c and the phase voltages u_a, u_b, u_c are transformed into the (d, q) coordinates as follows:

$$\begin{aligned}[i_d \;\; i_q]^T &= A_{d,q}^{a,b,c}[i_a \;\; i_b \;\; i_c]^T , \\ [u_d \;\; u_q]^T &= A_{d,q}^{a,b,c}[u_a \;\; u_b \;\; u_c]^T ,\end{aligned} \tag{10.2.18}$$

where matrix $A_{d,q}^{a,b,c}$ depends also on the electrical angular position of the rotor θ_e and is defined as

$$A_{d,q}^{a,b,c} = A_{d,q}^{\alpha,\beta} A_{\alpha,\beta}^{a,b,c} . \tag{10.2.19}$$

Matrix $A_{d,q}^{a,b,c}$ is a 2×3 matrix; hence, for the backward transformation, we need again its pseudo-inverse given as

$$\left(A_{d,q}^{a,b,c}\right)^+ = \left(A_{d,q}^{a,b,c}\right)^T \left(A_{d,q}^{a,b,c}\left(A_{d,q}^{a,b,c}\right)^T\right)^{-1} = \frac{3}{2}\left(A_{d,q}^{a,b,c}\right)^T , \tag{10.2.20}$$

resulting in

$$\begin{aligned}[i_a \;\; i_b \;\; i_c]^T &= \left(A_{d,q}^{a,b,c}\right)^+ [i_d \;\; i_q]^T , \\ [u_a \;\; u_b \;\; u_c]^T &= \left(A_{d,q}^{a,b,c}\right)^+ [u_d \;\; u_q]^T .\end{aligned} \tag{10.2.21}$$

The relationship between the control voltages u_d, u_q and the discontinuous controls u_1, u_2, u_3 can be established as

$$[u_d \;\; u_q]^T = A_{d,q}^{1,2,3}[u_1 \;\; u_2 \;\; u_3]^T , \tag{10.2.22}$$

where matrix $A_{d,q}^{1,2,3}$ is defined as

$$A_{d,q}^{1,2,3} = A_{d,q}^{\alpha,\beta} A_{\alpha,\beta}^{a,b,c} A_{a,b,c}^{1,2,3} . \tag{10.2.23}$$

Matrices $A_{\alpha,\beta}^{a,b,c}$ and $A_{a,b,c}^{1,2,3}$ satisfy the condition $A_{\alpha,\beta}^{a,b,c} A_{a,b,c}^{1,2,3} = A_{\alpha,\beta}^{a,b,c}$; therefore,

$$A_{d,q}^{1,2,3} = A_{d,q}^{\alpha,\beta} A_{\alpha,\beta}^{a,b,c} = A_{d,q}^{a,b,c} . \tag{10.2.24}$$

However, to maintain clarity, we prefer to use matrix $A_{d,q}^{1,2,3}$ denoting the transformation between the discontinuous controls u_1, u_2, u_3 and the control

voltages u_d, u_q. Matrix $A_{d,q}^{1,2,3}$ is a 2×3 matrix; hence, for the backward transformation, we need its pseudo-inverse as well:

$$\left(A_{d,q}^{1,2,3}\right)^{+} = \left(A_{d,q}^{1,2,3}\right)^{T}\left(A_{d,q}^{1,2,3}\left(A_{d,q}^{1,2,3}\right)^{T}\right)^{-1} = \frac{3}{2}\left(A_{d,q}^{1,2,3}\right)^{T}, \tag{10.2.25}$$

resulting in

$$[u_1 \; u_2 \; u_3]^T = \left(A_{d,q}^{1,2,3}\right)^{+}[u_d \; u_q]^T. \tag{10.2.26}$$

Finally, the generated motor torque τ_e and the mechanical power P of the motor are given by

$$\begin{aligned} \tau_e &= K_t i_q, \\ P &= \tau_e \omega_r, \end{aligned} \tag{10.2.27}$$

in which K_t is the torque constant, assumed to be equal to $(3/2)\lambda_0 N_r$ with N_r being the number of pole pairs of the motor, and ω_r is the mechanical angular speed of the motor rotor.

In developing the motor models, we assume that there is no reluctance torque in the PMSM motor. Under this assumption, the output torque of the motor is proportional to the q-axis stator current i_q. The mechanical motion equation of the motor can be written as

$$\begin{aligned} J\frac{d\omega_r}{dt} &= \tau_e - \tau_l, \\ \frac{d\theta_r}{dt} &= \omega_r, \end{aligned} \tag{10.2.28}$$

where τ_l and θ_r denote the load torque and the mechanical angular position of the motor rotor. For the electrical angular position/speed and the mechanical angular position/speed, the following relations hold:

$$\begin{aligned} \omega_e &= N_r \, \omega_r, \\ \theta_e &= N_r \theta_r. \end{aligned} \tag{10.2.29}$$

Usually, θ_r is measured, and ω_r, θ_e, ω_e are calculated according to Equations 10.2.28 and 10.2.29.

For stator windings connected at the neutral point n, the following balance conditions hold

$$\begin{aligned} I_a + I_b + I_c &= 0, \\ e_a + e_b + e_c &= 0, \\ u_a + u_b + u_c &= 0. \end{aligned} \tag{10.2.30}$$

Throughout this section, the motor parameters used to verify the design principles are as follows: L = 1.0 mH, R = 0.5 Ω, J = 0.001 kg·m^2, B = 0.001 Nm·sec/rad, $N_r = 4$, $\lambda_0 = 0.001$ V·s/rad, and kt = $(3/2)\lambda_0 N_r$ Nm/A. The supplied link voltage is $u_0 = 20$ V.

So far we have discussed the model descriptions in the different coordinate systems and the transformations of the state variables and the control signals between these reference frames. In the following sections, we deal with the sliding mode control issues of PMSMs.

10.2.3. Sliding Mode Current Control

The goal of the current control is to design a current controller to track the desired currents that are normally provided by an outer-loop speed/position controller. A current controller can be implemented with either pure hardware or a microprocessor. The so-called "chopper control" and "hysteresis control" are the hardware versions of a current controller attributable to the simplicity in the implementation. For the field-oriented current control, however, a microprocessor-based implementation is recommended. Current control based on the sliding mode approach can be implemented either with pure hardware or within a microprocessor, and, for both implementations, the control performance provided by the field orientation concept can be achieved.

In the context of sliding mode control of AC drives, there are two methods to determine the discontinuous controls u_1, u_2, u_3 as well as the on-off signals s_{w1}, s_{w2}, s_{w3}, s_{w4}, s_{w5}, s_{w6}. The on-off signals may also be called switching patterns. The switching patterns are the control signals feeding to the gates of the power converters, e.g., a voltage source inverter as shown in Figure 10.15.

The first method implies that the control voltages u_d and u_q are designed using the existence condition of sliding mode and mapping the resulting controls to the switching patterns of the inverter. The second method determines the switching patterns directly using the method of switching surface transformation (see Section 3.2). Both methods are able to generate switching commands for the voltage source inverter without involving the traditional PWM technique.

10.2.3.1. First Method for Current Control

Because the model in (d, q) coordinates gives clear physical interpretation in terms of a DC motor, we prefer to start with this model. Equation 10.2.14 is still a coupled nonlinear dynamic system with two control inputs u_d and u_q. However, as mentioned above, if we are able to reduce the current component i_d to zero, we would get exactly the same behavior as for a DC motor with constant excitation flux. Another difference from a DC motor is that all variables with subscripts d and q cannot be measured directly but rather are transformed from the variables measured in the (a, b, c) coordinate frame. For

performing this transformation, the electrical angular position of the rotor θ_e is required.

As in the DC motor case, for current control of a PMSM, we may design the switching functions as the difference between the desired and real currents. Select the switching functions for both current components i_d and i_q as

$$\begin{aligned} s_d &= i_d^* - i_d, \\ s_q &= i_q^* - i_q, \end{aligned} \tag{10.2.31}$$

where i_d^* and i_q^* denote the desired value for the currents i_d and i_q, respectively. Conventional field-oriented control of PMSMs uses linear control design techniques. The nonlinear model (Equation 10.2.14) has to be decoupled and linearized before linear control techniques can be applied. However, because the sliding mode control approach belongs to the category of nonlinear control techniques, no such decoupling and linearization procedures are necessary. Nevertheless, it can be shown that the controlled errors, i.e., s_d and s_q, vanish after finite time. As to the switching functions given by Equation 10.2.31, the existence condition of sliding mode (Equation 2.4.1) may be applied to find the controls. Select the control voltages as

$$\begin{aligned} u_d &= u_{d0}\,\mathrm{sign}(s_d), \\ u_q &= u_{q0}\,\mathrm{sign}(s_q), \end{aligned} \tag{10.2.32}$$

where u_{d0}, u_{q0} are the amplitudes of u_d, u_q, respectively. It follows from

$$\begin{aligned} s_d\dot{s}_d &= s_d\left(\frac{di_d^*}{dt} + \frac{R}{L}i_d - \omega_e i_q\right) - \frac{1}{L}u_{d0}\left|s_d\right|, \\ s_q\dot{s}_q &= s_q\left(\frac{di_q^*}{dt} + \frac{R}{L}i_q + \omega_e i_d + \frac{1}{L}\lambda_0\omega_e\right) - \frac{1}{L}u_{q0}\left|s_q\right| \end{aligned} \tag{10.2.33}$$

that the derivation from each of the switching surfaces and its time derivative have opposite signs if

$$\begin{aligned} u_{d0} &> \left|L\frac{di_d^*}{dt} + Ri_d - L\omega_e i_q\right|, \\ u_{q0} &> \left|L\frac{di_q^*}{dt} + Ri_q + L\omega_e i_d + \lambda_0\omega_e\right|. \end{aligned} \tag{10.2.34}$$

Obviously, unlike in the case of DC motors, in addition to the back EMF, the control voltages should suppress the coupling terms that are proportional to the angular speed of the motor rotor.

Remark 10.1

1. In the case of discontinuous reference currents i_d^* and i_q^* with associated "large" time derivatives, the real currents will not be able to follow their reference values. This can happen, for example, if the outer-loop controllers use high feedback gains. Because of the inductive nature of electric drives, discontinuous reference currents cannot be followed with any controller. However, a sliding mode controller is able to immediately use the full available control resources u_{d0} and u_{q0} such that the fastest possible response is guaranteed.
2. It is also possible to perform the decoupling and linearization procedure first and then apply the sliding mode technique to the resulting linear system. In this case, the resulting control voltages u_d and u_q will no longer be in the form of sign function but will contain an additive continuous part attributable to the decoupling procedure. Because the decoupling procedure involves the motor parameters, the resulting control is sensitive to these parameters.

Once the control voltages u_d and u_q are obtained, the next step is to map them into the switching patterns of the inverter. Lookup table techniques are often used for this purpose with the electrical angular position θ_e as the input of the table [Sabanovich and Utkin 1994]. This solution is simple but cannot implement arbitrary voltage vectors $[u_d\ u_q]^T$ because of the finite resolution of a lookup table. In the following, we propose a novel PWM technique using the sliding mode principle, which may be called "sliding mode PWM."

The basic problem is that the controls u_1, u_2, and u_3, required by the inverter, take only discrete values $-u_0$ or u_0. As a result, a direct implementation of the transformation $\left(A_{d,q}^{1,2,3}\right)^+$ is not possible. Instead, a second set of switching functions is defined for u_1, u_2, and u_3.

Define a set of desired controls according to transformation $\left(A_{d,q}^{1,2,3}\right)^+$ in Equation 10.2.25 as

$$\begin{bmatrix} u_1^* \\ u_2^* \\ u_3^* \end{bmatrix} = \left(A_{d,q}^{1,2,3}\right)^+ \begin{bmatrix} u_{d0}\,\mathrm{sign}(s_d) \\ u_{q0}\,\mathrm{sign}(s_q) \end{bmatrix}. \tag{10.2.35}$$

These controls cannot yet be applied to the inverter directly because matrix $\left(A_{d,q}^{1,2,3}\right)^+$ is a function of the electrical angular position θ_e, so that they do not take the values from the discrete set $\{-u_0, +u_0\}$. The second set of switching functions for controls u_1, u_2, and u_3 is chosen as

$$s_i^* = \int_0^t \left(u_i^*(\zeta) - u_i(\zeta)\right) d\zeta, \quad i = 1,\ 2,\ 3. \tag{10.2.36}$$

Note that the time derivatives $\dot{s}_i^*$ are linear in the inputs u_i (i = 1, 2, 3). Consequently, control laws

$$u_i = u_0 \,\text{sign}(s_i^*), i = 1,\ 2,\ 3 \tag{10.2.37}$$

enforce sliding mode in manifold $s_i^* = 0,\ (i = 1,\ 2,\ 3)$ if

$$u_0 > \max\left(\left|u_1^*\right|,\ \left|u_2^*\right|,\ \left|u_3^*\right|\right). \tag{10.2.38}$$

The sliding condition (Equation 10.2.38) is derived from the existence condition $s_i^* \dot{s}_i^* < 0$. Using the equivalent control method (see Section 2.3) by setting $\dot{s}_i^* = 0$ and solving for inputs u_i (for each i = 1, 2, 3) yields

$$u_{ieq} = u_i^*, i = 1,\ 2,\ 3, \tag{10.2.39}$$

which implies that the coordinate transformation (Equation 10.2.35) was implemented exactly by the proposed method.

As the last step of the control design, the resulting discontinuous controls u_1, u_2, and u_3 will be transformed to the switching patterns s_{w1}, s_{w2}, s_{w3}, s_{w4}, s_{w5}, s_{w6} using Equation 10.2.2.

At this point, we have completed the design procedure for the first version of the current control. For the implementation, phase currents i_a, i_b, i_c should be available. The design sequence assumes that an outer control loop provides desired currents i_d^* and i_q^* and can be summarized in the following steps.

Step 1: Transform the measured phase currents i_a, i_b, i_c into the (d, q) coordinate frame to obtain the torque current i_q and the field current i_d using Equation 10.2.18. In practice, only two components of the phase currents are measured; the third one is calculated according to the balance condition, e.g., $i_c = -(i_a + i_b)$.

Step 2: Design switching functions $s_d = i_d^* - i_d$, $s_q = i_q^* - i_q$ and associated control voltages u_d, u_q according to Equations 10.2.32 and 10.2.34. Because the maximum value of $\sqrt{u_{d0}^2 + u_{q0}^2}$ is limited by the DC link voltage, the selection of u_{d0} and u_{q0} is not arbitrary, i.e., u_{d0} and u_{q0} should be selected such that the inequalities in Equation 10.2.34 and $u_0 > \left|u_i^*\right|$ (i = 1, 2, 3) are satisfied.

Step 3: Transform the resulting discontinuous controls u_d and u_q to u_1^*, u_2^*, u_3^* according to Equation 10.2.35.

Step 4: Calculate the integral of Equation 10.2.36 to obtain the new switching functions s_1^*, s_2^*, s_3^*; compute the discontinuous controls u_1, u_2, and u_3 using Equation 10.2.37.

Step 5: Apply Equation 10.2.2 to the resulting controls u_1, u_2, and u_3 to derive the switching patterns of the inverter s_{w1}, s_{w2}, s_{w3}, s_{w4}, s_{w5}, s_{w6}.

Figure 10.17 shows an example of the proposed sliding mode PWM technique that modulates a sinusoidal voltage waveform to the width of a switching signal. Figure 10.18 gives the simulation result of the proposed current controller. The relatively high switching noise is attributable to the integration error of the sliding mode PWM, caused by the finite sampling period. Also, the integration action in closed loop may introduce additional dynamics that enlarge the high-frequency oscillations. The reference currents are selected as $i_d^* = 0$ and $i_q^* = 5.0sqw(15.7t)$, where sqw represents a square-wave function.

10.2.3.2. Second Method for Current Control

The second version of the current control is able to generate the discontinuous controls u_1, u_2, and u_3 directly without involving a PWM technique. Moreover, this design method is theoretically compact and straightforward (although no PWM technique is used, the implementation does not imply that the role of a power converter is reduced to amplifying some continuous control signal). This method may need high enough DC link voltage u_0 for every time instant.

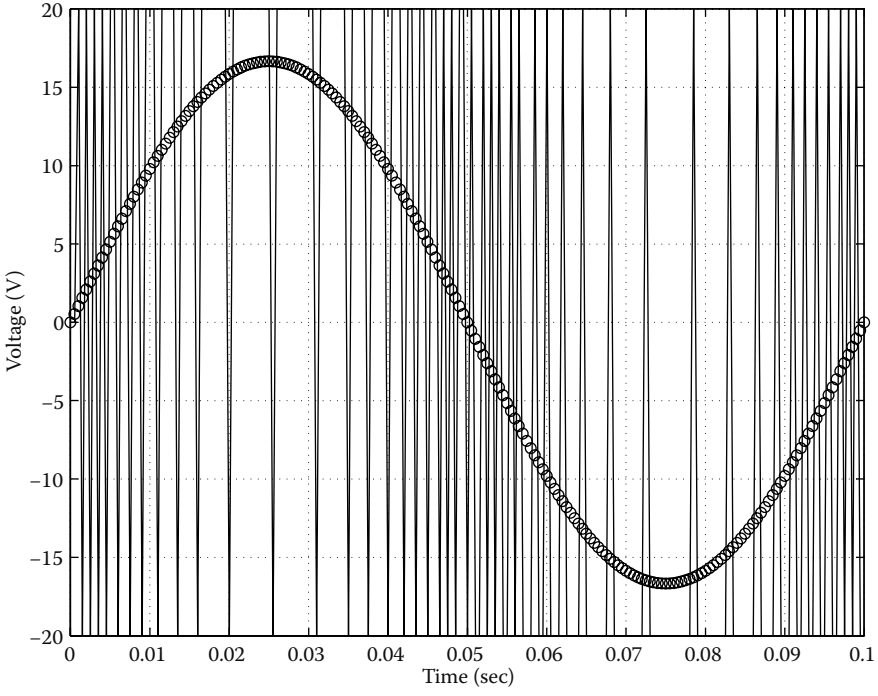

FIGURE 10.17
Example of the sliding mode PWM.

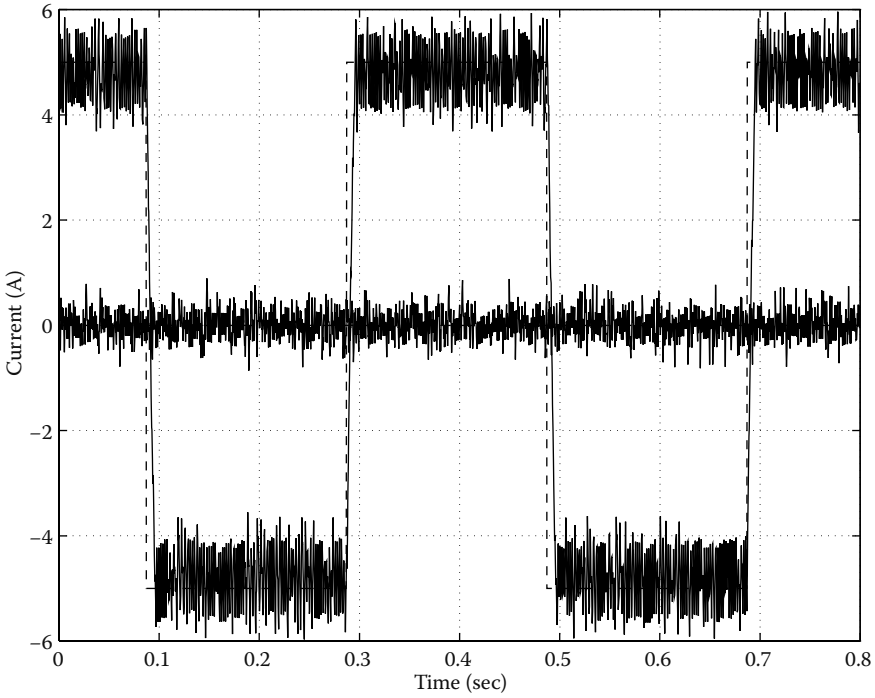

FIGURE 10.18
Responses of the proposed current controller. Dashed lines, reference currents; solid lines, real currents.

The second method also uses the (d, q) coordinate frame for ease of presentation. Given the desired currents i_d^* and i_q^*, provided by an outer control loop, design switching functions

$$\begin{aligned} s_d &= L(i_d^* - i_d), \\ s_q &= L(i_q^* - i_q), \end{aligned} \tag{10.2.40}$$

where L is the inductance of the stator windings. Note that L does not change the sign of s_d and s_q; it is involved here only for simplifying the derivations. The time derivatives of s_d and s_q in matrix-vector form are given by

$$\dot{\boldsymbol{S}}_{dq} = \boldsymbol{F}_{dq} - \boldsymbol{U}_{dq}, \tag{10.2.41}$$

where $\boldsymbol{S}_{dq} = [s_d\ s_q]^T$, $\mathbf{U}_{dq} = [u_d\ u_q]^T$, and

$$\boldsymbol{F}_{dq} = \begin{bmatrix} F_d \\ F_q \end{bmatrix} = \begin{bmatrix} L\dfrac{di_d^*}{dt} \\ L\dfrac{di_d^*}{dt} + \lambda\omega_e \end{bmatrix} + \begin{bmatrix} R & -L\omega_e \\ L\omega_e & R \end{bmatrix} \begin{bmatrix} i_d \\ i_q \end{bmatrix}. \tag{10.2.42}$$

Substitution of Equation 10.2.22 into Equation 10.2.41 yields

$$\dot{\boldsymbol{S}}_{dq} = \boldsymbol{F}_{dq} - \mathrm{A}_{d,q}^{1,2,3}\boldsymbol{U}_{gate}, \tag{10.2.43}$$

where $\boldsymbol{U}_{\text{gate}} = [u_1\ u_2\ u_3]^T$. The above equation establishes the direct relation between the controlled errors s_d, s_q and the discontinuous controls u_1, u_2, and u_3. Design controls u_1, u_2, and u_3 as follows

$$\boldsymbol{U}_{\text{gate}} = u_0\ \text{sign}(\boldsymbol{S}^*), \tag{10.2.44}$$

where $\boldsymbol{S}^* = \begin{bmatrix} s_1^* & s_2^* & s_3^* \end{bmatrix}^T$, is a vector of transformed switching functions to be determined later, and

$$\text{sign}(S^*) = \begin{bmatrix} \text{sign}(s_1^*) & \text{sign}(s_2^*) & \text{sign}(s_3^*) \end{bmatrix}^T. \tag{10.2.45}$$

Controls u_1, u_2, and u_3 take values from the discrete set $\{-u_0, +u_0\}$. The transformed vector $\boldsymbol{S}^*$ should be designed such that, under controls (Equation 10.2.44), s_d and s_q vanish in finite time. A proper candidate for $\boldsymbol{S}^*$ is

$$\boldsymbol{S}^* = \left(A_{d,q}^{1,2,3}\right)^+ \boldsymbol{S}_{dq} = \frac{3}{2}\left(A_{d,q}^{1,2,3}\right)^T \boldsymbol{S}_{dq}, \tag{10.2.46}$$

where matrix $\left(A_{d,q}^{1,2,3}\right)^+$ can be found as

$$\left(A_{d,q}^{1,2,3}\right)^+ = \begin{bmatrix} \cos\theta_a & -\sin\theta_a \\ \cos\theta_b & -\sin\theta_b \\ \cos\theta_c & -\sin\theta_c \end{bmatrix}, \tag{10.2.47}$$

with $\theta_a = \theta_e$, $\theta_b = \theta_e - 2\pi/3$, and $\theta_c = \theta_e + 2\pi/3$. Matrix $A_{d,q}^{1,2,3}\left(A_{d,q}^{1,2,3}\right)^+$ is a 2×2 identity matrix.

Theorem 10.1

For high enough link voltage u_0, system Equation 10.2.43 under control Equation 10.2.44 via transformation Equation 10.2.46 converges to its origin $s_d = 0$, $s_q = 0$ in finite time. □

Proof 10.1

Design a Lyapunov function candidate

$$V = \frac{1}{2} \boldsymbol{S}_{dq}^T \boldsymbol{S}_{dq} \tag{10.2.48}$$

and take the time derivative of V along the solutions of Equation 10.2.43 to yield

$$\dot{V} = (\boldsymbol{S}^*)^T \boldsymbol{F}^* - (\boldsymbol{S}^*)^T \left(A_{d,q}^{1,2,3} \right)^T A_{d,q}^{1,2,3} \boldsymbol{U}_{gate}, \tag{10.2.49}$$

where $\boldsymbol{F}^* = \begin{bmatrix} \boldsymbol{F}_1^* & \boldsymbol{F}_2^* & \boldsymbol{F}_3^* \end{bmatrix}^T = \left(A_{d,q}^{1,2,3} \right)^T \boldsymbol{F}_{dq}$. Substitution of controls in Equation 10.2.44 into Equation 10.2.49 results in

$$\dot{V} = (\boldsymbol{S}^*)^T \boldsymbol{F}^* - u_0 (\boldsymbol{S}^*)^T \left(A_{d,q}^{1,2,3} \right)^T A_{d,q}^{1,2,3} \operatorname{sign}(\boldsymbol{S}^*), \tag{10.2.50}$$

where matrix $\left(A_{d,q}^{1,2,3} \right)^T A_{d,q}^{1,2,3}$ is a singular matrix and can be calculated as

$$\left(A_{d,q}^{1,2,3} \right)^T A_{d,q}^{1,2,3} = \frac{4}{9} \begin{bmatrix} 1 & -\frac{1}{2} & -\frac{1}{2} \\ -\frac{1}{2} & 1 & -\frac{1}{2} \\ -\frac{1}{2} & -\frac{1}{2} & 1 \end{bmatrix}. \tag{10.2.51}$$

Depending on the signs of s_1^*, s_2^*, and s_3^*, there are eight possible combinations of values of $\operatorname{sign}(s_1^*)$, $\operatorname{sign}(s_2^*)$, and $\operatorname{sign}(s_3^*)$. Evaluation of Equation 10.2.46 shows that $\operatorname{sign}(s_1^*)$, $\operatorname{sign}(s_2^*)$, and $\operatorname{sign}(s_3^*)$ can never be all +1 or all –1 simultaneously. The remaining six combinations can be summarized as

$$\operatorname{sign}(s_l^*) \neq \operatorname{sign}(s_m^*) = \operatorname{sign}(s_n^*), \text{ with } l \neq m \neq n \text{ and } l, m, n \in \{1,\ 2,\ 3\}. \tag{10.2.52}$$

Starting from this notion, Equation 10.2.50 can be expanded based on Equation 10.2.51 to yield

$$\dot{V} = \left(s_1^* F_1^* + s_2^* F_2^* + s_3^* F_3^* \right) - (2/3)^2 u_0 \left(2\left| s_l^* \right| + \left| s_m^* \right| + \left| s_n^* \right| \right), \tag{10.2.53}$$

with $l \neq m \neq n$ and $l, m, n \in \{1, 2, 3\}$.

Apparently, as long as $\|\boldsymbol{S}^*\| \neq 0$ and the DC link voltage u_0 is selected as

$$u_0 > (3/2)^2 \max\left(\left| F_1^* \right|,\ \left| F_2^* \right|,\ \left| F_3^* \right| \right), \tag{10.2.54}$$

$\dot{V} < 0$ will be guaranteed for all possible l, m, n. This proof implies that $s_d = 0$, $s_q = 0$ can be reached in finite time by switching directly the discontinuous controls u_1, u_2, and u_3 in sign according to Equation 10.2.44. □

Similar to the first version of the current control, the next step is to map the resulting controls u_1, u_2, and u_3 into the switching patterns applied to the inverter. For this purpose, Equation 10.2.2 can be used.

For the implementation, matrix $\left(A_{d,q}^{1,2,3}\right)^{+}$ is needed to carry out the transformation (Equation 10.2.46), and the exact values of $\boldsymbol{F}_{dq}$ are not required. It is interesting to point out the physical meaning of the transformed switching functions s_1^*, s_2^*, and s_3^*. From Equations 10.2.46 and 10.2.21, we have

$$\begin{bmatrix} s_1^* & s_2^* & s_3^* \end{bmatrix}^T = L\begin{bmatrix} i_a^* - i_a & i_b^* - i_b & i_c^* - i_c \end{bmatrix}^T, \tag{10.2.55}$$

where i_a^*, i_b^*, and i_c^* are the reference currents in the (a, b, c) coordinate frame transformed from the reference currents i_d^*, i_q^*, usually determined by an outer-loop speed controller. From Equations 10.2.55 and 10.2.44, controls u_1, u_2, and u_3 can be found as

$$\begin{aligned} u_1 &= u_0 \operatorname{sign}(i_a^* - i_a), \\ u_2 &= u_0 \operatorname{sign}(i_b^* - i_b), \\ u_3 &= u_0 \operatorname{sign}(i_c^* - i_c). \end{aligned} \tag{10.2.56}$$

The reader familiar with conventional current control of AC motors will immediately recognize that Equation 10.2.56 is similar to the conventional techniques, in which, for reducing heat loss and electric-magnetic disturbances caused by the switching actions, a hysteresis circuit is usually added after each sign function, or, alternatively, the switching actions are synchronized with a fixed clock source. The former is called hysteresis control and the latter chopper control.

The sliding mode method presented here gives a condition, inequality Equation 10.2.54, for the current controller to be effective. Furthermore, it provides a way of transforming the reference currents i_d^*, i_q^* to the (a, b, c) coordinate frame to track the reference currents i_a^*, i_b^*, i_c^* (see Equation 10.2.46). In the (d, q) coordinate frame, reference current i_d^* is set to zero if no field weakening operation (see Section 10.2.4) is required. For field weakening operations of a PMSM, reference current i_d^* should be varied depending on the current motor speed. Reference current i_q^*, provided by an outer-loop controller, corresponds to the required motor torque.

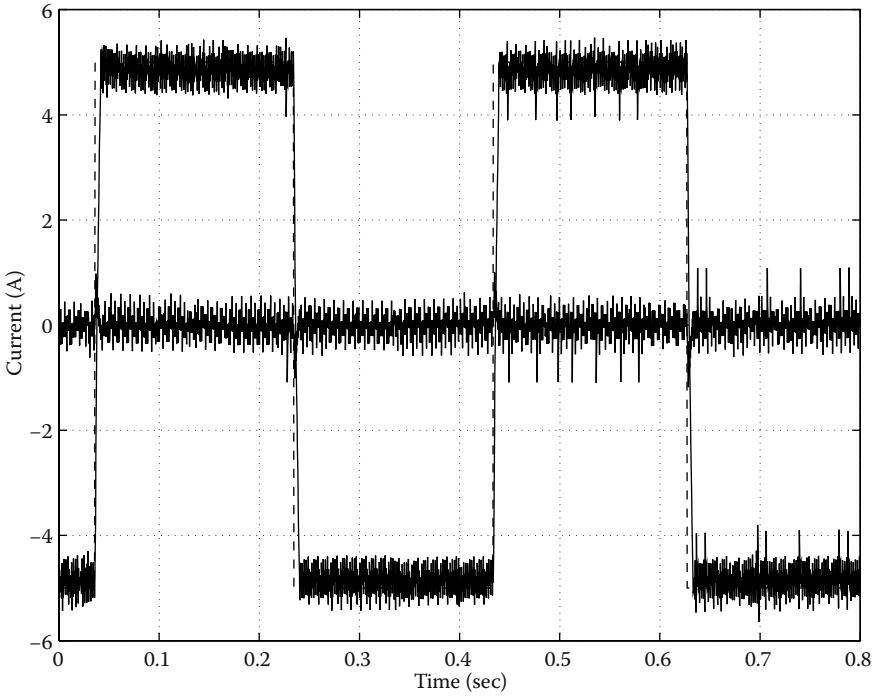

FIGURE 10.19
Responses of the second version current controller. Dashed lines, reference currents; solid lines, real currents.

Figure 10.19 shows the simulation results of the second version of the current control. The reference currents are the same as in the case of the first version of the current control.

10.2.4. Speed Control

Similar to DC motors, speed control of permanent-magnet synchronous motors can be realized in a cascaded control structure, with a current controller in an inner loop and a speed controller in an outer loop, providing the reference currents i_d^* and i_q^* for the inner loop. As discussed in the preceding section, reference current i_d^* is normally set to zero such that the motor is able to provide a constant torque. However, in some applications, high torque or high-speed performance is desired. For high-speed operation, the reference current i_d^* may be varied from zero to some negative value depending on the current motor speed. This technique is called field-weakening technique and is able to extend the operation range of the motor speed several times larger than in the case of zero i_d^*. See the work of Shi and Lu [1996] for details of the field-weakening operation of PMSMs.

For the outer speed control loop, most control techniques may be applied, with the exception of high gain and sliding mode techniques, because the reference input of the inner control loop should have a bounded time derivative. This may explain why some researchers argue that sliding mode control techniques do not work properly for some mechanical systems such as robotics manipulators. In general, a high gain or a sliding mode controller may only be used once in a cascaded control structure, namely, in the most internal control loop.

A suitable solution for designing the speed controller is to apply sliding mode control directly to the motor model to achieve the discontinuous controls u_1, u_2, and u_3 without explicitly involving a current control loop. This control scheme may be called "direct speed control." The advantages of such a control scheme have already been stated in the section on speed control of DC motors. Because we deal with sliding mode control applications, we are interested in the details of the direct speed control for permanent-magnet synchronous motors.

Let ω_r^* be the desired mechanical angular speed of the motor rotor. Design two switching functions for the speed control as

$$\begin{aligned} s_d &= \frac{K_t}{J}\left(i_d^* - i_d\right), \\ s_\omega &= c[\omega_r^* - \omega_r] + \frac{d}{dt}[\omega_r^* - \omega_r], \end{aligned} \tag{10.2.57}$$

where c is a positive constant determining the motion performance in sliding mode, positive coefficient K_t/J is introduced to simplify the derivations, reference current i_d^* is normally set to zero, and, for field-weakening operation, i_d^* is a function of the motor speed and motor parameters [Shi and Lu 1996]. From the above equations, if $s_\omega \equiv 0$ can be achieved after a finite time interval, then ω_r will converge to ω_r^* exponentially.

The motion projection of the system onto the subspaces s_ω, s_d is

$$\dot{\boldsymbol{S}}_{d\omega} = \boldsymbol{F}_{d\omega} - D_\omega \boldsymbol{U}_{gate}, \tag{10.2.58}$$

where $\boldsymbol{U}_{gate}$ is the same as for the current control; $\boldsymbol{S}_{d\omega} = [s_d\ s_\omega]^T$, and

$$\begin{aligned} \boldsymbol{F}_{d\omega} &= \begin{bmatrix} F_d \\ F_\omega \end{bmatrix} = \begin{bmatrix} \dfrac{K_t}{J}\dfrac{di_d^*}{dt} \\ c(\dot{\omega}_r^* - \dot{\omega}_r) + \ddot{\omega}_r^* + \dfrac{\dot{\tau}_l}{J} + \dfrac{K_t}{JL}\lambda N_r \omega_r \end{bmatrix} + \frac{K_t}{J}\begin{bmatrix} \dfrac{R}{L} & -N_r\omega_r \\ N_r\omega_r & \dfrac{R}{L} \end{bmatrix}\begin{bmatrix} i_d \\ i_q \end{bmatrix}, \\ D_\omega &= \frac{K_t}{JL} A_{d,q}^{1,2,3}, \end{aligned} \tag{10.2.59}$$

where matrix $A_{d,q}^{1,2,3}$ is defined by Equation 10.2.23.

From this stage on, we may follow the same procedure as in the second version of the current control. At first, the switching function transformation should be performed by

$$\boldsymbol{S}^* = D_\omega^+ \boldsymbol{S}_{d\omega}, \tag{10.2.60}$$

where $\boldsymbol{S}^* = \begin{bmatrix} s_1^* & s_2^* & s_3^* \end{bmatrix}^T$ is again the vector representing the transformed switching functions, and D_ω^+ is the pseudo-inverse of matrix D_ω and given as

$$D_\omega^+ = D_\omega^T (D_\omega D_\omega^T)^{-1} = \frac{3}{2}\frac{JL}{K_t}\left(A_{d,q}^{1,2,3}\right)^T. \tag{10.2.61}$$

Matrix D_ω^+ can be expanded to

$$D_\omega^+ = \frac{3}{2}\frac{JL}{K_t}\left(A_{d,q}^{1,2,3}\right)^T = \frac{JL}{K_t}\begin{bmatrix} \cos\theta_a & -\sin\theta_a \\ \cos\theta_b & -\sin\theta_b \\ \cos\theta_c & -\sin\theta_c \end{bmatrix}, \tag{10.2.62}$$

where $\theta_a = \theta_e$, $\theta_b = \theta_e - 2\pi/3$ and $\theta_c = \theta_e + 2\pi/3$. Matrix $D_\omega D_\omega^+$ is a 2×2 identity matrix.

The controls u_1, u_2, and u_3 have the same form as the second version of the current control,

$$\boldsymbol{U}_{\text{gate}} = u_0 \,\text{sign}(\boldsymbol{S}^*), \tag{10.2.63}$$

with $\text{sign}(\boldsymbol{S}^*) = \begin{bmatrix} \text{sign}(s_1^*) & \text{sign}(s_2^*) & \text{sign}(s_3^*) \end{bmatrix}^T$.

Theorem 10.2

For high enough link voltage u_0, system Equation 10.2.58 under control Equation 10.2.63 via transformation Equation 10.2.60 converges to its origin $s_d = 0$, $s_\omega = 0$ in finite time. □

Proof 10.2

Following the same procedure as for the current control, select a Lyapunov function candidate as

$$V = \frac{1}{2}\boldsymbol{S}_{d\omega}^T \boldsymbol{S}_{d\omega}. \tag{10.2.64}$$

Differentiation of V along the system trajectories yields

$$\dot{V} = \left(s_1^* F_1^* + s_2^* F_2^* + s_3^* F_3^*\right) - \left(\frac{2}{3}\frac{K_t}{JL}\right)^2 u_0 \left(2\left|s_l^*\right| + \left|s_m^*\right| + \left|s_n^*\right|\right), \tag{10.2.65}$$

with $l \neq m \neq n$ and $l, m, n \in \{1, 2, 3\}$.

F_1^*, F_2^*, and F_3^* are defined by $D_\omega^T \boldsymbol{F}_{d\omega} = \begin{bmatrix} F_1^* & F_2^* & F_3^* \end{bmatrix}^T$. Assume that di_d^*/dt, $\dot{\tau}_l$, and $\ddot{\omega}_r^*$ are bounded, then $\left\| D_\omega^T \boldsymbol{F}_{d\omega} \right\|$ is bounded as well (see Equation 10.2.59).

Obviously, as long as $\|S^*\| \neq 0$ and the DC link voltage u_0 satisfies

$$u_0 > \left(\frac{3}{2}\frac{JL}{K_t}\right)^2 \max\left(\left|F_1^*\right|, \left|F_2^*\right|, \left|F_3^*\right|\right) \tag{10.2.66}$$

the condition $\dot{V} < 0$ holds for all possible l, m, n. It means that the surfaces $s_d = 0$, $s_\omega = 0$ are reached in finite time in the system with the discontinuous controls u_1, u_2, and u_3 given in Equation 10.2.63. □

By high enough u_0, the proposed speed controller is robust with respect to the terms included in $D_\omega^T \boldsymbol{F}_{d\omega}$. For example, under condition Equation 10.2.66, the speed controller is robust with respect to the load torque variation, because $\dot{\tau}_l$ is contained in $D_\omega^T \boldsymbol{F}_{d\omega}$. Again, the knowledge on exact values of $\boldsymbol{F}_{d\omega}$ is not needed for the implementation. Only matrix D_ω^+ is relevant, because we need this matrix for calculating the switching function transformation.

To construct the sliding surface $s_w = 0$, the acceleration signal of the motor rotor is needed. Normally, this variable cannot be obtained directly but rather has to be obtained by a state observer based on the measured rotor speed and stator currents. Similar techniques as in Section 10.1.6 for the control of DC motors can be applied to retrieve the acceleration signal.

Figures 10.20 and 10.21 show the simulation results of the proposed sliding mode speed controller. The transition time of the speed control is about 0.1 sec. Figure 10.21 gives the smoothed wave forms of the motor currents. Bear in mind that the current i_q is not controlled explicitly; the ordinary behavior of the current components is the result of the acceleration control. The control gain c in Equation 10.2.57 is selected as $c = 50$.

10.2.5. Current Observer

From the viewpoint of practical applications, it is of interest to design a control system with no current transducers. In practice, there are two difficulties to obtain the stator currents i_d and i_q in the field-oriented coordinate frame.

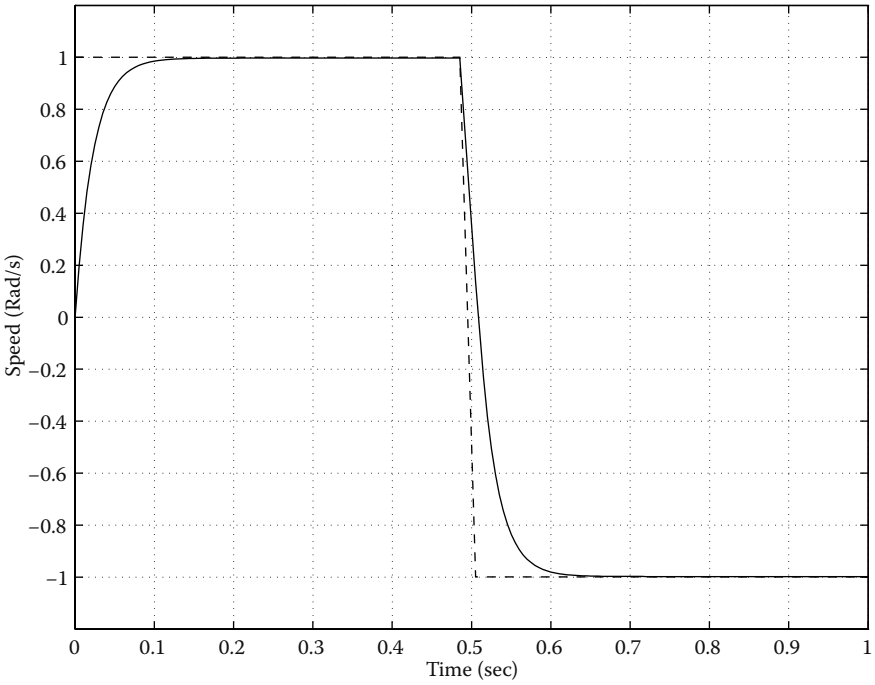

FIGURE 10.20
Response of the sliding mode speed control. Dashed line, reference speed; solid line, real speed.

The first one is attributable to the noise in the measured phase currents i_a and i_b, and the second one is attributable to the coordinate transformation. The noise problem is evident, whereas the second difficulty lies in the speed limitation of the calculation unit used for the transformation. Usually, i_a and i_b are high-frequency signals compared with the current components i_d and i_q, especially for PMSMs with a large number of pole pairs. These high-frequency signals must be sampled with a high enough sampling rate; otherwise, information will be lost. Furthermore, to transform the measured phase currents into the field-oriented coordinate frame, the rotor position signal with high enough resolution must be available. This is normally achieved by involving a high-resolution incremental encoder.

As a result, it is meaningful to design a current observer using the rotor speed measurement. Examination of the motor model leads to the conclusion that online simulation of the motor model suffices to achieve a stable observation of the stator currents. Let $\hat{i}_d$ and $\hat{i}_q$ be the estimates of the stator currents; the observer equations are just a copy of the motor model (Equation 10.2.14),

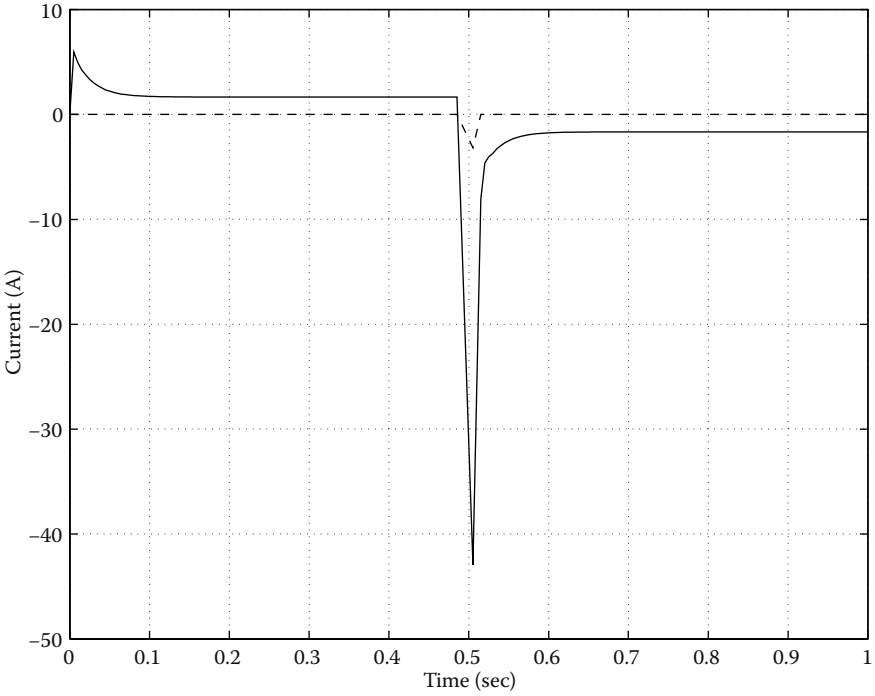

FIGURE 10.21
Currents response of the speed control. Dashed line, current i_d; solid line, current i_q.

$$\begin{aligned}\frac{d\hat{i}_d}{dt} &= -\frac{R}{L}\hat{i}_d + \omega_e\hat{i}_q + \frac{1}{L}u_d,\\ \frac{d\hat{i}_q}{dt} &= -\frac{R}{L}\hat{i}_q - \omega_e\hat{i}_d - \frac{1}{L}\lambda_0\omega_e + \frac{1}{L}u_q.\end{aligned} \tag{10.2.67}$$

It is proven below that this current observer is stable, and the observer errors will tend to zero asymptotically. The mismatch dynamics can be obtained as

$$\begin{aligned}\frac{d\bar{i}_d}{dt} &= -\frac{R}{L}\bar{i}_d + \omega_e\bar{i}_q,\\ \frac{d\bar{i}_q}{dt} &= -\frac{R}{L}\bar{i}_q - \omega_e\bar{i}_d,\end{aligned} \tag{10.2.68}$$

where $\bar{i}_d = \hat{i}_d - i_d$, $\bar{i}_q = \hat{i}_q - i_q$. Under the assumption that the electrical rotor speed $\omega_e = N_r\omega_r$ varies much slower than currents observation errors $\bar{i}_d$ and $\bar{i}_q$, Equation 10.2.68 can be treated as a linear system with characteristic polynomial

$$p^2 + 2\frac{R}{L}p + \frac{R^2}{L^2} + \omega_e{}^2 = 0, \tag{10.2.69}$$

which is stable for any physically plausible R, $L > 0$. Thus, $\hat{i}_d$ and $\hat{i}_q$ will tend to i_d and i_q asymptotically.

Figure 10.22 shows the responses of the proposed current observer while a current controller is working. The real currents i_d and i_q should follow their given references: $i_d^* = 0$ and $i_q^* = 5.0A$, respectively. The initial conditions of the observed currents are selected as $\hat{i}_d(0) = 20A$ and $\hat{i}_q(0) = -20A$ to see the convergence process. Because the current observer is just the online simulation of the motor model, no observer gain is to be adjusted.

10.2.6. Observer for Speed Sensorless Control

In the section concerning the DC-motor control, we have discussed the issue of sensorless control. Sensorless control of AC machines is more difficult than the control of DC motors because of the coupling effects in the motor dynamics.

The terminology sensorless control indicates that some internal states of a dynamic system are available, measured or estimated, but the output

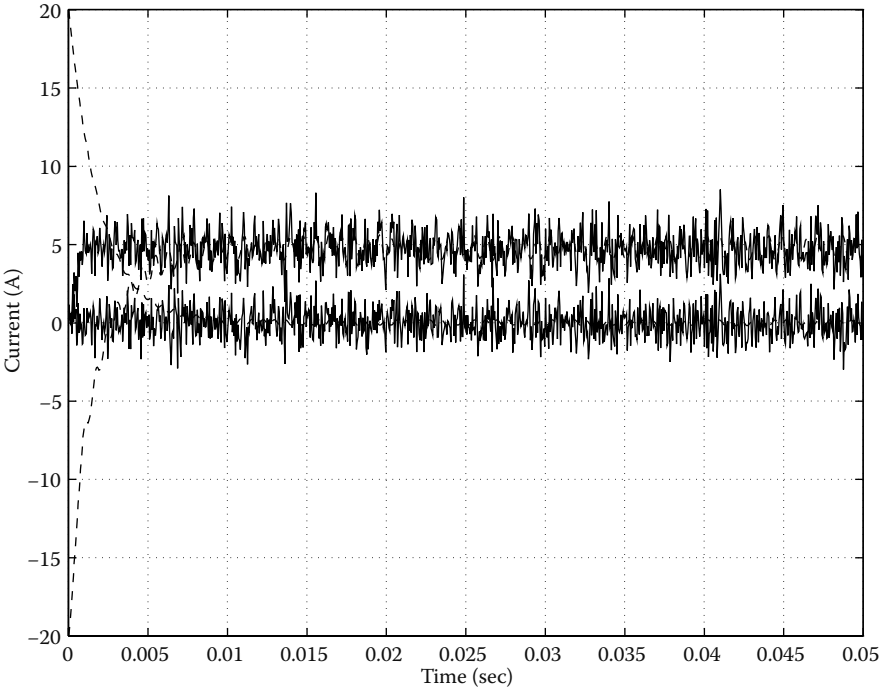

FIGURE 10.22
Responses of the current observer. Solid lines, real currents; dashed lines, observed currents.

measurements are unknown; however, these unmeasured output variables serve as principal control variables. In the case of PMSMs, the phase voltages (or the line voltages) and the phase currents are normally measured, whereas the motor speed ω_r as well as the motor position θ_r are unknown, despite being the principal control variables of a PMSM drive system.

To estimate these variables, the motor model in the field-oriented coordinate frame (i.e., the (d, q) coordinate frame) is usually not used, because the state variables in this coordinate frame are transformed from the fixed coordinate frames (i.e., from (a, b, c) coordinate frame through (α, β) coordinate frame) using transformation matrix $A_{dq}^{a,b,c}$ defined by Equation 10.2.19 for which the electrical angular position of the motor rotor θ_e is essential. As a result, the model in (α, β) coordinate frame is usually used. Rewriting the motor model in this coordinate system yields

$$\begin{aligned} \frac{di_\alpha}{dt} &= -\frac{R}{L} i_\alpha - \frac{1}{L} e_\alpha + \frac{1}{L} u_\alpha, \\ \frac{di_\beta}{dt} &= -\frac{R}{L} i_\beta - \frac{1}{L} e_\beta + \frac{1}{L} u_\beta, \end{aligned} \tag{10.2.70}$$

where $e_\alpha = -\lambda_0 \omega_e \sin\theta_e$ and $e_\beta = \lambda_0 \omega_e \cos\theta_e$ are the induced EMF components. Assuming the motor speed changes slowly, implying that $\dot{\omega}_e \approx 0$, the model of these induced EMF components, is

$$\begin{aligned} \dot{e}_\alpha &= -\omega_e e_\beta, \\ \dot{e}_\beta &= \omega_e e_\alpha. \end{aligned} \tag{10.2.71}$$

Conventional approaches to sensorless control of PMSMs usually follow a two-step procedure. First, the induced EMF components are observed. The electrical angular speed and position are then derived in a second step. Furthermore, in conventional sensorless control designs, the mechanical motion equation is normally involved in the observation algorithms. This model contains inaccurate mechanical parameters as well as the unknown load torque that are recognized to be major obstacles. Here, we propose a sliding-mode-based observer design technique using only the electrical motion equations.

10.2.6.1. Current Observer for EMF Components

Design a set of observer equations for the model in Equation 10.2.70 as

$$\begin{aligned} \frac{d\hat{i}_\alpha}{dt} &= -\frac{R}{L} \hat{i}_\alpha + \frac{1}{L} u_\alpha - \frac{l_1}{L} \text{sign}(\hat{i}_\alpha - i_\alpha), \\ \frac{d\hat{i}_\beta}{dt} &= -\frac{R}{L} \hat{i}_\beta + \frac{1}{L} u_\beta - \frac{l_1}{L} \text{sign}(\hat{i}_\beta - i_\beta), \end{aligned} \tag{10.2.72}$$

where $l_1 > 0$ is a constant observer gain. Assume that the parameters R and L are known exactly and thus are identical with those in the model. Subtracting the above equations from the model equations (Equation 10.2.70) yields the mismatch dynamics

$$\begin{aligned}\frac{d\bar{i}_\alpha}{dt} &= -\frac{R}{L}\bar{i}_\alpha + \frac{1}{L}e_\alpha - \frac{l_1}{L}\text{sign}(\bar{i}_\alpha),\\ \frac{d\bar{i}_\beta}{dt} &= -\frac{R}{L}\bar{i}_\beta + \frac{1}{L}e_\beta - \frac{l_1}{L}\text{sign}(\bar{i}_\beta),\end{aligned} \tag{10.2.73}$$

where $\bar{i}_\alpha = \hat{i}_\alpha - i_\alpha$ and $\bar{i}_\beta = \hat{i}_\beta - i_\beta$ denote the observation errors. The mismatch dynamics are disturbed by the unknown induced EMF components. However, because the EMF components are bounded, they can be suppressed by discontinuous inputs with $l_1 > \max(|e_\alpha|, |e_\beta|)$. Then, sliding mode with $\bar{i}_\alpha = 0$, $\bar{i}_\beta = 0$ will occur after a finite time interval. To examine the system behavior during sliding mode, the equivalent control method (see Section 2.3) is exploited. We formally set $\frac{d\bar{i}_\alpha}{dt} = 0$ and $\frac{d\bar{i}_\beta}{dt} = 0$ in Equation 10.2.73, resulting in

$$\begin{aligned}\left(l_1 \text{sign}(\bar{i}_\alpha)\right)_{eq} &= e_\alpha,\\ \left(l_1 \text{sign}(\bar{i}_\beta)\right)_{eq} &= e_\beta.\end{aligned} \tag{10.2.74}$$

Again, to extract e_α, e_β from the corresponding equivalent control values in Equation 10.2.74, we use low-pass filters with z_α, z_β as the filter outputs

$$\begin{aligned}z_\alpha(t) &= e_\alpha(t) + \Delta_\mu(t),\\ z_\beta(t) &= e_\beta(t) + \Delta_\mu(t),\end{aligned} \tag{10.2.75}$$

where $\Delta_\mu(t)$ is the error determined by the distortions of both slow and fast components of the discontinuous filter input. Filter time constant μ directly determines the amount of error $\Delta_\mu(t)$. It should be chosen small enough to have filter dynamics faster than those of the system (Equation 10.2.70) and at the same time not too small, to filter out the high-frequency components of the discontinuous switching actions.

10.2.6.2. Observer for EMF Components

For high-performance applications, z_α, z_β cannot be used directly as the estimation of the induced EMF components, because they contain disturbance $\Delta_\mu(t)$. Model Equations 10.2.71 are thus needed to design the observer for better filtering and simultaneously estimating the rotation speed. The following observer is designed to undertake this filtering task

$$\begin{aligned}
\dot{\hat{e}}_\alpha &= -\hat{\omega}_e \hat{e}_\beta - l_2(\hat{e}_\alpha - z_\alpha),\\
\dot{\hat{e}}_\beta &= \hat{\omega}_e \hat{e}_\alpha - l_2(\hat{e}_\beta - z_\beta),\\
\dot{\hat{\omega}}_e &= (\hat{e}_\alpha - z_\alpha)\hat{e}_\beta - (\hat{e}_\beta - z_\beta)\hat{e}_\alpha,
\end{aligned} \tag{10.2.76}$$

where $l_2 > 0$ is a constant observer gain. The observer is expected to have high filtering properties. Therefore, additional analysis will be performed under the assumption $\Delta_\mu(t) = 0$. Bearing in mind that $\omega_e = \text{const.}$, the mismatch equations are

$$\begin{aligned}
\dot{\bar{e}}_\alpha &= -\hat{\omega}_e \hat{e}_\beta + \omega_e e_\beta - l_2(\hat{e}_\alpha - e_\alpha),\\
\dot{\bar{e}}_\beta &= \hat{\omega}_e \hat{e}_\alpha - \omega_e e_\alpha - l_2(\hat{e}_\beta - e_\beta),\\
\dot{\hat{\omega}}_e &= (\hat{e}_\alpha - e_\alpha)\hat{e}_\beta - (\hat{e}_\beta - e_\beta)\hat{e}_\alpha,
\end{aligned} \tag{10.2.77}$$

where $\bar{e}_\alpha = \hat{e}_\alpha - e_\alpha$, $\bar{e}_\beta = \hat{e}_\beta - e_\beta$ and $\bar{\omega}_e = \hat{\omega}_e - \omega_e$ are the observation errors. Substituting $\hat{\omega}_e = \omega_e + \bar{\omega}_e$ into Equation 10.2.77 yields a simplified equation system:

$$\begin{aligned}
\dot{\bar{e}}_\alpha &= -\bar{\omega}_e \hat{e}_\beta - \omega_e \bar{e}_\beta - l_2(\hat{e}_\alpha - e_\alpha),\\
\dot{\bar{e}}_\beta &= \bar{\omega}_e \hat{e}_\alpha + \omega_e \bar{e}_\alpha - l_2(\hat{e}_\beta - e_\beta),\\
\dot{\hat{\omega}}_e &= (\hat{e}_\alpha - e_\alpha)\hat{e}_\beta - (\hat{e}_\beta - e_\beta)\hat{e}_\alpha.
\end{aligned} \tag{10.2.78}$$

To prove the convergence of observer (Equation 10.2.76), we design a Lyapunov function candidate:

$$V = \frac{1}{2}\left(\bar{e}_\alpha^2 + \bar{e}_\beta^2 + \bar{\omega}_e^2\right). \tag{10.2.79}$$

Its time derivative along the solutions of Equation 10.2.77 can be calculated as

$$\dot{V} = -l_2(\bar{e}_\alpha^2 + \bar{e}_\beta^2) \le 0, \tag{10.2.80}$$

implying that $\hat{e}_\alpha$, $\hat{e}_\beta$ tend to e_α, e_β asymptotically. Now, in the first two equations of Equation 10.2.78, all terms except for $\bar{\omega}_e \hat{e}_\alpha$ and $\bar{\omega}_e \hat{e}_\beta$ are equal to zero. Because $\hat{e}_\alpha(t) \neq 0$ and $\hat{e}_\beta(t) \neq 0$, the speed estimation error $\bar{\omega}_e$ should be equal to zero as well. Thus, the convergence of $\hat{\omega}_e$ to ω_e is proven.

For field-oriented control of PMSMs, transformation matrix $A_{d,q}^{\alpha,\beta}$ is needed that is based on the electrical angular position θ_e for PMSMs. Denoting the estimated matrix as $\hat{A}_{d,q}^{\alpha,\beta}$, we have

$$\hat{A}_{d,q}^{\alpha,\beta} = \begin{bmatrix} \cos\hat{\theta}_e & \sin\hat{\theta}_e \\ -\sin\hat{\theta}_e & \cos\hat{\theta}_e \end{bmatrix}, \tag{10.2.81}$$

where $\hat{\theta}_e$ is an estimate of θ_e. Considering relations

$$\begin{aligned} \hat{e}_\alpha &= -\lambda_0 \hat{\omega}_e \sin\hat{\theta}_e, \\ \hat{e}_\beta &= \lambda_0 \hat{\omega}_e \cos\hat{\theta}_e, \end{aligned} \tag{10.2.82}$$

the matrix elements $\sin\hat{\theta}_e$ and $\cos\hat{\theta}_e$ can be obtained as

$$\begin{aligned} \sin\hat{\theta}_e &= -\frac{1}{\lambda_0}\frac{\hat{e}_\alpha}{\hat{\omega}_e}, \\ \cos\hat{\theta}_e &= \frac{1}{\lambda_0}\frac{\hat{e}_\beta}{\hat{\omega}_e}, \end{aligned} \tag{10.2.83}$$

with $\sin\hat{\theta}_e \to \sin\theta_e$ and $\cos\hat{\theta}_e \to \cos\theta_e$ as $t \to \infty$.

The estimate of mechanical rotor speed, denoted as $\hat{\omega}_r$, can be obtained from Equation 10.2.29 as

$$\hat{\omega}_r = \frac{\hat{\omega}_e}{N_r}, \tag{10.2.84}$$

and $\hat{\omega}_r \to \omega_r$ as $t \to \infty$.

Remark 10.2

To develop the EMF model discussed in this section, we assumed that the motor speed varies slowly. Under this assumption, the observation problem can be simplified significantly. For the case of variable speed, it is also possible to design an observer; however, the convergence proof is a considerably more complicated problem. □

Figures 10.23 through 10.25 show the simulation results of the proposed observers for the speed sensorless control, i.e., from Equations 10.2.72 to 10.2.76. As shown in Figure 10.23, the observed speed converges to the true speed rapidly. To show the convergence process, the initial conditions of the observed EMF components are selected differently from those of the real EMF components: $\hat{e}_\alpha(0) = 0.002$ and $\hat{e}_\beta(0) = -0.002$, whereas $e_\alpha(0) = 0$ and $e_\beta(0) = 0$. The observer gains in Equations 10.2.72 and 10.2.76 are selected as $l_1 = 20{,}000$ and $l_2 = 20{,}000$. The low-pass filters used to obtain the equivalent controls in Equation 10.2.74 are of Butterworth type, with a cutoff frequency of 10,000 rad/s.

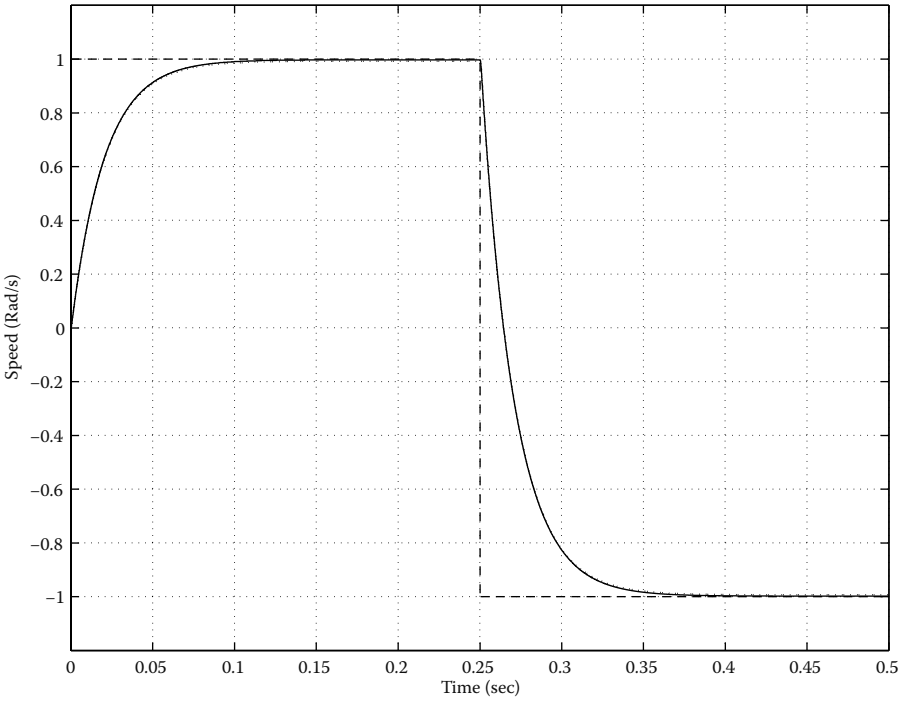

FIGURE 10.23
Speed response of the observer. Dashed line, reference speed; solid line, real speed; dotted line, observed speed.

10.2.7. Discussion

Dynamic models in each coordinate frame have been given as the starting point of this section. Two versions of current controllers have been presented. The first version is a standard method of sliding mode current control except the last part for deriving the control voltages: instead of the standard table lookup approach, the so-called sliding mode PWM technique has been introduced.

The second version of the current control is actually an open-loop approach of field-oriented control, i.e., the current controller is actually implemented in phase coordinates rather than in (d, q) coordinates, only the reference currents are transformed from the field-oriented coordinates. As has been shown, if the link voltage is high enough, it is equivalent to the closed-loop approach (pure field-oriented approach). Moreover, the stability condition is given and the resulting control algorithm is very simple. For speed control, we have not followed the traditional control structure, i.e., the cascade control structure, because it has been discussed in many textbooks. Instead, motor speed and acceleration are controlled simultaneously without an inner current control loop. The advantages are fast response and robustness with respect to the

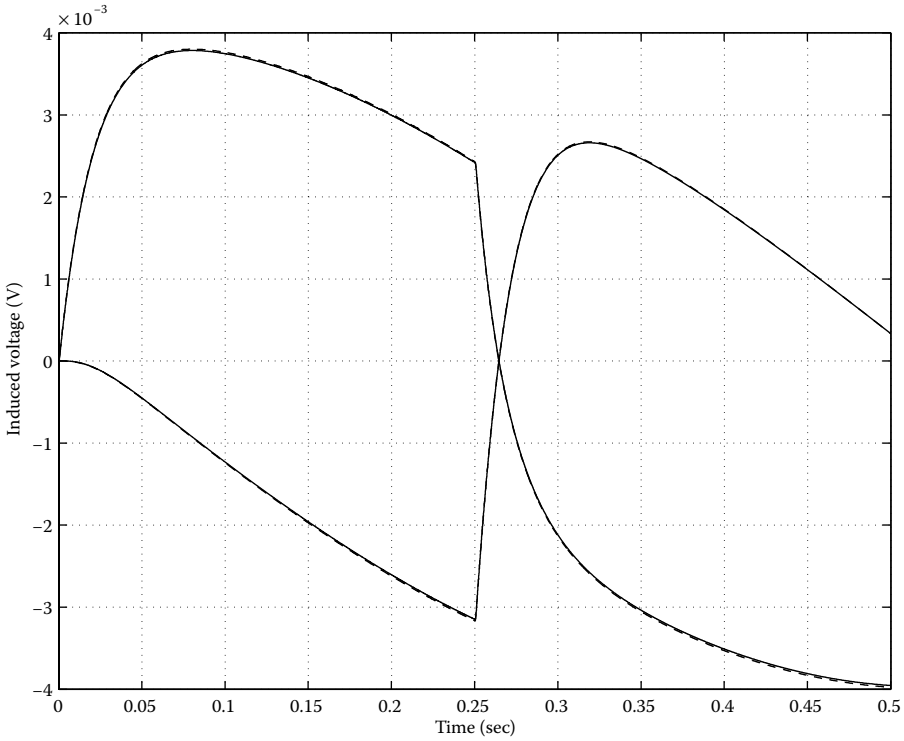

FIGURE 10.24
Responses of the induced voltages. Solid lines, real induced voltages e_α and e_β; dashed lines, observed induced voltages $\hat{e}_\alpha$ and $\hat{e}_\beta$.

mechanical parameters, but the motor acceleration has to be available. The motor acceleration can be estimated based on the motor model and the speed measurements, which involves a larger calculation overhead.

To avoid using (often noisy) current sensors, a current observer may be implemented in field-oriented coordinates. However, the dynamic response of this observer is sensitive to the motor parameters and relies on the voltage vector that is usually not measured. Instead, the reference voltages feeding to the power converter, i.e., the outputs of the current controllers, are normally used, which may be slightly different from the real voltages applied to the motor windings.

As the last part of this section, the sensorless control issue has been treated based on a sliding mode observer combined with a conventional asymptotic observer. Any algorithm for sensorless control problem will rely on model parameters. In the presence of modeling uncertainties, the control performance may not be as good as expected.

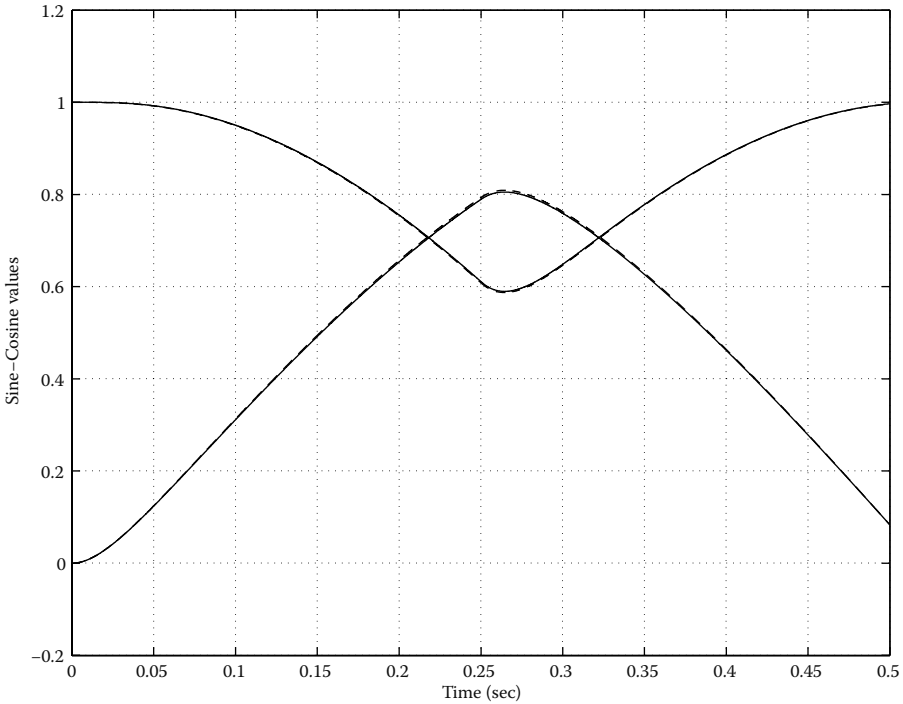

FIGURE 10.25
Responses of the commutation signals. Solid lines, real commutation signals $\sin(\theta_e)$ and $\cos(\theta_e)$; dashed lines, observed commutation signals $\sin(\hat{\theta}_e)$ and $\cos(\hat{\theta}_e)$.

10.3. Induction Motors

10.3.1. Introduction

From a control point of view, induction motors are nonlinear, high-order dynamic systems of considerable complexity. They are quite amenable to a formal mathematical analysis. However, it is not a trivial matter to comprehend the principles of their operation in an imaginative way, especially under transient conditions. Conversely, induction motors are widely used in practical systems because of their simple mechanical construction, low maintenance requirements, and lower cost compared with other types of motors, such as brushless DC motors. Therefore, it is of great significance to investigate the dynamic control problems of these kinds of drive systems.

As discussed in the previous section on permanent-magnet synchronous motors, the field-oriented coordinate frame coincides with the rotor coordinate frame, such that only three frames of reference are considered. For

an induction motor, however, the field (normally the rotor flux)-oriented coordinate frame differs from the rotor coordinate frame; hence, there are four different frames of reference to be considered.

For an induction motor, the angular difference between the rotor flux and the electrical angular position of the rotor is called "slip." Its time derivative is called "slip frequency," which is proportional to the developed motor torque. All state and control variables in the field-oriented coordinate frame are transformed based on the rotor-flux angular position ρ, called "rotor-flux angle" in the sequel, instead of the electrical rotor angle θ_e. To calculate the rotor flux angle, a "flux observer" is used because flux measurements are usually not available. If the electrical angular speed of the rotor, ω_e, is available, as proven later, the flux observer is simply an online simulation of the flux dynamics in the stator coordinate frame (the α, β coordinates); the rate of convergence depends on the rotor time constant. However, it is recognized that this time constant may vary slowly with changing ambient temperature. As a result, some online adaptation mechanisms are often involved, making the control problem of induction motors more complicated than the control of permanent-magnet synchronous motors. Moreover, if the rotor speed is not available, so-called sensorless control techniques have to be used. Currently, sensorless control techniques are not mature enough for application in high-performance industrial systems.

The current research in the control of induction motors is characterized by a great variety of control methodologies with different control/observation/adaptation algorithms combined with different coordinate systems, different state variables, and different notations. For the sliding mode control design described in this section, we mainly use the dynamic model given in the orthogonal stator coordinate frame (the α, β coordinates), with stator current components and rotor flux components as state variables, complemented by the mechanical equation.

10.3.2. Model of the Induction Motor

The structure of an induction motor drive system is shown in Figure 10.26. For sliding mode control design, it is convenient if the control inputs take values from the discrete set $\{-u_0, u_0\}$ instead of on-off signals from the discrete set $\{0, 1\}$. Let the six on-off signals be $s_w = [s_{w1}\ s_{w2}\ s_{w3}\ s_{w4}\ s_{w5}\ s_{w6}]^T$ with $s_{w4} = 1 - s_{w1}$, $s_{w5} = 1 - s_{w2}$, $s_{w6} = 1 - sw_3$, and the control inputs for sliding mode control design be $\boldsymbol{U}_{\text{gate}} = [u_1\ u_2\ u_3]^T$; then the following relation holds:

$$\boldsymbol{U}_{\text{gate}} = u_0 \boldsymbol{L}_w \boldsymbol{s}_w \text{ with } \mathbf{L}_w = \begin{bmatrix} 1 & 0 & 0 & -1 & 0 & 0 \\ 0 & 1 & 0 & 0 & -1 & 0 \\ 0 & 0 & 1 & 0 & 0 & -1 \end{bmatrix}. \tag{10.3.1}$$

The backward transformation can be obtained as

$$s_{w1} = 0.5(1 + u_1/u_0), \quad s_{w4} = 1 - s_{w1},$$
$$s_{w2} = 0.5(1 + u_2/u_0), \quad s_{w5} = 1 - s_{w2}, \tag{10.3.2}$$
$$s_{w3} = 0.5(1 + u_3/u_0), \quad s_{w6} = 1 - s_{w3}.$$

Four frames of reference are normally used for describing the dynamic behavior of the motor (see Figure 10.27): the phase frame in (a, b, c) coordinates, the stator frame in (α, β) coordinates, the rotor frame in (x, y) coordinates, and the field-oriented frame in (d, q) coordinates.

The relationship between the phase voltages u_a, u_b, u_c and the discontinuous controls u_1, u_2, u_3 can be given as follows:

$$[u_a\ u_b\ u_c]^T = G[u_1\ u_2\ u_3]^T, \tag{10.3.3}$$

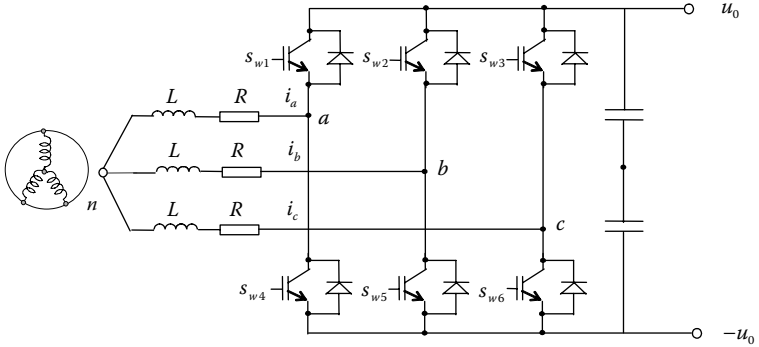

FIGURE 10.26
Structure of an induction motor drive system. n is the neutral point of the stator windings; u_a, u_b and u_c are the potential difference between points a, b, c and the neutral point n, respectively. i_a, i_b and i_c are the phase currents.

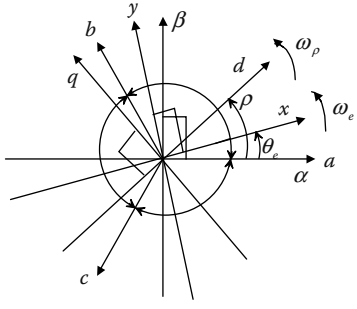

FIGURE 10.27
Coordinate systems of induction motor model. θ_e is the electrical rotor angular position and ω_e is the electrical rotor angular speed; ρ is the angular position of the rotor flux and ω_ρ is the angular speed of the rotor flux.

where matrix G is defined as

$$G = \frac{1}{3}\begin{bmatrix} 2 & -1 & -1 \\ -1 & 2 & -1 \\ -1 & -1 & 2 \end{bmatrix}. \tag{10.3.4}$$

Note that matrix G is a singular matrix implying that the phase voltages u_a, u_b, u_c are not linearly independent. In fact, the sum of u_a, u_b, u_c is equal to zero because of the physical configuration given in the Figure 10.26. The motor model in (α, β) coordinates is important for our control design and can be written as

$$\begin{aligned}
\frac{di_\alpha}{dt} &= \beta\eta\lambda_\alpha + \beta\omega_e\lambda_\beta - \gamma i_\alpha + \frac{1}{\sigma L_s}u_\alpha, \\
\frac{di_\beta}{dt} &= \beta\eta\lambda_\beta - \beta\omega_e\lambda_\alpha - \gamma i_\beta + \frac{1}{\sigma L_s}u_\beta, \\
\frac{d\lambda_\alpha}{dt} &= -\eta\lambda_\alpha - \omega_e\lambda_\beta + \eta L_h i_\alpha, \\
\frac{d\lambda_\beta}{dt} &= -\eta\lambda_\beta + \omega_e\lambda_\alpha + \eta L_h i_\beta, \\
\tau &= \frac{3P}{2}\frac{L_h}{L_r}(i_\beta\lambda_\alpha - i_\alpha\lambda_\beta), \\
\frac{d\omega_r}{dt} &= \frac{1}{J}(\tau - \tau_l),
\end{aligned} \tag{10.3.5}$$

with

$$\eta = \frac{R_r}{L_r}, \sigma = 1 - \frac{L_h^2}{L_s L_r}, \beta = \frac{L_h}{\sigma L_s L_r}, \gamma = \frac{1}{\sigma L_s}\left(R_s + \frac{L_h^2}{L_r^2}R_r\right), \tag{10.3.6}$$

where the parameters are defined in Table 10.1.

The stator currents i_α, i_β and the stator voltages u_α, u_β are transformed from the phase currents i_a, i_b, i_c and the phase voltages u_a, u_b, u_c by

$$\begin{aligned}
[i_\alpha \;\; i_\beta]^T &= A_{\alpha,\beta}^{a,b,c}[i_a \;\; i_b \;\; i_c]^T, \\
[u_\alpha \;\; u_\beta]^T &= A_{\alpha,\beta}^{a,b,c}[u_a \;\; u_b \;\; u_c]^T,
\end{aligned} \tag{10.3.7}$$

TABLE 10.1
Parameters of the Induction Motor

u_α, u_β	Stator voltages in (α β) coordinates
i_α, i_β	Stator currents in (α β) coordinates
λ_α, λ_β	Rotor flux components in (α β) coordinates
L_r, L_s, L_h	Rotor, stator, and manual inductance
R_r, R_s	Rotor and state resistance
P	Number of pole pairs
ω_e	Electrical rotor speed
J	Mass of inertia
τ	Motor torque
τ_l	Load torque

where $A_{\alpha,\beta}^{a,b,c}$ denotes the transformation matrix

$$A_{\alpha,\beta}^{a,b,c} = 2/3\begin{bmatrix} 1 & -1/2 & -1/2 \\ 0 & \sqrt{3}/2 & -\sqrt{3}/2 \end{bmatrix}. \tag{10.3.8}$$

Because the rank of this matrix is two, the backward transformation has no unique solution; hence, the pseudo-inverse concept is used. The pseudo-inverse of matrix $A_{\alpha,\beta}^{a,b,c}$, denoted as $\left(A_{\alpha,\beta}^{a,b,c}\right)^+$, is calculated as

$$\left(A_{\alpha,\beta}^{a,b,c}\right)^+ = \left(A_{\alpha,\beta}^{a,b,c}\right)^T \left(A_{\alpha,\beta}^{a,b,c}\left(A_{\alpha,\beta}^{a,b,c}\right)^T\right)^{-1} = \frac{3}{2}\left(A_{\alpha,\beta}^{a,b,c}\right)^T = \begin{bmatrix} 1 & -1/2 & -1/2 \\ 0 & \sqrt{3}/2 & -\sqrt{3}/2 \end{bmatrix}^T. \tag{10.3.9}$$

It is easy to show that $A_{\alpha,\beta}^{a,b,c}\left(A_{\alpha,\beta}^{a,b,c}\right)^+$ is a 2×2 identity matrix. As a result, the backward transformation of the stator currents/voltages to the phase currents/voltages can be given as

$$\begin{aligned} [i_a \;\; i_b \;\; i_c]^T &= \left(A_{\alpha,\beta}^{a,b,c}\right)^+ [i_\alpha \;\; i_\beta]^T \\ [u_a \;\; u_b \;\; u_c]^T &= \left(A_{\alpha,\beta}^{a,b,c}\right)^+ [u_\alpha \;\; u_\beta]^T. \end{aligned} \tag{10.3.10}$$

The motor model in (d, q) coordinates, which fixes on the rotor flux vector, can also be obtained by transforming the motor model from (α, β) coordinates to (d, q) coordinates using the rotor flux angle $\rho = arctg(\lambda_\beta/\lambda_\alpha)$:

$$\begin{aligned}
\frac{di_d}{dt} &= -\gamma i_d + \eta\beta\lambda_d + \omega_e i_q + \eta\frac{L_h i_q^2}{\lambda_d} + \frac{1}{\sigma L_s}u_d,\\
\frac{di_q}{dt} &= -\gamma i_q - \omega_e\beta\lambda_d - \omega_e i_d - \eta\frac{L_h i_d i_q}{\lambda_d} + \frac{1}{\sigma L_s}u_q,\\
\frac{d\lambda_d}{dt} &= -\eta\lambda_d + \eta L_h i_d,\\
\frac{d\rho}{dt} &= \omega_\rho = \omega_e + \omega_s, \text{ with } \omega_s = \eta\frac{L_h i_q}{\lambda_d},\\
\tau &= \frac{3P}{2}\frac{L_h}{L_r}\lambda_d i_q,\\
\frac{d\omega_r}{dt} &= \frac{1}{J}(\tau - \tau_l),
\end{aligned} \tag{10.3.11}$$

where i_d and i_q are the stator currents in (d, q) coordinates, u_d and u_q are the associated stator voltages, and λ_d is the d component of the rotor flux (the q component of the rotor flux is equal to zero, i.e., $\lambda_q = 0$). Currents i_d, i_q and voltages u_d, u_q are transformed from (α, β) coordinates by

$$\begin{aligned}
[i_d \;\; i_q]^T &= A_{d,q}^{\alpha,\beta}[i_\alpha \;\; i_\beta]^T,\\
[u_d \;\; u_q]^T &= A_{d,q}^{\alpha,\beta}[u_\alpha \;\; u_\beta]^T,
\end{aligned} \tag{10.3.12}$$

in which matrix $A_{d,q}^{\alpha,\beta}$ is defined as

$$A_{d,q}^{\alpha,\beta} = \begin{bmatrix} \cos\rho & \sin\rho \\ -\sin\rho & \cos\rho \end{bmatrix}. \tag{10.3.13}$$

This matrix is an orthogonal matrix whose inverse is equal to its transpose. As a result, the backward transformation can be written as

$$\begin{aligned}
[i_\alpha \;\; i_\beta]^T &= \left(A_{d,q}^{\alpha,\beta}\right)^T [i_d \;\; i_q]^T,\\
[u_\alpha \;\; u_\beta]^T &= \left(A_{d,q}^{\alpha,\beta}\right)^T [u_d \;\; u_q]^T.
\end{aligned} \tag{10.3.14}$$

The relationship between (d, q) coordinates and (a, b, c) coordinates can also be established. The phase currents i_a, i_b, i_c and the phase voltages u_a, u_b, u_c can be transformed into (d, q) coordinates using

$$\begin{aligned}
[i_d \;\; i_q]^T &= A_{d,q}^{a,b,c}[i_a \;\; i_b \;\; i_c]^T,\\
[u_d \;\; u_q]^T &= A_{d,q}^{a,b,c}[u_a \;\; u_b \;\; u_c]^T,
\end{aligned} \tag{10.3.15}$$

where matrix $A_{d,q}^{a,b,c}$ depends on the rotor flux angle ρ and is defined as

$$A_{d,q}^{a,b,c} = A_{d,q}^{\alpha,\beta} A_{\alpha,\beta}^{a,b,c}. \tag{10.3.16}$$

Matrix $A_{d,q}^{a,b,c}$ is a 2×3 matrix; hence, for the backward transformation, we again need its pseudo-inverse given as

$$\left(A_{d,q}^{a,b,c}\right)^{+} = \left(A_{d,q}^{a,b,c}\right)^{T} \left(A_{d,q}^{a,b,c}\left(A_{d,q}^{a,b,c}\right)^{T}\right)^{-1} = \frac{3}{2}\left(A_{d,q}^{a,b,c}\right)^{T}, \tag{10.3.17}$$

leading to the backward transformation

$$\begin{aligned} [i_a \;\; i_b \;\; i_c]^T &= \left(A_{d,q}^{a,b,c}\right)^{+} [i_d \;\; i_q]^T, \\ [u_a \;\; u_b \;\; \boldsymbol{u}_c]^T &= \left(A_{d,q}^{a,b,c}\right)^{+} [u_d \;\; u_q]^T. \end{aligned} \tag{10.3.18}$$

The relationship between the control voltages u_d, u_q and the discontinuous controls u_1, u_2, u_3 can be established as

$$[u_d \;\; u_q]^T = A_{d,q}^{1,2,3}[u_1 \;\; u_2 \;\; u_3]^T, \tag{10.3.19}$$

where matrix $A_{d,q}^{1,2,3}$ is defined as

$$A_{d,q}^{1,2,3} = A_{d,q}^{\alpha,\beta} A_{\alpha,\beta}^{a,b,c} A_{a,b,c}^{1,2,3}. \tag{10.3.20}$$

Following the properties of matrices $A_{\alpha,\beta}^{a,b,c}$ and $A_{a,b,c}^{1,2,3}$, we have $A_{\alpha,\beta}^{a,b,c} A_{a,b,c}^{1,2,3} = A_{\alpha,\beta}^{a,b,c}$, such that

$$A_{d,q}^{1,2,3} = A_{d,q}^{\alpha,\beta} A_{\alpha,\beta}^{a,b,c} = A_{d,q}^{a,b,c}. \tag{10.3.21}$$

However, to maintain clarity, we prefer to use matrix $A_{d,q}^{1,2,3}$ denoting the transformation between the discontinuous controls u_1, u_2, u_3 and the control voltages u_d, u_q. Matrix $A_{d,q}^{1,2,3}$ is a 2×3 matrix; hence, for the backward transformation, we need its pseudo-inverse as well:

$$\left(A_{d,q}^{1,2,3}\right)^{+} = \left(A_{d,q}^{1,2,3}\right)^{T} \left(A_{d,q}^{1,2,3}\left(A_{d,q}^{1,2,3}\right)^{T}\right)^{-1} = \frac{3}{2}\left(A_{d,q}^{1,2,3}\right)^{T}, \tag{10.3.22}$$

leading to the backward transformation

$$[u_1 \;\; u_2 \;\; u_3]^T = \left(A_{d,q}^{1,2,3}\right)^{+} [u_d \;\; u_q]^T. \tag{10.3.23}$$

If not specified in associated context, the default parameters of the induction motor used to verify the design principles are: $L_r = 650 \times 10^{-6} H$, $L_s = 650 \times 10^{-6} H$, $L_h = 610 \times 10^{-6} H$, $R_r = 0.015\Omega$, $R_s = 0.035\Omega$, $P = 2$, $J = 4.33 \times 10^{-4}\, kg \cdot m^2$ and $\tau_l = B\omega_r$, with B being the coefficient of viscous friction equal to 0.01 Nm·sec/rad. The DC-bus voltage is $u_0 = 12$ V.

Thus far, the induction motor model in the (α, β) and in the (d, q) coordinate systems has been presented. Current and voltage transformations between the different coordinate systems were also given. They are very important for the control design of induction motors.

Rotor flux-oriented current control of induction motors is very similar to that of permanent-magnet synchronous motors (see Section 10.2.3). The major difference lies in the angle used for the current/voltage transformations. Here, the rotor flux angle ρ is used instead of the electrical rotor angle θ_e. It is recognized that, for high control performance, angle ρ should be available. For a sliding mode-based control design, the angle ρ is needed as well.

We begin with the rotor flux observation problem with known rotor angular speed. Then, simultaneous observation of rotor flux and rotor speed is discussed, which is essential for sensorless control of an induction motor. In the next step, we deal with rotor speed and rotor time constant estimation. Finally, we discuss direct torque and flux control based on the sliding mode control principle. The topics of sliding mode current control and direct speed control are omitted here because of the similarity with permanent-magnet synchronous motors (see Sections 10.2.3 and 10.2.4).

10.3.3. Rotor Flux Observer with Known Rotor Speed

10.3.3.1. Online Simulation of Rotor Flux Model

The original motion equation of the rotor flux can be used directly as the observer equation. The implementation of such a flux observer is just the online simulation of the controlled induction motor. As proven below, this observer is stable in the large with the rate of convergence depending on the rotor time constant. In this case, the observer equations are given by

$$\begin{aligned}\frac{d\hat{\lambda}_\alpha}{dt} &= -\eta\hat{\lambda}_\alpha - \omega_e\hat{\lambda}_\beta + \eta L_h i_\alpha,\\ \frac{d\hat{\lambda}_\beta}{dt} &= -\eta\hat{\lambda}_\beta + \omega_e\hat{\lambda}_\alpha + \eta L_h i_\beta,\end{aligned} \tag{10.3.24}$$

where $\hat{\lambda}_\alpha$, $\hat{\lambda}_\beta$ are the estimates of the rotor flux components. Defining the estimation errors as $\bar{\lambda}_\alpha = \hat{\lambda}_\alpha - \lambda_\alpha$ and $\bar{\lambda}_\beta = \hat{\lambda}_\beta - \lambda_\beta$ results in the following error dynamics:

$$\begin{aligned}\frac{d\bar{\lambda}_\alpha}{dt} &= -\frac{R_r}{L_r}\bar{\lambda}_\alpha - \omega_e\bar{\lambda}_\beta,\\ \frac{d\bar{\lambda}_\beta}{dt} &= -\frac{R_r}{L_r}\bar{\lambda}_\beta + \omega_e\bar{\lambda}_\alpha.\end{aligned} \tag{10.3.25}$$

For the stability proof, select a Lyapunov function candidate as

$$V = \frac{1}{2}(\bar{\lambda}_\alpha^2 + \bar{\lambda}_\beta^2) > 0 \tag{10.3.26}$$

and calculate the time derivative of V along the solution of Equation 10.3.25 to yield

$$\dot{V} = -\eta(\bar{\lambda}_\alpha^2 + \bar{\lambda}_\beta^2) = -2\eta V < 0. \tag{10.3.27}$$

This means that by simply integrating Equation 10.3.24, the mismatch between the real and estimated rotor flux will tend to zero asymptotically, and the rate of the convergence depends on the rotor time constant $1/\eta$. The rate of convergence may be improved by properly designed observer gains as usually done for reduced-order observers (see next approach given in the sequel).

With the estimates of the rotor flux components, the rotor flux angle $\hat{\rho}$ can be calculated as

$$\hat{\rho} = \arctan(\hat{\lambda}_\beta / \hat{\lambda}_\alpha). \tag{10.3.28}$$

Figure 10.28 depicts the simulation results of the rotor flux observer (Equation 10.3.24). To show the convergence process, the initial conditions of the observed flux components are selected differently from those of the real flux components: $\hat{\lambda}_\alpha(0) = -0.045$ and $\hat{\lambda}_\beta(0) = 0.045$, whereas $\lambda_\alpha(0) = 0$ and $\lambda_\beta(0) = 0$. Because the flux observer is just the online simulation of the motor model, no observer gain is to be adjusted.

10.3.3.2. Sliding Mode Observer with Adjustable Rate of Convergence

Now a flux observer based on the sliding mode approach with measurements of stator current, state voltages, and rotor speed is demonstrated. Compared with the open-loop flux observer discussed before, this observer has the advantage that its convergence rate is tunable.

The sliding mode observer is designed as

$$\begin{aligned}
\frac{d\hat{\lambda}_\alpha}{dt} &= -\eta\hat{\lambda}_\alpha - \omega_e\hat{\lambda}_\beta + \eta L_h i_\alpha + kV_\alpha \\
\frac{d\hat{\lambda}_\beta}{dt} &= -\eta\hat{\lambda}_\beta + \omega_e\hat{\lambda}_\alpha + \eta L_h i_\beta + kV_\beta \\
\frac{d\hat{i}_\alpha}{dt} &= \beta\eta\hat{\lambda}_\alpha + \beta\omega_e\hat{\lambda}_\beta - \gamma\hat{i}_\alpha + \frac{1}{\sigma L_s}u_\alpha + V_\alpha \\
\frac{d\hat{i}_\beta}{dt} &= \beta\eta\hat{\lambda}_\beta - \beta\omega_e\hat{\lambda}_\alpha - \gamma\hat{i}_\beta + \frac{1}{\sigma L_s}u_\beta + V_\beta,
\end{aligned} \tag{10.3.29}$$

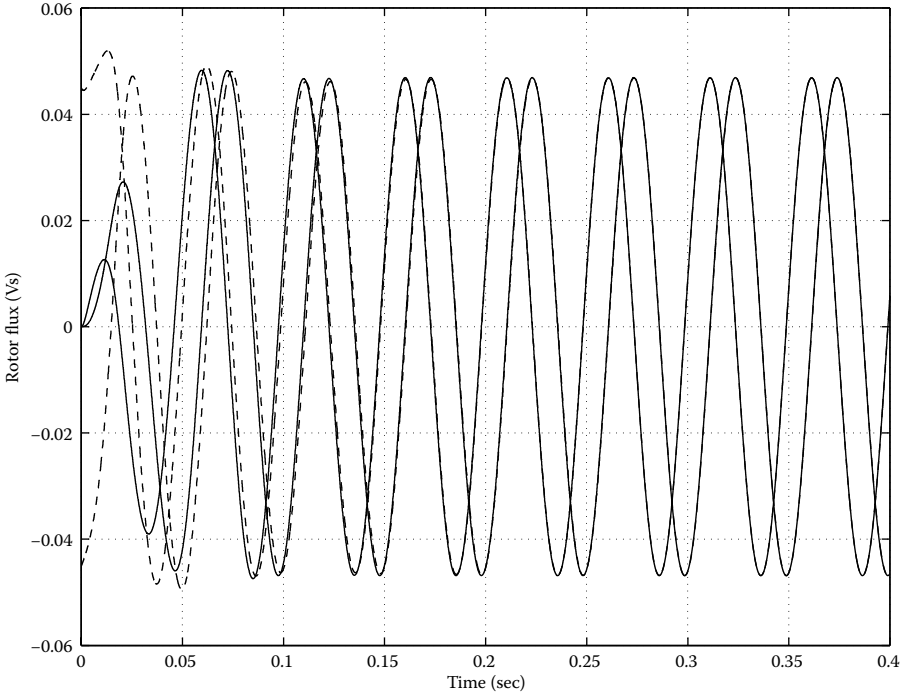

FIGURE 10.28
Responses of the flux observer with known rotor speed. Solid lines, real flux components λ_α and λ_β; dashed lines, observed flux components $\hat{\lambda}_\alpha$ and $\hat{\lambda}_\beta$.

where $\hat{i}_\alpha$, $\hat{i}_\beta$, $\hat{\lambda}_\alpha$, and $\hat{\lambda}_\beta$ are estimates of the stator current and rotor flux, and k is a positive gain to be chosen. V_α and V_β are discontinuous functions of the current errors,

$$\begin{aligned} V_\alpha &= -V_0 sign(\bar{i}_\alpha) = -V_0 sign(\hat{i}_\alpha - i_\alpha) \\ V_\beta &= -V_0 sign(\bar{i}_\beta) = -V_0 sign(\hat{i}_\beta - i_\beta) \end{aligned} \tag{10.3.30}$$

where V_0 is also a positive gain.

From Equation 10.3.29 and the induction motor model in Equation 10.3.5, the error dynamics for the current is obtained as

$$\begin{aligned} \frac{d\bar{i}_\alpha}{dt} &= \beta\eta\bar{\lambda}_\alpha + \beta\omega_e\bar{\lambda}_\beta - \gamma\bar{i}_\alpha + V_\alpha, \\ \frac{d\bar{i}_\beta}{dt} &= \beta\eta\bar{\lambda}_\beta - \beta\omega_e\bar{\lambda}_\alpha - \gamma\bar{i}_\beta + V_\beta. \end{aligned} \tag{10.3.31}$$

Let us select Lyapunov function candidate $V = \frac{1}{2}(\bar{i}_\alpha^2 + \bar{i}_\beta^2)$. Its time derivative along the state trajectories of current error system can be written as

$$\begin{aligned}\dot{V} &= \bar{i}_\alpha \dot{\bar{i}}_\alpha + \bar{i}_\beta \dot{\bar{i}}_\beta \\ &= \bar{i}_\alpha(\beta\eta\bar{\lambda}_\alpha + \beta\omega_e\bar{\lambda}_\beta - \gamma\bar{i}_\alpha - V_0 sign(\bar{i}_\alpha)) \\ &\quad + \bar{i}_\beta(\beta\eta\bar{\lambda}_\beta - \beta\omega_e\bar{\lambda}_\alpha - \gamma\bar{i}_\beta - V_0 sign(\bar{i}_\beta)) \\ &= -V_0(|\bar{i}_\alpha| + |\bar{i}_\beta|) - \gamma(\bar{i}_\alpha^2 + \bar{i}_\beta^2) + \bar{i}_\alpha f_\alpha + \bar{i}_\beta f_\beta,\end{aligned} \tag{10.3.32}$$

where $f_\alpha = \beta\eta\bar{\lambda}_\alpha + \beta\omega_e\bar{\lambda}_\beta$ and $f_\beta = \beta\eta\bar{\lambda}_\beta - \beta\omega_e\bar{\lambda}_\alpha$.

If $V_0 > max\{|f_\alpha|, |f_\beta|\}$, then $\dot{V} < 0$ until $\bar{i}_\alpha = 0$ and $\bar{i}_\beta = 0$, which means that sliding mode will occur in the intersection of the surfaces $\bar{i}_\alpha = 0$ and $\bar{i}_\beta = 0$. The estimated currents $\hat{i}_\alpha$ and $\hat{i}_\beta$ will converge to the real currents after sliding mode has been reached in $\bar{i}_\alpha = 0$ and $\bar{i}_\beta = 0$.

The equivalent control components V_{α_eq} and V_{β_eq} of the discontinuous functions V_α and V_β can be obtained by setting $\dot{\bar{i}}_\alpha = 0$, $\bar{i}_\alpha = 0$ and $\dot{\bar{i}}_\beta = 0$, $\bar{i}_\beta = 0$ in Equation 10.3.31:

$$\begin{aligned}V_{\alpha\_eq} &= -\beta\eta\bar{\lambda}_\alpha - \beta\omega_e\bar{\lambda}_\beta \\ V_{\beta\_eq} &= -\beta\eta\bar{\lambda}_\beta + \beta\omega_e\bar{\lambda}_\alpha.\end{aligned} \tag{10.3.33}$$

Note that the equivalent control V_{α_eq} and V_{β_eq} in Equation 10.3.33 are only for analysis of the proposed observer convergence. It is not necessary to obtain them in the observer implementation.

Substituting the above equivalent control into the flux observer (Equation 10.3.29) yields the dynamics for flux estimation in sliding mode:

$$\begin{aligned}\frac{d\hat{\lambda}_\alpha}{dt} &= -\eta\hat{\lambda}_\alpha - \omega_e\hat{\lambda}_\beta + \eta L_h i_\alpha + kV_{\alpha\_eq} \\ \frac{d\hat{\lambda}_\beta}{dt} &= -\eta\hat{\lambda}_\beta + \omega_e\hat{\lambda}_\alpha + \eta L_h i_\beta + kV_{\beta\_eq}.\end{aligned}, \tag{10.3.34}$$

The error dynamics for the flux estimation can then be derived as

$$\begin{aligned}\frac{d\bar{\lambda}_\alpha}{dt} &= -\eta(1+\beta k)\bar{\lambda}_\alpha - \omega_e(1+\beta k)\bar{\lambda}_\beta, \\ \frac{d\bar{\lambda}_\beta}{dt} &= -\eta(1+\beta k)\bar{\lambda}_\beta + \omega_e(1+\beta k)\bar{\lambda}_\alpha.\end{aligned} \tag{10.3.35}$$

To prove the convergence of the rotor flux estimation, let us choose the Lyapunov function candidate $V = \frac{1}{2}(\bar{\lambda}_\alpha^2 + \bar{\lambda}_\beta^2)$. Substituting Equation 10.3.35 gives the time derivative of V:

$$\dot{V} = -\eta(1+\beta k)(\bar{\lambda}_\alpha^2 + \bar{\lambda}_\beta^2), \tag{10.3.36}$$

from which we can see that the convergence rate of the flux observer is determined by $\eta(1 + \beta k)$. Increasing the tunable and positive observer gain k leads to faster convergence, in contrast to the open-loop flux observer with the convergence rate determined by the rotor time constant $1/\eta$.

The simulation results in Figure 10.29 show that the estimated rotor flux converges immediately to the real rotor flux after the observer equations being executed. In the simulation, $V_0 = 5000$ and $k = 0.004$ are selected. Note that $V_0 > max\{|f_\alpha|,|f_\beta|\}$ is required, but f_α and f_β are functions of rotor speed ω_e. To keep the chattering level (attributable to limited sample time) in the current observation within a reasonable range, V_0 may be selected to be rotor speed dependent.

The sliding mode flux observer is not the only way to achieve an adjustable convergence rate. Similar results can be achieved by an asymptotic observer (i.e., Luenberger observer) applied to the reduced order model $\dot{\lambda}_\alpha = \lambda_\alpha + Li_\alpha$ and $\dot{\lambda}_\beta = \lambda_\beta + Li_\beta$, where L is a constant gain to be determined.

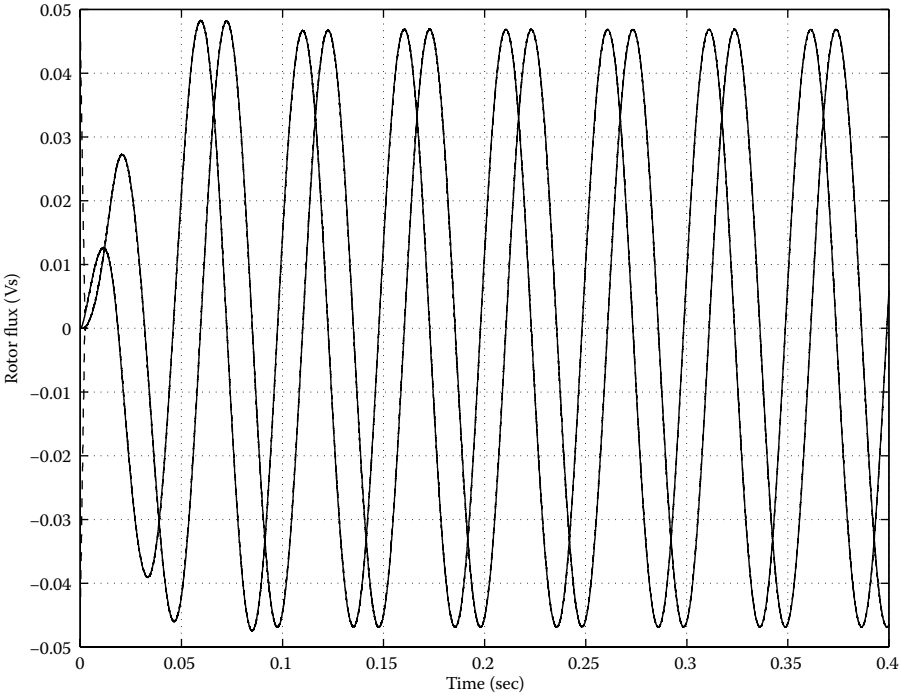

FIGURE 10.29
Responses of the flux observer with known rotor speed and adjustable rate of convergence. Solid lines, real flux components λ_α and λ_β; dashed lines, observed flux components $\hat{\lambda}_\alpha$ and $\hat{\lambda}_\beta$.

10.3.4. Simultaneous Observation of Rotor Flux and Rotor Speed

Simultaneous observation of rotor flux and rotor speed has been a challenging problem in the control of induction motors. Different approaches use the physical properties of induction motors, such as

- Structural modification of motor rotor [Lorenz 1995]
- Extraction of speed information from the harmonic components [Jiang and Holtz 1997]
- Test current method [Blaschke, Vandenput, and van der Burgt 1995]
- Involving stator flux estimation [Xu and Novotny 1993]

The above methods were tested in practical systems and shown to yield a well acceptable performance at very low rotor speed. Another trend in the research of sensorless control involves sophisticated control/estimation algorithms without additional source of information being exploited. These methods include some adaptive/robust algorithms, such as

- Kalman-Filter method [Henneberger, Brunsbach, and Klepsch 1991]
- Model reference adaptive control method [Tamai, Sugimoto, and Yano 1987]

The flux/speed observer discussed here is an extended version of [Isozimov 1983] and was presented by Yan, Jin, and Utkin [2000], in which some other important research works on this topic are referenced.

The objective in this subsection is to design a flux/speed observer to estimate the rotor flux and rotor speed simultaneously based on the measurement of the stator currents and voltages, under the natural assumption that there exists a torque/flux controller such that the estimated torque and estimated rotor flux are controlled and following their references.

The observer is designed as

$$\begin{aligned}
\frac{d\hat{\lambda}_\alpha}{dt} &= -\eta\hat{\lambda}_\alpha - \hat{\omega}_e\hat{\lambda}_\beta + \eta L_h i_\alpha + C\hat{\lambda}_\beta\mu \\
\frac{d\hat{\lambda}_\beta}{dt} &= -\eta\hat{\lambda}_\beta + \hat{\omega}_e\hat{\lambda}_\alpha + \eta L_h i_\beta - C\hat{\lambda}_\alpha\mu \\
\frac{d\hat{i}_\alpha}{dt} &= \beta\eta\hat{\lambda}_\alpha + \beta\hat{\omega}_e\hat{\lambda}_\beta - \gamma i_\alpha + \frac{1}{\sigma L_s}u_\alpha - \beta\hat{\lambda}_\alpha\mu \\
\frac{d\hat{i}_\beta}{dt} &= \beta\eta\hat{\lambda}_\beta - \beta\hat{\omega}_e\hat{\lambda}_\alpha - \gamma i_\beta + \frac{1}{\sigma L_s}u_\beta - \beta\hat{\lambda}_\beta\mu
\end{aligned} \tag{10.3.37}$$

where $\hat{\lambda}_\alpha$, $\hat{\lambda}_\beta$ represent the estimated rotor flux components, and $\hat{i}_\alpha$, $\hat{i}_\beta$ represent the estimated stator currents. C is a parameter to be selected. The

estimate of the rotor electrical angular speed $\hat{\omega}_e$ and the auxiliary variable μ are discontinuous quantities given by

$$\begin{aligned} \hat{\omega}_e &= n_0 sign(s_n) \\ \mu &= \mu_0 sign(s_\mu)' \end{aligned} \tag{10.3.38}$$

where n_0, μ_0 are constants, and s_n, s_μ are nonlinear functions of the stator current errors and estimated rotor flux components

$$\begin{aligned} s_n &= (\hat{i}_\beta - i_\beta)\hat{\lambda}_\alpha - (\hat{i}_\alpha - i_\alpha)\hat{\lambda}_\beta \\ s_\mu &= (\hat{i}_\alpha - i_\alpha)\hat{\lambda}_\alpha + (\hat{i}_\beta - i_\beta)\hat{\lambda}_\beta. \end{aligned} \tag{10.3.39}$$

Note that s_n and s_μ are actually proportional to the current estimation errors projected in the (d, q) coordinates based on the estimated rotor flux angle instead of the real rotor flux angle.

First, it will be shown that there exist constant values n_0 and μ_0 such that sliding mode occurs in the surfaces of $s_n = 0$ and $s_\mu = 0$, and, as a result, the estimation errors

$$\bar{i}_\alpha = \hat{i}_\alpha - i_\alpha, \quad \bar{i}_\beta = \hat{i}_\beta - i_\beta \tag{10.3.40}$$

are equal to zero. Then, under the natural assumption that a controller exists such that estimated motor torque and estimated rotor flux track their references, it will be shown that the flux estimation errors

$$\bar{\lambda}_\alpha = \hat{\lambda}_\alpha - \lambda_\alpha, \quad \bar{\lambda}_\beta = \hat{\lambda}_\beta - \lambda_\beta \tag{10.3.41}$$

will tend to zero as well, and, furthermore, the average value of the discontinuous variable $\hat{\omega}_e$ tends to the real speed ω_e.

10.3.4.1. Analysis of Current Tracking

To analyze the convergence of the estimates to the real values in the proposed observer structure, we first need to analyze the stator current tracking property. As it follows from the observer equations (Equation 10.3.37) and the motor model equations (Equation 10.3.5), the error dynamics with respect to the errors $\bar{i}_\alpha$, $\bar{i}_\beta$, $\bar{\lambda}_\alpha$, and $\bar{\lambda}_\beta$ can be written as

$$\begin{aligned} \frac{d\bar{\lambda}_\alpha}{dt} &= -\eta\bar{\lambda}_\alpha - \omega_e\bar{\lambda}_\beta - \bar{\omega}_e\hat{\lambda}_\beta + C\hat{\lambda}_\beta\mu \\ \frac{d\bar{\lambda}_\beta}{dt} &= -\eta\bar{\lambda}_\beta + \omega_e\bar{\lambda}_\alpha + \bar{\omega}_e\hat{\lambda}_\alpha - C\hat{\lambda}_\alpha\mu \\ \frac{d\bar{i}_\alpha}{dt} &= \beta\eta\bar{\lambda}_\alpha + \beta\omega_e\bar{\lambda}_\beta + \beta\bar{\omega}_e\hat{\lambda}_\beta - \beta\hat{\lambda}_\alpha\mu \\ \frac{d\bar{i}_\beta}{dt} &= \beta\eta\bar{\lambda}_\beta - \beta\omega_e\bar{\lambda}_\alpha - \beta\bar{\omega}_e\hat{\lambda}_\alpha - \beta\hat{\lambda}_\beta\mu \end{aligned} \tag{10.3.42}$$

Based on the error dynamics and the observer equations, the time derivative of s_n can be derived as

$$\dot{s}_n = \dot{\bar{i}}_\beta \hat{\lambda}_\alpha - \dot{\bar{i}}_\alpha \hat{\lambda}_\beta + \bar{i}_\beta \dot{\hat{\lambda}}_\alpha - \bar{i}_\alpha \dot{\hat{\lambda}}_\beta, \tag{10.3.43}$$

where

$$\begin{aligned} \dot{\bar{i}}_\beta \hat{\lambda}_\alpha - \dot{\bar{i}}_\alpha \hat{\lambda}_\beta &= -\beta \hat{\omega}_e \left\| \hat{\lambda} \right\|^2 + \beta \omega_e \left\| \hat{\lambda} \right\|^2 + \beta \eta e_2 - \beta \omega_e e_1 \\ \bar{i}_\beta \dot{\hat{\lambda}}_\alpha - \bar{i}_\alpha \dot{\hat{\lambda}}_\beta &= -\hat{\omega}_e s_\mu + \eta L_h (\bar{i}_\beta i_\alpha - \bar{i}_\alpha i_\beta) + C s_\mu \mu \end{aligned} \tag{10.3.44}$$

With the substitition of Equation 10.3.38 for $\hat{\omega}_e$, Equation 10.3.43 can be reformulated as

$$\dot{s}_n = -\left(\beta \left\| \hat{\lambda} \right\|^2 + s_\mu \right) n_0 sign(s_n) + f(\omega_e, \bar{i}_\alpha, \bar{i}_\beta, e_1, e_2), \tag{10.3.45}$$

with $\left\| \hat{\lambda} \right\| = \sqrt{\hat{\lambda}_\alpha^2 + \hat{\lambda}_\beta^2}$, $f(\omega_e, \bar{i}_\alpha, \bar{i}_\beta, e_1, e_2) = \beta \omega_e \left\| \hat{\lambda} \right\|^2 + \eta L_h (\bar{i}_\beta i_\alpha - \bar{i}_\alpha i_\beta) + \beta \eta e_2 - \beta \omega_e e_1 + C s_\mu \mu$, and

$$\begin{aligned} e_1 &= \bar{\lambda}_\alpha \hat{\lambda}_\alpha + \bar{\lambda}_\beta \hat{\lambda}_\beta \\ e_2 &= \bar{\lambda}_\beta \hat{\lambda}_\alpha - \bar{\lambda}_\alpha \hat{\lambda}_\beta \end{aligned}. \tag{10.3.46}$$

It follows from Equation 10.3.45 that, if the condition

$$\beta \left\| \hat{\lambda} \right\|^2 + s_\mu > 0, \tag{10.3.47}$$

holds, then for high enough n_0, $s_n \dot{s}_n < 0$, i.e., sliding mode will occur on the surface $s_n = 0$. Similarly, for s_μ, we have

$$\begin{aligned} \dot{s}_\mu &= \dot{\bar{i}}_\alpha \hat{\lambda}_\alpha + \dot{\bar{i}}_\beta \hat{\lambda}_\beta + \bar{i}_\alpha \dot{\hat{\lambda}}_\alpha + \bar{i}_\beta \dot{\hat{\lambda}}_\beta \\ &= \beta \eta e_1 + \beta \omega_e e_2 + \eta L_h (i_\alpha \bar{i}_\alpha + i_\beta \bar{i}_\beta) - \beta \mu_0 \left\| \hat{\lambda} \right\|^2 sign(s_\mu) \end{aligned}. \tag{10.3.48}$$

If μ_0 is high enough, $s_\mu \dot{s}_\mu < 0$, and sliding mode will occur on the surface $s_\mu = 0$.

After sliding mode arises on the intersection of both surfaces $s_n = \bar{i}_\beta \hat{\lambda}_\alpha - \bar{i}_\alpha \hat{\lambda}_\beta = 0$ and $s_\mu = \bar{i}_\alpha \hat{\lambda}_\alpha + \bar{i}_\beta \hat{\lambda}_\beta = 0$, $\bar{i}_\alpha = 0$ and $\bar{i}_\beta = 0$ are the unique solution under the assumption $\left\| \hat{\lambda} \right\|^2 \neq 0$, which means that the estimated currents $\hat{i}_\alpha$, $\hat{i}_\beta$ converge to the real currents i_α, i_β, respectively.

The equivalent control of the discontinuous functions $\hat{\omega}_e = n_0 sign(s_n)$ and $\mu = \mu_0 sign(s_\mu)$ are the solutions of the algebraic equations $\dot{s}_n = 0$ and $\dot{s}_\mu = 0$. For our case,

$$\hat{\omega}_{e\_eq} = \omega_e - \frac{\omega_e}{\left\|\hat{\lambda}\right\|^2} e_1 + \frac{\eta}{\left\|\hat{\lambda}\right\|^2} e_2. \tag{10.3.49}$$

As seen from Equation 10.3.49, if the estimated rotor flux converges to the real flux, which leads to $e_1 = 0$ and $e_2 = 0$ (see Equation 10.3.46), then, $\hat{\omega}_{e\_eq}$ will tend to the real rotor (electrical) speed. The next step is to prove $e_1 = 0$ and $e_2 = 0$. Before doing that, let us go through the following remarks.

Remark 10.3.1

Equation 10.3.49 is only for the theoretical analysis to show that the equivalent control of $\hat{\omega}_e = n_0 sign(s_n)$, i.e., $\hat{\omega}_{e\_eq}$ is indeed equal to the real rotor speed. In practice, however, $\hat{\omega}_{e\_eq}$ will be obtained through a low-pass filter with discontinuous term $\hat{\omega}_e = n_0 sign(s_n)$ as the input, i.e.,

$$t_c \dot{z} + z = n_0 sign(s_n), \; z \approx \hat{\omega}_{e\_eq}, \tag{10.3.50}$$

where the time constant of the low-pass filter, t_c, should be small compared with the slow component of $n_0 sign(s_n)$ but large enough to filter out the high rate component.

Remark 10.3.2

The condition Equation 10.3.47 for sliding mode to occur on the surface $s_n = 0$ is not very restrictive because the stator currents i_α and i_β are measurable. We can always choose the initial conditions $\hat{i}_\alpha(0)$ and $\hat{i}_\beta(0)$ close enough to the true stator currents $i_\alpha(0)$ and $i_\beta(0)$ such that the initial errors $\bar{i}_\alpha(0)$ and $\bar{i}_\beta(0)$, and hence s_μ, are small enough to guarantee that this condition holds.

Remark 10.3.3

Although the structure of the observer is selected in the framework of the work by Isozimov [1983], an extension is made to guarantee the convergence of the observer. It will be shown later that, under certain conditions, the asymptotic stability of the sliding mode observer can be guaranteed with the flux errors $\bar{\lambda}_\alpha$ and $\bar{\lambda}_\beta$ converging to zero and z tending to the real speed ω_e.

Remark 10.3.4

Although the flux/speed observer is of the fourth order, after sliding mode occurs on the surfaces $s_n = 0$ and $s_\mu = 0$, the error dynamics of the sliding mode observer are actually of second order. This order-reduction property of the sliding mode is very helpful for the stability analysis of the nonlinear time-varying error system.

10.3.4.2. Composite Observer-Controller Analysis

Now we will prove that $e_1 \to 0$ and $e_2 \to 0$ under certain conditions. In a control system based on observed state variables, the solutions of the observer will be under some constrains regarding the reference inputs of the control system. For a properly designed controller, the observed state variables closely follow their references and cannot become arbitrarily large.

Assumption

There exists a torque/flux controller such that the estimated torque and estimated rotor flux are controlled to follow their references starting from some time instant, i.e.,

$$\begin{aligned} \hat{\tau} &= \tau^* \\ \left\| \hat{\lambda} \right\| &= \lambda^* \end{aligned}. \tag{10.3.51}$$

As mentioned previously, the error system of the observer is of second order as a result of the order reduction of sliding mode. Calculate the time derivative of the transformed flux errors e_1 and e_2 to build the error system of the rotor flux estimation:

$$\begin{aligned} \dot{e}_1 &= \dot{\bar{\lambda}}_\alpha \hat{\lambda}_\alpha + \dot{\bar{\lambda}}_\beta \hat{\lambda}_\beta + \bar{\lambda}_\alpha \dot{\hat{\lambda}}_\alpha + \bar{\lambda}_\beta \dot{\hat{\lambda}}_\beta \\ \dot{e}_2 &= \dot{\bar{\lambda}}_\beta \hat{\lambda}_\alpha - \dot{\bar{\lambda}}_\alpha \hat{\lambda}_\beta + \bar{\lambda}_\beta \dot{\hat{\lambda}}_\alpha - \bar{\lambda}_\alpha \dot{\hat{\lambda}}_\beta \end{aligned} \tag{10.3.52}$$

and solve $\bar{\lambda}_\alpha$ and $\bar{\lambda}_\beta$ from Equation 10.3.46,

$$\begin{aligned} \bar{\lambda}_\alpha &= \frac{\hat{\lambda}_\alpha}{\left\| \hat{\lambda} \right\|^2} e_1 - \frac{\hat{\lambda}_\beta}{\left\| \hat{\lambda} \right\|^2} e_2 \\ \bar{\lambda}_\beta &= \frac{\hat{\lambda}_\beta}{\left\| \hat{\lambda} \right\|^2} e_1 + \frac{\hat{\lambda}_\alpha}{\left\| \hat{\lambda} \right\|^2} e_2 \end{aligned}. \tag{10.3.53}$$

Substituting the observer model (Equation 10.3.37) and the observer error dynamics (Equation 10.3.42) into Equation 10.3.52, by denoting

$$\begin{aligned} \hat{i}_d &= \frac{\hat{\lambda}_\alpha}{\left\| \hat{\lambda} \right\|} i_\alpha + \frac{\hat{\lambda}_\beta}{\left\| \hat{\lambda} \right\|} i_\beta \\ \hat{i}_q &= \frac{\hat{\lambda}_\alpha}{\left\| \hat{\lambda} \right\|} i_\beta - \frac{\hat{\lambda}_\beta}{\left\| \hat{\lambda} \right\|} i_\alpha \end{aligned}, \tag{10.3.54}$$

yields

$$\begin{aligned}\dot{e}_1 &= \left(-2\eta + \eta\frac{L_h\hat{i}_d}{\left\|\hat{\lambda}\right\|}\right)e_1 + \eta\frac{L_h\hat{i}_q}{\left\|\hat{\lambda}\right\|}e_2 + \bar{\omega}_e e_2 - C\mu e_2 \\ \dot{e}_2 &= \left(-\eta + \eta\frac{L_h\hat{i}_d}{\left\|\hat{\lambda}\right\|}\right)e_2 - \left(\omega_e + \eta\frac{L_h\hat{i}_q}{\left\|\hat{\lambda}\right\|}\right)e_1 + \bar{\omega}_e e_1 - C\left\|\hat{\lambda}\right\|^2\mu + C\mu e_1\end{aligned} \quad . \quad (10.3.55)$$

Note that the introduced auxiliary variables $\hat{i}_d$ and $\hat{i}_q$ in Equation 10.3.54 are actually stator currents projected onto the (d, q) coordinates, which aligns with the estimated rotor flux vector instead of the real (but unknown) rotor flux vector. The value of $\bar{\omega}_e$ is defined as $\bar{\omega}_e = \hat{\omega}_e - \omega_e$. After sliding mode occurs, $\hat{\omega}_e$ and $\hat{\omega}_{e\_eq}$ are equivalent. Hence, the speed deviation $\bar{\omega}_e$ can be calculated from Equation 10.3.49:

$$\bar{\omega}_e = -\frac{\omega_e}{\left\|\hat{\lambda}\right\|^2}e_1 + \frac{\eta}{\left\|\hat{\lambda}\right\|^2}e_2. \quad (10.3.56)$$

Substitution of Equation 10.3.56 into Equation 10.3.55 results in the error dynamics in matrix form:

$$\begin{bmatrix}\dot{e}_1 \\ \dot{e}_2\end{bmatrix} = \begin{bmatrix}-2\eta + \eta\dfrac{L_h\hat{i}_d}{\left\|\hat{\lambda}\right\|} & \eta\dfrac{L_h\hat{i}_q}{\left\|\hat{\lambda}\right\|} \\ -\left(\omega_e + \eta\dfrac{L_h\hat{i}_q}{\left\|\hat{\lambda}\right\|}\right) & -\eta + \eta\dfrac{L_h\hat{i}_d}{\left\|\hat{\lambda}\right\|}\end{bmatrix}\begin{bmatrix}e_1 \\ e_2\end{bmatrix} + \begin{bmatrix}-C\mu e_2 \\ -C\left\|\hat{\lambda}\right\|^2\mu + C\mu e_1\end{bmatrix} + \begin{bmatrix}\dfrac{\omega_e}{\left\|\hat{\lambda}\right\|^2}e_1e_2 + \dfrac{\eta}{\left\|\hat{\lambda}\right\|^2}e_2^2 \\ \dfrac{\omega_e}{\left\|\hat{\lambda}\right\|^2}e_1^2 - \dfrac{\eta}{\left\|\hat{\lambda}\right\|^2}e_1e_2\end{bmatrix}. \quad (10.3.57)$$

Because sliding mode on manifold $s_\mu = 0$ has also been enforced, we can solve the algebraic equation $\dot{s}_\mu = 0$ in Equation 10.3.48 with respect to μ to yield

$$\mu_{eq} = \frac{\eta}{\left\|\hat{\lambda}\right\|^2}e_1 + \frac{\omega_e}{\left\|\hat{\lambda}\right\|^2}e_2. \quad (10.3.58)$$

Equation 10.3.58 can be used to eliminate the discontinuous control μ from the error system in Equation 10.3.57. In the next step, we replace $\hat{i}_d$, $\hat{i}_q$ with the reference torque $\tau^*$and reference flux λ^*, using the assumption that the torque/flux controller will make τ^* and λ^* to be equal to $\hat{\tau}$ and $\left\|\hat{\lambda}\right\|$, respectively.

Similar to the induction motor model in (d, q) coordinates aligned with the real rotor flux vector, the flux and torque model in (d, q) coordinates aligned with the estimated rotor flux vector can also be found compared with Equation 10.3.11 under the notation $\|\lambda\| = \lambda_d$ (and also $\left\|\hat{\lambda}\right\| = \hat{\lambda}_d$):

$$\begin{aligned} \hat{\tau} &= \frac{3PL_h}{2L_r}\left\|\hat{\lambda}\right\|\hat{i}_q \\ \frac{d\left\|\hat{\lambda}\right\|}{dt} &= -\eta\left\|\hat{\lambda}\right\| + \eta L_h \hat{i}_d \end{aligned}. \tag{10.3.59}$$

Taking into account the assumption in Equation 10.3.51 and considering the steady-state solution of the flux model in Equation 10.3.59 (note that $\dot{\lambda}^* = 0$ is normally required), we have

$$\begin{aligned} \hat{i}_d &= \frac{\lambda^*}{L_h} \\ \hat{i}_q &= \frac{2L_r\tau^*}{3PL_h\lambda^*} \end{aligned}. \tag{10.3.60}$$

Finally, substituting Equations 10.3.58 (note that $\mu = \mu_{eq}$ in sliding mode), 10.3.60, and $\left\|\hat{\lambda}\right\| = \lambda^*$ into the error dynamic system (Equation 10.3.57) and performing linearization, yields

$$\begin{bmatrix} \dot{e}_1 \\ \dot{e}_2 \end{bmatrix} = \begin{bmatrix} -\eta & a \\ -(\hat{\omega}_{e\_eq} + a) - C\eta & -C\hat{\omega}_{e\_eq} \end{bmatrix} \begin{bmatrix} e_1 \\ e_2 \end{bmatrix}, \tag{10.3.61}$$

where $a = (2\tau^* R_r)/[3P(\lambda^*)^2]$.

Note that the linearized error system (Equation 10.3.61) does not depend on the real speed, real rotor flux, and real stator currents. It depends only on the reference torque τ^*, the reference flux λ^*, the equivalent rotor speed $\hat{\omega}_{e\_eq}$, and the adjustable parameter C. As follows from Equation 10.3.61, for large C, the motion of the error dynamic system can be classified into the slow and fast motion. The fast component $\eta e_1 + \hat{\omega}_{e\_eq} e_2$ decays rapidly with

$$\lim_{t\to\infty} e_2 = -\frac{\eta}{\hat{\omega}_{e\_eq}} e_1. \tag{10.3.62}$$

The slow motion is governed by

$$\dot{e}_1 = -\eta\left(1 + \frac{a}{\hat{\omega}_{e\_eq}}\right) e_1. \tag{10.3.63}$$

One of the sufficient conditions for the asymptotic stability of the slow motion for any time-varying speed is $1 + a/\hat{\omega}_{e\_eq} > 0$. It is clear that

$$\frac{a}{\hat{\omega}_{e\_eq}} > 0 \tag{10.3.64}$$

is a sufficient condition as well. This means that the solution to Equation 10.3.63 is stable and $\lim_{t\to\infty} e_1 = 0$ if the reference torque τ^* and the equivalent speed $\hat{\omega}_{e\_eq}$ have the same sign. Finally, according to Equation 10.3.62, $\lim_{t\to\infty} e_2 = 0$. We have described qualitatively the flux convergence issue based on the motion separation approach.

Remark 10.3.5

According to the theory of singularly perturbed systems, the asymptotic stability of the fast motion of the error dynamic (Equation 10.3.61) requires that the parameter C and $\hat{\omega}_{e\_eq}$ have the same sign. Because the equivalent speed $\hat{\omega}_{e\_eq}$ can be calculated through Equation 10.3.50 online, the sign of the parameter C can be adapted accordingly. At the instants when $\omega_{e\_eq} = 0$, the stability of the system in Equation 10.3.61 will depend on the signs of parameter C and parameter a, whereas a has the same sign as the reference torque. Thus, the sign of parameter C can be adapted to the sign of the reference torque, guaranteeing the stability of the system.

10.3.4.3. Simulation Results

The proposed estimation algorithm was first simulated using Matlab®. In the simulation, the torque/flux controller was also implemented besides the sliding mode observer to build up the whole closed-loop system. For the torque/flux control in the simulation, no PWM technique was used and the dynamics in the voltage source inverter were ignored.

Parameters used in the torque controller, the flux/speed observer, and the induction motor model for the simulations are listed in Table 10.2. Figures 10.30 through 10.34 show the piecewise continuous situation, and Figures 10.35 through 10.39 show the sinusoidal situation for torque tracking. From these simulation results, we can see that the proposed sliding mode flux/speed observer exhibits high accuracy. Note that convergence of estimations to real values of flux and speed takes place if torque estimate tracks the reference input.

10.3.4.4. Experimental Results

The proposed control scheme was also implemented in a laboratory experiment. The real-time control and estimation program was written in C. The proposed algorithm was tested at the experiment environment in PEEM

TABLE 10.2
Parameters Used in the Simulation

$L_s = 590 \times 10^{-6}\ H$	$\tau_l = BP\ \omega_e\ N.\ m$
$L_r = 590 \times 10^{-6}\ H$	$BP = 0.04\ N.\ m.\ s/rad$
$L_h = 555 \times 10^{-6}\ H$	$n_0 = 120$
$R_s = 0.0106\Omega$	$\mu_0 = 200$
$R_r = 0.0118\Omega$	$\lambda^* = 0.01$
$u_0 = 12V$	$\tau^* = 1.0\ N.m$
$P = 1.0$	$t_c = 0.0015$
$J = 4.33 \times 10^{-4}\ N.\ m.\ s^2$	

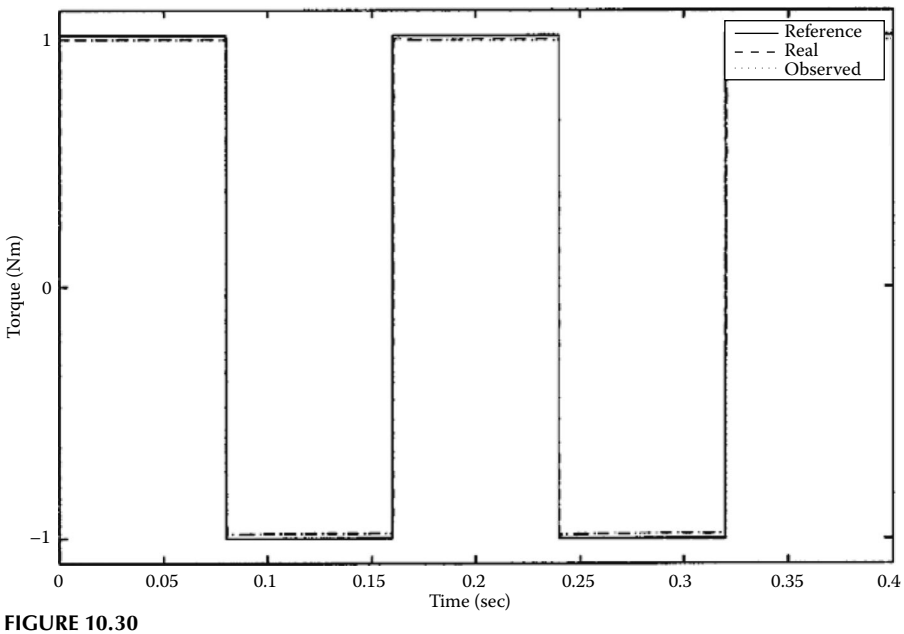

FIGURE 10.30
Torque tracking: reference τ^*, real τ, and observed $\hat{\tau}$.

(Power Electronics and Electrical Machines) Laboratory of The Ohio State University. The motor is a Westinghouse 5 hp, 220 V, Y-connected, four-pole induction machine with the parameters listed in Table 10.3.

Main components of the experiment environment include the following: a digital signal processor (DSP) system; the induction motor and associated voltage source inverters; an optical encoder attached to the motor shaft for

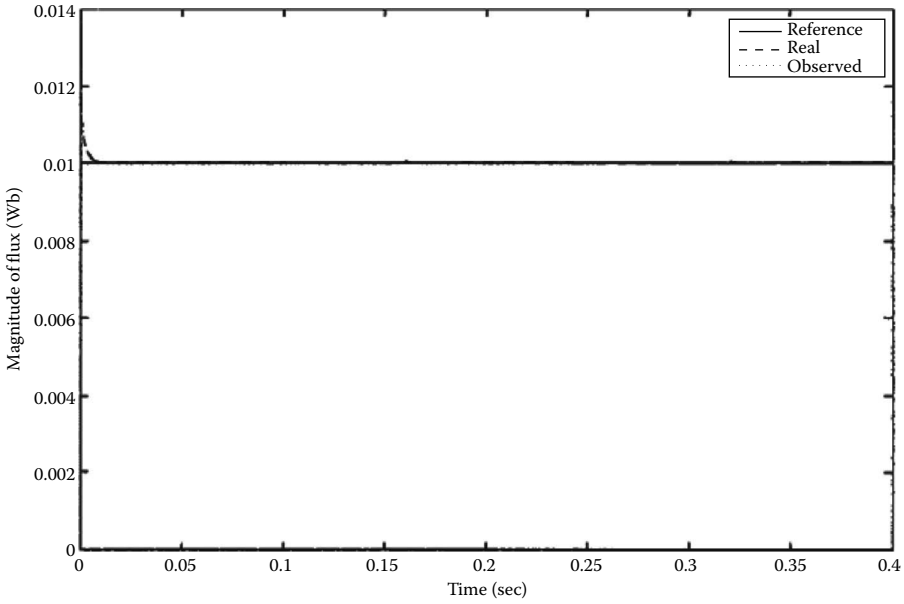

FIGURE 10.31
Magnitude of flux tracking: reference λ^*, real $\|\lambda\|$, and observed $\|\hat{\lambda}\|$.

the verification and comparison of the speed estimation; cables for connecting the whole analog/digital signals; and AC current sensors.

The torque control is executed every 100 μsec, which serves the insulated gate bipolar transistor (IGBT) inverter with a switching frequency of 10.5 kHz. Because the system was tested without load, we had to apply a sign-varying torque reference input.

To verify and compare the estimated flux of our sliding mode observer without using a rotor speed sensor, the reduced-ordered observer (Equation 10.3.24) with rotor speed sensor is used, because direct measurement of rotor flux is generally not possible. Figure 10.40 shows the result of the experiment in which only the torque/flux controller is implemented while the speed is measured by the optical sensor. $\hat{\tau}$ is defined as $\hat{\tau} = P(3/2)(L_h/L_r)(i_\beta \hat{\lambda}_\alpha - i_\alpha \hat{\lambda}_\beta)$. The rotor flux is from the reduced-ordered observer with known rotor speed. Figure 10.41 shows the flux estimations of the fourth-order sliding mode observer (Equation 10.3.37). We also compare them with the flux estimation from the reduced-ordered observer. Figure 10.42 shows the results for the system with both the torque/flux controller and sliding mode observer working together. In this case, we do not need to use the optical sensor to obtain the speed, i.e., we implemented the real sensorless control. All the variables needed for the controller implementation, such as flux components, their derivatives, and rotor speed, are obtained from the sliding mode observer.

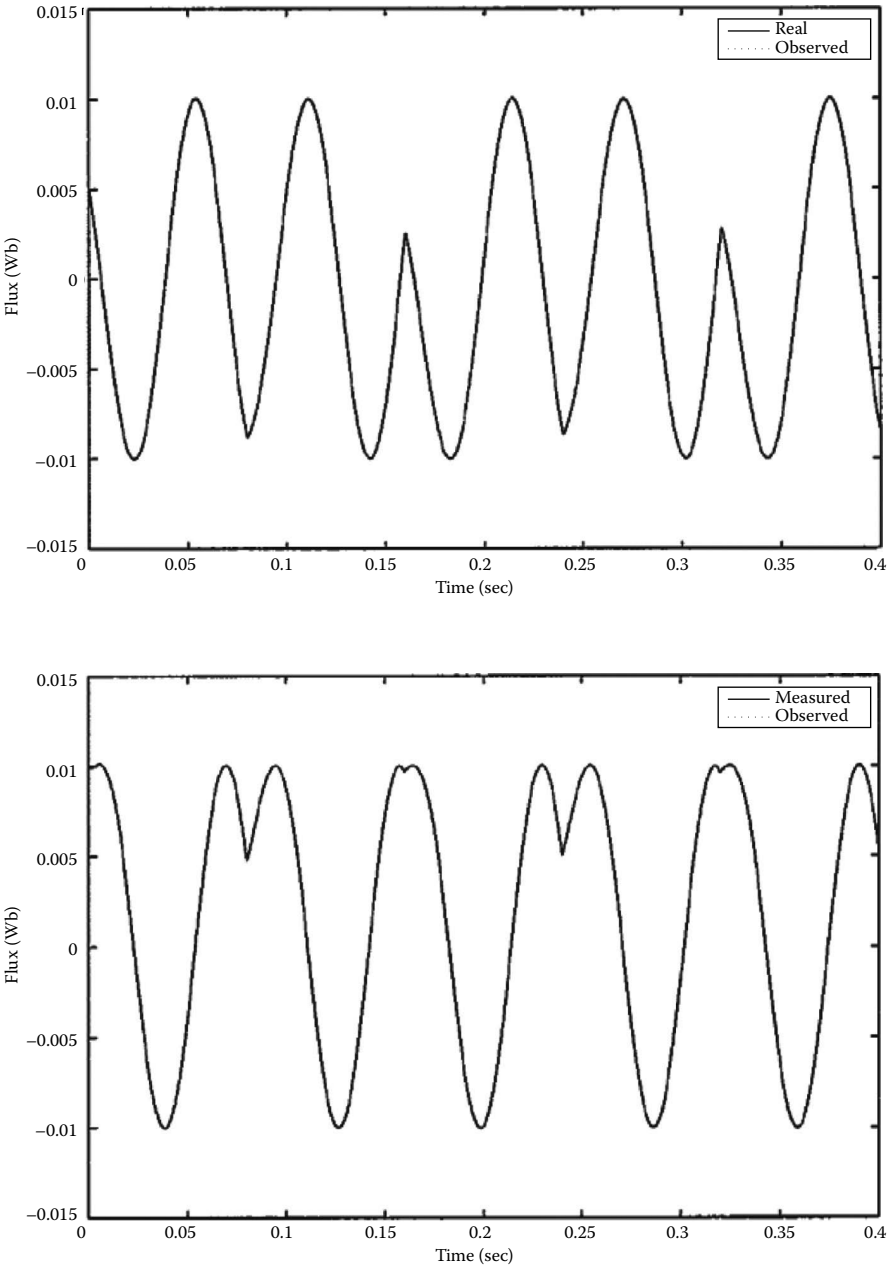

FIGURE 10.32
Flux convergence: observed $\hat{\lambda}_\alpha$ and real λ_α (upper plot) and observed $\hat{\lambda}_\beta$ and real λ_β (lower plot).

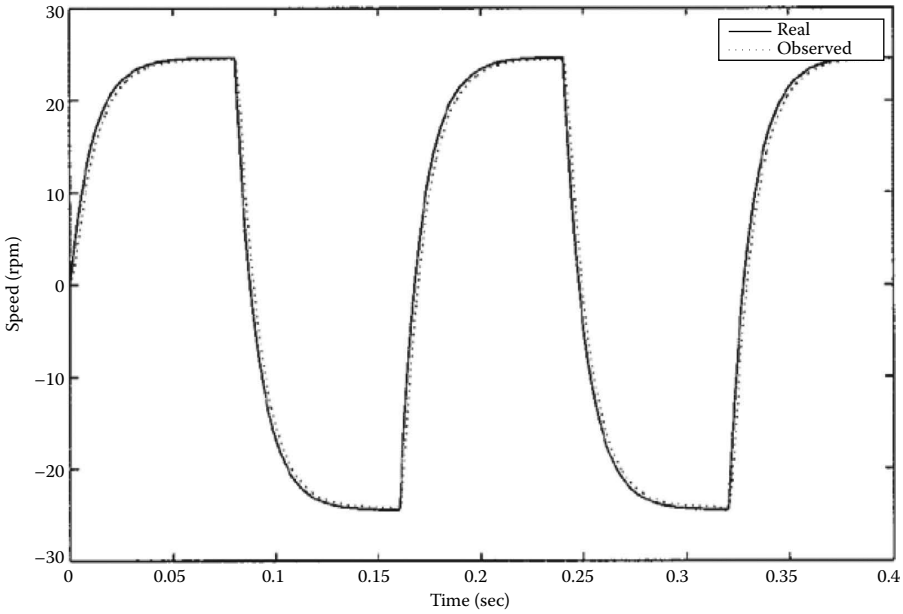

FIGURE 10.33
Speed estimation: observed speed ω_{e_eq} and real speed ω_e.

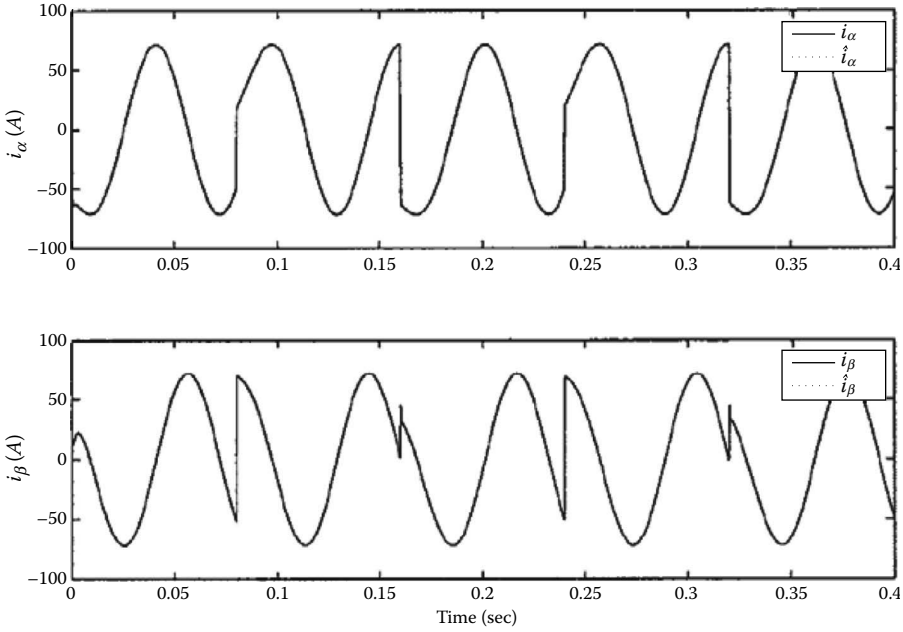

FIGURE 10.34
Current convergence for stator currents: observed and real (upper plot) and observed and real (lower plot).

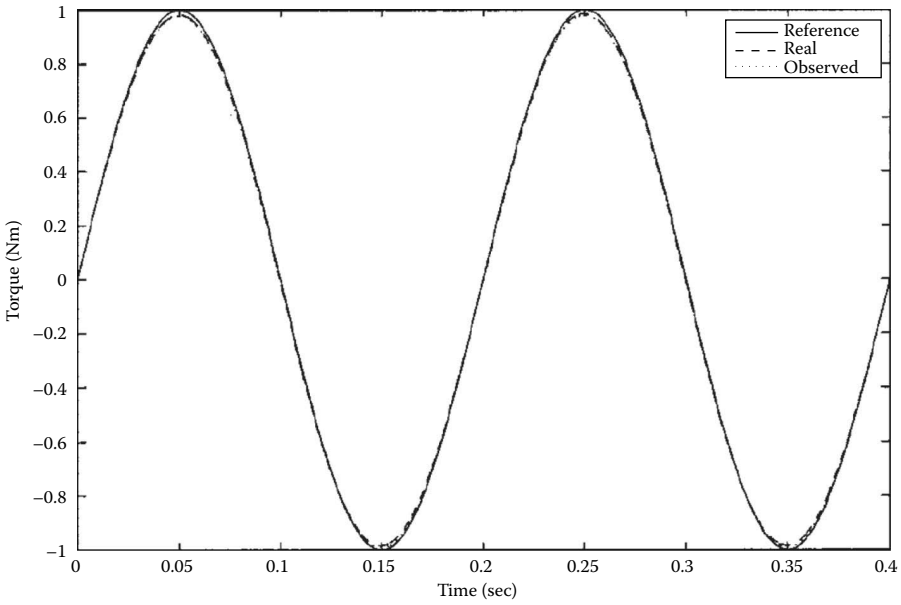

FIGURE 10.35
Torque tracking: reference τ^*, real τ, and observed $\hat{\tau}$.

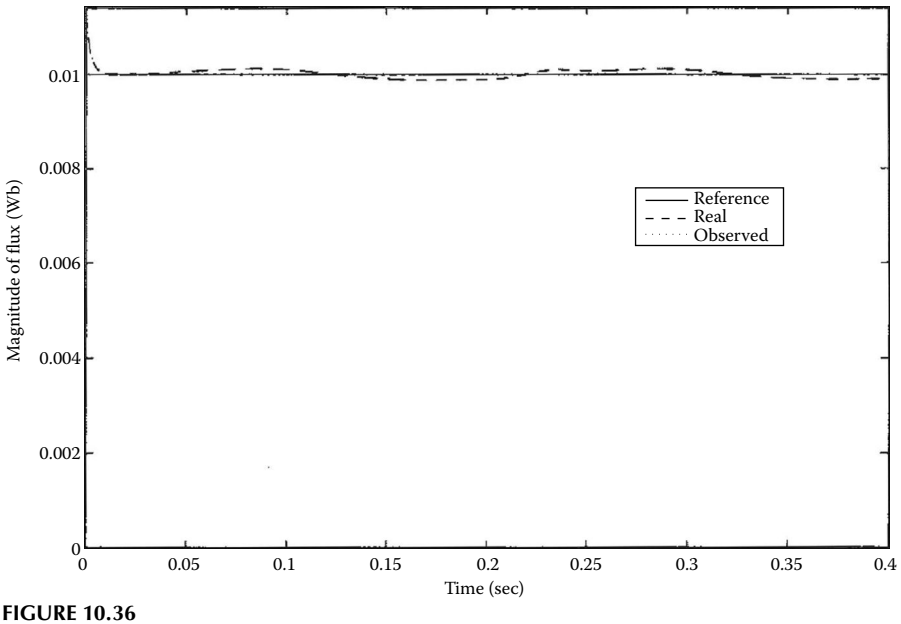

FIGURE 10.36
Magnitude of flux tracking: reference λ^*, real $\|\lambda\|$, and observed $\|\hat{\lambda}\|$.

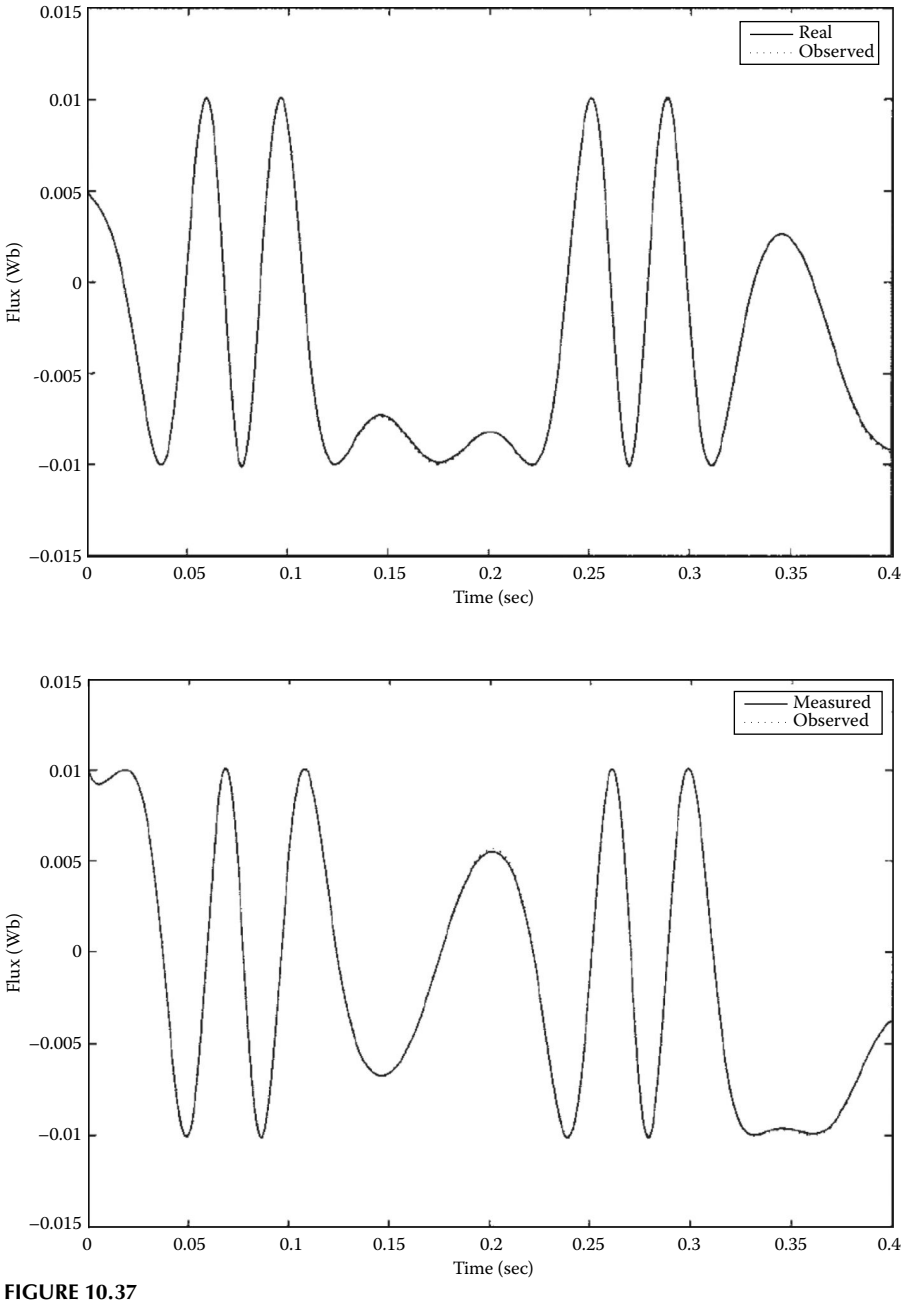

FIGURE 10.37
Flux convergence: observed $\hat{\lambda}_\alpha$ and real λ_α (upper plot) and observed $\hat{\lambda}_\beta$ and real λ_β (lower plot).

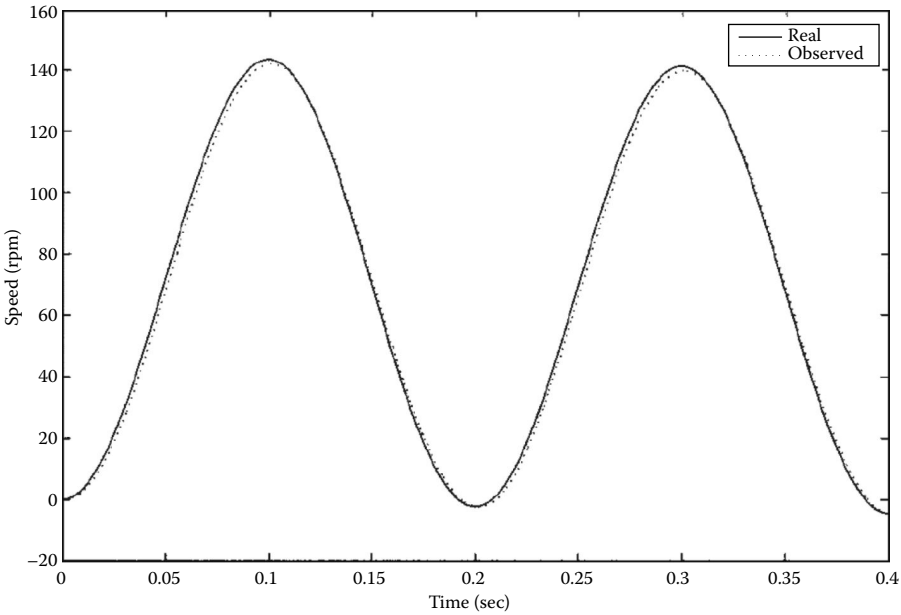

FIGURE 10.38
Speed estimation: observed speed ω_{e_eq} and real speed ω_e.

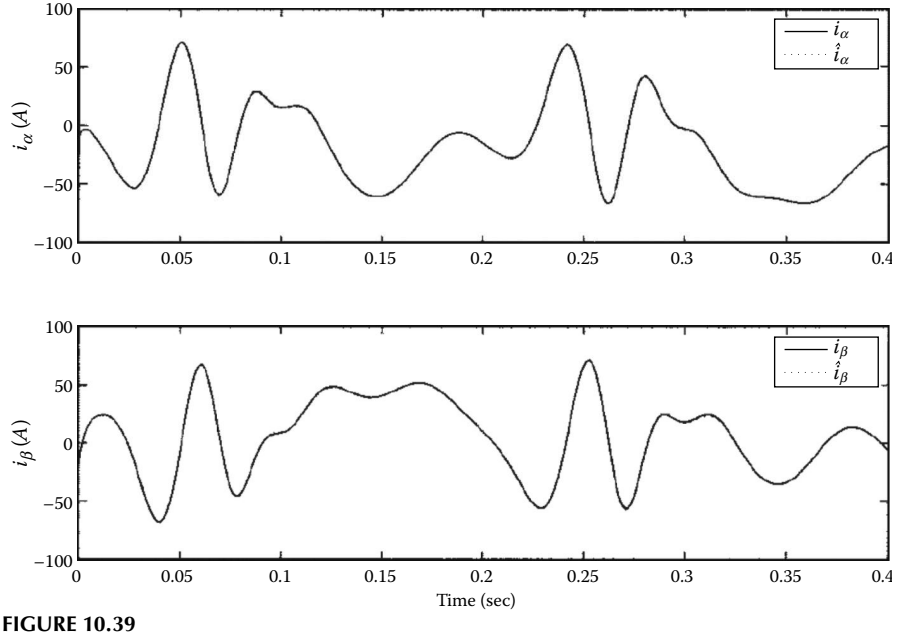

FIGURE 10.39
Current convergence for stator currents: observed and real (upper plot) and observed and real (lower plot).

TABLE 10.3
Parameters of the Induction Motor Used in Experiment

5 Hp	$R_s = 0.6\Omega$
4 poles	$R_r = 0.412\Omega$
14.8 A	$L_s = 0.0431H$
60 Hz	$L_r = 0.0431H$
1720 rpm	$L_h = 0.0412H$

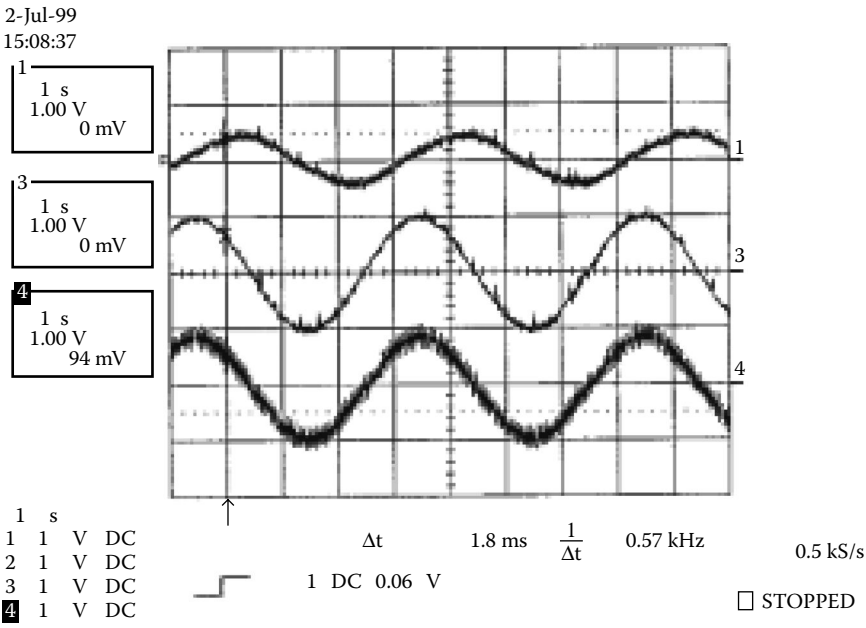

FIGURE 10.40
Torque control with speed sensor. Curve 1, ω_e; curve 3, $10\tau^*$; curve 4, 10τ.

In the experiment, the rotor speed control was also implemented. Speed control can be achieved based on the torque control using a cascaded structure. For the case of zero load, $d\omega_e/dt = (P/J)\tau$. As shown in the simulation and the experiment, the estimate ω_{e_eq} tends to ω_e; therefore, if the torque is set as $\tau = k(\omega_{e\_eq} - \omega_e^*)$, then $d\omega_e/dt = (kP/J)(\omega_{e\_eq} - \omega_e^*)$ and the motor speed converges to ω_e^* exponentially with the rate determined by the parameter kP/J. Figure 10.43 shows the case in which the speed is constant, and Figure 10.44 shows the case with time-varying speed reference input.

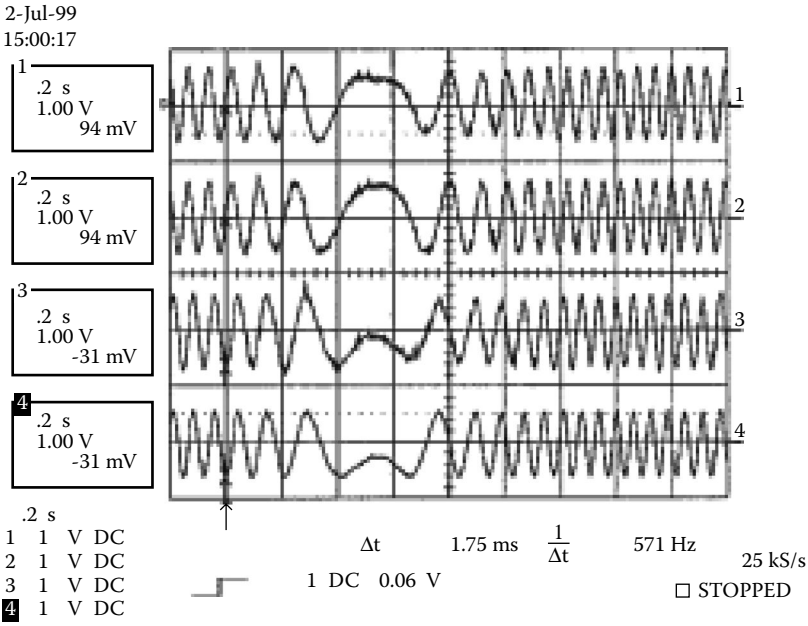

FIGURE 10.41
Flux estimation. Curves 1 and 3, $\hat{\lambda}_\alpha$ and $\hat{\lambda}_\beta$ from observer with speed sensor. Curves 2 and 4, $\hat{\lambda}_\alpha$ and $\hat{\lambda}_\beta$ from SM observer without speed sensor. SM, sliding mode observer.

10.3.5. Speed, Rotor Time Constant Observer, and Experimental Results

This section describes a new closed-loop approach to estimate the induction motor speed and rotor time constant from measured terminal voltages and stator currents [see also Derdiyok, Yan, Guven, and Utkin 2001]. A new state space system is defined without explicitly involving the flux information of the motor. A Lyapunov function is derived to determine the motor speed and the rotor time constant simultaneously, under the condition that these two quantities are unknown constant parameters. The rotor time constant estimation is useful to compensate the rotor resistance variation, especially in field-oriented control of induction motors. The proposed algorithms are validated by both simulation and experiment.

The stator current equations in the orthogonal stator frame ((α, β) coordinates) can be rewritten as follows:

$$\begin{aligned}\frac{di_\alpha}{dt} &= \beta\eta\lambda_\alpha + \beta\omega_e\lambda_\beta - \left(\frac{R_s}{\sigma L_s} + \beta L_h\eta\right)i_\alpha + \frac{1}{\sigma L_s}u_\alpha \\ \frac{di_\beta}{dt} &= \beta\eta\lambda_\beta - \beta\omega_e\lambda_\alpha - \left(\frac{R_s}{\sigma L_s} + \beta L_h\eta\right)i_\beta + \frac{1}{\sigma L_s}u_\beta\end{aligned} \quad . \tag{10.3.65}$$

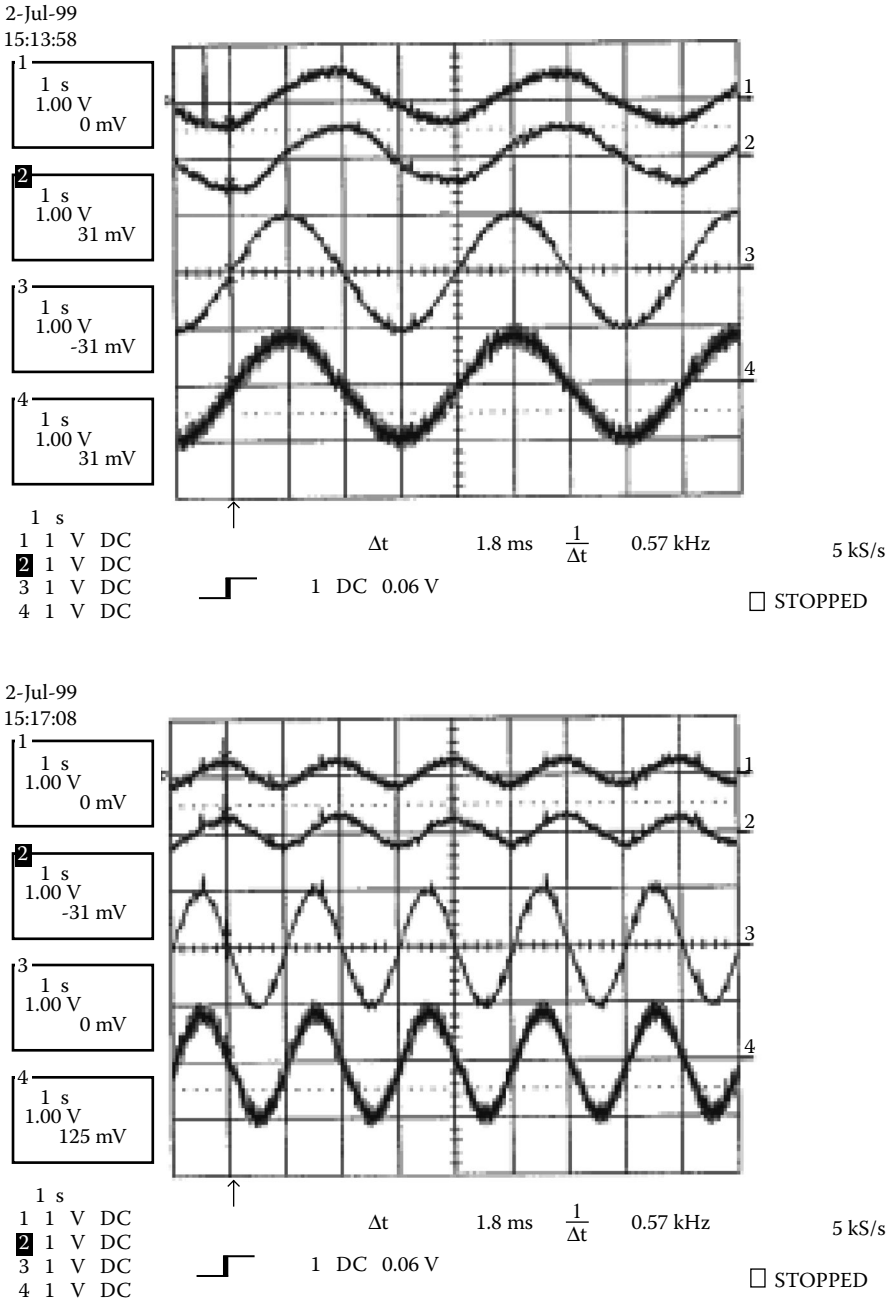

FIGURE 10.42
Sensorless torque control. Curve 1, ω_e from sensor; curve 2, ω_{e_eq} from observer; curve 3, $10\tau^*$; curve 4, $10\hat{\tau}$. Top plot, Case 1 (period time is 4 sec); bottom plot, case 2 (period is 2 sec).

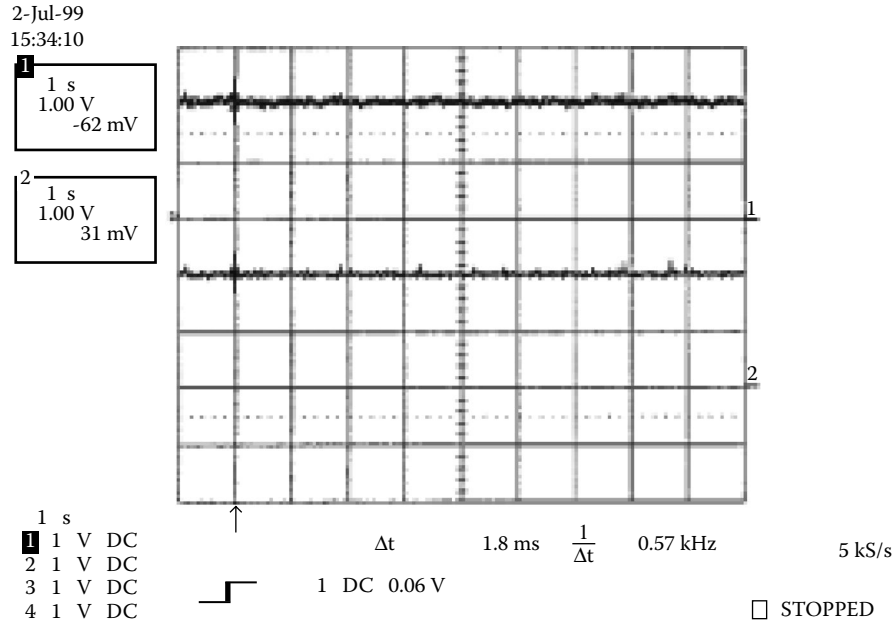

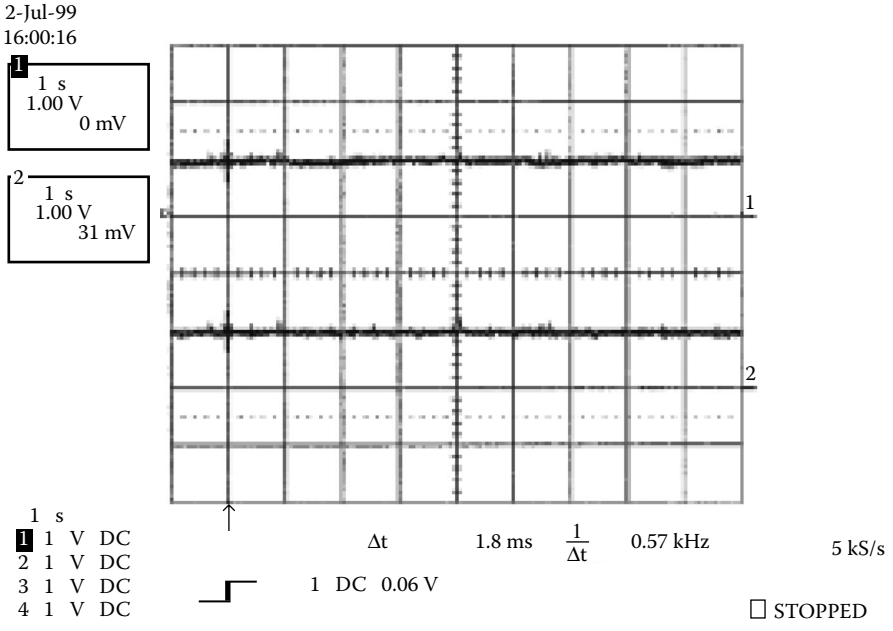

FIGURE 10.43
Sensorless speed control. Curve 1, ω_e; curve 2, ω_{e_eq}. Top plot, Case 1, $\omega_e^* = 0.2$ (600*r*/min); bottom plot, case 2, $\omega_e^* = 0.1$ (300*r*/min).

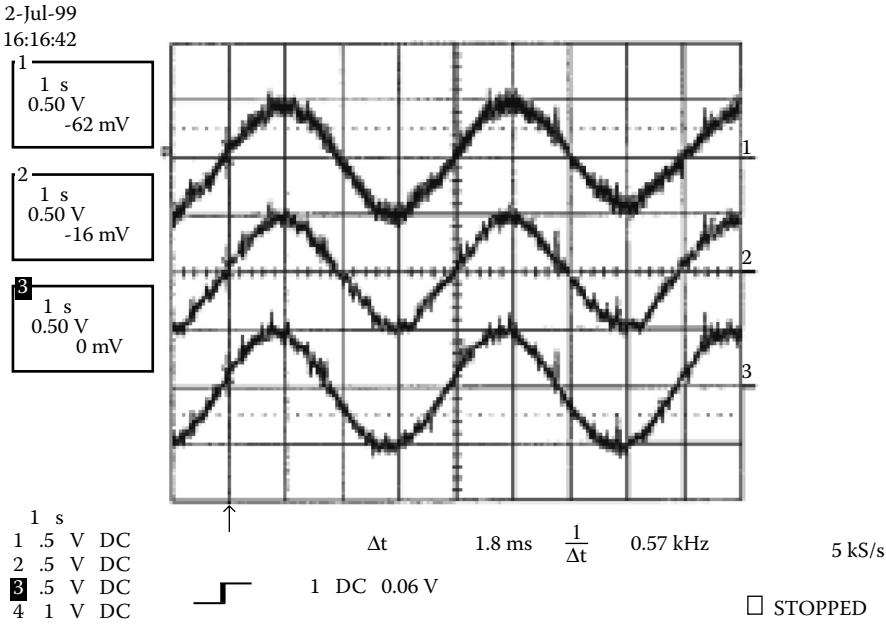

FIGURE 10.44
Sensorless speed control. Curve 1, ω_e; curve 2, ω_{e_eq}; curve 3, ω_e^*. Case 3, $\omega_e^* = 0.05 \sin[(\pi/2)t]$.

This form of equations is required because the rotor time constant η is now treated explicitly. These equations are obtained by substituting γ into the induction motor model (see Equations 10.3.5 and 10.3.6).

First, a stator current observer is designed with associated known parameters

$$\begin{aligned} \frac{d\hat{i}_\alpha}{dt} &= -\frac{R_s}{\sigma L_s} i_\alpha + \frac{1}{\sigma L_s} u_\alpha + V_\alpha \\ \frac{d\hat{i}_\beta}{dt} &= -\frac{R_s}{\sigma L_s} i_\beta + \frac{1}{\sigma L_s} u_\beta + V_\beta \end{aligned}, \tag{10.3.66}$$

where $\hat{i}_\alpha$, $\hat{i}_\beta$ are estimates of the two current components. V_α and V_β are discontinuous functions of the current errors

$$\begin{aligned} V_\alpha &= -V_0 sign(s_\alpha) = -V_0 sign(\hat{i}_\alpha - i_\alpha) \\ V_\beta &= -V_0 sign(s_\beta) = -V_0 sign(\hat{i}_\beta - i_\beta). \end{aligned} \tag{10.3.67}$$

It will be shown that there exists a constant value V_0 such that sliding mode occurs in the surfaces $s_\alpha = 0$ and $s_\beta = 0$. As a result, the estimation errors

$$\bar{i}_\alpha = \hat{i}_\alpha - i_\alpha, \quad \bar{i}_\beta = \hat{i}_\beta - i_\beta \tag{10.3.68}$$

tend to zero in finite time. Combining the above equations, the current estimation errors can be derived as

$$\begin{aligned}\frac{d\bar{i}_\alpha}{dt} &= V_\alpha - \beta\eta\lambda_\alpha - \beta\omega_e\lambda_\beta - \frac{R_s}{\sigma L_s}\bar{i}_\alpha + \beta L_h\eta i_\alpha \\ \frac{d\bar{i}_\beta}{dt} &= V_\beta - \beta\eta\lambda_\beta + \beta\omega_e\lambda_\alpha - \frac{R_s}{\sigma L_s}\bar{i}_\beta + \beta L_h\eta i_\beta.\end{aligned} \tag{10.3.69}$$

To find the discontinuous controls such that sliding mode is enforced in the manifolds $s_\alpha = 0$ and $s_\beta = 0$, select Lyapunov function candidate $V = \frac{1}{2}(s_\alpha^2 + s_\beta^2)$. Its time derivative along the state trajectories of system Equation 10.3.69 can be written as

$$\begin{aligned}\dot{V} &= s_\alpha\dot{s}_\alpha + s_\beta\dot{s}_\beta \\ &= s_\alpha\left(-V_0 sign(s_\alpha) - \beta\eta\lambda_\alpha - \beta\omega_e\lambda_\beta - \frac{R_s}{\sigma L_s}\bar{i}_\alpha + \beta L_h\eta i_\alpha\right) \\ &\quad + s_\beta\left(-V_0 sign(s_\beta) - \beta\eta\lambda_\beta + \beta\omega_e\lambda_\alpha - \frac{R_s}{\sigma L_s}\bar{i}_\beta + \beta L_h\eta i_\beta\right) \\ &= -V_0(|s_\alpha| + |s_\beta|) - \frac{R_s}{\sigma L_s}(s_\alpha^2 + s_\beta^2) + s_\alpha f_\alpha(t) + s_\beta f_\beta(t),\end{aligned} \tag{10.3.70}$$

where $f_\alpha(t)$ and $f_\beta(t)$ are continuous functions of the motor states i_α, i_β, λ_α, λ_β and ω_e but not dependent on the control signals V_α and V_β.

It is obvious that, if V_0 is large enough, $\dot{V} < 0$ can be guaranteed, i.e., sliding mode will occur in the intersection of the surfaces $s_\alpha = 0$ and $s_\beta = 0$. Hence, the estimated currents $\hat{i}_\alpha$ and $\hat{i}_\beta$ will converge to the real ones after sliding mode occurs.

As next step, the equivalent control of V_α and V_β will be investigated and associated auxiliary state variables are introduced. As we know from the previous sections, once sliding mode occurs, the equivalent control components, V_{α_eq} and V_{β_eq} can be obtained by setting $\dot{s}_\alpha = 0$ and $\dot{s}_\beta = 0$:

$$\begin{aligned}V_{\alpha\_eq} &= \beta\eta\lambda_\alpha + \beta\omega_e\lambda_\beta - \beta L_h\eta i_\alpha \\ V_{\beta\_eq} &= \beta\eta\lambda_\beta - \beta\omega_e\lambda_\alpha - \beta L_h\eta i_\beta.\end{aligned} \tag{10.3.71}$$

In practice, V_{α_eq} and V_{β_eq} cannot be calculated directly by the above two equations because they contain unknown information in the right-hand side. In fact, the two discontinuous controls V_α and V_β have slow and fast components, where the slow components are corresponding to V_{α_eq} and V_{β_eq}. As usually done in the previous sections, V_{α_eq} and V_{β_eq} can be obtained through a low-pass filter with discontinuous values V_α and V_β as the inputs, i.e.,

$$\begin{aligned}\mu\dot{z}_\alpha + z_\alpha &= V_\alpha, \quad & z_\alpha &\approx V_{\alpha\_eq}\\ \mu\dot{z}_\beta + z_\beta &= V_\beta, \quad & z_\beta &\approx V_{\beta\_eq},\end{aligned} \tag{10.3.72}$$

where μ is the time constant of the low-pass filters, which should be chosen small compared with the slow component of the real values V_α and V_β but large enough to filter out the high-frequency components. The output z_α and z_β of the low-pass filters are taken as V_{α_eq} and V_{β_eq}, respectively. Because z_α and z_β can be obtained directly, from now on we assume that V_{α_eq} and V_{β_eq} are available.

For the notation convenience, let us introduce auxiliary state variables $L_\alpha = V_{\alpha\_eq}$ and $L_\beta = V_{\beta\_eq}$ with unit $Volt{\cdot}H^{-1}$ (voltage/inductance). It is reasonable to assume that $\dot{\omega}_e = 0$ and $\dot{\eta} = 0$ because they vary much slower than the electrical variables such as stator currents and rotor flux. Hence,

$$\begin{aligned}\dot{L}_\alpha &= \beta\eta\dot{\lambda}_\alpha + \beta\omega_e\dot{\lambda}_\beta - \beta L_h\eta\dot{i}_\alpha\\ \dot{L}_\beta &= \beta\eta\dot{\lambda}_\beta - \beta\omega_e\dot{\lambda}_\alpha - \beta L_h\eta\dot{i}_\beta.\end{aligned} \tag{10.3.73}$$

Comparing the rotor flux model Equation 10.3.5 with Equation 10.3.71, it is obvious that

$$\dot{\lambda}_\alpha = -L_\alpha/\beta, \quad \dot{\lambda}_\beta = -L_\beta/\beta. \tag{10.3.74}$$

Substituting Equation 10.3.74 into Equation 10.3.73 yields the dynamics of L_α and L_β:

$$\begin{bmatrix}\dot{L}_\alpha\\ \dot{L}_\beta\end{bmatrix} = -\begin{bmatrix}\eta & \omega_e\\ -\omega_e & \eta\end{bmatrix}\begin{bmatrix}L_\alpha\\ L_\beta\end{bmatrix} - \beta L_h\eta\begin{bmatrix}\dot{i}_\alpha\\ \dot{i}_\beta\end{bmatrix}. \tag{10.3.75}$$

Finally, we are able to design the observer for L_α and L_β as well as the desired adaptation law for η and ω_e. The observer for L_α and L_β can be designed as

$$\begin{bmatrix}\dot{\hat{L}}_\alpha\\ \dot{\hat{L}}_\beta\end{bmatrix} = -\begin{bmatrix}\hat{\eta} & \hat{\omega}_e\\ -\hat{\omega}_e & \hat{\eta}\end{bmatrix}\begin{bmatrix}L_\alpha\\ L_\beta\end{bmatrix} - \beta L_h\hat{\eta}\begin{bmatrix}\dot{i}_\alpha\\ \dot{i}_\beta\end{bmatrix} - K\begin{bmatrix}\bar{L}_\alpha\\ \bar{L}_\beta\end{bmatrix}, \tag{10.3.76}$$

where $\hat{\eta}$, $\hat{\omega}_e$ are the estimates of η, ω_e and will be determined by an adaptation law, K is a positive constant to be chosen, and $\bar{L}_\alpha = \hat{L}_\alpha - L_\alpha$ and $\bar{L}_\beta = \hat{L}_\beta - L_\beta$ denote the observer errors.

Then the error dynamics read as follows:

$$\begin{bmatrix}\dot{\bar{L}}_\alpha\\ \dot{\bar{L}}_\beta\end{bmatrix} = -\begin{bmatrix}\bar{\eta} & \bar{\omega}_e\\ -\bar{\omega}_e & \bar{\eta}\end{bmatrix}\begin{bmatrix}L_\alpha\\ L_\beta\end{bmatrix} - \beta L_h\bar{\eta}\begin{bmatrix}\dot{i}_\alpha\\ \dot{i}_\beta\end{bmatrix} - K\begin{bmatrix}\bar{L}_\alpha\\ \bar{L}_\beta\end{bmatrix}. \tag{10.3.77}$$

Let us select the Lyapunov function candidate

$$V = \frac{1}{2}\bar{L}_\alpha^2 + \frac{1}{2}\bar{L}_\beta^2 + \frac{1}{2}\bar{\omega}_e^2 + \frac{1}{2}\bar{\eta}^2 \geq 0. \tag{10.3.78}$$

Combined with Equation 10.3.77, the time derivative of V is obtained as

$$\begin{aligned}\dot{V} &= \bar{L}_\alpha\dot{\bar{L}}_\alpha + \bar{L}_\beta\dot{\bar{L}}_\beta + \bar{\omega}_e\dot{\bar{\omega}}_e + \bar{\eta}\dot{\bar{\eta}} \\ &= \bar{\omega}_e\dot{\bar{\omega}}_e + \bar{\eta}\dot{\bar{\eta}} - K\bar{L}_\alpha^2 - K\bar{L}_\beta^2 + \bar{L}_\alpha(-\bar{\eta}L_\alpha - \bar{\omega}_e L_\beta - \beta L_h\bar{\eta}\dot{i}_\alpha) \\ &\quad + \bar{L}_\beta(\bar{\omega}_e L_\alpha - \bar{\eta}L_\beta - \beta L_h\bar{\eta}\dot{i}_\beta).\end{aligned} \tag{10.3.79}$$

To eliminate the unknown terms $\bar{\omega}_e$ and $\bar{\eta}$ in the right-hand side of $\dot{V}$, the adaptation law can be selected as

$$\begin{bmatrix}\dot{\hat{\eta}} \\ \dot{\hat{\omega}}_e\end{bmatrix} = \begin{bmatrix}\dot{\bar{\eta}} \\ \dot{\bar{\omega}}_e\end{bmatrix} = \begin{bmatrix}L_\alpha + \beta L_h\dot{i}_\alpha & L_\beta + \beta L_h\dot{i}_\beta \\ L_\beta & -L_\alpha\end{bmatrix}\begin{bmatrix}\bar{L}_\alpha \\ \bar{L}_\beta\end{bmatrix}. \tag{10.3.80}$$

In this case, $\dot{V}$ becomes

$$\dot{V} = -K(\bar{L}_\alpha^2 + \bar{L}_\beta^2) \leq 0, \tag{10.3.81}$$

which means that, under the adaptation law (Equation 10.3.80), the Lyapunov function V is diminishing until

$$\bar{L}_\alpha = 0, \quad \bar{L}_\beta = 0. \tag{10.3.82}$$

From Equations 10.3.80 and 10.3.82, we know $\dot{\bar{\omega}}_e = 0$ and $\dot{\bar{\eta}} = 0$, which means $\bar{\omega}_e$ and $\bar{\eta}$ are constant values. Conversely, substituting Equation 10.3.82 into Equation 10.3.77, we get

$$\begin{bmatrix}\bar{\eta} & \bar{\omega}_e \\ -\bar{\omega}_e & \bar{\eta}\end{bmatrix}\begin{bmatrix}L_\alpha \\ L_\beta\end{bmatrix} + \beta L_h\bar{\eta}\begin{bmatrix}\dot{i}_\alpha \\ \dot{i}_\beta\end{bmatrix} = \begin{bmatrix}0 \\ 0\end{bmatrix}, \tag{10.3.83}$$

which is equivalent to

$$\begin{bmatrix}L_\alpha + \beta L_h\dot{i}_\alpha & L_\beta \\ L_\beta + \beta L_h\dot{i}_\beta & -L_\alpha\end{bmatrix}\begin{bmatrix}\bar{\eta} \\ \bar{\omega}_e\end{bmatrix} = \begin{bmatrix}0 \\ 0\end{bmatrix}. \tag{10.3.84}$$

Because terms $L_\alpha + \beta L_h\dot{i}_\alpha$, L_β, $L_\beta + \beta L_h\dot{i}_\beta$, and L_α are all functions with respect to time and are not proportional to each other, they are linearly independent

time functions. As a result, the solution of Equation 10.3.84 will be $\bar{\eta} = 0$ and $\bar{\omega} = 0$, implying that $\hat{\eta} = \eta$ and $\hat{\omega}_e = \omega_e$.

The system is summarized as follows. For the observer (Equation 10.3.76), under the adaptation law (Equation 10.3.80), the estimated rotor speed and rotor time constant will converge to their real values.

The proposed observer was verified by simulation and experiment. The parameters of the induction motor used for the simulation and the experiment were taken from a real induction motor, which is a Westinghouse 5 hp, 220 V, Y-connected, four-pole induction machine, as listed in Table 10.4. The performance of the observer is verified by using it in an open loop, i.e., in the feedback loop, the actual speed from an encoder is used and the observer structure works parallel to the overall system without affecting the closed-loop system. The closed-loop system follows the commanded reference trajectories (in the speed control loop, a PI controller is used). The observer estimates the speed and the rotor time constant of the motor in parallel to the control loop.

Here only the experimental results are presented. The proposed algorithm was tested at the experiment environment in the PEEM Laboratory of The Ohio State University. The experimental results for different commanded speed trajectories in Figures 10.45 through 10.55 show that the observer system works satisfactorily in the experiment. For more details of the proposed observer system in this subsection, readers are referred to the work of Derdiyok, Yan, Guven, and Utkin [2001].

10.3.6 Direct Torque and Flux Control

In this section, the motor torque and the amplitude of rotor flux will be controlled directly by the inverter On-Off gating signals, without explicitly involving the stator current control and conventional PWM techniques.

TABLE 10.4
Parameters of the Induction Motor Used for the Simulation and the Experiment

5 Hp	$R_s = 0.6\Omega$
4 poles	$R_r = 0.412\Omega$
14.8 A	$L_s = 1.9\ mH$
60 Hz	$L_r = 1.9\ mH$
1800 rpm	$L_h = 41.2\ mH$

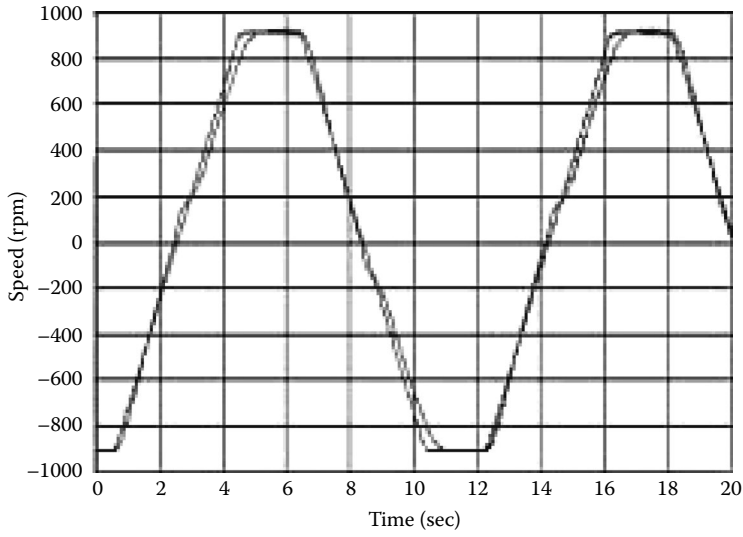

FIGURE 10.45
Measured and estimated speed.

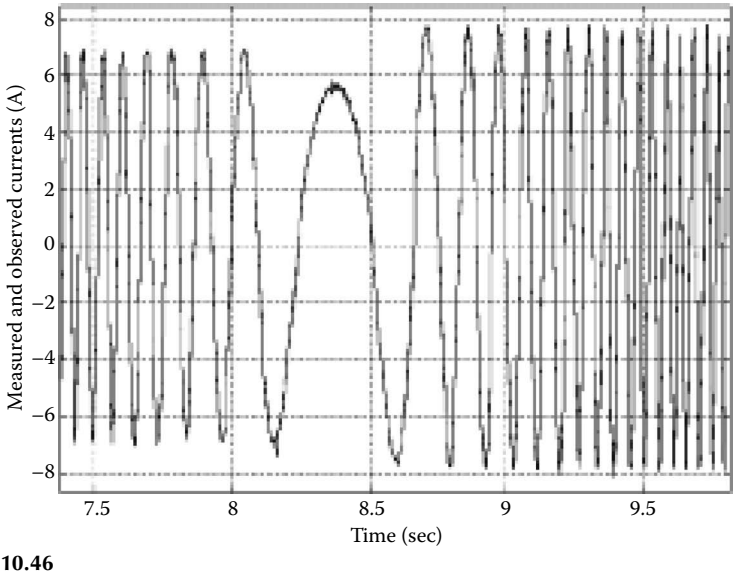

FIGURE 10.46
Measured and observed currents (between 7.5 and 9.5 sec) i_α and $\hat{i}_\alpha$.

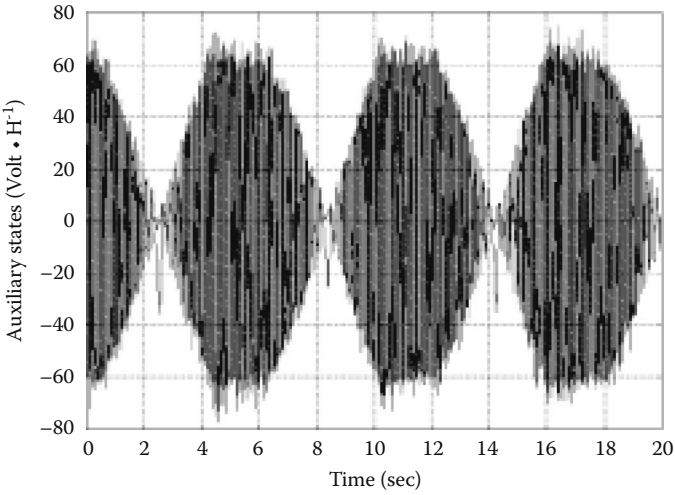

FIGURE 10.47
Calculated and observed states L_α and $\hat{L}_\alpha$.

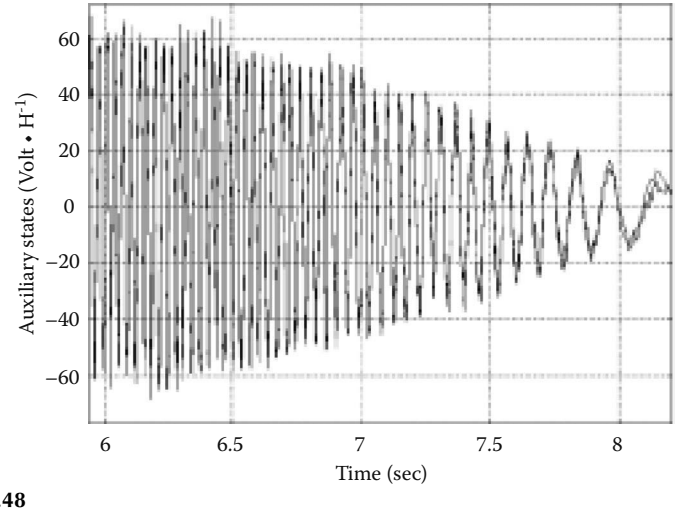

FIGURE 10.48
Enlargement of Figure 10.47 for 6-8 sec interval.

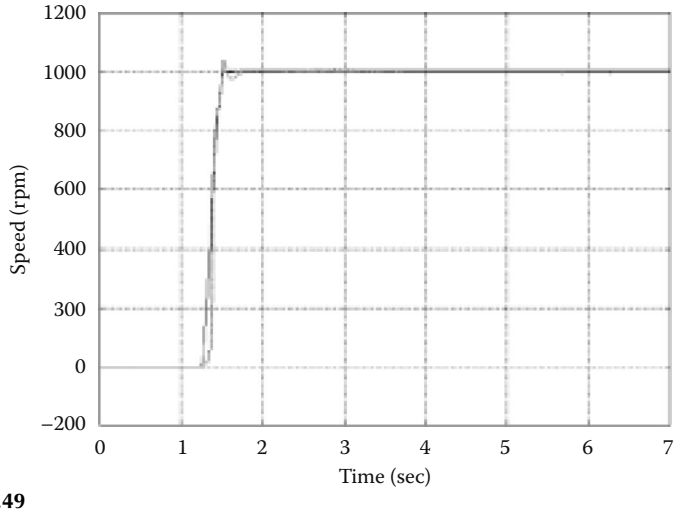

FIGURE 10.49
Measured and estimated speed.

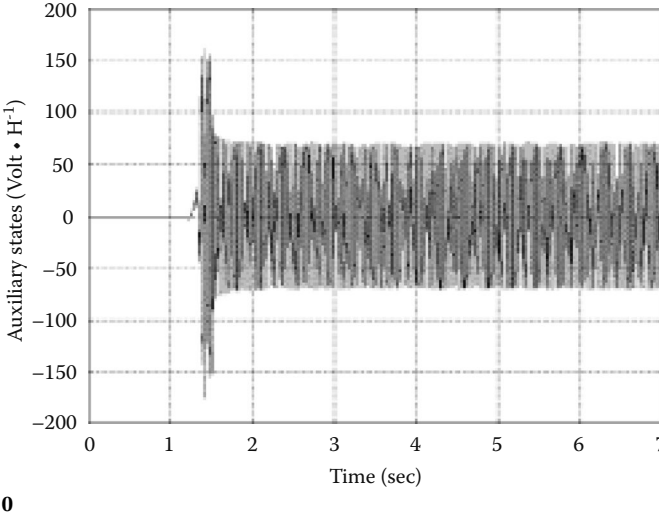

FIGURE 10.50
Calculated and observed states L_α and $\hat{L}_\alpha$.

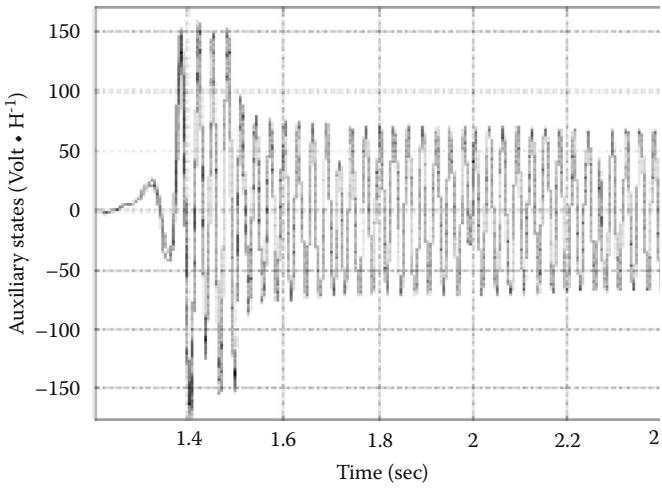

FIGURE 10.51
Enlargement of Figure 10.50 (between 1.2 and 2.4 sec).

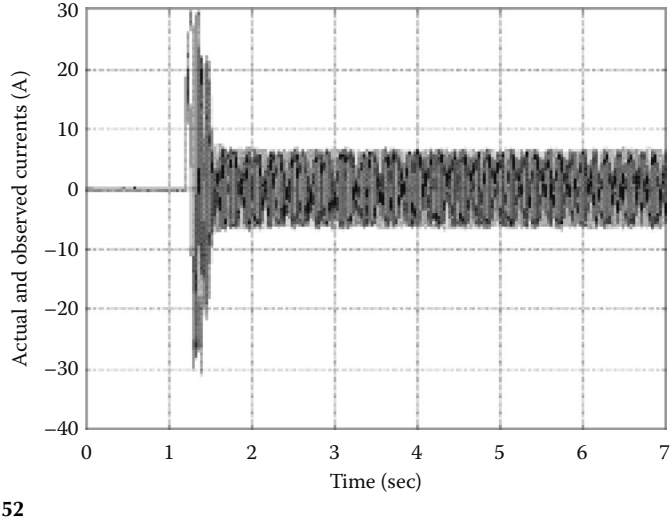

FIGURE 10.52
Measured and observed currents i_α and i_α.

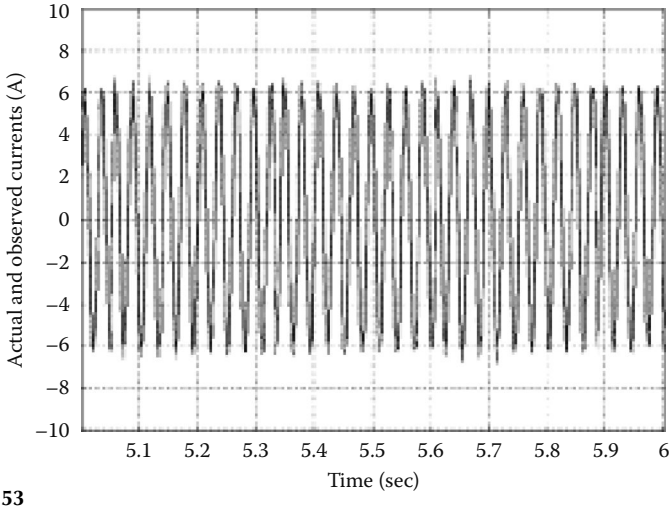

FIGURE 10.53
Enlargement of Figure 10.52 (between 5 and 6 sec).

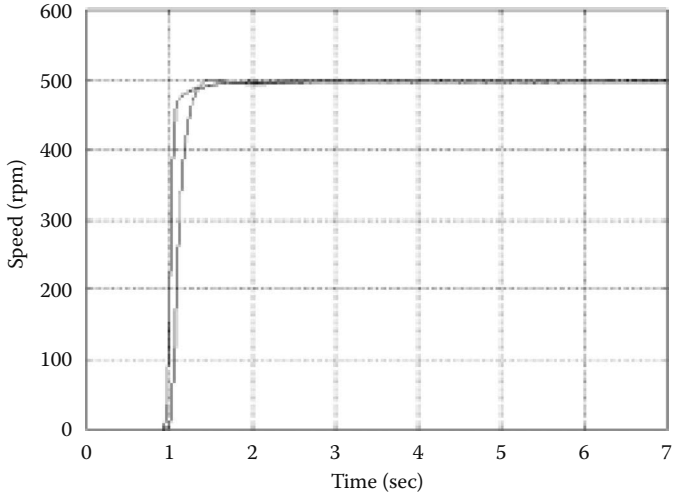

FIGURE 10.54
Measured and estimated speed.

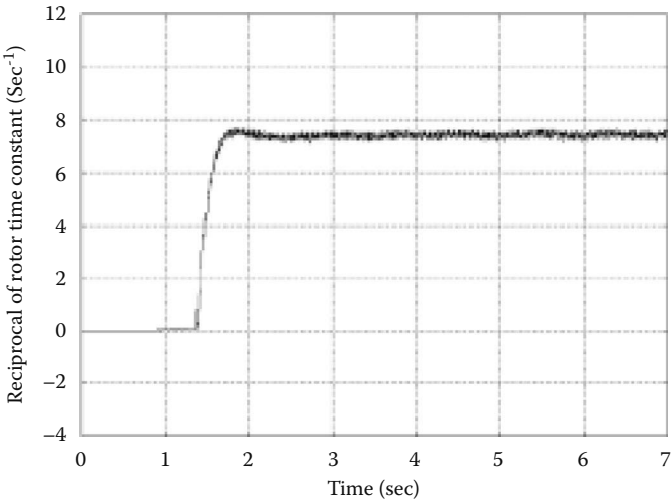

FIGURE 10.55
Estimated $\hat{\eta}$.

Let $\mathbf{S}_{\tau\lambda} = [s_\tau \; s_\lambda]^T$ be the vector contains sliding surfaces of torque and flux:

$$\begin{cases} s_\tau &= \tau - \tau^* \\ s_\lambda &= (\|\lambda\| - \lambda^*)c + (\left\|\dot{\lambda}\right\| - \dot{\lambda}^*) \end{cases} \tag{10.3.85}$$

where $\|\lambda\| = \sqrt{\lambda_\alpha^2 + \lambda_\beta^2}$, $\left\|\dot{\lambda}\right\|$ denotes $d\|\lambda\|/dt$, c is a designed positive constant and τ^*, λ^* are the reference value of motor torque and rotor flux, respectively. If $s_\tau = 0$, then $\tau = \tau^*$ and if $s_\lambda = 0$, then λ tends to λ^* at the rate defined by c. Time derivatives of s_τ and s_λ can be obtained by substituting the induction motor model Equation 10.3.5.

$$\begin{aligned} \dot{s}_\tau &= \dot{\tau} - \dot{\tau}^* \\ &= \frac{3PL_h}{2L_r}(\dot{i}_\beta\lambda_\alpha + i_\beta\dot{\lambda}_\alpha - \dot{i}_\alpha\lambda_\beta - i_\alpha\dot{\lambda}_\beta) - \dot{\tau}^* \\ &= f_1(i_\alpha, i_\beta, \lambda_\alpha, \lambda_\beta, \omega_e, \dot{\tau}^*) + \frac{3PL_h}{2\sigma L_r L_s}(u_\beta\lambda_\alpha - u_\alpha\lambda_\beta) \end{aligned} \tag{10.3.86}$$

$$\begin{aligned} \dot{s}_\lambda &= (\left\|\dot{\lambda}\right\| - \dot{\lambda}^*)c + (\left\|\ddot{\lambda}\right\| - \ddot{\lambda}^*) \\ &= f_2(i_\alpha, i_\beta, \lambda_\alpha, \lambda_\beta, \omega_e, \dot{\lambda}^*, \ddot{\lambda}^*) + \frac{1}{\sqrt{\lambda_\alpha^2 + \lambda_\beta^2}}(u_\alpha\lambda_\alpha + u_\beta\lambda_\beta) \end{aligned} \tag{10.3.87}$$

where f_1 and f_2 are continuous nonlinear functions of all arguments (note that they are not functions of u_α and u_β), and $\left\|\ddot{\lambda}\right\|$ denotes $d^2\|\lambda\|/d^2t$. Vector $\dot{\boldsymbol{S}}_{\tau\lambda}$ can be expressed in matrix form

$$\dot{\boldsymbol{S}}_{\tau\lambda} = \begin{bmatrix} \dot{s}_\tau \\ \dot{s}_\lambda \end{bmatrix} = \boldsymbol{F} + C_1 \begin{bmatrix} -\lambda_\beta & \lambda_\alpha \\ \dfrac{\lambda_\alpha}{\sqrt{\lambda_\alpha^2+\lambda_\beta^2}} & \dfrac{\lambda_\beta}{\sqrt{\lambda_\alpha^2+\lambda_\beta^2}} \end{bmatrix} \begin{bmatrix} u_\alpha \\ u_\beta \end{bmatrix} \tag{10.3.88}$$

where $\boldsymbol{F} = [f_1\ f_2]^T$, C_1 is a diagonal matrix with elements $C_1^{11} = 3PL_h/(\sigma L_r L_s)$ and $C_1^{22} = 1$. Note that stator voltages u_α, u_β can be handled as the control inputs of the induction motor system, but they cannot be implemented directly, since only the switching elements of the inverter (they receive the PWM signals in the conventional motor control techniques) can be controlled. Thus the control inputs should be formulated in terms of phase voltages as well as of gating signals of the inverter. As follows from Equation 10.3.8, the relation between u_α, u_β and the phase voltages is

$$\begin{bmatrix} u_\alpha \\ u_\beta \end{bmatrix} = \frac{2}{3} \begin{bmatrix} 1 & -1/2 & -1/2 \\ 0 & \sqrt{3}/2 & -\sqrt{3}/2 \end{bmatrix} \begin{bmatrix} u_a \\ u_b \\ u_c \end{bmatrix} \tag{10.3.89}$$

where the phase voltages u_a, u_b, u_c are the potential differences between points a, b, c and the neutral point n, respectively, as defined in Figure 10.26.

From Equations 10.3.88 and 10.3.89,

$$\begin{aligned} \dot{\boldsymbol{S}}_{\tau\lambda} = \begin{bmatrix} \dot{s}_\tau \\ \dot{s}_\lambda \end{bmatrix} &= \boldsymbol{F} + C_1 \begin{bmatrix} -\lambda_\beta & \lambda_\alpha \\ \dfrac{\lambda_\alpha}{\sqrt{\lambda_\alpha^2+\lambda_\beta^2}} & \dfrac{\lambda_\beta}{\sqrt{\lambda_\alpha^2+\lambda_\beta^2}} \end{bmatrix} \begin{bmatrix} u_\alpha \\ u_\beta \end{bmatrix} \\ &= \boldsymbol{F} + \frac{2}{3} C_1 \begin{bmatrix} -\lambda_\beta & \lambda_\alpha \\ \dfrac{\lambda_\alpha}{\sqrt{\lambda_\alpha^2+\lambda_\beta^2}} & \dfrac{\lambda_\beta}{\sqrt{\lambda_\alpha^2+\lambda_\beta^2}} \end{bmatrix} \begin{bmatrix} 1 & -1/2 & -1/2 \\ 0 & \sqrt{3}/2 & -\sqrt{3}/2 \end{bmatrix} \begin{bmatrix} u_a \\ u_b \\ u_c \end{bmatrix} \\ &= \boldsymbol{F} + \frac{2}{3} C_1 \begin{bmatrix} -\lambda_\beta & \left(\dfrac{\lambda_\beta+\sqrt{3}\lambda_\alpha}{2}\right) & \left(\dfrac{\lambda_\beta-\sqrt{3}\lambda_\alpha}{2}\right) \\ \dfrac{\lambda_\alpha}{\sqrt{\lambda_\alpha^2+\lambda_\beta^2}} & \dfrac{-\lambda_\alpha+\sqrt{3}\lambda_\beta}{2\sqrt{\lambda_\alpha^2+\lambda_\beta^2}} & \dfrac{-\lambda_\alpha-\sqrt{3}\lambda_\beta}{2\sqrt{\lambda_\alpha^2+\lambda_\beta^2}} \end{bmatrix} \begin{bmatrix} u_a \\ u_b \\ u_c \end{bmatrix} \\ &= \boldsymbol{F} + \frac{2}{3} \begin{bmatrix} Q_1 \\ Q_2 \end{bmatrix} \end{aligned} \tag{10.3.90}$$

where $[Q_1 \;\; Q_2]^T$ is a vector that represents the product of 2×2 matrix C_1, the 2×3 matrix (depending on the flux components), and the 3×1 vector in the penultimate step in Equation 10.3.90. Now consider the Lyapunov function candidate

$$V = \frac{1}{2} S_{\tau\lambda}^T S_{\tau\lambda} \tag{10.3.91}$$

Its time derivative is

$$\begin{aligned} \dot{V} &= S_{\tau\lambda}^T \dot{S}_{\tau\lambda} \\ &= f_V + \frac{2}{3}(s_\tau Q_1 + s_\lambda Q_2) \\ &= f_V + \frac{2}{3}\begin{bmatrix}\Omega_1 & \Omega_2 & \Omega_3\end{bmatrix}\begin{bmatrix} u_a \\ u_b \\ u_c \end{bmatrix} \end{aligned} \tag{10.3.92}$$

where f_V is a continuous function of all the possible arguments, and

$$\begin{cases} \Omega_1 &= -C_1^{11}\lambda_\beta s_\tau + \dfrac{\lambda_\alpha}{\sqrt{\lambda_\alpha^2+\lambda_\beta^2}} s_\lambda \\ \Omega_2 &= C_1^{11}(\dfrac{1}{2}\lambda_\beta + \dfrac{\sqrt{3}}{2}\lambda_\alpha)s_\tau + \dfrac{-\frac{1}{2}\lambda_\alpha + \frac{\sqrt{3}}{2}\lambda_\beta}{\sqrt{\lambda_\alpha^2+\lambda_\beta^2}} s_\lambda \\ \Omega_3 &= C_1^{11}(\dfrac{1}{2}\lambda_\beta - \dfrac{\sqrt{3}}{2}\lambda_\alpha)s_\tau + \dfrac{-\frac{1}{2}\lambda_\alpha - \frac{\sqrt{3}}{2}\lambda_\beta}{\sqrt{\lambda_\alpha^2+\lambda_\beta^2}} s_\lambda \end{cases} \tag{10.3.93}$$

From Equations 10.3.3 and 10.3.4, we have

$$\begin{bmatrix} u_a \\ u_b \\ u_c \end{bmatrix} = \frac{1}{3}\begin{bmatrix} 2 & -1 & -1 \\ -1 & 2 & -1 \\ -1 & -1 & 2 \end{bmatrix}\begin{bmatrix} u_1 \\ u_2 \\ u_3 \end{bmatrix} \tag{10.3.94}$$

Note that the control variables u_1, u_2, u_3 take values from the discrete set $\{-u_0, u_0\}$ with u_0 being the DC-bus voltage (as showed in Figure 10.26).

Substitute Equation 10.3.94 into Equation 10.3.92 and denote

$$\begin{bmatrix}\Lambda_1 & \Lambda_2 & \Lambda_3\end{bmatrix}=\begin{bmatrix}\Omega_1 & \Omega_2 & \Omega_3\end{bmatrix}\begin{bmatrix}2 & -1 & -1\\ -1 & 2 & -1\\ -1 & -1 & 2\end{bmatrix} \tag{10.3.95}$$

Then $\dot{V}$ is of the form

$$\dot{V}=f_V+\frac{2}{9}(\Lambda_1 u_1+\Lambda_2 u_2+\Lambda_3 u_3) \tag{10.3.96}$$

Define the control logic signals as $g_1=u_1/u_0$, $g_2=u_2/u_0$, $g_3=u_3/u_0$ which take values from the discrete set $\{-1, 1\}$, $\dot{V}$ can be further derived as

$$\dot{V}=f_V+\frac{2}{9}u_0[(\Lambda_1)g_1+(\Lambda_2)g_2+(\Lambda_3)g_3] \tag{10.3.97}$$

Select control logic of the inverter as

$$\begin{cases} g_1 &= -\text{sign}(\Lambda_1)\\ g_2 &= -\text{sign}(\Lambda_2)\\ g_3 &= -\text{sign}(\Lambda_3)\end{cases} \tag{10.3.98}$$

resulting in

$$\dot{V}=f_V-\frac{2}{9}u_0[|\Lambda_1|+|\Lambda_2|+|\Lambda_3|] \tag{10.3.99}$$

When the DC-bus voltage $u_0>0$ has enough magnitude, $\dot{V}<0$ can be guaranteed, implying that $s_\tau=0$ and $s_\lambda=0$ in finite time. It means that the real torque is equal to the reference torque $(\tau=\tau^*)$, and $\|\lambda\|$ tends to λ^* at the desired rate c.

Finally, the On-Off signals, which take values from the discrete set $\{0, 1\}$ (with 0=Off and 1=On), can be generated based on Equation 10.3.2

$$\begin{aligned} s_{w1}&=0.5(1+g_1), & s_{w4}&=1-s_{w1},\\ s_{w2}&=0.5(1+g_2), & s_{w5}&=1-s_{w2},\\ s_{w3}&=0.5(1+g_3), & s_{w6}&=1-s_{w3}. \end{aligned} \tag{10.3.100}$$

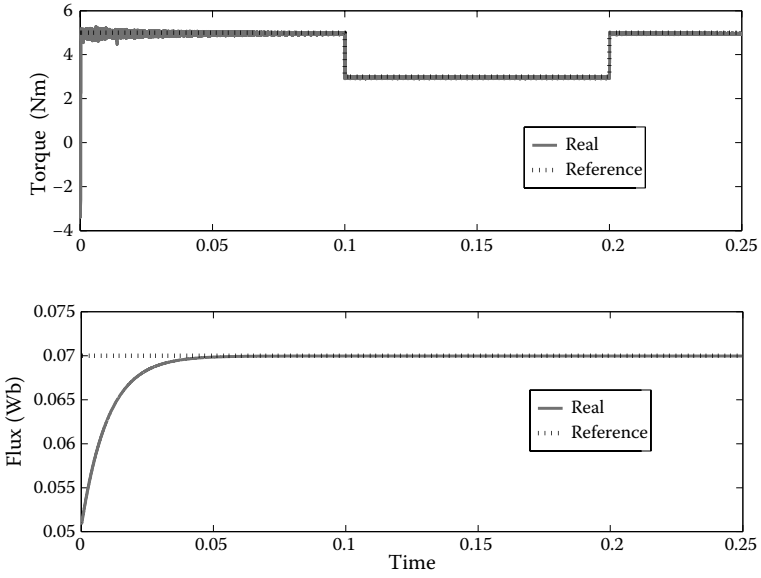

FIGURE 10.56
Torque tracking (upper plot) and flux tracking (lower plot).

These On-Off signals are illustrated in Figure 10.26. Note that in the practical implementation, s_{w4}, s_{w5}, s_{w6} should have several microsecond time delay with respect to s_{w1}, s_{w2}, s_{w3}, respectively, in order to prevent short circuits (during the switching state exchange between the upper and lower power-transistors, see Figure 10.26) in inverters such as IGBTs. In the stability proof given above, the control law Equation 10.3.98 is sensitive to the sign of the terms Λ_1, Λ_2, Λ_3. Thus some practical treatments, e.g. a hysteresis band, may be required to implement the control algorithm.

Figure 10.56 shows the simulation results of proposed torque/flux controller. The simulation uses the default motor parameters as given in 10.3.2 except that $u_0 = 50V$ instead of $u_0 = 12V$.

10.3.6.1. Supplement: Cascaded Torque and Flux Control Via Phase Currents

In the method described above, the motor torque and the amplitude of rotor flux are controlled directly by the inverter gating signals, without explicitly involving the stator current control and conventional PWM techniques. A conventional approach called "cascade control method" can be used to achieve the same goal. In the cascade method, given reference torque and reference flux, the corresponding phase currents are generated, and the latter are realized by conventional PWM or by sliding mode current control. The concept of cascade control method is sketched here without going into the details of the current control.

Suppose the reference torque and the reference flux τ^*, λ^* are given. Substituting τ^* into the torque equation of induction motor model (Equation 10.3.5), an algebraic equation of the desired torque control error can be derived as

$$F_1(i_\alpha, i_\beta, \lambda_\alpha, \lambda_\beta, \tau^*) = \tau^* - \frac{3PL_h}{2L_r}(i_\beta\lambda_\alpha - i_\alpha\lambda_\beta) = 0. \tag{10.3.101}$$

Note that, in the above equation, $i_\beta\lambda_\alpha - i_\alpha\lambda_\beta = \lambda_d i_q$, with $\lambda_d = \|\lambda\| = \sqrt{\lambda_\alpha^2 + \lambda_\beta^2}$, according to the motor model in (d, q) coordinates (Equation 10.3.11). Also, the desired flux dynamics can be given as

$$(\|\lambda\| - \lambda^*)c + \left(\|\dot{\lambda}\| - \dot{\lambda}^*\right) = 0, \tag{10.3.102}$$

which corresponds to $s_\lambda = 0$ in Equation 10.3.85. The time derivative of the flux amplitude can be calculated as

$$\|\dot{\lambda}\| = \frac{1}{\sqrt{\lambda_\alpha^2 + \lambda_\beta^2}}(\lambda_\alpha\dot{\lambda}_\alpha + \lambda_\beta\dot{\lambda}_\beta). \tag{10.3.103}$$

Substituting $\dot{\lambda}_\alpha$, $\dot{\lambda}_\beta$ from the motor model (Equation 10.3.5) into the above equation results in

$$\|\dot{\lambda}\| = -\eta\sqrt{\lambda_\alpha^2 + \lambda_\beta^2} + \eta L_h \frac{i_\alpha\lambda_\alpha + i_\beta\lambda_\beta}{\sqrt{\lambda_\alpha^2 + \lambda_\beta^2}}. \tag{10.3.104}$$

Note that this equation is actually the flux model $\dot{\lambda}_d = -\eta\lambda_d + \eta L_h i_d$ in (d, q) coordinates (see Equation 10.3.11). Substituting Equation 10.3.104 into Equation 10.3.102 results in the second algebraic equation

$$F_2(i_\alpha, i_\beta, \lambda_\alpha, \lambda_\beta, \lambda^*) = (c - \eta)\sqrt{\lambda_\alpha^2 + \lambda_\beta^2} + \eta L_h \frac{i_\alpha\lambda_\alpha + i_\beta\lambda_\beta}{\sqrt{\lambda_\alpha^2 + \lambda_\beta^2}} - (c\lambda^* + \dot{\lambda}^*) = 0. \tag{10.3.105}$$

For the equation system

$$F_1(i_\alpha, i_\beta, \lambda_\alpha, \lambda_\beta, \tau^*) = 0$$

$$F_2(i_\alpha, i_\beta, \lambda_\alpha, \lambda_\beta, \lambda^*) = 0, \tag{10.3.106}$$

the flux components λ_α, λ_β can be obtained by the flux observer (see Section 10.3.3). There are therefore two unknown variables i_α, i_β in the two equations. The solution is actually the desired i_α^*, i_β^*, corresponding to the references τ^*,

λ^*. If necessary, the corresponding values of three-phase currents i_a^*, i_b^*, i_c^* can also be found using transformation Equation 10.3.10.

Therefore, given the reference torque and reference flux, the desired currents in (α, β) coordinates and in (a, b, c) coordinates can be calculated. Then, conventional techniques can be used to control the phase currents in either (α, β) coordinates or (a, b, c) coordinates.

It should be pointed out that, technically, the desired i_α^*, i_β^* can be found through the currents components in (d, q) coordinates, i.e., i_d^*, i_q^* (see transformation Equation 10.3.14), and i_d^*, i_q^* are the solution of the following equation system:

$$\begin{aligned} \tau^* &= \frac{3PL_h}{2L_r}\lambda_d i_q^* \\ (c-\eta)\lambda_d &+ \eta L_h i_d^* - (c\lambda_d^* + \dot{\lambda}_d^*) = 0 \end{aligned} \tag{10.3.107}$$

where $\lambda_d^* = \lambda^*$ and $\lambda_d = \|\lambda\| = \sqrt{\lambda_\alpha^2 + \lambda_\beta^2}$. The above equation system is the same equation system (Equation 10.3.106) in (d, q) coordinates. Because now the two equations are decoupled, the solution for i_d^*, i_q^* is straightforward. The transformation from i_d^*, i_q^* to i_α^*, i_β^* needs rotor flux angle ρ or components sin ρ and cos ρ (see Equation 10.3.13 and 10.3.14), the latter can be obtained by

$$\begin{aligned} \sin\rho &= \frac{\lambda_\beta}{\sqrt{\lambda_\alpha^2 + \lambda_\beta^2}} \\ \cos\rho &= \frac{\lambda_\alpha}{\sqrt{\lambda_\alpha^2 + \lambda_\beta^2}} \end{aligned}. \tag{10.3.108}$$

The design approaches given above are actually the conventional rotor flux oriented control of induction motors from another point of view.

10.4. Summary

In this chapter, control algorithms for DC motors, permanent-magnet synchronous motors, and induction motors using the sliding mode design principle have been presented. Beside the advantages provided by the sliding mode approach in the sense of control techniques, this unified design principle also provides a deeper understanding of the functionality and mechanism of electric drive systems. For AC motors, the ultimate object of field-oriented control is to enable a decoupling between the motor torque and the motor flux, resulting in a system similar to a separately excited DC

motor. However, the traditional decoupling characteristic is sensitive to motor parameter variations. The design goals of sliding mode control are also given in the field-oriented coordinates, and the field orientation is realized by the switching surface transformation. Because no exact decoupling is required for sliding mode control, the resulting system is insensitive to the motor parameters and the solutions are quite simple. In this sense, sliding mode control may be considered as an extension of the traditional control techniques such as hysteresis control but with the following advantages: achieving field-oriented control performance, providing stability conditions, and extension beyond current control to outer-loop control such as speed and flux control.

Another impressive feature of sliding mode techniques is the combination with asymptotic observers and even the observer design itself. In these applications, the concept of equivalent control plays a key role. This concept originated from the observation of physical systems, providing an additional source of information to the control design and thus reducing the complexity of the overall system. Based on the concept of equivalent control, numerous estimation algorithms, i.e., observer designs, were presented in this chapter. Because the mathematical model of an electric motor matches the real motor quite well, the presented estimation algorithms open a wide range of practical applications.

References

Blaschke F. 1974. *Das Verfahren der Feldorientierung zur Regelung der Drehfeldmaschine.* Ph.D. thesis, Technische Universität Braunschweig, Braunschweig, Germany.

Blaschke F, Vandenput A, van der Burgt J. 1995. "Feldorientierung der geberlosen Drehfeldmaschine." *Elektromotoren* 21:14–23.

Derdiyok A, Yan Z, Guven M, Utkin VI. 2001. "A Sliding Mode Speed and Rotor Time Constant Observer for Induction Machines." Proceedings of the IEEE Conference on Industrial Electronics, Control, and Instrumentation, 27th Annual Conference of the IEEE Industrial Electronics Society, Denver, CO.

Filippov AF. 1961. "Application of the Theory of Differential Equations with Discontinuous Right-Hand Sides to Non-Linear Problems of Automatic Control." Proceedings of the First IFAC Congress. London: Butterworths, 923–927.

Henneberger G, Brunsbach BJ, Klepsch T. 1991. "Field-Oriented Control of Synchronous and Asynchronous Drives without Mechanical Sensors using a Kalman Filter." Proceedings of the European Conference on Power Electronics and Applications, Florence, Italy.

Isozimov DB. 1983. "Sliding Mode Nonlinear State Observer of an Induction Motor." In *Control of Multiconnected Systems* (in Russian), edited by M. V. Meerov and N. A. Kuznetsov. Moscow: Nauka, 133–139.

Jiang J, Holtz J. 1997. "High Dynamic Speed Sensorless AC Drive with On-Line Model Parameter Tuning for Steady-State Accuracy." *IEEE Trans Ind Electron* 44:240–246.

Kokotovic PV, O'Malley RB, Sannuti P. 1976. "Singular Perturbations and Order Reduction in Control Theory." *Automatica* 12:123–132.

Lorenz R. 1995. "Future Trends in Power Electronic Control of Drives: Robust, Zero Speed Sensorless Control and New Standard Approaches for Field Orientation." Proceedings of the IEEE International Conference on Power Electronics, Kurukhetra, India.

Sabanovic A, Utkin VI. 1994. "Sliding Mode Applications in Switching Converters and Motion Control Systems." Materials Workshop at the International Conference on Industrial Electronics, Control, and Instrumentation, Bologna, Italy.

Sabanovic A, Sabanovic N, Ohnishi K. 1993. "Sliding Mode in Power Converters and Motion Control Systems." *Int J Control* 57:1237–1259.

Shi J, Lu Y. 1996. "Field-Weakening Operation of Cylindrical Permanent-Magnet Motors." Proceedings of the IEEE Conference on Control Applications, Dearborn, MI.

Tamai S, Sugimoto H, Yano M. 1987. "Speed Sensorless Vector Control of Induction Motor with Model Reference Adaptive System." Proceedings of the IEEE/ Industrial Applications Society Annual Meeting, Atlanta, GA.

Utkin VI. 1992. *Sliding Modes in Control and Optimization*. London: Springer-Verlag.

Utkin VI. 1993. "Sliding Mode Control Design Principle and Applications to Electric Drives." *IEEE Trans Ind Electron* 40:23–36.

Xu X, Novotny DW. 1993. "Implementation of Direct Stator Flux Oriented Control on a Versatile DSP Based System." *IEEE Trans Ind Appl* 29:344–348.

Yan Z, Jin C, Utkin VI. 2000. "Sensorless Sliding-Mode Control of Induction Motors." *IEEE Trans Ind Electron* 47:1286–1297.

11

Power Converters

This chapter presents a sliding mode approach for the design of control systems for power converters. A cascaded control structure is chosen for ease of control realization and to exploit the motion separation property of power converters. For power converters, the fast motion is dominated by the dynamics of the loop current, whereas the slow motion stems from the dynamics of the output voltage. Because power converters inherently include switching devices, it is straightforward to implement sliding mode control design, yielding a discontinuous control law. Detailed control design and numeric simulations will demonstrate the efficiency of sliding mode control design principle in this field as a powerful alternative to the existing PWM techniques.

11.1. DC/DC Converters

For circuits controlled by switching devices, in which the control variable can take only values from a discrete set, it is natural to consider sliding mode strategies to synthesize the switching policy, from both a technological and a theoretical point of view. In the past, the method of state-space averaging has been widely used to analyze DC/DC converters. In the state-space averaging method, the linear circuit models and the state-space equation are identified for each of the possible switch positions of the converter during the switching period. These state-space equations are then averaged over the switching period, leading to a low-frequency equivalent model of the converter. The low-frequency model thus obtained may be linearized to apply linear control theory to design feedback compensators. In essence, state-space averaging provides a method of low-frequency characterization of converters such that frequency domain design approaches may be applied. Sliding mode control theory belongs to the category of time domain techniques and can be used to characterize the system under both small signal and large signal conditions. Sliding mode control uses state feedback and sets up directly the desired closed-loop response in time domain or in terms of differential equations. The most important feature of the sliding mode approach is the low sensitivity to system parameter variations.

11.1.1. Bilinear Systems

Commonly used DC/DC converters can be classified into "buck," "boost," "buck-boost," and "cuk" converters. Some of these DC/DC converters can be summarized with a unified state-space formulation in the form of a bilinear system defined on $\Re^n$:

$$\dot{x} = Ax + uBx, \tag{11.1.1}$$

where $x \in \Re^n$ is the state vector; $A \in \Re^{n\times n}$ and $B \in \Re^{n\times n}$ are matrices with constant real entries, and u is a scalar control taking values from the discrete set U =:{0, 1}. For system Equation 11.1.1, we may design a discontinuous control as

$$u = \frac{1}{2}\left(1 - \text{sign}(s)\right), \tag{11.1.2}$$

where s is a scalar switching function in the sense of sliding mode theory, defined by

$$s = c^T x, \tag{11.1.3}$$

with vector $c = [\partial s/\partial x]$ and $c \in R^n$ denoting the gradient of the scalar function s with respect to state space vector x. The motion projection of system Equation 11.1.1 onto the subspace s can be obtained as

$$\begin{aligned} \dot{s} &= c^T \dot{x} = c^T Ax + uc^T Bx \\ &= c^T Ax + \frac{1}{2}c^T Bx - \frac{1}{2}\text{sign}(s)c^T Bx. \end{aligned} \tag{11.1.4}$$

For sliding mode to exist in the manifold $s = 0$, system Equation 11.1.4 needs to satisfy the sliding condition $s\dot{s} < 0$, which implies that

$$s\dot{s} = s\left(c^T Ax + \frac{1}{2}c^T Bx\right) - \frac{1}{2}|s|c^T Bx < 0. \tag{11.1.5}$$

From the above inequality, the necessary condition for sliding mode to exist may be obtained.

If sliding mode exists, then in the vicinity of $s = 0$, the following relations hold:

$$\begin{aligned} \dot{s}_{s>0} &= C^T Ax < 0, \\ \dot{s}_{s<0} &= C^T Bx > -C^T Ax. \end{aligned} \tag{11.1.6}$$

The motion equation of system Equation 11.1.1 in sliding mode can be derived using the equivalent control method (see Section 2.3). The equivalent control of the discontinuous control u is calculated by formally setting $\dot{s} = 0$ and solving Equation 11.1.4 for u to yield

$$u_{eq} = -\frac{c^T Ax}{c^T Bx}. \tag{11.1.7}$$

The motion equation of the sliding motion is governed by

$$\dot{x} = Ax + u_{eq} Bx (s = 0). \tag{11.1.8}$$

Theorem 11.1

For sliding mode to locally exist on $s = 0$, the corresponding equivalent control satisfies

$$0 < u_{eq} = -\frac{c^T Ax}{c^T Bx} < 1. \tag{11.1.9}$$

□

Proof 11.1

For sliding mode to exist, $s\dot{s} < 0$ holds. The second line of Equation 11.1.4 states that

$$\frac{1}{2} c^T Bx > \left| \frac{1}{2} c^T Bx + c^T Ax \right|. \tag{11.1.10}$$

Solving this inequality leads to

$$0 < u_{eq} = -\frac{c^T Ax}{c^T Bx} < 1. \tag{11.1.11}$$

□

Note that condition $s\dot{s} < 0$ defines an attraction domain of the sliding manifold. It is the task of the control designer to ensure that this condition is always fulfilled in both transient behavior and steady state. This may also involve careful choices of initial conditions, as will become clearer during the study of different types of power converters.

In the remainder of this chapter, the control problems of buck and boost converters are investigated. The design approaches can be naturally extended to the buck-boost and cuk converters.

Boost converters are used for applications in which the required output voltage is higher than the source voltage. Conversely, buck converters are

used for applications with the output voltage being smaller than the source voltage. From a control design point of view, the boost converters are more difficult than the buck converters, because the standard design model of a boost converter is a nonminimum phase system [Venkataramanan, Sabanovic, and Slobodan 1985]. In the following, the control problems regarding the output-voltage regulation of both types of DC/DC converters will be discussed.

Traditionally, the control problems of the DC/DC converters are solved by using PWM techniques. Sira-Ramirez [1988] demonstrated the equivalence between sliding mode control and PWM control in the low-frequency range for a boost converter. Generally speaking, hardware implementation of a sliding mode control is much easier than a PWM control. Because the maximum frequency of commercially available switching elements increases higher and higher, the sliding mode approach is expected to become increasingly popular in the field of power converter control.

11.1.2. Direct Sliding Mode Control

For DC/DC converters, the input inductor (the word "inductor" is often used in the literature for DC/DC converters instead of "inductance") current and the output capacitor voltage are normally selected as the state variables. For most converters used in practice, the motion rate of the current is much faster than the motion rate of the output voltage. Calling on the theory of singular perturbations [Kokotovic, O'Malley, and Sannuti 1976], the control problem can be solved by using a cascaded control structure with two control loops: an inner current control loop and an outer voltage control loop. The latter is usually realized with standard linear control techniques, whereas the current control is implemented using either PWM or hysteresis control. Here,

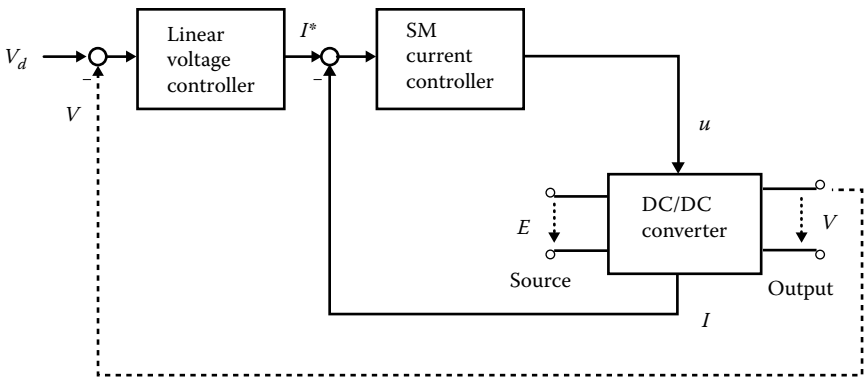

FIGURE 11.1
Cascaded control structure of DC/DC converters.

we use the sliding mode approach for the control of inductor current. Figure 11.1 shows the general structure of control system for DC/DC converters.

11.1.2.1. Buck-Type DC/DC Converter

The circuit structure of a buck DC/DC converter is shown in Figure 11.2, where the variables are defined as follows: L, loop inductor; C, storage capacitor; R, load resistance; E, source voltage; I, input current; V, output voltage; and u, switching signal taking value from discrete set U =:{0,1}.

The dynamic model of the buck type converter is given by

$$\begin{aligned} \dot{x}_1 &= -\frac{1}{L}x_2 + u\frac{E}{L}, \\ \dot{x}_2 &= \frac{1}{C}x_1 - \frac{1}{RC}x_2, \end{aligned} \tag{11.1.12}$$

with $x_1 = I$ and $x_2 = V$.

The goal of control is to achieve a constant output voltage denoted by V_d. In other words, the steady-state behavior of the buck converter (Equation 11.1.12) should be given by

$$\begin{aligned} x_2 &= V_d, \\ \dot{x}_2 &= \dot{V}_d = 0. \end{aligned} \tag{11.1.13}$$

The control design follows a two-step procedure known as integrator backstepping [Krstic, Kanellakopoulos, and Kokotovic 1995] or regular form control (see Section 3.3). First, it is assumed that x_1 in the second equation of Equation 11.1.12 can be handled as a control input. However, because x_1 is the output of the current loop in the first equation of Equation 11.1.12, this first

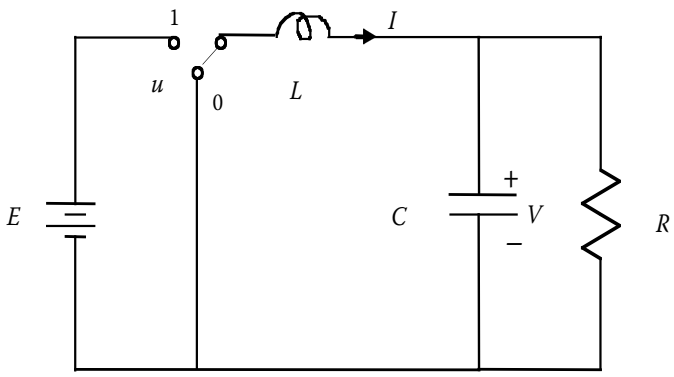

FIGURE 11.2
Buck DC/DC converter.

design step yields desired current x_1^*. The control goal (Equation 11.1.13) is substituted into the voltage loop, i.e., the second equation of Equation 11.1.12, to yield the desired current:

$$x_1^* = V_d / R. \tag{11.1.14}$$

The task of the second design step is to ensure that the actual current x_1 tracks the desired current (Equation 11.1.14) exactly. Because of its exact tracking properties, the sliding mode approach is an ideal tool for this task. If sliding mode is enforced in

$$s = x_1 - x_1^* = 0, \tag{11.1.15}$$

then $x_1 = V_d/R$. To enforce sliding mode in the manifold $s = 0$ in Equation 11.1.15, control u (taking only two values, 0 or 1) in the first equation of Equation 11.1.12 is defined as

$$u = \frac{1}{2}\left(1 - \text{sign}(s)\right). \tag{11.1.16}$$

The condition for sliding mode to exist is derived from $s\dot{s} < 0$. In compliance with the derivations in Section 11.1.1, sliding mode exists if

$$0 < x_2 < E. \tag{11.1.17}$$

This condition defines an attraction domain of the sliding manifold. Because the control (Equation 11.1.16) contains no control gain to be adjusted, the domain of attraction (Equation 11.1.17) is predetermined by the system architecture. In steady state, Equation 11.1.17 is fulfilled by the definition of a buck converter: the output voltage is smaller than the source voltage.

After the state of the inner current loop has reached the sliding manifold, i.e., converged to $s = 0$ at time $t = t_h$, $x_1 = x_1^* = V_d/R$ holds for $t > t_h$, and the outer voltage loop is governed by

$$\dot{x}_2 = -\frac{1}{RC} x_2 + \frac{1}{RC} V_d. \tag{11.1.18}$$

The solution of the above system,

$$x_2(t) = V_d + \left(x_2(t_h) - V_d\right) e^{-\frac{1}{RC}(t - t_h)}, \tag{11.1.19}$$

tends to V_d exponentially. Hence, the design goal of control is achieved.

Figures 11.3 and 11.4 show the simulation results of proposed control algorithm for the buck DC/DC converter. In the simulation, the converter parameters are selected as: $E = 20$ V, $C = 4$ μF, $R = 40$ Ω, and $L = 40$ mH. The desired

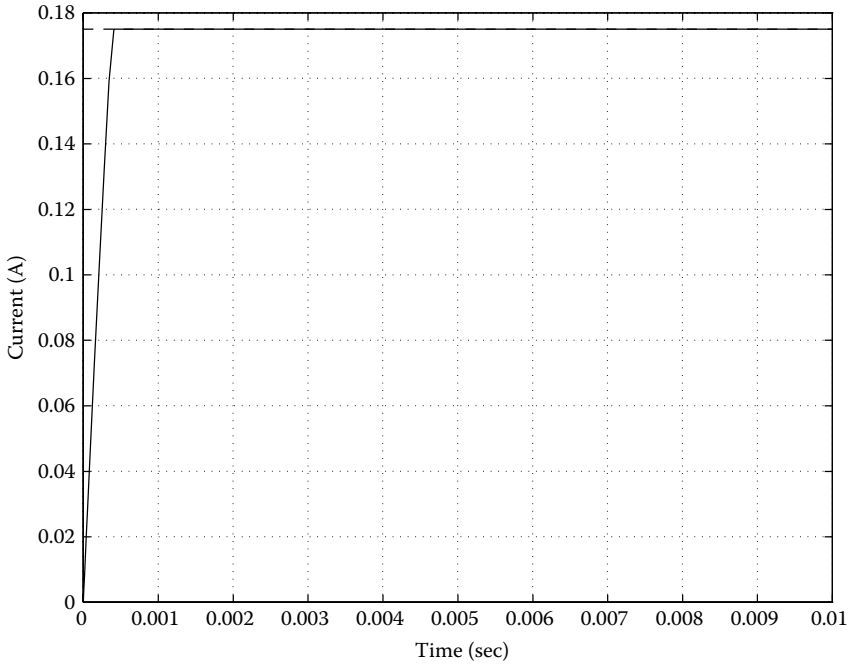

FIGURE 11.3
Current response of a sliding-mode-controlled buck DC/DC converter.

output voltage is $V_d = 7$ V. As can be seen from the figures, both the inductor current and the output capacitor voltage converge rapidly to their reference values.

11.1.2.2. Boost-Type DC/DC Converter

Figure 11.5 shows the principle of a boost type converter, in which the variables are defined as follows: L, loop inductor; C, storage capacitor; R, load resistance; E, source voltage; I, input current; V, output voltage; and u, switching signal taking value from discrete set $U =:\{0, 1\}$.

The main difference of the boost converter in Figure 11.5 compared with the buck converter in Figure 11.2 is the location of inductor L. The dynamic model of the boost converter is given as

$$\begin{aligned} \dot{x}_1 &= -(1-u)\frac{1}{L}x_2 + \frac{E}{L}, \\ \dot{x}_2 &= (1-u)\frac{1}{C}x_1 - \frac{1}{RC}x_2, \end{aligned} \tag{11.1.20}$$

with $x_1 = I$ and $x_2 = V$.

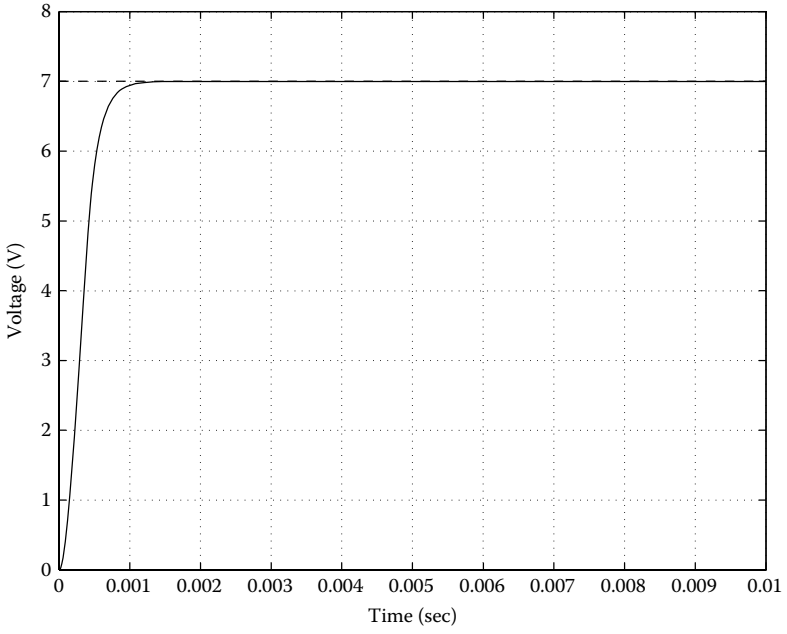

FIGURE 11.4
Voltage response of a sliding-mode-controlled buck DC/DC converter.

The topological modification of locating the inductor before the switching element rather than after it, as in the buck converter, enables a higher output voltage than the source voltage. However, from a control point of view, the boost converter is more difficult to control than the buck converter. This lies in the fact that the control u appears in both the current and voltage

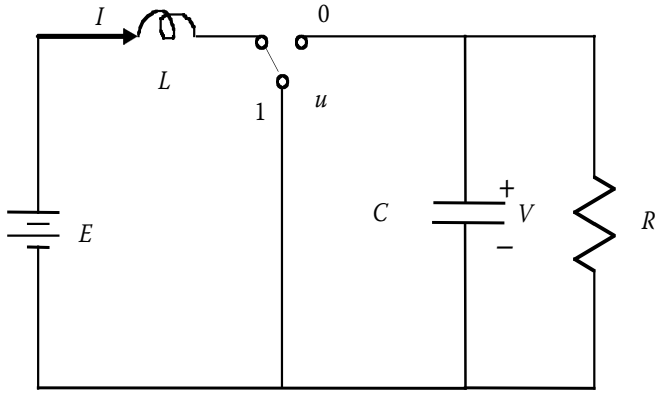

FIGURE 11.5
Boost DC/DC converter.

equations and both in bilinear fashion. Such a configuration implies a highly nonlinear system with associated difficulties in control design.

Just like buck converters, boost converters satisfy the motion-separation principle, which originates from the singular perturbation theory. In engineering words, the motion rate of the current is much faster than the motion rate of the output voltage. Consequently, the control problem can again be solved by using two cascaded control loops: an inner current loop and an outer voltage control loop. Again, a design of the current control loop based on sliding mode control techniques is presented.

Similar to the control design for the buck converter in the previous section, a desired current is obtained from the outer voltage loop as

$$x_1^* = V_d^2 / RE, \tag{11.1.21}$$

where V_d is the desired output capacitor voltage. The switching function for the inner current control is defined as

$$s = x_1 - x_1^*, \tag{11.1.22}$$

to enforce the current x_1 to track the desired current x_1^*. Control u can be designed as

$$u = \frac{1}{2}\big(1 - \text{sign}(s)\big). \tag{11.1.23}$$

Under the above control scheme, the equivalent control of u is derived by solving $\dot{s} = \dot{x}_1 = 0$ for the control input u with the substitution of Equation 11.1.20

$$u_{eq} = 1 - \frac{E}{x_2}, \tag{11.1.24}$$

where x_2 is the output voltage of the slow voltage loop. The motion equation of the outer voltage loop during sliding mode in the inner current loop is obtained by substituting the equivalent control (Equation 11.1.24) into the second line of Equation 11.1.20

$$\dot{x}_2 = -\frac{1}{RC}\left(x_2 - \frac{V_d^2}{x_2}\right). \tag{11.1.25}$$

The above equation can be solved explicitly as

$$x_2(t) = \sqrt{V_d^2 + \left(x_2^2(t_h) - V_d^2\right)e^{-\frac{2}{RC}(t-t_h)}}, \tag{11.1.26}$$

where t_h stands for the reaching instant of the sliding manifold $s = 0$, and $x_2(t_h)$ is the output voltage at time t_h. Apparently, x_2 tends to V_d asymptotically as t goes to infinity.

The attraction domain of the sliding manifold $s = 0$ is found by applying the convergence condition $s\dot{s} < 0$ to the system Equation 11.1.20, yielding

$$x_2 > E, \text{ or } 0 < u_{eq} = 1 - \frac{E}{x_2} < 1. \tag{11.1.27}$$

Condition Equation 11.1.27 implies that, as long as the output voltage is higher than the source voltage, sliding mode can be enforced. This requirement is essential for a boost-type DC/DC converter, and careful consideration of the initial conditions is required to guarantee the convergence to $s = 0$.

Figures 11.6 and 11.7 show the simulation results of proposed control algorithm for the boost DC/DC converter. In the simulation, the converter parameters are selected as $E = 20$ V, $C = 4$ μF, $R = 40$ Ω, and $L = 40$ mH. The desired output voltage is $V_d = 40$ V. As can be seen from the figures, both the inductor current and the output capacitor voltage converge rapidly to their reference values.

11.1.3. Observer-Based Control

Recently, research on sliding mode control theory has revealed great advantages by introducing certain dynamics into a sliding mode controller (see

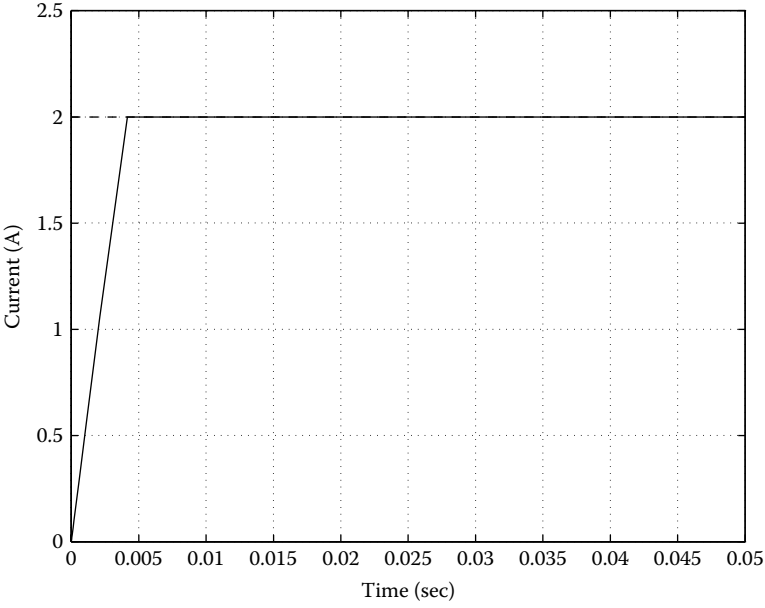

FIGURE 11.6
Current response of a sliding-mode-controlled boost DC/DC converter.

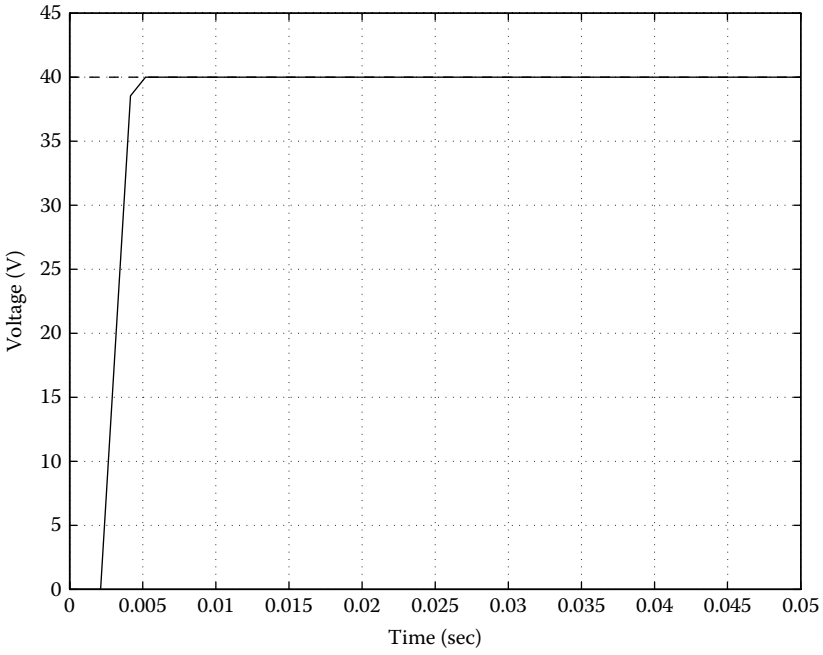

FIGURE 11.7
Voltage response of a sliding-mode-controlled boost DC/DC converter.

Chapter 6 through Chapter 8). These approaches fall into the category of dynamic feedback control. For observer-based sliding mode control, an ideal model is simulated in the controller in parallel to the real plant. For the sliding mode control itself, measurements of real plant states are substituted by observer states, reducing the number of plant states to be measured. The mismatch between some measurable plant output(s) and the observer output(s) is the "bridge" to keep both systems operating "closely." This mismatch has been used in different ways to improve the control performance. In general, an observer can be viewed as an artificially introduced auxiliary dynamic system to improve the control performance.

As seen from the previous derivations, for DC/DC converters, there is no control gain to be adjusted. The attraction domain of the sliding manifold $s = 0$ is bounded. The remaining degrees of freedom for the control design are the initial conditions of the auxiliary system. It has been shown that, by proper selection of the initial conditions of the auxiliary system, the performance of an observer-based sliding mode controller may be improved significantly [Sira-Ramirez, Escobar, and Ortega 1996].

It is worth pointing out the evolution process of sliding mode control theory. Originally, sliding mode control theory, as a general control design methodology for a large class of nonlinear systems, fell into the field of nonlinear control with order reduction and decoupling capabilities. The order reduction

and decoupling issues were some of the most difficult problems in the control of high-order nonlinear dynamic systems. Applications of sliding mode techniques in the fields of robotics and electric drives have confirmed the validity of this compact, uniform, and straightforward design methodology. In recent years, researchers have started to incorporate the dynamic feedback into the sliding mode controller to achieve higher control performance. Dynamic feedback increases the system order in the controller space and establishes coupling between the plant system space and the controller space. As a result, the complexity of the overall system will be increased in return.

Similar to the direct sliding mode control of DC/DC converters, the following sections investigate inductor current control and subsequently output capacitor voltage regulation based on observed states. Figure 11.8 shows the structure of the observer-based control system for DC/DC converters.

The price for observer-based control strategy is a more involved control design and an increasingly complex stability analysis. A general design strategy proceeds as follows:

1. The observer dynamics are derived with a similar structure as the plant model.
2. The stability of the observer system is examined to ensure that the observer states converge to the states of the real system (asymptotic stability).
3. A sliding mode current controller is designed based on the observed current rather than the measured current. Supposing sliding mode exists, observed current tracks the desired reference current and associated equivalent control can be obtained.
4. As motion in sliding mode, a reduced-order system consisting of the real plant model and the output voltage equation of the observer system can be derived by substitution of the equivalent control.
5. It is proven that, under the equivalent control, the reduced order-system provides (a) the real current convergence to the desired

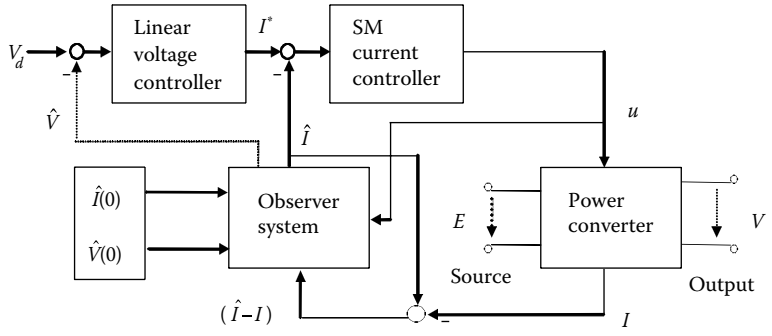

FIGURE 11.8
Observer-based control structure.

reference current and (b) the real output voltage convergence to the observed output voltage.

6. The observed output voltage converges to the desired output voltage, and so does the real output voltage.
7. The existence of sliding mode is established by proper selection of the initial conditions of the observer dynamics.

11.1.3.1. Observer-Based Control of Buck Converters

The observer equations, or the auxiliary system, are designed as

$$\dot{\hat{x}}_1 = -\frac{1}{L}\hat{x}_2 + u\frac{E}{L} - l\,(\hat{x}_1 - x_1),$$
$$\dot{\hat{x}}_2 = \frac{1}{C}\hat{x}_1 - \frac{1}{RC}\hat{x}_2, \tag{11.1.28}$$

where l is a positive scalar observer gain, and $\hat{x}_1$, $\hat{x}_2$ are the observed inductor current and output voltage, i.e., the outputs of the observer. Note that only measurement of the inductor current x_1 is required; there is no need to measure the output voltage x_2.

Theorem 11.2

Observer Equation 11.1.28 is an asymptotic observer whose outputs $\hat{x}_1$, $\hat{x}_2$ converge to the real states x_1, x_2 asymptotically. □

Proof 11.2

Defining the observer errors as $\bar{x}_1 = \hat{x}_1 - x_1$ and $\bar{x}_2 = \hat{x}_2 - x_2$, the error dynamics can be derived by subtracting Equation 11.1.12 from Equation 11.1.28:

$$\dot{\bar{x}}_1 = -\frac{1}{L}\bar{x}_2 - l\bar{x}_1,$$
$$\dot{\bar{x}}_2 = \frac{1}{C}\bar{x}_1 - \frac{1}{RC}\bar{x}_2. \tag{11.1.29}$$

Because control u is applied to both the observer system and the real plant model, it is canceled out in the error dynamics. The characteristic polynomial of the above linear system is

$$p^2 + \left(l + \frac{1}{RC}\right)p + \left(\frac{l}{RC} + \frac{1}{LC}\right) = 0. \tag{11.1.30}$$

Because all coefficients in Equation 11.1.30 are positive, system Equation 11.1.29 is stable, implying that observer errors $\bar{x}_1$ and $\bar{x}_2$ tend to zero asymptotically. □

The switching function for the sliding mode current control will be designed based on the observed current $\hat{x}_1$ instead of measured current x_1 as done in Equation 11.1.15:

$$\hat{s} = \hat{x}_1 - V_d/R. \tag{11.1.31}$$

The control u, applied to both the real plant and the observer system, is of the same form as in the case of the control scheme without an observer (see Equation 11.1.16):

$$u = \frac{1}{2}\left(1 - \text{sign}(\hat{s})\right). \tag{11.1.32}$$

Suppose that sliding mode can be enforced in the vicinity of the sliding manifold $\hat{s} = 0$, which results in

$$\hat{x}_1(t) \equiv V_d/R \text{ with } (\forall t > t_h) \tag{11.1.33}$$

where t_h denotes the reaching instant of the sliding manifold $\hat{s} = 0$. The equivalent control of u can be obtained by solving $\dot{\hat{s}} = 0$:

$$u_{eq} = \left(\frac{1}{L}\hat{x}_2 + l\left(\hat{x}_1 - x_1\right)\right)\frac{L}{E}. \tag{11.1.34}$$

Substituting u_{eq} into the real plant model (Equation 11.1.12) and considering the observer model (Equation 11.1.28), the motion in sliding mode can be represented as a reduced-order system, comprising the motion of the real plant and the slow dynamics (about output voltage) of the observer:

$$\begin{aligned}
\dot{x}_1 &= -\frac{1}{L}x_2 + \left(\frac{1}{L}\hat{x}_2 + l\left(\frac{V_d}{R} - x_1\right)\right), \\
\dot{x}_2 &= \frac{1}{C}x_1 - \frac{1}{RC}x_2, \\
\dot{\hat{x}}_2 &= \frac{1}{C}\frac{V_d}{R} - \frac{1}{RC}\hat{x}_2.
\end{aligned} \tag{11.1.35}$$

By defining errors $\bar{x}_1^* = V_d/R - x_1$ and $\bar{x}_2 = \hat{x}_2 - x_2$, the above equations can be transformed into a second-order error system:

$$\dot{\bar{x}}_1^* = -\frac{1}{L}\bar{x}_2 - l\bar{x}_1^*,$$

$$\dot{\bar{x}}_2 = \frac{1}{C}\bar{x}_1^* - \frac{1}{RC}\bar{x}_2, \tag{11.1.36}$$

where $\bar{x}_2$ has the same meaning as defined for Equation 11.1.29 but $\bar{x}_1^*$ represents the difference between the desired reference current and the real current rather than the difference between the observed current and the real current, denoted by $\bar{x}_1$. Formally, system Equation 11.1.36 is the same as the observer error system Equation 11.1.29, which is proven to be stable, implying that the real current converges to the desired reference current asymptotically.

So far, we have proven that, after sliding mode occurs, i.e., for $t \geq t_h$, observed current is equal to the desired reference current, and the real current will also tend to the desired reference current. It means that

$$\lim_{t\to\infty} x_1(t) = \hat{x}_1(t)\big|_{t\geq t_h} = \frac{V_d}{R}. \tag{11.1.37}$$

As the next step, we should prove that the observed output voltage converges to the desired output voltage, and so does the real output voltage. Substitute Equation 11.1.33 into the second equation of Equation 11.1.28 and solve the resulting equation with a similar procedure as used for Equation 11.1.18; this gives

$$\lim_{t\to\infty} \hat{x}_2(t) = V_d. \tag{11.1.38}$$

Following Theorem 11.2, the real output voltage and the observed output voltage are identical as $t \to \infty$. Finally, we achieve

$$\lim_{t\to\infty} x_2(t) = \lim_{t\to\infty} \hat{x}_2(t) = V_d. \tag{11.1.39}$$

The remaining task is to find the condition under which the occurrence of the sliding mode can be guaranteed. Applying the existence condition of sliding mode to the first line of Equation 11.1.28 with the substitution of Equations 11.1.32 and 11.1.31 yields

$$-Ll(\hat{x}_1 - x_1) < \hat{x}_2 < E - Ll(\hat{x}_1 - x_1). \tag{11.1.40}$$

This condition is consistent with the statement in Theorem 11.1, i.e.,

$$0 < u_{eq} = \left(\frac{1}{L}\hat{x}_2 + l\left(\hat{x}_1 - x_1\right)\right)\frac{L}{E} < 1. \tag{11.1.41}$$

Because x_1 is measured and $\hat{x}_1$, $\hat{x}_2$ are state variables in the controller space, i.e., variables in the control algorithm, the initial conditions of the observer $\hat{x}_1(0)$ and $\hat{x}_2(0)$ can be designed such that the occurrence of the sliding mode can always be guaranteed.

As an important specification of DC/DC converters, the so-called "stored error energy" has been defined previously [Sira-Ramirez, Escobar, and Ortega 1996]. For the buck converter, this quantity is defined as

$$H(t) = \frac{1}{2}\left(L\left(\frac{V_d}{R} - x_1(t) \right)^2 + C\left(V_d - x_2(t) \right)^2 \right), \tag{11.1.42}$$

where $H(t)$ represents the energy difference between the desired value and the real value providing to the load. For a well-controlled DC/DC converter, this energy difference should converge to zero smoothly.

Figures 11.9 through 11.11 show the simulation results of the observer-based control algorithm for the buck DC/DC converter. In the simulation, the converter parameters are selected as E = 20 V, C = 4 μF, R = 40 Ω, and L = 40 mH. The desired output voltage is V_d = 7 V. The observer gain is designed as l = 200. The initial conditions of the observer are selected as $\hat{x}_1(0)$ = 0.12 A, $\hat{x}_2(0)$ = 5.0 V and $\hat{x}_1(0)$ = 0.07 A, $\hat{x}_2(0)$ = 2.5 V, respectively.

Note that both the inductor current and the output capacitor voltage converge rapidly to their reference values, and the system response can be influenced by the design of the observer initial conditions.

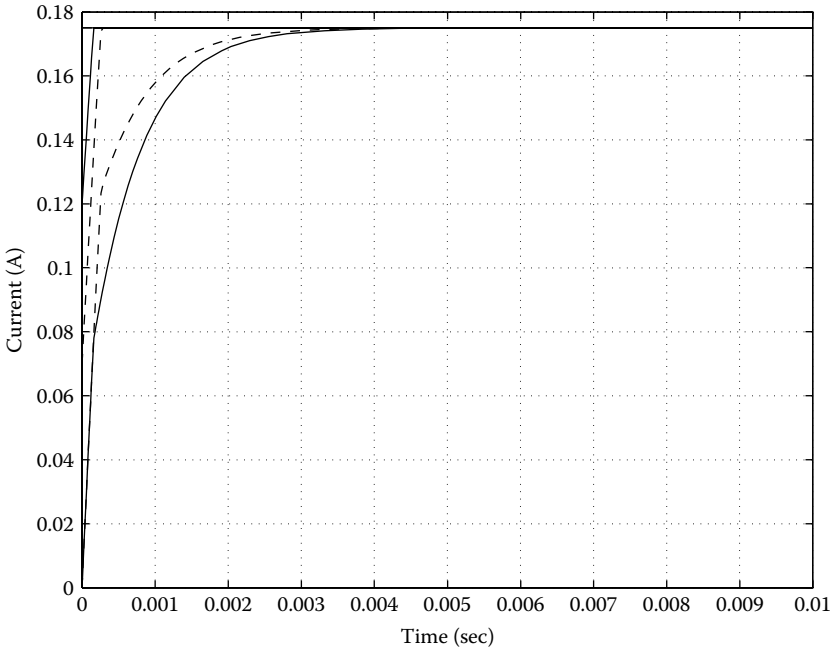

FIGURE 11.9
Response of real (curves starting from zero) and estimated current under different initial conditions. Solid line $\hat{x}_1(0)$ = 0.12, $\hat{x}_2(0)$ = 5.0; dashed line, $\hat{x}_1(0)$ = 0.07, $\hat{x}_2(0)$ = 2.5.

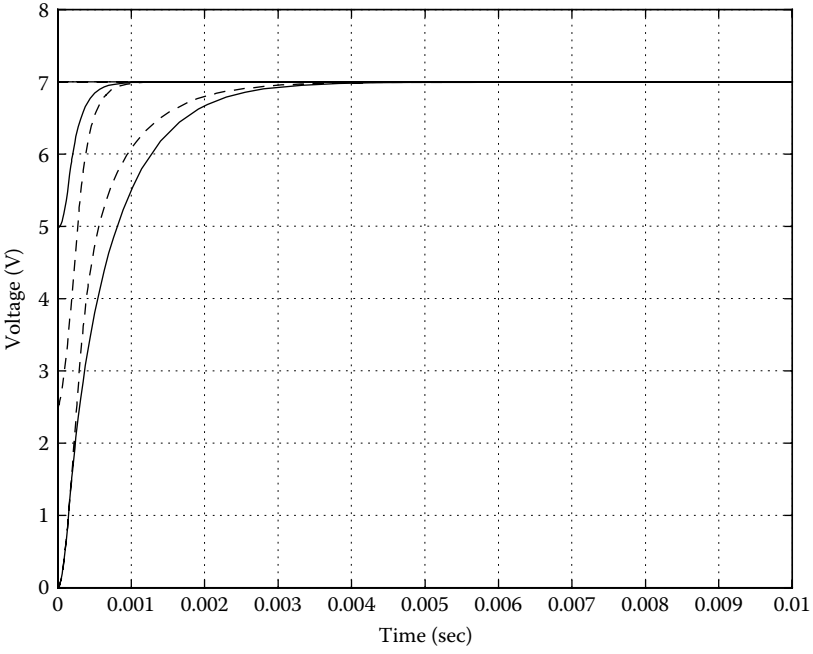

FIGURE 11.10
Response of real (curves starting from zero) and estimated voltage under different initial conditions. Solid line, $\hat{x}_1(0) = 0.12$, $\hat{x}_2(0) = 5.0$; dashed line, $\hat{x}_1(0) = 0.07$, $\hat{x}_2(0) = 2.5$.

11.1.3.2. Observer-Based Control of Boost Converters

To simplify the derivation, a new control input is defined as $v = (1 - u)$. The observer dynamics designed for a boost converter are governed by

$$\dot{\hat{x}}_1 = -v\frac{1}{L}\hat{x}_2 + \frac{E}{L} - l\,(\hat{x}_1 - x_1),$$
$$\dot{\hat{x}}_2 = v\frac{1}{C}\hat{x}_1 - \frac{1}{RC}\hat{x}_2, \tag{11.1.43}$$

where $\hat{x}_1$, $\hat{x}_2$ are the observed inductor current and output voltage, i.e., the outputs of the observer, and l is a positive scalar observer gain.

Theorem 11.3

Observer Equation 11.1.43 is an asymptotic observer whose outputs $\hat{x}_1$, $\hat{x}_2$ converge to the real states x_1, x_2 asymptotically. □

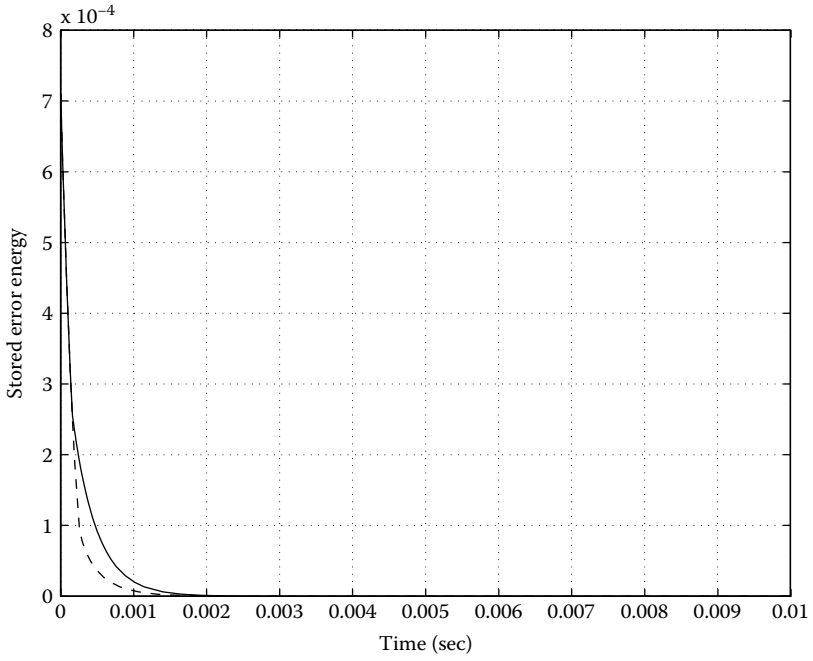

FIGURE 11.11
Stored error energy. Solid line, $\hat{x}_1(0) = 0.12, \hat{x}_2(0) = 5.0$; dashed line, $\hat{x}_1(0) = 0.07, \hat{x}_2(0) = 2.5$.

Proof 11.3

Defining the observer errors as $\bar{x}_1 = \hat{x}_1 - x_1$ and $\bar{x}_2 = \hat{x}_2 - x_2$, the error dynamics can be derived by subtracting Equation 11.1.20 from Equation 11.1.43:

$$\dot{\bar{x}}_1 = -v\frac{1}{L}\bar{x}_2 - l\bar{x}_1,$$
$$\dot{\bar{x}}_2 = v\frac{1}{C}\bar{x}_1 - \frac{1}{RC}\bar{x}_2. \tag{11.1.44}$$

Equation 11.1.44 is a nonlinear system, because the system states are multiplied by the control input v. For the convergence proof, we design a Lyapunov function candidate as

$$V = \frac{1}{2}\left(L\bar{x}_1^2 + C\bar{x}_2^2\right) > 0. \tag{11.1.45}$$

Its time derivative along the solutions of Equation 11.1.44 can be found as

$$\dot{V} = -Ll\bar{x}_1^2 - \frac{1}{R}\bar{x}_2^2 < 0; \tag{11.1.46}$$

therefore, system Equation 11.1.44 is stable for any $l > 0$. As a result, observer errors $\bar{x}_1$ and $\bar{x}_2$ tend to zero asymptotically. The convergence rate for the inductor current estimation can be adjusted by the observer gain l. □

The switching function for the sliding mode current control will be designed based on the observed current $\hat{x}_1$ instead of measured current x_1 as in Equation 11.1.22, i.e.,

$$\hat{s} = \hat{x}_1 - \frac{V_d^2}{RE}. \tag{11.1.47}$$

The control u applied to both the real plant and the observer is of the same form as in the case of the control scheme without an observer,

$$u = \frac{1}{2}\left(1 - \text{sign}(\hat{s})\right). \tag{11.1.48}$$

In terms of the new control input $v = (1 - u)$, we have

$$v = \frac{1}{2}\left(1 + \text{sign}(\hat{s})\right). \tag{11.1.49}$$

Suppose that sliding mode is enforced in the manifold $\hat{s} = 0$; then, according to Equation 11.1.47,

$$\hat{x}_1 \equiv \frac{V_d^2}{RE} \quad \text{with } (\forall t > t_h) \tag{11.1.50}$$

where t_h denotes the reaching instant of the sliding manifold $\hat{s} = 0$. The equivalent control of v can be obtained by solving $\dot{\hat{s}} = 0$:

$$v_{eq} = \frac{E - Ll(V_d^2/RE - x_1)}{\hat{x}_2}. \tag{11.1.51}$$

The motion of the system in sliding mode is of a reduced order and comprises the motion of the real plant and the slow dynamics (about output voltage) of the observer,

$$\begin{aligned}
\dot{x}_1 &= -v_{eq}\frac{1}{L}x_2 + \frac{E}{L}, \\
\dot{x}_2 &= v_{eq}\frac{1}{C}x_1 - \frac{1}{RC}x_2, \\
\dot{\hat{x}}_2 &= v_{eq}\frac{1}{C}\frac{V_d^2}{RE} - \frac{1}{RC}\hat{x}_2.
\end{aligned} \tag{11.1.52}$$

By defining errors $\bar{x}_1^* = V_d^2/RE - x_1$ and $\bar{x}_2 = \hat{x}_2 - x_2$, with the substitution of Equation 11.1.51, the above equations can be transformed into a second-order error system

$$\begin{aligned}\dot{\bar{x}}_1^* &= -\frac{x_2}{\hat{x}_2} l \bar{x}_1^* + \frac{E}{L}\frac{x_2}{\hat{x}_2} - \frac{E}{L},\\ \dot{\bar{x}}_2 &= \frac{E}{C}\frac{1}{\hat{x}_2}\bar{x}_1^* - \frac{Ll}{C\hat{x}_2}(\bar{x}_1^*)^2 - \frac{1}{RC}\bar{x}_2,\end{aligned} \tag{11.1.53}$$

where $\bar{x}_2$ has the same meaning as defined for Equation 11.1.44, but $\bar{x}_1^*$ represents the difference between the desired reference current and the real current rather than the difference between the observed current and the real current, denoted by $\bar{x}_1$.

Substituting $x_2 = \hat{x}_2 - \bar{x}_2$ into Equation 11.1.53 further simplifies the equations to

$$\begin{aligned}\dot{\bar{x}}_1^* &= -l\bar{x}_1^* + \frac{l}{\hat{x}_2}\bar{x}_1^*\bar{x}_2 - \frac{E}{L}\frac{\bar{x}_2}{\hat{x}_2},\\ \dot{\bar{x}}_2 &= -\frac{1}{RC}\bar{x}_2 - \frac{Ll}{C\hat{x}_2}(\bar{x}_1^*)^2 + \frac{E}{C}\frac{1}{\hat{x}_2}\bar{x}_1^*.\end{aligned} \tag{11.1.54}$$

For the convergence proof, we design a Lyapunov function candidate as

$$V = \frac{1}{2}\left(L(\bar{x}_1^*)^2 + C\bar{x}_2^2\right) > 0. \tag{11.1.55}$$

Its time derivative along the solutions of Equation 11.1.54 can be found as

$$\dot{V} = -Ll(\bar{x}_1^*)^2 - \frac{1}{R}\bar{x}_2^2 < 0; \tag{11.1.56}$$

therefore, the system Equation 11.1.54 is stable for any $l > 0$. As a result, errors $\bar{x}_1^*$ and $\bar{x}_2$ tend to zero asymptotically, showing that the real current converges to the desired reference current.

So far, we have proven that, after sliding mode occurs, i.e., for $t \geq t_h$, observed current is equal to the desired reference current and the real current will also tend to the desired reference current. Mathematically, this statement can be expressed as

$$\lim_{t\to\infty} x_1(t) = \hat{x}_1(t)\big|_{t\geq t_h} = \frac{V_d^2}{RE}. \tag{11.1.57}$$

The next task is to prove that $\hat{x}_2$ converges to the desired voltage value V_d. With the substitution of Equation 11.1.51, the third line of Equation 11.1.52 can be transformed to

$$\dot{y} = -\frac{2}{RC}y - \frac{2}{RC}\frac{V_d^2}{E}Ll\,\bar{x}_1^*, \quad \text{with } y = \hat{x}_2^2 - V_d^2. \tag{11.1.58}$$

This equation is a linear asymptotically stable system, with the input $\bar{x}_1^*$ tending to zero; hence, its output y tends to zero as well. Consequently, $\hat{x}_2 = \pm V_d$. Because $\hat{x}_2 > 0$ is required for generating sliding mode (proven below), the unique steady-state solution is $\hat{x}_2 = V_d$.

Following Theorem 11.3, the real output voltage and the observed output voltage are identical as $t \to \infty$. Finally, we achieve

$$\lim_{t\to\infty} x_2(t) = \lim_{t\to\infty} \hat{x}_2(t) = V_d. \tag{11.1.59}$$

So far, we have proven that the real inductor current x_1 tends to the desired reference current V_d^2/RE if sliding mode can be enforced in the manifold $\hat{s} = \hat{x}_1 - V_d^2/RE = 0$. As a consequence, both the observed output voltage $\hat{x}_2$ and the real output voltage x_2 converge to the desired output voltage V_d.

The remaining task is to find the condition under which the occurrence of the sliding mode can be guaranteed. Applying the existence condition of sliding mode to Equation 11.1.47 with the substitution of Equations 11.1.43 and 11.1.49 yields

$$0 < E - Ll(\hat{x}_1 - x_1) < \hat{x}_2. \tag{11.1.60}$$

This condition is consistent with Theorem 11.1, i.e.,

$$0 < v_{eq} = \frac{E - Ll\left(\hat{x}_1 - x_1\right)}{\hat{x}_2} < 1. \tag{11.1.61}$$

Bearing in mind that $v = 1 - u$, from the above inequality, we have also

$$0 < u_{eq} < 1. \tag{11.1.62}$$

Because x_1 is measured and $\hat{x}_1$, $\hat{x}_2$ are state variables in the controller space, i.e., variables in the control algorithm, the initial conditions of the observer, $\hat{x}_1(0)$ and $\hat{x}_2(0)$, can be designed such that the occurrence of sliding mode can always be guaranteed. The stored error energy for boost DC/DC converters is defined as

$$H(t) = \frac{1}{2}\left(L\left(\frac{V_d^2}{RE} - x_1(t)\right)^2 + C\left(V_d - x_2(t)\right)^2 \right), \tag{11.1.63}$$

where $H(t)$ represents the energy difference between the desired value and the real value provided to the load. For a well-controlled DC/DC converter, this energy difference should converge to zero smoothly.

Figures 11.12 through 11.14 show the simulation results of the observer-based control algorithm for the boost DC/DC converter. In the simulation, the converter parameters are selected as $E = 20$ V, $C = 4$ μF, $R = 40$ Ω, and $L = 40$ mH. The desired output voltage is $V_d = 40$ V. The observer gain is designed as $l = 200$. The initial conditions of the observer are selected as $\hat{x}_1(0) = 0$ A, $\hat{x}_2(0) = 0$ V and $\hat{x}_1(0) = 1.95$ A, $\hat{x}_2(0) = 38.5$ V, respectively. As can be seen from the figures, both the inductor current and the output capacitor voltage converge rapidly to their reference values, and the system response can be influenced by selection of the observer initial conditions.

For zero initial conditions, i.e., $\hat{x}_1(0) = 0$ A, $\hat{x}_2(0) = 0$ V, the observer-based control system converges to the non-observer-based control system. In this case, the stored error energy is not smooth (see Figure 11.14); the time derivative of $H(t)$ has discontinuous points. However, if the initial conditions of the observer are designed properly, the stored error energy decreases to zero smoothly, as illustrated by Figure 11.14. This important improvement to the boost DC/DC converter is produced by the observer-based control design.

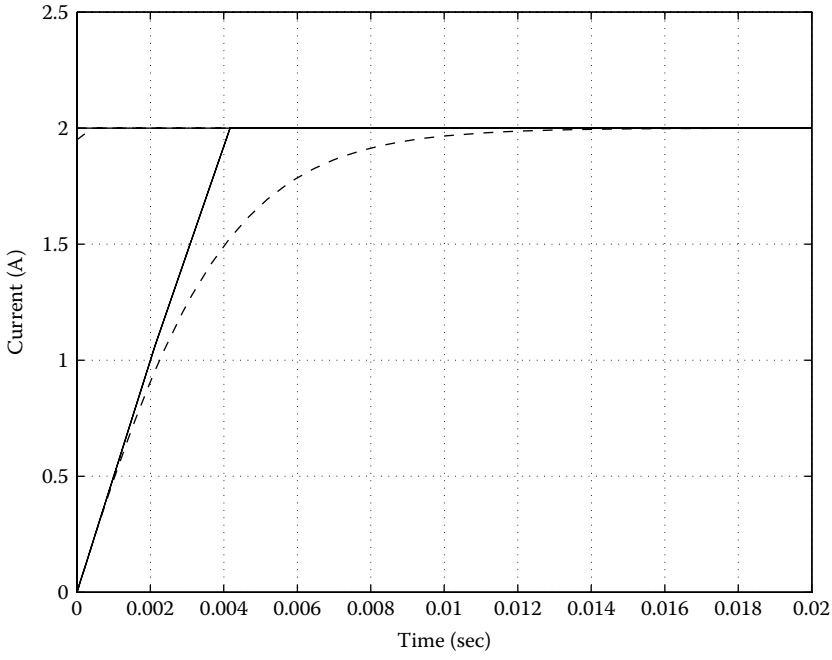

FIGURE 11.12
Current response. Solid line, $\hat{x}_1(0) = 0$, $\hat{x}_2(0) = 0$; dashed line, $\hat{x}_1(0) = 1.95$, $\hat{x}_2(0) = 38.5$.

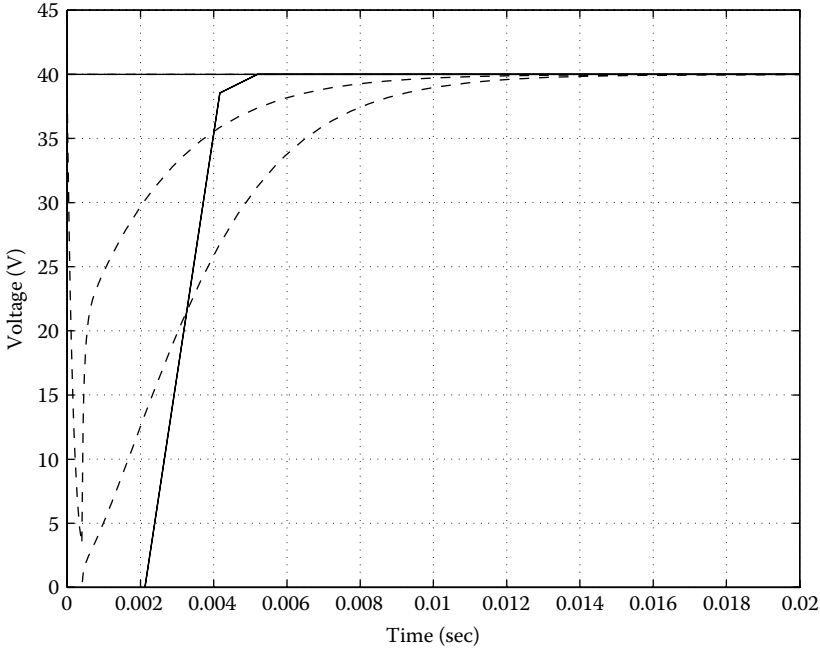

FIGURE 11.13
Response of real (curves starting from zero) and estimated voltage under different initial conditions. Solid line, $\hat{x}_1(0) = 0$, $\hat{x}_2(0) = 0$; dashed line, $\hat{x}_1(0) = 1.95$, $\hat{x}_2(0) = 38.5$.

11.1.4. Multiphase Converters

The design methodology developed in Section 8.8 is applied for a DC/DC multiphase buck converter. A converter with two phases is depicted in Figure 11.15. The objective is to demonstrate via simulation to what extent chattering can be suppressed in multiphase power converters using the proposed phase shift control methodology and to check the range of the function a for which the chattering suppression takes place. In simulation, the master-slave method is accepted. The gain K is selected as in Equation 8.8.15 as $K = 1/\alpha$ to maintain the switching frequency at the desired level in all phases even if a is beyond the admissible domain (Equation 8.8.14). Simulation results are presented for the two parameter sets in Table 11.1.

For simulation, the governing equations of m-phase converter are assumed as follows:

$$\begin{aligned} \dot{I}_k &= \frac{1}{L}(-I_k R_a + u_k - V_L)(k = 1, 2, \ldots, m) \\ V_L &= \frac{1}{C}\left(\sum_{k-1}^{m} I_k - \frac{V_L}{R_L}\right). \end{aligned} \tag{11.1.64}$$

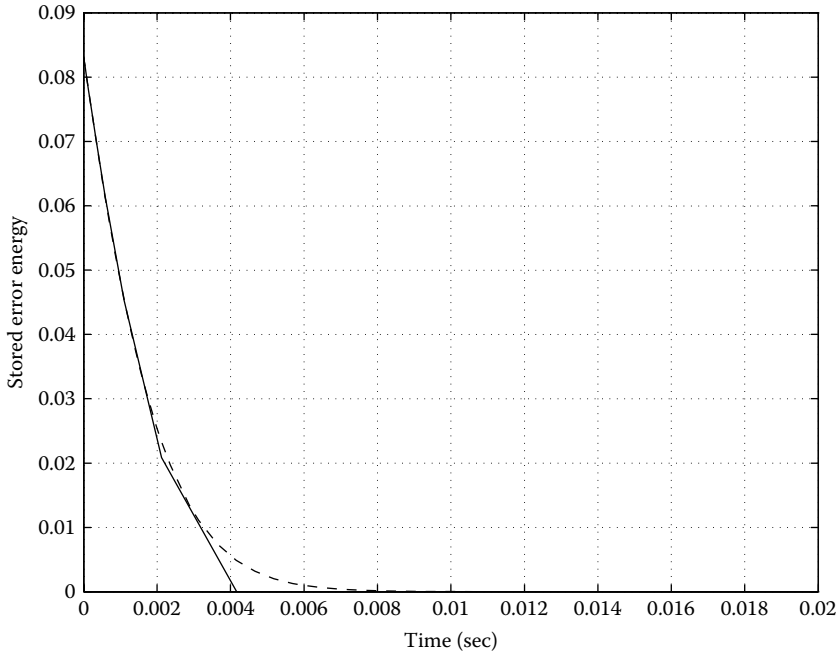

FIGURE 11.14
Stored error energy. Solid line, $\hat{x}_1(0) = 0$, $\hat{x}_2(0) = 0$; dashed line, $\hat{x}_1(0) = 1.95$, $\hat{x}_2(0) = 38.5$.

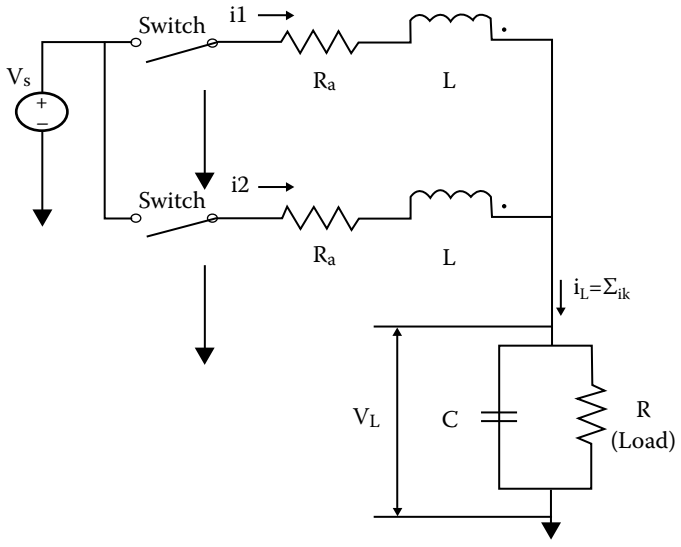

FIGURE 11.15
A two-phase DC/DC converter.

TABLE 11.1

Parameter Values for Simulation

Parameters	L (H)	C(F)	R_a(Ω)	R_L(Ω)	V_s(V)
Set I	1	1	1	1	12
Set II	5×10^{-8}	1×10^{-3}	3×10^{-4}	1×10^{-2}	12

The following control law is used for a two-phase power converter (m = 2) represented in Equation 11.1.64:

$$\begin{aligned} s_1 &= I_1 - \frac{I_{ref}}{m},\ I_{ref} = \frac{V_{ref}}{R_L} \\ u_1 &= V_s\frac{1-sign(s_1)}{2},\ u_2 = V_s\frac{1-sign(s_3^*)}{2}, \end{aligned} \tag{11.1.65}$$

where V_{ref} and I_{ref} are the reference voltage input and the corresponding reference load current, respectively. The desired phase shift $T/2$ is obtained by using two additional blocks, providing a phase of shift $T/4$ to each of them:

$$\begin{aligned} \dot{s}_1 &= \frac{1}{L}\left[-R_a s_1 - \frac{V_s}{2}sign(s_1) + \left(\frac{V_s}{2} - \frac{I_{ref}R_a}{m} - V_L\right)\right] \\ &= -Msign(s_1) - bs_1 + a \\ \dot{s}_2^* &= M[sign(s_1) - sign(s_2^*)] \\ \dot{s}_3^* &= M[sign(s_2^*) - sign(s_3^*)], \end{aligned} \tag{11.1.66}$$

where $a = \frac{V_s}{2L} - \frac{I_{ref}R_a}{mL} - \frac{V_L}{L}$, $M = \frac{V_s}{2L}$, and $b = \frac{R_a}{L}$. As follows from Equation 8.8.14, the only admissible value of a is equal to zero for m = 2. As shown in Figure 11.16, chattering is suppressed in the output current.

The four-phase converter (m = 4) is simulated with switching frequency control of the first phase by appropriate choice of hysteresis width or hysteresis loop gain K_h as a function of V_{ref} to maintain switching frequency at 50 Hz. The selected function $K_h(V_{ref}) = -0.0013V_{ref}^2 + 0.0127V_{ref} - 0.0007$ is shown in Figure 11.17.

Simulations in Figures 11.18 through 11.20 are performed for several values of a in the admissible domain with the following control law:

$$\begin{aligned} u_1 &= V_s\frac{1-sign(s_1)}{2}, u_k = V_s\frac{1-sign(s_k^*)}{2}, (k = 1,\ldots,m) \\ s_1 &= -Msign(s_1) - bs_1 + a \\ s_2^* &= KM[sign(s_1) - sign(s_2^*)] \\ s_3^* &= KM[sign(s_{k-1}^*) - sign(s_k^*)]. \end{aligned} \tag{11.1.67}$$

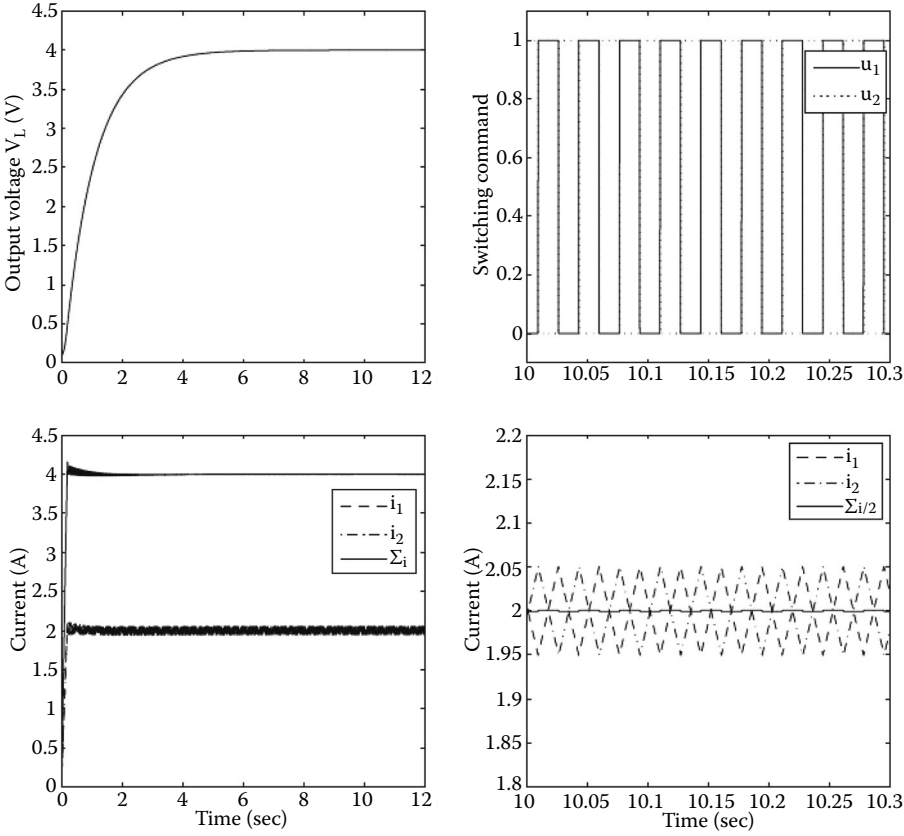

FIGURE 11.16
Simulation results for the two-phase converter ($a = 0$) with parameters of Set I in Table 11.1.

Because a can be out of the admissible range during transients, chattering appears at the beginning of the process. Note that, in the simulation, control (Equation 11.1.67) is without the modification given in Equation 8.8.15. Again, chattering suppression is observed, and the switching frequency is maintained at the same level.

The design methodology is developed under the assumption that state variables are constant within one period of oscillation. Additional simulation is performed for time-varying reference input with control (Equation 11.1.67) and modification (Equation 8.8.17). Simulation results in Figure 11.21 demonstrate efficient chattering suppression for both transient time intervals and steady-state modes.

Next, a set of simulation results for a six-phase converter with control law Equation 11.1.67 ($m = 6$) are shown. In Figures 11.22 through 11.24, it can be seen that the admissible range of reference input is wider for six-phase

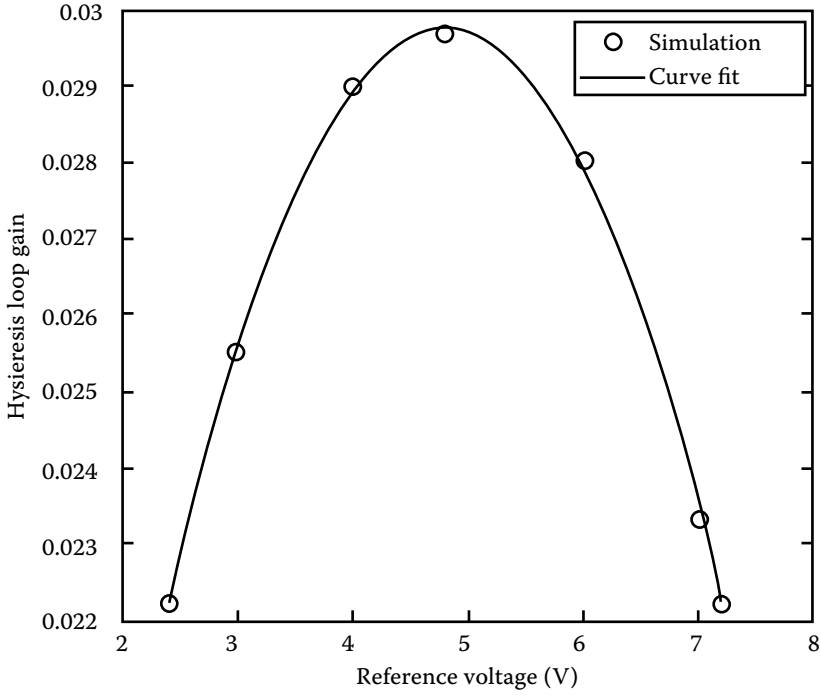

FIGURE 11.17
Hysteresis loop gain K_h.

converter compared with the four-phase converter ($V_{ref,min}$ is equal to 1.714 and 2.4 V, respectively). The chattering suppression effect demonstrated for four-phase converter with time-varying V_{ref} can be observed for six-phase converter as well (see Figure 11.24). For both cases, the modified control Equation 8.8.17 instead of Equations 8.8.12 or 8.8.19 decreases chattering considerably in transient intervals.

For the real-life four-phase DC/DC power converters with parameters from Set II in Table 11.1, simulations are performed for different reference inputs. The effect of chattering suppression for reference inputs 3, 6, and 8 V is demonstrated in Figures 11.25 through 11.27. Note that the inductance is relatively small to have fast converter dynamics. This leads to a high level of chattering in each phase, but it is practically suppressed in the output signal.

Finally, it is demonstrated that chattering can be reduced considerably following the "master-slave method" even if for a given number of phases m, parameter a is beyond the admissible domain (Equation 8.8.14) and the desired phase shift cannot be guaranteed by varying the width of the hysteresis loop. For the master-slave implementation, each phase can be complimented by several sequentially connected slaves, as illustrated in

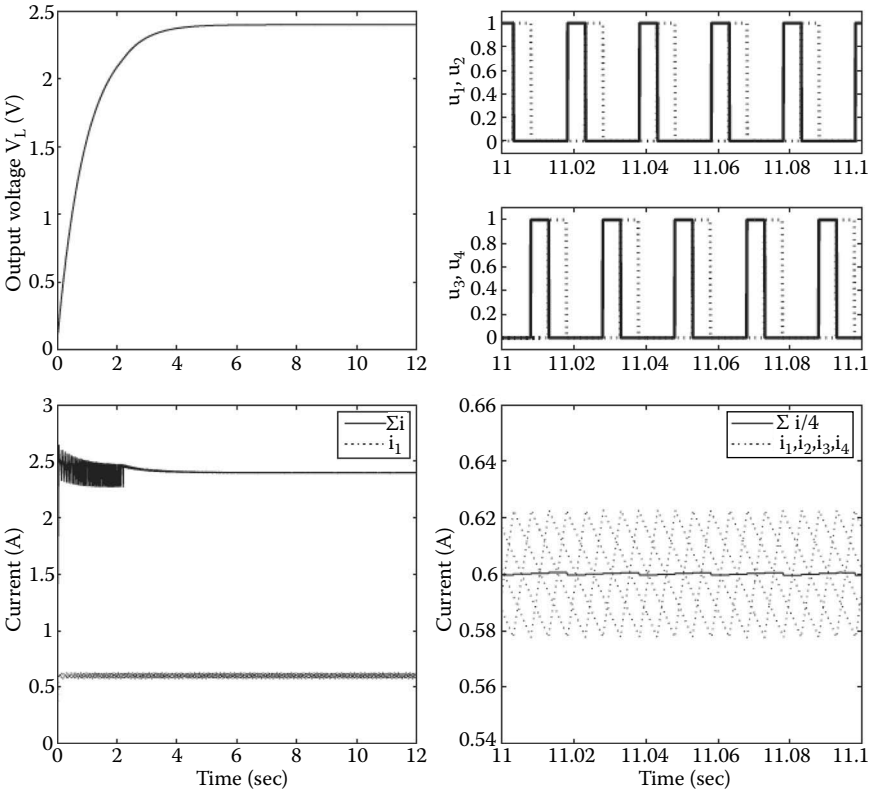

FIGURE 11.18
Simulation results for four phases, $V_{ref} = 2.4V$ (parameters of Set I), $a/b_1 = 0.5$.

Figure 11.28 for two-phase converter, such that the total phase shift is equal to the desired value.

In the general case, each of the m phases, except for the last one, is complemented, for example, by three slaves.

$$
\begin{aligned}
&u_1 = V_s \frac{1 - sign(s_1)}{2}, \dot{s}_1 = -Msign(s_1) - bs_1 + a \\
&u_k = V_s \frac{1 - sign(s^*_{k,3})}{2}, (k = 2, \ldots, m) \\
&\dot{s}^*_{k,i} = K^* \{-sign(s^*_{k,i}) + sign(s^*_{k,i-1})\}, (i = 1, 2, 3) \\
&s^*_{k,0} = s^*_{k-1,3}, s^*_{1,3} = s_1
\end{aligned}
\tag{11.1.68}
$$

and $K^* = 3K$.

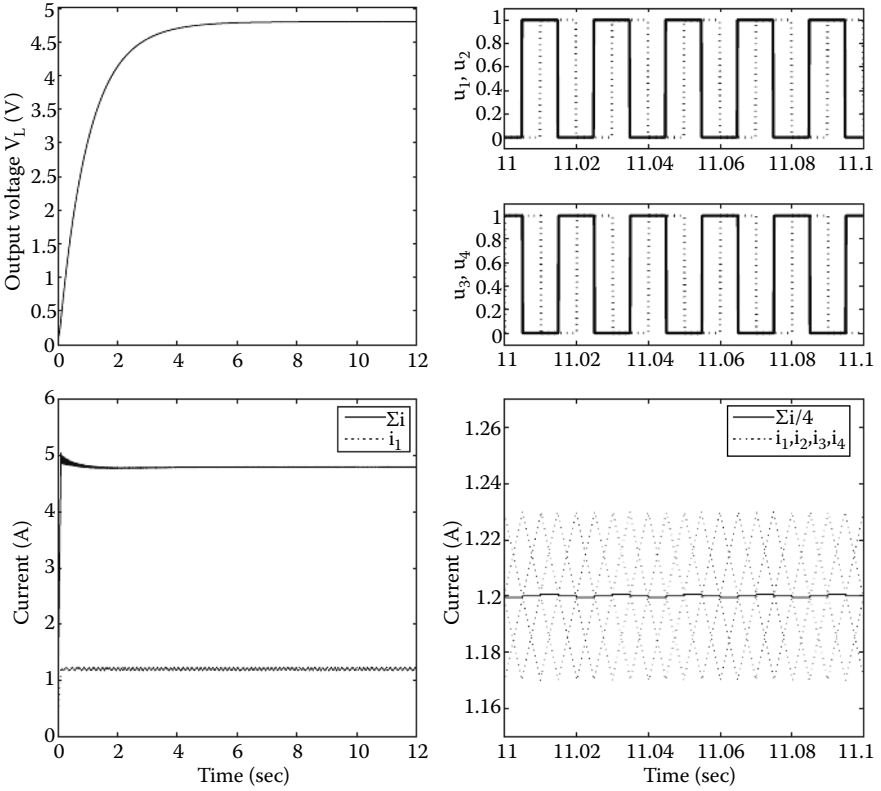

FIGURE 11.19
Simulation results for four phases, $V_{ref} = 4.8V$ (parameters of Set I), $a/b_1 = 0$.

To get the necessary phase shift $T/m = \Delta/2KM$ between the first and second phases, the gain K for the master-slave mode should be as follows (Equation 8.8.19):

$$K = \frac{m\left(1 - \left(\frac{a}{M}\right)^2\right)}{4}.$$

However, because it cannot be implemented with one slave in each phase if a does not satisfy Equation 8.8.14, assume that one-third of the phase can be obtained by one slave.

The periods of oscillations in s_1 and s_2^* are the same, and, according to Equation 8.8.18, the phase difference between corresponding switching of v_1 and $v_{2,1}$ is found as $\frac{\Delta}{2K^*M} = \frac{\Delta}{6KM}$.

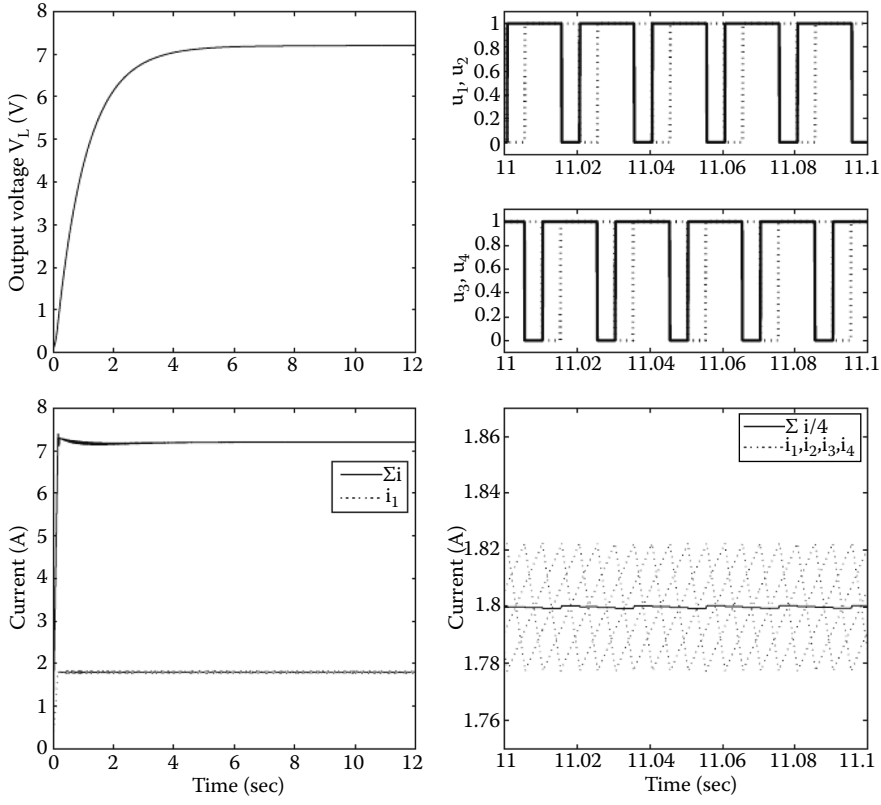

FIGURE 11.20
Simulation result for four phases, $V_{ref} = 7.2V$ (parameters of Set I), $a/b_1 = -0.5$.

As a result, the desired phase shift between v_1 and v_{23} (control command for the second phase),

$$\phi = \frac{\Delta}{2KM} = \frac{T}{m},$$

is obtained.

A simulation is performed for a 4-phase power converter. As can be seen in Figure 11.29, the performance is not acceptable for a 4-phase converter with only one slave in each phase, such that $\frac{a}{M} > 0.5$ and condition Equation 8.8.14 does not hold. Of course, chattering can be suppressed by increasing the number of phases preserving the "one slave in one phase" approach, as shown in Figure 11.30 for an eight-phase converter. Simulation results for a four-phase power converter with application of the proposed methodology are shown in Figure 11.31.

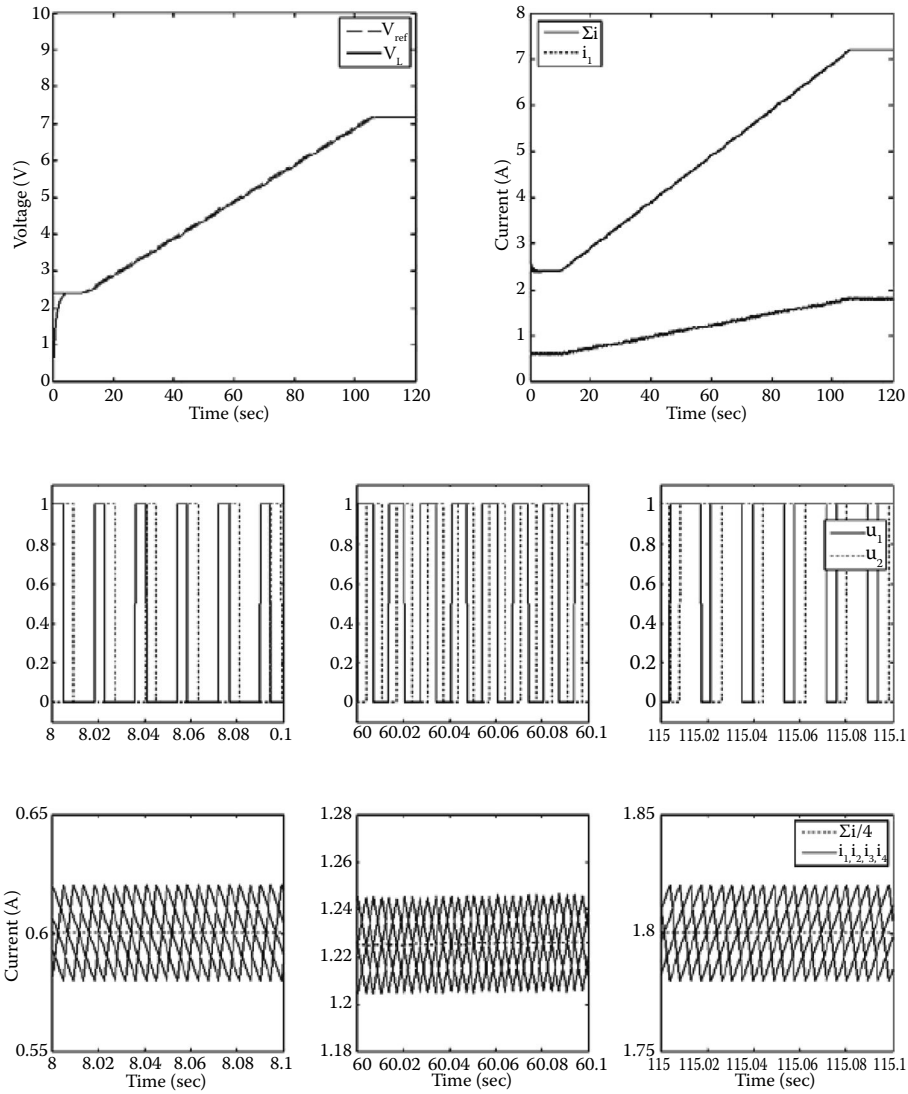

FIGURE 11.21
Simulation results for four phases with time-varying $V_{ref}(t)$.

Comparing the results shown in Figure 11.31 with those in Figure 11.30, it is observed that the effect of chattering reduction is improved significantly by the suggested method, although the ripple magnitude is higher than that of the eight-phase converter model in Figure 11.30. This effect can be explained easily: the relative weight of higher harmonics is increasing with decreasing duty cycle (it is equal to ⅛ for $V_{ref} = 1.5V$); the first three

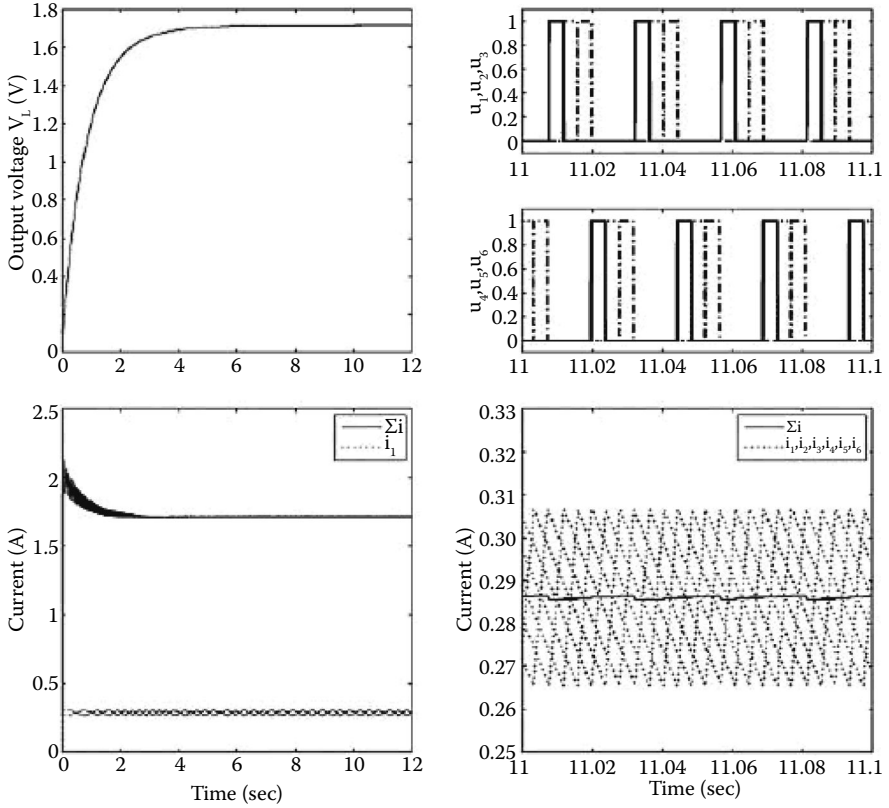

FIGURE 11.22
Simulation results for six phases, $V_{ref} = 1.714V$ (parameter of Set I), $a/b_1 = 2/3$.

harmonics are suppressed only for the four-phase converter, whereas seven harmonics are cancelled for the eight-phase converter.

11.2. Boost-Type AC/DC Converters

Nowadays, semiconductors using high-frequency switching devices such as MOSFET (metal oxide semiconductor field effect transistor), IGBT, and MCT (metal oxide semiconductor-controlled thyristor) are commonly used for drive systems. One of the main control techniques used is voltage modulation. The behavior of phase currents and output voltage as well as switching losses and dynamic responses not only depend on the choice of power semiconductor used but also on the choice of pulse-width modulation (PWM). This explains why PWM techniques have been the subject of intensive

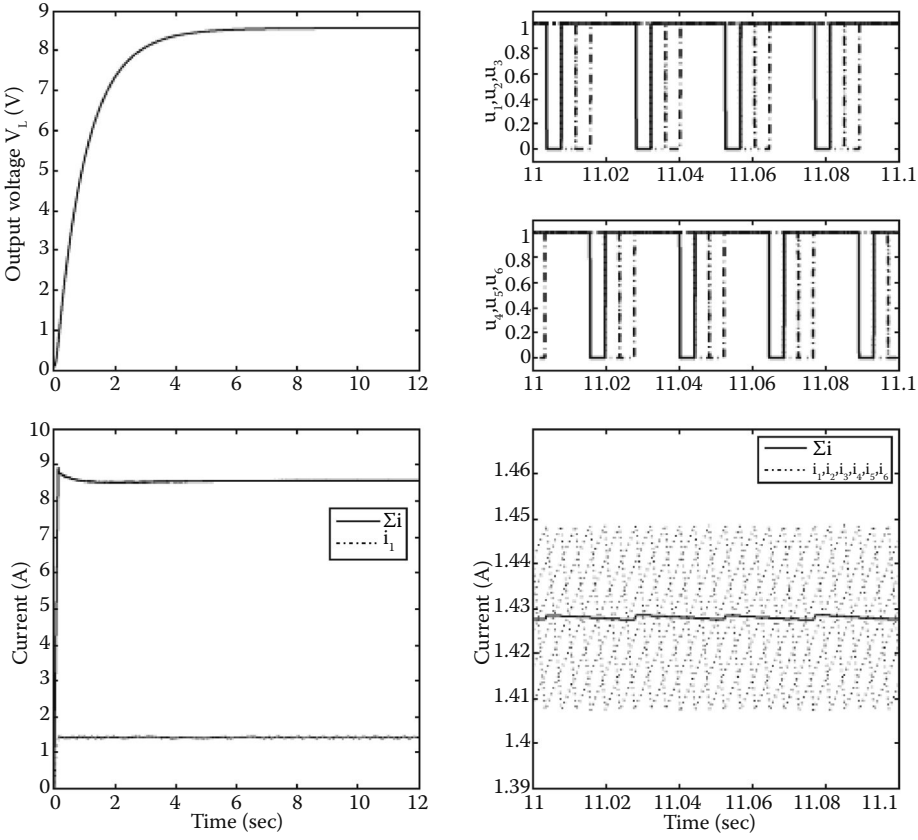

FIGURE 11.23
Simulation results for six phases, $V_{ref} = 8.571V$ (parameters of Set I), $a/b_1 = -2/3$.

research during the past few decades. A large variety of methods, different in concept and performance, have been developed.

These modulation approaches can be classified into two categories depending on the control techniques used: feedforward pulse width modulation based on the so called space-vector method and feedback modulation based on sliding mode or bang-bang control methods. The feedforward PWM technique is characterized by formation of the output voltage via an open-loop control structure. In this case, the drive system does not exhibit high dynamic performance, and the effect of disturbances, which exist always in a drive system, are not automatically reduced. On the other hand, it is very simple to realize a minimum loss PWM strategy. The feedback modulation approach allows an online realization of the switching pattern. This control technique ensures that the frequency and the pulse width are generated automatically together in solving the control task. Feedback control systems possess good dynamic performance because they use all available control

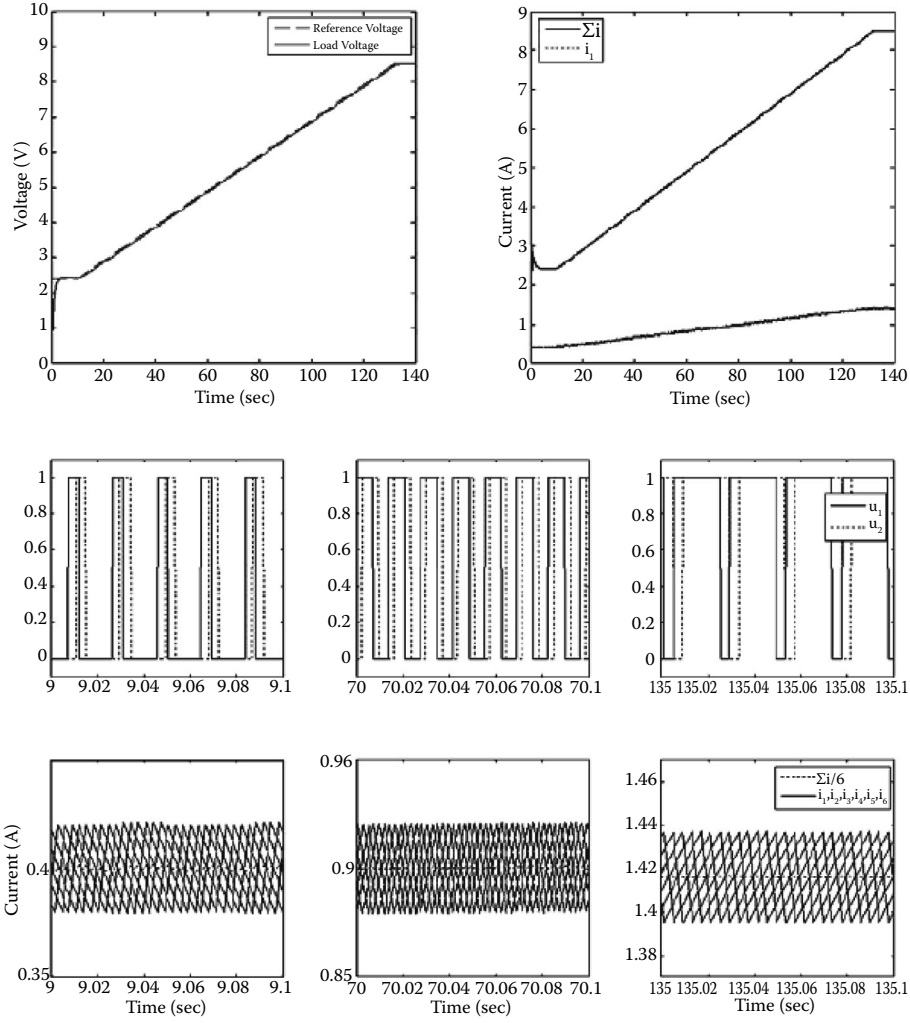

FIGURE 11.24
Simulation result for six phases with time-varying $V_{ref}(t)$.

resources to reduce the error. The influence of disturbances to the system is thus minimized. Many researchers demonstrated the effectiveness of the sliding mode control scheme [see Sabanovic, Sabanovic, and Ohnishi 1993; Vilathgamuwa, Wall, and Jackson 1996].

Compared to conventional PWM techniques, the sliding mode approach has no fixed switching frequency, resulting in a wider spectrum of acoustic noise. Sliding mode control under constant switching frequencies and with minimized switching losses for three-phase converters has also been developed [Sergy and Izosimov 1997].

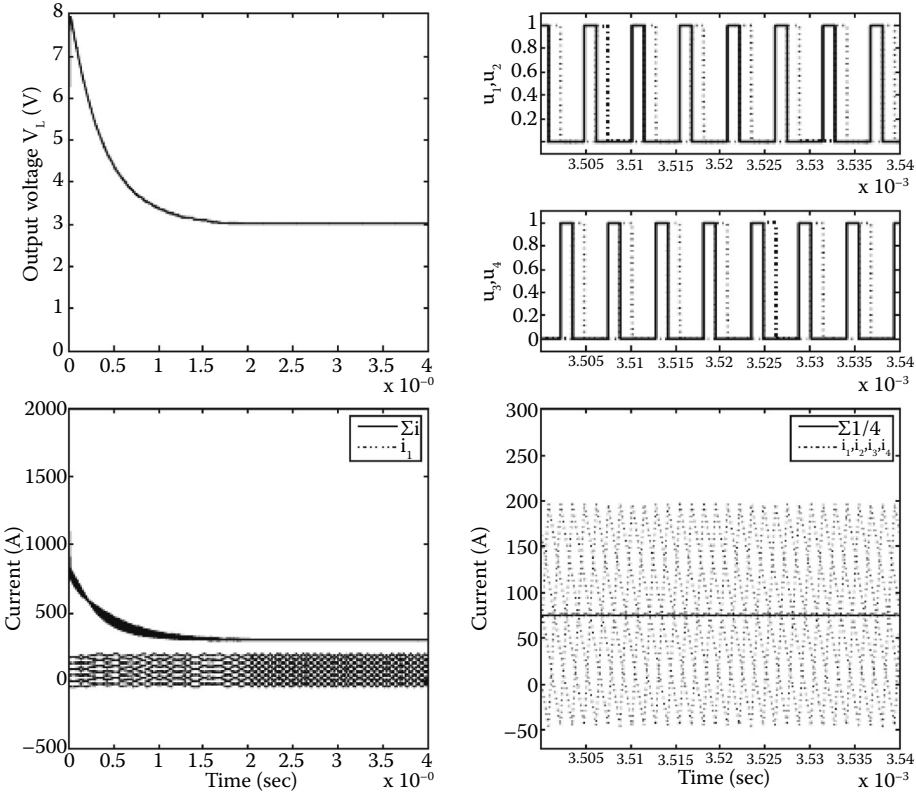

FIGURE 11.25
Simulation result for four phases, $V_{ref} = 3V$ (parameters of Set II).

Three distinguished characteristics may be used to classify multiple-phase converters. First, there are two types of tasks for multiple-phase converters: "rectification" and "inversion." Rectification transforms AC power into DC power, whereas inversion transforms DC power into AC power. Second, the power supply on the DC side may be in the form of either a voltage source or a current source. Third, similar to DC/DC converters, multiple-phase converters can also be classified into buck type and boost type depending on the circuit topology. As a result, there are eight possible combinations to form different types of multiple phase power converters as illustrated in Table 11.2.

An exhaustive study of all these types of converters goes beyond the scope of this text. In this section, we give an example of sliding mode control for a three-phase boost AC/DC converter, a typical converter used in industrial applications.

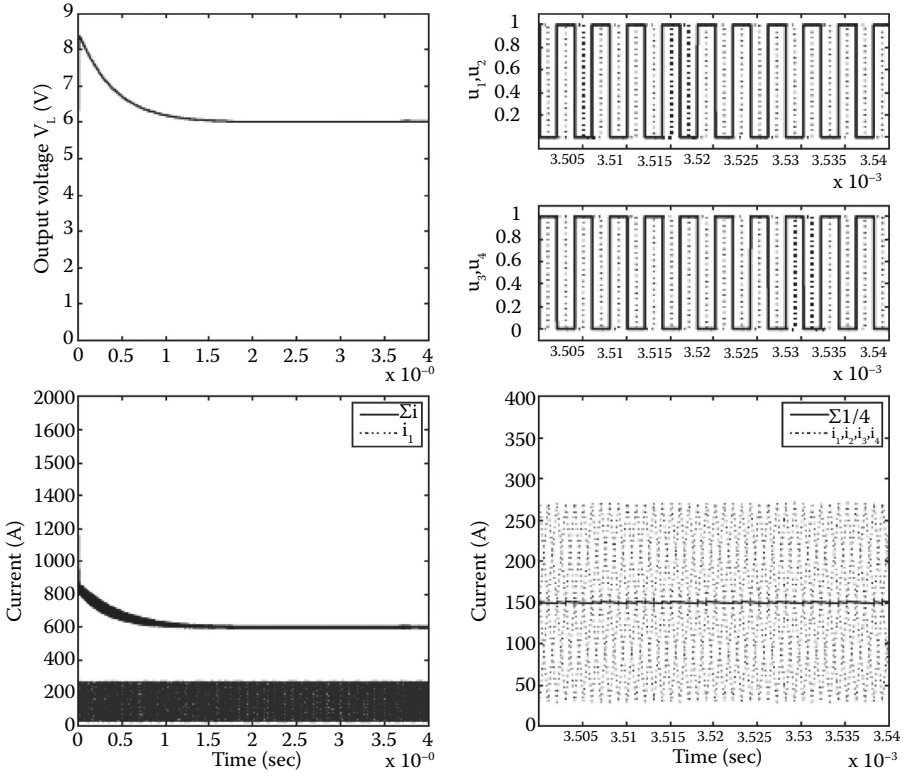

FIGURE 11.26
Simulation result for four phases, $V_{ref} = 6V$ (parameters of Set II).

11.2.1. Model of the Boost-Type AC/DC Converter

Figure 11.32 shows the structure of a boost-type AC/DC converter, in which the variables are defined as follows: L, phase inductance; R_w, phase resistance; C, storage capacitor; i_1, i_2, i_3, phase currents; i_{link}, link current; i_1, load current; u_{g1}, u_{g2}, u_{g3}, source voltages and u_0, output voltage.

For sliding mode control design, symmetric control inputs from discrete set {–1, 1} are more convenient than the on-off signals from discrete set {0, 1}. Let the six on-off signals of an AC/DC converter be denoted by

$$s_w = [s_{w1}\ s_{w2}\ s_{w3}\ s_{w4}\ s_{w5}\ s_{w6}]^T. \tag{11.2.1}$$

The control inputs, as they appear in the converter model, are defined as $U_{gate} = [u_1\ u_2\ u_3]^T$. Note that U_{gate} does not represent some control voltages

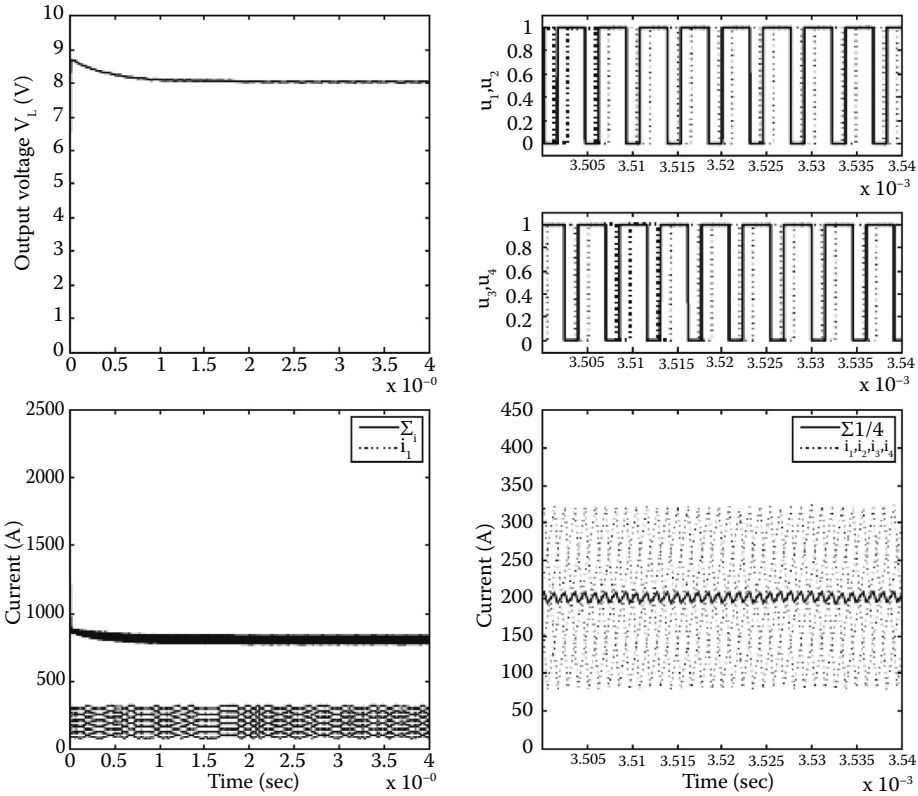

FIGURE 11.27
Simulation result for four phases, $V_{ref} = 8V$ (parameter Set II).

but rather a set of transformed control inputs taking values from the discrete set {–1, 1} instead of {0, 1} as done by s_w. Thus, the following relation holds:

$$\boldsymbol{U}_{gate} = \boldsymbol{G}_w \boldsymbol{s}_w \text{ with } \boldsymbol{G}_w = \begin{bmatrix} 1 & 0 & 0 & -1 & 0 & 0 \\ 0 & 1 & 0 & 0 & -1 & 0 \\ 0 & 0 & 1 & 0 & 0 & -1 \end{bmatrix}. \tag{11.2.2}$$

In the following, the dynamic model of the boost AC/DC converter will be given in both the phase coordinate frame and the field-oriented coordinate frame. The models in these two coordinate frames are useful for our sliding mode controller and observer design.

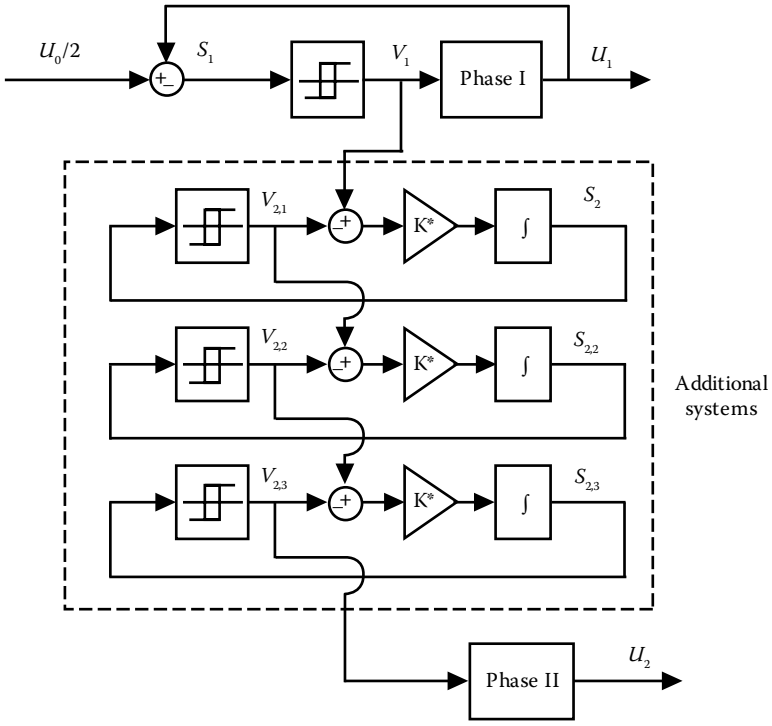

FIGURE 11.28
A modified master-slave mode schematic with two more additional systems. $v_{2,3}$ is the switching command for the second channel.

11.2.1.1. Model in Phase Coordinate Frame

Starting from the notation given in Equation 11.2.2, the dynamic model of a boost AC/DC converter in phase coordinate frame can be obtained using the theory of switched electric circuits,

$$\begin{aligned}
\frac{di_1}{dt} &= -\frac{R_w}{L} i_1 - \frac{u_0}{6L}(2u_1 - \sum_{j=2}^{3} u_j) + \frac{1}{L} u_{g1}, \\
\frac{di_2}{dt} &= -\frac{R_w}{L} i_2 - \frac{u_0}{6L}(2u_2 - \sum_{j=1,\, j\neq 2}^{3} u_j) + \frac{1}{L} u_{g2}, \\
\frac{di_3}{dt} &= -\frac{R_w}{L} i_3 - \frac{u_0}{6L}(2u_3 - \sum_{j=1}^{2} u_j) + \frac{1}{L} u_{g3}, \\
\frac{du_0}{dt} &= -\frac{i_l}{C} + \frac{1}{2C} \sum_{i=1}^{3} u_k i_k.
\end{aligned} \tag{11.2.3}$$

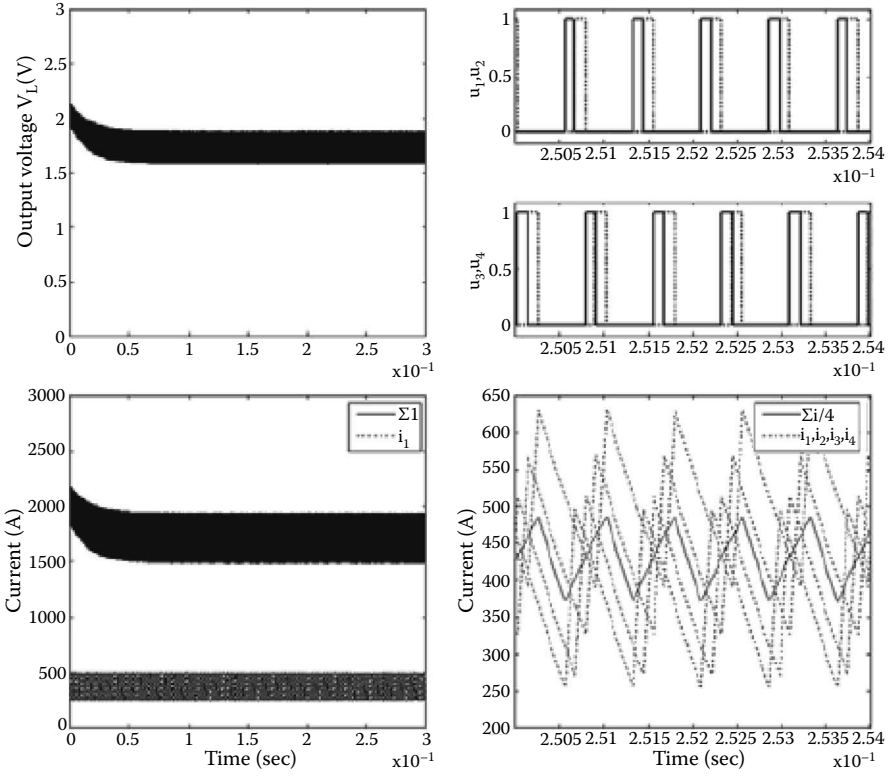

FIGURE 11.29
Simulation results for four-phase converter, $V_{ref} = 1.5V$, $R_L = 1m\Omega$, (parameters of Set II).

11.2.1.2. Model in (d, q) Coordinate Frame

As shown in Chapter 10, the control design of an AC motor is often performed in a field-oriented coordinate system, usually called (d, q) coordinates. For the control of an AC synchronous motor, the field-oriented coordinate system is simply the rotor coordinates. Similarly, for the control of three-phase AC/DC converters, it is convenient to design the control in the rotating reference frame synchronized with the supply frequency, i.e., the (d, q) coordinate system. In this case, all state variables should be transformed into the (d, q) coordinate system using the following relations:

$$\begin{aligned} x_\alpha + jx_\beta &= \sqrt{2/3}(x_1 + e^{j2\pi/3}x_2 + e^{j4\pi/3}x_3), \\ x_d + jx_q &= (x_\alpha + jx_\beta)e^{-j\theta}, \\ \theta &= \int \omega(t)dt, \end{aligned} \tag{11.2.4}$$

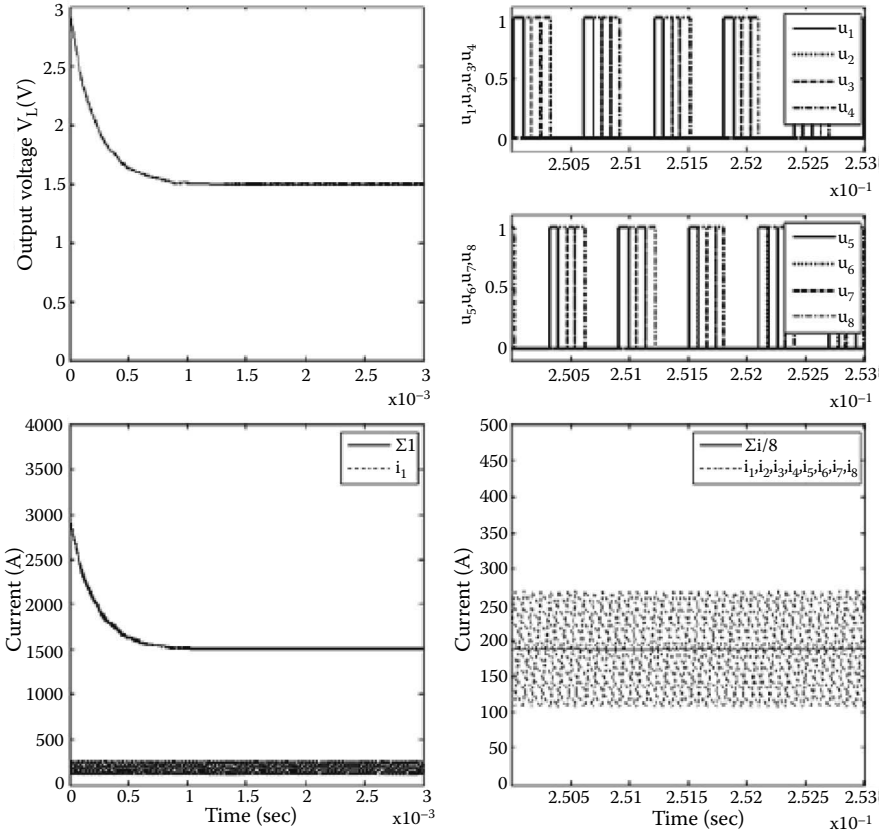

FIGURE 11.30
Simulation results for eight-phase converter, $V_{ref} = 1.5V$, $R_L = 1m\Omega$, (parameters of Set II).

where $\omega(t)$ is the supply frequency; (x_1, x_2, x_3) denote the state variables in phase coordinates, e.g., the phase currents (i_1, i_2, i_3), the source voltages (u_{g1}, u_{g2}, u_{g3}), and the switching controls (u_1, u_2, u_3); (x_α, x_β) represent the state variables, i.e., (i_α, i_β), $(u_{g\alpha}, u_{g\beta})$, and (u_α, u_β) in a fixed orthogonal coordinate system with the α-axis aligned with the axis of phase 1; and (x_d, x_q) are the state variables, i.e., (i_d, i_q), (u_{gd}, u_{gq}), and (u_d, u_q), in the (d, q) coordinate frame.

Remark 11.1

Here u_d, u_q are the transformed switching controls u_1, u_2, u_3 rather than transformed phase voltages as in the case of AC motors.

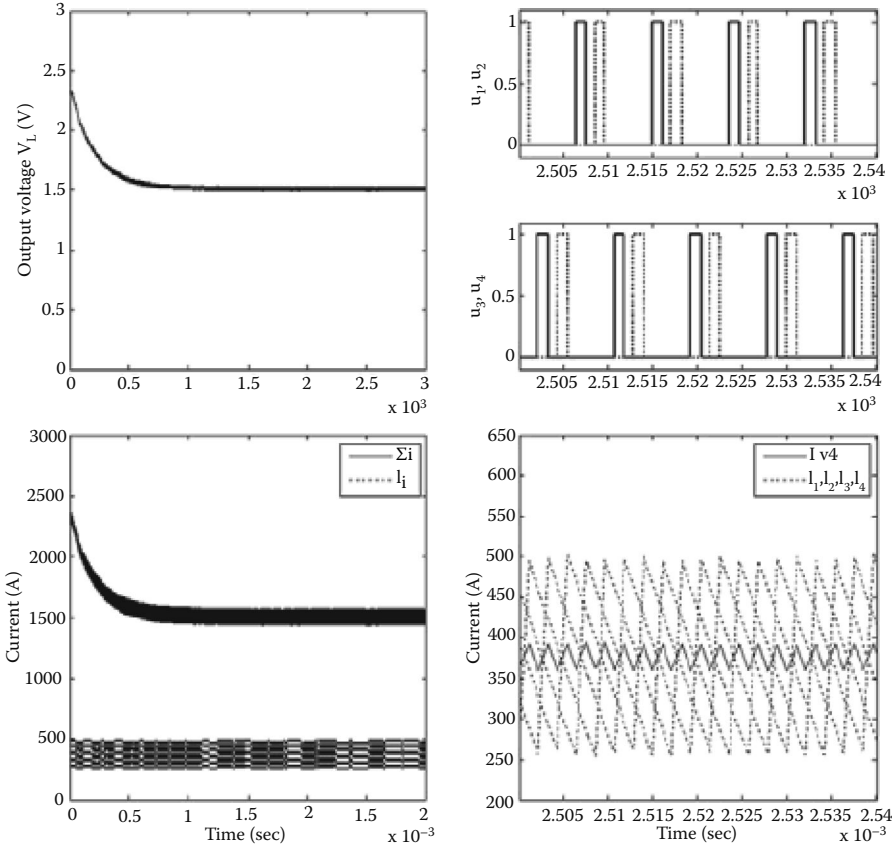

FIGURE 11.31
Simulation results for a four-phase converter, $V_{ref} = 1.5V$, $R_L = 1m\Omega$, (parameters of Set II) with triple slave method.

Equation (11.2.4) can be rewritten in matrix form:

$$\begin{bmatrix} x_d \\ x_q \end{bmatrix} = A_{d,q}^{\alpha,\beta} A_{\alpha,\beta}^{1,2,3} \begin{bmatrix} x_1 \\ x_2 \\ x_3 \end{bmatrix}, \tag{11.2.5}$$

where the transformation matrices are defined as

TABLE 11.2
Characteristics Used to Classify Multiple-Phase Converters

Type of transform	Rectification (AC to DC)	Inversion (DC to AC)
Power supply DC side	Voltage source	Current source
Circuit topology	Buck	Boost

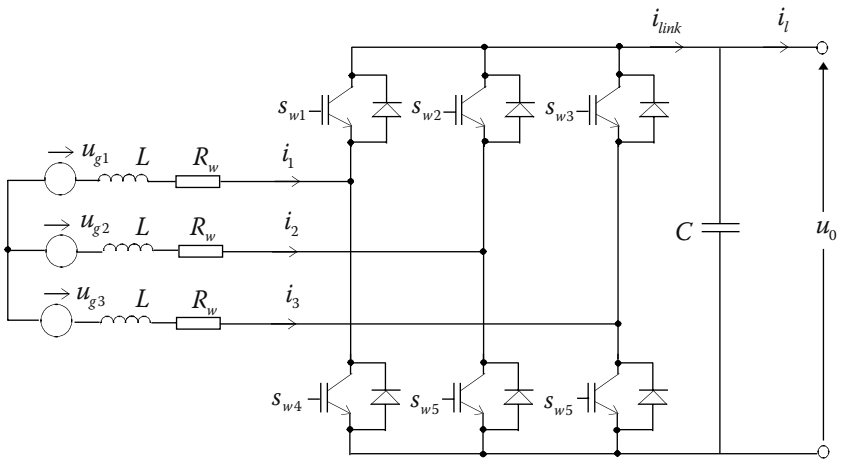

FIGURE 11.32
Boost type AC/DC converter.

$$A_{\alpha,\beta}^{1,2,3} = \frac{2}{3}\begin{bmatrix} 1 & -1/2 & -1/2 \\ 0 & \sqrt{3}/2 & -\sqrt{3}/2 \end{bmatrix},\ A_{d,q}^{\alpha,\beta} = \begin{bmatrix} \cos\theta & \sin\theta \\ -\sin\theta & \cos\theta \end{bmatrix}. \tag{11.2.6}$$

The inverse transformation is given by

$$\begin{bmatrix} x_1 \\ x_2 \\ x_3 \end{bmatrix} = \frac{3}{2}(A_{\alpha,\beta}^{1,2,3})^T (A_{d,q}^{\alpha,\beta})^T \begin{bmatrix} x_d \\ x_q \end{bmatrix}. \tag{11.2.7}$$

Using the above relations, the dynamic model (Equation 11.2.3) can be transformed into the (d, q) coordinate frame:

$$\begin{aligned} \frac{du_{0d}}{dt} &= -\frac{i_l}{C} + \frac{i_d u_d + i_q u_q}{2C}, \\ \frac{di_d}{dt} &= -\frac{R_w}{L} i_d + \frac{u_{gd}}{L} + \omega i_q - \frac{u_{od}}{2L} u_d, \\ \frac{di_q}{dt} &= -\frac{R_w}{L} i_q + \frac{u_{gq}}{L} - \omega i_d - \frac{u_{od}}{2L} u_q, \end{aligned} \tag{11.2.8}$$

where $u_{0d} = u_0$ ($u_{0q} = 0$ as a result of the field orientation).

11.2.2. Control Problems

A well-controlled three-phase AC/DC power converter should have the following characteristics:

- Unity power factor
- Sinusoidal input currents
- Regenerative capability
- Ripple free output voltage

From an electromagnetic interference point of view, fixed switching frequency is also an important characteristic that is inherently induced in a PWM-controlled converter. For a sliding mode-controlled converter, however, fixed switching frequency cannot be guaranteed because the switching action occurs according to the value of a sliding function and is not synchronized with a frequency source. In fact, varying switching frequencies are a distinct feature of sliding mode control systems.

In industrial power converter systems, one of the major design challenges is an unknown varying load that requires sufficient control robustness. Moreover, not all state variables that are necessary for the control purpose are measured or are measurable. As a result, a control engineer has to face the problem of designing a robust control system with observed state variables as well as achieving a high performance of the closed-loop system.

Control design of power converters is usually performed in two steps: current control in an inner loop and voltage control in an outer loop. In the frame of this cascaded control structure, sliding mode method is usually applied to the current control, whereas the outer-loop control, i.e., the output voltage regulation, is designed using linear control techniques. This holds for both DC/DC converters and AC/DC converters (Figure 11.33).

11.2.2.1. Sliding Mode Current Control

Similar to the control design for electric motors, the current control of a boost-type AC/DC converter can be designed in either phase coordinates or the (d, q) coordinate frame. Because the control criteria (as listed in the performance

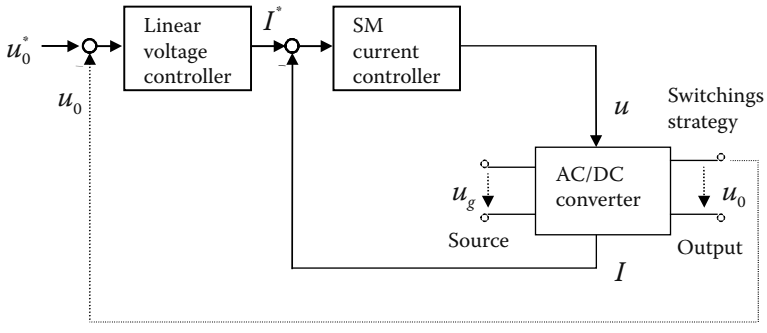

FIGURE 11.33
Cascaded control structure of AC/DC converters.

characteristics) are normally given in the (d, q) coordinate frame, it is more convenient to design the current control in the (d, q) coordinate frame than in phase coordinates.

Rewrite the current dynamics in Equation 11.2.8 as follows:

$$\begin{aligned}\frac{di_d}{dt} &= -\frac{R_w}{L}i_d + \frac{u_{gd}}{L} + \omega i_q - \frac{u_{od}}{2L}u_d,\\ \frac{di_q}{dt} &= -\frac{R_w}{L}i_q + \frac{u_{gq}}{L} - \omega i_d - \frac{u_{od}}{2L}u_q.\end{aligned} \tag{11.2.9}$$

These equations are the starting point for the current control. To simplify the derivations and to use the results developed for the electric motors, Equation 11.2.9 is represented in a generalized matrix form:

$$\dot{\boldsymbol{I}}_{dq} = \boldsymbol{f}_{dq}(\boldsymbol{I}_{\mathbf{dq}}, \boldsymbol{U}_{\mathbf{g}}, \boldsymbol{\omega}) - b\boldsymbol{U}_{dq}, \tag{11.2.10}$$

where $b = \dfrac{u_{0d}}{2L}$, $\boldsymbol{I}_{dq} = \begin{bmatrix} i_d & i_q \end{bmatrix}^T$, $\boldsymbol{U}_{dq} = \begin{bmatrix} u_d & u_q \end{bmatrix}^T$, and

$$\boldsymbol{f}_{dq}(\boldsymbol{I}_{\mathbf{dq}}, \boldsymbol{U}_{\mathbf{g}}, \omega) = \begin{bmatrix} -\dfrac{R_w}{L}i_d + \dfrac{u_{gd}}{L} + \omega i_q \\ -\dfrac{R_w}{L}i_q + \dfrac{u_{gq}}{L} - \omega i_d \end{bmatrix}. \tag{11.2.11}$$

The switching functions for the current control are designed as

$$\begin{aligned} s_d &= i_d^* - i_d,\\ s_q &= i_q^* - i_q,\end{aligned} \tag{11.2.12}$$

where i_d^* and i_q^* are the desired values of the currents in the (d, q) coordinate frame to be determined by the outer control loop for the output voltage regulation. The next task is to find the condition under which sliding mode can be enforced. As for the AC/DC converters, no control gain can be adjusted. The solution is to find a domain in the system space from which any state trajectory converges to the sliding manifold defined by $s_d = 0$, $s_q = 0$. Defining $\boldsymbol{S}_{dq} = \begin{bmatrix} S_d & S_q \end{bmatrix}^T$ and taking the time derivative of $\boldsymbol{S}_{dq}$ yields

$$\dot{\boldsymbol{S}}_{dq} = \dot{\boldsymbol{I}}_{dq}^* - \boldsymbol{f}_{dq}(\boldsymbol{I}_{dq}, \boldsymbol{U}_g, \omega) + b\boldsymbol{U}_{dq} = \boldsymbol{F}_{dq} + D\boldsymbol{U}_{gate}, \tag{11.2.13}$$

in which $\boldsymbol{I}_{dq}^* = \begin{bmatrix} i_d^* & i_q^* \end{bmatrix}^T$, $\boldsymbol{F}_{dq} = \dot{\boldsymbol{I}}_{dq}^* - \boldsymbol{f}_{dq}(\boldsymbol{I}_{dq}, \boldsymbol{U}_g, \omega)$ and

$$D = bA_{d,q}^{\alpha,\beta} A_{\alpha,\beta}^{1,2,3}. \tag{11.2.14}$$

Design controls $U_{gate} = [u_1\ u_2\ u_3]^T$ as follows:

$$\boldsymbol{U}_{\text{gate}} = -\text{sign}(\mathbf{S}^*), \tag{11.2.15}$$

where $\boldsymbol{S}^* = \begin{bmatrix} s_1^* & s_2^* & s_3^* \end{bmatrix}^T$ is a vector of transformed switching functions being determined later, and

$$\text{sign}(\boldsymbol{S}^*) = \begin{bmatrix} \text{sign}(s_1^*) & \text{sign}(s_2^*) & \text{sign}(s_3^*) \end{bmatrix}^T. \tag{11.2.16}$$

Apparently, controls u_1, u_2, u_3 take values from the discrete set {–1, +1}. The transformed vector $\boldsymbol{S}^*$ should be designed such that, under controls (Equation 11.2.15), s_d and s_q vanish in finite time. Vector $\boldsymbol{S}^*$ is selected as

$$\boldsymbol{S}^* = \frac{3}{2b^2} D^T \boldsymbol{S}_{dq}. \tag{11.2.17}$$

Note that $\boldsymbol{S}_{dq} = D\boldsymbol{S}^* = (3/2b^2)\text{DD}^T\boldsymbol{S}_{dq} = \boldsymbol{S}_{dq}$.

Theorem 11.4

Under control Equation 11.2.15 and transformation Equation 11.2.17, there exist a domain of $s_d(0)$ and $s_q(0)$ in which the state vector of system Equation 11.2.13 converges to the origin $s_d = 0$, $s_q = 0$ in finite time. □

Proof 11.4

Design a Lyapunov function candidate,

$$V = \frac{1}{2} \mathbf{S}_{dq}^T \mathbf{S}_{dq}. \tag{11.2.18}$$

Its time derivative along the solutions of Equation 11.2.13 is of form

$$\dot{V} = (\boldsymbol{S}^*)^T \boldsymbol{F}^* + (\boldsymbol{S}^*)^T D^T D \boldsymbol{U}_{gate}, \tag{11.2.19}$$

where $\boldsymbol{F}^* = \begin{bmatrix} F_1^* & F_2^* & F_3^* \end{bmatrix}^T = D^T \boldsymbol{F}_{dq}$. Substituting control Equation 11.2.15 into Equation 11.2.19 results in

$$\dot{V} = (\boldsymbol{S}^*)^T \boldsymbol{F}^* - (\boldsymbol{S}^*)^T D^T D\, \text{sign}(\boldsymbol{S}^*), \tag{11.2.20}$$

where matrix D^TD is a singular matrix and can be calculated as

$$D^T D = b^2 \frac{4}{9} \begin{bmatrix} 1 & -\frac{1}{2} & -\frac{1}{2} \\ -\frac{1}{2} & 1 & -\frac{1}{2} \\ -\frac{1}{2} & -\frac{1}{2} & 1 \end{bmatrix}. \tag{11.2.21}$$

Similar to the case of electric motor control (see Chapter 10), depending on the signs of s_1^*, s_2^* and s_3^*, there are eight possible combinations of values of sign(s_1^*), sign(s_2^*), and sign(s_3^*). Evaluation of Equation 11.2.17 shows that two of these combinations are not possible, i.e., sign(s_1^*), sign(s_2^*), and sign(s_3^*) are never all +1 or all –1. The remaining six combinations can be summarized as

$$\text{sign}(s_l^*) \neq \text{sign}(s_m^*) = \text{sign}(s_n^*), \text{ with } l \neq m \neq n \text{ and } l, m, n \in \{1,\ 2,\ 3\}. \tag{11.2.22}$$

Starting from this notation, Equation 11.2.20 can be expanded as

$$\dot{V} = \left(s_1^* F_1^* + s_2^* F_2^* + s_3^* F_3^*\right) - (2/3)^2 b^2 \left(2\left|s_l^*\right| + \left|s_m^*\right| + \left|s_n^*\right|\right), \tag{11.2.23}$$

with $l \neq m \neq n$ and $l, m, n \in \{1, 2, 3\}$. This equation can be further represented as

$$\dot{V} = \left(s_1^* F_1^* + s_2^* F_2^* + s_3^* F_3^*\right) - (2/3)^2 b^2 \left(\left|s_l^*\right| + \left|s_m^*\right| + \left|s_n^*\right|\right) - (2/3)^2 b^2 \left|s_l^*\right|. \tag{11.2.24}$$

Apparently, inequality

$$(2/3)^2 b^2 \geq \max\left(\left|F_1^*\right|,\ \left|F_2^*\right|,\ \left|F_3^*\right|\right) \tag{11.2.25}$$

is a sufficient condition for $\dot{V} < 0$. □

Inequality Equation 11.2.25 defines a subspace in the system space in which the state trajectories converge to the sliding manifold $\boldsymbol{S}_{dq} = \mathbf{0}$ in finite time. This is to show that the attraction domain of the sliding manifold is bounded in the state space. Note that parameter $b = \frac{u_{0d}}{2L}$ should be high enough at initial time instant. Because $u_{0d} = u_0$, the output voltage should not be zero at the initial time instant. In critical applications, this can be achieved by starting the converter operation with an open-loop control. In fact, as discussed in the DC/DC converter part, an observer-based control scheme can also be applied here such that sliding mode occurs starting from the initial time

instant. However, the associated convergence proof is rather involved and thus goes beyond this text.

As the last step of the control design, the resulting controls u_1, u_2, and u_3 should be mapped into the switching patterns applying to the power converter using the following relations:

$$\begin{aligned} s_{w1} &= \frac{1}{2}(1+u_1),\ s_{w4} = 1 - s_{w1}, \\ s_{w2} &= \frac{1}{2}(1+u_2),\ s_{w5} = 1 - s_{w2}, \\ s_{w3} &= \frac{1}{2}(1+u_3),\ s_{w6} = 1 - s_{w3}. \end{aligned} \tag{11.2.26}$$

For implementation of the proposed current control, matrix D^T is needed for transformation Equation 11.2.17 (exact values of F_{dq} are not required for the implementation). Matrix D^Tcan be found as

$$D^T = b\begin{bmatrix} \cos\theta_a & -\sin\theta_a \\ \cos\theta_b & -\sin\theta_b \\ \cos\theta_c & -\sin\theta_c \end{bmatrix}, \tag{11.2.27}$$

where $\theta_a = \theta$, $\theta_b = \theta - 2\pi/3$ and $\theta_c = \theta + 2\pi/3$.

11.2.2.2. Output Voltage Regulation

In this section, the reference currents feeding to the current controller, i_d^* and i_q^*, will be determined to ensure asymptotic stability of the output voltage regulation in the outer loop. Neglecting the voltage drop over the phase resistance R_w, the system model in the (d, q) reference frame can be simplified to

$$\begin{aligned} \frac{du_{0d}}{dt} &= -\frac{i_l}{C} + \frac{i_d u_d + i_q u_q}{2C}, \\ L\frac{di_d}{dt} &= u_{gd} + \omega L\, i_q - \frac{u_{0d}}{2} u_d, \\ L\frac{di_q}{dt} &= u_{gq} - \omega L\, i_d - \frac{u_{0d}}{2} u_q. \end{aligned} \tag{11.2.28}$$

Normally, the value of the inductance satisfies $L \ll 1$, and the right-hand sides of the equations in Equation 11.2.28 have the values of the same order. Hence, di_d/dt, $di_q/dt \gg du_{0d}/dt$, implying that the dynamics of i_d and i_q are much faster than those of u_{0d}. Provided that the fast dynamics are stable,

the outer-loop control can be simplified considerably. Based on the singular perturbation theory, we can formally let the left-hand sides of the second and third equations in Equation 11.2.28 be equal to zero and then solve the algebraic equations for u_d and u_q. As a result, the following equation system is valid for control design of the slow-manifold:

$$\begin{aligned} u_d &= 2(u_{gd} + \omega L\, i_q^*)/u_{0d}, \\ u_q &= 2(u_{gq} - \omega L\, i_d^*)/u_{0d}, \\ \frac{du_{0d}}{dt} &= -\frac{i_l}{C} + \frac{i_d^* u_d + i_q^* u_q}{2C}, \end{aligned} \tag{11.2.29}$$

where i_d^* and i_q^* are the reference values of i_d and i_q, respectively. Note that we replaced the real currents with their reference values, because we assume that the inner current control loop is in sliding mode with $s_d = i_d^* - i_d = 0$, $s_q = i_q^* - i_q = 0$. Based on Equation 11.2.29, these reference currents will be determined depending on the desired system performance.

The design goals have been given in the performance characteristics at the beginning of Section 11.2.2. The demand of sinusoidal input currents has been fulfilled automatically by involving the (d, q) transformation. The following characteristics will cover the major requirements of a well-controlled boost AC/DC converter:

1. The output voltage should converge to its reference value u_0^*.
2. The input current phase-angle should trace its reference value $\rho^* = \arctan(i_q^*/i_d^*)$.
3. The power-balance condition should be satisfied, i.e., $u_{gd} i_d^* + u_{gq} i_q^* = u_0^* i_l = u_{0d}^* i_l$.

The reference currents i_d^* and i_q^* will be calculated satisfying these requirements. Substitution of the first and second equations of Equation 11.2.29 into the third equation yields

$$\frac{du_{0d}}{dt} = -\frac{i_l}{C} + \frac{u_{gd} i_d^* + u_{gq} i_q^*}{C u_{0d}}. \tag{11.2.30}$$

Considering the power-balance condition, the above equation can be simplified to

$$\frac{du_{0d}}{dt} = -\frac{i_l}{C} + \frac{u_{0d}^* i_l}{C u_{0d}}. \tag{11.2.31}$$

For simplicity, only the case of a pure resistance load R_l is considered here, thus load current i_l in Equation 11.2.31 can be replaced by $i_l = u_{0d}/R_l$. Consequently, linear dynamics for output voltage u_{0d} can be obtained

$$\frac{du_{0d}}{dt} = \frac{u_{0d}^* - u_{0d}}{R_l C}. \tag{11.2.32}$$

Defining the voltage regulation error as $\bar{u}_{0d} = u_{0d}^* - u_{0d}$ with a constant desired voltage $\dot{u}_{0d}^* = 0$, we have

$$\bar{u}_{0d} + R_l C \dot{\bar{u}}_{0d} = 0. \tag{11.2.33}$$

Obviously, the voltage error tends to zero asymptotically with the time constant $R_l C$. The above derivations mean that, if the power-balance condition is fulfilled, the output voltage converges to its reference value automatically. Solving the equations for requirements 2 and 3 with respect to i_d^* and i_q^* yields

$$\begin{aligned} i_d^* &= \frac{u_0^* i_l}{u_{gd} + u_{gq} \tan \rho^*}, \\ i_q^* &= \frac{u_0^* i_l \tan \rho^*}{u_{gd} + u_{gq} \tan \rho^*}. \end{aligned} \tag{11.2.34}$$

The input current phase-angle ρ^* defined in the second requirement is usually determined by the control designer.

11.2.2.3. Simulation Results

The proposed sliding mode current controller and output voltage regulator are validated by the following simulation results. Parameters of the AC/DC converter are preset as $R_w = 0.45\Omega$, $L = 7.5$ mH, $C = 820\mu$F, and load resistance $R_l = 182\Omega$. The amplitude of the supply voltage is selected as $E = 50/\sqrt{3}$ V. The frequency of the supply voltage ω is 377 rad/sec. The simulation results are shown in Figures 11.34 through 11.37.

11.2.3. Observer for Sensorless Control

In the previous section, we developed a cascaded control structure to control the phase currents, output voltage, power factor, and the input current phase angle of boost-type AC/DC converters. Sliding mode current control ensures fast convergence of the real currents to their reference counterparts. However, this control structure is based on the assumption that the following information is available:

- Phase currents i_1, i_2, i_3
- Source voltages u_{g1}, u_{g2}, u_{g3}
- Supply frequency ω
- Load current i_l

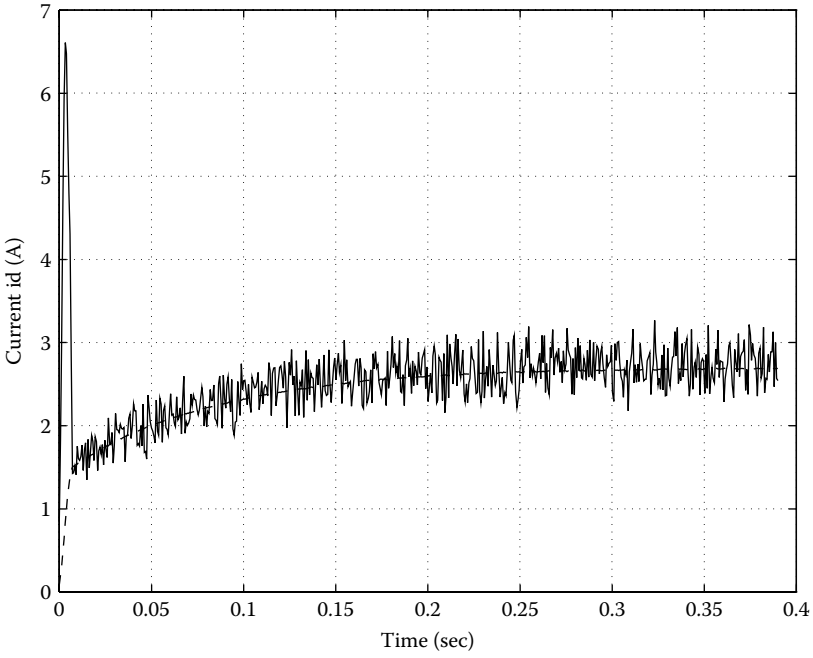

FIGURE 11.34
Current component $i_{d.}$

In industrial systems, the source voltages, assumed to have sinusoidal form, may come from a synchronous generator; transducers are needed for sensing their amplitude and frequency. The same holds for the phase currents and the load current. To minimize the number of sensors and hence the maintenance costs, a link current sensor may be integrated nearby the storage capacitor (see Figure 11.32). Based on this link current sensor, all state variables needed for the proposed control structure can be estimated using a sliding mode observer combined with the design techniques of a conventional observer.

We have made the assumption that the source voltages are of sinusoidal form; their frequency, however, may not be constant. This is the case for source voltages coming from a synchronous generator that might be started, stopped, accelerated, or decelerated. Suppose that the frequency of the source voltages changes, approximately, linearly with respect to time, i.e.,

$$\omega(t) = \alpha t + \beta, \tag{11.2.35}$$

where α, β are constant values. The phase of the source voltages is thus given by

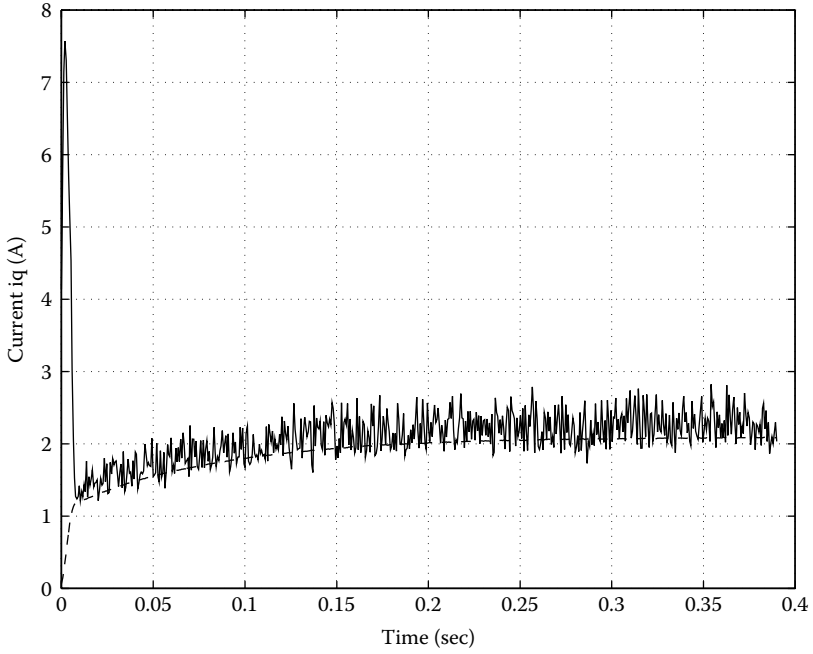

FIGURE 11.35
Current component i_q.

$$\theta(t) = \frac{1}{2}\alpha t^2 + \beta t + \gamma, \tag{11.2.36}$$

with γ also being a constant value. The model of the source voltage of phase $i = 1$ can then be obtained as

$$u_{g1} = \frac{d}{dt}(E\cos\theta(t)) = -E(\alpha t + \beta)\sin\left(\frac{1}{2}\alpha t^2 + \beta t + \gamma\right), \tag{11.2.37}$$

where E is a constant. Let us define new state variables as $x_1 = u_{g1}$ and $x_2 = \dot{x}_1$. It may be checked that u_{g1} in Equation 11.2.3 is a solution to the system

$$\begin{aligned} \dot{x}_1 &= x_2, \\ \dot{x}_2 &= -\left(\omega^2 + \frac{3\alpha^2}{\omega^2}\right)x_1 + \frac{3\alpha}{\omega}x_2, \end{aligned} \tag{11.2.38}$$

for any E and α. In other words, we have derived the model of the source voltage for one phase.

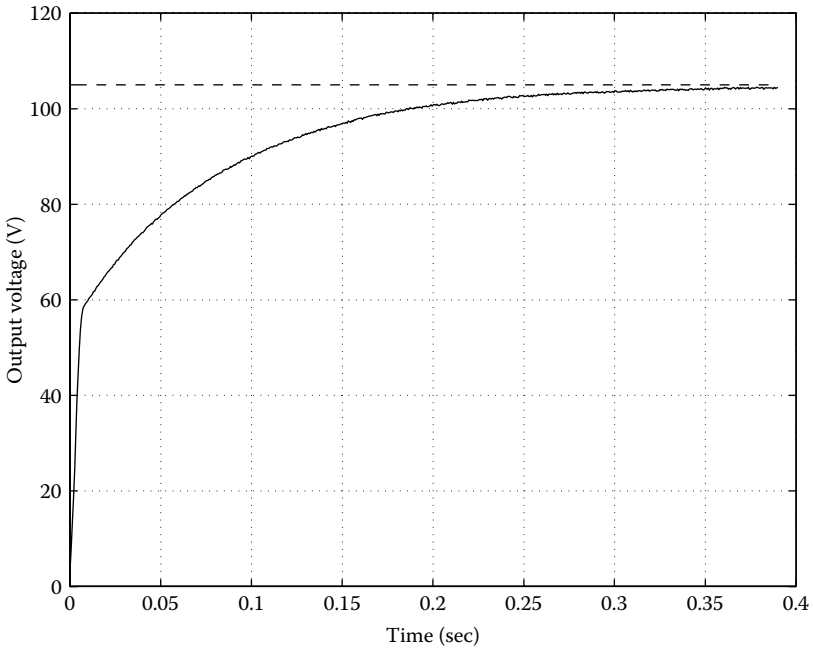

FIGURE 11.36
Output voltage u_0.

In the following, we propose to design observers for the state variables of phase $i = 1$. The state variables associated with phase $i = 2$ and $i = 3$ can be obtained in a similar manner. Note that state variable x_2 stands for the time derivative of $x_1 = u_{g1}$ and should not be mixed with the phase $i = 2$.

As mentioned before, the link current is assumed to be measurable as a function of i_i and u_i, $i = 1, 2, 3$,

$$i_{link} = f(i_1, i_2, i_3, u_1, u_2, u_3) \tag{11.2.39}$$

where function $f(\cdot)$ is defined as

$$i_{link} = \begin{cases} i_1 & \text{if } u_1 \neq u_2 = u_3 \\ i_2 & \text{if } u_2 \neq u_1 = u_3 \\ i_3 & \text{if } u_3 \neq u_1 = u_2 \end{cases}. \tag{11.2.40}$$

Therefore, the link current consists of sequential "windows" during which the phase currents can be observed sequentially. In other words, the link current is equal to one of the phase currents in certain windows, which are determined by the combination of the switching signals u_1, u_2, u_3. The lengths of the windows depend on the switching policy used.

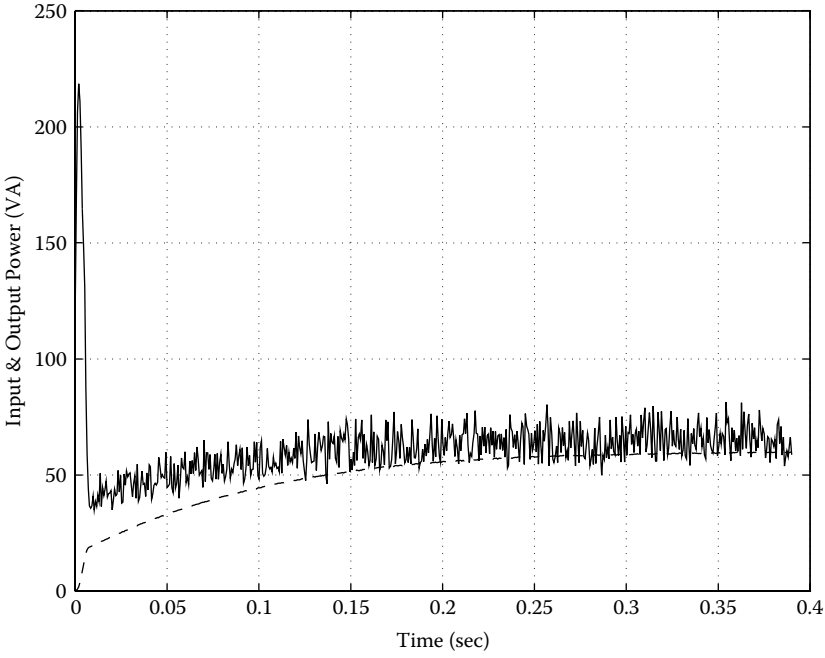

FIGURE 11.37
Input and output power.

11.2.3.1. Current Observer for Source Phase Voltage

Design a sliding mode current observer as

$$\dot{\hat{i}}_1 = -\frac{R_w}{L}\hat{i}_1 - \frac{u_0}{6L}(2u_1 - u_2 - u_3) + \frac{1}{L}M\,\text{sign}(u_1 i_{link} - \hat{i}_1), \tag{11.2.41}$$

where M is a constant observer gain. Assuming that the parameters R_w and L are identical with those in model Equation 11.2.3 and subtracting Equation 11.2.41 from Equation 11.2.3 leads to the mismatch dynamics:

$$\dot{\bar{i}}_1 = -\frac{R_w}{L}\bar{i}_1 + \frac{1}{L}x_1 - \frac{1}{L}M\,\text{sign}(\bar{i}_1), \tag{11.2.42}$$

where $\bar{i}_1 = i_1 - \hat{i}_1$. For a sufficiently large observer gain M, sliding mode can be enforced in Equation 11.2.42 with $\bar{i}_1 = 0$. Using the equivalent control method for $\dot{\bar{i}}_1 = 0$ and $\bar{i}_1 = 0$ leads to

$$\left(M\,\text{sign}(\bar{i}_1)\right)_{eq} = x_1. \tag{11.2.43}$$

To extract the equivalent control from Equation 11.2.42, we use a first-order linear filter (Section 2.4) with filter output z and filter time constant μ:

$$\mu\dot{z} + z = M\,\mathrm{sign}(\bar{i}_1) \tag{11.2.44}$$

implying that $\lim_{\mu\to 0} z = x_1 = u_{g1}$ asymptotically. Hence, the source voltage of phase $i = 1$ can be reconstructed by using the sliding mode observer and exploiting the equivalent control method.

11.2.3.2. Observer for Source Voltage

The source voltage $x_1 = u_{g1}$ obtained above is often corrupted by high-frequency noise because the time constant of the low-pass filter is required to be small enough. Otherwise, the associated phase lag as well as time delay would destroy the information in u_{g1} equal to the average value of $M\,\mathrm{sign}(\bar{i}_1)$. In addition, the voltage u_{g1} is estimated only within the windows when the link current is equal to the current of phase $i = 1$.

11.2.3.3. Known Supply Frequency

First, let us discuss a simple case to gain some theoretical insight of the EMF observer, i.e., the source voltage observer. Assuming that the frequency ω and the acceleration α of the EMFs are known and assuming that the link current can be measured continuously without the restriction of the watching windows, design the EMF observer as follows:

$$\begin{aligned}\dot{\hat{x}}_1 &= \hat{x}_2 - L_1\bar{x}_1,\\ \dot{\hat{x}}_2 &= -\left(\omega^2 + \frac{3\alpha^2}{\omega^2}\right)\hat{x}_1 + \frac{3\alpha}{\omega}\hat{x}_2 - L_2\bar{x}_1,\end{aligned} \tag{11.2.45}$$

where $\bar{x}_1 = \hat{x}_1 - z$ (z denotes the output of the low-pass filter (Equation 11.2.44) and we assume that $z = x_1$); L_1 and L_2 are the observer gains. The stability of the observer Equation 11.2.45 can be proven by a proper choice of a Lyapunov function. Subtracting Equation 11.2.38 from Equation 11.2.45 yields

$$\begin{aligned}\dot{\bar{x}}_1 &= \bar{x}_2 - L_1\bar{x}_1,\\ \dot{\bar{x}}_2 &= -\left(\omega^2 + \frac{3\alpha^2}{\omega^2}\right)\bar{x}_1 + \frac{3\alpha}{\omega}\bar{x}_2 - L_2\bar{x}_1,\end{aligned} \tag{11.2.46}$$

with $\bar{x}_2 = \hat{x}_2 - x_2$. Design the Lyapunov function candidate as

$$V = \frac{1}{2}\omega_0^2\bar{x}_1^2 + \frac{1}{2}\left(\bar{x}_2 - L_1\bar{x}_1\right)^2, \text{ with } V = 0 \text{ at } \bar{x}_1 = \bar{x}_2 = 0, \tag{11.2.47}$$

where ω_0 is a constant. The time derivative of Equation 11.2.47 along the solutions of Equation 11.2.46 is given by

$$\dot{V} = -\left(L_1 - \frac{3\alpha}{\omega}\right)\left(\bar{x}_2 - L_1\bar{x}_1\right)^2 + \left[\omega_0^2 - \left(\omega^2 + \frac{3\alpha^2}{\omega^2}\right) + \frac{3\alpha}{\omega}L_1 - L_2\right]\bar{x}_1\left(\bar{x}_2 - L_1\bar{x}_1\right). \tag{11.2.48}$$

We assume that time varying ω is lower bounded; then $\dot{V}(t)$ is negative semidefinite if

$$L_1 > 3\left|\frac{\alpha}{\omega}\right|, \text{ and } L_2(t) = \omega_0^2 - \left(\omega^2 + \frac{3\alpha^2}{\omega^2}\right) + \frac{3\alpha}{\omega}L_1. \tag{11.2.49}$$

The surface $\bar{x}_2 - L_1\bar{x}_1 = 0$ does not contain whole trajectories; the solution is $\bar{x}_1 = 0$, $\bar{x}_2 = 0$. Therefore, the EMF observer with the time-varying gain $L_2(t)$ is shown to be asymptotically stable.

If a crude measurement of the supply frequency is available, the acceleration α may be found using a linear observer:

$$\begin{aligned} \dot{\hat{\omega}} &= \hat{\alpha} - L_3(\hat{\omega} - \omega), \\ \dot{\hat{\alpha}} &= -L_4(\hat{\omega} - \omega). \end{aligned} \tag{11.2.50}$$

For constant positive parameters L_3 and L_4, both $\hat{\omega} \to \omega$ and $\hat{\alpha} \to \alpha$ as $t \to \infty$. It is preferable to use the estimated frequency $\hat{\omega}$ instead of the measured value ω if the crude measurement of the supply frequency is corrupted by noise.

11.2.3.4. Unknown Supply Frequency

In real applications, the supply frequency as well as the acceleration signals may not be measured. To meet this requirement, we need to additionally estimate ω and α. The convergence proof of this kind of observer will become involved. However, simulations and experimental results showed that the observer converges.

The following nonlinear observer for the EMFs and their frequency is proposed:

$$\begin{aligned} \dot{\hat{x}}_1 &= \hat{x}_2 - L_1 W_1 \bar{x}_1, \\ \dot{\hat{x}}_2 &= -\left(\hat{\omega}^2 + \frac{3\hat{\alpha}^2}{\hat{\omega}^2}\right)\hat{x}_1 + \frac{3\hat{\alpha}}{\hat{\omega}}\hat{x}_2 - L_2 W_1 \bar{x}_1, \\ \dot{\hat{\omega}} &= \hat{\alpha} + L_3 W_1 \bar{x}_1 \hat{x}_1, \\ \dot{\hat{\alpha}} &= -L_4 W_1 \bar{x}_1 \hat{x}_2, \end{aligned} \tag{11.2.51}$$

where $L_i (i = 1, 2, 3, 4)$ are the observer gains, and W_1 is the window signal defined by

$$W_1 = \begin{cases} 1 & \text{if } u_1 \neq u_2 = u_3 \\ 0 & \text{otherwise} \end{cases} . \tag{11.2.52}$$

Readers who are interested in the convergence proof under certain assumptions should consult previous works [Utkin and Drakunov 1995; Chen 1998].

The state variables associated with phase $i = 2$ and phase $i = 3$ can be obtained in a similar manner. Several factors will deteriorate the performance of the proposed observers:

1. There exist parameter uncertainties, e.g., in parameter R_w or L.
2. The sampling rate of a digital implementation is too low; in this case, we need a discrete-time version of the observer design [Utkin, Chen, Zarei, and Miller 1997].
3. The time constant of the low-pass filter μ (see Equation 11.2.44) is selected inappropriately.

11.2.3.5. Simulation Results

The proposed sliding mode observer for the case of varying, and unknown, supply frequency is validated by the following simulation results. Parameters of the AC/DC converter are preset as $R_w = 0.033\Omega$, $L = 1.55 \times 10^{-4}$H, $C = 40$F, and load resistance Rl = 0.12Ω. The amplitude of the supply voltage is selected as $E = 10$. The frequency of the supply voltage ω is assumed to vary in the range of 150–250 Hz, and the rate of frequency change, i.e., the acceleration α, may change within a range of ±1000 Hz/sec. Results of the estimated signals are shown in Figures 11.38 through 11.41. The desired rate of convergence can be obtained by the choice of observer gains. In the simulations, the observer gains are designed as $L_1 = 4000$, $L_2 = 4{,}000{,}000$, $L_3 = 500$, and $L_4 = 20{,}000$.

For all simulations, the information of the phase current is available only within the time windows in which link current is equal to the phase current. Beyond the windows, the observer operates in the open loop mode.

Section 13.3 will show experimental results for a similar problem for automotive applications, using a different form of back-EMF/frequency observer.

11.3. DC/AC Converter

After the intensive discussion of three-phase AC/DC converters in the previous section, this section presents sliding mode pulse width modulation (SMPWM) control methodologies for a three-phase DC/AC converter, i.e., current-controlled inverter. Two novel approaches adopting the sliding mode concept are proposed to make the system track the reference inputs.

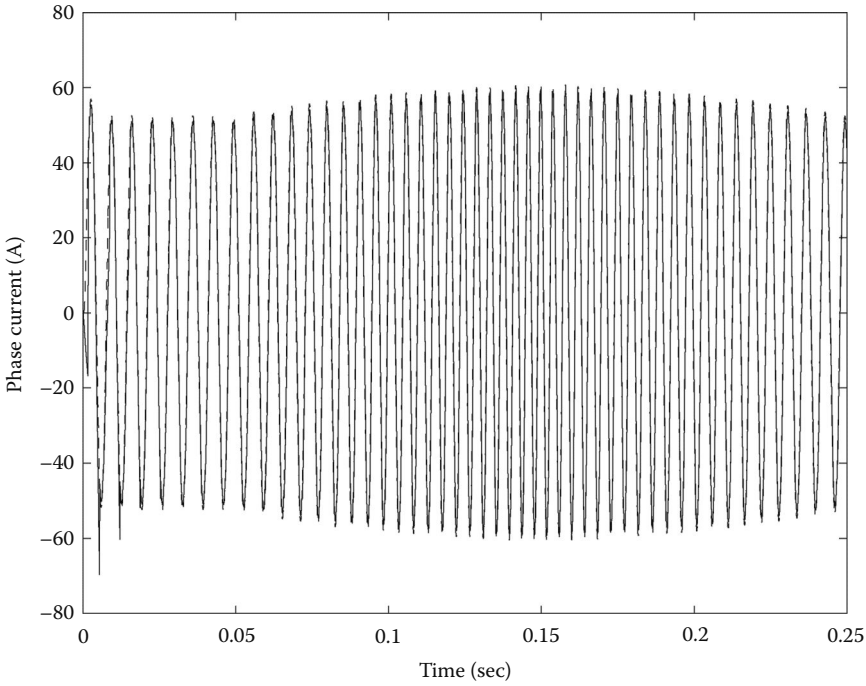

FIGURE 11.38
Estimation of the phase current $\hat{i}_1$.

Phase currents and the neutral point voltage are controlled simultaneously. Simulations and experiments are performed to confirm the effectiveness of the proposed control algorithms. Some considerations concerning the optimization of different operational criteria offered by SMPWM via the control of the neutral point voltage are also given. The main contents of this section are based on the work of Yan, Utkin, and Xu [2007].

11.3.1. Dynamic Model

Consider the system in Figure 11.42. The three-phase full-bridge inverter under control is to provide desired currents to the load, taking into account that they can be dependent.

Based on circuit analysis, the system equations are

$$\begin{aligned} L\frac{di_a}{dt} + Ri_a + e_a &= H_1 U_{dc} - v_n \\ L\frac{di_b}{dt} + Ri_b + e_b &= H_3 U_{dc} - v_n \\ L\frac{di_c}{dt} + Ri_c + e_c &= H_5 U_{dc} - v_n \end{aligned} \tag{11.3.1}$$

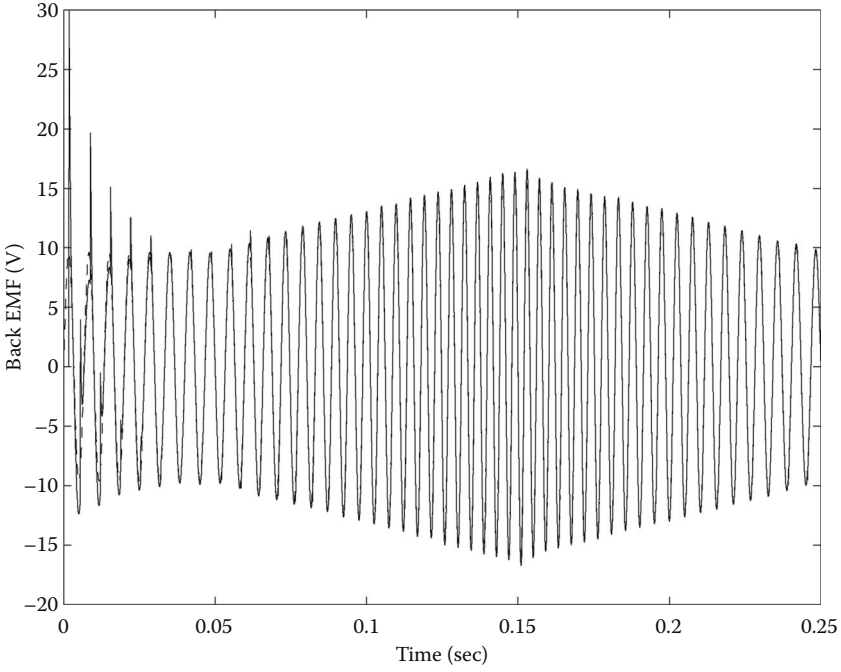

FIGURE 11.39
Estimation of the supply voltage $\hat{x}_1$.

where $H_1, H_3, H_5 \in \{\pm 1\}$ represent the switching control signals for six switching devices of the three-phase full-bridge converter. If a switching device is conducting, a value of 1 is assigned to it; otherwise, –1 is assigned. v_n is the voltage at neutral point n. e_a, e_b, e_c are voltages, for example, three back EMF in AC motors. It is assumed that $e_a + e_b + e_c = 0$. Because the sum of the phase currents is equal to zero as well, v_n of the three-phase system can be found from Equation 11.3.1:

$$v_n = \frac{U_{dc}}{3}(H_1 + H_3 + H_5) \tag{11.3.2}$$

Because H_1, H_3, H_5 are discontinuous signals, v_n is discontinuous as well. However, its average value changes continuously, and the control of v_n will be discussed later.

11.3.2. Control Design: Sliding Mode PWM

The objective of control algorithm is to track proper selected current references. Some existing PWM techniques use three-phase current errors as inputs to its controller, for example, hysteresis band PWM. Denote

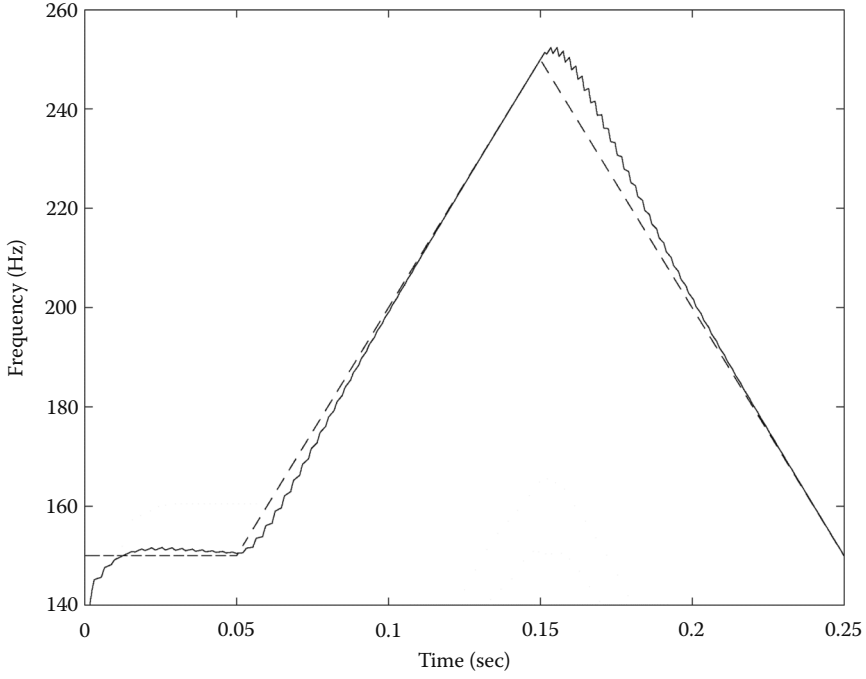

FIGURE 11.40
Estimation of the supply frequency $\hat{\omega}$.

$$\begin{aligned} f_a &= -(R/L)i_a - e_a/L \\ f_b &= -(R/L)i_b - e_b/L \\ f_c &= -(R/L)i_c - e_c/L. \end{aligned} \tag{11.3.3}$$

Substitute Equation 11.3.2 into Equation 11.3.1 and use the notation in Equation 11.3.3, gives

$$\begin{aligned} \frac{di_a}{dt} &= f_a + \frac{2}{3}\frac{U_{dc}}{L}H_1 - \frac{1}{3}\frac{U_{dc}}{L}H_3 - \frac{1}{3}\frac{U_{dc}}{L}H_5 \\ \frac{di_b}{dt} &= f_b + \frac{2}{3}\frac{U_{dc}}{L}H_3 - \frac{1}{3}\frac{U_{dc}}{L}H_1 - \frac{1}{3}\frac{U_{dc}}{L}H_5 \\ \frac{di_c}{dt} &= f_c + \frac{2}{3}\frac{U_{dc}}{L}H_5 - \frac{1}{3}\frac{U_{dc}}{L}H_1 - \frac{1}{3}\frac{U_{dc}}{L}H_3. \end{aligned} \tag{11.3.4}$$

Equation 11.3.4 can be written in matrix form:

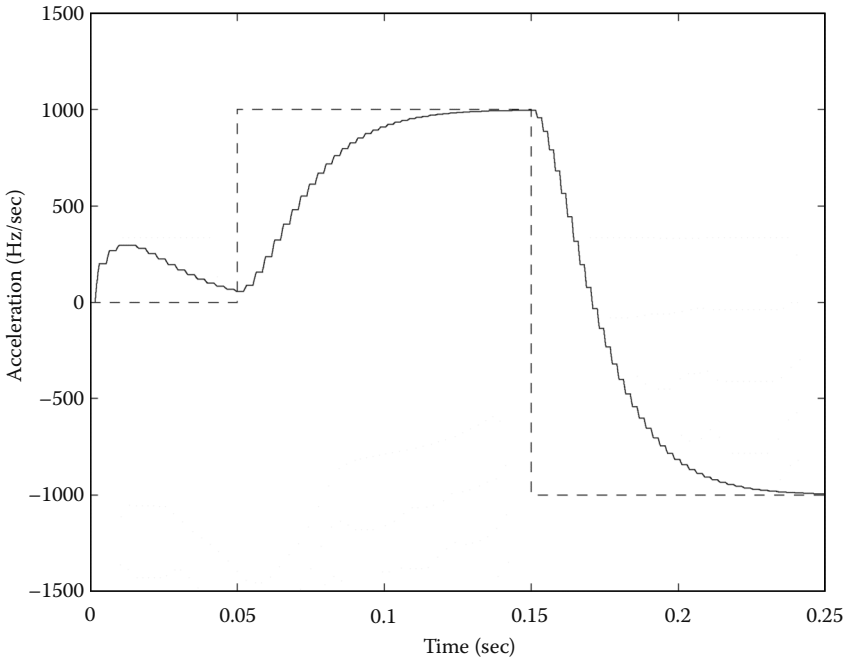

FIGURE 11.41
Estimation of the supply acceleration $\hat{\alpha}$.

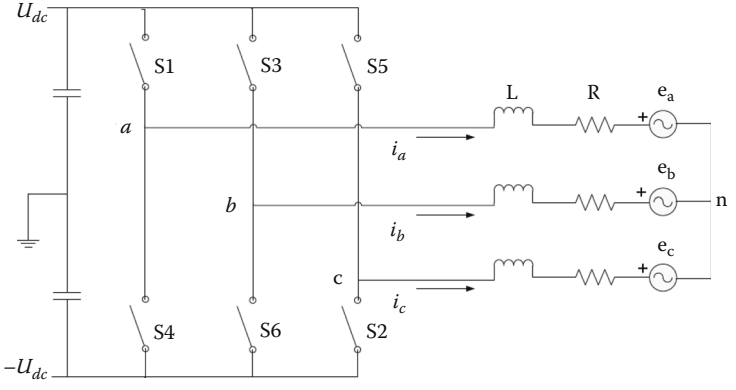

FIGURE 11.42
Circuit diagram of three-phase inverter and load.

$$\begin{bmatrix} \frac{di_a}{dt} \\ \frac{di_b}{dt} \\ \frac{di_c}{dt} \end{bmatrix} = \begin{bmatrix} f_a \\ f_b \\ f_c \end{bmatrix} + \frac{U_{dc}}{3L} \begin{bmatrix} 2 & -1 & -1 \\ -1 & 2 & -1 \\ -1 & -1 & 2 \end{bmatrix} \begin{bmatrix} H_1 \\ H_3 \\ H_5 \end{bmatrix} \tag{11.3.5}$$

which can be summarized to

$$\Rightarrow \frac{d\mathbf{i}}{dt} = \boldsymbol{f} + \frac{U_{dc}}{3L} B_1 \mathbf{H}, \tag{11.3.6}$$

where $\boldsymbol{i} = [i_a\ i_b\ i_c]^T$, $\boldsymbol{f} = [f_a\ \ f_b\ \ f_c]^T$, $\boldsymbol{H} = [H_1\ \ H_3\ \ H_5]^T$, and

$$B_1 = \begin{bmatrix} 2 & -1 & -1 \\ -1 & 2 & -1 \\ -1 & -1 & 2 \end{bmatrix}. \tag{11.3.7}$$

Note that matrix B_1 is singular because of $i_a + i_b + i_c = 0$, hence only two phase currents of i_a, i_b, i_c can be controlled independently. As a result, although the three currents are equal to the desired values, the motion of system is not unique. For example, the voltage v_n in Equation 11.3.2 can be equal to different values. In fact, we have three control inputs H_1, H_3, H_5 but only two independent controlled variables. Thus we have one superfluous degree of freedom to do some additional task, e.g., to minimize the number of inverter switching, as shown later. In the following, we assume that reference inputs i_a^* and i_b^* are given and discuss how to use the additional degree of freedom.

Let us complement the original system by the first-order equation

$$\dot{s}_3 = v_n^* - v_n. \tag{11.3.8}$$

See Equation 11.3.2 for the definition of v_n. Equation 11.3.8 can be implemented using an integrator. Define the sliding manifold $\boldsymbol{s} = [s_a\ s_b\ s_3]^T$ as

$$\begin{aligned} s_a &= i_a^* - i_a \\ s_b &= i_b^* - i_b \\ s_3 &= \int (v_n^* - v_n) d\tau \end{aligned} \tag{11.3.9}$$

where i_a^*, i_b^*, v_n^* are reference signals. Note that, if $s_a = s_b = 0$, $i_c^* = -(i_a^* + i_b^*) = -(i_a + i_b) = i_c$ is automatically satisfied. The selection of v_n^* will be discussed later. The time derivative of vector $\boldsymbol{s}$ can be found from Equations 11.3.2, 11.3.4, and 11.3.9:

$$\begin{aligned}
\dot{s}_a &= \dot{i}_a^* - f_a - \frac{2}{3}\frac{U_{dc}}{L}H_1 + \frac{1}{3}\frac{U_{dc}}{L}H_3 + \frac{1}{3}\frac{U_{dc}}{L}H_5 \\
\dot{s}_b &= \dot{i}_b^* - f_b - \frac{2}{3}\frac{U_{dc}}{L}H_3 + \frac{1}{3}\frac{U_{dc}}{L}H_1 + \frac{1}{3}\frac{U_{dc}}{L}H_5 \\
\dot{s}_3 &= v_n^* - \frac{U_{dc}}{3}(H_1 + H_3 + H_5)
\end{aligned} \tag{11.3.10}$$

Three-dimensional discontinuous control $\boldsymbol{H}$ can be designed such that sliding mode is enforced on $\boldsymbol{s} = 0$, implying that all three components of $\boldsymbol{s}$ are equal to zero and the tracking problem is solved. Because the system performance in sliding mode depends on v_n^*, it can be selected in correspondence with some performance criterion.

Two control methods that can be used to enforce sliding mode will be shown here. The first one is to design a Lyapunov function. The second one is to decouple the three dynamic equations in Equation 11.3.10 with respect to three controls by coordinate transformation. In the later approach, the frequency analysis can be performed for each phase independently.

11.3.2.1. Lyapunov Approach

Having proposed the sliding surface **s**, the control algorithm should be designed such that vector $\boldsymbol{s}$ goes to zero after finite time. Define the Lyapunov function candidate

$$V = \frac{1}{2}\boldsymbol{s}^T\boldsymbol{s}. \tag{11.3.11}$$

Its time derivative is

$$\begin{aligned}
\dot{V} &= \boldsymbol{s}^T\dot{\boldsymbol{s}} \\
&= s_a\dot{s}_a + s_b\dot{s}_b + s_3\dot{s}_3 \\
&= f_V - \frac{U_{dc}}{3L}[\alpha H_1 + \beta H_3 + \gamma H_5],
\end{aligned} \tag{11.3.12}$$

where $f_V = s_a(\dot{i}_a^* - f_a) + s_b(\dot{i}_b^* - f_b) + s_3\dot{v}_n^*$ is a bounded function with $\partial f_V/\partial H_i = 0$ ($i = 1, 3, 5$), and

$$\begin{aligned}
\alpha &= (2s_a - s_b + s_3L) \\
\beta &= (2s_b - s_a + s_3L) \\
\gamma &= (-s_a - s_b + s_3L)
\end{aligned} \tag{11.3.13}$$

Select the control logic for the inverter switches as

$$\begin{aligned} H_1 &= \text{sign}(\alpha) \\ H_3 &= \text{sign}(\beta) \\ H_5 &= \text{sign}(\gamma) \end{aligned} \tag{11.3.14}$$

$\dot{V}$ now becomes

$$\dot{V} = f_V - \frac{U_{dc}}{3L}\left[|\alpha| + |\beta| + |\gamma|\right]. \tag{11.3.15}$$

If U_{dc} is large enough, f_V can be suppressed, and $\dot{V} < 0$ can be guaranteed, then the sliding manifold is reached after finite time. SMPWM with the Lyapunov approach takes into account all sliding surfaces directly for each phase's control. Although the convergence of system states to corresponding sliding surfaces requires the DC-bus voltage to be high enough, SMPWM does not require the U_{dc} to be constant. Note that, in the calculation of v_n, the value of U_{dc} is required (see Equation 11.3.2).

11.3.2.2. Decoupling Approach

The Lyapunov approach is rather simple, but it does not let us analyze the motion in the vicinity of the sliding manifold, because three equations in Equation 11.3.10 are interconnected. The decoupling approach is a little bit more complex than the Lyapunov approach, but it provides some benefits. In this approach, three transformed sliding surfaces are introduced, and each switching control will correspond only to one sliding surface, i.e., the system is decoupled. Equation 11.3.10 can be written in matrix form:

$$\dot{\boldsymbol{s}} = \boldsymbol{f}_D + \frac{U_{dc}}{3L} B\boldsymbol{H}, \tag{11.3.16}$$

where the vector $\boldsymbol{f}_D = [\dot{i}_a^* - f_a,\ \dot{i}_b^* - f_b, v_n^*]^T$ includes terms without control variables, and

$$B = \begin{bmatrix} 2 & -1 & -1 \\ -1 & 2 & -1 \\ L & L & L \end{bmatrix}. \tag{11.3.17}$$

Because B is a nonsingular matrix it can be transformed into a diagonal matrix, and the control variables can be decoupled for each sliding surface. Introduce new switching manifold

$$\boldsymbol{s}^* = B^{-1}\boldsymbol{s} = 0, \tag{11.3.18}$$

where B^{-1} can be calculated as

$$B^{-1} = \frac{1}{9L}\begin{bmatrix} 3L & 0 & 3 \\ 0 & 3L & 3 \\ -3L & -3L & 3 \end{bmatrix} \tag{11.3.19}$$

Then $\boldsymbol{s}^*$ can be further expended as

$$\begin{aligned} \boldsymbol{s}^* &= B^{-1}\boldsymbol{s} \\ &= \frac{1}{9L}\begin{bmatrix} 3L & 0 & 3 \\ 0 & 3L & 3 \\ -3L & -3L & 3 \end{bmatrix}\begin{bmatrix} s_a \\ s_b \\ s_3 \end{bmatrix} \\ &= \frac{1}{9L}\begin{bmatrix} 3Ls_a + 3s_3 \\ 3Ls_b + 3s_3 \\ -3Ls_a - 3Ls_b + 3s_3 \end{bmatrix} = \begin{bmatrix} s_1^* \\ s_2^* \\ s_3^* \end{bmatrix} \end{aligned} \tag{11.3.20}$$

Differentiation of Equation 11.3.18 gives $\dot{\boldsymbol{s}}^* = B^{-1}\dot{\boldsymbol{s}}$, and $\dot{\mathbf{s}}$ can be found from Equation 11.3.10. Thus,

$$\begin{aligned} \dot{\boldsymbol{s}}^* &= B^{-1}\dot{\boldsymbol{s}} \\ &= \frac{1}{9L}\begin{bmatrix} 3L\dot{s}_a + 3\dot{s}_3 \\ 3L\dot{s}_b + 3\dot{s}_3 \\ -3L\dot{s}_a - 3L\dot{s}_b + 3\dot{s}_3 \end{bmatrix} \\ &= \boldsymbol{f}^* - \frac{U_{dc}}{3L}\begin{bmatrix} H_1 \\ H_3 \\ H_5 \end{bmatrix} \end{aligned} \tag{11.3.21}$$

where $\boldsymbol{f}^* = [f_1^*, f_2^*, f_3^*]^T$ is a 3×1 vector whose elements have bounded values

$$\begin{aligned} f_1^* &= \frac{1}{3L}(L\dot{i}_a^* - Lf_a + v_n^*) \\ f_2^* &= \frac{1}{3L}(L\dot{i}_b^* - Lf_b + v_n^*) \\ f_3^* &= \frac{1}{3L}(-L\dot{i}_a^* + Lf_a - L\dot{i}_b^* + Lf_b + v_n^*) \end{aligned} \tag{11.3.22}$$

Note that $\boldsymbol{f}^*$ does not contain control variables H_1, H_3, and H_5. Equation 11.3.21 shows that the dynamics of $\boldsymbol{s}^*$can be decoupled into three individual motions (with respect to control). Select the control logic for inverter switches as

$$\begin{aligned} H_1 &= \text{sign}(s_1^*) \\ H_3 &= \text{sign}(s_2^*) \\ H_5 &= \text{sign}(s_3^*) \end{aligned} \tag{11.3.23}$$

To enforce the sliding mode $\boldsymbol{s}^* = 0$, U_{dc} should be designed high enough, i.e., $U_{dc}/(3L) > \sup \|\boldsymbol{f}^*\|$, for the sliding mode existence conditions $s_1^* \dot{s}_1^* < 0$, $s_2^* \dot{s}_2^* < 0$, $s_3^* \dot{s}_3^* < 0$ to hold. Sliding manifold $\boldsymbol{s}^* = 0$ is reached after finite time. Because $\boldsymbol{s} = B\boldsymbol{s}^*$ and B is nonsingular, sliding manifold $\boldsymbol{s} = 0$ is reached at the same time instant, thus tracking control performance is guaranteed.

11.3.2.3. Possible Applications of v_n Control

Reference input v_n^* may be selected depending on some operation criteria: control of switching frequency, minimization of this frequency with given accuracy, and so on.

As follows from Equation 11.3.10, the time derivative of s_3 depends on v_n varying at high frequency in sliding mode. Because of the integration in s_3, the high frequency will be rejected on the sliding surface and s_3 will depend on average value of v_n.

As mentioned previously, the reference currents are tracked. At the same time, the average value of v_n can be controlled using SMPWM. To take advantage of this extra degree of freedom, proper v_n^* can be found to optimize some performance criterion. For example, the switching frequency (i.e., the number of switching) can be minimized to reduce switching losses.

Ideally, sliding mode is a mathematical abstraction in which the sliding motion trajectories are strictly on sliding surfaces. However, sliding mode in a real-life system occurs not strictly on the sliding surfaces. Instead, it occurs within some boundary layer. Assuming that switching devices have hysteresis loop Δ, then Δ defines the accuracy of the system, as shown in Figure 11.43. In the control system, the switching frequency depends on state velocities; it is not a constant value (unlike the case of conventional PWM, in

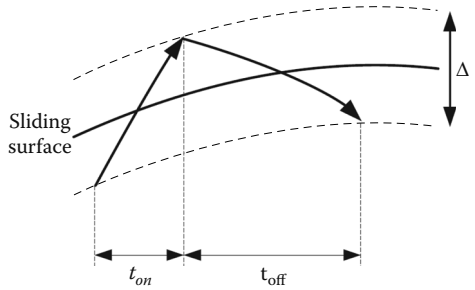

FIGURE 11.43
Sliding manifold of SMPWM.

which the switching frequency is fixed). We consider the system using the decoupling approach, in which each surface s_i^*, $i \in \{1, 2, 3\}$ can be handled independently by the corresponding control H_{2i-1}. The switching frequency of one transformed sliding surface is determined by two time intervals with $\dot{s}_i^* > 0$ and $\dot{s}_i^* < 0$.

Consider the switching behavior of the ith motion in Equation 11.3.21 where $i \in \{1, 2, 3\}$. The function f^* in Equation 11.3.21 depends on v_n^*, as shown in Equation 11.3.22. For each motion in Equation 11.3.21, the time duration of "switch on," i.e., $H_i = 1$, and the time duration of "switch off," i.e., $H_i = -1$, can be written as functions of v_n^*:

$$t_{\text{on}i}(v_n^*) = \frac{\Delta}{\left| f_i^*(v_n^*) - \frac{U_{dc}}{3L} \right|}, \tag{11.3.24}$$

$$t_{\text{off}i}(v_n^*) = \frac{\Delta}{\left| f_i^*(v_n^*) + \frac{U_{dc}}{3L} \right|}. \tag{11.3.25}$$

It means that the switching frequency of the ith motion is a function of v_n^* as well:

$$f_{\text{switch}\_i}(v_n^*) = \frac{1}{t_{\text{on}i}(v_n^*) + t_{\text{off}i}(v_n^*)}. \tag{11.3.26}$$

Taking into account all three motions in Equation 11.3.21, the overall switching frequency of the system can be measured by

$$f_{\text{switch}}(v_n^*) = \sum_{i=1}^{3} f_{\text{switch}\_i}(v_n^*). \tag{11.3.27}$$

Let $f_{\text{switch}}(v_n^*)$ be the function to be minimized under the constraint $U_{dc}/(3L) > \sup\|f^*\|$. Then the optimal v_n^* can be found from Equations 11.3.22 and 11.3.24 through 11.3.27, such that $f_{\text{switch}}(v_n^*)$ is minimized while tracking $v_n = v_n^*$ is provided, besides tracking of $i_i^* = i_i$ with $i \in \{a, b, c\}$.

11.3.2.4. Simulation Results

To evaluate the proposed control algorithm, computer simulations have been conducted. Parameters used in simulation are listed in Table 11.3. The simulation used the sliding surface decoupling approach. Results of three-phase current tracking (zoomed in) are shown in Figure 11.44. After a brief transient stage, phase currents track the references very well. In Figure 11.45, the average value of v_n tracks a time-varying reference. This average value is obtained by a first-order low-pass filter, $\mu\dot{x} = -x + v_n$ and $\mu = 0.001$. The filter is used only to calculate the average value of v_n to illustrate how close is this value to v_n^*. For the implementation of the system, this filter is not required. In the simulation, the reference v_n^* is a randomly selected time-varying function.

TABLE 11.3

Simulation Parameters

U_{dc}	650 (V)
$E_{abc,rms}$	200 (V)
$i^*_{abc,peak}$	18 (A)
R	0.06 (Ω)
L	12 (mH)
Simulation step	10 (μsec)
Frequency (fundamental)	60 (Hz)

It is not optimized according to some criterion. The only objective of Figure 11.45 is to show the ability to track a time-varying $v_n^*(t)$.

A point worth noting is that SMPWM has an advantage over conventional PWM techniques, e.g., the space vector PWM (SVPWM), because SMPWM does not require the control device to have a timing functionality, because it controls directly the gating signals of the inverter depending on the tracking errors.

11.3.2.5. Experimental Results

The purpose of the experiment is to confirm the effectiveness of SMPWM in a real-time environment under the influence of disturbances and nonideal circuit components. The control objective is to track a reference voltage at the neutral point of a three-phase load; at the same time, reference currents at the output of the three-phase full-bridge inverter are also tracked.

A block diagram of the experimental setup is shown in Figure 11.46. The switches of the inverter are 1200 V/100 A IGBT (2MBI100NC-12). Parameters of the system are shown in Table 11.4.

Results of the experiment are shown in Figures 11.47 through 11.53. Figure 11.47 shows the result of current tracking of one phase of the converter. The frequency content of this switching signal (shown in Figure 11.48) has two peaks in frequency domain: one at 60 Hz (fundamental frequency) and one at 10 kHz. Different from the space vector PWM, the switching action of the SMPWM is not fixed by a PWM frequency. The time-varying switching of SMPWM can be seen from Figures 11.49 and 11.50. The 10 kHz component can be measured in the time domain of the fast switching intervals in the waveforms shown in Figure 11.50. In Figure 11.51, the first waveform shows the current tracking, and the second waveform shows the tracking of a time-varying voltage reference $v_n^*(t)$ at the neutral point of the Y-connected load. In this experiment, the $v_n^*(t)$ is selected as a sinusoidal signal. In real applications, this reference can be selected according to different criteria. This experiment only demonstrates SMPWM's ability to

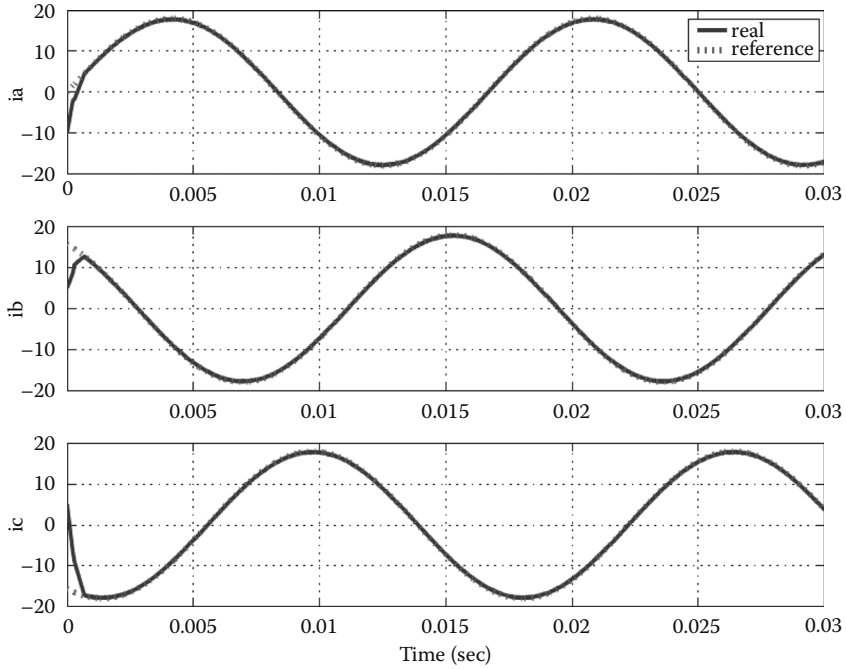

FIGURE 11.44
Current tracking using SMPWM.

track a time-varying $v_n^*(t)$. Figure 11.52 shows the load current (one of the phase current) and SMPWM's control signal. Figure 11.53 shows the output voltage (one of the phase voltage) of the converter and the load current.

For comparison, the SVPWM is also implemented to track the same current references without changing the hardware setup. Only the software generating PWM switching signal was changed. The load current and the SVPWM switching signal of one phase are shown in Figure 11.54. Compare the first waveform of Figure 11.54 with that of Figure 11.52; the ripples of sinusoidal load currents are approximately at the same level. Figure 11.55 shows the zoomed switching action of SVPWM in figure 11.54.

The spectrum of the SVPWM switching signal is shown in Figure 11.56. The SVPWM switching is concentrated at 20 kHz, which is determined by

TABLE 11.4

Experimental Parameters

DC supply	50 V	Load resistance	0.272Ω
Interrupt frequency	20 kHz	Load inductance	13.9 mH

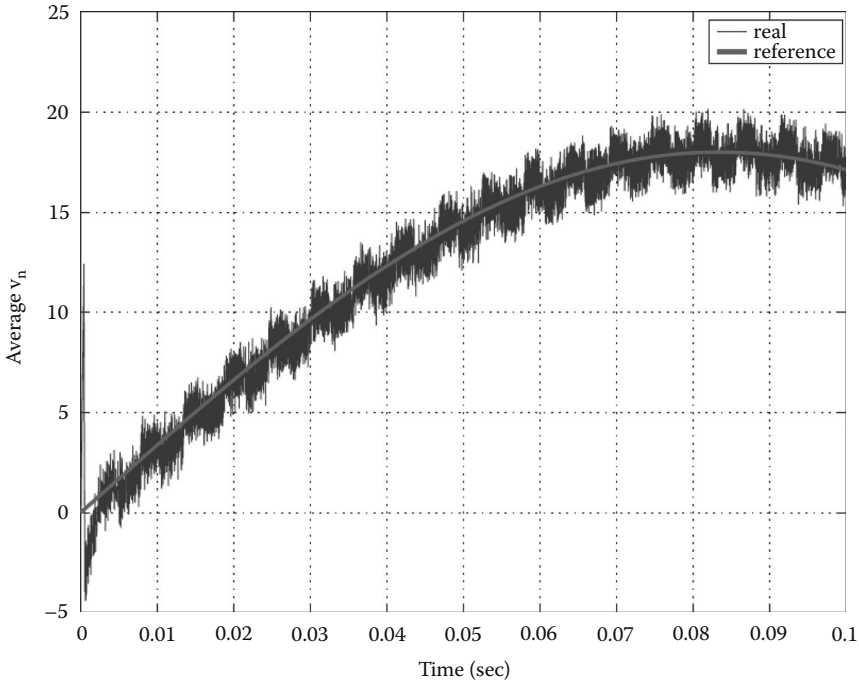

FIGURE 11.45
Tracking a time-varying $v_n^*(t)$ using SMPWM.

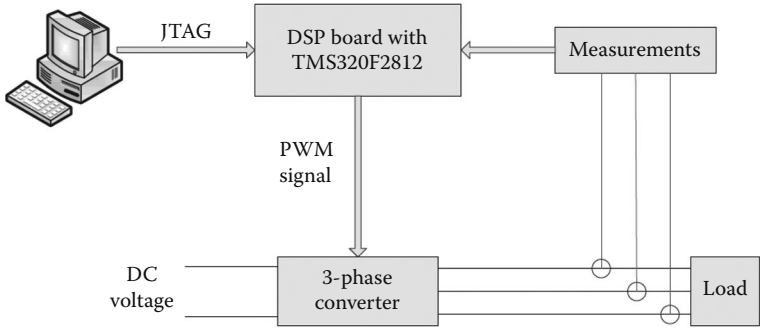

FIGURE 11.46
Sliding mode PWM experimental setup.

the interrupt frequency of the closed-loop controller. This 20 kHz switching can be measured directly in the time domain, as shown in Figure 11.55. Compared with the 10 kHz switching of using SMPWM (shown in Figure 11.48), it can be observed that SMPWM can use a much slower switching signal to track the same reference current with the same accuracy. In this

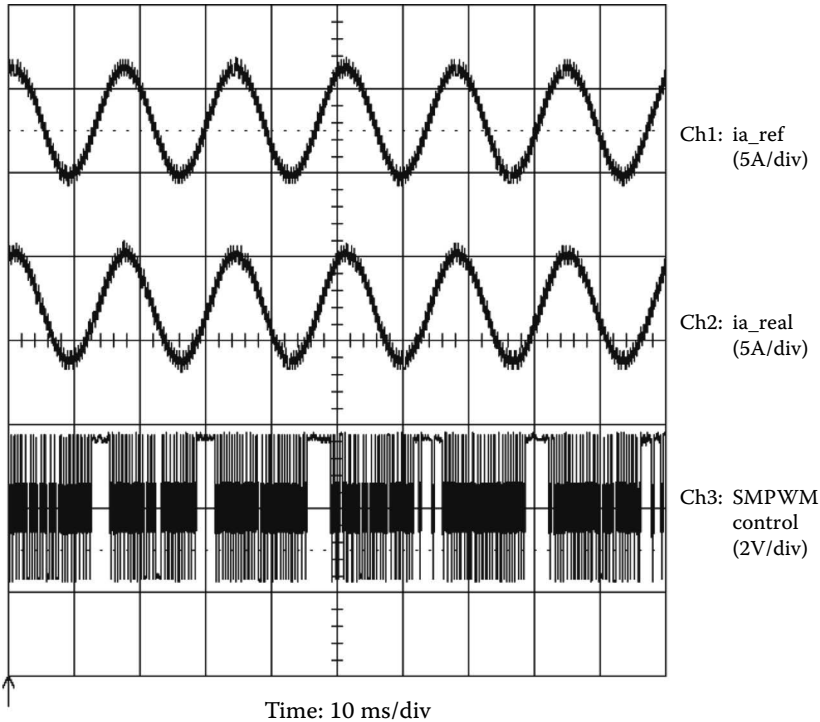

FIGURE 11.47
Current tracking and SMPWM control signal. The first waveform (ch1) is the reference current given by digital signal processor (DSP). The second waveform (ch2) is the real current measurement. The third waveform (ch3) shows the switching action on the corresponding phase..

experiment, the accuracy is judged by observing the level of ripples on the sinusoidal currents at the load. The experimental results verified the effectiveness of the SMPWM approach.

11.4. Summary

Sliding mode approaches to switching power converters were discussed in this chapter. The proper selection of the switching manifolds and a cascaded control structure was shown to have interesting features:

1. Sliding motion is performed in the inner current loop. The structure of this loop is similar for all types of power converters.
2. Because switching is the only way for controlling power converters, the sliding mode approach does not introduce any additional complexity or chattering.

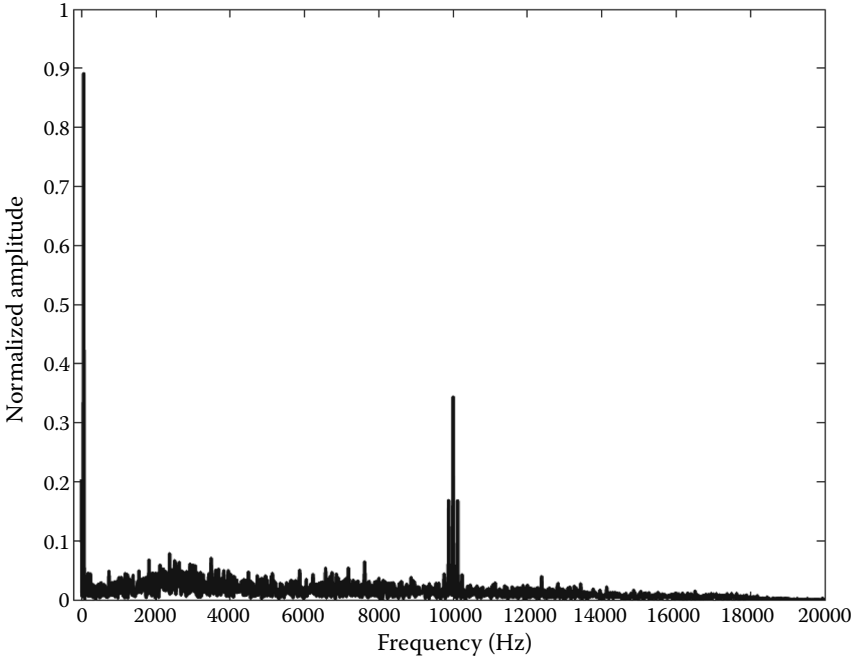

FIGURE 11.48
Frequency content of the SMPWM control signal.

3. In all systems, the reference currents are calculated to be continuous variables. There are a few application-dependent parameters such that the controller can easily be realized in industrial systems.
4. The solutions for all types of converters are global, implying that no linearization procedure is necessary.

As a very important aspect of this chapter, observer-based control approaches have been presented, either asymptotic observers or sliding mode observers. It was shown that an observer-based control system may achieve a higher control performance than a non-observer-based control system. To reduce the number of sensors, sliding mode observers play an important role in the control design. The information is extracted through the concept of equivalent control; thus, no high-order time derivatives of the internal state are necessary. Simulation and experimental results confirmed the effectiveness of the proposed control approaches.

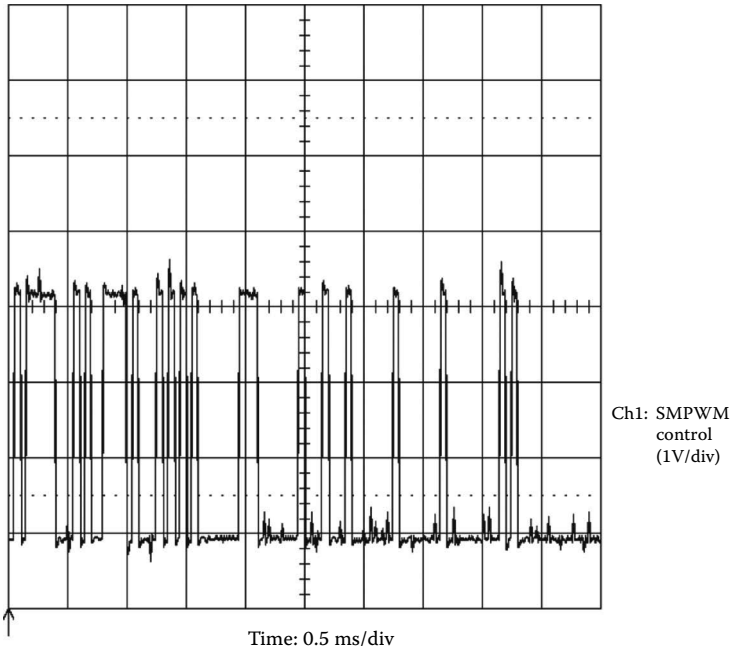

FIGURE 11.49
Time-varying switching action of the SMPWM.

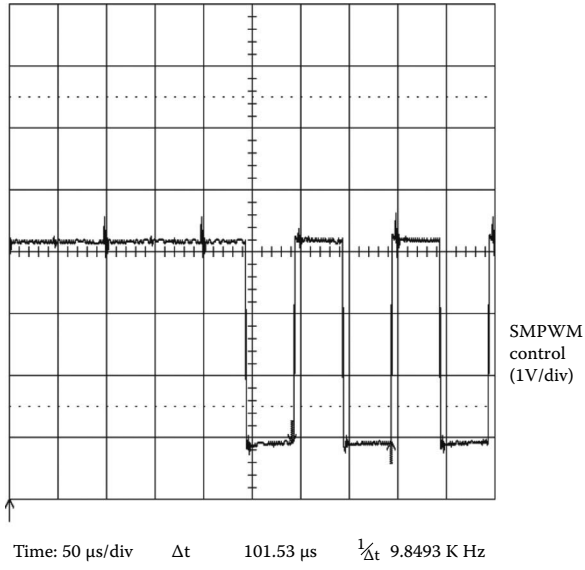

FIGURE 11.50
Zoomed-in experimental result of switching action of the SMPWM.

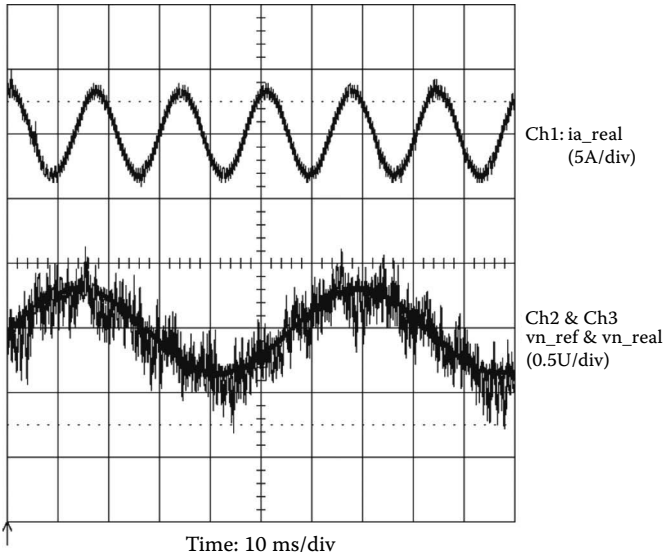

FIGURE 11.51
Current tracking and time-varying $v_n^*(t)$ tracking using SMPWM.

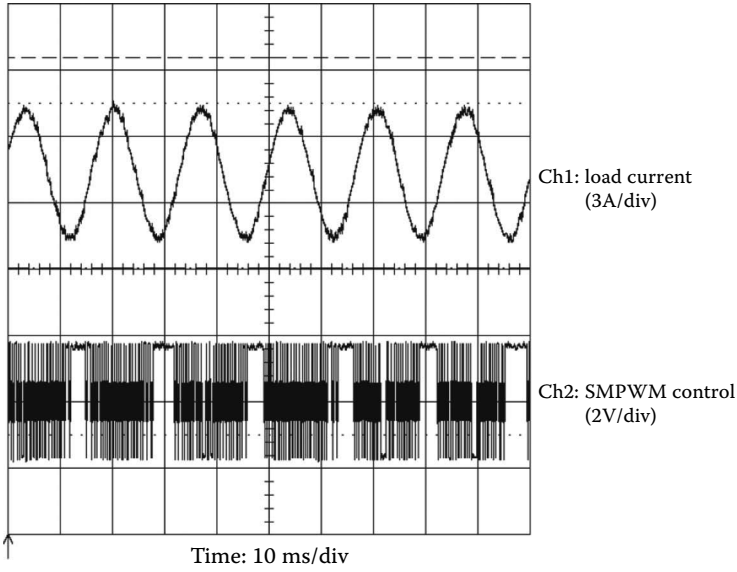

FIGURE 11.52
SMPWM control signal and current in load.

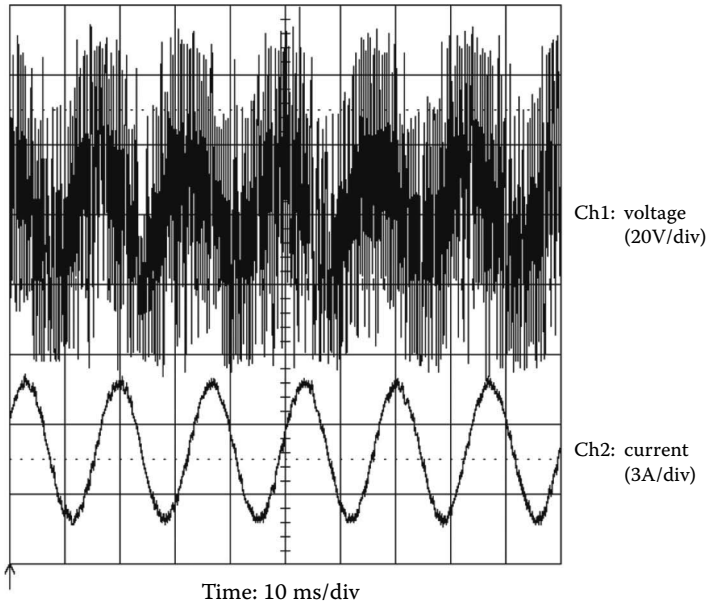

FIGURE 11.53
Output voltage and load current using SMPWM.

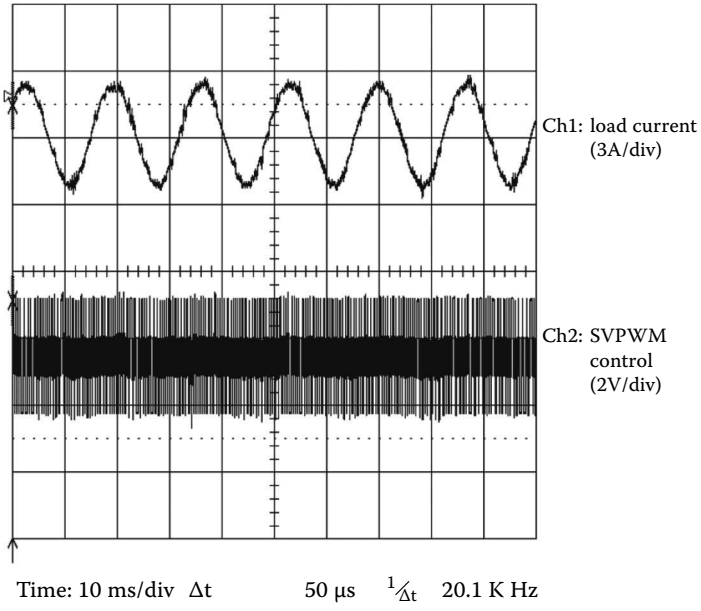

FIGURE 11.54
Current in load and the control signal using SVPWM.

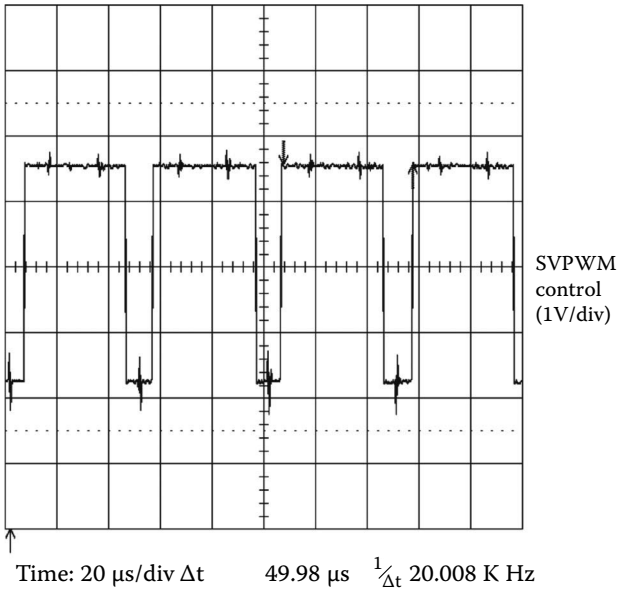

FIGURE 11.55
Zoomed-in switching action of the SVPWM.

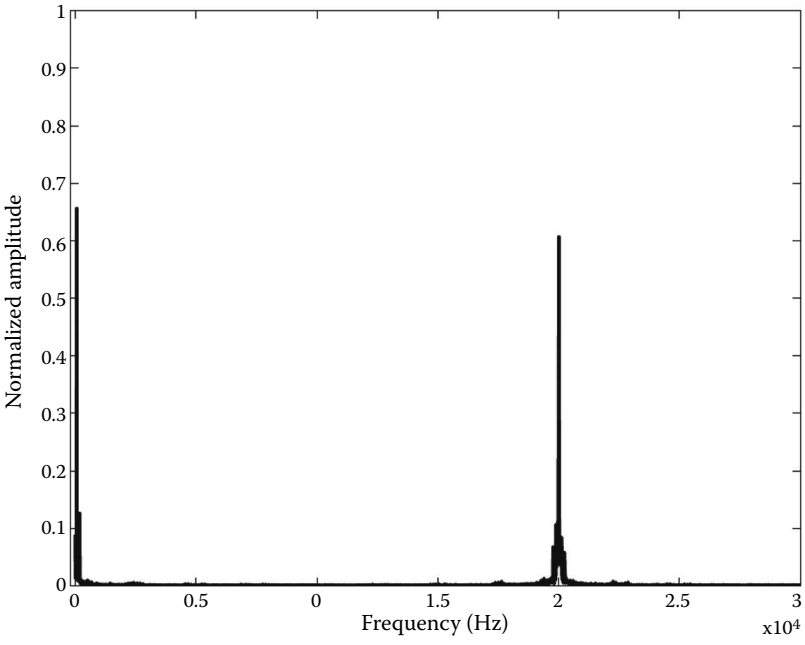

FIGURE 11.56
Frequency content of the SVPWM control signal.

References

Chen DS. 1998. *Discrete Time Sliding Mode Observer for Automotive Alternator.* Ph.D. thesis, The Ohio State University, Columbus, OH.

Kokotovic PV, O'Malley RB, Sannuti P. 1976. "Singular Perturbations and Order Reduction in Control Theory." *Automatica* 12:123–132.

Krstic M, Kanellakopoulos I, Kokotovic P. 1995. *Nonlinear and Adaptive Control Design*. New York: Wiley-Interscience.

Sabanovic A, Sabanovic N, Ohnishi K. 1993. "Sliding Mode in Power Converters and Motion Control Systems." *Int J Control* 57:1237–1259.

Sergy R, Izosimov D. 1997. "Novel Switching Losses Optimal Sliding Mode Control Technique for Three-Phase Voltage Source." Proceedings of the IEEE Symposium on Industrial Electronics, Guimarães, Portugal.

Sira-Ramirez H. 1988. "Sliding Mode Control on Slow Manifolds of DC/DC Power Converters." *Int J Control* 47:1323–1340.

Sira-Ramirez H, Escobar G, Ortega R. 1996. "On Passivity-Based Sliding Mode Control of Switched DC-to-DC Power Converters." Proceedings of the 35th IEEE Conference on Decision and Control, Kobe, Japan.

Utkin VI. 1992. *Sliding Modes in Control and Optimization*. London: Springer-Verlag.

Utkin VI, Drakunov S. 1995. "Sliding Mode Observer for Automotive Applications." Technical Report, Ford Motor Company.

Utkin VI, Chen DS, Zarei S, Miller J. 1997. "Discrete Time Sliding Mode Observer for Automotive Alternator." Proceedings of the European Control Conference, Brussels, Belgium.

Venkataramanan R, Sabanovic A, Slobodan C. 1985. "Sliding Mode Control of DC-to-DC Converters." Proceedings of the IEEE Conference on Industrial Electronics, Control, and Instrumentation, San Francisco, CA.

Vilathgamuwa DM, Wall SR, Jackson RD. 1996. "Variables Structure Control of Voltage Sourced Reversible Rectifiers." *Proc IEEE Conf Electron Power Appl* 143:18 –24.

Yan W, Utkin VI, Xu L. 2007. "Sliding Mode Pulse Width Modulation." Proceedings of the American Control Conference, New York, NY.

12

Advanced Robotics

The control of robots, mobile robots, and manipulator arms alike, has fascinated control engineers for several decades. Robots are complex mechanical systems with highly nonlinear dynamics. Hence, high-performance operation requires nonlinear control designs to fully exploit a robot's capabilities.

After describing the dynamic models for robots, this chapter first discusses four basic sliding mode control design alternatives for the classic trajectory tracking problem, in which the robot is asked to follow a prescribed trajectory. Next, advanced robot control is studied using the example of gradient tracking control, in which the robot motion is guided online by the gradient of an artificial potential field to avoid collisions with obstacles in its workspace. The chapter concludes with four practical examples of sliding mode control in advanced robotics.

12.1. Dynamic Modeling

A large number of control problems for mechanical systems are based on controlling the position or location of a mass using a force or a torque as the input variable. Instead of the pure regulation problem of driving the output location to a specified value, the position of the mass often is required to follow a prescribed trajectory. Levels of complexity may be added by introducing sets of masses with coupled dynamics, to be controlled by sets of force/torque inputs. The standard "fully actuated" case then features one control force/torque input associated with each primary mass and additional forces/torques arising from static and dynamic coupling between the different masses. A typical example is a robotic arm or robot manipulator with n links connected by n joints with force/torque-generating actuators. Usually, an end-effector tool is mounted at the tip of the last link for manipulating objects according to the specific robot application. The case of less control inputs than primary masses is called underactuation and requires extra consideration. Examples were given in Chapter 4.

The input force(s)/torque(s) are the output(s) of, often electrical, actuators with their own complex dynamics. These actuator dynamics are usually neglected in the first step of control design for the electromechanical system, assuming that they are stable and considerably faster than the inertial

dynamics of the mass(es). Because of the large variety of actuators, we refer for the treatment of actuator control to Chapter 10. Also, other dynamics such as structural flexibilities are often neglected when deriving a basic model for the mechanical system. In practice, this leads to the chattering problem described in Chapter 8, and one of the solutions discussed there should be used on top of the basic control designs outlined in this chapter.

Before designing control strategies for a mechanical system, a dynamic model describing the principle physical behavior should be derived. In this section, we consider holonomic mechanical systems in unconstrained motion and planar mobile robots with nonholonomic motion constraints. Several methods have been developed to obtain a dynamic model based on the physical properties of the system. A popular methodology is the Euler-Lagrange formulation for an energy-conserving system:

$$\frac{d}{dt}\frac{\partial L}{\partial \dot{q}} - \frac{\partial L}{\partial q} = \tau, \tag{12.1.1}$$

where $q \in \Re^{n\times 1}$ is a vector of generalized configuration coordinates, $\tau \in \Re^{n\times 1}$ is a vector of generalized external (input) forces/torques (excluding gravity), and the Lagrangian $L = K - P$ is the difference between the total kinetic (K) and potential (P) energies of the system. For details and alternative formulations, please refer to textbooks on the dynamics of mechanical systems; for robotic systems, see Craig [1986] and Spong and Vidyasagar [1989].

12.1.1. Generic Inertial Dynamics

For the purpose of general control design considerations in the first part of this chapter, consider a continuous-time model of a generic, fully actuated n-dimensional robotic system with inertial dynamics of the form

$$M(q)\ddot{q} + N(q,\dot{q}) = \tau, \tag{12.1.2}$$

where $q \in \Re^{n\times 1}$ is a vector of generalized configuration variables (translational or rotational), $M(q) \in \Re^{n\times n}$ denotes an inertial mass matrix, $N(q,\dot{q}) \in \Re^{n\times 1}$ comprises coupling forces/torques between the masses as well as gravity and friction, and $\tau \in \Re^{n\times 1}$ are the generalized input forces/torques. Equation 12.1.2 describes the principle relationship between inertial motion of the system masses, internal forces/torques $N(q,\dot{q}) \in \Re^{n\times 1}$, and external input forces/torques τ, and hence is well-suited for control design.

Traditionally, robots have been categorized into "robot manipulators" and "mobile robots." Robot manipulators usually have a fixed base and consist of a number of rigid links, connected by translational or rotational joints. A set of $q \in \Re^{n\times 1}$ configuration variables of the n joints prescribes a robot configuration, also called robot posture. The set of all possible configurations

within the physical joint limitations defines the robot configuration space. The robot "kinematics" provide a mapping between joint coordinates and world coordinates. The associated locations of a given point of the manipulator, e.g., the tip of its end-effector in a world coordinate system, define the robot workspace. Note that multiple configurations may result in similar end-effector positions. Because consequently, the inverse kinematic mapping between end-effector location in world coordinates and the configuration vector $q \in \Re^{n\times 1}$ is not unique, we omit here the treatment of "inverse kinematics" and concentrate on control design in configuration space. Again, the interested reader is referred to textbooks on robotics for a detailed treatment of robot kinematics and inverse kinematic mappings.

Most manipulator arms have serial links, but there are also designs with parallel linkages. Conversely, mobile robots possess wheels or other means to move about. Their workspace is defined by the set of points reachable via their means of mobility. Position and possibly orientation variables with respect to a workspace-fixed coordinate system define the configurations of a mobile robot. Recently, robot manipulators and mobile robots have been combined to form mobile manipulators, for instance, with three degrees of freedom for mobility in the plane and six degrees of freedom for manipulation.

For control design, we distinguish "holonomic" and "nonholonomic" robots. The motion of a holonomic robot is usually unconstraint. All joints may move arbitrarily within their physical limitations and the constraints of the robot workspace, i.e., only limits of the position variables exist. This class of robots, described in Section 12.1.2, incorporates both manipulators and so-called "onmidirectional" mobile robots. Special cases include interaction between a robot and components of its workspace, and cooperative action of two or more robots, requiring special treatment beyond the scope of this text. "Nonholonomic" robots face additional constraints of the time derivatives $\dot{q} \in \Re^{n\times 1}$ of their position variables, i.e., constraints on the velocity variables. Section 12.1.3 describes a kinematic and dynamic model for nonholonomic robots.

12.1.2. Holonomic Robot Model

A well-known example of highly nonlinear, fully actuated mechanical systems with coupled dynamics is a robot manipulator with rigid links. For a large class of holonomic robot systems, the generic dynamics in Equation 12.1.2 can be rewritten in configuration space as

$$M(q)\ddot{q} + V_m(q,\dot{q})\dot{q} + F(\dot{q}) + G(q) = \tau, \tag{12.1.3}$$

where $q \in \Re^{n\times 1}$ denotes the joint configurations (translational or rotational) of the n robot links, $M(q)$ stands for the inertial mass matrix, $V_m(q,\dot{q}) \in \Re^{n\times n}$ comprises Coriolis and centripetal forces, vector $F(\dot{q}) \in \Re^{n\times 1}$ describes viscous friction, and vector $G(q) \in \Re^{n\times 1}$ contains the gravity terms. The formulation

Equation 12.1.3 follows directly from the Euler-Lagrange equations of motion and encompasses robot manipulators operating freely without motion constraints. Craig [1988] revealed the following three properties: mass matrix, skew symmetry, and boundedness of dynamic terms.

12.1.2.1. Mass Matrix

The square mass matrix $M(q)$ is symmetric, positive definite, and can be written as

$$M(q) = \begin{bmatrix} m_{11}(q) & \cdots & m_{1n}(q) \\ \vdots & \ddots & \vdots \\ m_{1n}(q) & \cdots & m_{nn}(q) \end{bmatrix}, \tag{12.1.4}$$

with bounded parameters $m_{ij}^{-} \le m_{ij}(q) \le m_{ij}^{+}, 1 \le i, j \le n$. Hence, $M(q)$ can be bounded by

$$M^{-} \le \left\| M(q) \right\|_2 \le M^{+}, \tag{12.1.5}$$

where any induced matrix norm may be used to define two known scalars $0 < M^{-} \le M^{+}$ as bounds. The known scalars M^{-} and M^{+} also bound the inverse of $M(q)$ as shown,

$$\frac{1}{M^{+}} \le \left\| M^{-1}(q) \right\|_2 \le \frac{1}{M^{-}}. \tag{12.1.6}$$

In Equation 12.1.5 and in the sequel, the induced two norm will be used as an example of bounding norms, but many other norms may be used instead. The induced two norm of matrix $M(q)$ is defined as

$$\left\| M(q) \right\|_2 = \sqrt{\max\{\lambda(M^T M)\}}, \tag{12.1.7}$$

where $\lambda(M^T M)$ denotes the eigenvalues of matrix $M^T M$.

12.1.2.2. Skew Symmetry

The time derivative of the mass matrix, $\dot{M}(q) = \dfrac{d}{dt} M(q) = \dfrac{\partial M(q)}{\partial q} \dot{q}$, and the Coriolis/centripetal matrix, $V_m(q, \dot{q})\dot{q}$, are skew symmetric, i.e.,

$$y^T \left(\dot{M}(q) - 2V_m(q, \dot{q}) \right) y = 0 \tag{12.1.8}$$

holds for any nonzero vector $y \in \Re^{n \times 1}$.

12.1.2.3. Boundedness of Dynamic Terms

The Coriolis/centripetal vector $V_m(q,\dot{q})\dot{q}$ is bounded by

$$\left\|V_m(q,\dot{q})\dot{q}\right\|_2 \le V^+ \left\|\dot{q}\right\|_2, \tag{12.1.9}$$

where V_m^+ is a positive scalar. Viscous friction may be bounded by positive scalars F^+ and F_0 as shown:

$$\left\|F(\dot{q})\right\|_2 \le F^+ \left\|\dot{q}\right\|_2 + F_0. \tag{12.1.10}$$

The gravity vector likewise is bounded by a positive scalar G^+ according to

$$\left\|G(q)\right\|_2 \le G^+. \tag{12.1.11}$$

Example 12.1: Holonomic Model of a Two-Link Manipulator

A planar, two-link manipulator with revolute joints will be used as an example throughout the control development in Section 12.2. The manipulator and the associated variables are depicted in Figure 12.1.

Examination of the geometry in Figure 12.1 reveals the "forward kinematics" of the two-link manipulator. The end-effector position, (x_w, y_w), i.e., the location of mass M_2 in world coordinate frame (x, y), is given by

$$\begin{aligned} x_W &= L_1 \cos q_1 + L_2 \cos(q_1 + q_2), \\ y_W &= L_1 \sin q_1 + L_2 \sin(q_1 + q_2), \end{aligned} \tag{12.1.13}$$

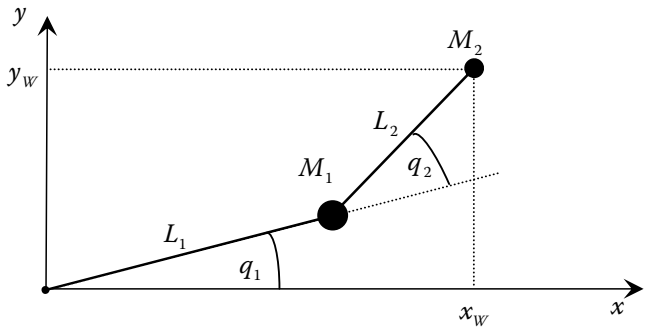

FIGURE 12.1
Two-link manipulator with link lengths L_1 and L_2 and concentrated link masses M_1 and M_2. The manipulator is shown in joint configuration (q_1, q_2), which leads to end-effector position (x_W, y_W) in world coordinates. The manipulator is operated in the plane, i.e., gravity acts along the *z*-axis.

where (q_1, q_2) denotes the joint displacements, and L_1, L_2 are the link lengths. Solving Equation 12.1.13 for the joint displacements as a function of the end-effector position (x_W, y_W) yields the "inverse kinematics" as

$$\begin{aligned} q_2 &= \operatorname{atan2}(D, C), \quad \text{with} \quad C = \frac{x_W^2 + y_W^2 - L_1^2 - L_2^2}{2L_1L_2}, \; D = \pm\sqrt{1-C^2} \\ q_1 &= \operatorname{atan2}(y_W, x_W) - \operatorname{atan2}(L_2 \sin q_2, L_1 + L_2 \cos q_2) \end{aligned} \tag{12.1.14}$$

which obviously is not unique because of the two sign options of the square root in variable D. The function "atan2(.)" describes the arctan function normalized to the range ±180°.

Applying a standard modeling technique such as the Euler-Lagrange equations yields the dynamic model according to Equation 12.1.2 as

$$\begin{bmatrix} \tau_1 \\ \tau_2 \end{bmatrix} = \begin{bmatrix} m_{11} & m_{12} \\ m_{21} & m_{22} \end{bmatrix} \begin{bmatrix} \ddot{q}_1 \\ \ddot{q}_2 \end{bmatrix} + \begin{bmatrix} n_1 \\ n_2 \end{bmatrix}, \tag{12.1.15}$$

with

$$\begin{aligned} m_{22} &= L_2^2 M_2, \\ m_{12} &= m_{21} = m_{22} + L_1 L_2 M_2 \cos q_2, \qquad M(q) = \begin{bmatrix} m_{11} & m_{12} \\ m_{21} & m_{22} \end{bmatrix}, \\ m_{11} &= L_1^2 (M_1 + M_2) + 2m_{12} - m_{22}, \\ n_2 &= L_1 L_2 M_2 \dot{q}_1^2 \sin q_2, \qquad N(q, \dot{q}) = \begin{bmatrix} n_1 \\ n_2 \end{bmatrix}, \\ n_1 &= -L_1 L_2 M_2 (2\dot{q}_1 \dot{q}_2 - \dot{q}_2^2) \sin q_2. \end{aligned} \tag{12.1.16}$$

Note the absence of gravity terms in Equation 12.1.16 because the manipulator is operated in the plane, perpendicular to gravity. For the control design examples in the following sections, we will use the parameters shown in Table 12.1.

TABLE 12.1
Geometric and Inertial Parameters of Planar Two-Link Manipulator Used for Control Design Examples

M_1	M_2	L1	L2
10 kg	1 kg	1 m	1 m

To examine the skew symmetry property in Equation 12.1.8, take the derivative of mass matrix $M(q)$ in Equation 12.1.16 to yield

$$\dot{M}(q, \dot{q}) = \begin{bmatrix} 2\dot{m}_{12} & \dot{m}_{12} \\ \dot{m}_{12} & 0 \end{bmatrix}, \qquad \dot{m}_{12}(q, \dot{q}) = L_1 L_2 M_2 \dot{q}_2 \sin q_2. \tag{12.1.17}$$

Then separate matrix $N(q, \dot{q})$ into its components according to Equation 12.1.3. Because of the assumptions of planar operation and no friction, the gravity and frictions terms are equal to zero and we obtain

$$N(q, \dot{q}) = V(q, \dot{q}) = V_m(q)\dot{q}, \quad \text{with}$$
$$V_m(q) = \begin{bmatrix} -L_1 L_2 M_2 \dot{q}_2 \sin q_2 & -L_1 L_2 M_2 (\dot{q}_1 + \dot{q}_2) \sin q_2 \\ L_1 L_2 M_2 \dot{q}_1 \sin q_2 & 0 \end{bmatrix}. \tag{12.1.18}$$

Skew symmetry follows from Equations 12.1.17 and 12.1.18 as

$$y^T \left(\dot{M}(q) - 2V_m(q, \dot{q})\right) y =$$
$$L_1 L_2 M_2 \sin q_2 \begin{bmatrix} y_1 & y_2 \end{bmatrix} \left(\begin{bmatrix} -2\dot{q}_2 & -\dot{q}_2 \\ -\dot{q}_2 & 0 \end{bmatrix} - 2 \begin{bmatrix} -\dot{q}_2 & -\dot{q}_1 - \dot{q}_2 \\ \dot{q}_1 & 0 \end{bmatrix} \right) \begin{bmatrix} y_1 \\ y_2 \end{bmatrix} = \tag{12.1.19}$$
$$L_1 L_2 M_2 \sin q_2 \begin{bmatrix} y_1 & y_2 \end{bmatrix} \left(\begin{bmatrix} 0 & 2\dot{q}_1 + \dot{q}_2 \\ -2\dot{q}_1 - \dot{q}_2 & 0 \end{bmatrix} \right) \begin{bmatrix} y_1 \\ y_2 \end{bmatrix} = 0$$

Assuming exact knowledge of the parameters in Table 12.1 but ignoring all dependencies on joint positions, yields upper and lower bounds for the elements of the matrices $M(q)$ and $N(q, \dot{q})$ in Equation 12.1.16 as listed in Table 12.2.

Using the two norm according to Equation 12.1.7 results in upper and lower bounds for mass matrix $M(q)$ as described in Equation 12.1.5 as $M^- = 0.957$ kg/m^2 and $M^+ = 204.511$ kg/m^2. Matrix $N(q, \dot{q})$ can be upper bounded as $G(q)\dot{q} = 0$.

TABLE 12.2
Lower and Upper Bounds of Matrix Elements in Geometric and Inertial Parameters

m_{11}^-	m_{11}^+	$m_{12}^- = m_{21}^-$	$m_{12}^+ = m_{21}^+$	m_{22}^-	m_{22}^+	n_1^+	n_2^+
12 kg/m^2	14 kg/m^2	1 kg/m^2	2 kg/m^2	1 kg/m^2	1 kg/m^2	$\left(2\left\|\dot{q}_1 \dot{q}_2\right\| + \dot{q}_2^2\right) \cdot 1\text{kg/m}^2$	$\dot{q}_2^2 \cdot 1\text{kg m}^2$

12.1.3. Nonholonomic Robots: Model of Wheel-Set

Robots whose motion is subjected to a set of p nonintegrable constraints involving time derivatives of the configuration vector q are classified as nonholonomic systems [see Neimark and Fufaev 1972]. The constraints usually take the form

$$G(q)\dot{q} = 0, \tag{12.1.20}$$

with the $(n - p)$ independent columns of the $p \times n$ matrix $G(q)$ forming the base for the nonholonomic constraint condition

$$\dot{q} = K(q)u. \tag{12.1.21}$$

Note that the number of control inputs is less than the dimension of the system, i.e., underactuation with $u \in \Re^{n-p}$ follows from Equation 12.1.20. Consider a set of wheels with a common axle but independent wheel actuators as an example of a mobile robot with nonholonomic kinematics, as shown in Figure 12.2. Assuming no slip at the tires, the motion of each wheel is restricted to its longitudinal direction with velocities ν_R and ν_L, respectively, by a single nonholonomic constraint ($p = 1$). In other words, no motion can occur along the lateral robot coordinate axis y_R. Also shown in Figure 12.2 is the robot configuration $q = (x, y, \phi) \in \Re^3$ in the world coordinate frame (x_w, y_w). Control inputs are the two wheel velocities ν_R and ν_L, which may be translated into the translational and rotational velocity variables $u = (\nu_c, \omega) \in \Re^2$ for convenience. The motion of the wheel set in the world coordinate frame is given by

$$\begin{aligned} \dot{x} &= \nu_c \cos\phi, \\ \dot{y} &= \nu_c \sin\phi, \\ \dot{\phi} &= \omega, \end{aligned} \tag{12.1.22}$$

which form the forward kinematics for this case.

For the wheel set shown in Figure 12.2, we assume inertial dynamics of the form

$$M\dot{v}_C + N_t(v_C, \omega) = \tau_t, \tag{12.1.23}$$

$$J\dot{\omega} + N_r(v_C, \omega) = \tau_r, \tag{12.1.24}$$

with positive scalars M and J denoting mass and rotational inertia about the vertical z_w-axis, $\tau = (\tau_t, \tau_r) \in \Re^2$ being the control inputs, and scalars $N_t(\dot{v}_C, \omega)$ and $N_r(\dot{v}_C, \omega)$ comprising all additional dynamics. A more involved dynamic modeling was discussed by Bloch, Reyhanoglu, and McClamroch [1992].

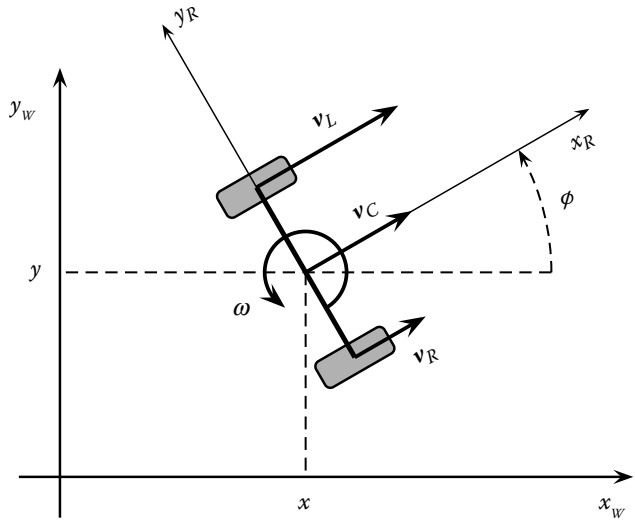

FIGURE 12.2
Wheel set with common fixed axis as example of nonholonomic robot kinematics. Wheels are constrained to longitudinal velocities v_R (right) and v_L (left) along robot axis x_R. Lateral motion along axis y_R is impossible. Wheel velocities v_R and v_L result in translational robot motion v_C and rotational motion ω. Also shown is the robot position (x, y, ϕ) of Equation 12.1.22 in the world coordinate frame (x_W, y_W).

12.2. Trajectory Tracking Control

The control task commonly arising in robot control is to track a time-dependent trajectory described by

$$[q_d(t), \dot{q}_d(t), \ddot{q}_d(t)], \tag{12.2.1}$$

with bounded desired configurations $q_d(t) = [q_{d_1}(t), \ldots, q_{d_i}(t), \ldots, q_{d_n}(t)]$, velocities $\dot{q}_d(t) = [\dot{q}_{d_1}(t), \ldots, \dot{q}_{d_i}(t), \ldots, \dot{q}_{d_n}(t)]$, and accelerations $\ddot{q}_d(t) = [\ddot{q}_{d_1}(t), \ldots, \ddot{q}_{d_i}(t), \ldots, \ddot{q}_{d_n}(t)]$ for each component of an n-dimensional system like that in Equation 12.1.2. Control of a second-order mechanical system with a force/torque input as in Equation 12.1.2 requires position and velocity feedback as a basis for stabilization, i.e., PD-type control. This requirement can be met by either measurement and feedback of both position and velocity variables or a lead compensator for position measurements in the linear sense [see Arimoto and Miyazaki 1984]. In sliding mode control designs, this requirement is reflected in the choice of the sliding manifold with a stable motion, designed as a (linear) combination of position and velocity variables.

Since the first set-point sliding mode controller for robot manipulators suggested by Young [1978], numerous variations have been presented in the literature. In the sequel, we seek to outline the set of principle design choices to be made when designing a sliding mode tracking controller for a mechanical system like that in Equation 12.1.2. First, the designer may choose between componentwise control and vector control. Second, a pure discontinuous controller has to be compared with a continuous feedback/feedforward controller with an additional discontinuity term to achieve robustness by generating sliding mode. For overviews, see Tables 12.6 and 12.7, respectively, at the end of this section.

Example 12.2: Circular Trajectory for Planar Two-Link Manipulator

For the control design examples in this section, we will demand the planar two-link manipulator detailed in Example 12.1 to follow a circular trajectory in its workspace. The circle with center (x_d, y_d) and radius r_d is given in world coordinates (x_w, y_w) by

$$\begin{aligned} x_d(t) &= x_{d_0} + r_d \cos\psi_d \\ y_d(t) &= y_{d_0} - r_d \sin\psi_d \\ \psi_d(t) &= \frac{2\pi}{t_f} t - \sin\left(\frac{2\pi}{t_f} t\right), \quad 0 \le t \le t_f, \end{aligned} \tag{12.2.2}$$

where the operation is assumed to start at time $t = 0$ and to be completed at final time $t = t_f$. The parameters for the examples are chosen as shown in Table 12.3. Bounds over the time interval $0 \le t \le t_f$ can be obtained by using the inverse kinematics (Equation 12.1.14) as summarized in Table 12.4. The desired trajectory is depicted in Figure 12.3.

TABLE 12.3
Parameters of Desired Circular Trajectory

x_d	y_d	r_d	t_f
1 m	1 m	0.5 m	5 s

TABLE 12.4
Bounds of Desired Circular Trajectory

$\lvert\psi_d\rvert \le \frac{2\pi}{5}$	$\lvert\dot{\psi}_d\rvert \le \frac{4\pi}{5}$	$\lvert\ddot{\psi}_d\rvert \le \frac{4\pi^2}{25}$	$\lvert\dot{q}_{d_1}\rvert \le 1$ rad/s	$\lvert\dot{q}_{d_2}\rvert \le 1$ rad/s

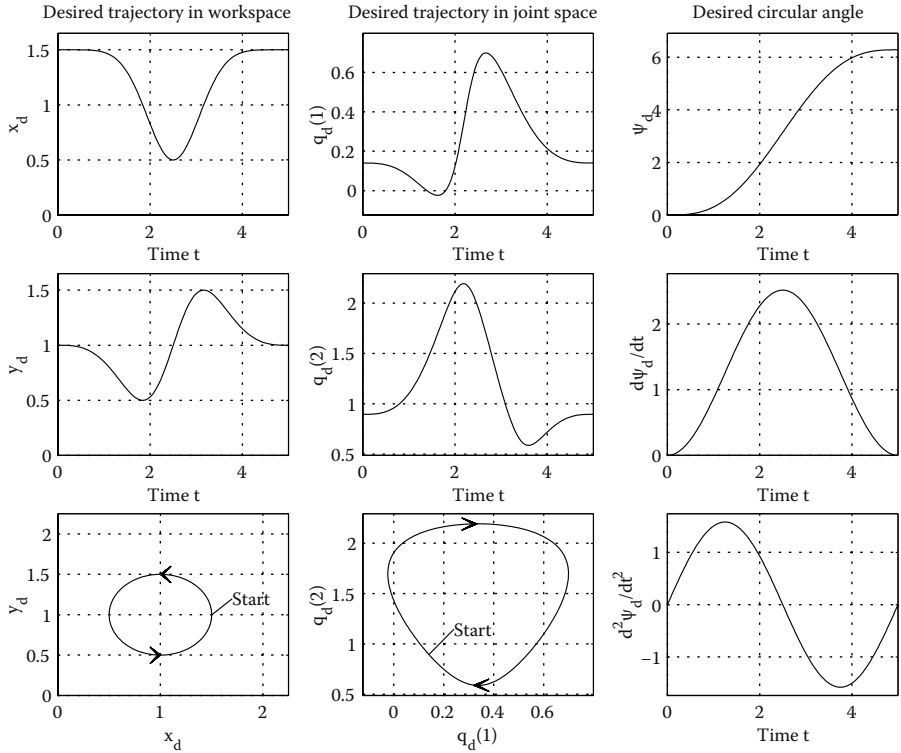

FIGURE 12.3
Desired circular trajectory for example control designs. Workspace trajectory in world coordinates (x_W, y_W) is shown in left column. Center column depicts associated joint space trajectories in (q_1, q_2) coordinates. Right column shows time trajectory of angle Ψ_d.

12.2.1. Componentwise Control

The first choice is mainly concerned with the structure of the sliding manifold(s). Because in system Equation 12.1.2 n force/torque inputs are assumed to control n configuration outputs of the $2n$-dimensional dynamics, each component i of the n components of the output vector may be assigned its own sliding manifold and hence be controlled independently. Alternatively, the n components are dealt with as a vector (see Section 12.2.2). For componentwise control, the structure of the n sliding manifolds is

$$s_i = c_i q_{e_i} + \dot{q}_{e_i}, \quad i = 1, \ldots, n, \tag{12.2.3}$$

where $c_i > 0$ are scalar gains to determine the rate of exponential convergence of the tracking error $q_{e_i} = q_{d_i} - q_i$ to zero after reaching the sliding manifold $s_i = 0$. Each component of the control input vector τ_i is responsible for ensuring

sliding mode to occur along its respective manifold (Equation 12.2.3), e.g., by choosing

$$\tau_i = \tau_{0_i} \text{sign}(s_i), \quad i = 1, \ldots, n. \tag{12.2.4}$$

Sliding mode is established independently in each manifold $s_i = 0$ and finally in the intersection $s = [s_1, \ldots, s_n]^T = 0_{n\times 1}$. The controller gains τ_{0_i} are to be determined from the stability analysis sketched in Theorem 12.1.

Theorem 12.1

The states of system (Equation 12.2.5) with components (Equation 12.2.6) under control (Equation 12.2.8) will reach the sliding manifolds (Equation 12.2.7) in finite time.

Total System $$\ddot{q} = M^{-1}\left(\tau - N(q, \dot{q})\right) \tag{12.2.5}$$

System component $$\ddot{q}_i = \left(M^{-1}\left(\tau - N(q, \dot{q})\right)\right)_i = \frac{1}{m_{ii}}\left(\tau_i - n_i - \sum_{j=1, j\neq i}^{n} m_{ij}\ddot{q}_j\right) \tag{12.2.6}$$

Manifolds $$s_i = c_i q_{e_i} + \dot{q}_{e_i} = c_i(q_{d_i} - q_i) + (\dot{q}_{d_i} - \dot{q}_i) \tag{12.2.7}$$

Control $$\tau_i = \tau_{0_i} \text{sign}(s_i) \tag{12.2.8}$$

□

Proof 12.1

Consider a Lyapunov function candidate for each component,

$$V_i = \frac{1}{2} s_i^2, \tag{12.2.9}$$

with its time derivative along the system trajectories

$$\begin{aligned} \dot{V}_i &= s_i\left(c_i\dot{q}_{e_i} + \ddot{q}_{d_i} - \frac{1}{m_{ii}}\left(\tau_{0_i}\text{sign}(s_i) - n_i - \sum_{j=1, j\neq i}^{n} m_{ij}\ddot{q}_j\right)\right) \\ &\leq -\frac{\tau_{0_i}}{m_{ii}^{+}}|s_i| + |s_i|\left(c_i|\dot{q}_{e_i}| + |\ddot{q}_{d_i}| + \frac{1}{m_{ii}^{-}}\left(n_i^{+} + \sum_{j=1, j\neq i}^{n} m_{ij}^{+}|\ddot{q}_j|\right)\right). \end{aligned} \tag{12.2.10}$$

Boundedness of the desired trajectory in Equation 12.2.1 of the elements m_{ij} of the mass matrix in Equation 12.1.4 and of the elements n_i of vector $N(q)$ by Equations 12.1.9 through 12.1.11 ensures the existence of a

$$\tau_{0_i} > m_{ii}^{+}\left(c_i\left|\dot{q}_{e_i}\right| + \left|\ddot{q}_{d_i}\right| + \frac{1}{m_{ii}^{-}}\left(n_i^{+} + \sum_{j=1,\, j\neq i}^{n} m_{ij}^{+}\left|\ddot{q}_j\right|\right)\right) \tag{12.2.11}$$

to yield

$$\dot{V}_i \leq -\xi_i \left| s_i \right|, \tag{12.2.12}$$

for some scalar $\xi_i > 0$. Consequently, finite convergence of the system Equation 12.2.6 to the manifold $s_i = 0$ in Equation 12.2.7 is established. □

The assumption of boundedness of the terms $\frac{m_{ji}}{m_{ii}}\ddot{q}_j, j = 1,\ldots,n, j \neq i$, implies bounded coupling forces/torques attributable to bounded accelerations of the other masses. In practical mechanical systems with one mass m_i being associated with each control input τ_i, a hierarchical boundedness of coupling terms is inherent. In particular, robot manipulators tend to be constructed with stronger and hence heavier links and joints near the base and with increasingly lighter links and joints toward the tip and the end effector. For an explicit stability analysis, the hierarchy of masses has to be solved reversely, a process that may become tedious for higher-dimensional systems. The details of the hierarchical design method may be found in previous work [Utkin 1992].

Alternatively to the individual design of components τ_i of control vector τ pursued in Theorem 12.1, the design may be based on a Lyapunov function constructed for the whole system instead for each subsystem. The main advantage of such a closed representation in vector form is the avoidance of hierarchical mass requirements attributable to the positive-definite property of the mass matrix M. It will be shown in Section 12.2.2 that using a control vector τ likewise enforces sliding mode.

Example 12.3: Componentwise Control of Two-Link Manipulator

Solving Equation 12.2.6 for the planar two-link manipulator with dynamics Equation 12.1.15 yields

$$\ddot{q}_1 = \frac{1}{m_{11}}\left(\tau_1 - n_1 - m_{21}\ddot{q}_2\right),$$
$$\ddot{q}_2 = \frac{1}{m_{22}}\left(\tau_2 - n_2 - m_{12}\ddot{q}_1\right). \tag{12.2.13}$$

According to Equation 12.2.7, the sliding manifolds are defined as

$$\begin{aligned} s_1 &= c_1 q_{e_1} + \dot{q}_{e_1} = 0, \quad q_{e_1} = q_{d_1} - q_1, \\ s_2 &= c_2 q_{e_2} + \dot{q}_{e_2} = 0, \quad q_{e_2} = q_{d_2} - q_2, \end{aligned} \tag{12.2.14}$$

leading to a control vector

$$\tau = \begin{bmatrix} \tau_1 \\ \tau_2 \end{bmatrix} = \begin{bmatrix} \tau_{0_1} \operatorname{sign} s_1 \\ \tau_{0_2} \operatorname{sign} s_2 \end{bmatrix}. \tag{12.2.15}$$

For proving stability, a Lyapunov function candidate is used for each component. As an example, consider the first joint controller:

$$V_1 = \frac{1}{2} s_1^2. \tag{12.2.16}$$

The time derivative along the system dynamics (Equations 12.2.3 through 12.2.14) under control Equation 12.2.15 is given by

$$\begin{aligned} \dot{V}_1 &= s_1 \dot{s}_1 \\ &= s_1 (c_1 \dot{q}_{e_1} + \ddot{q}_{d_1} - \ddot{q}_1) \\ &= s_1 \left(-\frac{\tau_{0_1} \operatorname{sign} s_1}{m_{11}} + c_1 \dot{q}_{e_1} + \ddot{q}_{d_1} + \frac{n_1}{m_{11}} + \frac{m_{21}}{m_{11}} \ddot{q}_2 \right). \end{aligned} \tag{12.2.17}$$

The requirement $\dot{V}_1 < -\xi_1 |s_1|$ leads to a condition for the required control resources τ_{0_1} as

$$\tau_{0_1} \geq m_{11}^+ \left(c_1 \left| \dot{q}_{e_1} \right| + \left| \ddot{q}_{d_1} \right| + \frac{n_1^+}{m_{11}^-} + \frac{m_{21}^+}{m_{11}^-} \left| \ddot{q}_2 \right| \right) + \xi_1, \quad \xi_1 > 0. \tag{12.2.18}$$

The parameter bounds can be found from Tables 12.2 and 12.4. The second joint controller can be treated in a similar manner.

Often, the link accelerations $\ddot{q}_i$ are not available. In such a case, the desired link accelerations $\ddot{q}_{d_i}$ can be substituted under the assumption of close tracking.

For robots with on-off control inputs, i.e., control torques that may only take two values $\tau_i = -\tau_{0_1}$ or $\tau_i = +\tau_{0_1}$, the maximum of Equation 12.2.18 over the whole desired trajectory in the interval $0 \le t \le t_f$ should be taken. If the required control resources calculated from Equation 12.2.18 exceed the actual control resources of a given robot, the desired trajectory should be modified to decrease the required joint accelerations.

Also, because the starting point of the robot manipulator often coincides with the starting point of the desired trajectory, the initial errors are zero and sliding mode may occur immediately at the start. Thus, all errors and their derivatives are zero throughout the entire operation.

Figures 12.4 and 12.5 show the time trajectory in the robot workspace, the distances to the sliding manifolds, and the required control resources for the circular example trajectory (Equation 12.2.2). The initial conditions were chosen to be nonzero for illustration purposes. Convergence to the sliding manifolds in finite time is illustrated by the top graph in Figure 12.5. Note the difference in required control resources for the two joints in the bottom graph of Figure 12.5.

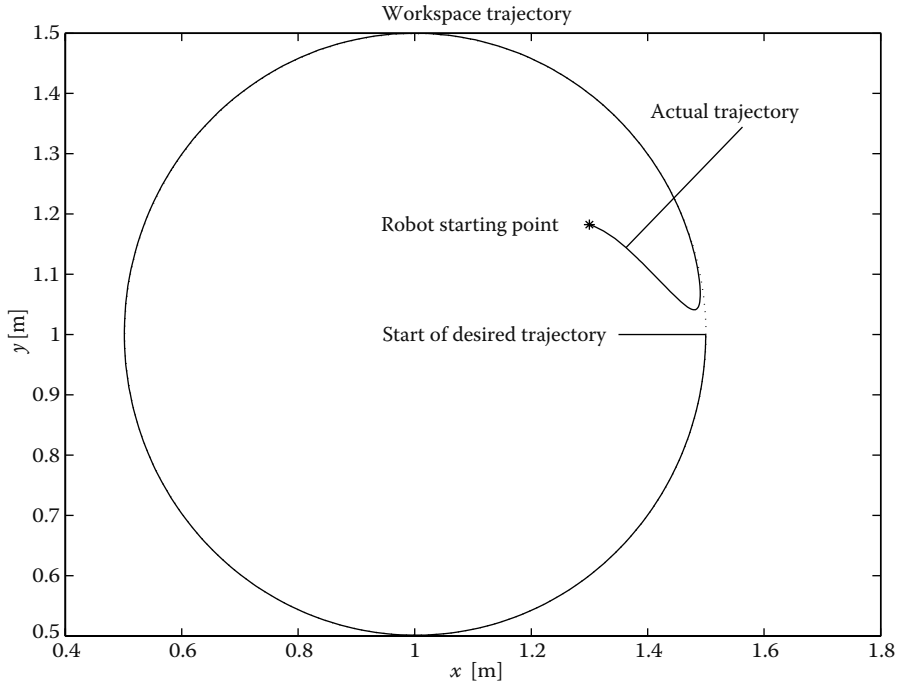

FIGURE 12.4
Robot trajectory and desired trajectory in world coordinates for componentwise control design.

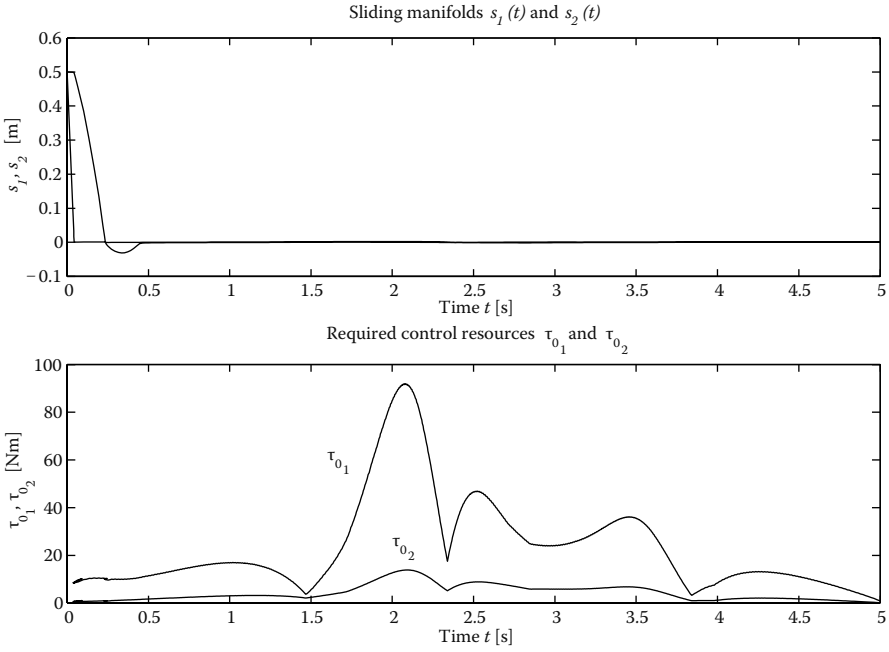

FIGURE 12.5
Top graph: Distance to sliding manifolds $s_1(t)$ and $s_2(t)$. Bottom graph: Required control resources τ_{0_1} and τ_{0_2} for each joint.

12.2.2. Vector Control

The above componentwise control is most suitable for systems with dominant terms in the diagonal of the mass matrix $M(q)$ and with truly discontinuous control inputs, i.e., inputs τ_i that may only take two values $\tau_i = -\tau_{0_i}$ and $\tau_i = +\tau_{0_i}$. For other systems, in particular for those with range control inputs $-\tau_{0_i} \le \tau_i \le +\tau_{0_i}$, vector control is an elegant alternative.

In contrast to the set of n one-dimensional sliding manifolds $s_i = 0$ for componentwise control design, vector control is based on a single n-dimensional vector sliding manifold

$$s = Cq_e + \dot{q}_e, s \in \Re^{n\times 1}, \tag{12.2.19}$$

where $C \in \Re^{n\times n}$ is a Hurwitz and preferably diagonal gain matrix, $q_e(t) = q_d(t) - q(t)$ is the tracking error vector, and input vector τ is defined as

$$\tau = \tau_0 \frac{s}{\|s\|_2}, \tau \in \Re^{n\times 1}. \tag{12.2.20}$$

Sliding mode only occurs when all components of s in Equation 12.2.19 are equal to zero instead of occurring in each component separately as for componentwise control. Likewise, $s = 0_{n\times 1}$ is the only discontinuity in control Equation 12.2.20, whereas Equation 12.2.4 features n control discontinuities in vector $\tau = [\tau_1, \tau_2, \ldots, \tau_n] \in \Re^{n\times 1}$. Note that the control vector has always length τ_0, which led to the name "unit control" for this approach [Ryan and Corless 1984; Dorling and Zinober 1986]. The stability analysis in the following theorem is also vector based.

Theorem 12.2

The system in Equation 12.2.21 with the bounds given in Equations 12.1.5 and 12.1.9 through 12.1.11 under control Equation 12.2.23 will reach the sliding manifold Equation 12.2.22 in finite time.

System $$\ddot{q} = M^{-1}\left(\tau - N(q,\dot{q})\right) \tag{12.2.21}$$

Manifold $$s = Cq_e + \dot{q}_e = C(q_d - q) + (\dot{q}_d - \dot{q}) = 0 \tag{12.2.22}$$

Control $$\tau = \tau_0 \frac{s}{\|s\|_2} \tag{12.2.23}$$

□

Proof 12.2

Consider the Lyapunov function candidate

$$V = \frac{1}{2} s^T s, \tag{12.2.24}$$

with its derivative along the system trajectories in Equation 12.2.21 under control given in Equation 12.2.23,

$$\begin{aligned} \dot{V} &= s^T \left(C\dot{q}_e + \ddot{q}_d - M^{-1}(q)\left(\tau_0 \frac{s}{\|s\|_2} - N(q,\dot{q}) \right) \right) \\ &\leq -\frac{\tau_0}{M^+}\|s\| + \|s\|\left(C\|\dot{q}_e\| + \frac{N^+}{M^-} + \|\ddot{q}_d\| \right). \end{aligned} \tag{12.2.25}$$

Use of the boundedness assumptions on the desired trajectory in Equation 12.2.1 and of the bounds given in Equations 12.1.5 and 12.1.9 through 12.1.11 enables to find a sufficiently large τ_0 to guarantee

$$\dot{V} \leq -\xi \|s\|_2 \tag{12.2.26}$$

and henceforth finite converge to the manifold $s = 0_{n\times 1}$ in Equation 12.2.22. □

Compared with componentwise control design as in Theorem 12.1, vector control exploits matrix/vector norms for bounds in Equations 12.1.5 and 12.1.9 through 12.1.11 in the stability analysis rather than single-parameter bounds. Although matrix/vector norms yield a more elegant and more concise mathematical formulation, they are known to be conservative and may result in overestimation of the required control resources. In particular, because $\tau_0 \geq \tau_{0_i}, \forall i = 1,\ldots,n$ in Equations 12.2.8 and 12.2.23, all components τ_i of the control input vector τ in Equation 12.2.21 are required at least resources τ_0. For mechanical systems with inhomogeneous masses and actuators, such a requirement may considerably exceed the system capabilities and componentwise control design is advisable. An example is a multilink robot manipulator with heavy base links with strong joint actuators but smaller links near the end effector with preferably less powerful actuators.

Example 12.4: Vector Control of Two-Link Manipulator

Adaptation of the control design in Theorem 12.2 to the planar two-link manipulator example of Equation 12.1.15 yields a sliding manifold as shown

$$s = \begin{bmatrix} c_1 & 0 \\ 0 & c_2 \end{bmatrix} \begin{bmatrix} q_{e_1} \\ q_{e_2} \end{bmatrix} + \begin{bmatrix} \dot{q}_{e_1} \\ \dot{q}_{e_2} \end{bmatrix}, \tag{12.2.27}$$

which in fact is similar to the componentwise control design (Equation 12.2.14) for this choice of gain matrix $C = \begin{bmatrix} c_1 & 0 \\ 0 & c_2 \end{bmatrix}$. The difference in control design becomes apparent when defining the vector controller according to Equation 12.2.23 as

$$\tau = \tau_0 \frac{s}{\|s\|_2} = \frac{\tau_0}{\sqrt{(c_1 q_{e_1} + \dot{q}_{e_1})^2 + (c_2 q_{e_2} + \dot{q}_{e_2})^2}} \left(\begin{bmatrix} c_1 & 0 \\ 0 & c_2 \end{bmatrix} \begin{bmatrix} q_{e_1} \\ q_{e_2} \end{bmatrix} + \begin{bmatrix} \dot{q}_{e_1} \\ \dot{q}_{e_2} \end{bmatrix} \right), \tag{12.2.28}$$

compared with Equation 12.2.15.

Stability can be established using Lyapunov function candidate

$$V = \frac{1}{2} s^T s = \frac{1}{2} \left(s_1^2 + s_2^2 \right), \tag{12.2.29}$$

which also differs from the componentwise Lyapunov function (Equation 12.2.16). Differentiation along the system trajectories in Equation 12.1.15 with manifold Equation 12.2.27 and under control Equation 12.2.28 yields

$$\dot{V} = s_1\dot{s}_1 + s_2\dot{s}_2 =$$

$$= -\frac{\tau_0}{M^+}\|s\| + \|s\|\left(\sqrt{c_1^2\dot{q}_{e_1}^2 + c_1^2\dot{q}_{e_1}^2} + \frac{N^+}{M^-} + \sqrt{\ddot{q}_1^2 + \ddot{q}_2^2}\right). \tag{12.2.30}$$

Substituting the matrix bounds of the example in Section 12.1.2 leads to an upper bound on the required control resources as

$$\tau_0 \geq M^+\left(\sqrt{c_1^2\dot{q}_{e_1}^2 + c_1^2\dot{q}_{e_1}^2} + \frac{N^+}{M^-} + \sqrt{\ddot{q}_1^2 + \ddot{q}_2^2}\right) + \xi,\ \xi > 0. \tag{12.2.31}$$

Again, the desired link acceleration $\|q_d\| = \sqrt{\ddot{q}_{d_1}^2 + \ddot{q}_{d_2}^2}$ may be substituted for the actual link acceleration $\|q\| = \sqrt{\ddot{q}_1^2 + \ddot{q}_2^2}$ under the assumption of exact tracking. Note that vector control design requires both joints to provide resources according to Equation 12.2.31.

Simulation results are shown in Figures 12.6 and 12.7. Because the matrix bounds are more conservative than the bounds on the single matrix elements in Table 12.2, the requirement for τ_0 is considerably larger than for τ_{0_1} and τ_{0_2} in the

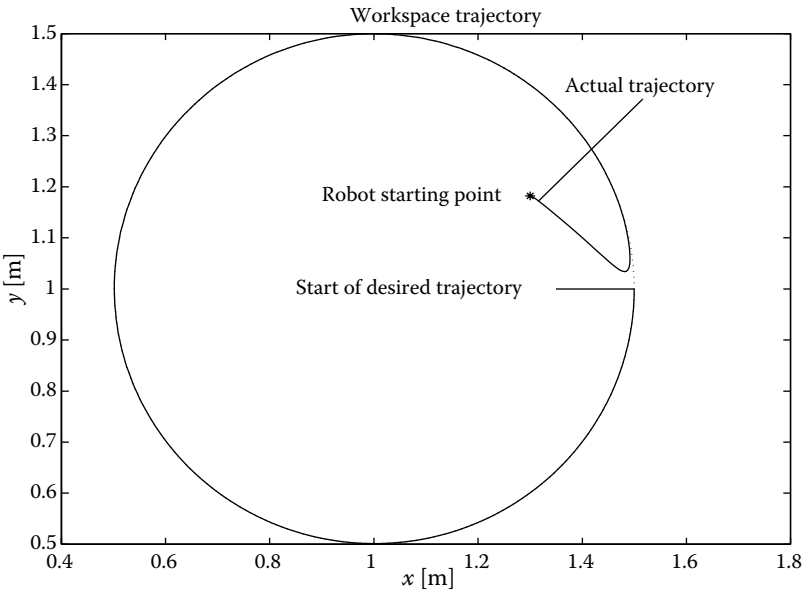

FIGURE 12.6
Robot trajectory and desired trajectory in world coordinates for vector control design.

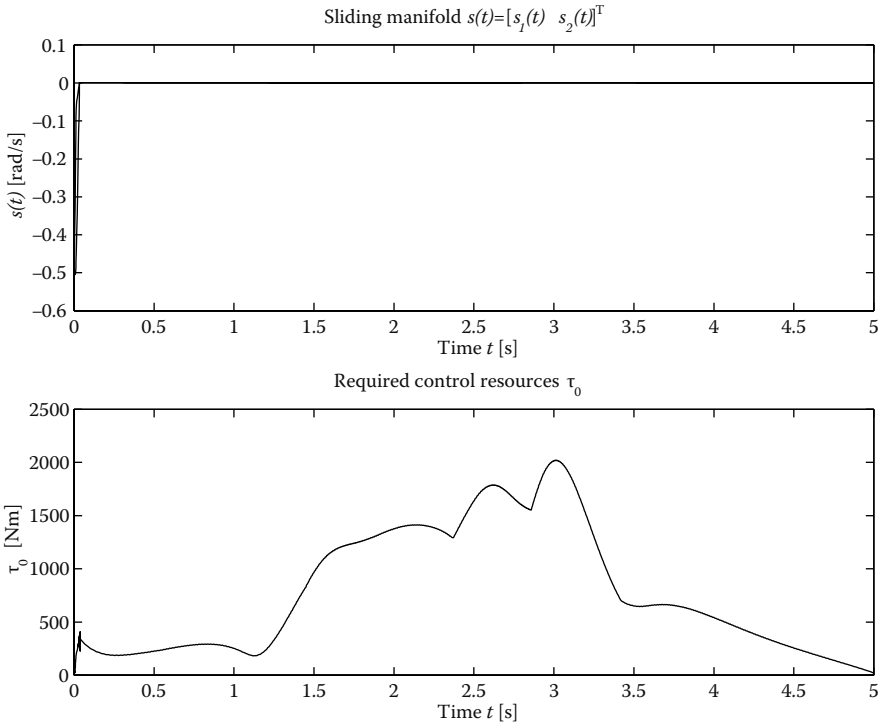

FIGURE 12.7
Top graph: Distance to sliding manifold $s(t) = [s_1(t)\ s_2(t)]^T$. Bottom graph: Required control resources τ_0 for both joints.

case of componentwise control design (compare Figures 12.5 and 12.7). Because of the increase of control resources, convergence to the sliding manifold from the initial conditions is significantly faster. Also note that sliding mode occurs simultaneously in both components of vector $s = \begin{bmatrix} s_1 & s_2 \end{bmatrix}^T$.

12.2.3. Continuous Feedback/Feedforward Control with Additional Discontinuity Term for Sliding Mode

The two designs in Theorems 12.1 and 12.2 yield purely discontinuous controllers. All system dynamics are treated as unknown disturbances and are suppressed by the control inputs. Only bounds on the system parameters are assumed to be known and are necessary for guaranteeing stability of the design. This approach is well suited for systems with in fact mostly unknown or highly uncertain parameters and with direct implementability of a sliding mode controller. In cases of at least partially known parameters and in the presence of additional unmodeled dynamics, requiring one of the

methods of Chapter 8 to prevent chattering, a more complex feedback/feedforward structure is advisable. Another advantage of this second alternative choice is the possibility to exploit the physical properties of the system to the benefit of the control performance. In particular, for robot manipulators with dynamics described by Equation 12.1.3, the skew-symmetry property (Equation 12.1.8) can be used. Although this approach is suitable for both componentwise control and vector control, we focus on the latter for ease and clarity of presentation. Componentwise control was discussed previously [Slotine 1985; Chen, Mita, and Wahui 1990].

Assume that there exist estimates for the matrices and vectors in Equation 12.1.3 with similar structures and estimated parameters, denoted by $\hat{M}(q), \hat{V}_m(q,\dot{q}), \hat{F}(\dot{q})$, and $\hat{G}(q)$. In addition to Equation 12.2.19, we define

$$\dot{\lambda} = Cq_e + \dot{q}_d = s + \dot{q} \tag{12.2.32}$$

and present the following control design.

Theorem 12.3

The system in Equation 12.2.33 with bounds given in Equations 12.1.5 and 12.1.9 through 12.1.11 under control in Equation 12.2.35 will reach the sliding manifold Equation 12.2.34 in finite time.

System $$\ddot{q} = M^{-1}(q)\left(\tau - V_m(q,\dot{q})\dot{q} - F(\dot{q}) - G(q)\right) \tag{12.2.33}$$

Manifold $$s = \dot{\lambda} - \dot{q} = 0, \quad \lambda = C(q_d - q) + \dot{q}_d \tag{12.2.34}$$

Control $$\tau = \hat{M}(q)\ddot{\lambda} + \hat{V}_m(q,\dot{q})\dot{\lambda} + \hat{F}(\dot{q}) + \hat{F}(\dot{q}) + \hat{G}(q) + \tau_0 \frac{s}{\|s\|_2} \tag{12.2.35}$$

□

Proof 12.3

Consider the Lyapunov function candidate

$$V = \frac{1}{2} s^T M(q) s, \tag{12.2.36}$$

which is positive semi-definite with respect to q because the mass matrix $M(q)$ is positive definite. Differentiation along the system trajectories under control Equation 12.2.35 and using the skew-symmetry property (Equation 12.1.8) yields

$$\begin{aligned}\dot{V} &= s^T\left(-\tau_0\frac{s}{\|s\|_2}+\bar{M}(q)\ddot{\lambda}+\bar{V}_m(q,\dot{q})\dot{\lambda}+\bar{F}(\dot{q})+\bar{G}(q)\right)\\ &\le -\tau_0\|s\|+\|s\|\left(\bar{M}^+\left\|\ddot{\lambda}\right\|+\bar{V}_m^+\left\|\dot{\lambda}\right\|+\bar{F}_0+\bar{F}^+\|\dot{q}\|+\bar{G}^+\right).\end{aligned} \tag{12.2.37}$$

Because estimates $\hat{M}(q), \hat{V}_m(q,\dot{q}), \hat{F}(\dot{q})$, and $\hat{G}(q)$ have similar structures as their equivalents in Equation 12.1.3, they also fulfill the boundedness properties described in Section 12.1.2. Hence, the estimation errors $\bar{M}(q) = M(q) - \hat{M}(q)$, $\bar{V}_m(q,\dot{q}) = V_m(q,\dot{q}) - \hat{V}_m(q,\dot{q})$, $\bar{F}(\dot{q}) = F(\dot{q}) - \hat{F}(\dot{q})$, and $\bar{G}(q) = G(q) - \hat{G}(q)$ may be bounded similarly to Equations 12.1.5 through 12.1.11 by appropriate scalars $\bar{M}^-$, $\bar{M}^+$, $\bar{V}_m^+$, $\bar{F}_0$, $\bar{F}^+$, and $\bar{G}^+$. For a bounded trajectory with $|q_d(t)| \le q_d^+$, $|\dot{q}_d(t)| \le \dot{q}_d^+$ and $|\ddot{q}_d(t)| \le \ddot{q}_d^+$, and bounded link positions $q(t)$ and velocities $\dot{q}(t)$, $\dot{\lambda}(t)$ and $\ddot{\lambda}(t)$ are also bounded and there exists a finite

$$\tau_0 > \bar{M}^+\left\|\ddot{\lambda}\right\| + \bar{V}_m^+\left\|\dot{\lambda}\right\| + \bar{F}_0 + \bar{F}^+\|\dot{q}\| + \bar{G}^+ \tag{12.2.38}$$

such that the sliding condition is fulfilled, i.e.,

$$\dot{V} \le -\xi\|s\|_2, \tag{12.2.39}$$

and reaching of the sliding manifold Equation 12.2.34 in finite time is guaranteed. □

The first four continuous terms in Equation 12.2.35 fulfill both feedback and feedforward tasks by compensating for dynamic terms in Equation 12.2.33 according to the current error and the desired trajectory as comprised in the variable λ in Equation 12.2.32. Note that $\ddot{\lambda}(t)$ in controller Equation 12.2.35 does not require measurement of link acceleration $\ddot{q}(t)$ (see also definition Equation 12.2.32). In the case of exact knowledge of all model parameters, i.e., $\bar{M}(q) = 0_{n\times n}$, $\bar{V}_m(q,\dot{q}) = 0_{n\times n}$, $\bar{F}(\dot{q}) = 0_{n\times 1}$, and $\bar{G}(q) = 0_{n\times 1}$, a small discontinuous term $\tau_0\frac{s}{\|s\|_2}$ would suffice to guarantee stability. In practice, the sliding mode term also has to cope with uncertainties in the estimates $\hat{M}(q), \hat{V}_m(q,\dot{q}), \hat{F}(\dot{q})$, and $\hat{G}(q)$ and possibly also with additive external disturbance forces/torques not accounted for in model Equation 12.1.3.

The feedback/feedforward terms follow the ideas of feedback linearization: to obtain a basically linearized outer control loop by appropriate cancellation of all nonlinear terms in an inner control loop. In robotic applications, this technique is referred to as "computed torque control" [Hunt, Su, and

Meyer 1983; Gilbert and Ha 1984]. Related approaches directly use energy considerations derived from the Euler-Lagrange formulation [Takegaki and Arimoto 1981] or the "natural motion" of the mechanical system [Koditschek 1991]. An advantage over classical feedback linearization is the possibility to exploit the dynamics of the system, such as the skew-symmetry property of robot manipulators, rather than canceling all nonlinear terms via feedback regardless of their possibly beneficial influence in closed loop. Various other approaches in this class of controllers have been proposed in the literature to improve the accuracy of the feedback/feedforward terms, e.g., reducing the estimation error by adaptive or robust adaptive control. The underlying idea is to minimize control action in the outer loop. For a more detailed treatment of feedback/feedforward strategies , the interested reader is encouraged to study textbooks on robot control [such as Craig 1988; Spong and Vidyasagar 1989; Lewis, Abdallah, and Dawson 1993].

Example 12.5: Feedback/Feedforward Control of Two-Link Manipulator

To design a feedback/feedforward controller, estimates of the model parameters are required. For clarity, the parameter estimates in this example are chosen as the average of the lower and upper bounds of the model parameters as given in Table 12.2. The estimated parameters are denoted with circumflexes (^); their numeric values are given in Table 12.5. Note that the estimates for Coriolis/centripetal effects are set to zero because of the contained trigonometric functions.

Furthermore, auxiliary variable $\lambda(t)$ needs to be calculated in addition to sliding manifold Equation 12.2.34:

$$\dot{\lambda} = \begin{bmatrix} c_1 & 0 \\ 0 & c_2 \end{bmatrix} \begin{bmatrix} q_{d_1} - q_1 \\ q_{d_2} - q_w \end{bmatrix} + \begin{bmatrix} \dot{q}_{d_1} \\ \dot{q}_{d_2} \end{bmatrix}. \tag{12.2.40}$$

Given the parameter estimates in Table 12.5 and the definition of λ in Equation 12.2.40, a control vector according to Equation 12.2.35 can be defined as

$$\tau = \begin{bmatrix} \hat{m}_{11} & \hat{m}_{12} \\ \hat{m}_{21} & \hat{m}_{22} \end{bmatrix} \begin{bmatrix} \ddot{\lambda}_1 \\ \ddot{\lambda}_2 \end{bmatrix} + \hat{V}_m(q, \dot{q}) \begin{bmatrix} \dot{\lambda}_1 \\ \dot{\lambda}_2 \end{bmatrix} + \tau_0 \frac{s}{\|s\|_2}. \tag{12.2.41}$$

TABLE 12.5
Estimates for the Matrix Elements in Geometric and Inertial Parameters

$\hat{m}_{11}$	$\hat{m}_{12} = \hat{m}_{21}$	$\hat{m}_{22}$	$\hat{V}_m$
13 kg/m^2	1.5 kg/m^2	1.5 kg/m^2	$0_{2\times2}$

Note that, because the example manipulator operates in the plane without the influence of gravity and no friction was included in model Equation 12.1.15, $N(q,\dot{q}) = V_m(q,\dot{q})\dot{q}$ holds.

The stability proof exploits Lyapunov function candidate Equation 12.2.36 with its time derivative given in Equation 12.2.37. Matrix bounds for the estimation errors are obtained in a similar manner as in the example in Section 12.1.2. For example, the estimation error of the mass matrix, $\bar{M} = M - \hat{M}$, can be bounded by $\bar{M}^- = 3.177\,\text{kg/m}^2$ and $\bar{M}^+ = 5.323\,\text{kg/m}^2$. Note that especially the value for the upper bound is considerably smaller than the corresponding value of $M^+ = 205.511\,\text{kg/m}^2$. Consequently, the amplitude of the control discontinuity term, τ_0 in Equation 12.2.41, can be chosen significantly smaller than in Equation 12.2.28.

Figures 12.8 and 12.9 illustrate the performance of the continuous feedback/feedforward controller with a small discontinuity term in a similar manner as in the previous examples in Sections 12.2.1 and 12.2.2. However, because the continuous feedback/feedforward part also requires control resources, the bottom graph of Figure 12.9 depicts a low-pass-filtered average of the total control torques τ_1 and τ_2. The simulation example suggests that the required control resources are in the same order of magnitude as in the case of componentwise control in Section 12.2.1. Note that convergence to the sliding manifold is slower than in the previous examples, but both components reach the manifold simultaneously because of the unit vector characteristic of the discontinuity term in Equation 12.2.41.

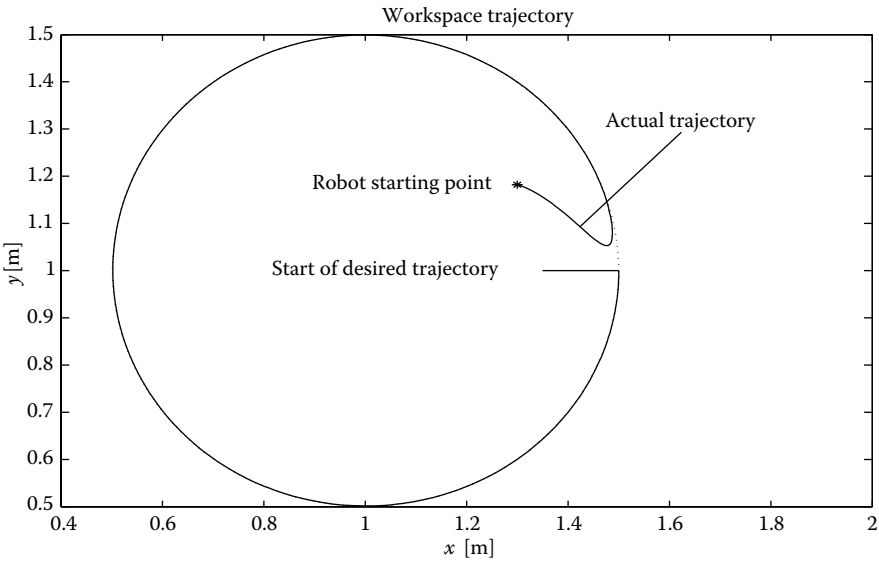

FIGURE 12.8
Robot trajectory and desired trajectory in world coordinates for continuous feedback/feedforward control design with additional discontinuity term.

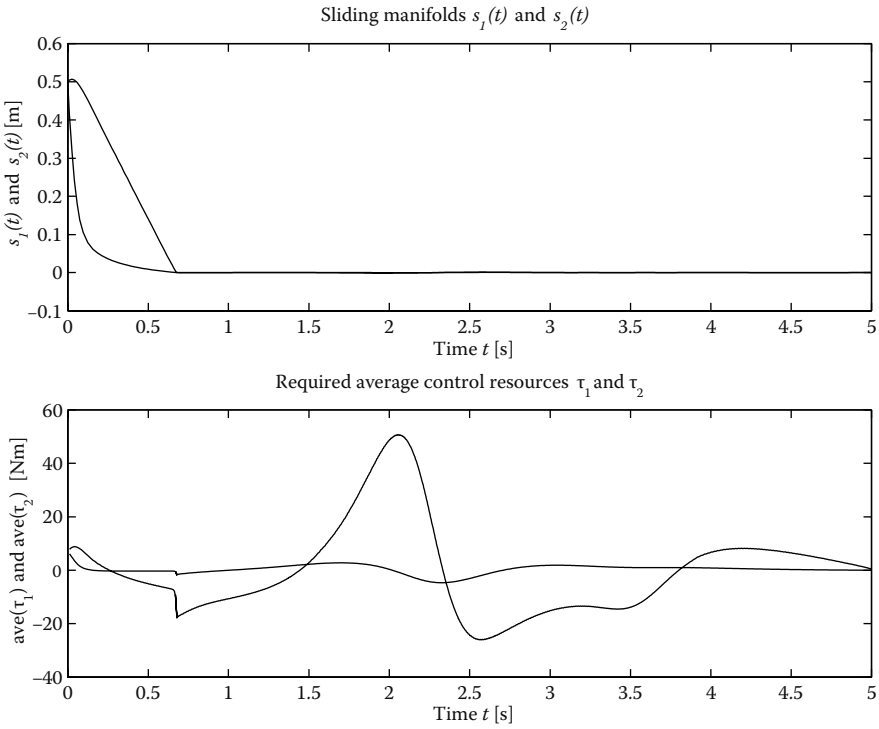

FIGURE 12.9
Top graph: Distances to sliding manifolds $s_1(t)$ and $s_2(t)$. Bottom graph: Required average control resources τ_1 and τ_2 for each joint.

12.2.4. Discussion of Sliding Mode Control Design Choices

The previous three sections presented three control design alternatives for mechanical systems based on two choices: componentwise control or vector control, and purely discontinuous control versus continuous feedback/feedforward control with an additional discontinuity term. The fourth possible control alternative, continuous feedback/feedforward control with an additional, componentwise discontinuity term, is omitted here for brevity. The interested reader is encouraged to study a simple design example such as the planar two-link manipulator given in Section 12.1.2 for this combination of choices.

All four control design alternatives have one feature in common: they enforce sliding mode in some manifold and thus achieve exact tracking of the desired trajectory. Besides the differences in control design methodologies,

the four alternatives differ in the required control resources for each joint. Whereas componentwise control seeks to determine the necessary resources for each joint but requires tedious derivations, vector control is more concise at the expense of higher control resource requirements.

In all four control alternatives, the control discontinuities are used to suppress model uncertainties and, in practice, external disturbances. Continuous feedback/feedforward control reduces the amount of model uncertainty to be suppressed by the control discontinuity. However, for the choice "componentwise control versus vector control," the uncertainty to be suppressed remains the same, and the difference in amplitude of the discontinuity terms arises from the stability proof rather than from system requirements.

For ideal sliding mode control systems with direct implementation of the discontinuity term, pure discontinuous control as in Theorem 12.2 is equivalent to the continuous feedback/feedforward control with additional discontinuous control in Theorem 12.3. After reaching the sliding manifold, the motions of the two systems are identical. This can be established using the equivalent control method discussed in Section 2.3. In fact, the equivalent control torques during sliding mode are similar for all four alternatives: all control algorithms on average apply the torques necessary to follow the desired trajectory. Higher amplitudes of the discontinuity only shorten the transient phase for approaching the sliding manifold.

For sliding mode designs in systems with unmodeled dynamics, the feedback/feedforward structure enables to use "smaller" sliding gains τ_0, thought to cause chattering. Even with the chattering problem being solved reliably, a similar qualitative argumentation holds for most chattering prevention schemes, in particular for the saturation function method in Section 8.2 and the observer-based approach in Section 8.3. These methods avoid excitation of unmodeled dynamics by replacing the infinite gain of an ideal sliding mode controller with a finite gain in the linear zone of the saturation function or in the observer loop, respectively.

For a given system, the nature of the unmodeled dynamics, especially their frequency range, determines a practical upper bound for the finite gain. This bound on the saturation feedback gain implies bounded ability to suppress uncertainties and disturbances. In general, the smaller the possible gains, the larger the errors, i.e., the larger the boundary zone introduced by the saturation function or the larger the observer errors. Consequently, feedback of estimated dynamics and feedforward of the desired trajectory improves the performance of the control system by reducing the amount of uncertainty to be suppressed by the sliding mode term. Tables 12.6 and 12.7 contrast the general choices for sliding mode control design for mechanical systems.

TABLE 12.6
Comparison Between Componentwise Sliding Mode Control Design and Vector Control/Unit Control (Equations are Given for Purely Discontinuous Control Approach)

	Component-Wise Control	**Vector Control/Unit Control**
Preferred systems	Truly discontinuous inputs in each component that can take only two values, $-\tau_{0_i}$ or $-\tau_{0_i}$	Ability to vary inputs in a continuous range, i.e., $-\tau_{0_i} \leq \tau_i \leq \tau_{0_i}$
Sliding manifold(s)	n $(2n–1)$-dimensional manifolds $s_i = 0$, $i = 1,...,n$ in $2n$-dimensional state space $\Re^{2n \times 1}$	One n-dimensional manifold $s = 0$, $s \in \Re^{n \times 1}$, for the entire system vector $q \in \Re^{n \times 1}$
Control	Discontinuous in each component, $\tau_i = \tau_{0_i} \operatorname{sign}(s_i)$, $i = 1,..., n$	Unit vector with one discontinuity in the origin, $\tau = \tau_0 \dfrac{s}{\|s\|_2}$, $\tau \in \Re^{n \times 1}$
Stability analysis	Separate Lyapunov functions $V_i = \frac{1}{2} s_i^2$ for each component $i = 1,...,n$; often tedious analysis of coupling terms for higher-dimensional or complex systems based on bounds for each system parameter	One Lyapunov function $V = \frac{1}{2} s^T s$ for the entire system; often conservative analysis based on vector/matrix bounds for the whole system model

12.3. Gradient Tracking Control

Trajectory tracking control as discussed in the previous section implies an a priori designed trajectory q_d to be given for the entire robot operation. Expansion of the range of robot tasks and an increase in robot autonomy led to the need to generate trajectories online, for example, to avoid collisions with obstacles in the workspace while approaching a given goal point. A popular tool for online trajectory generation with inherently included collision avoidance is the artificial potential field method, pioneered by Khatib [1986] and refined by many others. The key idea is to design an artificial potential field in the control computer with a global minimum at the goal point of the robot operation and local maxima at workspace obstacles. Robot motion then is guided by the gradient of the computer-generated artificial potential field instead of by a predetermined trajectory.

TABLE 12.7
Comparison Between Pure Discontinuous Control and Continuous Feedback/Feedforward Control with Additional Discontinuity Term (Equations are Given for the Unit Control Approach, Using Generic Robot Manipulator Dynamics as an Example)

	Pure Discontinuous Control	**Feedback/Feedforward with Additional Discontinuity Term**
Preferred systems	Ideal systems with truly discontinuous inputs and no unmodeled dynamics	Mechanical systems with continuous inputs and additional unmodeled dynamics
Sliding manifold	$s = Cq_e + \dot{q}_e = 0,\ q_e = q_d - q$	$s = Cq_e + \dot{q}_e = 0,\ q_e = q_d - q,\ \dot{\lambda} = s + \dot{q}_e$
Control	$\tau = \tau_0 \dfrac{s}{\|s\|_2}$	$\tau = \hat{M}(q)\ \dot{\lambda} + \hat{V}_m(q, \dot{q})\ \dot{\lambda} + \hat{F}(\dot{q}) + \hat{G}(q) + \tau = \tau_0 \dfrac{s}{\|s\|_2}$
Stability analysis	Straightforward Lyapunov analysis with $V = \frac{1}{2}\ s^T s$; discontinuous term suppresses all systems dynamics	Includes system dynamics in a Lyapunov function like $V = \frac{1}{2}\ s^T M(q) s$; discontinuous term suppresses uncertainty in estimated feedback/feedforward terms

This method is an early form of virtual reality, because the potential field is generated "artificially" in the control computer without any physical relevance. However, many approaches exploit physical phenomena to design the artificial potential field, e.g., electrostatics, fluid dynamics, or stress mechanics. To avoid additional local minima away from the goal point, which may trap the robot and cause premature termination of the operation, harmonic Laplace fields are often used, using either the von-Neumann or the Dirichlet boundary conditions.

A number of methods to guide the robot motion using artificial potential fields have been presented in the literature, including the following.

- ***Coupling of the Gradient of the Artificial Potential Field into the Robot Dynamics Via the Control Input:*** The control force/torques are applied colinear to the gradient, implementing a dynamic relationship between the robot and its environment in the general framework of impedance control of mechanical systems [Hogan 1985]. Effectively, the robot acceleration vector $\ddot{q}(t)$ is oriented along the gradient, which obviously does not lead to tracking of the gradient because of the robot's inertial dynamics. However, safe collision avoidance can be guaranteed for potentials tending to infinity

at obstacle boundaries, even for bounded actuator resources [Rimon and Koditschek 1992].

- ***Accounting for the Robot Dynamics and Actuator Limitations in the Design of the Potential Field:*** Krogh's "generalized potential field" [Krogh 1984] considers the *time* needed to reach the goal point or an obstacle rather than the respective distance. The control design is based on a double integrator to model a mobile robot and takes into account limited actuator resources, but no additional dynamics.
- ***Using Feedback for Tracking the Gradient of the Potential Field:*** Khatib [1986] proposed a feedback linearization strategy, similar to the continuous feedback/feedforward control discussed in Section 12.2.3, assuming exact parametric knowledge of all robot dynamics. This rather restrictive requirement was relieved by Koditschek's [1991] "natural motion" approach for dissipative mechanical systems and a related, energy-based approach by Takegaki and Arimoto [1981]. However, in Koditschek's approach, the gradient of the artificial potential field implicitly takes into account the robot mass/inertia matrix for generating natural motion and hence cannot be designed independently of the robot dynamics.
- ***Using Sliding Mode Control for Exact Tracking of a Gradient:*** Utkin, Drakunov, Hashimoto, and Harashima [1991] proposed to orient the robot's velocity vector along the gradient of the artificial potential field to achieve exact tracking. The method was later generalized by Guldner and Utkin [1995] and will be the basis for control design in this section. The primary advantage is the exact gradient tracking property, which allows an artificial gradient field to be designed independently.

Let the gradient of an artificial potential field $U(q)$ be denoted by

$$E(q) = -\nabla U(q),\ E(q) \in \Re^n. \tag{12.3.1}$$

For each point $q \in \Re^n$ in the robot workspace, the gradient Equation 12.3.1 defines a vector of a desired direction of motion. Integration along the gradient vector via

$$\frac{\partial q(t)}{\partial t} = E(q(t)) \tag{12.3.2}$$

with integration variable t (not necessarily denoting time) yields a continuous trajectory from the starting point $q_0 \in \Re^n$, called a "gradient line." A set of gradient lines is depicted in Figure 12.10 for a planar example of the harmonic dipole potential method [Guldner, Utkin, and Hashimoto 1997] with a

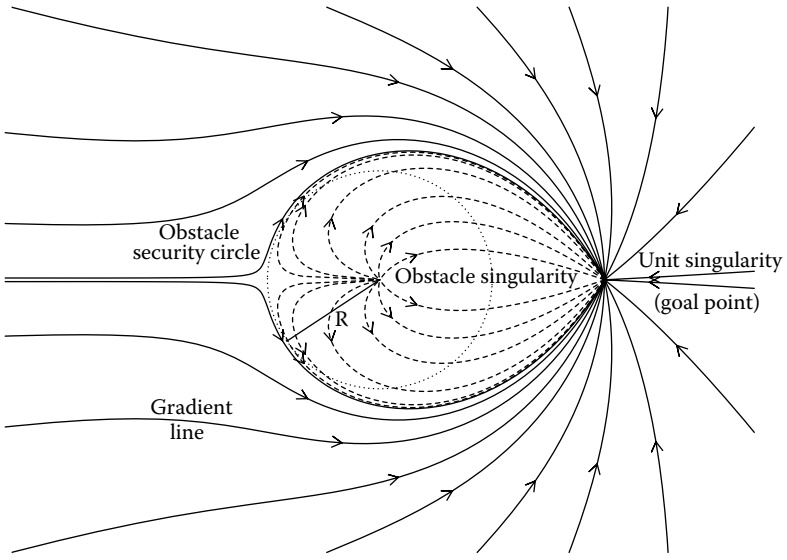

FIGURE 12.10
Gradient lines of harmonic dipole potential field (solid and dashed lines) with negative unit singularity in goal point and positive obstacle singularity in center of obstacle security circle (dotted line). For details, see Sections 12.4.2 and 12.4.3.

single obstacle being protected by a circular security zone. All gradient lines starting in the robot free space continuously approach the goal point without entering the security zone. However, a number of gradient lines come close to the security circle, which can only result in safe operation if exact tracking is guaranteed via robust sliding mode control.

12.3.1. Control Objectives

The goal of control is to track the gradient of an arbitrary artificial potential field (Equation 12.3.1) with a robot manipulator described by Equation 12.1.3 or a mobile robot such as Equations 12.1.22 through 12.1.24. Exact tracking can be achieved by orienting the velocity vector $\dot{q}(t)$ of Equation 12.1.3 colinear to the gradient vector E in Equation 12.3.1. To avoid singularities at equilibrium points $E = 0_{n\times 1}$, we define the desired motion vector $\dot{q}_d(q) \in \Re^n$ as

$$\dot{q}_d(q) = v_d(q,t)\frac{\mathbf{E}(q)}{\max(\|\mathbf{E}(q)\|, \varepsilon)} \tag{12.3.3}$$

for some small scalar $\varepsilon > 0$. The task of the controller to be designed in Section 12.3.2 is to guarantee $\dot{q}(t) = \dot{q}_d(q(t))$ at all times. In the previous section, a sliding mode controller was designed for tracking a given trajectory. According

to the characteristics of this desired trajectory, required control resources were calculated from the stability analysis. Here, we choose a different path: the control resource limitations are assumed to be given. Then, the motion profile (velocity and acceleration) is derived online together with the desired trajectory, i.e., the gradient of the artificial potential field. The desired scalar tracking velocity $v_d(q, t)$ thus should be adjusted to enable exact tracking with limited control resources. Given a maximal possible acceleration a_0, to be determined in the sequel from the available control resources, suitable starting and goal-approach phases are given by

$$v_d(q,t) = \min\left(a_0 t, v_0(q,t), \sqrt{2a_0\zeta}\right), \tag{12.3.4}$$

where $v_0(q, t)$ is the desired "traveling" velocity, to be determined below, and ζ is the remaining distance to the goal point q_G, i.e.,

$$\zeta = \|q(t) - q_G\|. \tag{12.3.5}$$

Starting from initial time $t = 0$, the desired velocity $v_d(q, t)$ is increased using maximal acceleration a_0 until the traveling velocity $v_0(q, t)$ is reached.

Required acceleration a_0 during "normal traveling" with $v_d(q, t) = v_0(q, t)$ is found from Equation 12.3.3 as

$$\begin{aligned}\ddot{q}_d(q,t) &= \dot{v}_0(q,t)\frac{\mathbf{E}(q)}{\|\mathbf{E}(q)\|} + v_0(q,t)\frac{\partial}{\partial q}\left(\frac{\mathbf{E}(q)}{\|\mathbf{E}(q)\|}\right)\dot{q}(t) \\ &= \left(\dot{v}_0(q,t) + v_0^2(q,t)\frac{\partial}{\partial q}\left(\frac{\mathbf{E}(q)}{\|\mathbf{E}(q)\|}\right)\right)\frac{\mathbf{E}(q)}{\|\mathbf{E}(q)\|},\end{aligned} \tag{12.3.6}$$

assuming $\|\mathbf{E}(q)\| > \varepsilon$ and exact tracking with $\dot{q} = v_0(q,t)\dfrac{\mathrm{E}(q)}{\|\mathrm{E}(q)\|}$. An upper bound for desired acceleration $\ddot{q}_d(q,t)$ in Equation 12.3.6 is given by

$$\|\ddot{q}_d(q,t)\| = |\dot{v}_0(q,t)| + v_0^2(q,t)\left\|\frac{\partial}{\partial q}\left(\frac{\mathrm{E}(q)}{\|\mathrm{E}(q)\|}\right)\right\| \le a_0. \tag{12.3.7}$$

For given maximum acceleration a_0, determined by the available control resources in the subsequent section, a suitable traveling velocity $v_0(q, t)$ is dynamically determined by the solution of

$$\dot{v}_0(q,t) = a_0 - v_0^2(q,t)\left\|\frac{\partial}{\partial q}\left(\frac{\mathrm{E}(q)}{\|\mathrm{E}(q)\|}\right)\right\|. \tag{12.3.8}$$

Because E(q) is time independent, its derivatives with respect to vector q are known in closed form, and dynamic Equation 12.3.8 can be solved online. A similar procedure can be followed for $\|\mathbf{E}(q)\| \le \varepsilon$. Note that $v_0(t)$ is automatically decreased in areas of high curvature of the gradient E(q), i.e., for large values of $\left\| \frac{\partial}{\partial q}\left(\frac{\mathrm{E}(q)}{\|\mathrm{E}(q)\|} \right) \right\|$. In practice, the traveling velocity $v_0(t)$ will be bounded by $0 \le v_0(t) \le v_{0_{\max}}$, where $v_{0_{\max}}$ is selected according to physical limitations of the robot and the maximum change of curvature of the gradient encountered for the specific robot task.

When approaching the goal point q_G, the trajectory can be approximated by the remaining scalar distance $\zeta(t)$ under the assumption of an approach with $q(t) = q_d\left(q(t)\right)$ as proposed previously [Utkin, Drakunov, Hashimoto, and Harashima 1991],

$$\dot{\zeta}(t) = -\sqrt{2a_0\zeta(t)}. \tag{12.3.9}$$

Using Equations 12.3.4 and 12.3.9, a bound on scalar $\dot{v}_d(q,t)$ can be established for the goal approaching phase as

$$|\, v_d(q,t)\,| \;=\; \left| \frac{d}{d_t}\sqrt{2a_0\zeta(t)} \right| \;=\; \left| \frac{1}{2}\frac{2a_0\zeta(t)}{\sqrt{2a_0\zeta(t)}} \right| \le a_0. \tag{12.3.10}$$

The choice of $v_d(q,t) = \sqrt{2\alpha_0\zeta(t)}$ during the goal approaching phase also prevents overshoot at the goal point and results in a finite reaching time. By virtue of definition Equation 12.3.5, $\zeta \ge 0$ holds at all times. Integrating Equation 12.3.9 from $\zeta_s = \zeta(q(t_s)) = \zeta(_s)$ at some starting position q_s at time t_s

$$\int_{\zeta_s}^{\zeta} \frac{\mathrm{d}\zeta}{\sqrt{2\mathrm{a}_0\zeta}} = -\int_{t_s}^{t} \mathrm{d}t \tag{12.3.11}$$

directly yields

$$\sqrt{2a_0\zeta} - \sqrt{2a_0\zeta_s} = -a_0(t - t_s). \tag{12.3.12}$$

Because the right-hand side of Equation 12.3.12 is negative for $t > t_f$, $\zeta < \zeta_s$ is decreasing monotonously to reach $\zeta_f = 0$ after finite time

$$t_f = t_s + \sqrt{\frac{2\zeta_s}{a_0}}. \tag{12.3.13}$$

12.3.2. Gradient Tracking Control Design for Holonomic Robots

Among the four choices of control design outlined for trajectory tracking control in Tables 12.6 and 12.7, purely discontinuous vector control features the most concise mathematical formulation and hence will be used here to reveal the basic principle structure of gradient tracking control design. The design presented below can be easily reformulated in terms of one of the three other methods described in Section 12.2.

The control objective defined in the preceding section is to guarantee $\dot{q}(t) = \dot{q}_d(t)$ given in Equations 12.3.3 and 12.3.4 at all times. The main difference between trajectory tracking control and gradient tracking control is that in the latter, velocity vector $\dot{q} \in \Re^n$ rather than position vector $q \in \Re^n$, is used as the control variable. Desired velocity $\dot{q}_d(t)$ implicitly depends on position vector $q \in \Re^n$ via the gradient vector $\mathrm{E}(q) \in \Re^n$ and hence can be regarded as an outer control loop encompassing the robot and its environment. For gradient tracking control on velocity scale, an n-dimensional sliding variable $s \in \Re^n$ is chosen as

$$s(\dot{q}, \dot{q}_d) = \dot{q}_d(t) - \dot{q}(t). \tag{12.3.14}$$

The following theorem exemplifies the gradient tracking control design for purely discontinuous vector control.

Theorem 12.4

The system in Equation 12.3.15 with bounds as given in Equation 12.1.5 and 12.1.9 through 12.1.11 under control in Equation 12.3.17 will reach the sliding manifolds of Equation 12.3.16 in finite time.

System
$$\ddot{q} = M^{-1}\left(\tau - N(q, \dot{q})\right) \tag{12.3.15}$$
$$s = \dot{q}_d(t) - \dot{q}(t) = 0$$

Manifold
$$\dot{q}_d(q) = v_d(q,t)\frac{\mathrm{E}(q)}{\max(\|\mathrm{E}(q)\|, \varepsilon)} \tag{12.3.16}$$

Control
$$\tau = \tau_0 \frac{s}{\|s\|_2} \tag{12.3.17}$$

□

Proof 12.4

Consider the Lyapunov function candidate

$$V = \frac{1}{2} s^T s \tag{12.3.18}$$

with the following time derivative along Equations 12.3.15 and 12.3.16 and control Equation 12.2.23:

$$\begin{aligned} \dot{V} &= s^T \left(\ddot{q}_d(t) - \ddot{q}(t) \right) \\ &\leq -\frac{\tau_0}{M^+} \|s\| + \|s\| \left(a_0 + \frac{N^+}{M^-} \right), \end{aligned} \tag{12.3.19}$$

where the bounds in Equations 12.3.7 and 12.3.10 for $\ddot{q}_d(t)$ helped to reduce the expression in Equation 12.3.19. For given control resources τ_0, maximum acceleration for determining traveling velocity $v_0(t)$ in Equation 12.3.8 and the goal approach in Equation 12.3.9 is calculated as

$$a_0 < \frac{\tau_0 - N^+}{M^-} \tag{12.3.20}$$

such that $\dot{V} \leq -\xi \|s\|_2$ is ensured. Stability and finite approach of the sliding manifold $s(\dot{q}, \dot{q}_d) = 0$ in Equation 12.3.14 then follows along standard arguments for Equation 12.3.19, guaranteeing exact tracking of the gradient lines. □

12.3.3. Gradient Tracking Control Design for Nonholonomic Robots

Gradient tracking control for nonholonomic robots also follows the control objectives given in Section 12.3.1. As an example, we will discuss control design for a mobile robot modeled as a nonholonomic wheel set as shown in Figure 12.2 in Section 12.1.3. The kinematic and dynamic models were given in Equations 12.1.22 and 12.1.23 through 12.1.24, respectively. The task of orienting the motion vector of the wheel set along the gradient vector according to Equations 12.3.3 through 12.3.5 can be split into two subtasks because of the definition of the input vector u in Equation 12.1.22: orientation control using ω and velocity control using v_C. Hence, componentwise control design is most suitable. The sliding manifold for velocity control along the gradient lines, the translational motion, is defined as

$$s_t = v_d(q, t) - v_C = 0 \tag{12.3.21}$$

for the case $\|E(q)\| > \varepsilon$.

The orientation error for control of the rotational motion component is given by

$$\phi_e = \phi_d - \phi,\ \phi_d = \text{Atan}\frac{E_y(q)}{E_x(q)}, \tag{12.3.22}$$

where the arcus-tangent function Atan(.) returns angles in all four quadrants, i.e., $\phi_d \in [-\pi, \pi]$, and $E = [E_x(q)\ E_y(q)]^T$ is the gradient vector in the plane. The control of the robot's orientation again is a position control, and thus the associated sliding manifold is defined as for second-order systems:

$$s_r = C\phi_e + \dot{\phi}_e = 0 \tag{12.3.23}$$

The control designs are summarized in the following theorem.

Theorem 12.5

Systems described by Equations 12.3.24 and 12.3.25 with bounds $0 < M^- \le M \le M^+$, $0 < J^- \le J \le J^+$, $0 < |N_t(v_C, \omega)| \le N_t^+$, and $0 < |N_t(v_C, \omega)| \le N_r^+$ under controls given in Equations 12.3.28 and 12.3.29 will reach the sliding manifolds in Equation 12.3.26 and 12.3.27 in finite time.

System $$M\dot{v}_C + N_t(v_C, \omega) = \tau_t \tag{12.3.24}$$

$$J\dot{\omega} + N_r(v_C, \omega) = \tau_r \tag{12.3.25}$$

Manifolds $$s_t = v_d(q,t) - v_C = 0 \tag{12.3.26}$$

$$s_r = C\phi_e + \dot{\phi}_e = 0,\ \phi_e = \phi_d - \phi,\ \phi_d = \text{Atan}\frac{E_y}{E_x} \tag{12.3.27}$$

Control $$\tau_t = \tau_{t0}\ \text{sign}\ s_t \tag{12.3.28}$$

$$\tau_r = \tau_r 0\ \text{sign}\ s_r \tag{12.3.29}$$

□

Proof 12.5

Consider the Lyapunov function candidates

$$V_t = \frac{1}{2} s_t^T s_t \tag{12.3.30}$$

and

$$V_r = \frac{1}{2} s_r^T s_r. \tag{12.3.31}$$

Differentiation of Equation 12.3.30 along Equations 12.3.24 and 12.3.26 under control Equation 12.3.28 with the above bounds yields

$$\begin{aligned} \dot{V}_t &= s\left(\dot{v}_d(t) + \frac{N_t(v_C, \omega)}{M} - \frac{\tau_t}{M} \right) \\ &\le |s|\left(a_0 + \frac{N_t^+}{M^-} \right) - |s| \frac{\tau_{t0}}{M^+}, \end{aligned} \tag{12.3.32}$$

where Equation 12.3.7 was used to reduce the expression. Stability follows from Equation 12.3.32 for sufficiently large τ_{t0} for a suitable choice of a_0. Similarly, stability of the orientation controller with manifold Equation 12.3.27 is shown by differentiation of Equation 12.3.31 with system Equation 12.3.25 under control Equation 12.3.29:

$$\begin{aligned} \dot{V}_t &= s\left(C\dot{\phi}_e + \ddot{\phi}_d + \frac{N_r(v_C, \omega)}{J} - \frac{\tau_r}{J} \right) \\ &\le |s|\left(C\left|\dot{\phi}_e\right| + \left|\ddot{\phi}_d\right| + \frac{N_r^+}{J^-} \right) - |s| \frac{\tau_{r0}}{J^+}. \end{aligned} \tag{12.3.33}$$

Boundedness of $\dot{\phi}_e = \dot{\phi}_d - \omega$ and $\ddot{\phi}_d$ is established for $\|E\| > \varepsilon$ attributable to

$$\dot{\phi}_d = \frac{d}{dt}\left(\operatorname{Atan} \frac{E_y(q)}{E_x(q)} \right) = H_0 v_C \tag{12.3.34}$$

$$\ddot{\phi}_d = \frac{d^2}{dt^2}\left(\operatorname{Atan} \frac{E_y(q)}{E_x(q)} \right) = H_1 + \frac{H_0}{M} \tau_t, \tag{12.3.35}$$

where

$$H_0 = \frac{\mathrm{E}_x^2\left[D_x + D_y\right]\left(\mathrm{E}_y\right) - \mathrm{E}_x\mathrm{E}_y\left[D_x + D_y\right]\left(\mathrm{E}_x\right)}{\|\mathrm{E}\|^2}$$

$$H_1 = v_C^2 H_2 - \frac{N_t(v_C, \omega)}{M} H_0$$

$$\begin{aligned} H_2 = \mathrm{E}_x \Bigg\{ & \frac{1}{\|\mathrm{E}\|^4}\Big[2\mathrm{E}_x\left[D_x\right]\left(\mathrm{E}_x\right)\left[D_x + D_y\right]\left(\mathrm{E}_y\right) + \mathrm{E}_x^2\left[D_{xx} + D_{xy}\right]\left(\mathrm{E}_y\right) \\ & -\mathrm{E}_y\left[D_x^2 + D_x D_y\right]\left(\mathrm{E}_x\right) - \mathrm{E}_x\left[D_x\right]\left(\mathrm{E}_y\right)\left[D_x + D_y\right]\left(\mathrm{E}_x\right) - \mathrm{E}_x\mathrm{E}_y\left[D_{xx} + D_{xy}\right]\left(\mathrm{E}_x\right)\Big] \\ & -\frac{3}{\|\mathrm{E}\|^6}\Big[\mathrm{E}_x^2\left[D_x + D_y\right]\left(\mathrm{E}_y\right) - \mathrm{E}_x\mathrm{E}_y\left[D_x + D_y\right]\left(\mathrm{E}_x\right)\Big]\Big[\mathrm{E}_x\left[D_x\right]\left(\mathrm{E}_x\right) + \mathrm{E}_y\left[D_x\right]\left(\mathrm{E}_y\right)\Big]\Bigg\} \\ & + \mathrm{E}_y \Bigg\{ \frac{1}{\|\mathrm{E}\|^4}\Big[2\mathrm{E}_x\left[D_y\right]\left(\mathrm{E}_x\right)\left[D_x + D_y\right]\left(\mathrm{E}_y\right) + \mathrm{E}_x^2\left[D_{xy} + D_{yy}\right]\left(\mathrm{E}_y\right) \\ & -\mathrm{E}_y\left[D_x D_y + D_y^2\right]\left(\mathrm{E}_x\right) - \mathrm{E}_x\left[D_y\right]\left(\mathrm{E}_y\right)\left[D_x + D_y\right]\left(\mathrm{E}_x\right) - \mathrm{E}_x\mathrm{E}_y\left[D_{xy} + D_{yy}\right]\left(\mathrm{E}_x\right)\Big] \\ & -\frac{3}{\|\mathrm{E}\|^6}\Big[\mathrm{E}_x^2\left[D_x + D_y\right]\left(\mathrm{E}_y\right) - \mathrm{E}_x\mathrm{E}_y\left[D_x + D_y\right]\left(\mathrm{E}_x\right)\Big]\Big[\mathrm{E}_x\left[D_y\right]\left(\mathrm{E}_x\right) + \mathrm{E}_y\left[D_y\right]\left(\mathrm{E}_y\right)\Big]\Bigg\}. \end{aligned} \tag{12.3.36}$$

$[D_x](\cdot)$ denotes the first-order differential operator $\frac{\partial}{\partial x}(.)$, and $\left[D_{xy}\right](.)$ denotes the second-order differential operator $\frac{\partial^2}{\partial x \partial y}(.)$. Sliding mode was assumed to exist in the translational manifold Equation 12.3.26, enabling the use of the equivalent control methodology for τ_t. Solving $\dot{s}_t = 0$ for the translational control input yields

$$\left(\tau_t\right)_{eq} = N_t(v_C, \omega) + M\dot{v}_d(t), \tag{12.3.37}$$

which was substituted for τ_t into Equation 12.3.34 to reduce the expression. Bounds for the above terms can be determined to calculate the necessary control input τ_{r0} for Equation 12.3.29. □

Two application examples for gradient tracking control can be found in Sections 12.4.2. and 12.4.3.

12.4. Application Examples

In this section, we present a variety of examples for the use of sliding mode philosophy in advanced robotic systems. First, torque control of a flexible robot joint using integral sliding mode is presented. Next, we discuss the application of the gradient tracking control derived in Section 12.3 for collision avoidance of mobile robots and robot manipulators in known workspaces. Finally, we introduce fully automatic steering control for passenger cars as an extension of robotic systems.

12.4.1. Torque Control for Flexible Robot Joints

In many practical applications, robot joints and robot links exhibit flexibilities that need to be considered when designing advanced control algorithms. As an example [for details, see Shi and Lu 1993], consider a single revolute link with a flexible joint, i.e., a robot consisting of just one link actuated by one drive with flexibilities in the joint. Extension of this model to multilink robot arms follows along the lines of Equation 12.1.3 but is omitted here for ease of notation. Neglecting actuator dynamics, a flexible joint model can be derived as

$$\begin{aligned} J_l\ddot{q}_l + d_l &= \tau_l \\ J_m\ddot{q}_m + d_m &= \tau_m - \frac{\tau_l}{n}, \end{aligned} \tag{12.4.1}$$

where $J_l^- \le J_l \le J_l^+$ is the link inertia, q_l is the joint angular position, n is the gear ratio, $J_m^- \le J_m \le J_m^+$ is the motor/gear inertia, q_m is the angular motor position, $k^- \le k \le k^+$ denotes the joint stiffness, $\tau_l = k(q_m / n - q_l)$ is the link torque at the joint, and the motor torque τ_m represents the control input. Also, unknown but bounded torque disturbances $|d_l| \le d_l^+$ and $|d_m| \le d_m^+$ were added to Equation 12.4.1 at the link and motor sides, respectively.

Because we already introduced trajectory tracking control (position scale) in Section 12.2 and gradient tracking control (velocity scale) in Section 12.3, we will study torque tracking control (acceleration scale) in this example, i.e., the problem of controlling link torque τ_l to track a known desired profile $[\tau_d, \dot{\tau}_d, \ddot{\tau}_d]$.

A linear input/output representation of Equation 12.4.1 is given by

$$\ddot{\tau}_l + a\tau_l + d = b\tau_m, \tag{12.4.2}$$

with $a = \dfrac{k}{n^2 J_m} + \dfrac{k}{nJ_l}$, $b = \dfrac{k}{nJ_m}$, and $d = \dfrac{k}{nJ_m} d_m + \dfrac{k}{J_l} d_l$.

This example will exploit both the continuous feedback/feedforward technique discussed in Section 12.2.3 and integral sliding mode control presented

in Chapter 7 to reject the unknown disturbance $|d| < D^+$ and uncertainties in a and b.

The control law for τ_m hence is composed of a continuous controller of feedback-linearizing type with pole placement, τ_f, and a disturbance rejecting controller τ_r, i.e.,

$$\tau_m = \tau_f + \tau_r. \tag{12.4.3}$$

Define a continuous feedback/feedforward controller as

$$\tau_f = \hat{b}^{-1}(\hat{a}\tau_l + \ddot{\tau}_d + c_1\dot{\tau}_e + c_0\tau_e), \tag{12.4.4}$$

where $\hat{a}$ and $\hat{b}$ are estimates of a and b, respectively. The first term $\frac{\hat{a}}{\hat{b}}\tau_l$ in Equation 12.4.4 seeks to compensate the term $a\tau_l$ in the left-hand side of Equation 12.4.2 as a type of feedback linearization. The second term in Equation 12.4.4, $\frac{1}{\hat{b}}\ddot{\tau}_d$, is a feedforward term of acceleration of the desired torque. Finally, the last two terms in Equation 12.4.4, $\frac{1}{\hat{b}}(c_1\dot{\tau}_e + c_0\tau_e)$, are a linear pole placement controller. Substitution of Equation 12.4.4 into Equation 12.4.2 yields error dynamics for $\tau_e = \tau_d - \tau_l$, $\dot{\tau}_e = \dot{\tau}_d - \dot{\tau}_l$, and $\ddot{\tau}_e = \ddot{\tau}_d - \ddot{\tau}_l$ as

$$\ddot{\tau}_e + c_1\dot{\tau}_e + c_0\tau_e = \tau_p - \hat{b}\tau_r. \tag{12.4.5}$$

The left hand side of Equation 12.4.5 is linear with poles determined by c_1, $c_0 > 0$, but is subject to the perturbation torque:

$$\tau_p = \left(\frac{\hat{b}}{b} - 1\right)\ddot{\tau}_l + \left(\frac{\hat{b}}{b}a - \hat{a}\right)\tau_l + \frac{\hat{b}}{b}d + (b - \hat{b})\tau_r, \tag{12.4.6}$$

which may be simplified by substitution of $\ddot{\tau}_l = b\tau_m - a\tau_l - d$ from Equation 12.4.2 to

$$\tau_p = (a - \hat{a})\tau_l + (\hat{b} - b)\tau_m + d. \tag{12.4.7}$$

To improve the control performance, the disturbance in Equation 12.4.7 should be compensated by the additional disturbance rejection term τ_r in Equation 12.4.3. Because τ_p is not measurable, an estimate is obtained through a sliding mode observer of the form

$$\dot{\hat{z}} = \ddot{\tau}_d + c_1\dot{\tau}_e + c_0\tau_e + \hat{b}\tau_r - u, \tag{12.4.8}$$

with $\hat{z}$ being an estimate for $\dot{\tau}_l$. Basically, observer Equation 12.4.8 is a copy of Equation 12.4.5 with $\ddot{\tau}_l$ replaced by $\dot{\hat{z}}$ and observer feedback u as a replacement for τ_p being defined as

$$u = \left(\bar{a}^+ |\tau_l| + \bar{b}^+ |\tau_m| + \bar{d}^+\right) \text{sign}\, \bar{z}. \tag{12.4.9}$$

Here, $\bar{a}^+$, $\bar{b}^+$, and $\bar{d}^+$ denote upper bounds for $\bar{a} = a - \hat{a}$, $\bar{b} = b - \hat{b}$, and $\bar{d} = d - \hat{d}$, respectively, obtained from the bounds on the system parameters given above, e.g.,

$$\bar{a}^+ = \max\left\{\left(\frac{k^+}{n^2 J_m^-} + \frac{k^+}{nJ_l^-}\right) - \hat{a}, \hat{a} - \left(\frac{k^-}{n^2 J_m^+} + \frac{k^-}{nJ_l^+}\right)\right\}. \tag{12.4.10}$$

The control discontinuity is introduced along the observation error $\bar{z} = \hat{z} - \dot{\tau}_l$. Stability of the observer system is ensured via Lyapunov function candidate $V = \frac{1}{2}\bar{z}^2$; differentiation along the system trajectories Equation 12.4.8 with control Equation 12.4.9 yields

$$\begin{aligned} \dot{V} &= \left(\dddot{\tau}_d + c_1 \ddot{\tau}_e + c_0 \dot{\tau}_e + \hat{b}\dot{\tau}_r - (\bar{a}^+ |\tau_l| + \bar{b}^+ |\tau_m| + \bar{d}^+) \text{sign}\, \bar{z} - \dddot{\tau}_l\right)\bar{z} \\ &= \tau_p \bar{z} - \tau_p^+ |\bar{z}|, \end{aligned} \tag{12.4.11}$$

where $\tau_p^+ = \bar{a}^+ |\tau_l| + \bar{b}^+ |\tau_m| + \bar{d}^+ > \max(\tau_p)$ ensures the existence of sliding mode via

$$\dot{V} < -\xi |\bar{z}| \tag{12.4.12}$$

for some small scalar $\xi > 0$.

Because Equation 12.4.8 is generated in the control computer, the initial conditions can be set as

$$\hat{z}|_{t=0} = \dot{\tau}_l|_{t=0}, \tag{12.4.13}$$

such that $\bar{z} = 0$ for all $t \geq 0$, i.e., sliding mode is initiated immediately at $t = 0$. To estimate the disturbance torque τ_p to be compensated via disturbance rejection term τ_r in Equation 12.4.3, the equivalent control method (see Section 2.3) is exploited. In sliding mode, $\dot{\bar{z}} = \dot{\hat{z}} - \ddot{\tau}_l = 0$, i.e.,

$$\dot{\bar{z}} = \ddot{\tau}_e + c_1 \dot{\tau}_e + c_0 \tau_e + \hat{b}\tau_r - u_{eq} = 0. \tag{12.4.14}$$

The control signal u in Equation 12.4.9 contains two components: a high-frequency switching component resulting from the discontinuous sign

term and a low-frequency component, i.e., the equivalent control u_{eq}. As discussed in detail in Section 2.4, the equivalent control is equal to the average of u, obtained for example by a low-pass filter. With this in mind, $u_{eq} = u_{ave} = \tau_p$ follows from comparing Equations 12.4.5 and 12.4.14. Consequently, defining

$$\tau_r = \hat{b}u_{eq} = \hat{b}u_{ave} \tag{12.4.15}$$

and substituting in leads to closed-loop error dynamics

$$\ddot{\tau}_e + c_1\dot{\tau}_e + c_0\tau_e = 0. \tag{12.4.16}$$

Hence, the sliding mode estimator τ_r successfully rejects both the uncertainties in parameters a and b and additive disturbance d in Equation 12.4.2 and allows controller Equation 12.4.4 to perform exact pole placement. It should be noted that the low-pass filter time constant or bandwidth has to be carefully chosen to be faster than the perturbation dynamics in τ_p but at the same time to be slow enough not to excite unmodeled dynamics in the system such as the neglected actuator dynamics producing torque τ_m. In particular, the extreme case of direct implementation without averaging as $\tau_r = u$ with u defined in Equation 12.4.9 led to chattering in experiments reported by Lu and Chen [1993].

A simulation study of the controller discussed above is based on the mechanical model in Figure 12.11. The system parameters were chosen as

$$J_m = 1.0e-5,\ n = 600,\ J_l = nJ_m/4,\ k = 10, \tag{12.4.17}$$

and subject to a square-wave (sqw(·)) disturbance of the form

$$d_m = 1 + \text{sqw}(50t) \tag{12.4.18}$$

on the motor side. Assuming perfect parameter knowledge, i.e., known J_m, J_l, n and k, the poles were both assigned to –200 by defining $c_1 = 400$ and $c_0 = 40{,}000$. The disturbance was upper bounded by $d^+ = \dfrac{k}{nJ_m}\max d_m = 5000$. The averaging of u in Equation 12.4.9 is performed by a simple first-order low pass as shown

$$\frac{\dot{u}_{\text{ave}}}{2000} + u_{\text{ave}} = u, \tag{12.4.19}$$

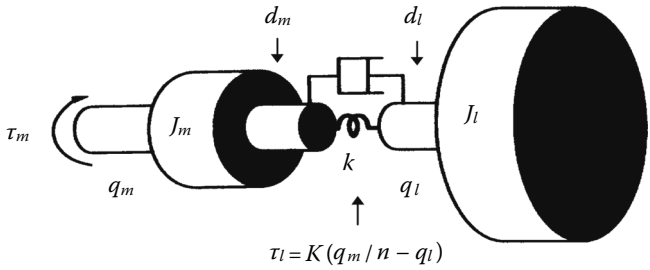

FIGURE 12.11
Definition of variable of flexible joint control problem.

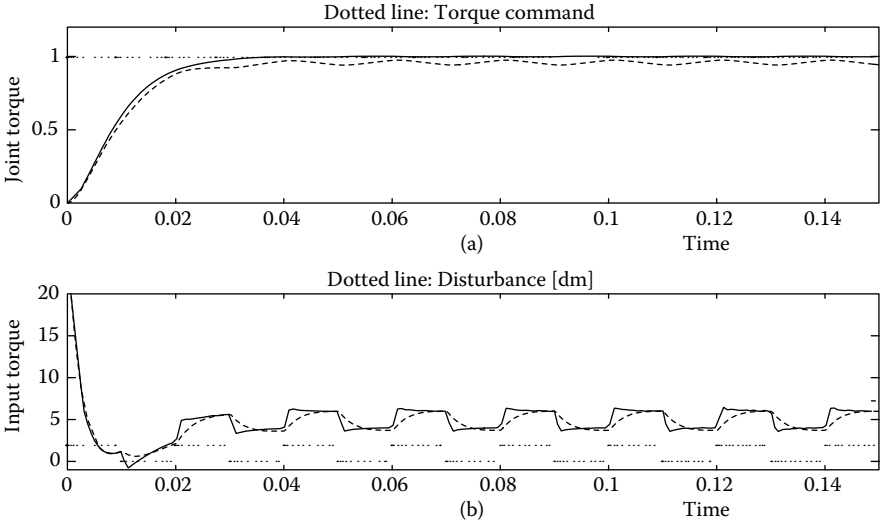

FIG. 12.12
Dynamical Responses. (a) Output torque: (Solid line) with disturbance compensation, (dashed line) without disturbance compensation, (dotted line) the torque command. (b) Input torque: (solid line) with disturbance compensation, (dashed line) without disturbance compensation, (dotted line) the disturbance torque on the motor side.

i.e., 10 times faster than the torque control loop. Simulation results in Figure 12.12 are shown for step responses of $\tau_d = 1$ and demonstrate the significant performance improvement achieved by the disturbance compensation.

12.4.2. Collision Avoidance for Mobile Robots in a Known Planar Workspace

In this section, we present an example of planar collision avoidance for mobile robots using the artificial potential field approach already mentioned in Section 12.3. A mobile robot is to be guided to a specified goal point through

a planar workspace with known obstacles. Workspaces of higher dimension are discussed in the subsequent section. The obstacle avoidance scheme with the gradient tracking algorithm of Section 12.3 form the core of a hierarchical path control scheme [see Guldner, Utkin, and Bauer 1995].

The known obstacles in the robot workspace are protected by security zones, which form the basis for the design of an artificial potential field. A set of diffeomorph transformations given by Rimon and Koditschek [1992] provides a mapping between arbitrary star-shaped security zones and security circles. Hence, the design of an artificial potential field may concentrate on obstacle security circles in transformed space. After calculating the artificial potential field and its gradient in the transformed space, an inverse mapping provides the back transformation into the real robot workspace. The obstacle security zones are assumed to be nonoverlapping, with the goal point lying outside of all security zones.

The main advantage of the transformation procedure is the possibility to concentrate the design of the artificial potential field on security circles for the obstacles rather than on security zones of complex shape. Thanks to the exact tracking capability of the gradient tracking controller discussed in Section 12.3, the artificial potential field can be designed independently of the robot dynamics, enabling a wide variety of applications.

An example of a possible choice of an artificial potential field is the harmonic dipole potential in $\Re^2$ suggested by Guldner and Utkin [1995]. For a singularity at the origin, the harmonic potential is given by

$$U = \rho \ln \frac{1}{r}, \tag{12.4.20}$$

where ρ denotes the "strength" of the singularity, and r is the distance from the origin. For convenience, a polar coordinate system (r, φ) is adopted here. The planar gradient is given by

$$\mathrm{E} = -\nabla U = \begin{cases} -\dfrac{\partial U(r,\varphi)}{\partial r} = \dfrac{\rho}{r} \\ -\dfrac{1}{r}\dfrac{\partial U(r,\varphi)}{\partial \varphi} = 0 \end{cases} \tag{12.4.21}$$

Consider a dipole for a single obstacle security circle formed by a unit singularity in the goal point and a singularity of opposite polarity in the center of the obstacle security circle with strength:

$$0 < \rho = \frac{R}{R+D} < 1, \tag{12.4.22}$$

where R is the radius of the security circle, and D is the distance between the two singularities. The total artificial potential field in a polar coordinate

system with the origin in the goal point with the negative unit singularity is given by

$$U(r,\varphi) = \frac{\rho}{2}\ln\left(\frac{1}{r^2 - 2Dr\cos\varphi + D^2}\right) - \ln\frac{1}{r}, \tag{12.4.23}$$

with the associated gradient derived from Equation 12.4.21 as

$$\mathrm{E} = \begin{cases} -\dfrac{\partial U(r,\varphi)}{\partial r} & = \rho\left(\dfrac{r - D\cos\varphi}{r^2 - 2Dr\cos\varphi + D^2}\right) - \dfrac{1}{r} \\ -\dfrac{1}{r}\dfrac{\partial U(r,\varphi)}{\partial \varphi} & = \rho\dfrac{2Dr\sin\varphi}{r^2 - 2Dr\cos\varphi + D^2} \end{cases} \tag{12.4.24}$$

The resulting gradient lines were already displayed in Figure 12.10. Note two properties of harmonic dipoles:

- All gradient lines beginning outside the security circle remain outside.
- Following any gradient line outside the security circle monotonously decreases the distance to the goal point.

These properties are preserved under the above mentioned diffeomorph transformations. For details and proofs, refer to the work of Guldner and Utkin [1995].

To reduce the computational complexity, many artificial potential field approaches only consider one obstacle at each time instance and switch between the potentials associated with different obstacles, e.g., when the robot gets closer to a different obstacle than the one currently considered. The switching between potentials of different obstacles led to oscillations in several approaches, for example, reported by Koren and Borenstein [1991], which are caused by the robot inertia and time delays in the closed-loop system "obstacle-potential field-robot." An example is shown in Figure 12.13 for a circular robot, oscillating around the equidistant line between two obstacle potentials. The obstacles themselves are omitted in this and the following figures.

An intuitive solution to the oscillation problem is the introduction of a low-pass filter for the artificial potential field or its gradient, leading to a time-dependent field. However, a low-pass filter is reactive, i.e., is only starting to consider the new potential when the robot crosses the equidistant line between the obstacles. Thus, the oscillations can only be damped but not be eliminated completely, as illustrated in Figure 12.14.

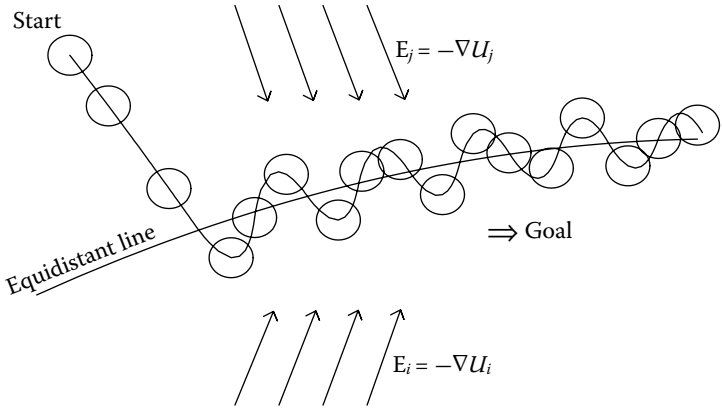

FIGURE 12.13
Robot, depicted by circles, oscillating along equidistant line between two obstacles *i* and *j*. Obstacles and goal point (located to the right of the graph) are not shown. Planar gradients $E_i = -\nabla U_i$ and $E_j = -\nabla U_i$ are symbolized by arrows.

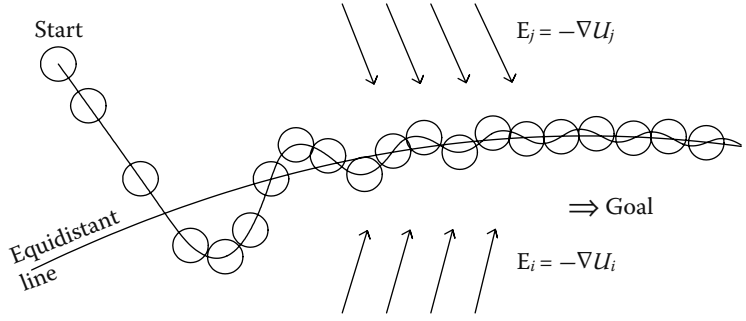

FIGURE 12.14
Robot, depicted by circles, oscillating along equidistant line between two obstacles *i* and *j*. The oscillations are damped by a low-pass filter applied to the gradient. Obstacles and goal point (located to the right of the graph) are not shown. Planar gradients $E_i = -\nabla U_i$ and $E_j = -\nabla U_i$ are symbolized by arrows.

A closer look at the oscillation phenomenon reveals that it is similar to chattering in variable structure systems as discussed in Chapter 8. In fact, the oscillations are caused by unmodeled dynamics in the closed-loop system "obstacle-potential field-robot": the switching between the potential fields of different obstacles neglects the robot dynamics. In the vicinity of the equidistant line, the gradient lines may be oriented toward this line (see Figure 12.15a), and the trajectory field resembles the state space of a dynamic system with sliding mode. Formally, sliding mode may appear along the line in our case with the robot trajectory coinciding with the equidistant line. In the course of this motion, the robot avoids collisions with obstacles and approaches the goal. Unfortunately, this ideal motion cannot

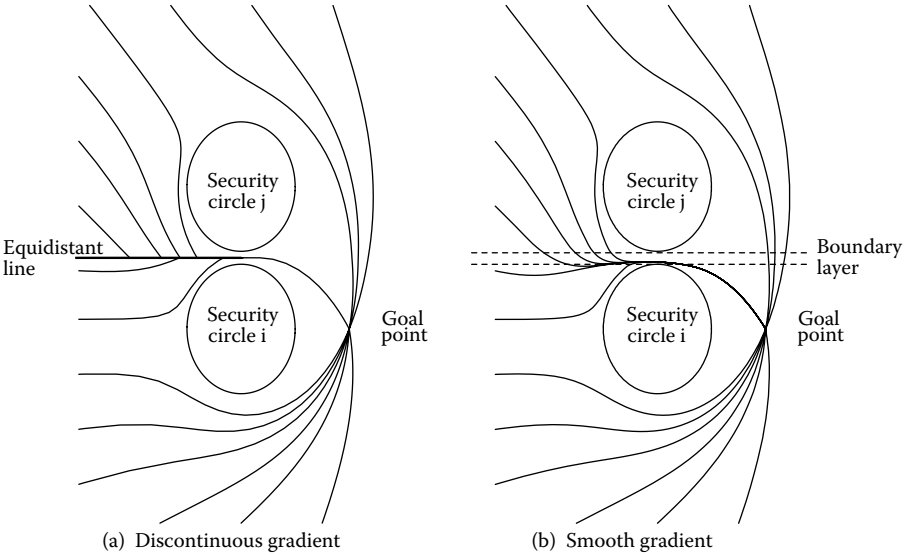

FIGURE 12.15
Effect of boundary layer for smoothing gradient lines along equidistant lines between obstacle security zones. (a) Discontinuous switching between gradients of obstacle security circles *i* and *j*. (b) Smooth switching in boundary layer along equidistant line.

be implemented. Indeed, ideal sliding mode would ask for the speed vector tracking the smooth gradient lines of each of two adjoining potential fields to undergo discontinuities on the equidistant line. This implies that the control force or torque should develop infinite acceleration, which is impossible because of physical constraints. As a result, the robot trajectory oscillates in the vicinity of the equidistant line (see Figure 12.10) as in a system with chattering. Because of this similarity, a reliable solution is the application of one of the methods discussed in Chapter 8 to prevent chattering.

As an example, the boundary layer approach as described in Section 8.2 is used in the sequel. Instead of switching the potential field abruptly when the robot crosses the equidistant line between two obstacles, both potentials $U_1(q)$ and $U_2(q)$ are considered simultaneously in a boundary layer of width δ along the equidistant line. The resulting total potential field is

$$U_{res}(q) = \begin{cases} U_1(q) & \text{for} \quad d < -\dfrac{\delta}{2} \\ \left(\dfrac{1}{2} + \dfrac{d}{\delta}\right) U_1(q) + \left(\dfrac{1}{2} - \dfrac{d}{\delta}\right) U_2(q) & \text{for} \quad |d| < \dfrac{\delta}{2} \\ U_2(q) & \text{for} \quad d > \dfrac{\delta}{2} \end{cases} \tag{12.4.25}$$

where d denotes the distance of the robot from the equidistant line. Figure 12.14 compares the gradient lines for an example with two obstacle security ellipses. Note the difference of the gradient lines in the vicinity of the equidistant line denoted by $s_{equi} = 0$. The discontinuities along $s_{equi} = 0$ visible in the left graph of Figure 12.15 are eliminated by the introduction of the boundary layer δ along $s_{equi} = 0$ in the right graph. Figure 12.16 illustrates that this application of sliding mode theory to the collision avoidance problem successfully eliminates the oscillations [see Guldner, Utkin, and Bauer 1994].

12.4.3. Collision Avoidance in Higher-Dimensional Known Workspaces

This section extends the results of the previous section for mobile robots in planar workspaces to robots in higher-dimensional workspaces $\Re^n$, $n > 2$, in particular to robot manipulators. Details of the development in this section may be found in previous work [Guldner, Utkin, and Hashimoto 1997]. The concept of transforming star-shaped obstacle security zones into security circles is carried over to $\Re^n$ by using security spheres (for $n = 3$) and security hyperspheres (for $n > 3$). However, it is beyond this book to generalize the diffeomorph transformations given previously [Rimon and Koditschek 1992] to $n > 2$. As in the planar case, obstacles are assumed to be known, with nonoverlapping security zones and a reachable goal point outside any security zone.

Instead of redesigning the harmonic potential in Equation 12.4.20 for $\Re^n$, $n > 2$, the aforementioned properties of the planar gradient (Equation 12.4.21) are further exploited. Because in any space $\Re^n$, $n > 2$, three points uniquely define a subspace of dimension $n = 2$, a projection onto such a planar subspace allows to continue to use the planar harmonic dipole potential

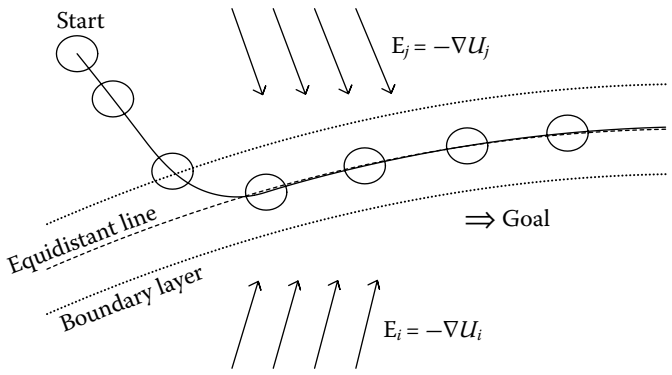

FIGURE 12.16
Robot, depicted by circles, follows the equidistant without oscillations when gradients are smoothed inside boundary layer. Obstacles and goal point (located to the right of the graph) are not shown. Planar gradients $E_i = -\nabla U_i$ and $E_j = -\nabla U_j$ are symbolized by arrows.

of Section 12.4.2. Let the goal point $q_G \in \Re^n$, the center of the obstacle (hyper)sphere $q_S \in \Re^n$, and the robot position $q_R \in \Re^n$ define a plane

$$\wp(q): q = q_R + \alpha_1 \frac{q_r - q_G}{\|q_R - q_G\|} + \alpha_2 \frac{q_R - q_S}{\|q_R - q_s\|} \forall \alpha_1, \alpha_2 \in \Re. \tag{12.4.26}$$

The plane $\wp(q)$ serves as a design platform for the planar harmonic dipole potential Equation 12.4.23 with gradient Equation 12.4.24. In $\Re^n$, the gradient is directly found as

$$\mathrm{E} = \frac{q_R - q_G}{\|q_R - q_G\|^2} - \rho \frac{q_R - q_S}{\|q_R - q_S\|^2} \in \Re^n, \tag{12.4.27}$$

where ρ is found according to Equation 12.4.22 with $D = \|q_R - q_S\|$ and q_G, q_R, $q_S \in \Re_n$ are taken as vectors. A three-dimensional example is shown in Figure 12.17 with a sphere-like robot traveling in plane $\wp(q)$ toward the goal point in the origin of the coordinate system.

For multiple obstacles in the workspace, a switching procedure similar to the planar case is designed. Each obstacle is assigned to its own security zone, each of which is separately transformed into a security (hyper)sphere. In $\Re^n$, $n > 2$, the switching between different artificial potentials for various obstacles takes place in subspaces of varying dimension. Consider the example of a three-dimensional situation. Between two obstacles, one two-dimensional equidistant subspace can be found, i.e., an equidistant

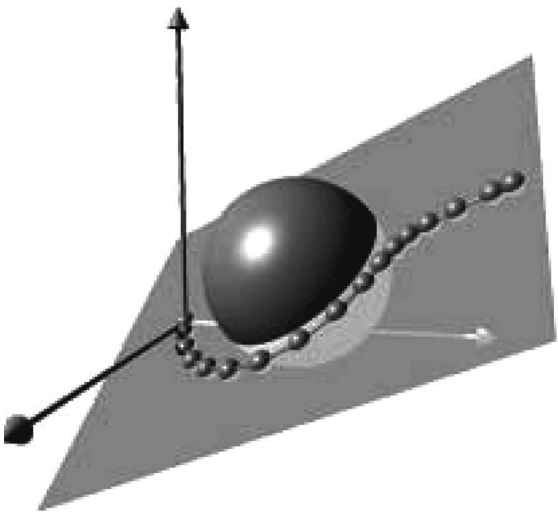

FIGURE 12.17
Sphere-like robot in three-dimensional space avoiding spherical obstacle. Gradient is defined in two-dimensional subspace, plane $\wp(q)$, similar to Figure 12.10.

plane. Introducing a third obstacle in this exemplary three-dimensional workspace leads to a total of three equidistant planes for each combination of two of the three obstacle security zones. Additionally, the points of equidistant to all three obstacles form a one-dimensional subspace, an equidistant line.

Generalizing the above to arbitrary $\Re^n$, $n > 2$, yields subspaces $\Re^{n-1}$ equidistant to exactly two of the obstacle security zones, subspaces $\Re^{n-2}$ equidistant to exactly three of the obstacle security zones, and subspaces $\Re^{n-k+1}$ equidistant to exactly $1 < k < n$ of the obstacle security zones, with k being the number of obstacles among all workspace obstacles that may have to be considered simultaneously. The equidistant subspaces for various obstacle security zones are equivalent to Voronoi planes [see Latombe 1991], often used for robot path planning. In contrast to Voronoi-based approaches, the equidistant subspaces do not have to be computed explicitly for the following switching strategy.

To avoid oscillations along the switching planes, i.e., the equidistant subspaces, boundary zones of appropriate dimension are introduced as an extension of Equation 12.4.25. Consider an $\Re^n$ situation with k obstacles in which the gradients in all adjacent regions converge to equidistant subspace $\Theta_k^n \in \Re^{n-k+1}$. An appropriate boundary zone of width $\delta > 0$ is defined as

$$B_k^n = \left\{ q \in \Re^n \,\middle|\, \left\| q \perp \Theta_k^n \right\| \le \delta \right\}, \tag{12.4.28}$$

where $\left\| q \perp \Theta_k^n \right\|$ denotes the length of the normal projection of vector $q \in \Re^n$ onto subspace $\Theta_k^n \in \Re^{n-k+1}$. Within boundary zone B_k^n, all k obstacles contribute to the resulting potential field $U_{res} \in \Re^n$. Let U_G be the unit potential of the goal point, which is common to all single obstacle potentials. The individual weights η_i of each obstacle potential U_{S_i} with appropriate strength ρ_i according to Equation 12.4.22 are given by

$$\eta_i = \frac{1}{k}\left(1 - \frac{1}{\delta}\left((k-1)d_i - \sum_{\substack{l=1 \\ l \neq i}}^{n} d_l\right)\right), \quad i = 1, 2, \ldots, k, \tag{12.4.29}$$

with d_i being the distance of the robot position $q_R \in \Re^n$ from the equidistant subspace with respect to obstacle i. The resulting potential field is found as

$$U_{res} = U_G + \sum_{i=1}^{k} \eta_i U_{S_i}. \tag{12.4.30}$$

The necessary condition $\sum_{i=1}^{k} \eta_i = 1$ ensures that the properties of the harmonic dipole potentials are preserved, and smooth transition between different

potentials enables tracking without oscillations. It should be noted that the robot motion is only confined to the boundary zone B_k^n as long as all k gradients in adjacent regions are directed toward the equidistant subspace Θ_k^n. When the robot has passed an obstacle, the boundary zone may be left, and new equidistant subspaces with a different number of obstacles considered simultaneously are found until the goal point is reached. There is no intention to create sliding motion along the equidistant subspaces, although the motion trajectories may temporarily resemble boundary layer sliding mode trajectories.

This section concludes with two examples in $\Re^3$. First, consider the spherical robot of Figure 12.17 in a workspace with three obstacles and the goal point in the origin of the coordinate system as shown in Figure 12.18. The varying number of obstacles is illustrated in Figure 12.19 according to the distance of the robot to the respective obstacles. Initially, only obstacle 1 in the bottom left corner is considered. After about 0.6 sec, the robot enters the boundary plane between the two lower obstacles 1 and 2. Finally, when the top obstacle 3 has the same distance from the robot as obstacle 2, all three obstacles are considered in the calculation of the resulting potential and the robot travels in the boundary zone of the equidistant line toward the goal point.

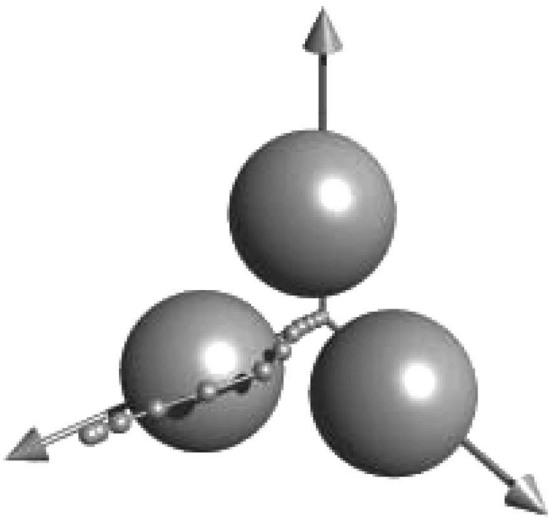

FIGURE 12.18
Sphere-like robot in three-dimensional space avoiding three spherical obstacles. The goal point is located in origin of the coordinate system. See also Figure 12.19. Obstacle 1 is in the bottom left corner. Obstacle 2 is in the bottom right corner. Obstacle 3 is in the top center.

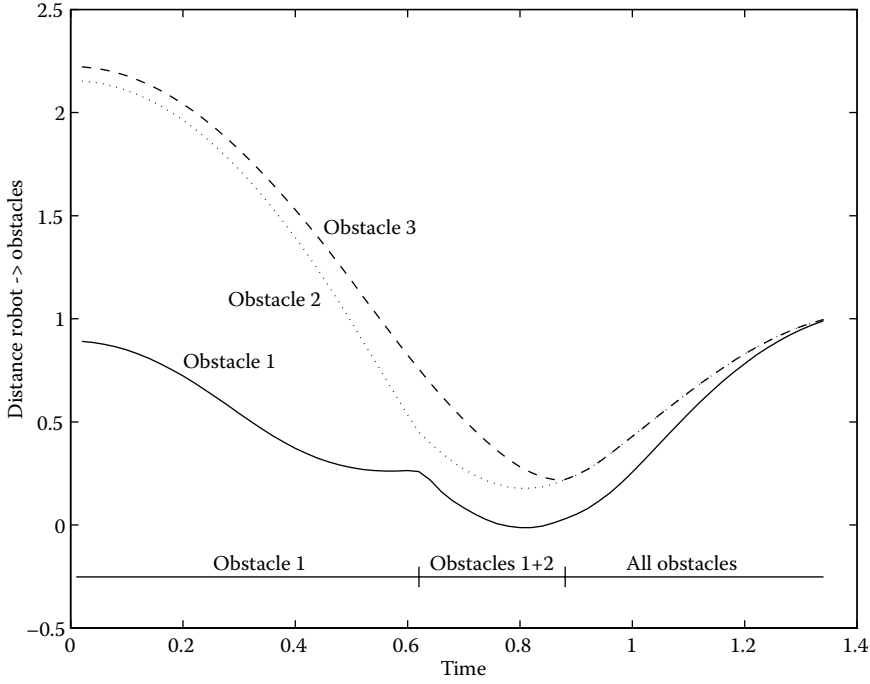

FIGURE 12.19
Distances between robot and obstacle security spheres of the simulation in Figure 12.18. Solid line, Distance to obstacle 1 (bottom left). Dotted line, Distance to obstacle 2 (bottom right). Dashed line, Distance to obstacle 3 (top center). Also noted in the bottom part of the graph are the respective obstacles considered for definition of potentials according to Equations 12.4.29 and 12.4.30.

Because the previous examples in Figures 12.17 through 12.19 are rather abstract, being based on "free-flying" spherical robots, the next example shows the application of the above algorithm to a more realistic problem of a revolute robot manipulator with three links and three joints, avoiding cylindrical obstacles in its three-dimensional workspace. The potential fields were calculated in the robot's $\Re^3$ configuration space rather than in the $\Re^3$ workspace. Figure 12.20 shows the robot motion in the actual workspace in nine snapshots. Details of this application have been described by Guldner, Utkin, and Hashimoto [1997].

12.4.4. Automatic Steering Control for Passenger Cars

Automatic steering control is the last example for the application of advanced robotics. Automation of vehicles, for example, for automated highways systems, has been discussed for several decades and is studied in various

FIGURE 12.20
Robot arm with three links avoiding two cylindrical obstacles. Obstacle security zones, depicted by ellipsoids, were transformed into configuration space, and the potential fields were calculated in this three-dimensional configuration space.

programs worldwide in the framework of intelligent transport systems [see Stevens 1996; Tsugawa, Aoki, Hosaka, and Seki 1996].

Two control subtasks arise for automated driving of "robot cars": steering control to keep the vehicle in the lane (controlling the lateral motion) and throttle/brake control to maintain speed and proper spacing between vehicles (controlling the longitudinal motion). Both subtasks have been solved using sliding mode control. The focus in this section will be on automatic steering control. Longitudinal control was studied previously [see Hedrick, Tomizuka, and Varaiya 1994; Pham, Hedrick, and Tomizuka 1994]. The automatic steering system of an automated vehicle consists of a reference system to determine the lateral vehicle position with respect to the lane center, sensors to detect the vehicle motion (typically yaw rate and lateral acceleration), and a steering actuator to steer the front wheels. The variety of reference systems used ranges from look-ahead systems, such as machine vision or radar, to look-down systems, such as electric wires or magnets embedded in the road surface. "Look-ahead/look-down" describes the point of measurement of lateral vehicle displacement from the reference to be ahead of the vehicle or directly down from the front bumper [for a more detailed treatment, see Patwardhan, Tan, and

Guldner 1997]. The control design below, however, is valid for any reference system.

Control design is usually based on the so-called single-track model, which concentrates on the main vehicle mass by combining the two wheels at each axle into a single wheel. The road-tire interaction forces are responsible for generating planar lateral and yaw vehicle motions, with the front wheel steering angle δ_f being the input variable. A linearized second-order model for constant speed v is given by

$$\begin{bmatrix} \dot{\beta} \\ \ddot{\psi} \end{bmatrix} = \mu \begin{bmatrix} -\dfrac{c_f + c_r}{Mv} & -1 - \dfrac{c_f l_f - c_r l_r}{Mv^2} \\ -\dfrac{c_f l_f - c_r l_r}{J} & -\dfrac{c_f l_f^2 + c_r l_r^2}{Jv} \end{bmatrix} \begin{bmatrix} \beta \\ \dot{\psi} \end{bmatrix} + \mu \begin{bmatrix} \dfrac{c_f}{Mv} \\ \dfrac{c_f l_f}{J} \end{bmatrix} \delta_f, \qquad (12.4.31)$$

with states side slip angle β and yaw rate $\dot{\Psi}$. For a detailed derivation of Equation 12.4.31, see the work of Peng [1992] or Ackermann et al. [1993]. Parameters are vehicle mass M and yaw inertia J, distances l_f and l_r of front and rear axles from the center of gravity (CG), front and rear tire cornering stiffness c_f and c_r, and road adhesion factor μ. All parameters are uncertain within known bounds, e.g., $0 < \mu^- \le \mu \le \mu^+ \le 1$.

When following a reference path with curvature ρ_{ref} as depicted in Figure 12.21, lateral vehicle displacement y_{e_S}, measured at some sensor position d_S ahead of CG, and angular error Ψ_e can be described by linearized dynamic model

$$\begin{aligned} \dot{y}_{e_S} &= v(\beta + \Psi_e) + d_S \dot{\Psi}, \\ \dot{\Psi}_e &= \dot{\Psi} - v\rho_{\text{ref}}. \end{aligned} \qquad (12.4.32)$$

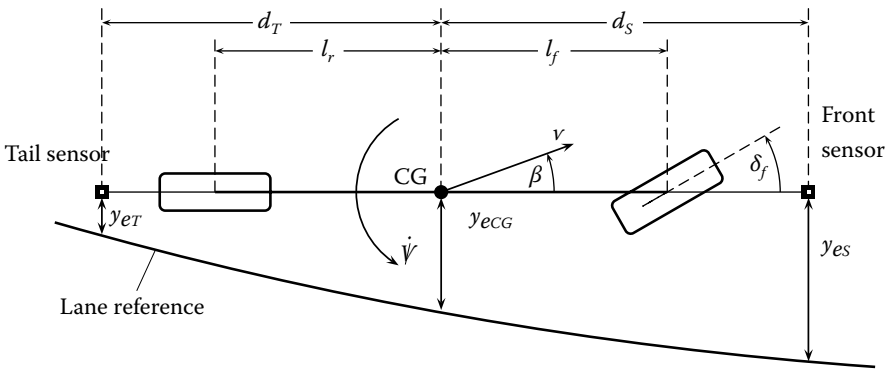

FIGURE 12.21
Single track model of a vehicle following a lane reference. Sensors at the front and tail bumpers measure lateral displacements y_{e_S} and y_{e_T}, respectively. Also shown are vehicle states, side slip angle β and yaw rate $\dot{\Psi}$, input steering angle δ_f, and various distances from CG.

Given Equations 12.4.31 and 12.4.32, various control design options are possible. As an example, we present a cascaded control design under the assumption that vehicle yaw rate $\dot{\Psi}$ is measurable by a gyroscope. The control design follows the regular form methodology (see Section 3.2) and considers the subsystem in Equation 12.4.31 as the input to the subsystem in Equation 12.4.32. Hence, the first design step assumes yaw rate $\dot{\Psi}$ to be a direct input to Equation 12.4.32 and derives a desired yaw rate $\dot{\Psi}_d$. The second step then ensures that the actual, measured vehicle yaw rate $\dot{\psi}$ follows $\dot{\Psi}_d$ exactly via appropriate control design for steering angle δ_f in Equation 12.4.31, the true system input. A suitable continuous feedback/feedforward "yaw rate" controller to stabilize the first equation in Equation 12.4.32 would be

$$\dot{\psi}_d = -\frac{1}{l_S}\left(v(\beta + \psi_e) + Cy_{e_S}\right), \tag{12.4.33}$$

with linear feedback gain $C > 0$. However, neither side slip angle β nor yaw angle error Ψ_e can be measured and hence have to be estimated by an observer [for details, see Guldner, Utkin, and Ackermann 1994]. Introducing auxiliary variable $z = \beta + \Psi_e$, an observer is designed as

$$\begin{bmatrix} \dot{\hat{y}}_{e_S} \\ \dot{\hat{z}} \end{bmatrix} = \begin{bmatrix} 0 & v \\ 0 & 0 \end{bmatrix} \begin{bmatrix} \hat{y}_{e_S} \\ \hat{z} \end{bmatrix} + \begin{bmatrix} l_S \\ 0 \end{bmatrix} \dot{\psi} + \begin{bmatrix} c_1 \\ c_2 \end{bmatrix} \overline{y}_{e_S}, \tag{12.4.34}$$

with feedback of the observation error $\overline{y}_{e_S} = y_{e_S} - \hat{y}_{e_S}$ via gains $c_1 > 0$ and $c_2 > 0$, chosen faster than the vehicle dynamics in Equation 12.4.31. With the help of the observed auxiliary variable $\hat{z} = \hat{\beta} + \hat{\Psi}_e$, a desired yaw rate is defined as

$$\dot{\psi}_d = -\frac{1}{l_S}\left(v(\hat{\beta} + \hat{\psi}_e) + Cy_{e_S}\right). \tag{12.4.35}$$

The second step of control design uses the steering angle δ_f as the input to Equation 12.4.31 to drive yaw rate error $\dot{\Psi}_e = \dot{\Psi}_d - \dot{\Psi}$ to zero, for example, by purely discontinuous sliding mode control

$$\delta_f = \delta_0 \operatorname{sign} \dot{\Psi}_e. \tag{12.4.36}$$

The stability analysis follows the previously discussed Lyapunov approach and is omitted here for brevity. Alternatively to Equation 12.4.36, a combination of continuous feedback/feedforward and a discontinuity term could be used, i.e.,

$$\delta_f = \delta_1 \operatorname{sign} \dot{\psi}_e + \frac{1}{\hat{c}_f \hat{l}_f}\left(\left(\left(\hat{c}_f \hat{l}_f - \hat{c}_r \hat{l}_r\right)\hat{\beta} + \frac{1}{v}\left(\hat{c}_f \hat{l}_f^2 + \hat{c}_r \hat{l}_r^2\right)\dot{\psi}\right) + \frac{\hat{J}}{\hat{\mu}}\ddot{\psi}_d\right), \tag{12.4.37}$$

where estimates of vehicle parameters are denoted with circumflexes (ˆ), the estimate of side slip angle, $\hat{\beta}$, stems from an observer similar to Equation 12.4.34, and the derivative of the desired yaw rate, $\ddot{\Psi}_d$, can be derived from Equation 12.4.35 by virtue of known observer dynamics. Because of the continuous feedback/feedforward terms in Equation 12.4.37, the gain of the discontinuity term can be reduced compared to Equation 12.4.36, i.e., $\delta_1 < \delta_0$.

The above control design neglects the dynamics of the steering actuator, which will lead to chattering in practical implementations. In addition to the chattering prevention methods discussed in Chapter 8, the introduction of an integrator in the control loop proved to be a promising approach. Originally, the integrator was a physical model of the actuator dynamics [see Ackermann et al. 1993], with the steering rate u being the system input as

$$\dot{\delta}_f = u, \tag{12.4.38}$$

rather than the steering angle δ_f itself. The additional integrator only requires to alter the outer control loop (Equations 12.4.36 and 12.4.37). Define a second-order sliding variable

$$s = C_3 \dot{\Psi}_e + \ddot{\Psi}_e, \tag{12.4.39}$$

leading to a control law

$$\delta_f = \delta_0 \operatorname{sign} s \tag{12.4.40}$$

instead of Equation 12.4.36. The alternative feedback/feedforward controller term in Equation 12.4.37 has to be adjusted accordingly. If the real steering actuator is not an integrator as in Equation 12.4.38 but features more complex dynamics, for example, of an electrohydraulic actuator, two design alternatives are left to the control engineer. Either, a sliding mode controller is designed according to Equations 12.4.36 and 12.4.37 with appropriate measures to prevent chattering as discussed in Chapter 8 or an integrator like that in Equation 12.4.38 is introduced as part of the controller, i.e., realized in the controller software. The latter case follows the ideas of integral sliding mode by implementing sliding motion in an integral manifold rather than directly in the control input variable δ_f. Hence, the switching action of the sliding mode discontinuity is first filtered by integrator Equation 12.4.38 and thus does not directly reach the input δ_f, which inherently prevents chattering. A different integrator location in the control loop has been proposed by Pham, Hedrick, and Tomizuka [1994], before rather than after the switching discontinuity. For a comparison study of different integrator locations in the controller loop, the interested reader is referred to the work of Hingwe and Tomizuka [1995]. Experimental results from this work are displayed in Figure 12.22.

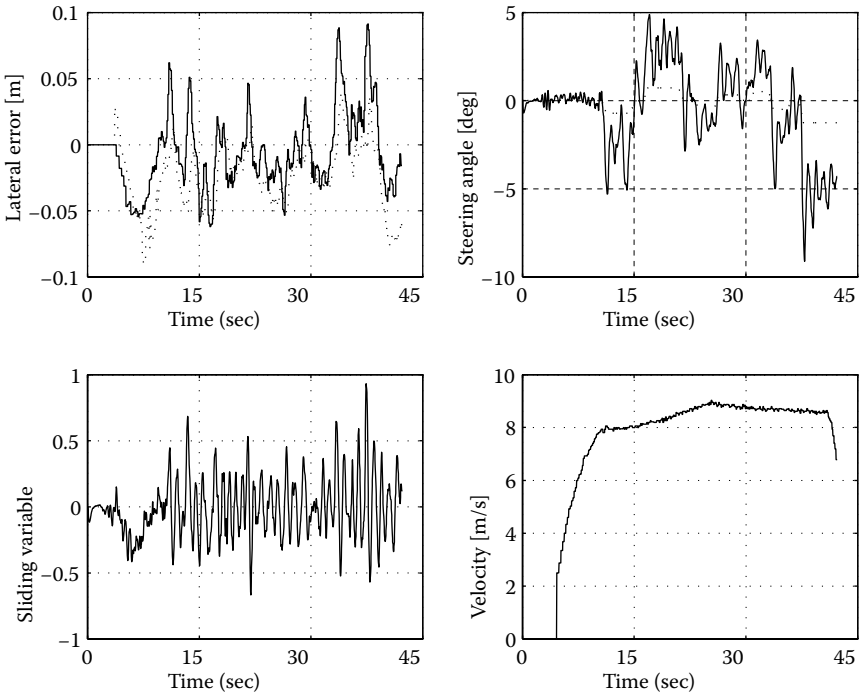

FIGURE 12.22
Experimental results of an automatic steering controller based on sliding mode design. The authors thanks Dr. Hingwe and Professor Tomizuka for providing this experimental data.

References

Ackermann J, Bartlett A, Kaesbauer D, Sienel W, Steinhauser R., 1993. *Robust Control: Analysis and Design of Linear Control Systems with Uncertain Physical Parameters.* London: Springer-Verlag.

Arimoto S, Miyazaki F. 1984. "Stability and Robustness of PID Feedback Control of Robot Manipulators of Sensory Capability." Proceedings of the First International Symposium on Robotics Research. Cambridge, MA: MIT Press, 783–799.

Bloch AM, Reyhanoglu M, McClamroch NH. 1992. "Control and Stabilization of Nonholonomic Dynamic Systems." *IEEE Trans Automat Contr* 37:1746–1757.

Chen Y-F, Mita T, Wahui S. 1990. "A New and Simple Algorithm for Sliding Mode Control of Robot Arms." *IEEE Trans Automat Contr* 35:828–829.

Craig J. 1986. *Introduction to Robotics: Mechanics and Control*. Reading, MA: Addison-Wesley.

Craig J. 1988. *Adaptive Control of Mechanical Manipulators*. Reading, MA: Addison-Wesley.

Dorling C, Zinober A. 1986. "Two Approaches to Hyperplane Design in Multivariable Variable Structure Control Systems." *Int J Control* 44:65–82.

Gilbert E, Ha I. 1984. "An Approach to Nonlinear Feedback Control with Applications to Robotics." *IEEE Trans Syst Man Cybern* 14:879–884.

Guldner J, Utkin VI. 1995. "Sliding Mode Control for Gradient Tracking and Robot Navigation Using Artificial Potential Fields." *IEEE Trans Rob Autom* 11:247–254.

Guldner J, Utkin VI, Ackermann J. 1994. "A Sliding Mode Approach to Automatic Car Steering." Proceedings of the American Control Conference, Baltimore, MD.

Guldner J, Utkin VI, Bauer R. 1994. "On the Navigation of Mobile Robots in Narrow Passages: A General Framework Based on Sliding Mode Theory." Proceedings of the International Federation of Automatic Control Symposium on Robot Control, Capri, Italy.

Guldner J, Utkin VI, Bauer R. 1995. "A Three-Layered Hierarchical Path Control System for Mobile Robots: Algorithms and Experiments." *Rob Auton Syst* 14:133–147.

Guldner J, Utkin VI, Hashimoto H. 1997. "Robot Obstacle Avoidance in *n*-Dimensional Space Using Planar Harmonic Artificial Potential Fields." *J Dyn Syst Meas Control* 119:160–166.

Hedrick JK, Tomizuka M, Varaiya P. 1994. "Control Issues in Automated Highway Systems." *IEEE Control Syst* 9:21–30.

Hingwe P, Tomizuka M. 1995. "Two Alternative Approaches to the Design of Lateral Controllers for Commuter Buses based on Sliding Mode Control," in *Advanced Automotive Technologies*. Presented at the American Society of Mechanical Engineers International Mechanical Engineering Congress and Exposition, San Francisco, CA.

Hogan N. 1985. "Impedance Control: An Approach to Manipulation (Parts I–III)." *J Dyn Syst Meas Control* 107:1–24.

Hunt L, Su R, Meyer G. 1983. "Global Transformation of Nonlinear Systems." *IEEE Trans Automat Contr* 28:24–31.

Khatib O. 1986. "Real-Time Obstacle Avoidance for Robot Manipulators and Mobile Robots." *Int J Rob Res* 5:90–98.

Koditscheck D. 1991. "The Control of Natural Motion in Mechanical Systems." *J Dyn Syst Meas Control* 113:547–551.

Koren Y, Borenstein J. 1991. "Potential Field Methods and Their Inherent Limitations for Mobile Robot Navigation." Proceedings of the IEEE Conference on Robotics and Automation, Sacramento, CA, pp. 1398–1404.

Krogh B. 1984. "A Generalized Potential Field Approach to Obstacle Avoidance Control." Proceedings of the Society of Manufacturing Engineers Conference on Robotics Research, Bethlehem, PA.

Latombe J-C. 1991. *Robot Motion Planning*. Amsterdam: Kluwer Academic Publishers.

Lewis F, Abdallah C, Dawson D. 1993. *Control of Robot Manipulators*. New York: Macmillan Publishers.

Lu Y, Chen J. 1993. "Sliding Mode Controller Design for a Class of Nonautonomous Systems: An Experimental Study." Proceedings of the IEEE International Conference of Industrial Electronics, Control, and Instrumentation, Honolulu, HI.

Neimark J, Fufaev N. 1972. "Dynamics of Nonholonomic Systems." Translation of *Mathematics Monographs*, Vol. 33. Providence, RI: American Mathematical Society.

Patwardhan S, Tan H-S, Guldner J. 1997. "A General Framework for Automatic Steering Control." Proceedings of the American Control Conference, Albuquerque, NM.

Peng H. 1992. *Vehicle Lateral Control for Highway Automation*. Ph.D. thesis, University of California, Berkeley, CA.

Pham H, Hedrick K, Tomizuka M. 1994. "Combined Lateral and Longitudinal Control of Vehicles for IVHS." Proceedings of the American Control Conference, Baltimore, MD.

Rimon E, Koditschek DE. 1992. "Exact Robot Navigation using Artificial Potential Functions." *IEEE Trans Rob Autom* 8:501–518.

Ryan EP, Corless M. 1984. "Ultimate Boundedness and Asymptotic Stability of a Class of Uncertain Systems via Continuous and Discontinuous Feedback Control." *IMA J Math Control Info* 1:223–242.

Shi J, Lu Y. 1996. "Chatter Free Variable Structure Perturbation Estimator on the Torque Control of Flexible Robot Joints with Disturbance and Parametric Uncertainties." Proceedings of the International Conference on Industrial Electronics, Control, and Instrumentation, Taipei, Taiwan.

Slotine J-J-E. 1985. "The Robust Control of Robot Manipulators." *Int J Rob Res* 4: 49–64.

Spong M, Vidyasagar M. 1989. *Robot Dynamics and Control*. New York: Wiley & Sons.

Stevens W. 1996. "The Automated Highway Systems Program: A Progress Report." Proceedings of the 13th International Federation of Automatic Control World Congress, San Francisco, CA.

Takegaki M, Arimoto S. 1981. "A New Feedback Method for Dynamic Control of Manipulators." *J Dyn Syst Meas Control* 102:119–125.

Tsugawa S, Aoki M, Hosaka A, Seki K. 1996. "A Survey of Present IVHS Activities in Japan." Proceeding of the 13th International Federation of Automatic Control World Congress, San Francisco, CA.

Utkin VI. 1992. *Sliding Modes in Control and Optimization*. London: Springer-Verlag.

Utkin VI, Drakunov S, Hashimoto H, Harashima F. 1991. "Robot Path Obstacle Avoidance via Sliding Mode Approach." Proceedings of the IEEE/Robotics Society of Japan International Workshop on Intelligent Robots and Systems, Osaka, Japan.

Young K-KD. 1978. "Controller Design for a Manipulator Using Theory of Variable Structure Systems." *IEEE Trans Syst Man Cybern* 8:210–218.

13

Automotive Applications

This chapter presents different applications of sliding modes to a wide range of control and estimation in automotive industry. Sliding mode is recognized as an efficient approach for design of robust controllers for complex nonlinear systems operating under uncertainty conditions, which is common for automotive systems. When designing such systems, high accuracy and dynamic properties should be associated with reliability, low cost, and ease of maintenance, which implies minimization of the number of sensors to acquire the information on the system state. Sliding mode state observers proved to be a promising way to simplify implementation of feedback systems. The items under study embrace three issues: control and estimation for combustion engine AFR (air-fuel ratio), camless combustion engines, and an automotive alternator.

13.1. Air/Fuel Ratio Control

The ratio of injected air and fuel into a cylinder (ARF) should be maintained at a specific level (called stoichiometric ratio, equal to 14.7 for gasoline), corresponding to the maximum efficiency of a combustion engine

$$ARF = \frac{\dot{m}_{ac}}{\dot{m}_{fc}}, \tag{13.1.1}$$

where $\dot{m}_{ac}$ is mass flow rate of air entering cylinder, and $\dot{m}_{fc}$ is fuel flow rate entering cylinder. The air mass flow rate depends on the intake manifold pressure and engine parameters [Kim, Rizzoni, and Utkin 1998]

$$\dot{m}_{ac} = \frac{\eta_v p_m V_d \omega}{4\pi R T_a} \tag{13.1.2}$$

where η_v is charge efficiency, p_m is intake manifold pressure assumed to be measured, V_d is displacement volume, π is engine speed, R is ideal gas constant (joules per kilogram per kelvin), and T_a is ambient temperature.

The charge efficiency is not available but can be estimated based on manifold pressure equation

$$\frac{dp_m}{dt} + \frac{\eta_v V_d \omega}{4\pi V_m} p_m = \frac{RT_a}{V_m} \dot{m}_{ath}, \tag{13.1.3}$$

where $\dot{m}_{ath}$ is the (measurable) air mass flow rate at the throttle. The fuel m_{fi} from an injector is not sent to the cylinder directly; it condensates and evaporates in the intake port. A commonly used model of the condensation and evaporation dynamics of fuel in an intake port [Kim, Rizzoni, and Utkin 1998] is based on the notion that a fraction of the fuel injected into the inlet port will condense to form a liquid fuel film in the inlet port walls. The mass of liquid fuel will then change as a result of the addition of fuel from the injection process and the evaporation of the condensed fuel according to

$$\begin{aligned} \dot{m}_{ff} &= -\frac{1}{\tau_f} m_{ff} + X\dot{m}_{fi} \\ \dot{m}_{fc} &= \frac{1}{\tau_f} m_{ff} + (1-X)\dot{m}_{fi}, \end{aligned} \tag{13.1.4}$$

where m_{ff} is mass of fuel in fuel film, $\dot{m}_{fi}$ is fuel flow rate from injector, X is fraction of injected fuel enter into the film, and τ_f is fuel evaporation time constant.

As follows from the above equations,

$$\phi = \frac{1}{\tau_f} \frac{m_{ff}}{\dot{m}_{ac}} + (1-X)\frac{\dot{m}_{fi}}{\dot{m}_{ac}}, \quad \phi = \frac{1}{AFR}. \tag{13.1.5}$$

An important aspect of the dynamics of a spark-ignition engine is the inherent delay of the combustion process and the transport of the exhaust gas between the exhaust valve and the oxygen sensor with only binary output readings. The total delay θ is the sum of combustion delay and transport delay. The sensor used to measure the concentration of oxygen in the exhaust gas can, to a first approximation, be modeled as a first-order lag with time constant τ_m and a delay

$$\tau_m \frac{d\phi_m}{dt} + \phi_m = \phi(t-\theta), \tag{13.1.6}$$

with the output

$$y = sign(\phi_m - \phi_s),\ (1/\phi_s) - \text{stoichiometric ratio.} \tag{13.1.7}$$

The fuel flow rate $\dot{m}_{fi}$ from the injector takes the role of the control variable and should be designed such that AFR is equal to the stoichiometric ratio.

First, the charge efficiency needed for calculation of $\dot{m}_{ac}$ (Equation 13.1.2) will be found from Equation 13.1.3 using a sliding mode observer:

$$\frac{d\tilde{p}_m}{dt} + \frac{\Psi V_d \omega}{4\pi V_m} p_m = \frac{RT_a}{V_m} \dot{m}_{ath},$$
$$\Psi = \Psi_0 sign(p_m - \tilde{p}_m),\ \Psi_0 = const > 0,\ \tilde{p}_m \text{ is an estimate of } p_m.$$

Because $s = p_m - \tilde{p}_m$ and $\dot{s} = \frac{V_d \omega}{4\pi V_m} p_m [\eta_v - \Psi_0 sign(s)]$ have different signs for $\Psi_0 > \eta_v$, sliding mode occurs on $s = 0$ and $\Psi_{eq} = \eta_v$. As shown in Section 2.4, the value of η_v is equal to average value of Ψ obtained by filtering out its high-frequency component with a low-pass filter. Then, the air flow rate entering the cylinder can be calculated from Equation 13.1.2.

A second sliding mode observer is intended to find $\dot{m}_{fc}$, the fuel flow rate entering cylinder. Bearing in mind that Equation 13.1.6 can be written as

$$\tau_m \frac{dz}{dt} + z = \phi(t),\ \ \phi_m = z(t - \theta),$$

The system (Equations 13.1.4 through 13.1.7) with control $\dot{m}_{fi}$ and output y can be represented in the form of Equation 6.4.1 with the modification in Remark 6.2 at the end of Section 6.4. Note that $\dot{m}_{ac}$ has been estimated by the first observer designed above. It means that the methodology developed in Section 6.4 is applicable and the states that m_{ff} and ϕ, or $1/AFR$, can be found.

After $\dot{m}_{ac}$ and m_{ff} are found, the control $\dot{m}_{fi}$ needed for maintaining the air/fuel ratio at the desired level $\left(\phi(t) = \phi_s = {}^{1}\!/_{AFR_s}\right)$ can be calculated from Equation 13.1.5:

$$\dot{m}_{fi} = \frac{1}{1 - X} \frac{\dot{m}_{ac}}{AFR_s} - \frac{1}{(1 - X)\tau_f} m_{ff}.$$

The estimation results are compared with experimental data obtained from a production mass air flow meter (only possible at steady state) and with the charge efficiency predicted by an empirical model [Krishnaswami and Rizzoni, 1997] consisting of a polynomial function of engine speed ω, manifold pressure p_m, and throttle opening α:

$$\eta_v = 1.9751 \times 10^{-1} - 3.6075 \times 10^{-3} \omega + 7.0125 \times 10^{-6} \omega^2 - 5.3226 \times 10^{-6} p_m + 4.8898\alpha$$

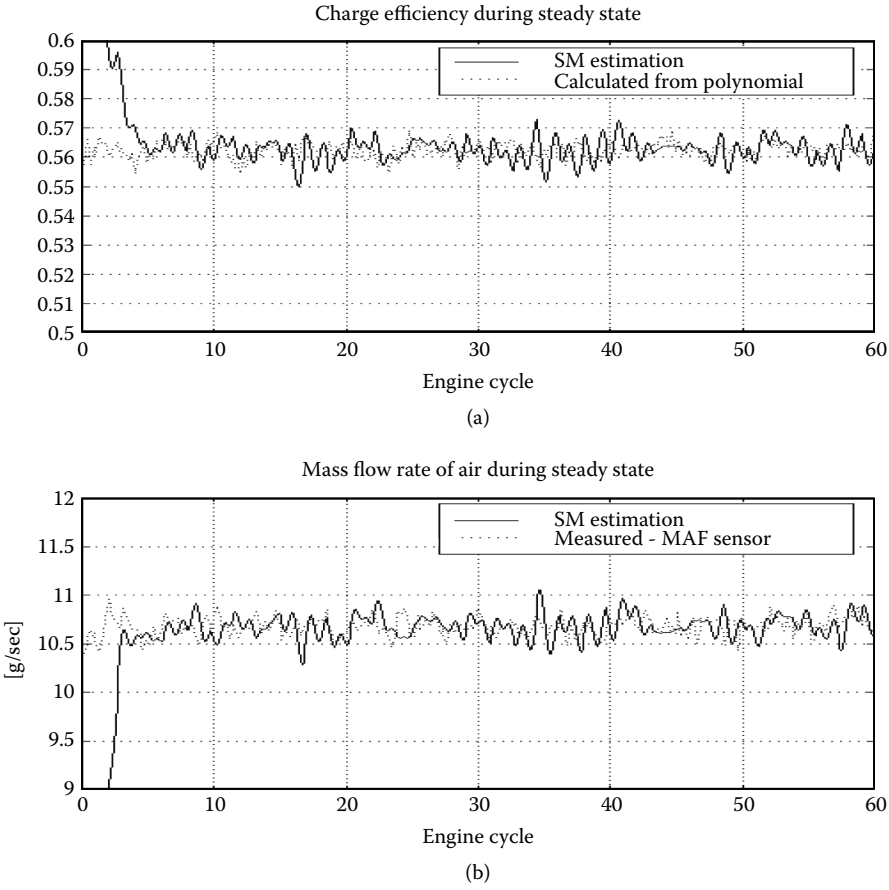

FIGURE 13.1
Estimation result during steady state ($\alpha = 5\%$, $\omega = 860$ rpm, $p_m = 50$ kPa).

Figure 13.1a compares the charge efficiency η_v estimated from the sliding mode observer with the estimate obtained using the polynomial approximation. Figure 13.1b repeats the comparison for the air charge variable, adding also the measured air charge by the mass flow sensor, for the same experimental conditions. The estimation results of the same variables during throttle transient are illustrated in Figure 13.3. Unfortunately, it is impossible to obtain a reliable measurement of the air flow rate during a transient.

Estimation of fuel film and AFR using a nonlinear oxygen sensor can be done by the observer proposed in this section: observer with binary measurement. With this observer, in addition to estimate of m_{ff}, the current value of AFR can also be estimated.

Figure 13.4 shows the estimation of the fuel flow in fuel film and linear AFR sensor. After initial transient attributable to the difference in initial

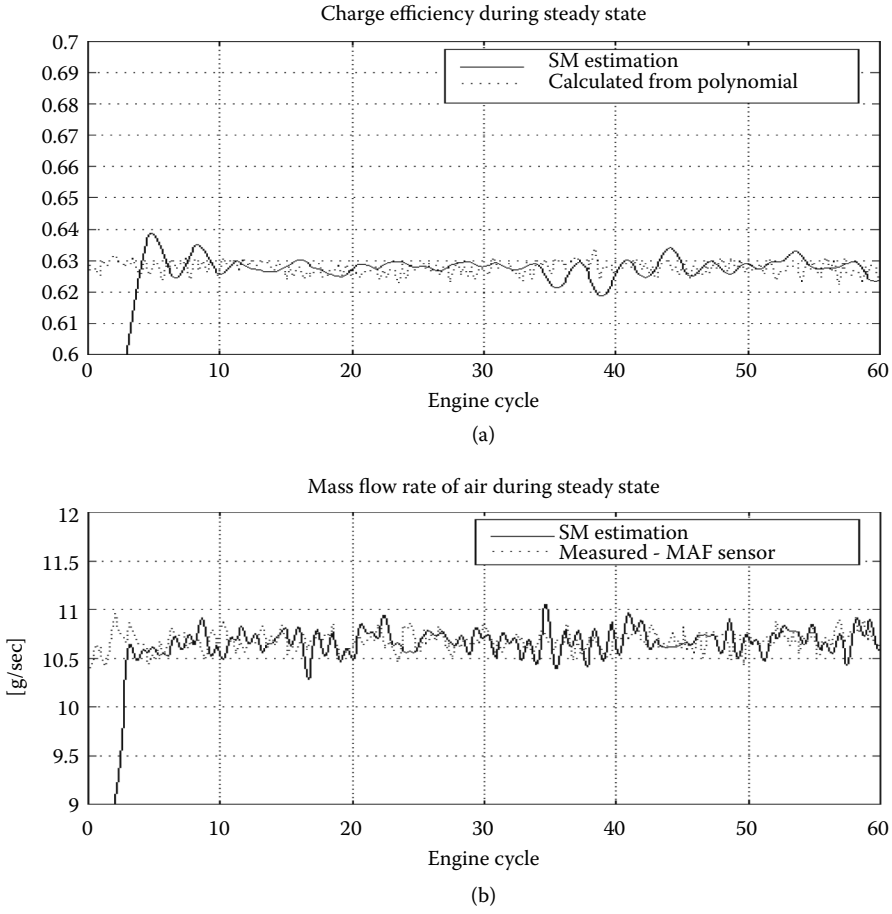

FIGURE 13.2
Estimation result at steady state (α =10%, ω = 1550 rpm, p_m = 50 kPa).

conditions, the estimated states converge to the actual states within a reasonable accuracy except during throttle tip-in.

The measurement was performed by the sensor with continuous reading, which is much more expensive than the binary oxygen sensor used for production vehicles.

The observers in this section are simulated using for the mean value model [Kim, Rizzoni, and Utkin, 1998]. Figure 13.5 shows a comparison between the response from a standard PI controller and the response with transient fuel compensation using the observer-based method. As can be seen in Figure 13.5, the AFR excursion during transient is improved remarkably with transient fuel compensation.

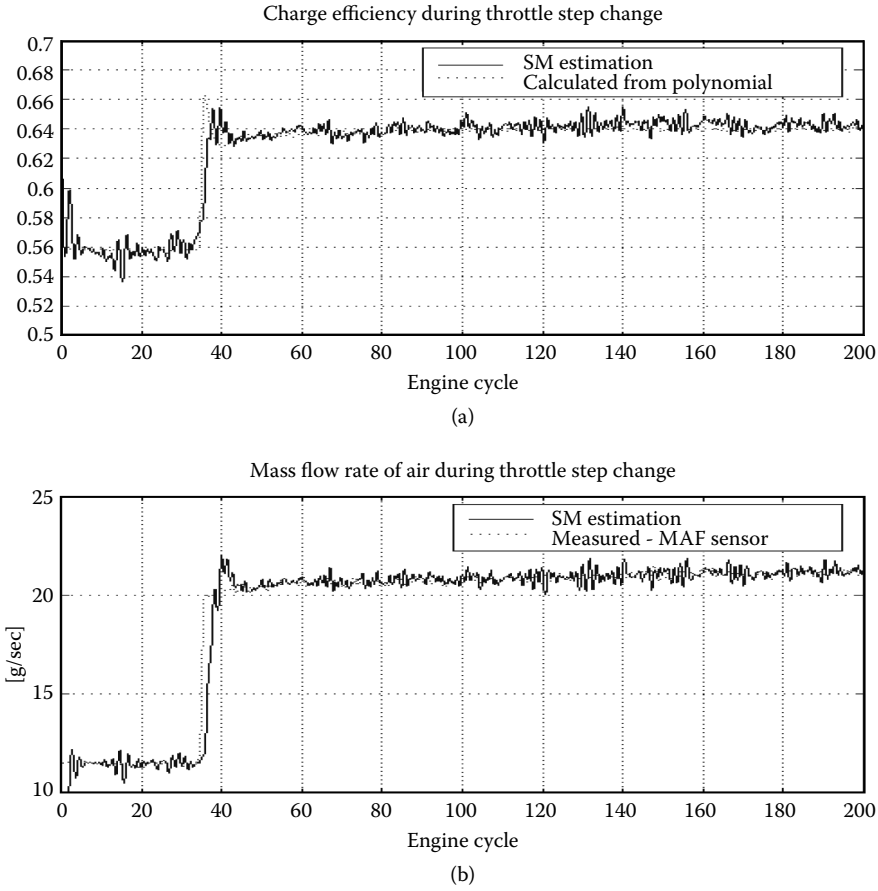

FIGURE 13.3
Estimation result during throttle tip-in (throttle step change 15° → 20° at the 35th cycle).

13.2. Camless Combustion Engine

Replacing a cam shaft by individual solenoid-type actuators for each cylinder is a new promising technological approach. It leads to fuel economy as a result of reduction of pumping losses and lower idle speed, can improve engine performance, and reduce nitrogen oxide and hydrocarbon in exhaust gas attributable to individual control of each cylinder [Holfman and Stefanopoulou 2001; Chun and Tsao 2003] .The position of each valve (Figure 13.6) is controlled by the input voltage of the solenoid; the valve is subjected to electromagnetic and spring forces. To avoid valve damage, the feedback control should be designed such that up and down travels of the valve are monotonous, called the soft-seating problem. The design idea will be illustrated for a simplified model without a spring (Figure 13.7).

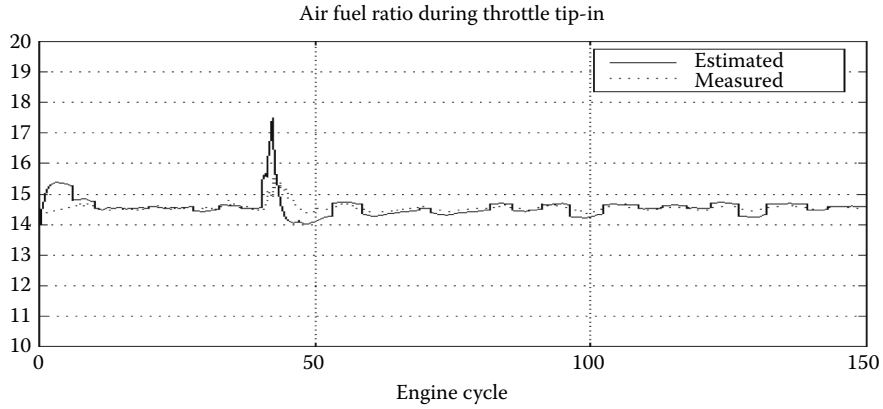

FIGURE 13.4
Observer responses during throttle tip-in.

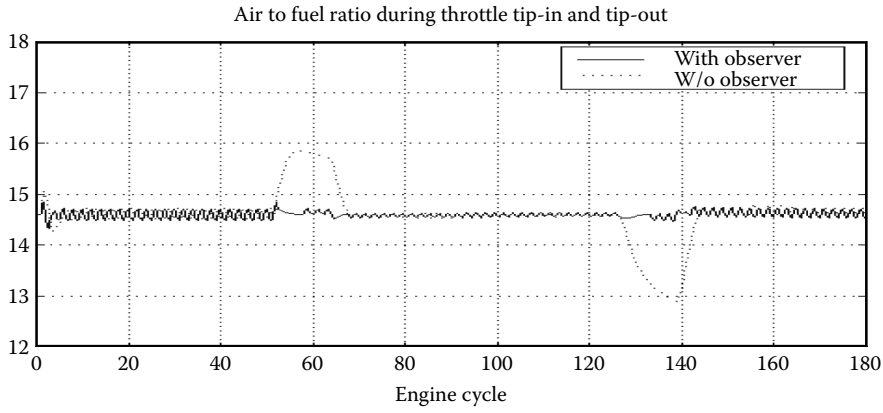

FIGURE 13.5
AFR during throttle step change: simulation results.

All coefficients in the system equations are set equal to 1:

$$\begin{cases} \ddot{z} = i\Psi - g \\ \dot{\Psi} = -iR + u \end{cases} \quad \Psi = \frac{i}{z+a} \Rightarrow \ddot{z} = \frac{i^2}{z+a} - g, \tag{13.2.1}$$

where flux Ψ is a monotonously decreasing function of the air gap z ($a = const > 0$) , and g is the gravitational force.

Steady state is described by

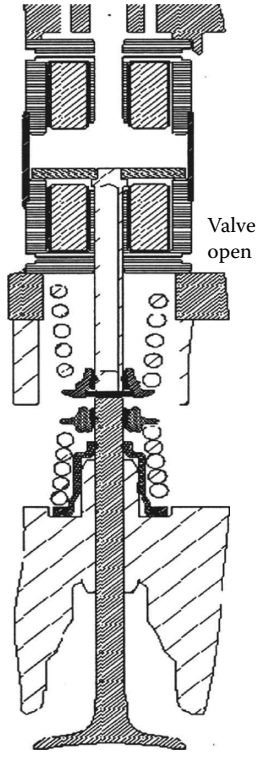

FIGURE 13.6
Solenoid-type actuator.

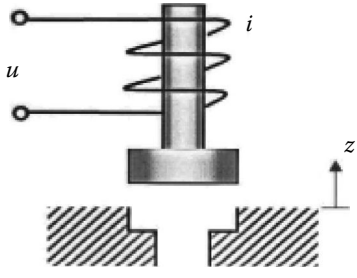

FIGURE 13.7
Simplified model.

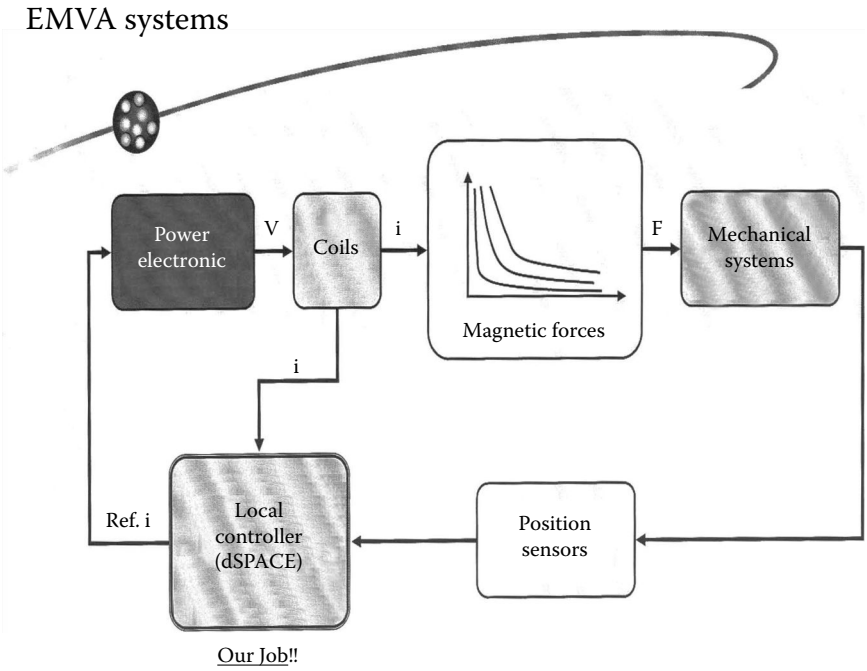

FIGURE 13.8
Block diagram of feedback control system.

$$z^* = 0, \quad i^* = \sqrt{ga}, \quad u^* = Ri^* = R\sqrt{ga}. \tag{13.2.2}$$

Represent Equation 13.2.1 as a system of three first-order equations

$$\begin{cases} \dot{z}_1 = z_2 & z_1 = z \\ \dot{z}_2 = \dfrac{i^2}{z_1 + a} - g & \\ \dot{i} = z_2 \dfrac{i}{z_1 + a} + (z_1 + a)(-iR + u) & \end{cases} \tag{13.2.3}$$

The force F developed by the electromagnetic coil is inversely proportional to the air gap for a constant current as shown in the block diagram (Figure 13.8). The aim of control u is to reduce the output variable z_1 to zero for any nonzero initial conditions.

The system Equation 13.2.3 is in the regular form (Section 3.3) with the current i as an intermediate control in the block consisting of the two first equations. If

$$\frac{i^2}{z_1 + a} - g = -k_1 z_1 - k_2 z_2, \quad \text{or } s = \frac{i^2}{z_1 + a} - g + k_1 z_1 + k_2 z_2 = 0, \tag{13.2.4}$$

the desired dynamics of z_1

$$\begin{cases} \dot{z}_1 = z_2 \\ \dot{z}_2 = -k_1 z_1 - k_2 z_2 \end{cases}$$

can be obtained by a proper choice of the coefficients k_1 and k_2. The final step of the design method based on the regular form enforces sliding mode on the surface $s = 0$ using the discontinuous control

$$u = -u_0 sign(s) \text{ or } u = -u_0 \frac{1 + sign(s)}{2}, \tag{13.2.5}$$

depending on the structure of the power converter. The coil current is always positive in real systems; therefore, only positive voltages are needed and the second version can be recommended.

In the time derivative of s,

$$\dot{s} = 2\frac{i}{z_1 + a} u + f(z_1, z_2, i),$$

$f(z_1, z_2, i)$ is a continuous function of the state variables. The magnitude of the control u_0 can be selected such that the values of s and $\dot{s}$ have different signs. Then, according to Equation 2.4.1, sliding mode occurs after a finite time interval, and condition in Equation 13.2.4 holds.

The control has been designed assuming that all state components are available. Two scenarios will be analyzed below: control design with position and current measurement, and control design with only current measurement.

First, when only current is measured, analyze local observability of the linearized system in the vicinity of the steady-state point (Equation 13.2.2) $z_1^* = z_2^* = 0$, $i = i^* + \Delta i$, $u = u^* + \Delta u$ with measurement of the current only:

$$\frac{i^2}{z_1+a}=\frac{(i^*+\Delta i)^2}{z_1+a}\approx g+2\sqrt{\frac{g}{a}}\Delta i-\frac{g}{a}z_1$$

$$z_2\frac{i^*+\Delta i}{z_1+a}\approx\sqrt{\frac{g}{a}}z_2,\quad (z_1+a)[-(i^*+\Delta i)R+u^*+\Delta u]\approx -aR\Delta i+a\Delta u,$$

$$\dot{x}=Ax+b\Delta u,\quad x=\begin{bmatrix}z_1\\ z_2\\ \Delta i\end{bmatrix},\quad A=\begin{pmatrix}0 & 1 & 0\\ -\frac{g}{a} & 0 & 2\sqrt{\frac{g}{a}}\\ 0 & \sqrt{\frac{g}{a}} & -aR\end{pmatrix},\ b=\begin{bmatrix}0\\ 0\\ a\end{bmatrix},$$

$$y=cx,\quad c=(0,0,1).$$

The system is observable because the observability matrix is not singular

$$\det\begin{pmatrix}c\\ cA\\ cA^2\end{pmatrix}=\det\begin{pmatrix}0 & 0 & 1\\ 0 & \sqrt{\frac{g}{a}} & -aR\\ -\left(\frac{g}{a}\right)^{3/2} & -aR\sqrt{\frac{g}{a}} & 2\frac{g}{a}+a^2R^2\end{pmatrix}\neq 0.$$

In the framework of a linear model, an asymptotic state observer can be designed to obtain both variables z_1 and z_2 with only measuring the coil current i (Section 6.1):

$$\dot{\hat{x}}=A\hat{x}+b\Delta u+L(\hat{i}-i),\quad L=\begin{bmatrix}l_1\\ l_2\\ l_3\end{bmatrix},\quad L=const, \tag{13.2.6}$$

where $\hat{x}$ tends to x at the desired rate, which means that $z_1$and z_2 are available for implementation of the discontinuous control Equation 13.2.5.

The observer design method (Equation 13.2.6) was applied to the nonlinear system directly:

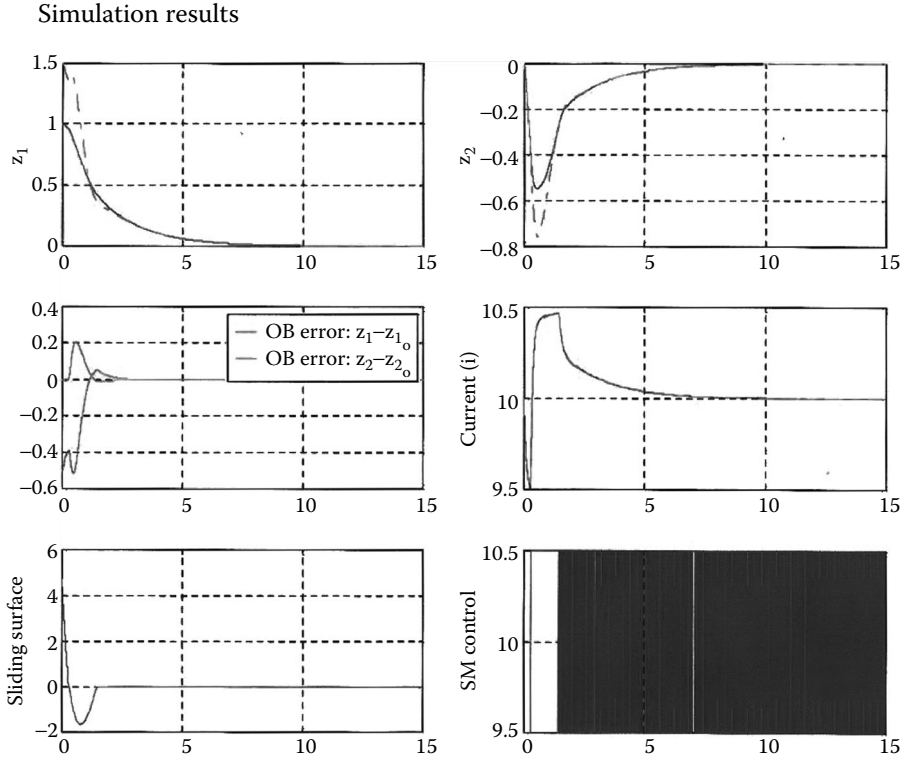

FIGURE 13.9
Simulations with measurement of current only.

$$\begin{cases} \dot{\hat{z}}_1 = \hat{z}_2 + l_1(\hat{i} - i) \\ \dot{\hat{z}}_2 = \dfrac{\hat{i}^2}{\hat{z}_1 + a} - g + l_2(\hat{i} - i) \\ \dot{\hat{i}} = \hat{z}_2 \dfrac{\hat{i}}{\hat{z}_1 + a} + (\hat{z}_1 + a)(-\hat{i}R + u) + l_3(\hat{i} - i). \end{cases}$$

The convergence of the estimates $\hat{z}_1$ and $\hat{z}_2$ to the real values of $z_1$and z_2 was verified by simulation as well the monotonous convergence of z_1 to zero (Figure 13.9).

The control method developed in this section was tested using an experimental setup of VISTEON. The control (Equations 13.2.4 and 13.2.5) was implemented using measurement of both the current and the valve position. The speed of the valve z_2 is found using the observer:

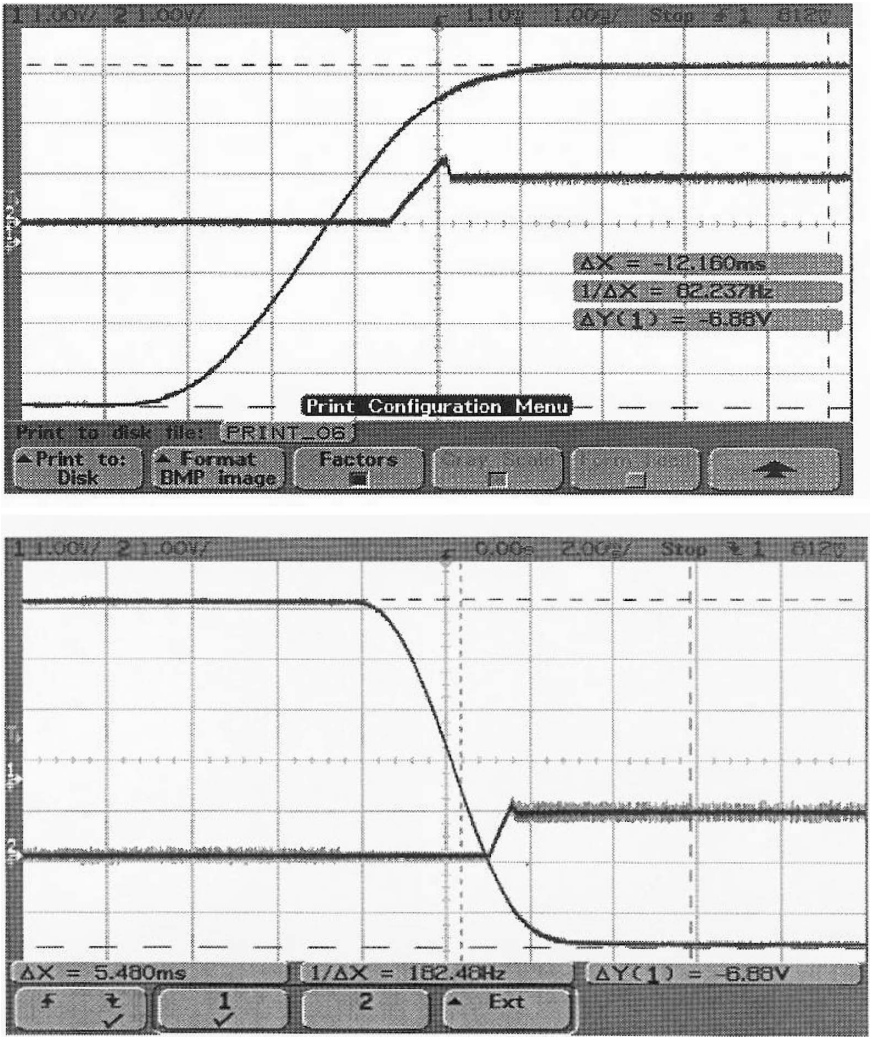

FIGURE 13.10
Soft-seating for both opening and closing processes.

$$\begin{cases} \dot{\hat{z}}_1 = \hat{z}_2 + l_1(\hat{z}_1 - z_1) \\ \dot{\hat{z}}_2 = \dfrac{i^2}{z_1 + a} - g + l_2(\hat{z}_1 - z_1). \end{cases}$$

The valve position and coil current as time functions are plotted in Figure 13.10. As the experiments showed, the processes for closing and opening the valve for air-fuel injection are monotonous.

13.3. Observer for Automotive Alternator

This section presents a method for estimating back-EMF without a direct mechanical sensor of the rotor position [Utkin, Chen, Zarei, and Miller 1997, 1999]. The back EMFs are needed to implement high-efficiency control of an automotive alternator (AC generator).

The electrical circuit of the automotive electrical power supply system is shown in Figure 13.11.

The AC generator is composed of three identical windings with inductance L and resistance R_w. The switching signals u_m (m = 1, 2, 3) represent the controllable rectifier, which can be either 1 or –1. A value of 1 means that the phase winding is connected to the "plus" terminal, and a value of –1 connects it to the "minus" terminal of the battery. The dynamic equations of the system are represented by

$$\frac{di_m}{dt} = -\frac{R_w}{L} i_m - \frac{v_o}{6L}(2u_m - \sum_{n \neq m} u_n) + \frac{1}{L} e_m(t), \tag{13.3.1}$$

$$\frac{R_L + R_b}{R_L(t)} \frac{du_c}{dt} = -\frac{1}{R_L(t)C} u_c + \frac{1}{2C} \sum_{m=1}^{3} u_m i_m, \tag{13.3.2}$$

where DC-bus voltage $v_o = CR_b(du_c/dt) + u_c$ and m = 1, 2, 3. Equation 13.3.2 is a simplified model of the battery charging system with capacitor C, internal resistance of the battery R_b, and consumer loads $R_L(t)$ in the automobile electric system. u_c stands for the voltage of the capacitor, and i_m refers to the AC phase currents.

The alternator's back EMFs $e_m(t)$ are needed for switching assignment of the controllable rectifier. The EMFs are sinusoidal functions with

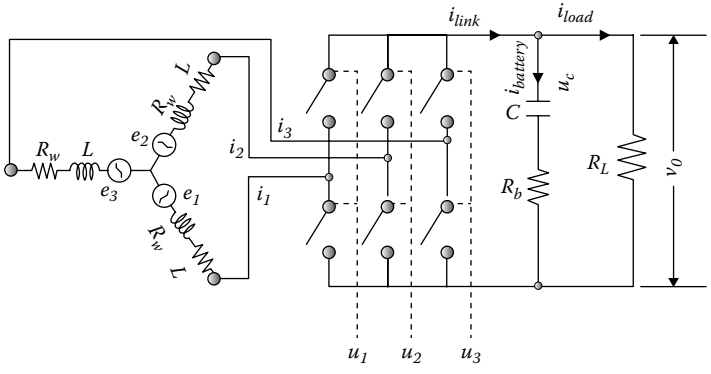

FIGURE 13.11
Automotive electric power supply system.

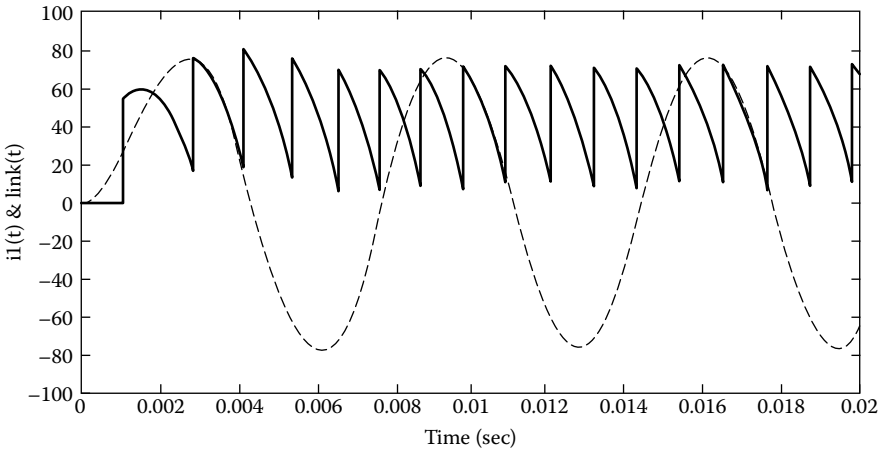

FIGURE 13.12
Phase and link currents.

frequency and amplitude depending on the engine speed, if the speed is constant.

In the following, observer design for the state variables of phase $m = 1$ will be presented. The state variables associated with the second and third phases can be obtained in a similar manner. Because measurement of the phase current may be prohibitive, the proposed observer uses only two sensors of the electrical variables: output DC voltage v_0 and DC-link current i_{link} of the rectifier. As shown in Figure 13.12, the phase current i_1 coincides with the link current only for short, reoccurring time intervals called observation windows.

Let us first design a sliding mode observer under the assumption that both phase current i_1 and v_o are available:

$$\frac{d\hat{i}_1}{dt} = -\frac{R_w}{L}\hat{i}_1 - \frac{v_o}{6L}(2u_1 - u_2 - u_3) + \frac{1}{L}Msign(i_1 - \hat{i}_1), \tag{13.3.3}$$

where M is a constant observer gain such that sliding mode with $\bar{i}_1 = i_1 - \hat{i}_1 = 0$ occurs. Having identical parameters R_w and L with those in model Equation 13.3.1, one obtains the equivalent value of the observer switching function

$$\{Msign(\bar{i}_1)\}_{eq} = e_1$$

by subtracting Equation 13.3.3 from Equation 13.3.1, for $m = 1$, and solving the mismatch equation $\dot{\bar{i}}_1 = 0$ for $Msign(\bar{i}_1)$ (Section 2.3). The equivalent value $\{Msign(\bar{i}_1)\}_{eq}$ or the EMF can be found by using a low-pass filter with time constant τ:

$$\tau\dot{z} = -z + Msign(\bar{i}_1), \tag{13.3.4}$$

implying that $lim_{\tau\to 0}(z) = e_1$, if the switching frequency tends to infinity (Section 2.3). Thus, the back EMF can be estimated by applying the equivalent control method. However, in real-life systems, for example, systems with discrete-time implementation of a controller, the switching frequency is finite and the tradeoff between filtering out the high-frequency component of control and distortion of its low-frequency component dictates selection of the time constant τ.

The simulation results for the proposed observer Equations 13.3.3 and 13.3.4 demonstrate dependence of the estimation accuracy on the time constant τ for the case of constant engine speed. The parameters of the rectifier are given in Table 13.1. Frequency and amplitude of the real EMF are equal to $\omega = 150$ Hz and $A = 9.6v$, the sampling interval $\delta = 1$ μsec, $M = 60$. A considerable phase shift between real value of e_1 and its estimate can be seen for the case $\tau = 0.2$ msec (Figure 13.13). To decrease the phase delay, it

TABLE 13.1

Parameters	Values	Parameters	Values
R_w	0.033 Ω	R_L	0.12 Ω
L	1.55×10^{-4} H	R_b	0.012 Ω
C	40 F		

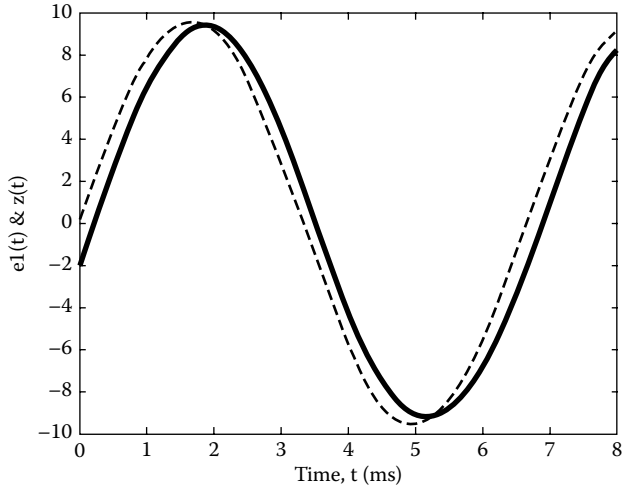

FIGURE 13.13
Estimated and real EMFs with time constant $\tau = 0.2$ msec.

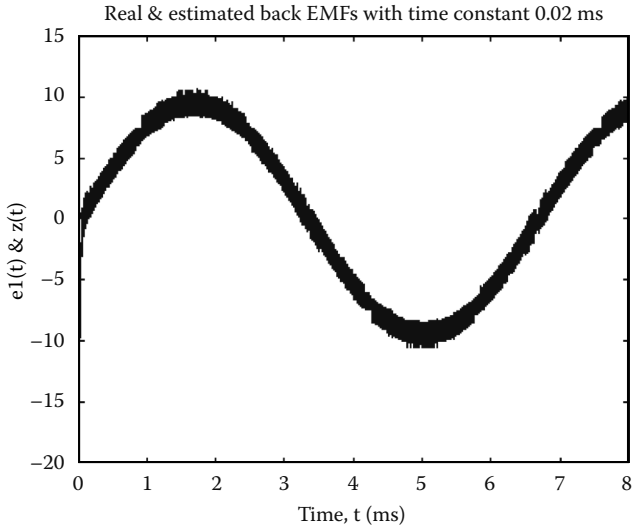

FIGURE 13.14
Estimated and real EMFs with time constant $\tau = 0.2$ msec.

is possible to reduce the time constant of the low-pass filter, for instance, to $\tau = 0.02$ msec. However, this may result in a high-frequency component of the chattering as shown in Figure 13.14.

To overcome the chattering problem, the linear back-EMF model of the sinusoidal function

$$\begin{cases} \dot{e}_1 = e_1' \\ \dot{e}_1' = -\omega^2 e_1 \end{cases} \tag{13.3.5}$$

with constant unknown frequency ω may be taken into account. The system Equation 13.3.5 is complemented by

$$\dot{\omega} = 0 \text{ or } \dot{\Omega} = 0, \quad \Omega = \omega^2. \tag{13.3.6}$$

The observer for estimation of the back EMF and speed is selected in the form

$$\begin{aligned} \frac{d\hat{i}_1}{dt} &= -\frac{R_w}{L}\hat{i}_1 - \frac{v_o}{6L}(2u_1 - u_2 - u_3) + \frac{1}{L}Msign(i_1 - \hat{i}_1) \\ \tau\dot{z} &= -z + Msign(i_1 - \hat{i}_1) \\ \dot{\hat{e}}_1 &= \hat{e}_1' - l_1(\hat{e}_1 - z) \\ \dot{\hat{e}}_1' &= -\hat{\Omega}\hat{e}_1 - l_2(\hat{e}_1 - z) \\ \dot{\hat{\Omega}} &= l_3\hat{e}_1(\hat{e}_1 - z) \end{aligned} \tag{13.3.7}$$

The observer input gains $M > 0$ and $l_i > 0$ ($i = 1, 2, 3$) are to be selected to provide convergence of all its states to the state of Equations 13.3.5 and 13.3.6. Observer stability analysis and selection of the observer parameters can be found in previous work [Chen 1998].

At a qualitative level, the design method can be explained in the following way. As mentioned, $z \approx e_1$; hence, the mismatch equations between states of the system and of the observer can be obtained from Equations 13.3.6 and 13.3.7:

$$\begin{aligned} \dot{\bar{e}}_1 &= \bar{e}_1' - l_1 \bar{e}_1 \\ \dot{\bar{e}}_1' &= -\hat{\Omega}\bar{e}_1 - l_2 \bar{e}_1 - \bar{\Omega}\hat{e}_1 \\ \dot{\bar{\Omega}} &= l_3 \hat{e}_1 \bar{e}_1 \end{aligned} \tag{13.3.8}$$

If $l_1 \gg 1$, then $\bar{e}_1' - l_1 \bar{e}_1 \approx 0$, $\bar{e}_1 \approx \bar{e}_1' / l_1$, and, as follows from Equation 13.3.8,

$$\begin{aligned} \dot{\bar{e}}_1' &= -\frac{\hat{\Omega} + l_2}{l_1} \bar{e}_1' - \bar{\Omega}\hat{e}_1 \\ \dot{\bar{\Omega}} &= \frac{l_3 \hat{e}_1}{l_1} \bar{e}_1' \end{aligned} \tag{13.3.9}$$

The time derivative of the positive definite Lyapunov function

$$V = 1/2 \left[\frac{l_3}{l_1} (\bar{e}_1')^2 + \bar{\Omega}^2 \right] \text{ is } \dot{V} = -\frac{l_3}{l_1} \frac{\hat{\Omega} + l_2}{l_1} (\bar{e}_1')^2 \le 0 \text{ for } l_2 + \hat{\Omega} > 0.$$

The values of $\bar{e}_1'$ cannot be equal to zero identically if $\bar{\Omega} \neq 0$, because e_1 and $\hat{e}_1 = e_1 + \bar{e}_1'$ are nonzero time functions. It means that both mismatches $\bar{e}_1'$ and $\bar{\Omega}$ as well as $\bar{e}_1$ tend to zero, and the back EMF, its time derivative, and frequency are found simultaneously. As can be seen in the simulation results (Figure 13.15), the observer Equation 13.3.7 exhibits much better chattering suppression properties than a low-pass filter of the equivalent control Equation 13.3.4.

In the case of link current measurements, the input i_1 in the first equation of Equation 13.3.7 should be replaced by $u_1 i_{link}$, and the coefficients l_1, l_2 l_3 are selected such that the estimates converge to the real values within the

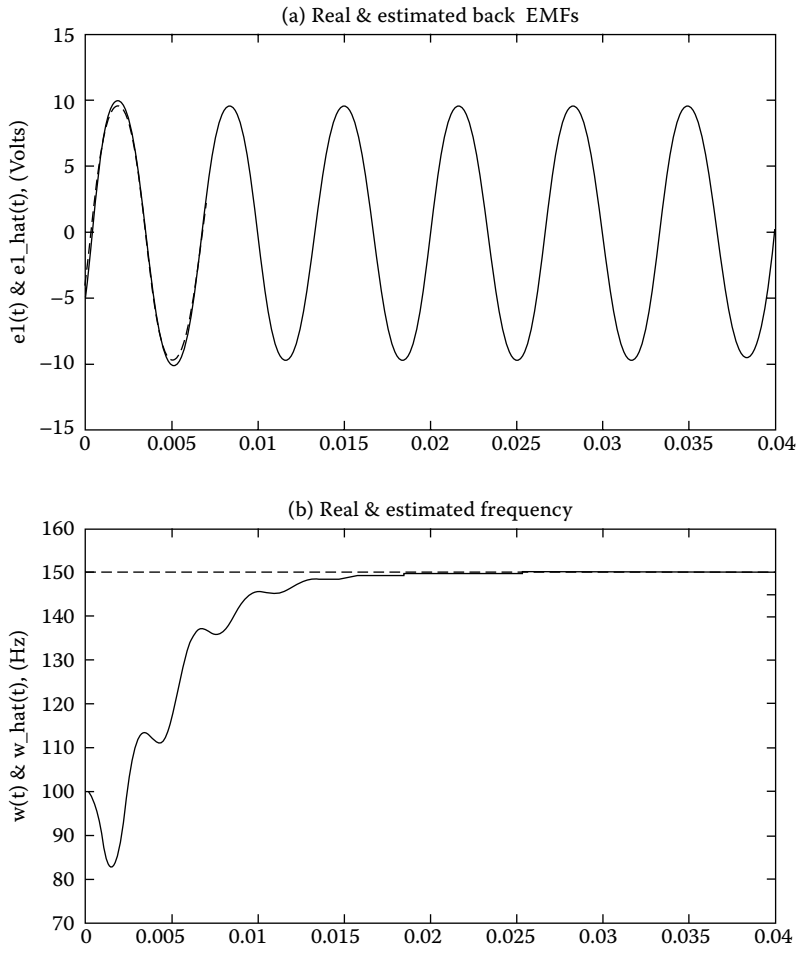

FIGURE 13.15
Observer for estimation of back EMF and frequency.

observation windows, when $u_1 \neq u_2 = u_3$, and they are equal to zero beyond the observation windows. The estimation method with link current measurement was tested at the experimental setup (Figure 13.16) in the Research Science Laboratory of Ford Motor Company.

The observation windows are indicated in Figure 13.17. The estimation result is close to the measured phase current. The estimation methods for time-varying engine speed with the battery current measurement, which is always available in commercially produced cars, and with discrete-time implementation can be found in previous works [Utkin, Chen, Zarei, and Miller 1997, 1999].

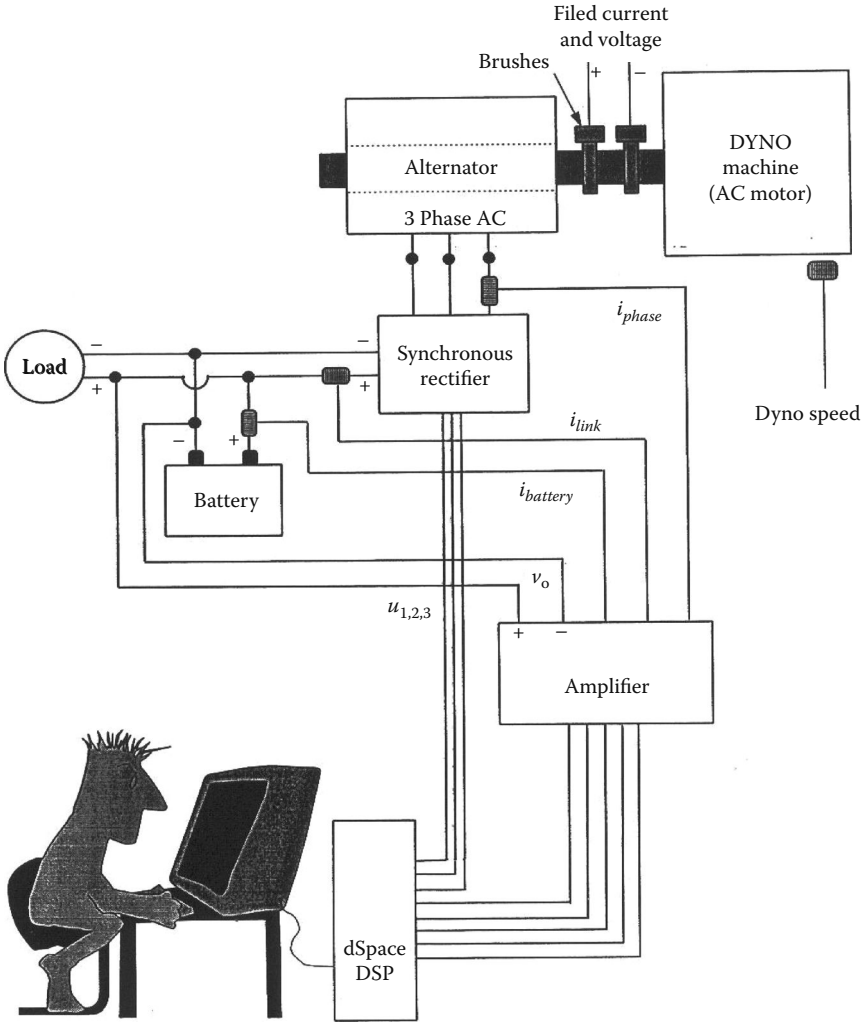

FIGURE 13.16
Schematic diagram of experimental setup.

References

Chen D-S. 1998. *Sliding Mode Observers for Automotive Alternator.* Ph.D. thesis, The Ohio State University, Columbus, OH.

Chun T, Tsao T-C. 2003, "Control of an Electromechanical Actuator for Camless Engines." Proceedings of the American Control Conference, Denver, CO.

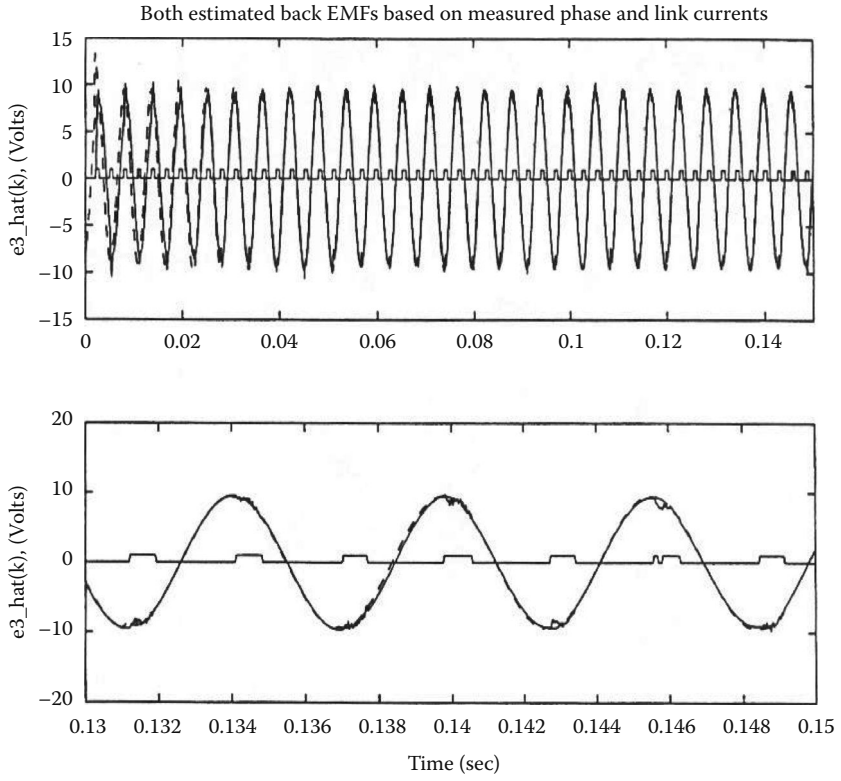

FIGURE 13.17
Comparison of estimated back EMF based on phase $(\hat{e}_{1p})$ and link currents $(\hat{e}_{1l})$.

Holfman W, Stefanopoulou A. 2001. "Iterative Learning Control of Electromechanical Camless Valve Actuator." Proceedings of the American Control Conference, Arlington, VA.

Kim Y-W, Rizzoni G, Utkin V. 1998. "Automotive Engine Diagnostics and Control via Nonlinear Estimation." *IEEE Control Syst* 18:84–89.

Krishnaswami V, Rizzoni G. 1997. "Robust Residual Generation for Nonlinear System Fault Detection and Isolation." Proceedings of the International Federation of Automatic Control/International Federation for Mathematics and Computer in Simulation Symposium on Fault Detection, Supervision, and Safety for Technical Processes, Hull, United Kingdom.

Utkin VI, Chen D-S, Zarei S, Miller J. 1997. "Synchronous Rectification of the Automotive Alternator using Sliding Mode Observer." Proceedings of the American Control Conference, Albuquerque, NM.

Utkin VI, Chen D-S, Zarei S, Miller J. 1999. "Sliding Mode Observers for Automotive Alternators." Proceedings of the American Control Conference, San Diego, CA.

Index

Electrical Engineering

Interest in Sliding Mode Control (SMC) has grown rapidly since the first edition of this book was published. This second edition includes new results that have occurred in SMC throughout the past decade relating to both control design methodology and applications.

In that time, SMC has continued to gain increasing importance as a universal design tool for the robust control of linear and nonlinear electro-mechanical systems. Its strengths result from its simple, flexible, and highly cost-effective approach to design and implementation. Most importantly, SMC promotes inherent order reduction and allows for the direct incorporation of robustness against system uncertainties and disturbances. These qualities lead to dramatic improvements in stability and help enable the design of high-performance control systems at low cost. SMC is particularly useful for the design of electromechanical systems because of its discontinuous structure. In fact, where the hardware of many electromechanical systems (such as electric motors) prescribes discontinuous inputs, SMC becomes the natural choice for direct implementation.

Reflecting developments in the field over the past decade, this new edition of **Sliding Mode Control in Electro-Mechanical Systems** builds on the solid fundamentals presented in the first edition to promote a deeper understanding of the conventional SMC methodology. It examines new design principles in order to broaden the application potential of SMC. Written by three of the most respected experts in the field, including one of its originators, this updated edition

- Details new theoretical developments, including the suppression of the high-frequency oscillations that were considered the main obstacle to SMC implementation
- Complements new developments with cutting-edge design principles
- Explores a wider range of applications, including cascade control of induction motors, control of multiphase power converters, new automotive applications
- Adds new methods of power converter control, as well as a new chapter on high-order SMC for implementations with continuous control actions
- Offers a simple and compact description of mathematical design principle

This book provides a unique combination of theory, implementation issues, and examples of real-life applications reflective of the authors' own industry-leading work in the development of robotics, hybrid automobiles, and other technological breakthroughs.

CRC Press
Taylor & Francis Group
an **informa** business
www.crcpress.com

6000 Broken Sound Parkway, NW
Suite 300, Boca Raton, FL 33487
270 Madison Avenue
New York, NY 10016
2 Park Square, Milton Park
Abingdon, Oxon OX14 4RN, UK

65602
ISBN: 978-1-4200-6560-2
90000
9 781420 065602